UNIVERSITEIT GENT
Faculteit Wetenschappen
Vakgroep Geologie en Bodemkunde
Renard Centre of Marine Geology

Structure and Evolution of Transfer Zones in Extensional Tectonic Basins — A Study based on Examples from Lake Baikal and Analogue Sandbox Models

Studie van de Structuur en Evolutie van Transferzones in Extensiebekkens aan de hand van Voorbeelden uit het Baikal-Meer en Analoge Zandbakmodellen

Robert Hus

Proefschrift voorgelegd tot het behalen van de graad van
Doctor in de Wetenschappen, richting Geologie

Promotor: **Prof. Dr. M. De Batist**
Co-Promotor: **Dr. J. Klerkx**

Academiejaar 2004–2005

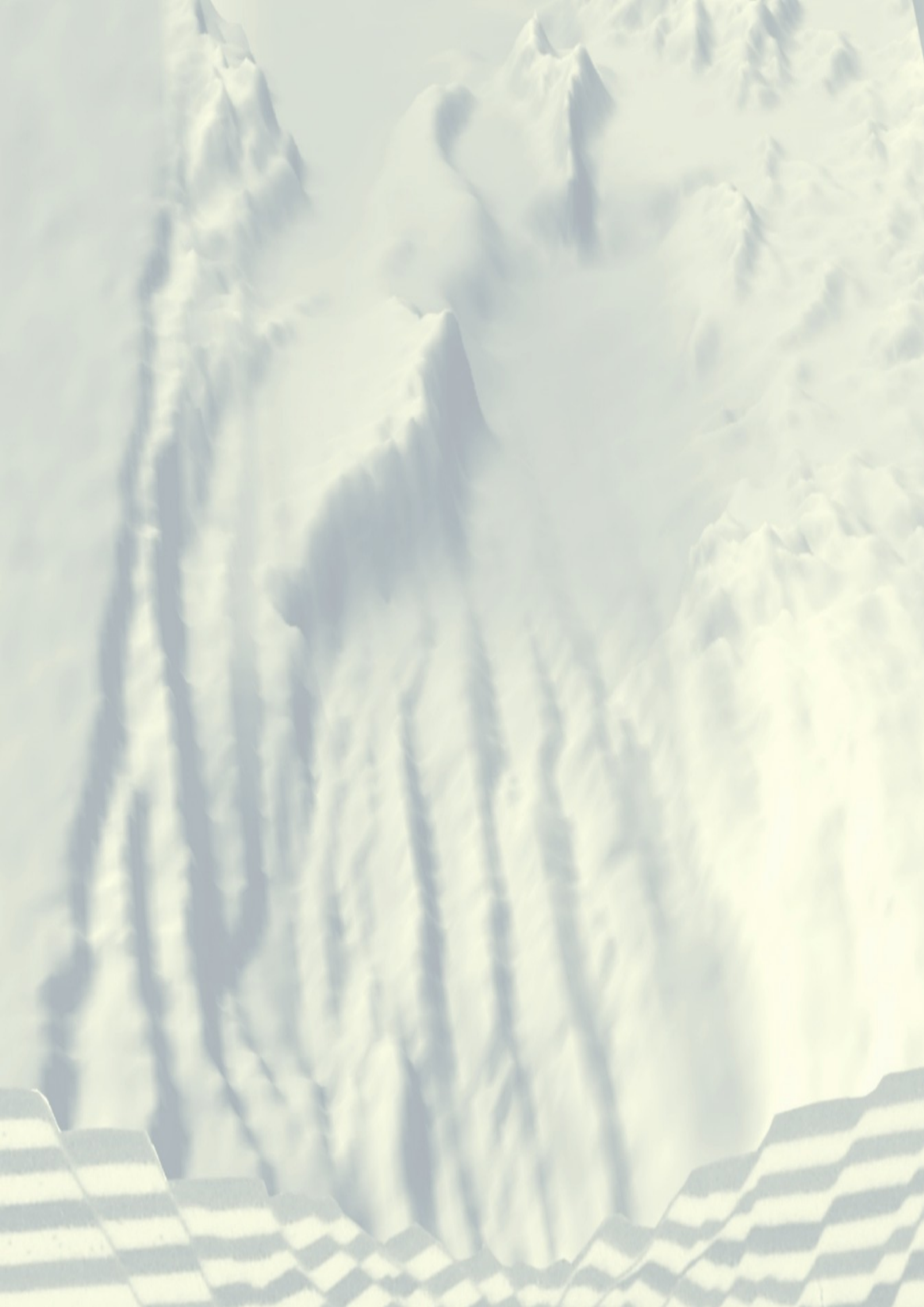

Structure and Evolution of Transfer Zones in Extensional Tectonic Basins — A Study based on Examples from Lake Baikal and Analogue Sandbox Models

UNIVERSITEIT GENT
Faculteit Wetenschappen
Vakgroep Geologie en Bodemkunde
Renard Centre of Marine Geology

Structure and Evolution of Transfer Zones in Extensional Tectonic Basins — A Study based on Examples from Lake Baikal and Analogue Sandbox Models

Studie van de Structuur en Evolutie van Transferzones in Extensiebekkens aan de hand van Voorbeelden uit het Baikal-Meer en Analoge Zandbakmodellen

Robert Hus

Proefschrift voorgelegd tot het behalen van de graad van
Doctor in de Wetenschappen, richting Geologie

Promotor: **Prof. Dr. M. De Batist**
Co-Promotor: **Dr. J. Klerkx**

Academiejaar 2004–2005

The correct citation is:

> Hus (2005). *Structure and Evolution of Transfer Zones in Extensional Tectonic Basins — A Study based on Examples from Lake Baikal and Analogue Sandbox Models.* PhD Thesis, Ghent University.

Gent, December 2004

The author
Robert HUS

The promotor
Prof. Dr. Marc DE BATIST

Dankwoord — Acknowledgements

From the very first moment when I started this PhD I've been realising how lucky I was to be surrounded by exactly the people whose help I needed to make progress, and to eventually finish this work. Since those early days I've been willing to thank many of them, but it is only now that I'm officially "allowed" to do so. I hope I'm forgiven for the delay.

Without any doubt the first person to thank is Marc De Batist, my supervisor, who has been a great help right from the start of this work up to the very last revision of this thank-you-note. He has given me a great opportunity to study a really exciting topic in geology. I owe him most credits for the scientific experience that I've gathered throughout these years.

But I guess I had never even met Marc if there were no Jan Klerkx, my co-supervisor. I think it is actually because of Jan's continuous enthusiasm that I've been pushed into research. As a graduate student he already involved me in 5 scientific missions in the former CIS, and I was sure I wanted more! I should also thank him for introducing me to this subject, as well as for his guidance along the way.

I would also like to acknowledge Ken McClay who gave me the opportunity to work for 5 months in his *Fault Dynamics Research Group* at Royal Holloway University of London. In London I had the use of all the facilities in his structural modelling laboratories, and it turned out to be a nice experience.

However, it has been Valerio Acocella who first introduced me in the world of sandbox modelling. Based on some obscure descriptions of the relay ramp in Zavarotny he was 100% prepared to investigate relay ramps by means of physical experiments. I thank Valerio and Renato Funiciello first of all for giving me the opportunity to use their modelling lab in Rome. But apart from that, I would like to thank Valerio in particular for the countless discussions, both during my stay in Rome as well as during the back-and-forward mailing afterwards.

A big "thank-you" also to Oleg Khlystov for his support on the Baikal trips. Thanks to him the seismic mission of 2001 and the fieldwork in 2002 finished without any problems. Of course Koen De Rycker has also been indispensable during that seismic mission as well as Sergey Baryshev and the crew of R/V Obruchev. Apart from Oleg I also need to thank Edik Osipov, Vadim Khoklov, Sergey, Vanessa, Sveta and Natasha for their contributions to the fieldwork.

I would also like to thank Nick Dobretsov Jr. and Sergey Krivonogov for helping me to process the RESURS-mk4 satellite images in the GIS-centre of Novosibirsk.

I owe much gratitude to my colleagues or past-colleagues at the RCMG:
First of all, Deevit who has been well-prepared to share an office for several years, but who for god-knows-what-reason found it time to finish his PhD and actually leave... Anyway, thanks for the discussions, the music, etc etc.
Pieter, Maarten and Ben have been involved in the beginning of this PhD. Thanks for the support and pep-talk in those early days.
Marc Faure is thanked for his help with almost all administration related to this PhD. And Wim Versteeg for the geophysical manipulation of most seismic profiles.
Yannick, François, Lieven, Davy, Anneleen, Jeroen and all the others, you have all been very pleasant colleagues and I've greatly enjoyed my time here.

In Royal Holloway I've had the pleasure to meet some interesting people as well, who either helped me with the modelling or who were there for TGIF's or other activities. I thank Paul Whitehouse, Tim Dooley and Kevin D'Souza — the Lab-guru's. Mike Craker is acknowledged for constructing the different base-plates as well as the modelling rigs. Also Mario, Liz, Alejandro, Jose, Diego and Sole kindly helped with some of the experiment. Special thanks to Gianluca Grando, Nicoletta and Yen for dragging me into the darkest places of London.

I also want to thank Boris Dehandschutter, Damien Delvaux, Karel Theunissen, Max Fernandez, Annie and Miranda for their caring during the first year of this thesis when I was working in the Royal Museum for Central Africa in Tervuren.

For the last year I've been neglecting some friends, but I'm confident they will forgive me in the weeks to come: Boris, Tinneke, Jouke, Fjo...?? Luckily Jeffrey and Johan worked in the same department otherwise the situation would have been problematic!!

Also a special "thank you" to Vanessa Coisne, through the years she has become a good friend, and she has been a great help to finish this work.

My sister, Els, is thanked for keeping an eye on my apartment while I was away, thanks for paying all my bills ☺. I also thank my brothers Jan and Luk.

I'm also greatly indebted to the Institute for the Promotion of Innovation through Science and Technology in Flanders (IWT), which generously funded this research project for 4 years. Hopefully they won't regret their financial support, which was indispensable for the development of this work.

Finally I would like to thank my parents, whose goodness I've been shamelessly abusing for yet another 5 years. And although they don't need any repayment in return, I insist to dedicate this work to my mum.

Rob Hus, December 2004

Abstract

In general, regional extensional strain isn't accommodated on one single major displacement fault, but rather distributed over different smaller faults. Transfer zones correspond to areas between such faults, where complex deformational features "transfer" the displacement from one fault to the other. Several types of transfer zones exist, determined by the geometry of the faults between which the displacement transfer occurs.

Notwithstanding the importance of large transfer zones in rift basins, their internal structure has mainly been investigated from small scale (metres to tens of metres) or meso scale (few 100 metres) examples. In a first part of this work the internal structure of two large scale natural transfer zones in Lake Baikal has been investigated (Zavarotny and Maloe More area's), and the process of linkage between two major synthetically dipping rift boundary faults is discussed. This part of the study provides additional insight in the evolution of border fault systems in rifts by (1) highlighting the complexity of the internal structure of large relay ramps, including the formation of smaller basins within such ramps; and (2) proposing new evolutionary models for the two transfer zone areas in Lake Baikal. Because the internal structure and evolution of large relay ramps has been determined, the observations can be compared to observations made on smaller scales to evaluate whether the internal structure of relay ramps depends on scale or not.

In a second part of this study, the derived conceptual evolution models are tested by means of scaled experimental sandbox simulations, where the kinematic evolution of similar structures has been observed in real time. A first set of experiments focused on the evolution of relay ramps between offset faults with an imposed geometry. In this modelling it has been evaluated how the structure and evolution of relay ramps depends on the geometry of the main faults (i.e. orientation, spacing, overlap,...).

In a second set of experiments it has been tested to what extent the geometry of pre-existing basement structures in a rift system can control the location of transfer zones. For this purpose several experiments were run — with differently shaped basal plates —, to evaluate whether the introduction of a preferred basement geometry in a model could reproduce a similar stepwise border fault deflection as observed in Lake Baikal, and whether relay zones develop between the different fault segments or not.

The overall conclusions of this work can be summarised as follows:

It has been possible to reconstruct the connection between major rift boundary faults in Zavarotny and Maloe More. These structural studies have illustrated that large relay ramps between major rift boundary faults are more complex than smaller scale relay ramps, for what concerns their evolution and internal structure. It has moreover been found that the evolution of relay ramps does not end when the initially offset faults become hard-linked, but that rather a considerable post-breaching evolution of relay ramps takes place. Further, it was found that the evolution and submergence of the Pri-Ol'khon Block was started much earlier than predicted by the existing evolution models for central Lake Baikal. This submergence was controlled by the reactivation of the Primorsky Fault, which comprised first the reactivation of different small segments that in a later stage connected.

The first set of analogue models has allowed to observe the evolution of relay ramps from the initiation of the faults upto their final connection. After the fault connection, also in the models often the post-breaching evolution of the relay ramps has been observed, similar to the situation in Zavarotny. Given the good correspondence between the geometry and evolution of the modelled relay ramps and that of natural examples, the sandbox models are considered good analogues of natural relay ramps.

Finally, in the second modelling study is has been observed that relay zones often developed at the locations where the introduced "basement structures" changed their orientation. This observation reflects a strong control of pre-existing basement structures on the location of relay zones in natural rift zones.

Contents

List of Figures

Chapter 1

Introduction

Our current understanding of large extensional areas — like, for example, rift systems — would never have reached its present level if geologists had not introduced the concept of *transfer zone*. Realising that different parts of rift systems — sometimes with completely different structural styles — interact with each other and form as such a coherent dynamical system, has been a big step forward.

Although the transfer zone concept had been known already from linked fault systems in thrust belts, it became only widely used in extensional studies since the beginning of the 1980's. Dahlstrom (1970) used the term transfer zone for *the structures that conserve shortening, or allow a regular change in shortening, between overstepping thrust faults* (figure 1.1). A general definition was later proposed by Morley et al. (1990) as: *a coordinated system of deformational features conserving regional strain*, which meant that for the upper (mechanically brittle) parts of the crust in areas of extension, a transfer zone would be *a coordinated system of deformational features that conserve fault displacement in 3 dimensions*, unless other crustal processes such as ductile flow or magma intrusion accommodate large parts of the extension in the shallow crust (Morley et al., 1990). Because regional extensional strain is in general not concentrated on one large fault, but rather distributed over different smaller faults, transfer zones are a common element in these extensional environments. Moreover, they often correspond to areas where the geometry of rift boundary faults changes considerably (fault orientation and/or polarity), and therefore transfer zones cannot be neglected if one wants to understand the complexities of rifting.

It is important to emphasise that the term transfer zone is usually restricted to so called *soft linkage* structures. Two faults are soft-linked, when the displacement transfer between them does not occur on a well-defined fault that connects both (ie. a *transfer fault* (e.g. Gibbs, 1984)), but rather is achieved by a ductile highly-strained zone in between the faults (Walsh and Watterson, 1991; Davison, 1994). A transfer fault is usually termed a *hard linkage* structure (figure 1.2). Morley et al. (1990) have somehow questioned the importance of real transfer faults in rifts. They argued that — before the importance of soft linkage transfer zones was recognised — such faults were more or less automatically inferred between off-set faults, although often an insufficient

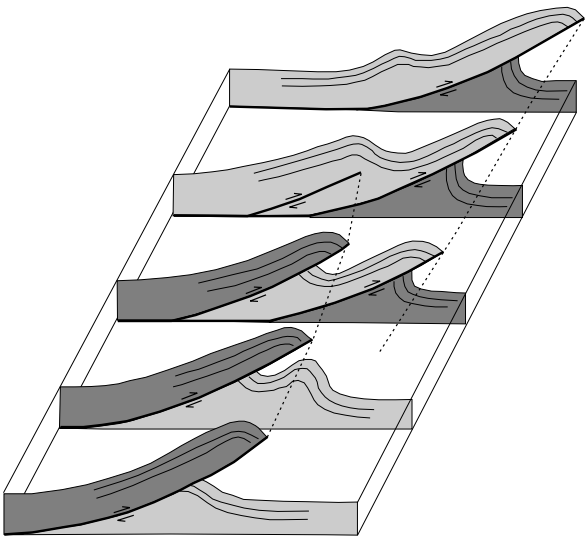

Figure 1.1: *The concept of transfer zones in thrust tectonics. Displacement is "transferred" from one thrust fault to the other. From Faulds and Varga (1998) modified after (Dahlstrom, 1970).*

data coverage didn't allow for distinguishing between transfer faults and transfer zones. Well-documented examples of real transfer faulting have nevertheless been reported in the Basin and Range Province (Faulds and Varga, 1998; Henry, 1998) and the Recôncavo-Tucano-Jatobá Rift (Milani and Davison, 1988; Destro et al., 2003).

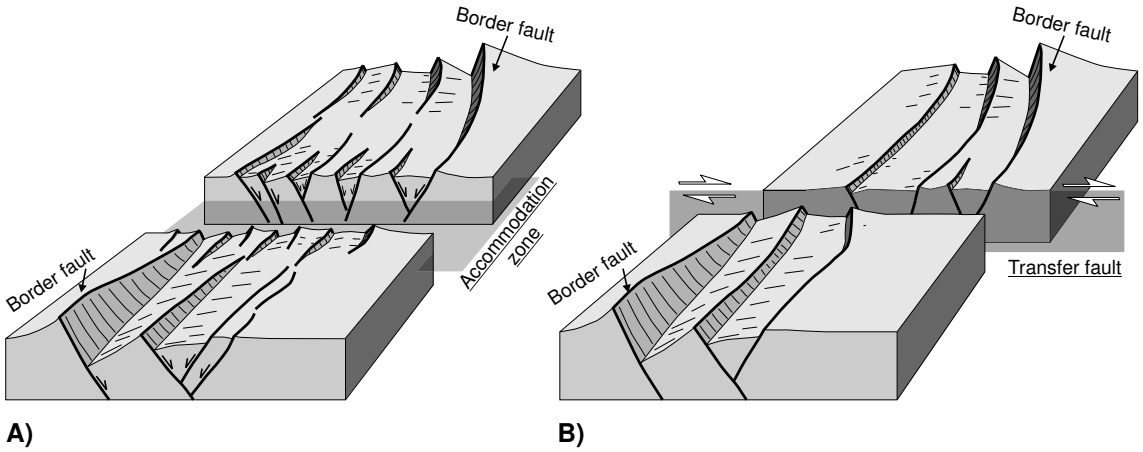

Figure 1.2: *Schematic illustration of the difference between a* soft-linked *accommodation zone or transfer zone, and a* hard-linked *transfer fault. In the former displacement transfer occurs over a relatively wide area, whereas for the latter a discrete zone links the different structures. Mark the change in polarity of the main half grabens in the rift. After McClay et al. (2002).*

1.1 Objectives and aims

Not only started the concept of transfer zone to become used in the studies of rift systems, transfer zones themselves on their turn became as well the topic of intense research to better understand the important role they play in fault system development (e.g. in rifts and extensional basin margins). They are known to influence:

- earthquakes and surface ruptures, and therefore they have a strong influence on further fault development (Schwartz and Coppersmith, 1984; dePolo et al., 1991; Anders and Schlische, 1994; McCalpin, 1996; Gupta and Scholz, 2000);
- displacement patterns on faults (Peacock and Sanderson, 1991; Bürgmann et al., 1994; Willemse et al., 1996);
- hydrocarbon trapping (Morley et al., 1990; Nelson et al., 1992; Peacock and Sanderson, 1994; Coskun, 1997; Dou and Chang, 2003);
- sedimentation patterns near major faults (Gawthorpe and Hurst, 1993; Gupta et al., 1999; Lezzar et al., 2002; McLeod et al., 2002);
- drainage patterns (Gawthorpe and Hurst, 1993; Gupta et al., 1999; Trudgill, 2002; Pivnik et al., 2003);
- basin development (Anders and Schlische, 1994; Contreras et al., 2000);
- the location of volcanic activity (Lambiase and Bosworth, 1995; Acocella et al., 1999b)

The studies referred to here above, can be classified in roughly 2 categories; one type addresses the internal structure of transfer zones (mainly *relay ramps* see section 1.2) but based on the description of mostly small-scale (metres to decametres) examples (Peacock and Sanderson, 1991; Peacock, 1991; Peacock and Sanderson, 1994) (figure 1.3). The work of Trudgill and Cartwright (1994) is an exception because it's based on meso-scale relay ramps in the Canyonlands Utah. The other type of studies focuses on larger scale examples (e.g. in rift basins), but does not touch on the internal structure of the transfer zones but rather addresses the geometry of the surrounding major faults, and how this geometry is influenced by the transfer zone (e.g. Ebinger, 1989; Morley et al., 1990; Gawthorpe and Hurst, 1993; Morley, 1999a). In these studies, the internal structure of transfer zones is often described as "a complex pattern of overlapping fault terminations". The development of mechanical models to try to infer fault interaction based on the interpretation of deep, but low-resolution, seismic profiles (e.g. Freeman et al., 1990; Maerten et al., 2000; Kattenhorn and Pollard, 2001), indicates that — notwithstanding that the most sophisticated modern research techniques have been applied — we are far from determining the detailed internal structure of transfer zones in possible hydrocarbon productive basins.

Despite the recent research attention given to transfer zones in continental rifts, several questions still need to be answered before a full understanding of all aspects of their evolution and their importance is attained. For example:

1. *What is the internal structure of large scale transfer zones in rift basins? And how do they evolve?*

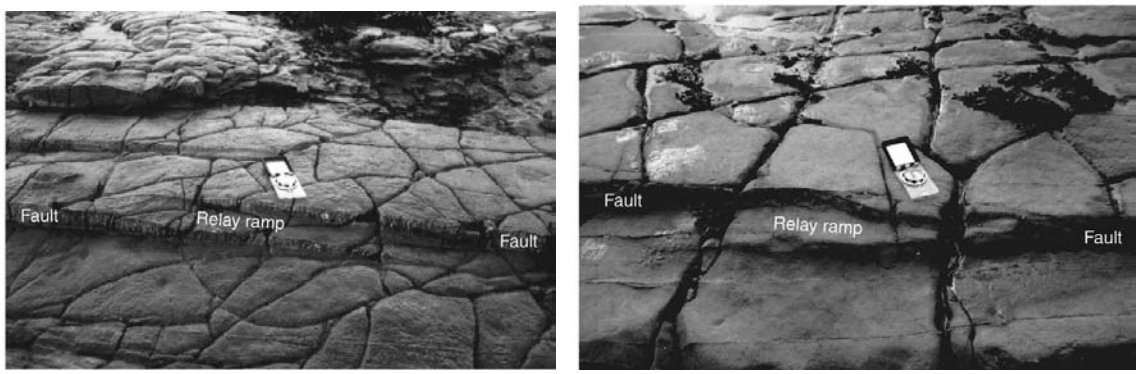

(a) (b)

Figure 1.3: *Photographs of small-scale relay ramps exposed on limestone bedding planes at East Quantoxhead, Somerset, UK. Bedding is tilted between two normal faults that overstep in map view. (a) The relay ramp is not breached, but veins link between the overstepping faults. (b) The relay ramp has been partially breached by small connecting faults. From Peacock (2002).*

Answering this question requires the availability of suitable transfer zone examples. They should be located near the surface, to allow for a high-resolution imaging, but they should also have reached a certain degree of maturity — preferably in a sedimentary environment — to be able to unravel their evolution history.

2. *Is the internal structure of large transfer zones and their evolution comparable to that of smaller scale examples? Or in other words, does a scale independency for transfer zones exist?*

   Such a structural independence of scale has been claimed, but before detailed comparisons with larger structures have been made, this remains rather speculative.

3. *Can we determine how an initial fault geometry — or the geometry of pre-existing basement structures — influences the further development of transfer zones? And what is the influence of the rifting process and the kinematics of rifting on the evolution of transfer zones?*

   This requires a systematic investigation of a sufficient amount of transfer zone examples which all evolved in an environment that, apart from the value of some starting parameters, was similar for all. Obviously a modelling study seems suitable for this purpose.

The aim of this work has been to help answering these standing questions. For this purpose, the internal structure of several transfer zones in a rift system has been investigated in detail, in order to develop a model for their formation and current role in the rift's evolution.

This work focused on transfer zone examples in the central part of Lake Baikal, which were investigated using different research techniques: high-resolution reflection seismic profiling, satellite image interpretations, constructions of digital terrain models,... Where possible, further

insight has been gained through experimental modelling of analogue structures in scaled sandbox simulations. This modelling roughly focused on two different scales: (1) a small-scale modelling of relay ramps, where the geometry of 2 faults was varied to see its influence on the ramp structure that formed between them, and (2) a larger scale modelling, aiming at understanding the interaction between the different faults in the central part of Lake Baikal.

1.1.1 Importance of this work

The transfer zones in Lake Baikal belong to the category of large scale examples, and therefore by studying their internal structure in detail, very useful information is obtained for comparing their architecture with published descriptions of small scale structures.

By choosing the transfer zones in Lake Baikal as the object for this study, important advantages were gained compared to other studies, and this for several reasons:

1. in Lake Baikal, different types of transfer zones occur relatively close to each other;
2. these transfer zones have reached a certain stage of maturity, however, they are at present still actively deforming;
3. the Baikal transfer zones are located partly onshore and partly offshore, which allows for the use of different research techniques, specific for both areas;
4. during the past decennium detailed data-sets have been collected in the transfer zone area's of lake Baikal, and this for the offshore parts as well as the onshore parts.

1.2 Classification of transfer zones

In the literature a wide collection of terms can be found that all refer to certain types of transfer zones. Examples include: *relay zone* (Huggins et al., 1995), *relay ramp* (Peacock and Sanderson, 1991; Trudgill and Cartwright, 1994; Barton et al., 1998), *accommodation zone* (Bosworth, 1985; Coffield, 1987; Faulds and Varga, 1998), *overlap zone* (Childs et al., 1995), *fault bridge* (Ramsay and Huber, 1987), *hinge zone* (Morley, 1995), *graben shift* (Kornsawan and Morley, 2002), etc... Often these terms have a different meaning, restricting their use to only a single type of transfer zone. For example, relay ramp is used for an area of tilted bedding between two normal faults with the same dip direction that overstep in map view (Peacock and Sanderson, 1994; Peacock et al., 2000a). Accommodation zones on the other hand have been mainly used for those areas in extensional domains, where tips overlap of faults that have different dip directions (e.g. Bosworth, 1985; Rosendahl, 1987). When the overlapping faults in an accommodation zone dip towards each other this results in a *low-relief accommodation zone*, whereas in case the faults dip away from each other a *high-relief accommodation zone* is formed (e.g. McClay et al., 2002). An accommodation zone is normally a structure between different rift basins — a so called interbasin transfer zone sensu Gawthorpe and Hurst (1993) — whereas a relay ramp is a transfer zone between different fault segments on the same side of a rift — or an intrabasin

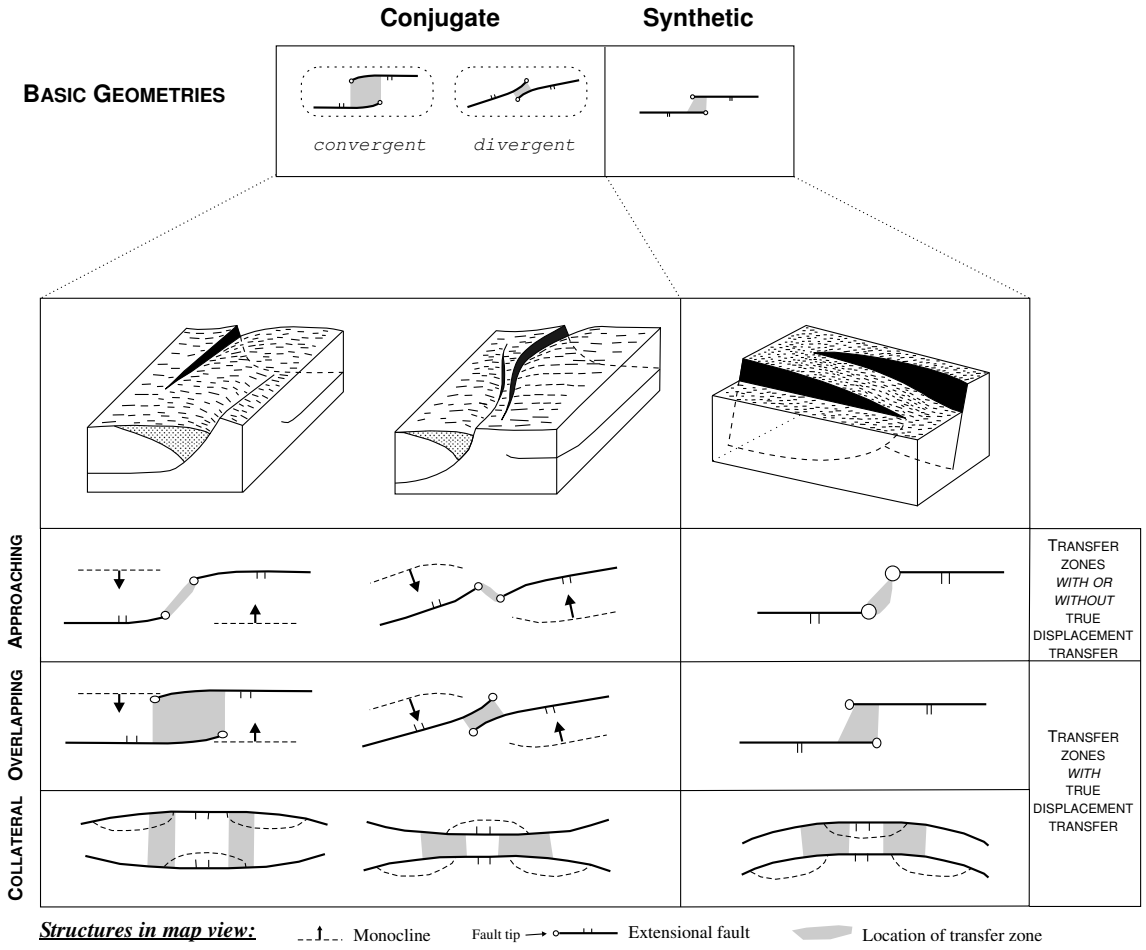

Figure 1.4: *Different types of transfer zones in the classification scheme of Morley et al. (1990). A further distinction can be made based on the degree of overlap of the main faults: e.g. approaching, overlapping and collateral (see text for explanation). Modified from Morley (1995) and Crider and Pollard (1998).*

transfer zone (Gawthorpe and Hurst, 1993). Although the term 'accommodation zone' has often been used to refer to a transfer zone, Morley (1995) emphasises that strictly speaking the overlapping faults of an accommodation zone need not to be active at the same time, whereas using the word 'transfer zone' automatically implies fault activity at the same time.

Morley et al. (1990) have introduced a systematic classification scheme for transfer zones, based on the geometry of the faults between which the displacement transfer occurs (figure 1.4). This classification scheme is based on observations from the East African Rift System and therefore applies for fault interactions between major boundary faults. In this classification, a first-order subdivision into *synthetic* and *conjugate* transfer zones is based on the relative dip direction of the faults. For the synthetic type, faults have to dip in the same direction, whereas for the conjugate type, faults have to dip in opposite directions. These conjugate transfer zones

can then be sub-divided again into *divergent* transfer zones, where the faults dip away from each other, and *convergent* transfer zones, where the faults dip towards each other. For every category a new subdivision can be made based on the degree of overlap of the main faults: (1) *approaching* transfer zones occur where two fault tips did not yet — or failed to — propagate past each other; (2) *overlapping* transfer zones occur where the two fault tips have propagated past each other, and a degree of overlap exists, and finally (3) *collateral* transfer zones occur where the two faults overlap completely, and displacement transfer between them occurs along the whole length of the fault segments. Finally a last category can be found in the divergent conjugate type of transfer zones when the two faults are *collinear*, ie. the two faults are located directly along strike of each other.

Recently, Peacock (2003) proposed that the term relay ramp should be used for relatively small structures, and that for basin bounding structures it is more appropriate to talk about *synthetic transfer zone*. By suggesting the need for this distinction, Peacock (2003) implicitly assumes a difference between structures on both scale. Moreover, by using a different terminology for similar structures on different scales, the usefulness of Morley et al. (1990)'s classification scheme gets lost. To my point of view it would be more appropriate to refer to a certain scale in Morley et al. (1990)'s classification by simply adding an appropriate adjective. For example *small-scale* for transfer zones with the shortest dimension <100m, *meso-scale* for relay structures with the shortest dimension >100m and <1km, and *large-scale* for structures exceeding >1km.

In their paper, Faulds and Varga (1998) used the word transfer zone for discrete zones of strike-slip and oblique-slip faults that strike parallel or slightly oblique to the extension direction. This definition is a bit confusing as this type of structures are often called *transfer faults*. They further used accommodation zone to refer to "real" transfer zones despite the slightly different meaning of the term (as mentioned above). Faulds and Varga (1998) proposed a similar classification scheme for accommodation zones as the one of Morley et al. (1990) for transfer zones.

Moustafa (2002) divided transfer zones in two categories, one being transfer zones between individual faults (fault-to-fault transfer zones [F-F TZ]) and the other being transfer zones between half grabens with different fault domains (half-graben–to–half-graben transfer zones [H-H TZ]). This distinction appears to be more or less similar to Gawthorpe and Hurst (1993)'s intrabasin transfer zones and interbasin transfer zones, respectively.

Throughout this work, the term *transfer zone* will be used as the most general term for a soft-linkage structure that transfers displacement between different faults. In those cases in which the transfer zone was a divergent conjugate transfer zone (figure 1.4), it will be referred to as an *accommodation zone*, because this is by far the most common term used in literature. The same is true for the overlapping synthetic transfer zone (figure 1.4), which will be termed in this work a *relay ramp* for the same reason. Relay ramp will only be used to refer to an overlap zone between more or less parallel fault tips. In case the overlapping fault tips have a different orientation I prefer to use the term *relay zone*.

To describe the geometry of transfer zones, *overlap* and *overlap length* have been used to

refer to the fault parallel distance over which two faults overlap. For relay ramps the overlap corresponds to the length of the relay ramp. When faults do not yet overlap, the term *underlap* is used which represents a negative overlap. The fault perpendicular distance between two overlapping fault tips will be referred to as *spacing*. For a relay ramp this corresponds to the width of the ramp. Often the geometry of overlap zones is described by their aspect ratio, which is the ratio between the overlap length and the spacing

1.3 Outline of this thesis

This thesis consists of 8 chapters and 4 appendices. *Chapter 1* is an introduction, that briefly introduces the transfer zone concept to the reader, including a general accepted classification scheme. The chapter contains a description of the aims of this work and it addresses its importance. *Chapter 2* is a short introduction to some of the characteristics of extensional faulting. It mainly focuses on the process of fault growth and linkage, and explains the current ideas of fault evolution. Towards the end it contains a simplified description of the geometry of rift related faults in the upper parts of the continental crust. *Chapter 3* is an introduction to the geology of the study area. It aims to provide the reader with a general background of the geological setting of the Baikal Rift Zone and Lake Baikal in particular. More detailed outlines of the studied transfer zones of Lake Baikal are included in later chapters.

In a first part of this study (chapters 4 and 5), two examples of natural relay zones from Lake Baikal are studied. In *chapter 4* the structure of a large ($\approx$400km^2) relay ramp is described in the area of Zavarotny between 2 fault segments in the northern part of Lake Baikal. The observations that were made are compared to existing models of relay ramp structure and evolution (as described in chapter 2), and therefore allow to make comparisons of structures on small and large scale. *Chapter 5* contains the structural interpretation of an even larger area in the central part of Lake Baikal (i.e. the area of Ol'khon Island and Maloe More). This area has classically been interpreted as being part of a major accommodation zone between the central and the northern Baikal basins. The chapter includes a new model for the evolution of this area, which before the final merging of the two boundary faults formed a large overlap zone.

In a second part of this work (chapters 6 and 7) the conceptual evolution models derived in the first part are tested by means of analogue models. The outcome of an experimental modelling study focussing on relay ramps is presented in *chapter 6*. For this chapter a systematic investigation was performed to analyse how an initial fault geometry affects the further evolution of relay ramp structures. *Chapter 7* presents a series of sandbox models that aimed to provide insight in the evolution of the fault segmentation in Lake Baikal. For this modelling pre-existing basement structures have been introduced in sandbox models, to see how this affects the deflection of the border faults and the creation of relay zones. Finally, the conclusions of this thesis are presented in *Chapter 8*.

Four appendices have been added to this work, one containing information about the geometries of natural overlap zones between normal faults. A second appendix contains detailed illustrations of the base-plates that were used in the modelling of chapter 7. The third appendix

describes the evolution of two 2D rift models, in which the evolution has been recorded in cross-section through a glass sidewall rather than at the model's top surface. A fourth appendix is a manual for the creation of 3D surface views of selected horizons in an analogue model.

Chapter 2

Characteristics of extensional faulting

2.1 Introduction

The most prominent way to accommodate extensional deformation in the brittle crust is by normal faulting (e.g. Jackson, 1987; Mandl, 1988; Cowie and Scholz, 1992a). During the last 20 years, numerous studies have addressed specific topics of extensional faulting, like describing the geometries of normal faults (e.g. McClay and Ellis, 1987; Roberts et al., 1991; Dresen et al., 1991) or proposing models for their development and growth (e.g. Watterson, 1986; Cowie and Scholz, 1992a; Morley, 2002). Such studies have emphasised the role that normal faults play in the development of extensional basins (e.g. Gibbs, 1984, 1987) and the input of sediments into such basins (e.g. Gawthorpe and Hurst, 1993; Leeder and Jackson, 1993; Allen and Densmore, 2000; Goldsworthy and Jackson, 2000; Pivnik et al., 2003). They also highlighted the importance of normal faults for mining and for hydrocarbon accumulation and exploration (e.g. Rippon, 1985; Hardman and Booth, 1991), as well as their significance for earthquake hazard assessment (e.g. Scholz, 1990; Collier et al., 1998; Meghraoui et al., 2000), etc...

In this chapter, some of the characteristics of extensional faulting are reviewed, and some of the structures associated with the growth of faults are described. This chapter should be seen as a short introduction for which specific topics have been selected that were deemed important in understanding the present knowledge of the growth process of faults. There has been no intention to cover all aspects of normal faulting.

2.2 The formation of faults

Whenever the formation of faults is discussed, two different time-scales can be considered. One being the time-scale of a single earthquake or slip event on a fault and the other one — often understood as the actual faulting itself — being the result of a cumulation of such small-scale phenomena on a single fault (Watterson, 1986; Sibson, 1989; Cowie and Scholz, 1992a).

2.2.1 Mechanical aspects of faulting

The limit condition of Mohr-Coulomb is a good approximation for describing the critical situations in which brittle faults can form (ie. shear failure can occur) in a regime of tri-axial compression (i.e. with the all principal stresses, σ_I, σ_{II} and σ_{III}, compressive). As this limit condition also applies for the formation of faults in brittle sandbox models (Hubbert, 1951; Waltham, 2002) (chapters 6 and 7), the theory of Mohr-Coulomb is shortly introduced in this section.

The formation of shear fractures or shear bands, in a rock sample or a rock volume, requires that the differential stress ($\sigma_I - \sigma_{III}$, which is twice the maximum shear stress τ_{max}) attains a critical value (e.g. Hubbert, 1951; Mandl, 2000). The limit condition of Mohr-Coulomb combines the state of stress in a point and the properties of the rock to evaluate failure.

The frictional criterion for the strength of cohesionless soils has been formulated as:

$$\frac{\tau}{\sigma\prime_\perp} \cong C^{te} \tag{2.1}$$

or

$$\tau = \sigma\prime_\perp . \tan\varphi \tag{2.2}$$

with φ the angle of internal friction, τ the shear stress and $\sigma\prime_\perp$ the effective normal stress (i.e. $\sigma - p$ with p the pore fluid pressure).

For materials that are cohesive, equation 2.2 can be modified by adding the initial shear strength (τ_0) to the relation:

$$\tau = \tau_0 + \sigma\prime_\perp . \tan\varphi \tag{2.3}$$

In Mohr's stress plane of normal effective stresses $\sigma\prime_\perp$ and shear stresses τ this criterion plots as a straight line that cuts the τ-axis at τ_0 and has a slope φ (figure 2.1). This line is termed the *line of fracture* or the *Coulomb Mohr limit line* (Hubbert, 1951; Mandl, 2000).

In Mohr's stress plane the state of stress on the other hand, is represented by a Mohr circle, which expresses $\sigma_\perp$ and τ as functions of σ_I, σ_{III} and the orientation of the plane on which they act (figure 2.1). Fracturing in the material occurs when the Mohr circle becomes tangential to the Coulomb-Mohr limit lines (figure 2.1b). As such the Coulomb-Mohr limit lines correspond to the envelopes of the set of all limit stress circles in Mohr's stress plane (see Mandl, 2000, for a detailed discussion).

Restrictions and limits: The limit condition of Mohr-Coulomb is based on several assumptions, which put major restrictions on the applicability of the criteria (Mandl, 2000):

- The limit condition can only be applied to brittle deformation and therefore only in the regions of the earth where tectonic deformation is mainly brittle.
- The regime in which the faulting occurs must be one of effective compression, i.e. where none of the effective stresses is tensile. In regimes where $\sigma_3 < 0$; faults of a dilational type form which have a slightly different failure line in Mohr's stress plane compared to real "shear" faults (see discussion in Mandl, 2000, pages 129–130).

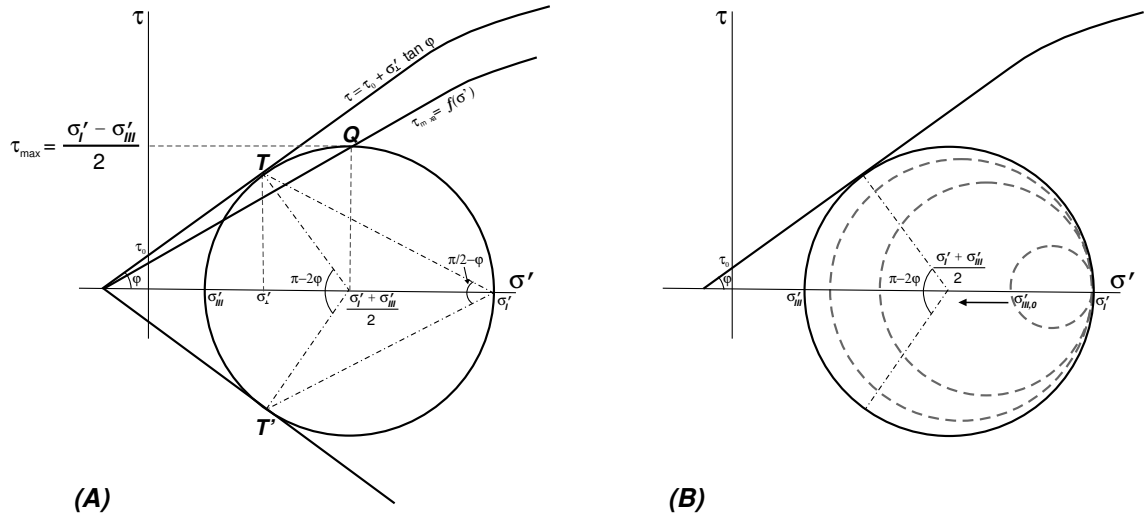

Figure 2.1: *Limit states of stress in Mohr's stress plane. The curvature in the failure lines symbolises the escape from the linear relation for high effective pressures. (A) illustrates the two types of failure lines, one that corresponds to the maximum shear stress ($\tau_{max} = f(\sigma')$) and the another one that is the Mohr-Coulomb failure envelope ($\tau = \tau_0 + \sigma'_\perp . \tan\varphi$) (from Mandl (1988)). (B) represents the condition for normal fault formation: σ'_{III} decreases, until the Mohr's circle reaches the Mohr-Coulomb failure envelope and a normal fault develops (modified from Hubbert (1951)).*

- The use of the limit condition is further restricted to materials in which no anisotropy in the shear strength exists (Mandl, 1988).
- Because the shear strength of the rock cannot increase infinitely in proportion to an increasing effective mean stress, the limit condition only applies to regimes of low to moderate effective mean stress.
- In deriving the limit condition the influence of σ'_{II} on the shear failure was neglected. Laboratory tests have shown that this influence is indeed minor in comparison to the influence of σ'_{III} but it is an approximation (See Mandl, 2000, for a detailed discussion).

Andersonian model

E. M. Anderson realised that the formation of tectonic faults was related to brittle fracturing, and he applied the criterion of Mohr-Coulomb to this problem. Anderson showed that faults often formed as planes that include the direction of principal intermediate stress (σ_{II}), and that are oriented with acute angles to the direction of maximum principal stress (σ_I). As the optimal orientation for the fault plane occurs on both sides of the σ_I direction, faults could form in conjugate sets. Anderson applied the condition that no shearing stresses exist at the earth's free surface, and therefore one of the major principal stresses should be vertical and the two other horizontal. This allowed him to distinguish between the three main types of faults: *normal, reverse* and *strike-slip* faulting (e.g. Anderson, 1951; Scholz, 2002; Turcotte and Schubert, 2002)

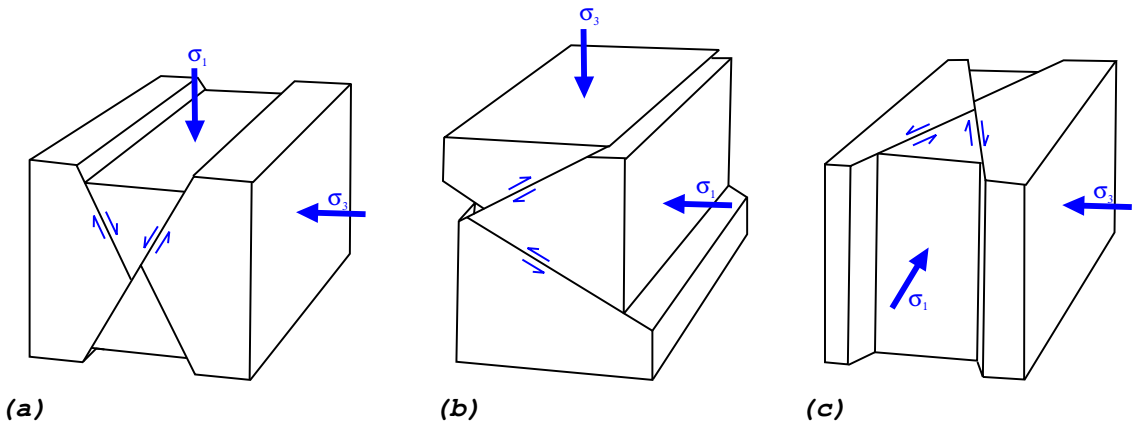

Figure 2.2: *The three main types of faults (here conjugate sets) expected to develop close to the surface of the earth, as predicted by Anderson's model: (a) normal faults, (b) reverse faults and (c) strike-slip faults. Modified from Ramsay and Huber (1987). In all cases one of the principle stresses is vertical, respectively σ_1, σ_3 and σ_2 for figures a, b and c. The direction of σ_2 is not marked in the figures, but it is perpendicular to σ_1 and σ_3.*

(figure 2.2). For normal faulting it is σ_I that is vertical, with the acute angle between the fault plane and σ_I typically being around 30°, which results in dip angles of normal faults around 60°.

Restrictions and limits: Because the model of Anderson is based on the criteria of Mohr-Coulomb, the same restrictions apply. Moreover, starting from the assumption that the surface of the earth has zero shear stress, the model's application is basically limited to the upper parts of the crust. Deeper in the crust the principal stress directions do no longer need to be parallel and perpendicular to the earth's surface (e.g. Ramsay and Huber, 1987). Also topographic relief and/or other tectonic deformations generally induce shear stresses that act on horizontal and vertical planes (e.g. Mandl, 2000). An ideal situation for applying Anderson's fault model would be for example a tectonically undisturbed horizontal rock layer that rests on a practically frictionless base and that is horizontally stressed or compressed, in the absence of topographic relief (Mandl, 2000).

Another restriction to Anderson's model is that the principal stresses have to remain unchanged during the loading period prior to the faulting (Mandl, 2000).

Recent advances

The Mohr-Coulomb limit condition links the onset of failure to the stress conditions in a rock mass, however, it does not describe the growth process of a fault, nor the displacement distribution along a fault, or the local stress fields around the fault.

Studies that have treated fault growth with a more mechanical approach can be classified in two important categories, one using the theory of *linear elastic fracture mechanics (LEFM)* (e.g.

Pollard and Segall, 1987; Peacock and Sanderson, 1996) and the other one using the *cohesive zone theory (CZT)*, either in 2D (e.g. Rudnicki, 1980; Cowie and Scholz, 1992b; Scholz et al., 1993) or 3D (e.g. Willemse, 1997; Martel and Boger, 1998). In the cohesive zone theory (often called the *post-yield fracture mechanics model*), faults are treated as shear cracks in which friction acts on their interior walls. In a *cohesive zone* just behind the fracture tip, elevated stresses exist that resist the opening or sliding of the fracture walls. This breakdown zone can involve inelastic deformations at the crack tips which results in a more realistic approximation compared to models for slip events in ideal elastic materials (e.g. Pollard and Segall, 1987), as the latter imply unrealistic infinite high stresses at the fault tips[1] (Rudnicki, 1980; Cowie and Scholz, 1992b). With the *CZT* the theoretical singularity in stresses at the fault tip can be eliminated if the resisting stresses are sufficiently strong and the cohesive zone is sufficiently large (Rudnicki, 1980; Martel and Boger, 1998).

Moreover, in the *LEFM* approach fractures are treated as perfectly sharp, something that doesn't match with the observed complex breakdown process of shear fractures in nature (Scholz et al., 1993). Rather than through the development of a well defined, fault plane, faults initially grow by the development of a process zone, where micro-fractures form that eventually coalesce (Cowie and Shipton, 1998). When a fault is formed, stress concentrations near the fault tip will cause the expansion of the process zone and eventually the lateral propagation of the fault. During this fault tip propagation, fractures that had formed aside of the tip are left behind and form a system of small fractures around the fault (e.g. d'Alessio and Martel, 2004). Such a zone of fracturing around and related to a fault is often termed a "damage zone" (McGrath and Davison, 1995; Peacock et al., 2000a; Kim et al., 2004).

The formation and growth of faults, however, cannot be described completely by this traditional fracture mechanical models, as it involves distributed inelastic deformation of the surrounding rocks (Cowie and Scholz, 1992a). Also the interaction and intersection of faults with other faults in a fault array, produce local stress inhomogeneities, that are accommodated by secondary faulting (Cowie and Scholz, 1992a).

Stress field around faults and cracks

So far, three terms have been used to refer to discrete breaks that result from brittle failure: *fracture, fault* and *crack*. Fracture is considered to be the most general term to refer to any such breaks ranging from micro-scale upto large-scale mega-lineaments (Ramsay and Huber, 1987). As such this term covers both the macro-scale shear fractures, usually referred to as faults, and micro-scale fractures, sometimes referred to as cracks.

There are three main modes of fracture loading and related fracture displacement (e.g Atkinson, 1987; Pollard and Aydin, 1988; Hertzberg, 1989) (see figure 2.3):

Mode I: the opening or tensile mode, where the crack surfaces move directly apart,

[1]The stresses near the crack tip have the following form: $\sigma_{ij} = K_L(2\pi r)^{-1/2} f_{ij}^L(\theta) + O(1)$ where r is the distance from the crack tip. At the crack tip ($r \to 0$) the singularity $r^{-1/2}$ exists (e.g. Rudnicki, 1980).

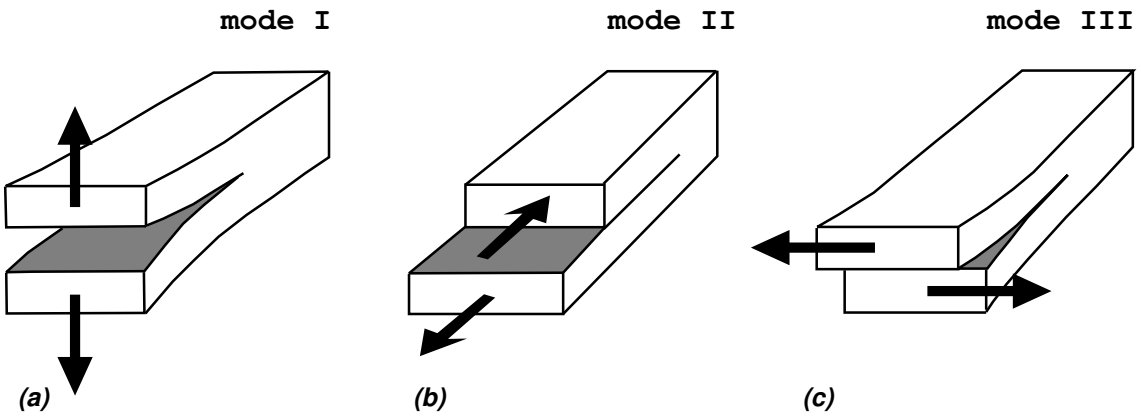

Figure 2.3: *Basic modes of loading and the corresponding fundamental modes of fracture. From Atkinson (1987). Mode I (a) is the opening or tensile mode, where the crack surfaces move directly apart. Mode II (b) is the sliding or in-plane shear mode where the crack surfaces slide over one another in a direction perpendicular to the leading edge of the crack. Mode III (c) is the tearing or antiplane shear mode, where the crack surfaces move relative to one another and parallel to the leading edge of the crack (e.g. Hertzberg, 1989).*

Mode II: the sliding or in-plane shear mode where the crack surfaces slide over one another in a direction perpendicular to the leading edge of the crack, and

Mode III: the tearing or antiplane shear mode, where the crack surfaces move relative to one another and parallel to the leading edge of the crack.

Fractures that have components of different loading modes are called *mixed mode fractures*.

When a fault is considered in a uniform far-field or remote stress field, its presence will cause this stress field to be locally perturbed. This perturbation is caused because along the fault and in its tip regions there is a decrease in the shear strength and Young's modulus, which limits the shear stress that can be carried by the fault (e.g. Mandl, 2000). Also the relative motion that occurs along structural discontinuities like faults in a rock mass, will perturb the local stress field (e.g. Pollard and Segall, 1987).

The stress pattern associated with a normal fault is qualitatively the same as that for a mode III crack (e.g. Cowie, 1998). Assuming cylindrical coordinates r and θ, a general expression for the stress field distribution for any mode of crack can be given as (e.g. Atkinson, 1987):

$$\sigma_{ij} = K_L \sqrt{2\pi r}.f_{ij}(\theta) \tag{2.4}$$

with $f_{ij}(\theta)$ a function that depends on the loading mode (I, II, or III), and K_L is the stress intensity factor that embodies the essential boundary conditions of the crack system, and that depends as well on the loading mode of the crack. In equation 2.4, r corresponds to the distance from the crack tip. More specific expressions describing the stress field around cracks are given by Du and Aydin (1991) for mode I cracks and by Poliakov et al. (2002) for mode II and mode III cracks.

Segall and Pollard (1980) calculated the perturbing stresses of a crack on the total stress field, and concluded that these perturbing stresses become less than a fraction ε of the applied stress outside a critical radius r_c (Segall and Pollard, 1980):

$$r_c \cong \frac{a}{\sqrt{2\varepsilon}} \tag{2.5}$$

For example for a radius $r_c = 2.25a$ the perturbing stresses become less than 10% of the applied stress. In equation 2.5 a is the crack's half length, and r is the radial distance to the crack's centre.

2.3 The growth and propagation of isolated normal faults

Because large faults are often made up of a connection of different fault segments (see section 2.4), the characteristics of isolated faults are shortly introduced here. This is important, as in determining whether or not interaction exists between two different faults, or whether a fault is made up of a series of connected segments, often the deviation of fault properties from those of isolated ones is observed.

Observations of displacement profiles of isolated normal faults show maximum displacement near the centre of the fault, and a gradual decrease in displacement to zero near the edges (Dawers et al., 1993) (figure 2.4). Whenever slip accumulates in the interior of the fault plane, stress concentrations at the fault tips will increase, resulting in the lateral growth of the fault to relax these stress concentrations (e.g. Scholz, 2002). This mechanism suggests that faults originate at a point and that they grow further with progressive slip, increasing both their length and their accumulated displacement. As the faults propagate in both directions relative to the centre of the fault, this mechanism is also referred to as *fault growth by radial propagation.*

2.3.1 The Walsh and Watterson cumulative slip model of fault growth

Walsh and Watterson (1987) have tried to quantify the growth of isolated blind normal faults (i.e. a fault that does not intersect a free surface) with an idealised elliptical shape of the slip surface. The maximum displacement on such a fault lies in the centre of the ellipse, with displacement decreasing in all directions away from the central maximum (Barnett et al., 1987) (figure 2.5). In their model, the total displacement on the fault resulted from a series of discrete slip events, with the slip vector parallel to the short axis of the fault plane. The basic assumption of the model was that the amount of slip in individual events increased in a simple arithmetic progression (Watterson, 1986). When successive slips increase by the constant number k, the amount of displacement D_N after N slip events is given by:

$$D_N = k + 2k + ... + Nk = \frac{N(n+1)k}{2} \approx \frac{N^2.k}{2} \tag{2.6}$$

or:

$$D_N = u^2/2k \tag{2.7}$$

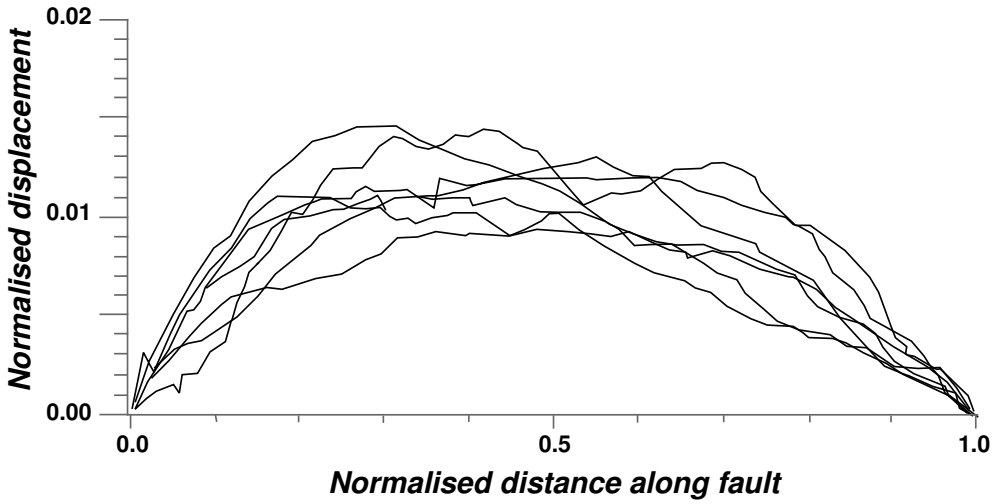

Figure 2.4: *Displacement profiles of different faults in the Volcanic Tableland, eastern California. The distance along the fault as well as the displacement are normalised to the fault length. The plotted faults had lengths that varied from 696m to 2210m and maximum displacements from 8.4m to 31m. Modified from Dawers et al. (1993).*

with u being the slip of the last slip event ($u = N.k$). As the amount of final slip is proportional

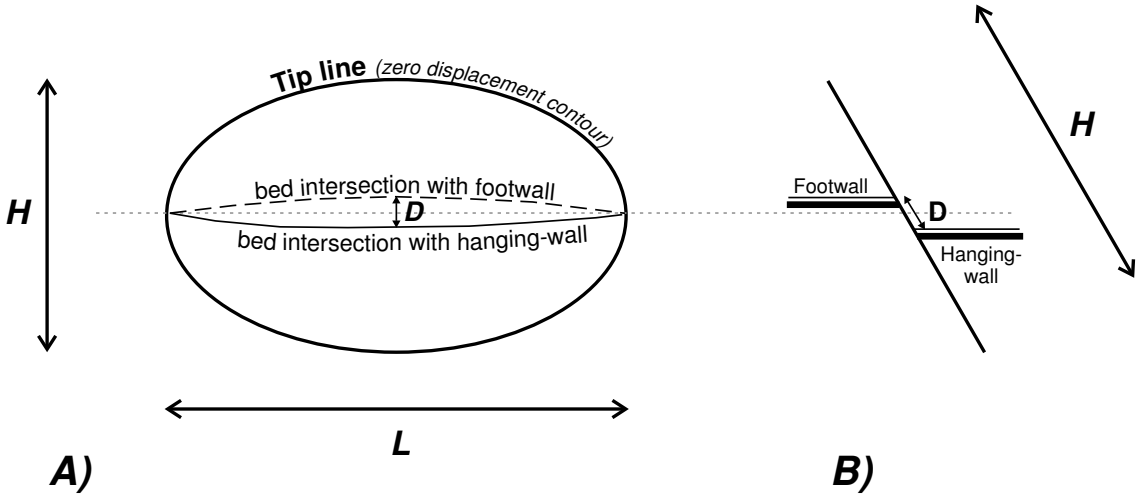

Figure 2.5: *Geometry of an idealised simple blind normal fault with elliptical tip line, or zero displacement contour. Figure A) is a view normal to the slip surface, and figure B) is a view along strike. In the latter, the displacement of an originally horizontal horizon on the fault plane is shown.* L *is the length of the fault plane (parallel to the strike-direction),* H *is the height of the fault (parallel to the slip direction) and* D *is the maximum displacement. Modified from Watterson (1986).*

to the width of the fault: $u \propto L$, equation 2.7 can be written as[2]:

$$D_N = C^{te}.L^2 \tag{2.8}$$

with the C^{te} being a material constant, or:

$$\log D_N = C^{te} + 2\log L \tag{2.9}$$

A fault growing by this model will therefore have a growth curve that plots as a straight line on a log-log plot of D_N vs. L, with its position at a given time being determined by the values of k and u/W (Watterson, 1986).

The model of Watterson (1986) and Walsh and Watterson (1987) is based on several simplifications, but despite this, it is consistent with observations from natural faults on varying scales (e.g. Walsh and Watterson, 1988; Gillespie et al., 1992).

2.3.2 Other models

Important in the Walsh and Watterson model for fault growth, is that the model does not incorporate an explanation for the fault growth. For example, the dislocation resulting from a single slip event on a fault, can be accommodated by elastic strains in the surrounding rocks. However for the Walsh and Watterson model, these strains should then be relaxed into permanent strains before the next slip event occurs (Walsh and Watterson, 1988; Gillespie et al., 1992).

Peacock and Sanderson (1996) developed a model for fault growth, where the total displacement of the fault — like in the model of Walsh and Watterson (1987) — is a result of a series of slip events. For Peacock and Sanderson (1996) these slip events all had characteristic displacement profiles of a fracture in an ideal elastic material. Such a characteristic displacement profile for a single slip event is given by (Pollard and Segall, 1987):

$$d = A\sqrt{r^2 - x^2} \tag{2.10}$$

With:
A = a constant depending on the driving stress and the elastic properties of the rock,
r = the crack's half length or radius, and
x = the distance from the crack centre.

However, Peacock and Sanderson (1996) introduced in their model a parametric representation of fault growth, which they called the *fault propagation rate*. The cumulation of slip events of type 2.10 results after N events in a displacement given by:

$$d = \sum_{n=0}^{N} \sqrt{(p^n c_1)^2 - x^2} \tag{2.11}$$

[2]Walsh and Watterson used in their publications the letter W for the width of the fault, where the width corresponded to the horizontal axis of the slip surface. Most other studies however refer to this parameter as the length of the fault. To be consistent with the symbols used later in this text, I prefer to use the symbol L rather than W.

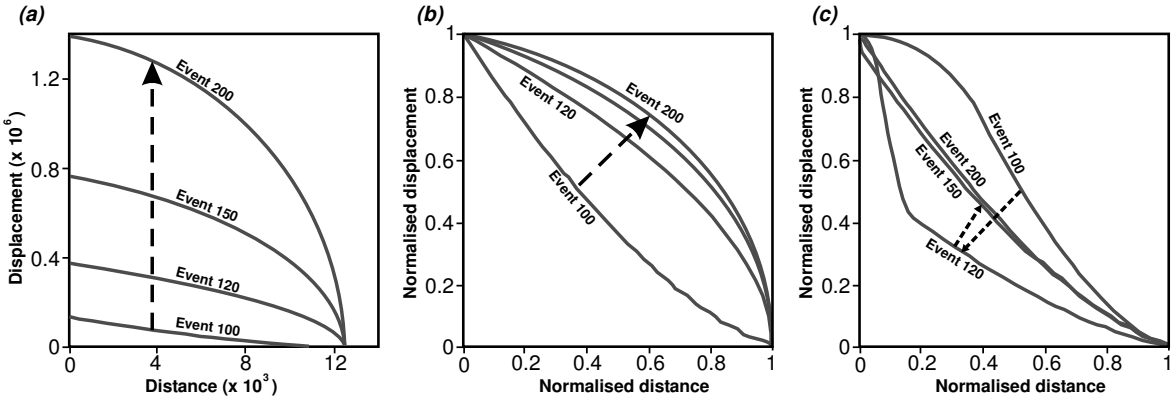

Figure 2.6: *Graphs illustrating the effects of variations in the propagation rate of a fault (p) on the final shape of the displacement profile. Figure (a) shows a non-normalised example of a fault where p decreases from $p = 1.1$ in the first 100 slip events to $p = 1$ in the next 100. This results in an increase of the displacement along the fault, without a further increase in the length. Figure (b) shows the displacement profile of the same fault as in (a), but normalised. Figure (c) is a graph of a normalised displacement profile, where the p increases from $p = 1.01$ for the first 100 slip events to $p = 1.1$ for the next 100 events. From Peacock and Sanderson (1996).*

In which, c_1 is the initial half length of the fault, x is the distance from the centre, n the number of slip events and p the fault propagation rate. Depending on its value the fault propagates ($p > 1$) or not ($p = 1$).

The introduction of the fault propagation rate allowed Peacock and Sanderson (1996) to change the amount of propagation associated with a slip event and to calculate resulting displacement profiles (eg. 100 slip events with $p = 1.01$ followed by 100 slip events with $p = 1.1$ etc.). The final displacement profile of the fault in this model is therefore only little affected by the last slip event, but strongly influenced by the propagation history of the fault (see figure 2.6). This means that inferring the displacement profile of a single slip event is not possible from the total displacement profile of a fault (Peacock and Sanderson, 1996). Variations in the propagation rate of a fault can for example be related to interaction with neighbouring faults, but this is discussed in more detail in section 2.4 on page 45.

2.3.3 Fault scaling

Displacement-length scaling

As suggested by the Walsh and Watterson model of fault growth (section 2.3.1) a relation exists between the length of a fault and its maximum displacement (equation 2.8). As, other studies have reported different values for the exponent in equation 2.8 than 2, the most general displacement-length scaling law for faults becomes:

$$D = c \times L^n \tag{2.12}$$

The existence of scaling laws for faults, be it for their displacement-length relation or for their spatial distribution (see later in this section on page 44), has important practical uses. They can be used for example to calculate the total strain resulting from faulting in an area (Scholz and Cowie, 1990; Marrett and Allmendinger, 1991; Poulimenos, 2000), or to determine the presence of so-called "sub-resolution" faults (Groshong Jr et al., 2003), or they can for example be used to evaluate the geometric coherence of an interpreted fault map from seismic data (Freeman et al., 1990; Walsh and Watterson, 1991; Gauthier and Lake, 1993). The existence of universal scaling laws for faults would mean that data gathered on faults of only a limited range of lengths could then be used to determine accurately the fault characteristics, fault spacings and the contribution of faults to the total strain across several orders of magnitude (e.g. Wojtal, 1994; Needham et al., 1996).

The importance of general fault scaling laws motivates the different attempts that have been made to characterise the values of n and c, however so far no consensus exists. Watterson (1986) and Walsh and Watterson (1988) believe that the value of n should be around 2 which they deem consistent with observations in nature. Cowie and Scholz (1992b) and Scholz et al. (1993) on the other hand calculated the value of n based on their fracture mechanical model. They found theoretical values for the exponent of 1. Gillespie et al. (1992) studied ca. 1350 individual faults with maximum displacement values ranging over 8 orders of magnitude. They found from these data that the value of n should be between 1.5 and 2, and that a value of 1 for the power-law exponent was not consistent with the observations. Also Marrett and Allmendinger (1991) found values for n of around 1.5 from the study of a similar data-set. Later Scholz (2002) argued that the values reported in the previous studies were all culled from the literature and that they contained systematic errors. Scholz (2002) still believes that for physical reasons one should expect a linear relation as proposed by Cowie and Scholz (1992b). Natural observations supporting the linear relation between the length and the maximum displacement of a fault have been published by for example Dawers et al. (1993); Schlische et al. (1996) and Koukouvelas et al. (1999) (Figure 2.7). Also from observations of analogue models, maximum displacement to length relations have been calculated with an n value of 0.93 (Mansfield and Cartwright, 2001).

It has however been demonstrated from numerical models that the maximum displacement on a fracture is not only dependent on the length of the fracture, but as well on the height (Willemse, 1997; Schultz and Fossen, 2002) (figure 2.5). It has been proposed by several studies that the shortest dimension of a fault or fracture determines the displacement magnitude (e.g. Willemse, 1997). According to linear elastic fracture mechanics (LEFM), the maximum relative displacement on a fracture surface is given by (e.g. Schultz and Fossen, 2002):

$$D_{max} = \left[\frac{2(1-\nu)}{G}\sigma_d\right]\left(\frac{b}{E(a,b)}\right) \tag{2.13}$$

with a and b being respectively the semi-major and semi-minor axis of the ellipse that represents the fracture shape. σ_d is the driving stress on the fracture. ν is the Poisson's ratio and G the shear modulus of the host rock. The function $E(a,b)$ in 2.13 is the complete elliptic integral of

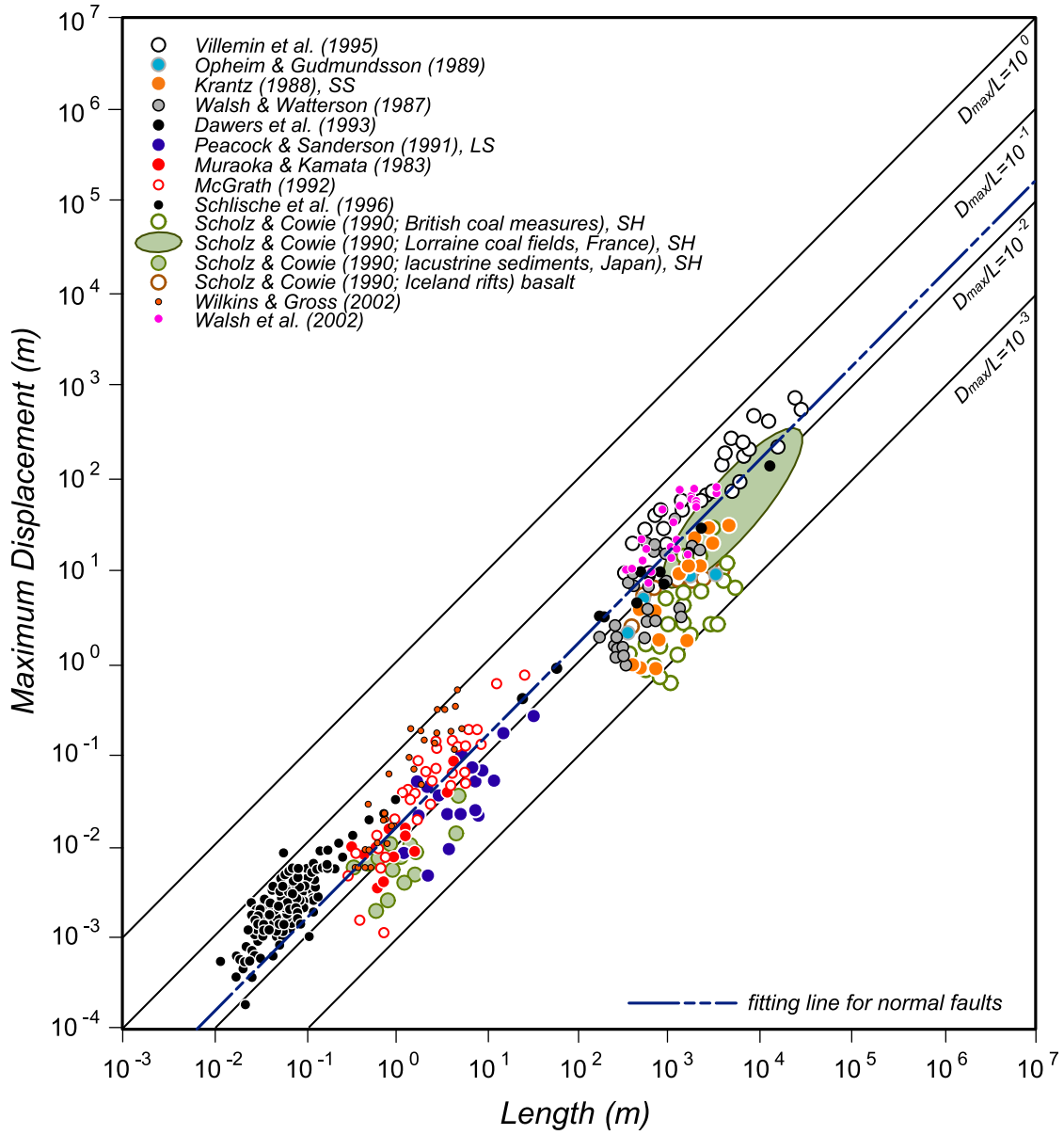

Figure 2.7: *Maximum displacement D_{max} of a fault plotted versus fault length L for normal faults. From Kim and Sanderson (2004).*

the second kind which is given by (Schultz and Fossen, 2002):

$$E(a,b) = \int_0^{\frac{\pi}{2}} \sqrt{1 - \left(\frac{a^2 - b^2}{a^2}\right)^2 \sin^2\varphi \; d\varphi} \tag{2.14}$$

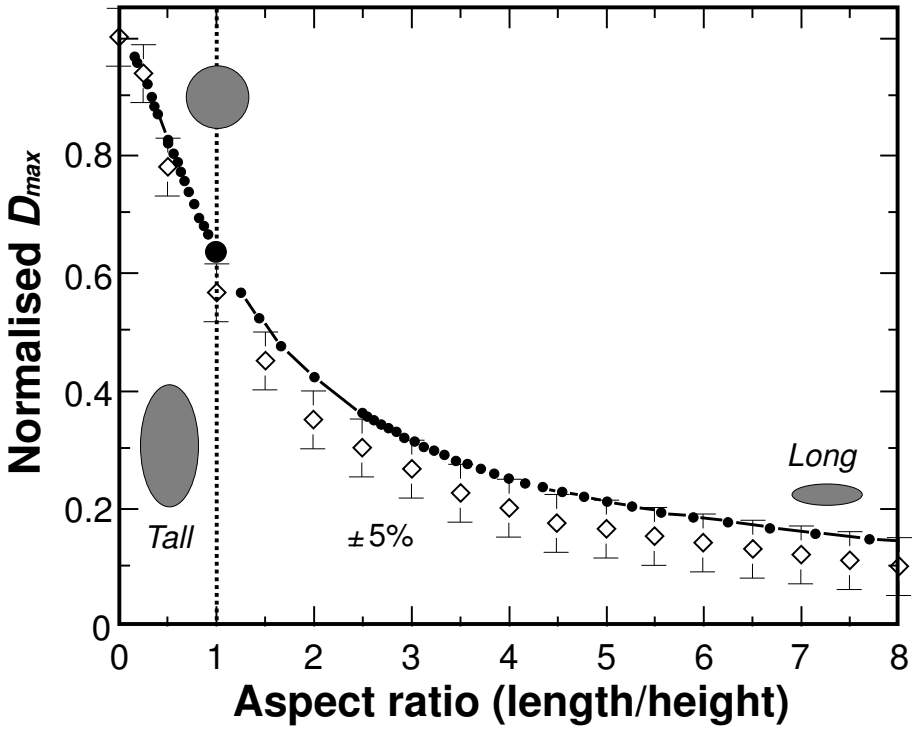

Figure 2.8: *Normalised maximum displacement (3-D relative to 2-D) on a fracture in relation to its aspect ratio. Filled symbols are from Schultz and Fossen (2002) and open symbols are from Willemse et al. (1996). Shaded ellipses represent the shape of the fracture in that zone of the graph, assuming constant values for the length. Calculations assumed a Poisson's ratio of 0.25 and a shear modulus of 6.25GPa. From Schultz and Fossen (2002).*

But which can be approximated within 5% of its numerical solution by:

$$E(a,b) = \Omega \cong \sqrt{1 + 1.464\left(\frac{a}{b}\right)^{1.65}} \tag{2.15}$$

The φ in equation 2.14 is the so called amplitude of the elliptic integral (Schultz and Fossen, 2002). In figure 2.8 the maximum displacement of a fracture is represented in function of the aspect ratio of that fracture (i.e. length/height). From equation 2.13 it is already clear that the expression of the maximum displacement along a fault contains apart from the fault length and fault height several material properties like the Poisson's ratio ν and the shear modulus G. The dependence of the l/D_{max} ratio of a fault (as well as the displacement profile) on several factors like the spatial stress variations along a fault, frictional strength along a fault, inelastic deformation at fault tips, etc. has already been demonstrated by Bürgmann et al. (1994). Peacock and Sanderson (1996) moreover found that this ratio also depends on the propagation history of the considered fault. The wide variety of factors that influence the scaling of faults, explains the large scatter that is usually observed in displacement vs. fault length plots of natural fault populations (Mansfield and Cartwright, 2001).

Fault populations

Faults are also believed to follow a power-law scaling for their size-frequency distribution. This assumption comes from the empirical Gutenberg-Richter relation between the frequency of earthquakes and their size (e.g. Scholz, 2002):

$$N(M_0) = a.M_0^{-B}$$

or:

$$\log N(M_0) = a - BM_0 \tag{2.16}$$

with $N(M_0)$ being the number of earthquakes of seismic moment $\geqslant M_0$ occurring during a given period, and a and B constants. The relation between the magnitude m of an earthquake[3] and the slip surface dimension w of that earthquake is given by $m \propto \log w^2$ (Walsh and Watterson, 1992). Thus, as large earthquakes do require large fault surfaces, this relationship also defines the size distribution of active faults in an area (e.g. Roberts and Yielding, 1994). For active faults, the power law scaling of the fault displacement can be presented as (e.g. Yielding et al., 1992; Needham et al., 1996; Nicol et al., 1996; Yielding et al., 1996):

$$N = aS^{-\mathfrak{D}} \tag{2.17}$$

With N the number of faults with a size greater than or equal to S, a a constant and $\mathfrak{D}$ the fractal dimension. Studies have shown that size populations obey a power-law relation over at least 2.5 orders of magnitude (Walsh et al., 1991; Yielding et al., 1992; Watterson et al., 1996). However, there appears to be a systematic variation in the fractal dimension, depending on the type of fault data used (e.g. Nicol et al., 1996). Values of $\mathfrak{D}$ obtained from outcrop studies usually lie between 0.4 and 0.6, whereas values from seismic data sets tend to be higher (0.8–1.0). This suggests that there is a general decrease in $\mathfrak{D}$ values with decreasing fault size (Nicol et al., 1996), meaning that different processes or controls might be effective on different scales. Such deviations might for example be related to distinct size populations of small faults that "cluster" immediately adjacent to larger ones. The review paper of Bonnet et al. (2001) includes a table of published power law exponents for fracture length distributions as well as discussions on the applicability of other statistical distributions in fracture characterisation.

A consequence of the size population scaling is that at any given time also inactive faults must exist in a fault population. This is because when faults grow according to a model like the one described in section 2.3.1 continuously new faults must be formed to satisfy the Gutenberg-Richter relation, as the earlier formed faults grow in size (Walsh and Watterson, 1992). If the Gutenberg-Richter relation is maintained for the active faults, this requires that a number of the faults must be inactive. Different strategies can be applied to calculate this so called *dead fault* population, and the results show that this population will comprise a greater amount of small faults than usually predicted by the Gutenberg-Richter relation (Walsh and Watterson, 1992).

[3] the magnitude of an earthquake and its seismic moment are related as: $m \propto C \log M_0$ with $C = 1.5$ (Walsh and Watterson, 1992)

This has also been observed in analysis of coal-mine plans (e.g. Childs et al., 1990). Therefore a significant proportion of the accumulated geological extension may occur on the smaller-scale structures, unlike the distribution of seismic slip, where the largest earthquakes account for an overwhelming amount of the seismic slip (Roberts and Yielding, 1994). Walsh and Watterson (1992) showed that also the dead fault population has a fractal size distribution.

It has been shortly mentioned above that there appears to be a difference in the fractal dimensions of fault populations of small faults and large faults. This suggested that there might be different processes or mechanisms involved on these different scales. Other studies have also reported departures from the power-law size-frequency distribution, for example when faults are part of duplex systems (Wojtal, 1994). Also for fault array evolution in large strain settings, the displacement-length scaling sometimes changes as faults start to accommodate increasing strains by larger displacements, without a considerable increase in fault length (e.g. Poulimenos, 2000) (see also section 2.4.2).

2.4 Fault interaction and linkage

Natural examples of large normal faults often show irregular traces with jogs along their path, which results in a clear segmentation of the faults (e.g. dePolo et al., 1991; Stewart and Hancock, 1991; Cartwright et al., 1996; Morewood and Roberts, 2000; Jackson et al., 2002, ...). This segmentation has been observed in nature over a whole range of scales, ranging from millimetres to several kilometres (Tchalenko and Ambraseys, 1970; Segall and Pollard, 1980; Pollard and Aydin, 1984; Vermilye and Scholz, 1999; Marchal et al., 2003; Walsh et al., 2003), as well as in small-scale sandbox models of fault formation (Tchalenko, 1970; Tron and Brun, 1991; McClay and White, 1995; Mansfield and Cartwright, 2001) (see also chapter 7).

Martel (1999) showed through mechanical analysis, that a variety of reasons could be responsible for the development of non-planar fault geometries in map view. Only faults characterised by a uniform shear stress drop and surrounded by uniform and isotropic rocks in a uniform far-field stress state would remain planar, and therefore non-planar faults are inevitable in the heterogeneities of the earth. Moreover in such stress fields it would be the rule, rather than the exception, that incipient faults consist of separate segments which do not lie on a smooth surface (Mandl, 1987). The most important reason for the mentioned irregularities in fault traces therefore is believed to be the result of the linkage of such different individual fault segments that existed and evolved as smaller structures before they actually connected (e.g. Segall and Pollard, 1980; Peacock and Sanderson, 1991; Davison, 1994; Peacock and Sanderson, 1994; Willemse, 1997; Morewood and Roberts, 2000). This process of *fault growth by segment linkage* therefore differs from the radial propagation model for fault growth as described in the introduction of section 2.3 (see also figure 2.9). Vermilye and Scholz (1999) argue that segmentation can also result from the uneven propagation of a fault tip when it encounters rock masses with a higher fracture toughness. However, this model has been proposed to explain observations from a microstructural analysis of a small fault, and therefore its applicability to explain larger

segmentation is not clear.

2.4.1 Fault growth by segment linkage

On page 35 it was explained, that cracks and faults perturb the remote stress field, and so create a different local stress field that is the sum of the applied stresses and the stress perturbation caused by the fault. Equation 2.5 allowed to calculate the radius around a fault for which the perturbing stress had a considerable influence on the stress field. When isolated fault segments evolve and grow, there can be a moment when two segments approach each other close enough so that their "perturbing areas" overlap. This means that their stress fields will interfere with

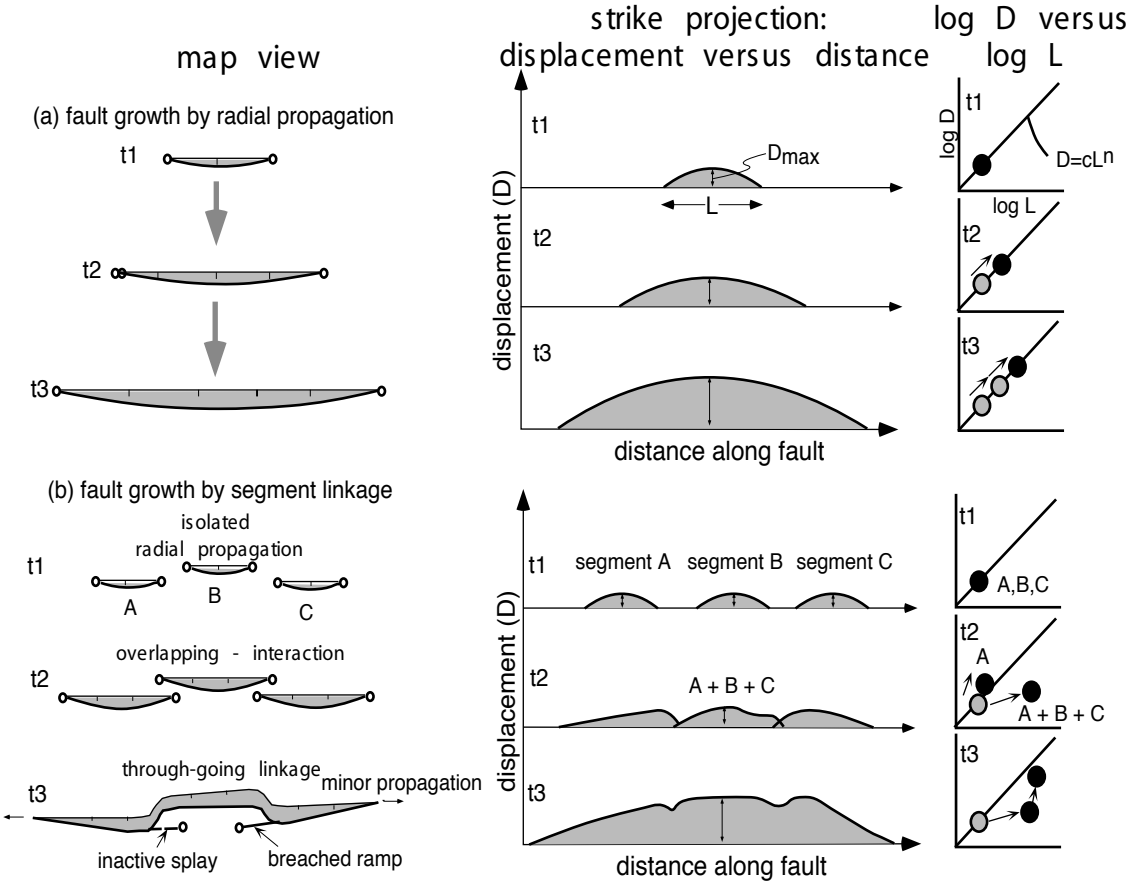

Figure 2.9: *Two models for the development of faults. Radial propagation (a) and fault growth by segment linkage (b). During the radial propagation process, individual faults lengthen and accumulate more displacement through time. This results in a linear growth curve on the log-log graph on the right. When faults grow by segment linkage, individual faults gradually link with each other as they grow further. This results in a sudden increase in the fault length. In a later stage, the displacement profile will be restored, as mainly displacement will be accumulated, without a further increase in propagation (see growth curve on the right). From Burbank and Anderson (2001) after Cartwright et al. (1995).*

each other and therefore fault interaction exists. From 2D studies fault interaction was assumed to be significant if 2 similar faults were spaced less than the horizontal fault length from each other (i.e. each fault having a "radius of influence" equal to half the horizontal fault length). 3D mechanical studies showed that this radius of influence depends on the 3-dimensional shape of the fault planes, and therefore a better rule of thumb would be that the radius is about equal to half the shortest in-plane dimension of the fault (Willemse, 1997).

Mechanical modelling of fault interaction has shown that as long as two neighbouring faults do not overlap, their tips are situated in a zone where movement on one fault enhances the shear stress on the other. On the other hand, when the fault tips overlap, they are situated in the "stress shadow zone" of the other fault, which results in a decrease of the shear stress on one fault caused by slip on the other (figure 2.10) (Segall and Pollard, 1980; Aydin and Schultz, 1990; Hodgkinson et al., 1996; Willemse et al., 1996; Willemse, 1997). Therefore, fault segments that have an under-lapped geometry will tend to grow further, whereas when segments overlap, they tend not to propagate (Willemse, 1997; Crider and Pollard, 1998). This was also demonstrated by Pollard and Aydin (1984) for the propagation of oceanic ridge segments, where they determined the *ridge propagation force* of a central ridge in a 3-ridge array, and calculated how the propagation force changed with varying overlap and spacings with neighbouring ridges. The results are shown in figure 2.11. This graph shows that for all geometries the propagation force increases as the ridges approach each other. As soon as an overlap exists, the ridge propagation force decreases, and reaches values below that of an isolated ridge, meaning that the propagation is impeded compared to those of isolated ones. With closer spacings, the magnitude

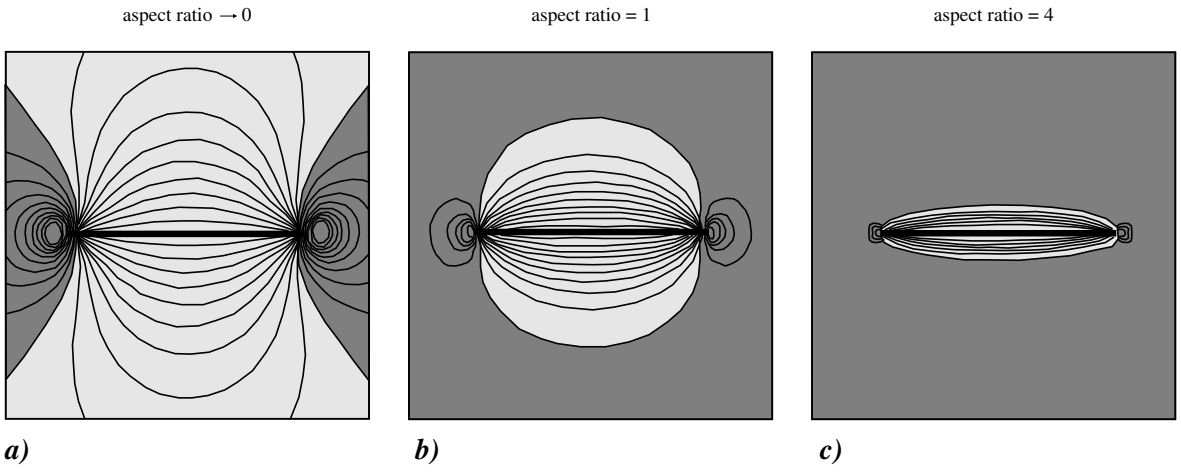

Figure 2.10: *Influence of the three-dimensional shape of a fault on the elastic stress around a vertical normal fault characterised by a uniform stress drop. The figure illustrates the perturbation of the shear stress component σ_{32} that acts in the direction of the fault slip vector. The contours are drawn on a horizontal plane through the centre of the fault. Dark shaded areas denote regions where the shear stress is enhances, and light shaded areas are marked by a reduction in the shear stress. Figure (a) represents a fault that has an almost infinite height, (b) represents a circular fault, and (c) is a fault where the length is four times larger than the height. From Willemse (1997).*

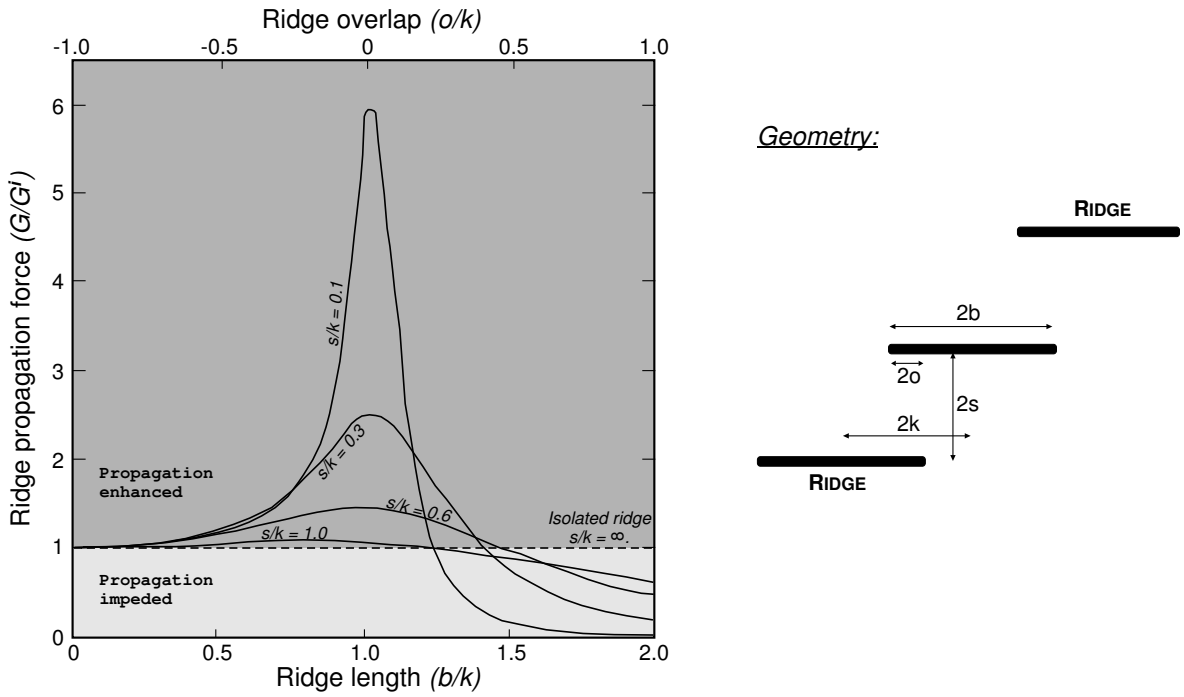

Figure 2.11: *Graph of ridge propagation force for the middle crack of a three-member array plotted against ridge length and overlap. Each solid line is for a different value of separation. The dashed line represents an isolated ridge. The ridge propagation force G is normalised to that of an isolated ridge G^i. b corresponds to half the ridge's length, o to half the overlap distance between ridges, s to half the spacing and k is half the distance between the midpoints of adjacent ridges. After Pollard and Aydin (1984).*

of the variations in ridge propagation force becomes larger, which indicates that closely spaced ridges are more subject to the propagation enhancement and impediment (figure 2.11). A similar type of curves was obtained by Willemse (1997) for normal faults, for which he plotted theoretical displacement gradients in function of the overlap distance of two faults (his figure 10). Similar graphs have also been obtained for the propagation energy in arrays of 3 dilatant echelon cracks or joints (Pollard et al., 1982; Pollard and Aydin, 1988) and of strike-slip faults Aydin and Schultz (1990).

The fact that the propagation of interacting faults is enhanced when they do not overlap and impeded as soon as an overlap zone has developed, is often used as an explanation for the only rare occurrence of two faults with such an underlapped geometry compared to that with an overlap geometry (e.g. Aydin and Schultz, 1990; Willemse et al., 1996). Acocella et al. (2000) found for example that only 7% of the fault pairs they studied in Iceland were in the underlapped geometry and Aydin and Schultz (1990) calculated only 10% for strike-slip faults.

In the region between two overstepping faults or cracks, values of the mean stress can be as large as 1.4 times the background value, and just outside that region, stress values are less than that in the far field (Segall and Pollard, 1980). These large stresses can cause secondary

fracturing in the area between two interacting cracks or faults. Moreover, it has been observed that between two overlapping normal faults areas of tilted bedding can develop (so called *relay ramps*, see section 2.5). This rotation often involves bending and the formation of minor faults within the ramp (Peacock and Sanderson, 1994; Cartwright et al., 1996; Crider and Pollard, 1998). At a certain critical limit, a through-going fault could pass the distribution of minor faults, resulting in a breaching of the ramp and the connection of the two originally isolated faults (Peacock and Sanderson, 1991, 1994; Cartwright et al., 1996).

When two neighbouring fault segments connect in this way, the "new" fault has a length that is about the sum of the individual segments, but it has a maximum displacement that is only equal to the largest displacement on both individual fault segments. Willemse et al. (1996) calculated with mechanical models that this maximum displacement is 9% larger than that of a similar isolated fault, for fault segments of length a that overlap when spaced $0.05a$ from each other. From the displacement to length relation between faults (equation 2.12) it is clear that even with a 9% increase in the displacement, the newly formed fault will still be *"under-displaced"* as compared to its new length (e.g. Cartwright et al., 1996). As a result displacement will increase mainly in the centre of the newly formed fault so that the shape of the displacement profile adapts to that of an isolated fault and the structure adapts its self-similar profile shape (Cartwright et al., 1995; Schlische, 1995; Cartwright et al., 1996; McLeod et al., 2000; Morley, 2002, etc.). This adaption of the displacement profile has often been observed (e.g. Gupta et al., 1998; Contreras et al., 2000; McLeod et al., 2000; Young et al., 2001), but in some areas no simple displacement pattern seems to develop after linkage (for example the Lupa Fault in the Rukwa Rift (Morley et al., 2000; Morley, 2002)). If no readjustment of the fault's displacement profile occurs, some regions along the fault remain stronger than others, and so prevent the new fault from slipping along its entire length (Cowie and Shipton, 1998; Morley, 2002).

The above described fault growth by segment linkage thus consists of different stages (figure 2.12):

stage 1: which consists of the *nucleation* of the faults, as simple isolated small faults. As extension continues these faults will accumulate displacement and their fault tips will propagate.

stage 2: in a second stage the fault tips have approached each other close enough to allow for a mechanical interaction. As fault tips first don't overlap, they experience an *enhanced growth* as a result of this interaction.

stage 3: In a last stage faults have formed overlap zones, and *linkage* has occurred, resulting in longer faults, able to carry more displacement than the originally isolated ones. In this stage, a readjustment of the displacement profile can occur.

From the described mechanical interaction between faults it is clear that faults which grow according to this model of fault growth by segment linkage evolve in locally heterogeneous stress and strain fields, as the slip and propagation of its segments will be influenced both, by the

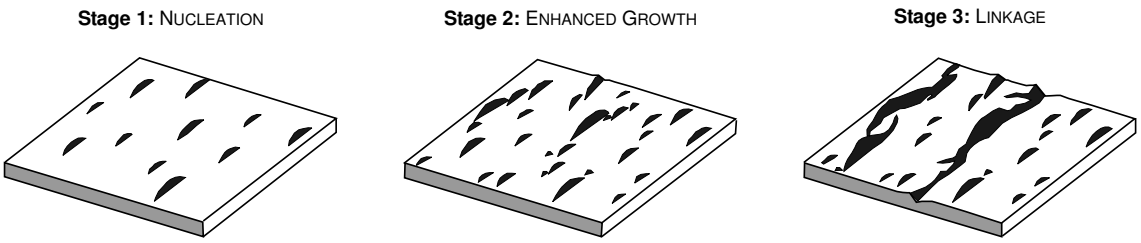

Figure 2.12: *Block diagram showing the evolution of a fault array. After Cowie (1998).*

tectonic loading, but also by the near-field stress perturbations of neighbouring segments (Crider and Pollard, 1998). Also secondary faulting or fracturing in the vicinity of such fault can be a result of stress perturbations related to that fault (e.g. Ackermann and Schlische, 1997; Bourne and Willemse, 2001; Maerten et al., 2002). A common example of such secondary fracturing is the development of so-called *tip faults*. Such faults are inferior to the principal fault plane, but they do have a slightly different orientation, resulting from the perturbed stress field near the termination of the principal fault (Willemse, 1997; Marchal et al., 2003). Marchal et al. (2003) argue that the secondary tip faults and the principal fault are part of one isolated fault system. As such three processes are involved in the growth and propagation of faults (Marchal et al., 2003) (figure 2.13):

1. Radial propagation,
2. Tip-to-parent fault connection, and
3. Isolated-to-isolated fault linkage.

Seen the likeliness for the development of tip faults, the fault planes of isolated normal faults are rarely as simple as mentioned in section 2.3, but rather show local complexities superimposed on the "elliptical" fault plane (Marchal et al., 2003).

2.4.2 Fault array evolution

Numerical models of fault array evolution have shown that large faults can develop from the growth and connection of smaller faults as extension continues (e.g. Cowie, 1998; Gupta et al., 1998; Cowie et al., 2000). In such models faults grow spontaneously, without a priori defined fault planes, at random positions. When a fault array starts to develop, some of the faults will form a geometry which is favoured by a positive feedback during rupture and reloading whereas others will experience a negative feedback. The former will therefore grow preferentially, while the latter stay minor (Cowie, 1998). This feedback mechanism is caused by the already explained propagation enhancement/impediment related to fault interaction. If for example an en echelon array of sub-parallel faults develops in the fault array, slip on these individual fault segments will enhance slip on the along-strike neighbours. This will cause the en echelon array to grow faster than for example isolated faults, and much faster than faults that are located in the shadow zones of another (Cowie, 1998) (See also figure 2.12 and figure 2 in Cowie (1998)).

This feedback mechanism causes a transition in the model from an initial distributed deformation, accommodated on widely spread small faults, to a stage of localised deformation, concentrated on less but larger faults (Cowie, 1998). Recently, a detailed study of 3D seismic data from the Timor Sea (NW Australia) has revealed similar behaviour for fault arrays in nature (Meyer et al., 2002), confirming the applicability of Cowie's model.

For the evolution of fault arrays involving more than 2 faults, the above described readjustment of the displacement profile seems to start already in the stage of mechanical interaction between the different fault segments, and not necessarily (as described by Cartwright et al. (1995)) after a real hard-linkage is achieved (e.g. Dawers and Anders, 1995). This is explained by Cowie (1998) as a result of the preferential growth of faults that are located at points of rupture symmetry. In an evolving en echelon fault array, this point of rupture symmetry is the central segment, by which it may achieve already greater lengths and accommodate larger displacements before any hard linkage takes place. Moreover, also the displacement-length ratio's of the central segments may increase as the interaction with overlapping neighbours inhibits further propagation (Cowie, 1998). This lead Cowie et al. (2000) to distinguish between an early linkage case, when linkage occurs before displacement readjustment, and a late linkage

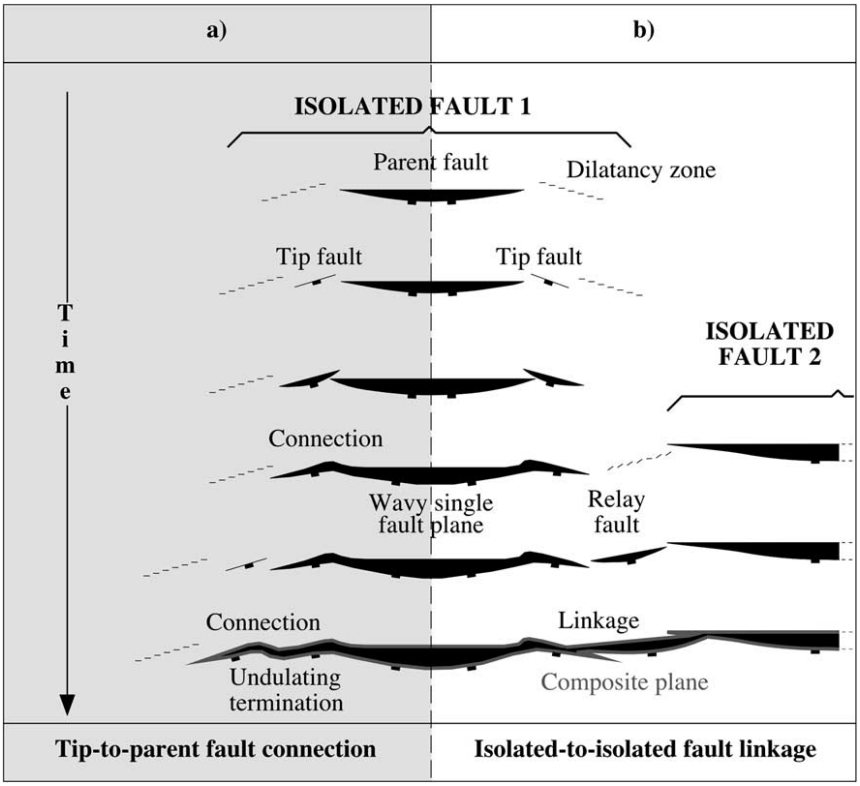

Figure 2.13: *Mechanisms of fault propagation: either tip-to-parent fault connection for isolated faults (a), or isolated-to-isolated fault connection for composite faults (b). From Marchal et al. (2003).*

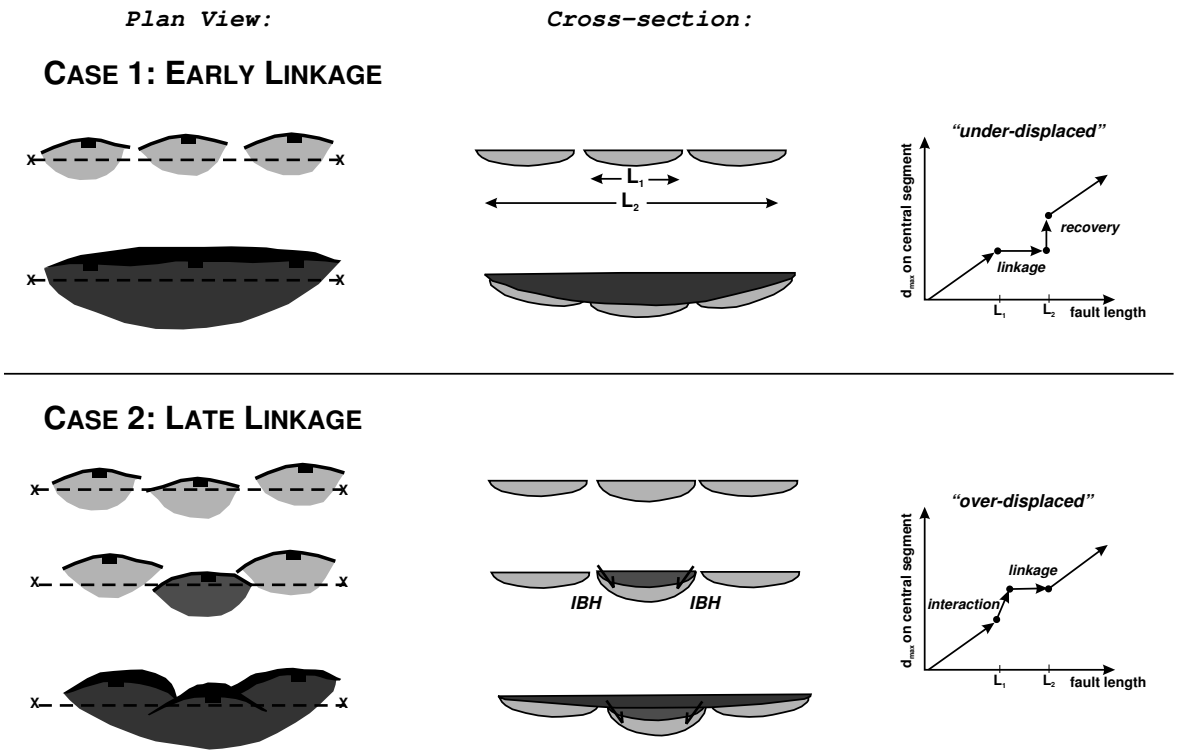

Figure 2.14: *Summary diagram of sub-basin coalescence due to growth by linkage for an array of three fault segments. The figure illustrates the difference between* early *and* late *linkage. Left-hand side: plan view of sub-basins. Centre: along-strike section through sub-basins. Right-hand side: maximum displacement on the central segment plotted as a function of fault length. For this graph a linear displacement-length scaling relationship was assumed.* Case 1: *linkage precedes interaction and displacement profile re-adjustment;* : Case 2: *pre-linkage interaction causes the displacement profile along the central segment to re-adjust without significant length change. In Case 1 a broad shallow basin develops on top of small sub-basins and the rate of subsidence increases until the pre-linkage displacement-length ratio is re-established. In Case 2 persistent intrabasin highs (IBH) develop which laterally confine the developing sub-basins. The central sub-basin temporarily experiences higher rates of subsidence due to interaction. Eventually displacement localises onto the one basin-bounding fault surface, the intrabasin highs become inactive and are on-lapped. The rate of subsidence returns to its pre-interaction rate. Modified from Cowie et al. (2000).*

case, when the fault system adopts already a displacement profile similar to that of an isolated fault before the actual linking. In the late linkage case the post-linkage displacement increase is minor (figure 2.14).

Once larger faults have developed by the linkage of different segments (stage 3 in figure 2.12), an increased subsidence can occur due to the increase in fault displacement that results from the readjustment of the displacement profiles of the newly linked faults (Gupta et al., 1998; Cowie et al., 2000). In such cases the increased subsidence therefore does not require an increase in the rate of extension. Gupta et al. (1998) suggested that this mechanism might explain the common observation of subsidence increase in the so-called *rift climax* stage of rift systems.

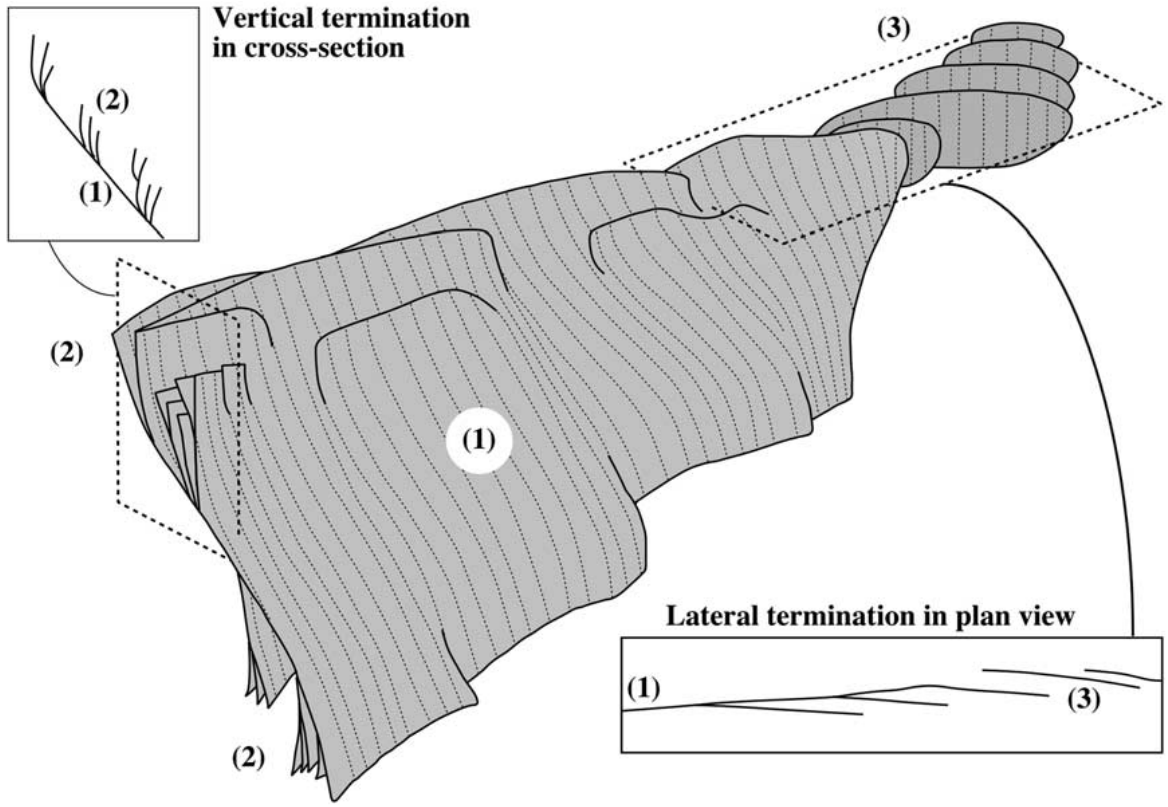

Figure 2.15: *The half-plane of a normal fault composed of a principal plane (1); branched secondary fault planes at the vertical termination (2) and en échelon secondary fault planes at the lateral termination (3). From Marchal et al. (2003).*

Combined with the development of larger (more dominant) faults, inactivity of an increasing number of smaller faults can occur (Cowie, 1998). This cessation of activity of smaller faults has also been observed in natural systems (e.g. Morley, 2002).

2.4.3 Fault linkage in 3 dimensions

Recently Walsh et al. (2003) suggested that for originally isolated faults the post-linkage displacement readjustment can only be significant if the displacement deficit has been maintained by elastic deformation. This maintenance is possible during seismic slip events, but it is unlikely over a time lapse of several million of years. In such cases displacement readjustment would indicate that the faults were initially already connected at depth rather than being really isolated in 3 dimensions (Walsh et al., 2003).

This idea is outlined in the coherent fault model of Childs et al. (1996) and Walsh et al. (2003), where seemingly isolated faults at the surface might form a single kinematically coherent system when the faults result from the bifurcation at depth of a single fault (figure 2.15).

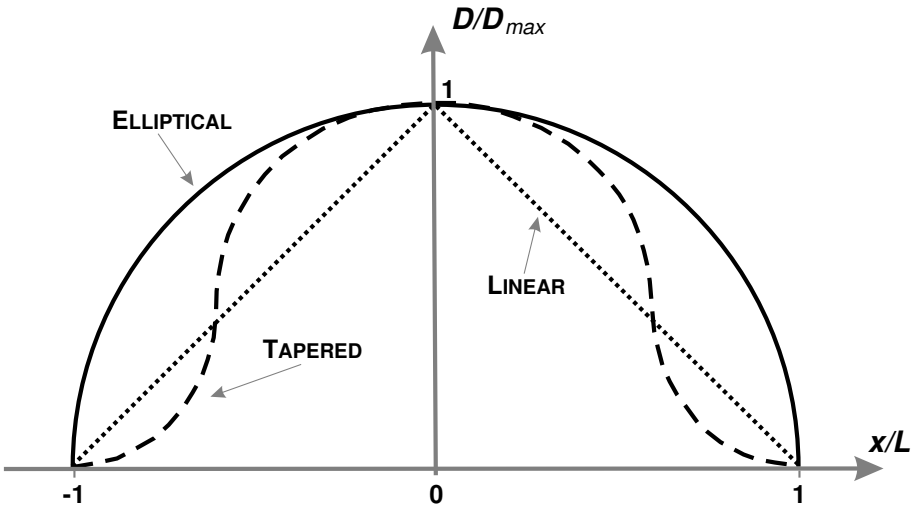

Figure 2.16: *Ideal displacement distributions for different types of fault models. Displacement is normalised to maximum displacement, and the position is normalised to half the fault length. Modified from Moore and Schultz (1999).*

2.4.4 Determining fault interaction

As demonstrated in section 2.3.3, knowledge of fault lengths and of the maximum displacement along faults (D_{max}) can be sufficient to discuss displacement-length scaling. However, this knowledge is insufficient to reveal displacement variations along the length of a fault, or to characterise displacement gradients in fault tip regions (Peacock and Sanderson, 1991; Moore and Schultz, 1999). For this purpose often displacement profiles are drawn in which displacement values are plotted against the position along a fault (e.g. figure 2.4) (e.g. Muroaka and Kamata, 1983; Dawers et al., 1993; Cartwright and Mansfield, 1998).

Variations in displacement profiles

Several "ideal" displacement profiles have been proposed, the shapes of which are mainly related to the model that is used to describe their fault slip (e.g. Scholz, 2002) (section 2.3.2). All shapes have in common that the maximum displacement occurs in the centre of the fault, with displacement decreasing towards the fault tips. This decrease can be described for example as linear, elliptical (for the elastic model) or as tapered (for the cohesive end-zone model) (figure 2.16). Displacement profiles in nature are controlled by twelve factors (Schultz, 1999; Peacock, 2002):

1. fault length (in map view and cross-section),
2. the aspect ratio of the fault (i.e. the ratio between fault length and fault height),
3. fault shape,
4. proximity of the fault to the free surface or other boundaries,
5. configuration of far-field stresses,

6. frictional and constitutive properties of the fault,
7. variations in elastic properties and lithology along the fault,
8. time-dependent faulted rheologies,
9. inter-fault plate deformation,
10. near-tip processes,
11. interaction with other faults, and
12. fault segment linkage.

As fault interaction and linkage are important causes for the deviation of the displacement profiles from the "ideal" one, these deviations are a useful criterion to infer fault interaction. Drawing throw profiles along the strike of a natural fault is an effective technique to visualise possible deviations from the ideal, isolated, displacement profile of a fault (Peacock and Sanderson, 1991; Dawers and Anders, 1995; Contreras et al., 2000). From such displacement profiles, it has been observed that along segmented faults slip can vary considerably along the trace, and that as such — at least in early stages of the evolution — a clear relation exists between the geometry of the segments and the displacement profiles of the fault (e.g. Contreras et al., 2000).

Peacock and Sanderson (1991, 1994) were among the first to notice that the displacement gradient of a fault increases in the zone where it overlaps with another fault, and that the displacement maximum is no longer in the centre of the trace, but located closer to the overlap zone (figure 2.17). Moreover, increasing displacement gradients occur with increasing fault interaction (Peacock and Sanderson, 1991; Gupta and Scholz, 2000). By using different seismic horizons to construct displacement profiles, Morley and Wonganan (2000) showed that the shape of the profiles along a fault could vary considerably, with some horizons having an asymmetric throw profile while others had a more symmetric shape.

Manighetti et al. (2001) classified 94% of the 255 faults they investigated in Afar in 8 categories, based on the first order shape of their displacement profiles (figure 2.18). They called only 4% of these faults completely "unrestricted", which means that the magnitude of the displacement gradient is more or less constant for the whole fault. The other 96% show an increased magnitude at least at one side of the fault trace, what they interpreted as being a result of a fault tip that did not further extend laterally, but which could still increase its displacement. This could possibly be the result of interaction with neighbouring faults (Manighetti et al., 2001). In section 2.4.1 it was already explained that interacting faults that overlap impede each other's propagation, which makes it a plausible cause for the observed tip restriction. This mechanism also explains the "shift" of the fault's maximum displacement towards the overlap zone. Indeed, if the displacement maximum stays at the same position along the fault, but only one of its fault tips (the unrestricted one) propagates laterally, this results in a final asymmetric displacement profile with the displacement maximum located closer to the restricted fault tip (figure 2.17). Based on mechanical models of interacting faults, theoretical displacement profiles have been constructed that closely resemble natural observations (Willemse et al., 1996; Willemse, 1997).

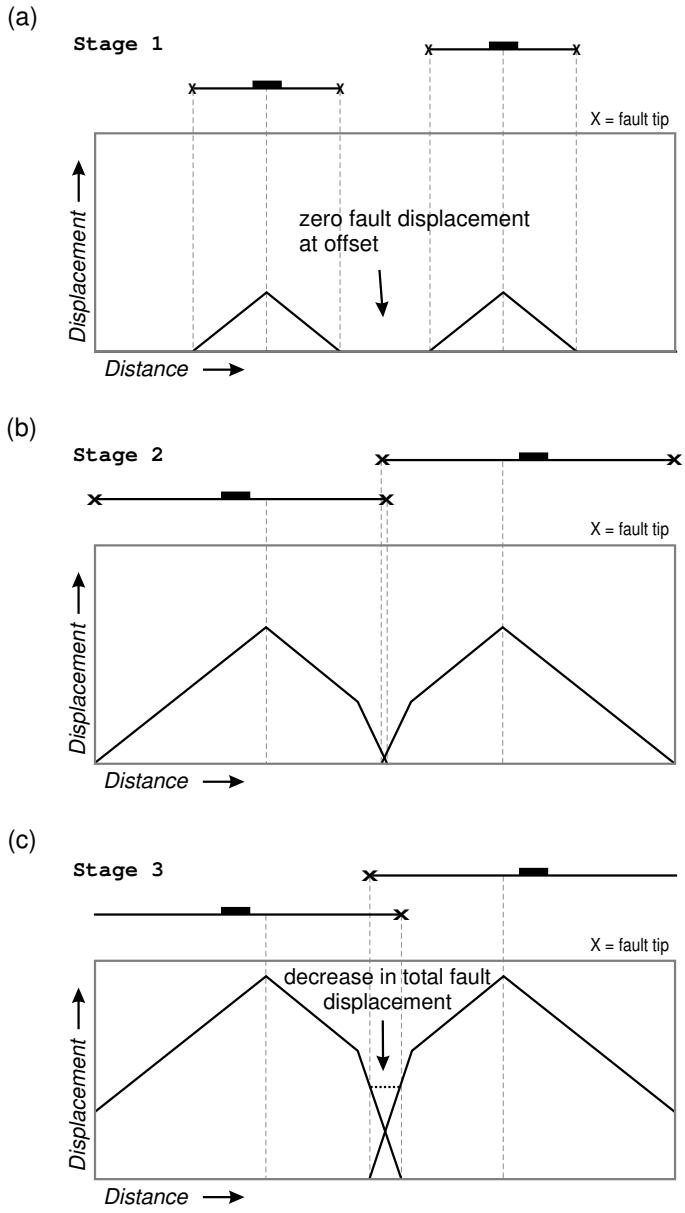

Figure 2.17: *Stages of offset development of normal faults, with corresponding displacement profiles. In this diagrams a linear displacement distribution is assumed for the faults. (a) Stage 1: two offset normal faults underlap. The displacement profiles are regular and symmetric, with maximum displacement in the centre of the profile. Fault tips will propagate in both directions. (b) Stage 2: a small area of overlap has formed between the two faults. The fault tips in the overlap zone propagate less than the other fault tips, which results in an increased displacement gradient inside the overlap zone. Because the displacement maximum is still located at the same position in the fault, the displacement profile adopts an asymmetric shape. (c) Stage 3: Further propagation of the outer fault tips accompanied by only a limited propagation inside the overlap zone increases the displacement profile asymmetry. The observed total fault displacement in the overlap zone is often smaller than the height difference between the footwall of the upper fault and the hanging-wall of the lower fault, because tilting of the layers between the two faults accounts for part of the height difference. After Peacock and Sanderson (1991).*

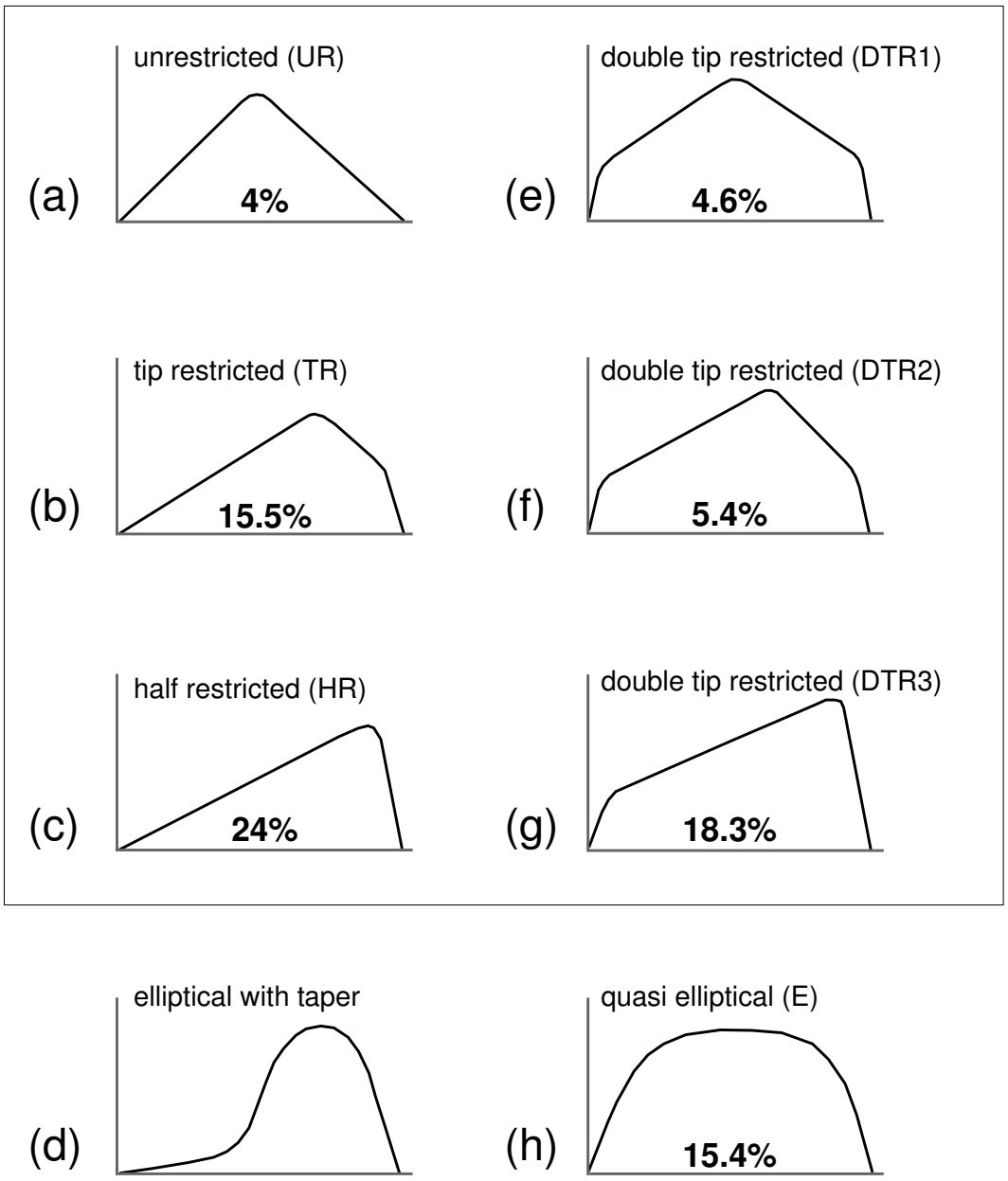

Figure 2.18: *Sketch of the first-order shapes of displacement profiles in the Afar region as identified by Manighetti et al. (2001). The numbers are percentages of faults with a given shape (with respect to the total number of faults that could be classified: 240). The remaining 12.5% have intermediate shapes. (a), (b) and (c) have at least one unrestricted side, whereas (e), (f) and (g) are restricted on both sides. Only 15% of the slip profiles exhibit the elliptical or bell-shaped patterns as predicted by the simple elastic theories (g) (see also figure 2.16). The tapered pattern as illustrated in (d) is only drawn for an elliptical displacement profile, but it has also been observed for the TR, HR and DTR profiles. From Manighetti et al. (2001).*

Spacing and overlap of faults

As explained in section 2.4.1 the stress field around a fault differs from the far-field stress field, with the difference remaining considerable within the radius of influence of the fault, but becoming negligible outside (Segall and Pollard, 1980; Willemse, 1997). This idea stimulated several authors to use the separation between faults and the degree of overlap to evaluate possible interaction, in natural examples (e.g. Huggins et al., 1995; Peacock, 2003) as well as in analogue modelling experiments (An, 1997). Although the overlap to spacing ratio is related to displacement anomalies along a fault, it cannot be used to quantify fault interaction as the above mentioned increase in displacement gradient (Gupta and Scholz, 2000). Usually fault interaction is assumed when the overlap to spacing ratio has values around 3.5 or 4 (Willemse, 1997; Acocella et al., 2000). An (1997) and Acocella et al. (2000) found that the interaction of faults depends not only on the overlap or spacing, but as well on the total length of the fault system. For example strike-slip faults in laboratory experiments interacted when the spacing between two faults was less than 10% of the combined fault length (An, 1997). Acocella et al. (2000) found from normal faults in Iceland that the minimum length of the fault system for interaction to occur was 14 times the value of the spacing. The qualitative aspect of this dependence is somehow evident, as the radius of influence of a fault depends on the fault's dimensions. Also from the energy curves in figure 2.11 (page 48) it was already clear that the spacing between large interacting faults could be larger than that for small faults with similar interaction, as the different curves were normalised to half the fault's length. As such, mechanical models support the observations of An (1997) and Acocella et al. (2000).

2.4.5 Importance for earthquake hazard assessment

The concept of fault segmentation has in the past been very appealing in seismic-hazard assessment, as segment boundaries of faults are locations where ruptures commonly stop or are impeded (Schwartz and Coppersmith, 1984; King, 1986; Thenhaus and Barnhard, 1989; Crone and Haller, 1991; Zhang et al., 1991). The early idea was that segments were *persistent* barriers, which meant that an earthquake rupture on a long fault zone would always be restricted to the individual segment on which it began (see references in McCalpin, 1996). This length restriction would therefore also mean a restriction in the magnitude of the earthquake. Later research, however, has also revealed the existence of *non-persistent* rupture barriers or *leaky* barriers (e.g. dePolo et al., 1991; Anders and Schlische, 1994), that inhibit but don't stop rupture propagation.

The segmentation for active faults is usually interpreted in a broader sense than just the segmentation revealed by geometric discontinuities along a fault trace (as used so far in this chapter). Initially, an *earthquake rupture segment* was identified based on the surface ruptures related to earthquakes along a fault, whereas the geometric discontinuities along a fault trace are "static" criteria. These concepts have been mingled with each other continuously, hoping that the static boundaries might act as rupture barriers in future earthquakes (McCalpin, 1996).

In general, the most common fault zone discontinuities can be classified into three major groups: *geometric, structural* and *behavioural*, but with considerable "gray areas" between them

(dePolo et al., 1991):

- Geometric discontinuities are marked by, for example, a change in fault orientation (bends) or by step-overs and separations or gaps in a fault zone,
- Structural discontinuities include fault branches, intersections with other faults and folds, and terminations at cross structures, and
- Behavioural discontinuities, on their turn or characterised by changes in slip rates or in the sense of displacement, or for example by a difference in creeping vs. locked behaviour.

It has been observed that segment boundaries identified using static geological or geometric criteria, can act as real rupture barriers (e.g. King and Nábělek, 1985), but even so ruptures can pass through them (e.g. Crone and Haller, 1991; dePolo et al., 1991; Anders and Schlische, 1994). Harris and Day (1993) showed with numerical simulations of strike-slip faults, that it is unlikely that strike-slip ruptures "jump" a fault step that is wider than 5km. They found that the "jumpable" distance depends on the stress drop along the fault and on the rupture velocity. The maximum "jumpable" spacing was in general also less for compressional steps than for corresponding dilatational steps (Harris and Day, 1993). This does not mean that it is possible to distinguish whether a geometric discontinuity is a real seismic barrier or not based solely on its geometry, as the behaviour of the fault step will be completely different in case the faults are connected at depth to a single one, or in case, for example, the zone between the two faults consists of already heavily fractured, or easy to fracture, material (Harris and Day, 1993).

In general the likelihood for relay zones in normal fault systems to be real earthquake segment boundaries is believed to be rather low (18% according to table 9.5 in McCalpin, 1996). This seems logical, as relay zones are regions in which fault displacement is accommodated on 2 or several faults that interact. Instead of stopping most ruptures, relay zones will cause ruptures to be transferred to a given fault one time, and to another fault the next time (Anders and Schlische, 1994). This displacement transfer therefore considerably complicates the assessment of seismic risks in a certain area (Scholz and Gupta, 2000). Moreover, in later stages of the evolution of segmented normal fault systems, the displacement deficit that formed between originally isolated faults is likely to gradually disappear. This would mean that if initially the geometric segment boundaries corresponded to real seismic rupture barriers, this would reverse in later stages, as the original overlap zones are expected to become the loci for new earthquakes when the fault's displacement profile readjusts. Such post-linkage earthquakes would as well have larger magnitudes because the size of the potential rupture zone will have increased (Soliva and Benedicto, 2003). Attempts to incorporate stress transfer and interaction between different earthquakes into probabilistic seismic hazard assessment have been presented by Stein (1999). Also Scholz and Gupta (2000) have addressed the problem of earthquake triggering between interacting faults, and they emphasised that because of the triggering the extent of the zone of damage of the aftershocks might be much larger than the zone in which the main-shock caused damage. Therefore, due to the triggering, the aftershocks might cause additional damage in zones which weren't affected by the main-shock. In older models, aftershock weren't considered that important for the assessment of seismic hazard, as they were believed to mainly affect areas

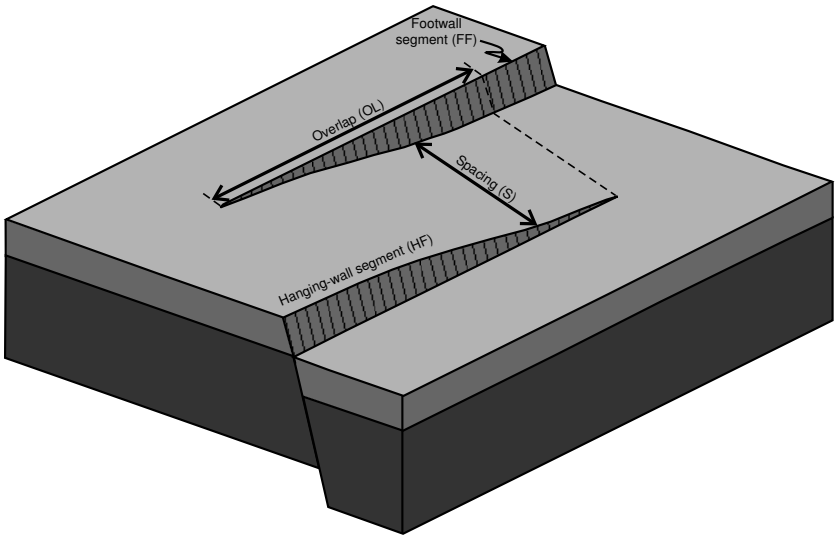

Figure 2.19: *Cartoon of a relay ramp between two overlapping synthetic normal faults. The terminology used in this work is indicated on the figure. After Peacock and Parfitt (2002).*

that were already destroyed in the first place (e.g. Scholz and Gupta, 2000).

2.5 Relay ramps

As already explained in section 1.2 on page 25, a *relay ramp* is a special kind of transfer zone (figure 2.19). The term is used for an area of tilted bedding between two overlapping synthetic normal faults (Larsen, 1988; Peacock and Sanderson, 1991; Peacock et al., 2000a) and therefore corresponds to a synthetic overlapping transfer zone in the classification of Morley et al. (1990). Similar structures can form between two overstepping strike-slip faults (Aydin and Nur, 1985; Westaway, 1995), but they should then be termed *strike-slip relay ramps* (Peacock and Sanderson, 1995). In this section the existing conceptual models for relay ramp structure and evolution are briefly explained. These models will be compared to observations of a large scale relay ramp in Lake Baikal (chapter 4), and to observations from experimental simulations (chapter 6).

Earlier in this chapter (page 48) it was mentioned that only a small amount of interacting faults are in an underlapped geometry compared to the amount of faults that overlap. This means that in the growth process of faults through segment linkage, relay ramps are common structures. The surface of relay ramps usually tilts towards the hanging-wall fault segment, and this tilt often causes a decrease in the total fault displacement in the overlap zone (Peacock and Sanderson, 1991) (figure 2.17). Peacock and Sanderson (1991) identified 4 main stages in the development and evolution of relay ramps, but as the formation of overlap zones has been discussed above, here will only be focused on the last two stages of this evolution, i.e. the development of secondary faults in the ramp and a final breaching of the ramp structure. According to Peacock and Sanderson (1994) and Peacock and Parfitt (2002), the different evolutionary

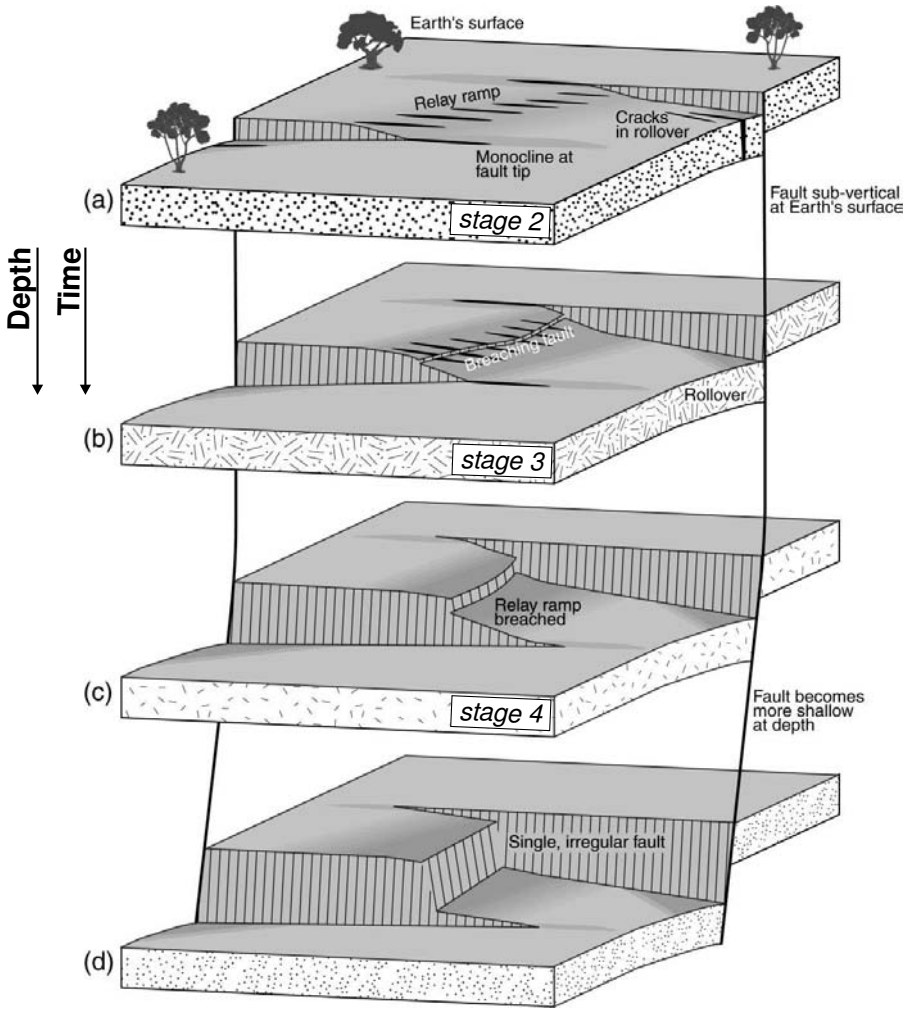

Figure 2.20: *Block diagram of the possible three-dimensional geometry of a relay ramp. This figure is based on examples from faults in the Koae and Hilina fault systems, but similar figures have been published by Peacock and Sanderson (1994); Peacock (2002). The evolutionary stages of the ramp can change both in time as well as in depth, because different levels of the fault have different displacements, and therefore mark a spatial development of the ramp. After Peacock and Parfitt (2002).*

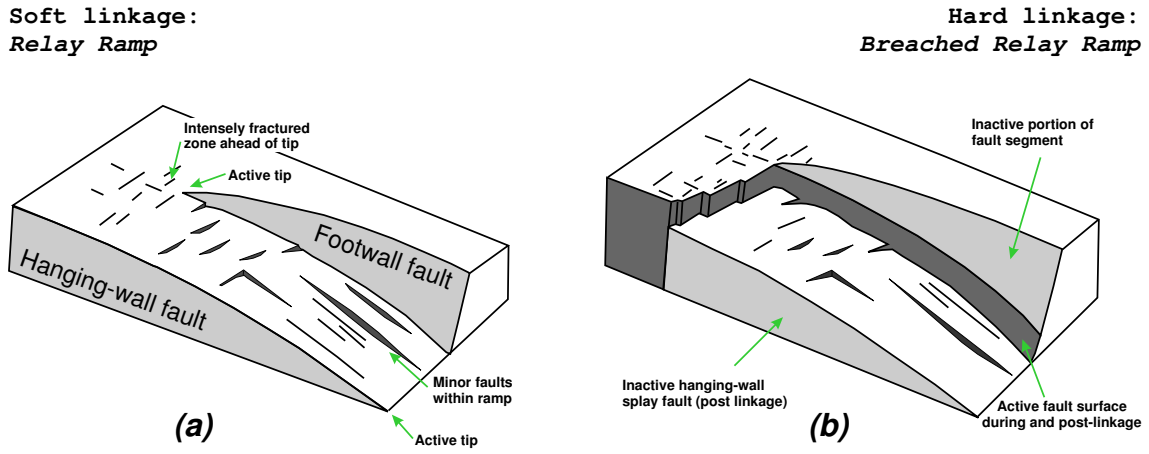

Figure 2.21: *Deformation in a relay ramp leads to the formation of secondary faults and fractures (a). At a certain stage a through-going fault can develop that cuts through the relay ramp and connects the two main faults. This through-going fracture tends to develop near the fault tip of one of the main faults (b). If the breaching is established at lower part of the ramp it's sometimes called a* lower ramp breach, *breaching at the upper part of the ramp (like in figure (b)) might be referred to as* upper ramp breach *(e.g. Crider, 2001). After Cartwright et al. (1996).*

stages of a relay ramp could be observed in nature, both in time and in depth (figure 2.20).

2.5.1 Breaching of relay ramps

Due to the progressive increase in fault displacement gradients towards the fault tips of overlapping faults (figure 2.17) the bedding in a relay ramp becomes tilted (Peacock and Sanderson, 1994). It was already explained above (section 2.4.1) that this reorientation of the bedding often involved bending which might lead to the development of secondary fracturing in the ramp (figure 2.21). The through-going fault that connects the offset faults in a final stage of the ramp evolution tends to develop either at the hanging-wall end of the ramp or at the footwall end (Trudgill and Cartwright, 1994; Cartwright et al., 1996). This was also noted by Childs et al. (1995) who distinguished 4 possible breaching mechanisms for relay ramps (figure 2.22):

1. Propagation of the footwall fault towards the hanging-wall to achieve linkage. In this case the tip of the hanging-wall fault becomes unused. Trudgill and Cartwright (1994) called such a ramp a *footwall breached ramp*.
2. Propagation of the hanging-wall fault towards the footwall fault to achieve linkage, and leaving the tip of the footwall fault unused. Such a ramp is also called a *hanging-wall breached ramp* (Trudgill and Cartwright, 1994).
3. Simultaneous propagation of the footwall fault towards the hanging-wall fault and of the hanging-wall fault towards the footwall fault. In this case no fault tips are short-cut.
4. The development of a new cross-cutting fault, that cuts through the ramp and leaves the fault tips of both main faults unused.

Although Childs et al. (1995) mentioned this fourth possibility of breaching, they did not know of any natural example where it had occurred. Also for extensional fractures linkage seems to result mostly from the propagation of one of the main fractures towards the other (Acocella et al., 2000). Ferrill et al. (1999) described examples where breaching resulted from the propagation of one of the main faults towards the other, but he also found examples where a new fault system cross-cuts the ramp (figure 2.23a). This connecting "fault" usually corresponds to a fault system that results from the interconnection of different fault clusters in the ramp, only rarely a continuous, well-defined, fault is observed (e.g. figure 2.23b; see also chapter 4). Also in the Koae and Hilina fault systems in Hawaii, several examples of breached relay ramps have been found, in which a connecting fault cuts through the centre of the ramp (Peacock and Parfitt, 2002).

Ferrill et al. (1999) explained the linkage of relay ramps in terms of the displacement gradient on the main faults. Where fault throw increases disproportionally to fault tip propagation, linkage by a connecting fault would be favoured. In such cases the displacement gradients at the fault tips would increase, causing steepening of the ramp structure. Such a steepening will involve an increase tilting and bending of the ramp along an axis perpendicular to the strike of the main faults. The extension that is associated with this bending is directed parallel to the main faults, and therefore favours the formation of faults striking at high angles to them. If the propagation of the main faults is proportional to the increase in displacement, lengthening of the relay ramp structure would occur rather than steepening, and this would result in the breaching by the propagation of one of the main faults towards the other (Ferrill et al., 1999). Peacock and Parfitt (2002) argue that a breaching crack might develop at much lower strains, when the faults or fractures are connected at depth. Such a connection could therefore also determine the style of breaching (Peacock and Parfitt, 2002).

As soon as a connection exists between the two off-set faults the relay ramp is *breached*. This will cause the unused fault parts (i.e. relict fault tips) to gradually disappear through erosion, as displacement in the ramp is taken over by the new connection. The replacement of

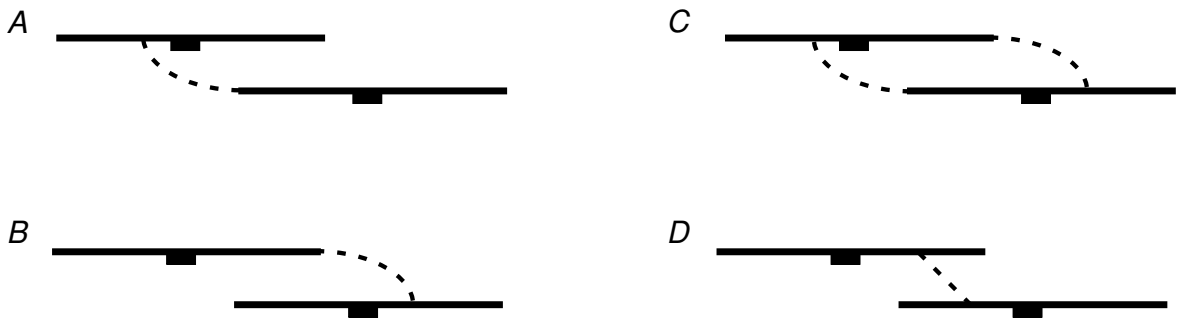

Figure 2.22: *Possible breaching geometries of relay ramps. See text for explanation. (a) footwall fault towards hanging-wall fault propagation, (b) hanging-wall fault to footwall fault propagation, (c) both faults propagate towards each other and (d) development of a new connecting fault. From Childs et al. (1995).*

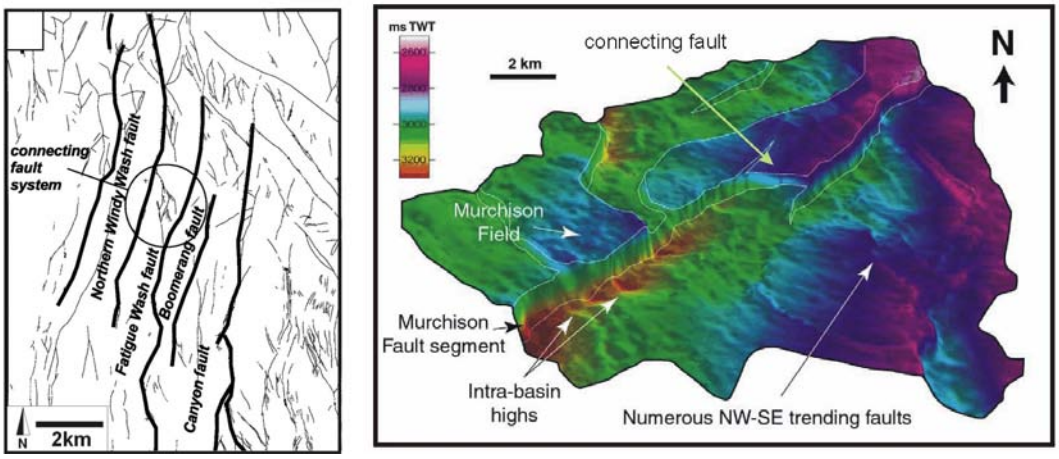

(a) (b)

Figure 2.23: *Two natural examples of the breaching of a relay ramp by the development of a connecting fault. a) In the western Yucca Mountain fault system a connection developed by several minor faults (from Ferrill et al. (1999)). b) In the Murchison-Stratfjord North Fault Zone in the East Shetland basin (northern North Sea), the connecting fault consists of a well-defined single fault that connects the major fault segments (from Young et al. (2001)).*

the ephemeral soft linkage relay ramp structure by a hard linkage connection corresponds to the final evolutionary stage of a relay ramp (Peacock and Sanderson, 1991; Trudgill and Cartwright, 1994) (see also figure 2.21).

2.5.2 Scaling of relay ramps

Not only is fault segmentation a phenomenon that is observed on different scales in a fault zone (see section 2.4 on page 45), also the geometries of the overlap zones seem to be invariant on a broad range of scales (e.g. Aydin and Nur, 1982; Aydin and Schultz, 1990; Acocella et al., 2000; Peacock, 2003). It has been found that the overlap distance of segments is roughly proportional to spacing between them, for strikes-slip fault (Aydin and Schultz, 1990) as well as for normal faults (Acocella et al., 2000) (see also appendix A). Peacock (2003) shows that relay ramps in the British Isles also obey a power-law scaling relation for their size-frequency distribution over ∼5 orders of magnitude. Peacock (2003) did, however, find a slightly lower fractal dimension for the regional scale faults (drawn on the Petroleum Exploration Society of Great Britain (2000) 1:1,500,000 scale map) and the smaller faults exposed on the Somerset coast (figure 2.24).

The invariance of scale for the geometry of relay ramps (as demonstrated by the references above), however, does not necessarily imply an invariance of the internal structure of the ramps on the different scales as well (as meant by question nr. 2 in section 1.1 on page 24). This will be discussed in further detail in later chapters.

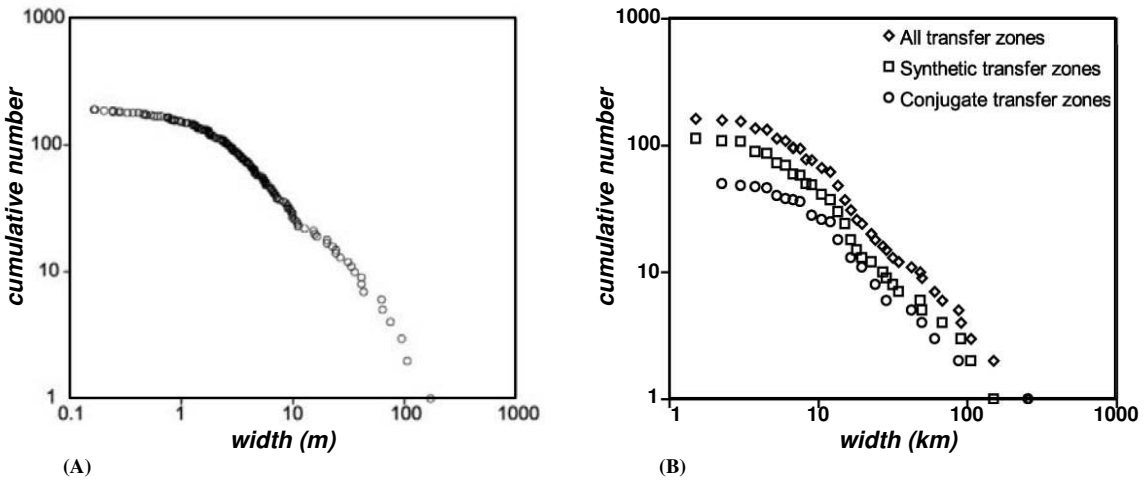

Figure 2.24: *Size-frequency curve of widths of relay ramps and conjugate transfer zones. From Peacock (2003). (a) Measured widths between Blue Ben and east of Lilstock (n = 192). These ramps obey a power-law up to ∼50m with a power-law exponent of ∼0.96. (b) widths of transfer zones measured off the Petroleum Exploration Society of Great Britain (2000) map, divided into synthetic and conjugate transfer zones. The total population of transfer zones obeys a power-law scaling relationship between widths of about 10 and 250 km, with a power-law exponent of ∼1.23 (n = 163).*

2.5.3 Overlap zones between dilatational cracks

Although overlap zones between extensional cracks do not form relay ramps, their geometry shows remarkable similarities with that of overlap zones between normal faults. Pollard and Aydin (1984) have shown a scale independence over 9 orders of magnitude for overlapping dilatational zones (ranging from extensional cracks to overlapping spreading centres). The typical hook-shaped pattern of overlapping extensional cracks (see examples in Pollard and Aydin, 1984; Olsen and Pollard, 1989) has also been observed for overlapping normal faults (e.g. Acocella et al., 2000).

2.6 Reactivation of faults

Inactive faults represent pre-existing weak zones that — when reactivated — may strongly influence the geometries of tectonic structures, as they tend to produce structural trends that are atypical for a given area (e.g Versfelt and Rosendahl, 1989; Huyghe and Mugnier, 1992; Le Turdu et al., 1999; Morley, 1999d, amongst others). Pre-existing faults are characterised by a lower shear strength, and therefore the reactivation of such older inactive fault structures can be a process that is preferred above the creation of new fractures in intact rocks (e.g. Etheridge, 1986; Holdsworth et al., 1997; Morley, 1999d). Fault zone hardening through extensive hydrothermal alteration can, on the other hand, greatly reduce the tendency for reactivation (see for example the discussion in Etheridge, 1986). Pre-existing discontinuities can also inhibit the propagation of fractures and faults (e.g. Morley, 1995).

A tectonic fault is *reactivated* if it undergoes renewed displacement after a prolonged period of inactivity (Peacock, 2002). For Holdsworth et al. (1997) the minimum time interval between the separable displacement events should be larger than 1Ma. Because pre-existing faults are discrete planes or zones of weakness, they can be classified as *discrete fabrics* in a more general classification for several kinds of pre-existing fabrics (e.g. Morley, 1999d). Different criteria to recognise fault reactivation in nature have been presented by Holdsworth et al. (1997).

The most obvious cause for the "death" of an active fault, is the rotation of the fault with time (either along a horizontal or a vertical axis), so that it becomes unfavourable oriented for movement in the prevailing stress field (e.g. Jackson, 1999). Other causes for the cessation of activity of faults can be related to changes in the prevailing stress conditions, for example as a result of fault interaction with neighbouring faults. The inhibition of fault movement caused by slip on a nearby fault is, however, believed to be mainly important for smaller faults (Jackson, 1999). The possibility that smaller faults become inactive as a result of the nearby development of larger faults that account for almost all of the displacement in an area (e.g. Cowie, 1998; Morley, 2002) was already mentioned on page 53.

2.6.1 Influence on fault orientation

Because of the difference in cohesive strength and sliding friction between a pre-existing fault and intact rock, it is possible that even with a non-optimal orientation, the shear stress along the pre-existing fault plane reaches the critical value for slippage before the critical value is attained for the formation of new (but optimally oriented) faults in intact rock (figure 2.25). As a result, pre-existing faults with a range of orientations are usually reactivated before new faults are formed in intact rock. It has been illustrated that the reactivation range of faults decreases with increasing depth and increases with increasing pore fluid pressure (e.g. Ranalli, 2000). The range is in general also larger for the reactivation of normal faults than for thrust faults (Ranalli, 2000).

2.6.2 Influence on fault shape

Recently Walsh et al. (2002) have suggested that the reactivation of faults, can cause a departure from the conventional fault scaling models. The reactivation of older faults might result in the formation of under-displaced faults; faults with a substantial larger length for a given displacement than predicted by fault scaling laws (section 2.3.3). Walsh et al. (2002) further argue that such fault systems will however rapidly acquire displacement-length scaling that is consistent with the ideas explained in section 2.3.3.

2.7 Large scale faulting

It is useful to make a distinction between large faults and smaller faults, because the way the rock volume deforms around both type of faults differs (e.g. Roberts and Yielding, 1994). Large scale extensional faults have been defined as those faults whose dimensions are sufficient to cut

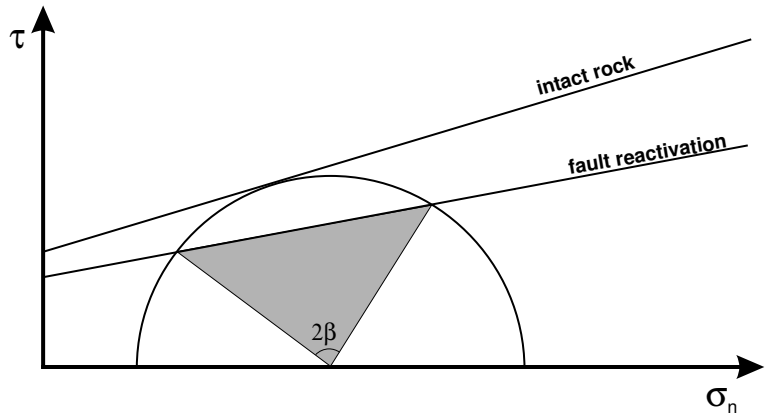

Figure 2.25: *Mohr circle representation for the state of stress in rock. Two failure envelopes are shown, one for fault formation (Coulomb failure) and one for slip on a pre-existing fault (friction criterion). Pre-existing faults with a range of orientation given by β will be reactivated before new faults are formed in intact rock. From from Etheridge (1986) and Scholz (1990).*

the entire seismogenic layer — the part of the crust that responds to stress by brittle failure (Roberts and Yielding, 1994). Large faults are thus the structures, that accommodate the upper-crustal part of a whole lithospheric deformation. In areas of extension this upper-crustal part or seismogenic layer is usually around 15 km thick (Roberts and Yielding, 1994). Jackson and White (1989) and Roberts and Yielding (1991) suggested that the maximum strike length of a normal fault surface that can accommodate seismic slip in a single rupture event is around 25km.

Different from small faults is that in the deformation produced by large normal faults, also a long term isostatic response should be included, apart from the shorter co-seismic deformation (e.g. Buck, 1988; Yielding and Roberts, 1992). The co-seismic deformation associated with large normal faulting produces an uplift of the footwall and a subsidence of the hanging-wall in the order of tens of centimetres. The magnitude of the hanging-wall subsidence is around 5 to 20 times larger than the footwall uplift (Roberts and Yielding, 1994; Morley, 1995). These values have been determined in few studies where the earth's surface was geodetically surveyed before and after a major earthquake (see references in Roberts and Yielding, 1994). Models have suggested that the uplift and subsidence ratio depends on the dip of the slip surface; a decreasing fault dip causes a decreasing ratio, which results in an increasing asymmetry (Savage and Hastie, 1966; Gibson et al., 1989). The subsequent post-seismic response associated with large scale faulting is driven by an isostatic imbalance introduced by the initial co-seismic deformation. This post-seismic response acts over a time scale of tens to hundreds of thousands of years (Morley, 1995) and it reduces the hanging-wall subsidence (where lower density sediments replace a similar volume of basement rocks) and enhances the footwall uplift (due to erosion of the already uplifted footwall region) (figure 2.26). The duration of the process depends on the viscosities of the lower crust and the uppermost mantle (Roberts and Yielding, 1994). The combined co- and post-

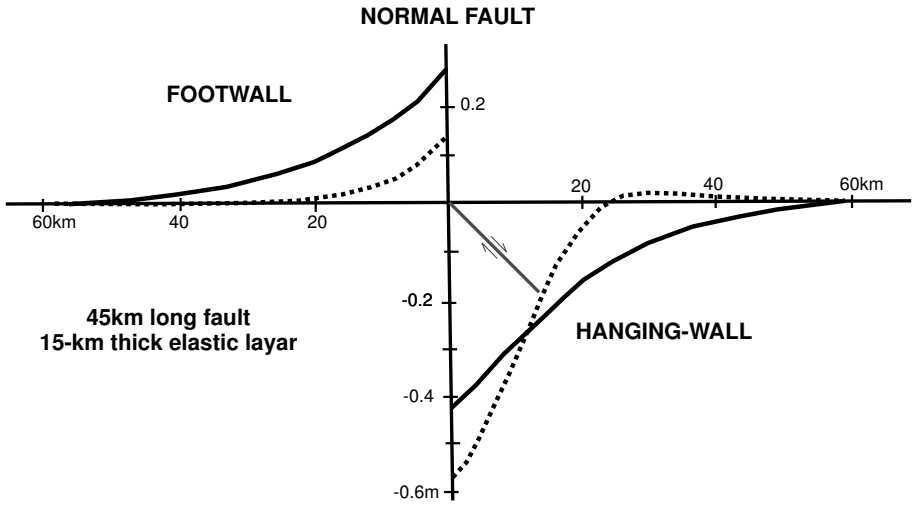

Figure 2.26: *Profile showing the co-seismic (dotted) and co-seismic plus post-seismic (solid) deformation associated with a modelled normal fault dipping at 45° that cuts a 15km thick elastic layer. From King et al. (1988).*

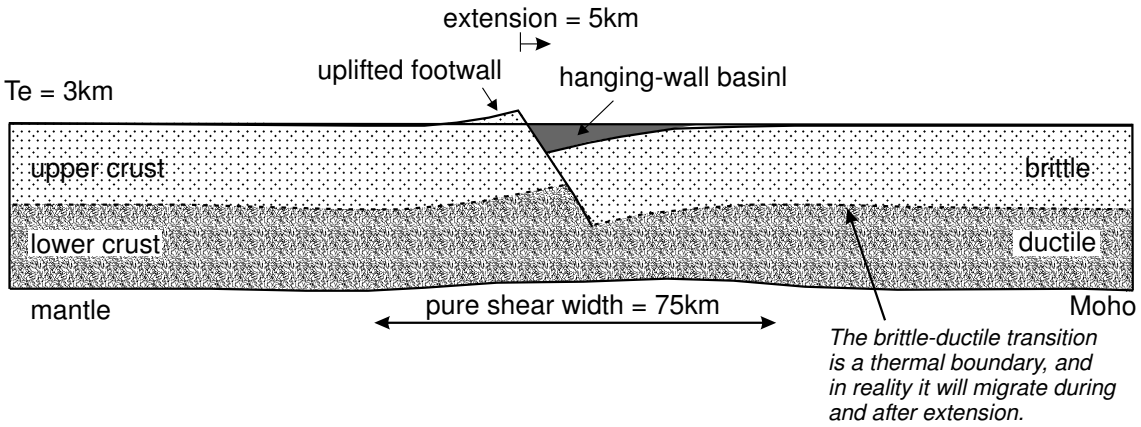

Figure 2.27: *Representation of a single fault in the flexural cantilever model, producing the hanging-wall subsidence and footwall uplift. From Roberts and Yielding (1991).*

seismic deformations can result in a footwall uplift that is approximately 50% of the hanging-wall subsidence (Morley, 1995). The co-seismic deformation can successfully be modelled as a purely elastic response to slip on a fault surface, whereas for the post-seismic response flexural/isostatic models of long-term deformation are used. The flexural cantilever model (figure 2.27), where fault controlled simple shear deformation of the upper crust is combined with bulk pure shear in the lower crust and lithospheric mantle is an example of the last category of models (Kusznir et al., 1991; Roberts and Yielding, 1994).

2.8 Listric faulting

Listric faults are extensional faults characterised by a concave upwards profile, in which steeply dipping faults flatten with depth. Listric faults are common in gravity-driven fault systems, where they form in unconsolidated or only partially-consolidated sediments (Ramsay and Huber, 1987; Roberts and Yielding, 1994).

Listric faults cause a distinct geometry in the hanging-wall strata that become tilted towards the footwall and form a so called "roll-over anticline" the geometry of which depends on the depth of the corresponding detachment (figure 2.28) (Williams and Vann, 1987; Darros de Matos, 1993; Xiao and Suppe, 1992; Withjack and Peterson, 1993). Nevertheless, for a given roll-over geometry a non-unique answer is obtained for the shape of the fault and the depth of the detachment, leaving successful listric geometry prediction a matter of selecting the most likely fault shape and depth (Withjack and Peterson, 1993). As a result of the roll-over, the hanging-wall is affected by complex strains, commonly accommodated on arrays of planar or listric growth faults that develop in the crest of the anticline (e.g. Erickson et al., 2001; Imber et al., 2003). Experimental simulations of the formation and deformation of the hanging-wall regions of listric faults have been performed by e.g. McClay and Ellis (1987); Vendeville et al. (1987); Vendeville and Cobbold (1988) (figure 2.29).

Listric fault systems usually propagate by footwall collapse, where new faults form in the undeformed footwall block of an older fault. This can result in a listric fault family that commonly links in one detachment fault (Gibbs, 1984; Imber et al., 2003) (figure 2.30).

Whether the listric fault geometry is also common for large scale faults as described in section 2.7 has been a matter of much debate. Huge amounts of earthquake data of large active faults reveal mainly planar fault geometries in the seismogenic layer. According to Roberts and Yielding (1994) there is no earthquake evidence for seismically active low-angle or listric normal faults. Models have suggested that extension is mostly accommodated on high-angle normal faults. As a result of the flexural response such faults will rotate and adopt a low-angle geometry. However, this rotation also seems to cause the cessation of the fault's activity (e.g. Buck, 1988; Lister and Davis, 1989). Ofoegbu and Ferrill (1998) indicated that as a result of geometric and dynamic effects, the slip rate on low-angle detachment faults can be several orders of magnitude smaller than the slip rate on steeply dipping faults. This lower slip rates can result in an aseismic behaviour of the detachment, but it does not imply that it becomes inactive (Ofoegbu and Ferrill, 1998).

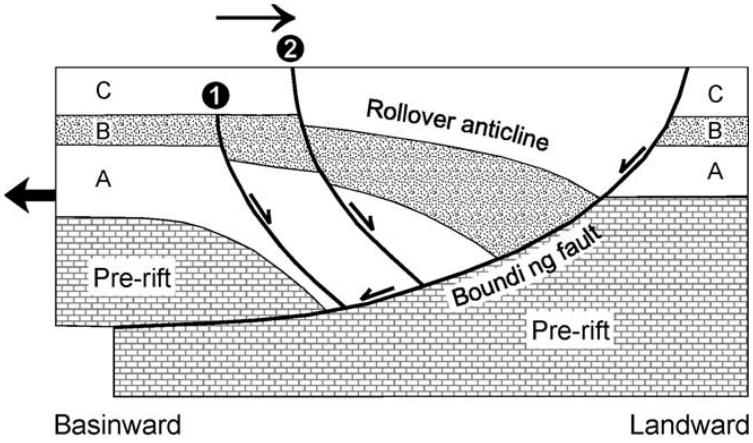

Figure 2.28: *Cartoon summarising the principal features in a listric fault system. Packages of syn-faulting sediments in the hanging-wall (units A, B and C) are deformed by a geometrically necessary roll-over anticline. Faults 1 and 2 are growth faults that cut the hanging-wall. From Imber et al. (2003).*

Processes that can cause the formation of vertical fault curvature are usually classified in two categories: (1) a first one which causes the formation of initially curved faults, and (2) processes that cause fault curvature after fault formation (Mandl, 1988; Vendeville, 1991; Mandl, 2000). The first category includes:

- Vertical changes in rheology, accompanied by possible shear stress along rheological interfaces.
- The presence of basal shear stresses, which can cause curved stress trajectories which on their turn can generate curved faults. Such basal shear stresses can for example result from gravity forces that act on tilted surfaces, or from ductile underflow (e.g. salt layers).
- The presence of large 'master' faults can cause stress fields to vary. As a result second-order faults in the hanging-walls of such faults show often curved geometries.

The creation of fault curvature after fault formation can be caused by:

- Straining of a block that contains a fault. This mechanism works when slip on the fault is not the only active deformation process.
- Fault curvature due to compaction. The volume of sedimentary rocks decreases downward due to compaction. This volume decrease can cause a decrease in dip of fault planes present. If the volume decrease occurs gradually, an initial planar fault attains a curved shape.
- The interplay of sedimentation and faulting. Vendeville and Cobbold (1988) argued that block rotation causes faults to rotate and attain smaller dip angles. The same fault will however propagate through syn-kinematic sediment layers with a $\approx 60^\circ$ dip angle. Further deformation would result in a tilting of the last — originally horizontal — layer as well accompanied by a slight further rotation of the fault plane. Again if new syn-kinematic layers are deposited they are cut again by the fault plane that dips with the $\approx 60^\circ$ angle. As

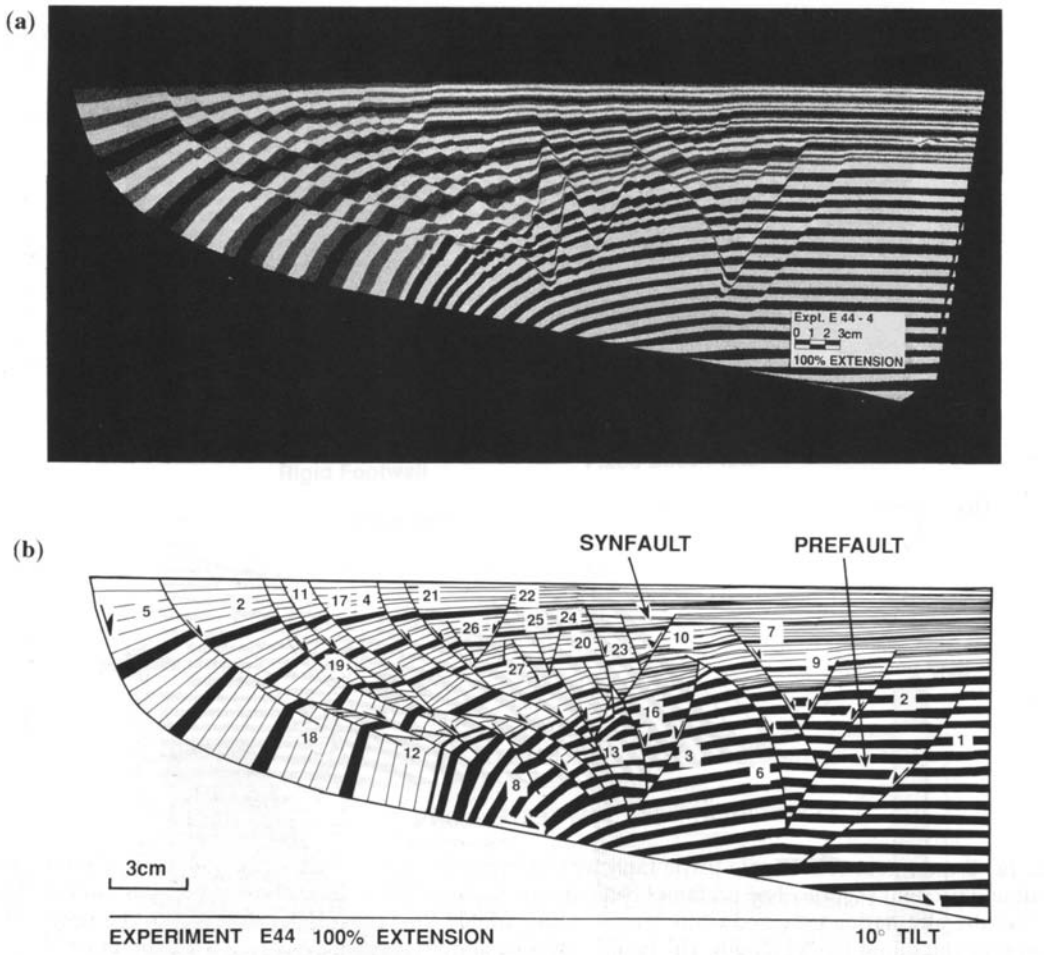

Figure 2.29: *Sandbox model of a simple listric fault with a 10° tilted lower detachment (a) and the interpretation (b). Extension was to the right, and 100% of the initial model length. Numbers in figure (b) indicate the fault sequence. From McClay et al. (1991).*

such the process results in growth fault profiles that become gradually more listric with continuing extension and syn-kinematic sedimentation (Vendeville and Cobbold, 1988) (e.g. figure 2.31)

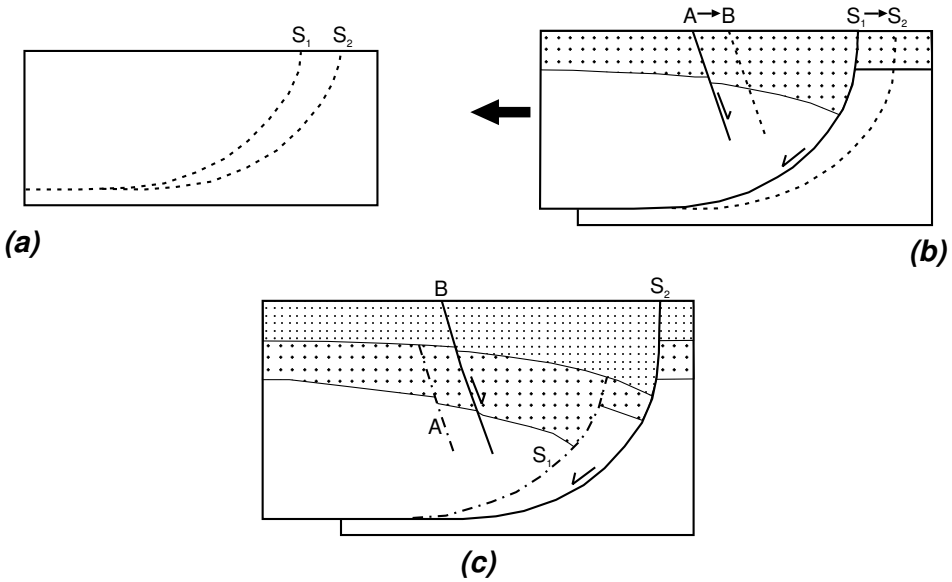

Figure 2.30: *Illustration of footwall collapse, and the associated growth fault migration in the hanging-wall. Bold solid lines are active faults, dashed lines are faults that have not yet formed and dot-dashed lines are faults that are inactive. (a) Undeformed 'template' showing the future positions of the future bounding faults. (b) The bounding fault (S_1) steps back into the footwall, causing the hanging-wall growth faults to step into the same direction. (c) The original position of the bounding fault is marked by a 'dead' splay (S_1) which is carried passively in the hanging-wall of the active bounding fault surface (S_2). From Imber et al. (2003)*

.

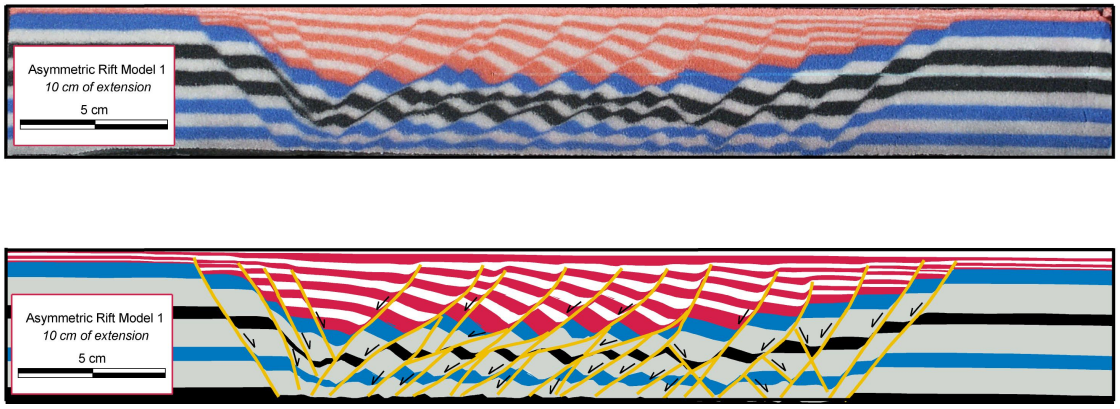

Figure 2.31: *Original photograph and an interpreted section of a sandbox rift model after 100% extension. In the centre of the model, a series of "left-dipping" listric shaped faults can be seen that result from the interplay of faulting and syn-kinematic infill of depocentres with new sand layers. Blue and black layers are pre-kinematic layers, and red layers are syn-kinematic. The model is described in Appendix C.*

2.9 Rifting

Continental rifts are regions characterised by vertical movements, crustal extension, faulting and seismic activity, as well as volcanism. Also a thinned lithosphere, abnormal heat flow values and regional Bouguer gravity lows are characteristic for rift systems (e.g. Neugebauer, 1983). Extension of the lithosphere can result in either the formation of narrow or discrete rifts (like the East African Rift System and the Baikal Rift), wide or diffuse rifts (like the Basin and Range Province) or metamorphic core complexes (see for example Buck, 1991; Ruppel, 1995) (figure 2.32). Metamorphic core complexes are in general associated with wide rifts (e.g. Wernicke, 1981; Wernicke and Axen, 1988), however, as discussed by Roberts and Yielding (1994), a quantitative test of the applicability of the model has yet to be found. Brun (1999) suggested that metamorphic core complexes correspond to local anomalies within wide rifts, and therefore they should not be considered as a different mode of extension. The rifting mechanism depends on factors like the thermal structure, the lithospheric rheology, the strain rate and temporal factors (e.g. Bassi, 1995; Ruppel, 1995). These factors have a strong influence on the mechanical processes involved in the rifting, ie. pure shear, simple shear, combination mechanisms or lower crustal flow (Ruppel, 1995).

Based on the architecture of the East African Rift System (EARS), Rosendahl (1987) has proposed a nomenclature to describe continental rifts. In his scheme, the *rift system* denotes the rift at its largest scale. Such a system can be subdivided in different *rift branches* (e.g. the eastern and western branch in the EARS), which on their turn consist of different *rift zones*. According to Rosendahl (1987) the subdivision of rift branches in rift zones, is done "in ways that are morphologically evident, but mechanically poorly understood". Rift zones have general lengths of 500-700km, they are built up of different "fundamental units": the *rift unit*, which are structural basins with typical lengths of 80-160 km and a length to width ratio of 2–4. Rift units often have a half-graben geometry (figure 2.33), although full-graben structures can occur as well (table 2.1). Yet another smaller rift entity is termed a *rift block*, which has a common width of ∼10 km and a length to width ratio rarely larger than 4.

The surface expression of many rift systems is determined by the geometry of the rift units and their bounding faults. Throughout the rift zone, half-grabens for example often change polarity along accommodation zones or transfer zones, located in between them (Gibbs, 1984; Bosworth, 1985; Rosendahl et al., 1986; Versfelt and Rosendahl, 1989; Younes and McClay, 2002) (figure 2.34). This results in the clearly segmented geometry of many natural rifts (e.g. Bosworth, 1985; Rosendahl et al., 1986; Ebinger, 1989; Faulds and Varga, 1998, and many others). Rosendahl et al. (1986) and Rosendahl (1987) have mapped the main boundary faults of such half grabens in Lake Tanganyika and Lake Malawi, and interpreted them as having a clear curvilinear geometry in plan view. The transfer zones over which displacement was transferred from one boundary fault to the other formed zones with important oblique or strike-slip movements, and passed from one side of the rift towards the other. Later Morley et al. (1990) and Morley (1999a) questioned this curvilinear shape of the boundary faults, based on more detailed seismic profiling studies. They also did not find evidence for the crossing of

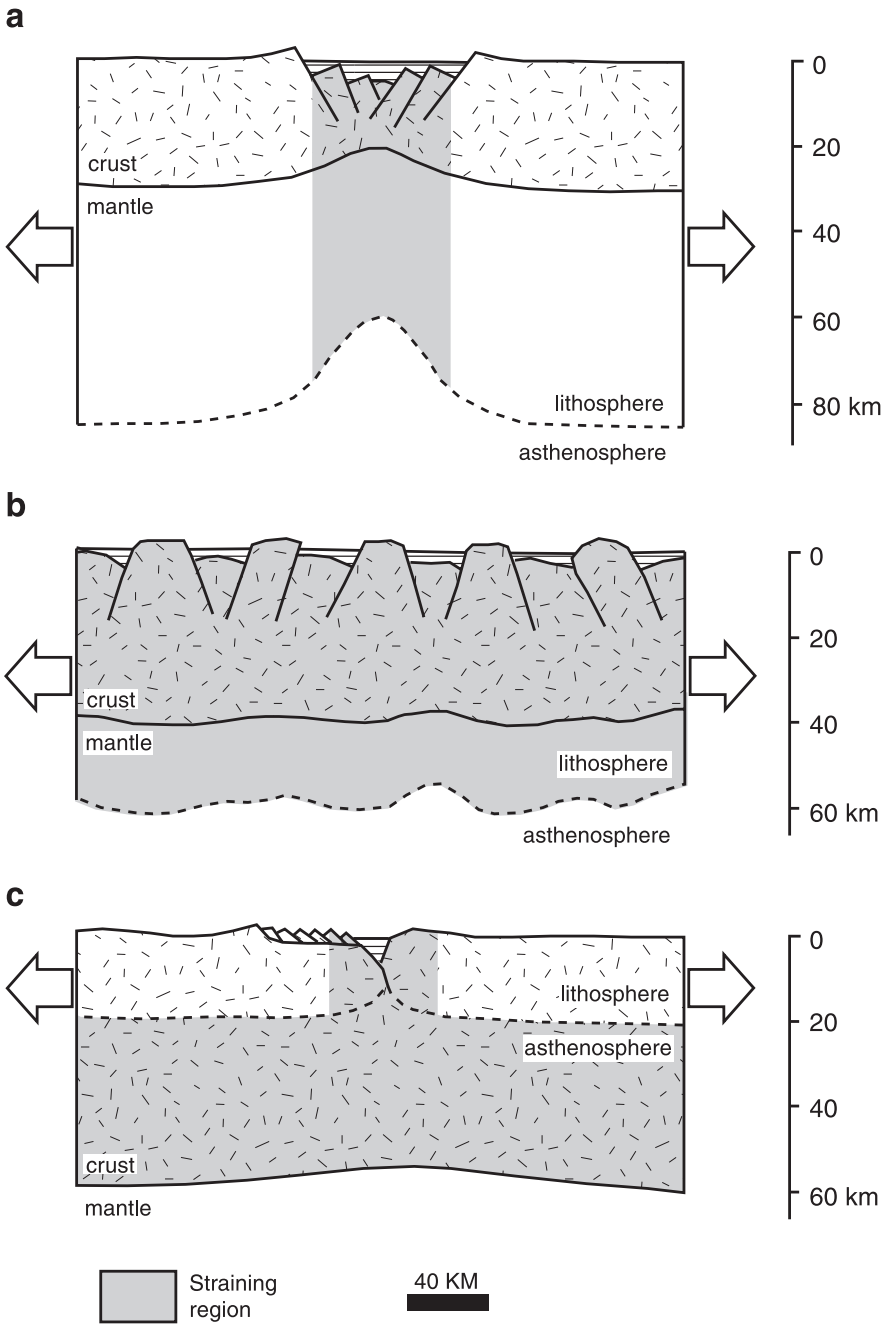

Figure 2.32: *Different modes of continental extension, emphasising the regions undergoing the greatest amounts of extensional strain. Lithosphere connotes areas with effective viscosities of $>10^{21}$ Pa.s. Hatchured lines show the base of the lithosphere. After Buck (1991).*

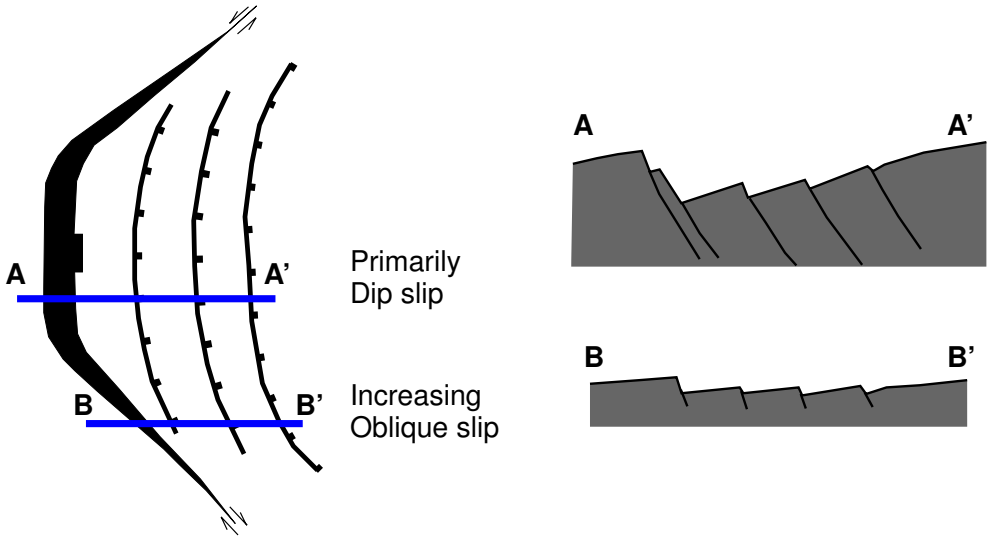

Figure 2.33: *Plan view and hypothetical cross-sections of an idealised half-graben. From Scott and Rosendahl (1989).*

the major boundary faults from one side of the rift towards the other. Rather than being associated with oppositely dipping faults along a rift segment with a single axis, Morley (1999a) interpreted the accommodation zones (or divergent transfer zones) to be caused by offsets or changes in orientation of the rift axis (e.g. figure 2.35b). In Lake Tanganyika the 2 important transfer zones occur where pre-existing fabrics depart from a north-south orientation (Morley, 1999a) (figure 2.35a).

Also in the evolution of the Suez rift, pre-existing structures are believed to have influenced the location and geometry of accommodation zones in the early evolutionary stages. The at that time relatively small boundary faults were stopped or deflected at older major basement shear zones oriented at high-angle to the faults. At this stage the transverse basement shear zones acted as accommodation zones. Later, when the boundary faults grew larger, the faults seem to have cut through the basement discontinuities, giving rise to the development of long, relatively straight boundary faults, and the gradual disappearing of the accommodation zone (Khalil and McClay, 2001; Younes and McClay, 2002) (figure 2.36). Also in the East-African Rift System, border fault reorganisation has occurred with increasing extension (figure 2.37), this results in a change in the basin geometries and a change in the type of transfer zones between them. This illustrates that in rift systems, pre-existing basement fabrics can control — apart from the location of the rift and the geometry of the rift segments and bounding faults — also the locations of transfer zones (Versfelt and Rosendahl, 1989; Morley, 1995, 1999d). Acocella et al. (1999a) further showed that the trend of a transfer zone is not only dependent on the orientation of inherited structures, but even so on the spacing between the offset rift basins.

Accommodation zones in rift systems have typical widths of 15–30 km and are cut by many steeply dipping faults. Accommodation zones can form structural highs relative to the surround-

	Half-Graben	Full-Graben
	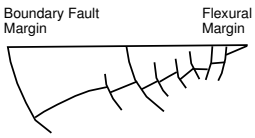	
Timing between major and minor faults:	Minor faults are commonly abandoned prior to cessation of activity on boundary fault.	Minor faults are commonly abandoned prior to cessation of activity on boundary fault.
Mixture of antithetic and synthetic minor faults:	Synthetic minor faults tend to be more numerous and take up the highest percentage of extension.	More even mixture of minor faults dipping in both directions.
Partitioning of the extension between major and minor faults:	Relatively high percentage of extension (20–50%) distributed on minor faults.	Relatively low percentage (<20%) of extension distributed on minor faults.
Minor fault spacing:	Relatively closely spaced.	Relatively widely spaced.
Minor fault distribution:	Minor faulting more intense towards flexural margin (FM). Antithetic faults more common towards FM.	Minor faults more frequent in central part of rift, less frequent approaching boundary faults.

Table 2.1: Difference between fault distributions in half- and full-grabens based on data from Lake Tanganyika. From Morley (1995).

ing rift basins (Younes and McClay, 2002). Fault deflection at an accommodation zone can be the result of a local variation in direction of extension. This explains why the arcuate fault tips near the accommodation zones often display dominant dip-slip movements, although they are almost sub-parallel to the regional direction of extension (Younes and McClay, 2002; Corti et al., 2003). Acocella et al. (1999a) have demonstrated that in early stages displacement transfer in a transfer is accomplished by strain partitioning between strike-slip faults and normal faults whereas in later stages the transfer zone evolves in an area of mainly oblique-slip faulting.

Because border faults of rift basins are usually the longest faults, characterised by the greatest displacements, they are the principal tectonic component in rifts (Crider and Pollard, 1998; Ebinger et al., 1999). The variation in border fault length between different rift systems can be attributed to the elastic thickness of the continental lithosphere (Ebinger et al., 1999).

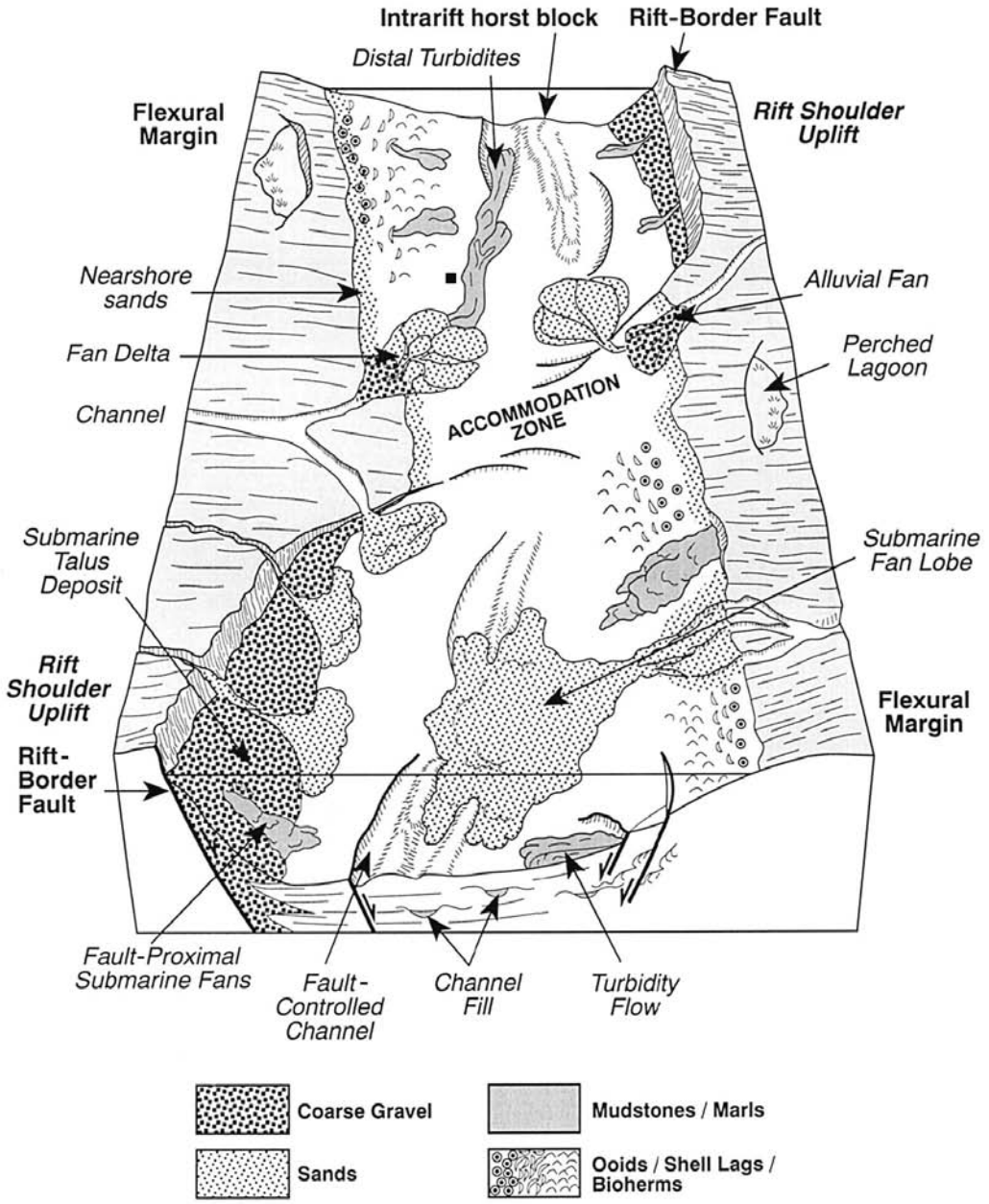

Figure 2.34: *Conceptual model of a narrow rift system (shallow marine intra-continental) showing an along-strike change in half-graben polarity. The possible variations in syn-rift sediment patterns and input points are shown. From Younes and McClay (2002).*

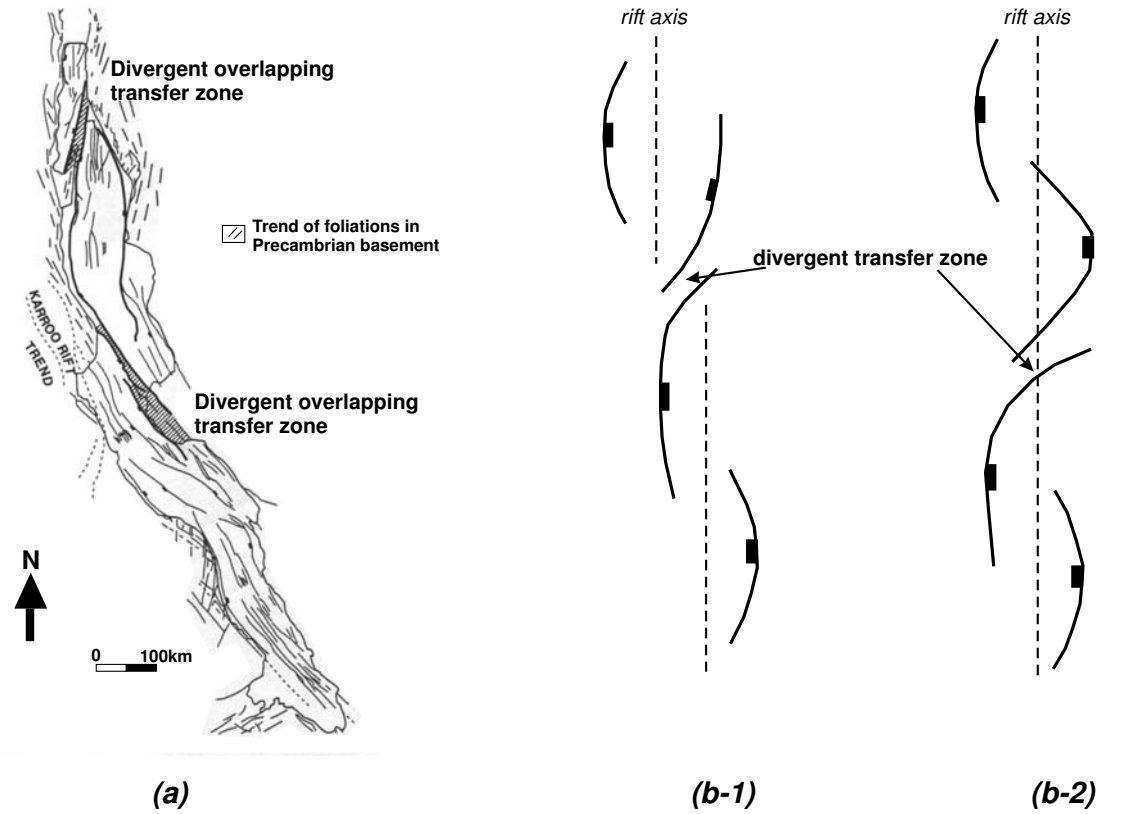

Figure 2.35: *Schematic map of Lake Tanganyika (a), the divergent transfer zones occur at regions where the pre-existing fabrics depart from a north-south orientation. Transfer zones tend to be associated with offsets or changes in rift axis (b-1), rather than with faults that occur along a rift segment with a single axis (b-2). From Morley (1999a).*

2.9.1 Active vs. passive rifting

As already mentioned above, two different time scales can be applied for describing the process of faulting (section 2.2). For the scale of lithospheric extension, yet another scale is observed in which lithospheric deformation can be described by continuum models (Cowie and Scholz, 1992a). Therefore, in such models the role of faults as deformation mechanism cannot explicitely be included. And although strictly speaking this chapter deals with extensional faulting, some of these large scale models of lithospheric extension will be mentioned in this section as they are important in understanding the underlying processes of rifting.

Over the years, classically two main categories of rifting have been considered: active rifting and passive rifting (e.g. Şengör and Burke, 1978; Ruppel, 1995; Huismans et al., 2001). The difference between the two relates to the driving mechanism that causes the rifting. For the active rifting this driving mechanism is an ascending mantle plume that causes a thermal thinning of the lithosphere and isostatic crustal doming, which results in the development of deviatoric tensional stresses in the region of uplift (Ziegler and Cloetingh, 2004). For the passive rifting

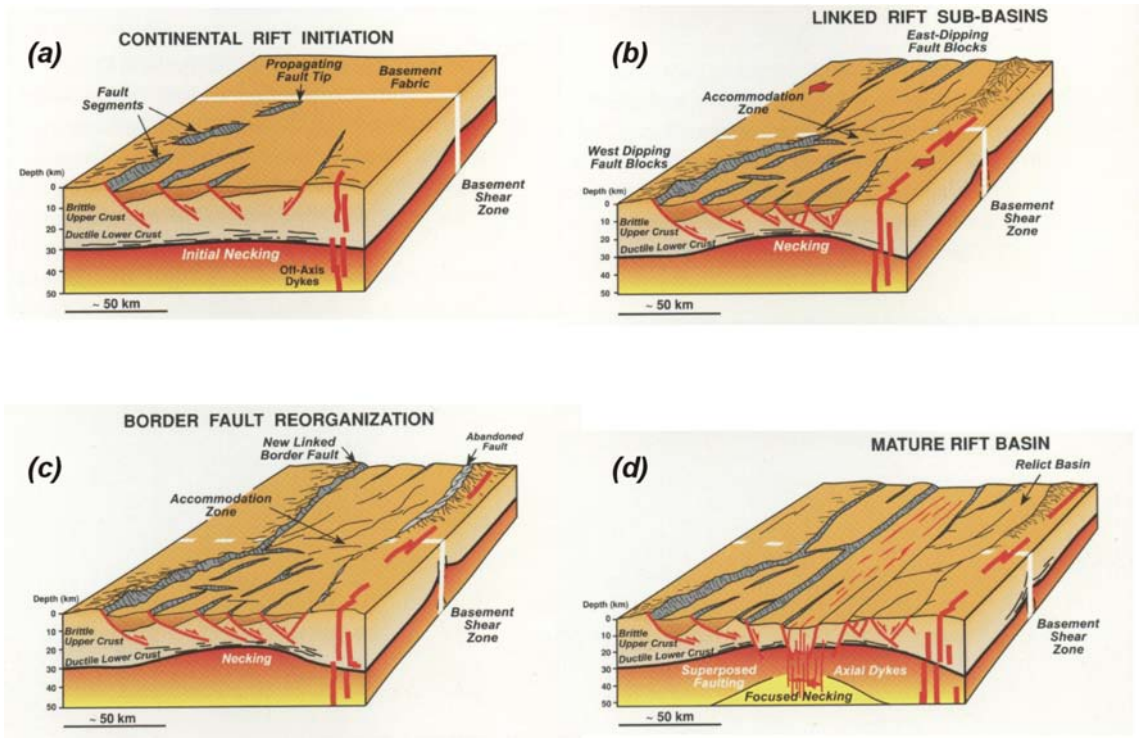

Figure 2.36: *Schematic evolution of the Suez rift, from the initiation of the rift (a) to the mature rift (d). Initially small faults are formed that are stopped or deflected along major (pre-existing) basement shear zones (a and b). Only after faults have grown large enough, they propagate through these shear zones, to evolve in more or less straight border faults (c and d). From Khalil and McClay (2001).*

the extensional stresses result from a regional stress field, often assumed to originate from remote boundary forces (e.g. Corti et al., 2003). In this case, the lithospheric thinning is caused first in response to extension, giving rise to a passive asthenospheric up-welling, which can cause many secondary processes.

Because intra-oceanic hot spots such as Hawaii and intra-continental ones such as the Cenozoic Hoggar and Tibesti volcanic centres are not associated with major extensional faulting, Ziegler and Cloetingh (2004) argue that hot spot activity on its own is unlikely to cause the development of major rifts. The bending associated with the active rifting is an unrealistic process for the rifting as a whole, because it is unable to produce the amount of crustal extension that is often observed in continental rifts. According to Buck (1991) the active mechanism can only account for $\sim$10% extension. To produce larger deformations, favourable plate kinematics are likely to have accompanied the active rifting process (Mulugeta, 1985).

The distinction between active and passive rifting is mainly important during the initial stages of crustal thinning, as the evolution of both mechanisms "converges" in later stages (Corti et al., 2003).

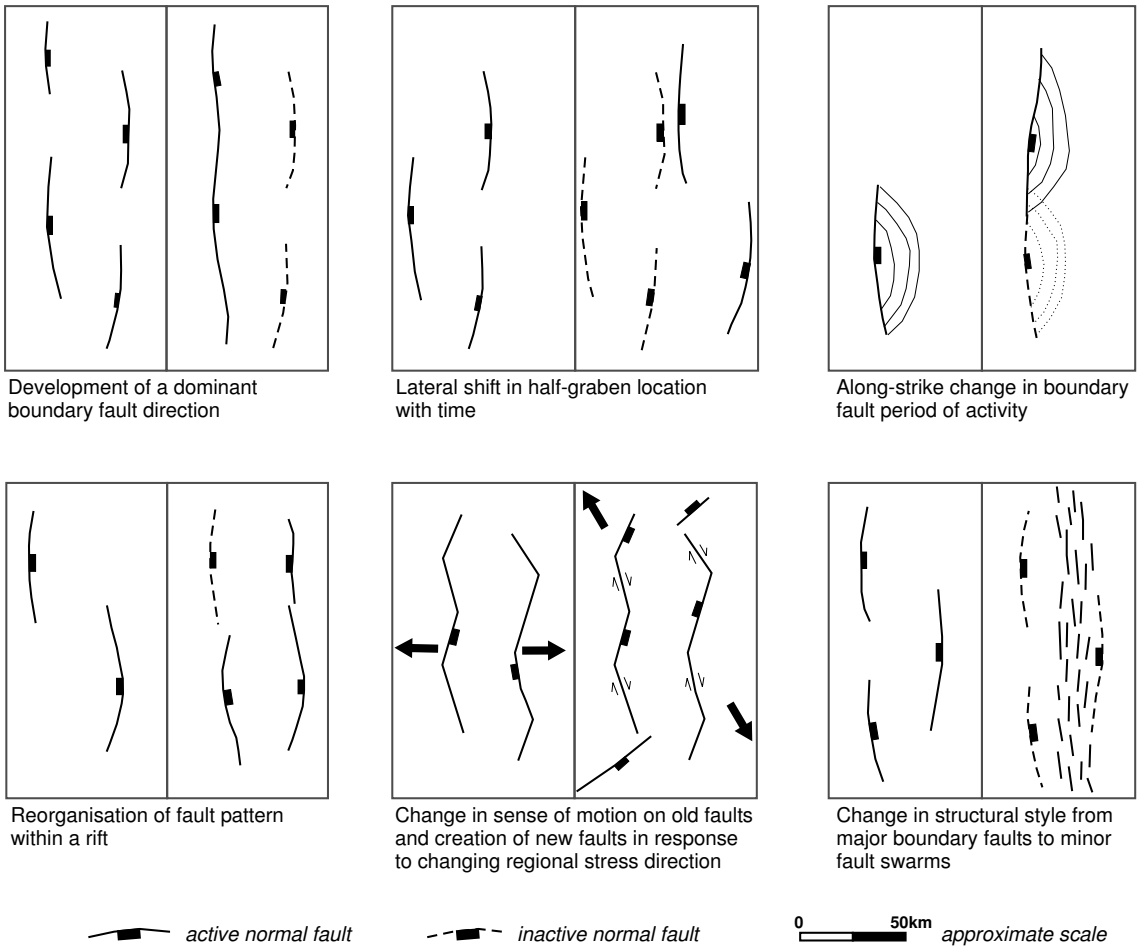

Figure 2.37: *Schematic illustrations of the main modes of basin evolution in the East African Rift System. From Morley (1999b).*

2.9.2 Fault controlled sedimentation patterns in rifts

Because fault growth and fault interaction have a major influence on basin development, they form the primary control on the creation of accommodation space in rifts (Schlische, 1991; Contreras et al., 1997; McLeod et al., 2002). The lateral propagation of a normal fault for example will cause the expansion of the hanging-wall depocentre. A linkage between two originally isolated faults and a subsequent displacement readjustment will cause the amalgamation of 2 depocentres, and a shift of the maximum basin depth towards the centre of the new fault (figure 2.38).

Apart from controlling the accommodation space, faults and fault growth structures also affect drainage patterns (Gawthorpe and Hurst, 1993; Trudgill, 2002). As described in section 2.7, large faults usually generate a considerable amount of uplift of their footwall regions as a flexural and isostatic response to the faulting (figure 2.26 and 2.39a). This means that where fault

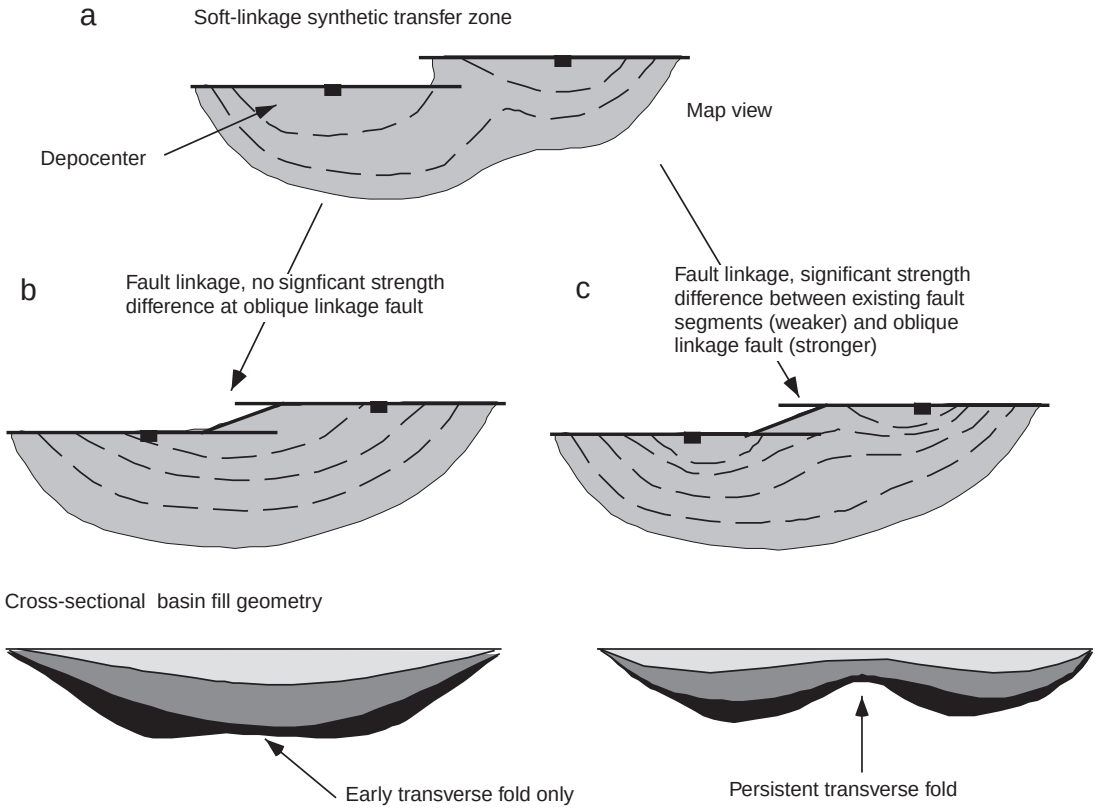

Figure 2.38: *Schematic evolution of fault-controlled half-graben basins at a relay ramp or synthetic transfer zone. Once the two faults are linked, the fault system can adjust its displacement profile (b), or the central displacement minimum can remain, what results in a persistent intrabasin high (c). From Morley (2002).*

displacements are low, the amount of footwall uplift is expected to be low as well. As such, footwall elevation and hanging-wall subsidence both decrease towards fault tips and transfer zones (Morley et al., 1990; Gawthorpe and Hurst, 1993). It has been demonstrated that such topographic changes that are associated with transfer zone are important in determining where drainage networks enter rift systems (Leeder et al., 1991; Gawthorpe and Hurst, 1993; Leeder and Jackson, 1993) (figure 2.39b and 2.40). Figure 2.41 summarises the tectono-sedimentary evolution of a fault array of like dipping faults.

High-relief accommodation zones or divergent transfer zones on the other hand, can form barriers for sediment transport between different rift basins. In young rifts accommodation zones usually are sub-aerial, and they prevent drainage networks to pass from one rift basin into the other. In more mature rifts, where accommodation zones can be submerged and where rift lakes often encompass several rift basins, only a fraction of the suspended sediments is carried shallow enough to be transported over an accommodation zone (Lambiase and Bosworth, 1995). As a

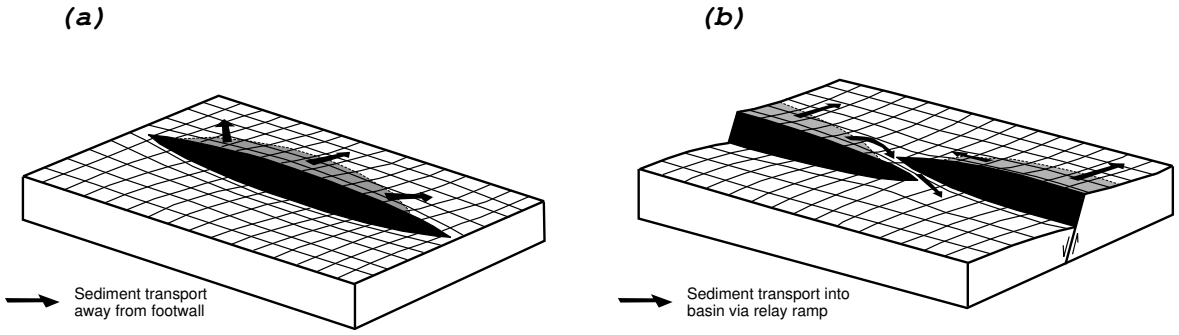

Figure 2.39: *Cartoons illustrating how the amount of footwall uplift varies along a single major fault (a) and along two faults with an en échelon geometry (b). The relay ramp in (b) necessarily has a lower footwall elevation than the central parts of each fault, and therefore it acts as a sediment transport route from the footwall to the hanging-wall basin. Syn-rift sands will be preferentially deposited near these transfer zones. Arrows indicate expected sediment transport. Grey areas correspond to erosion zones. From Yielding and Roberts (1992).*

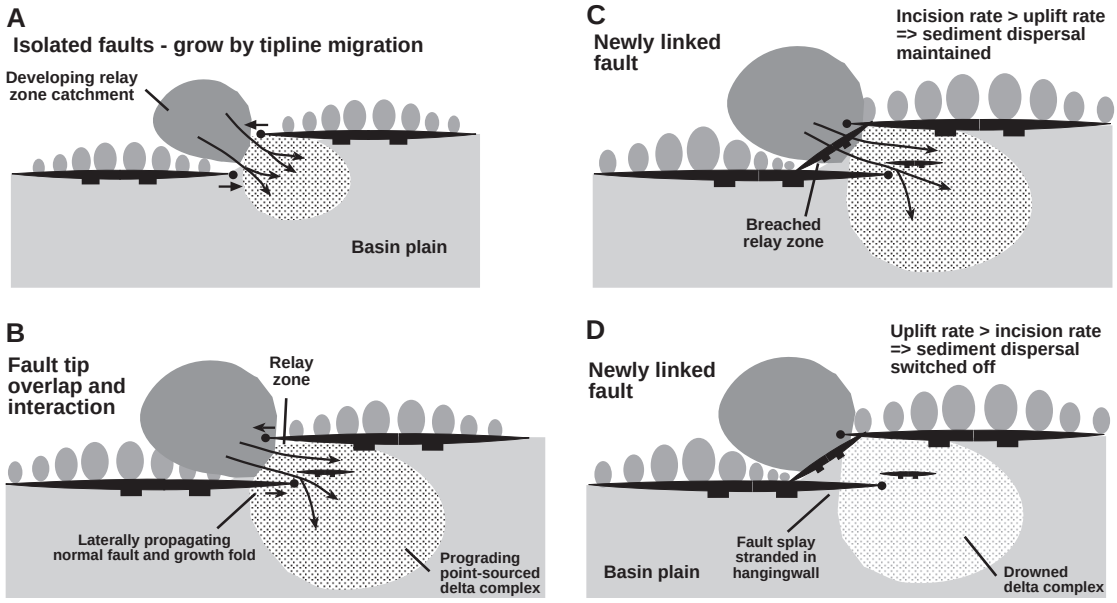

Figure 2.40: *Cartoon illustrating conceptual model for spatial and temporal variation in coarse clastic input from the footwall margin of an extensional basin in response to patterns of fault growth and linkage. From Gupta et al. (1999).*

result, most sediments will be deposited in the same basin in which they entered the rift, and produce a distinct stratigraphy (Lambiase and Bosworth, 1995). Evidently, this barrier effect is only important in case the accommodation zone stands as a clear positive topographic feature in the rift.

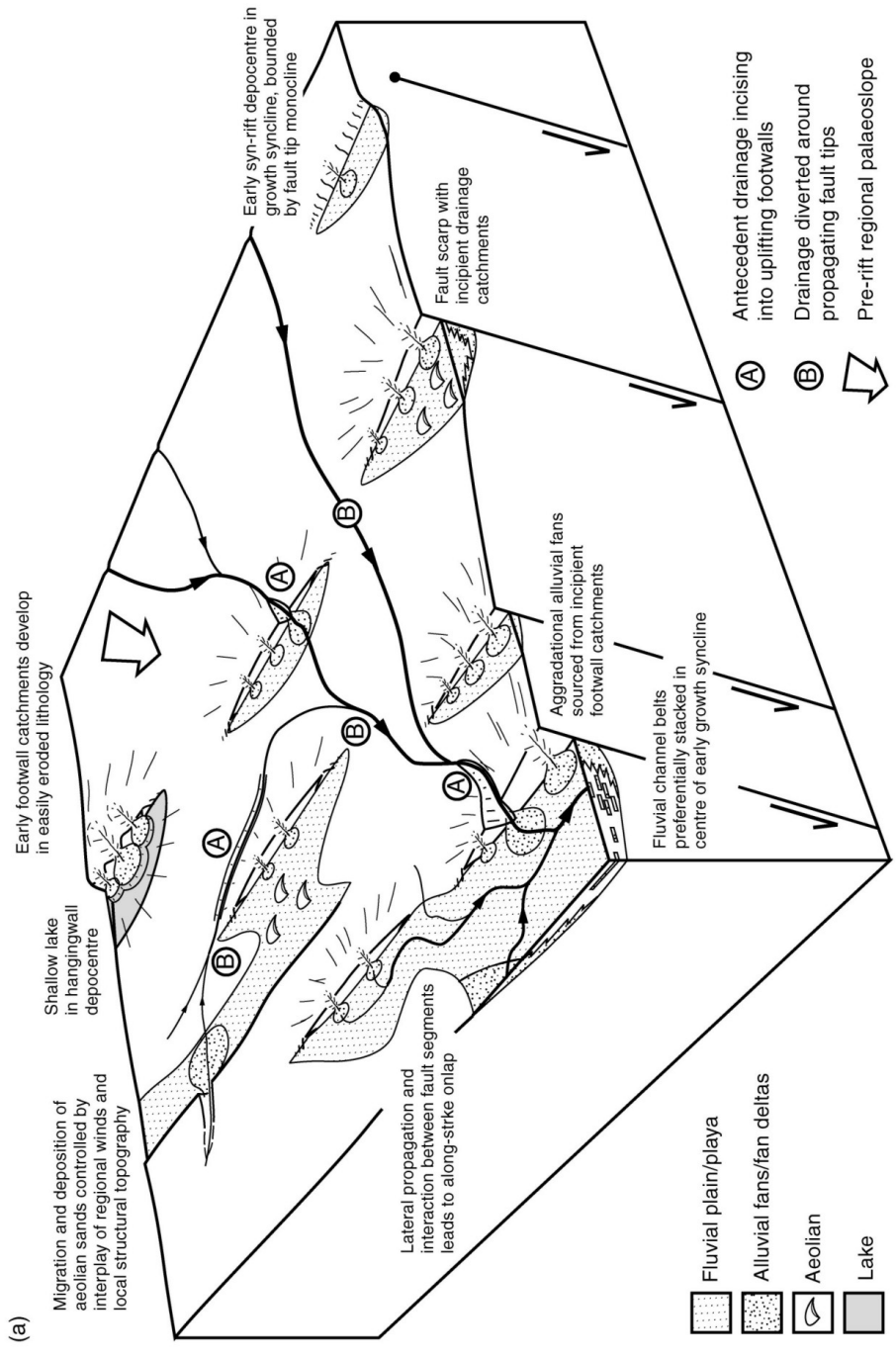

Figure 2.41: *Tectono-sedimentary of a normal fault array during the* initiation stage. *Numerous isolated fluvio-lacustrine sub-basins in the hanging-walls of propagating normal faults segments. Major sediment transport pathways are dominated by antecedent drainage networks that are locally modified by surface topography associated with fault breaks and growth folds. Stratigraphic variability between individual basins is high, due to the difference in sediment supply. From Gawthorpe and Leeder (2000).*

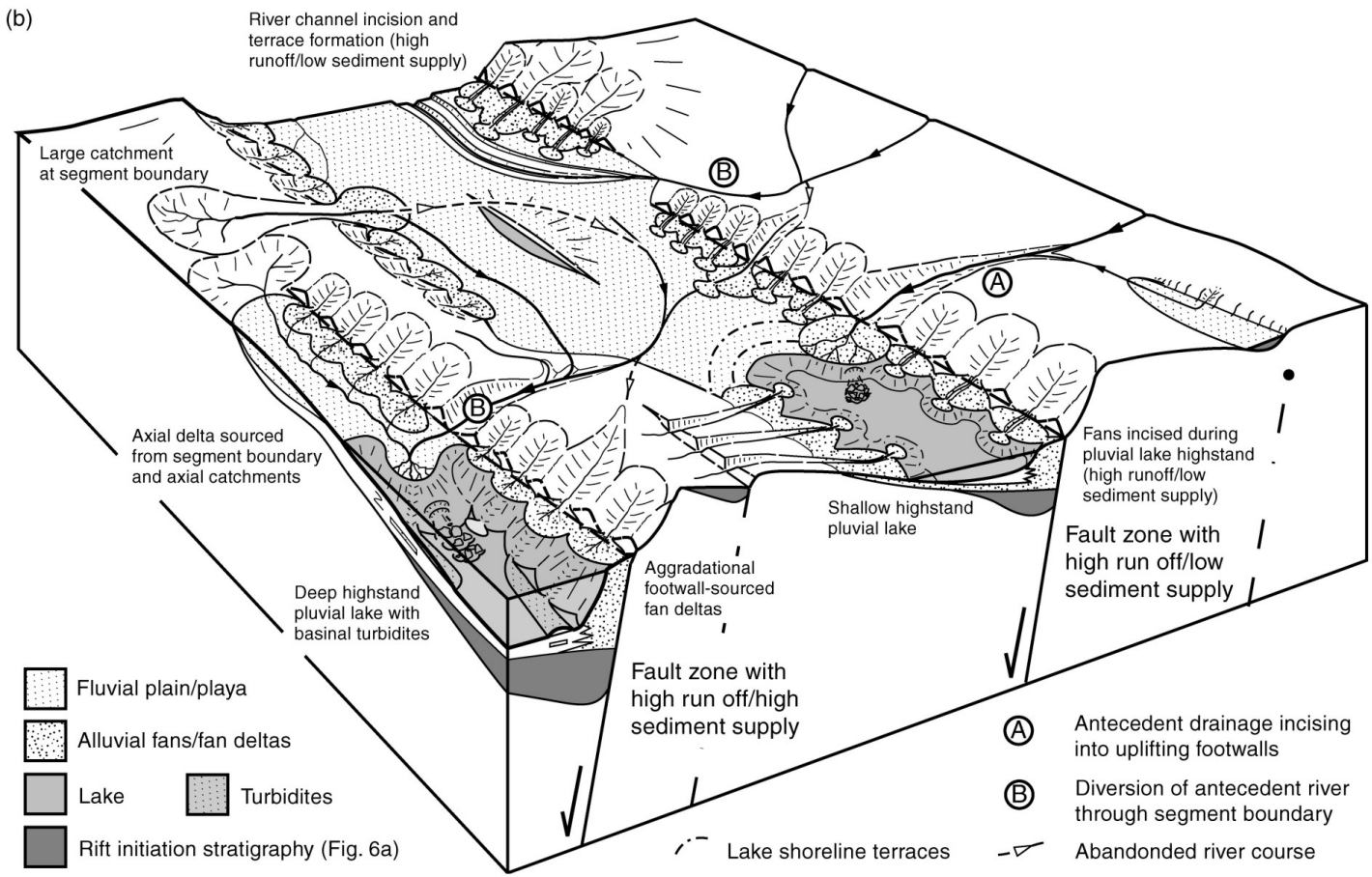

Figure 2.41: ***(continued)*** — *Tectono-sedimentary evolution of a normal fault array during the* interaction and linkage stage. *Lateral propagation and interaction between fault segments leads to enlargement and coalescence of early fault depocentres, whilst other fault segments become inactive (dashed on front face). Basin fills adjacent to inactive faults are buried and preserved if located close to the hanging-wall of a major fault, or are uplifted, incised and reworked if near footwall crest. Consequent drainage catchments continue to develop along faceted footwall scarps and hanging-wall dip-slopes and act as transverse sediment sources to developing half-graben depocentres. Note decrease in size of footwall catchments and associated fans towards fault tips. Location of isolated lakes is largely controlled by fault segmentation. Right-hand fault zones are shown for Basin and Range style interglacial with high run off and low sediment yields. Left-hand fault zones are shown for interglacial with high run off and high sediment yields.*

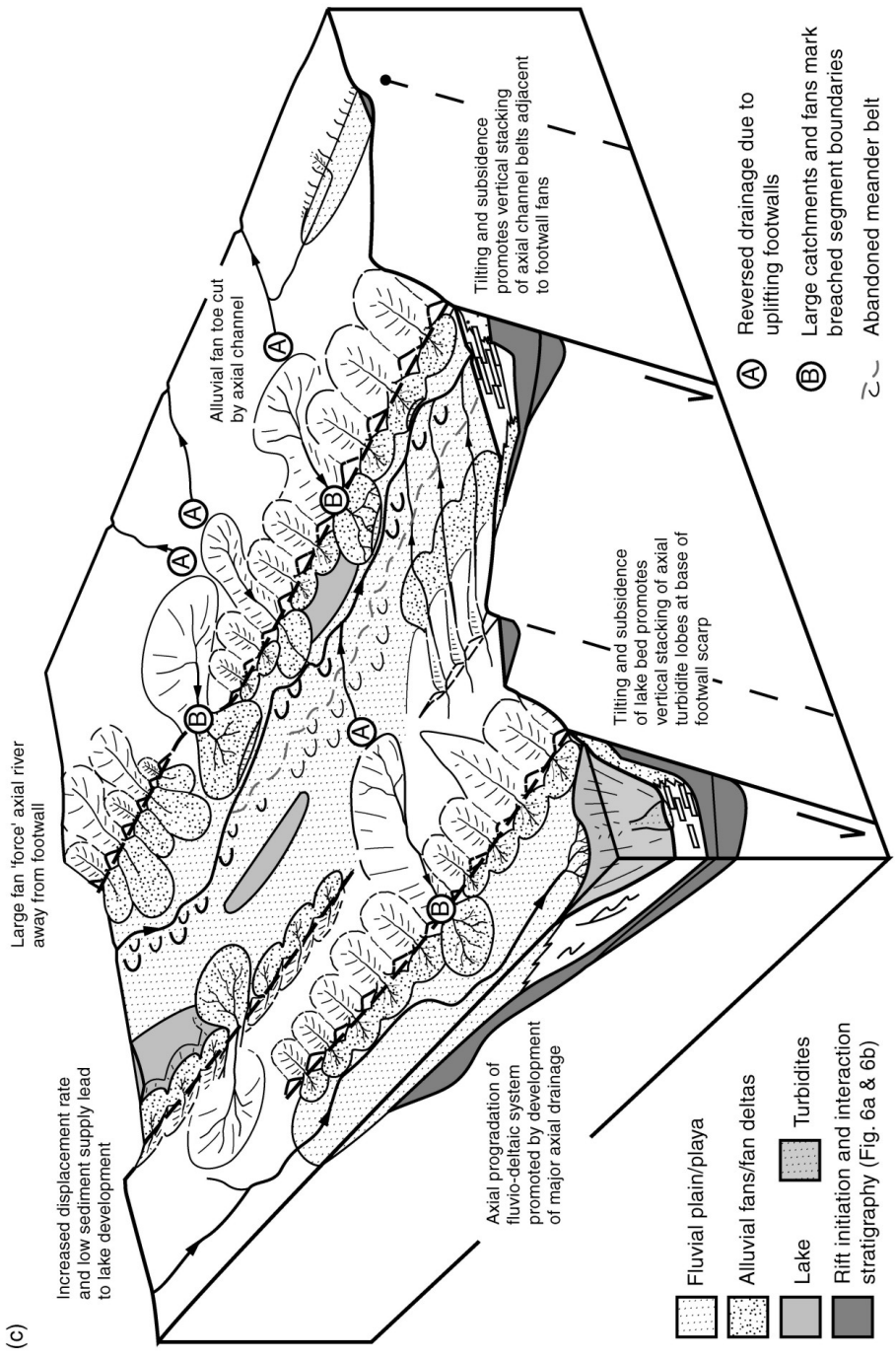

Figure 2.41: ***(continued)*** — *Tectono-sedimentary evolution of a normal fault array during the* through-going fault stage. *Linkage of adjacent fault segments creates major linked fault zones defining half-graben basins. Displacement on linked faults reduces topography of former intrabasin highs, allowing axial river to flow between former isolated basin segments. Localisation of displacement causes increased displacement rates on active faults leading to the development of pronounced footwall topography and reversed antecedent drainage.*

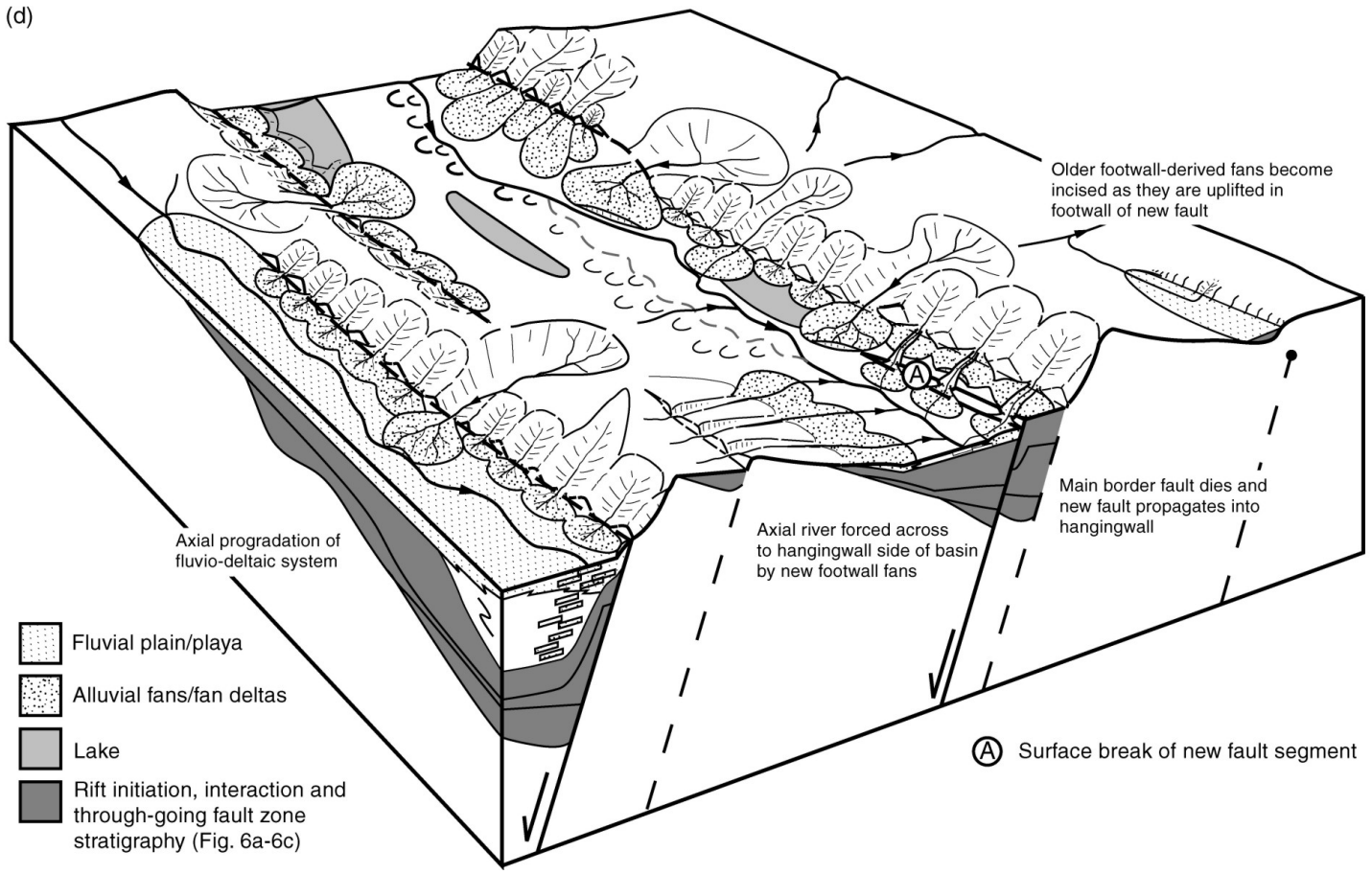

Figure 2.41: ***(continued)*** — *Tectono-sedimentary evolution of a normal fault array during the* fault death stage. *Locus of active faulting migrates into hanging-wall of right-hand fault zone causing uplift and incision of former footwall-derived fans and a shift of the axial river away from the rift shoulder.*

Chapter 3

Lake Baikal: Geological setting

The Baikal Rift Zone — of which Lake Baikal occupies the central part — developed since the Late-Oligocene along the margins of the Siberian craton within the weaker crust of the Baikal-Sayan mobile belt (e.g. Zonenshain and Savostin, 1981). Before its Cenozoic reactivation, the *pre-rift* structure of this folded belt had been shaped during several stages of compression and extension from Late Proterozoic to Mesozoic times, mainly linked to the evolution of the Central Asian fold belt (Delvaux et al., 1995). Because a significant inheritance of pre-rift tectonic structures has strongly influenced the Cenozoic evolution of the Baikal Rift Zone, it's appropriate to shortly outline the evolution of the Central Asian fold belt. A more complete review of this matter can be found in the work of De Grave (2003).

3.1 Regional geology: The Central Asian Fold Belt

The Central Asian fold belt has a length of over 5000 km and is considered the world's largest intra-continental fold belt. The present morphology of the Central Asian fold belt is one of alternating mountain ranges and tectonic depressions (figure 3.1) (e.g. Dobretsov et al., 1996). The Central Asian fold belt can be subdivided into a western part (Tarim-Kazakhstan, including the Ural, Kazakhstan, Tien Shan, Tarim and northwestern China) and an eastern part (Siberia-Mongolia, including Taimyr, Yenisei Range, Altay-Sayan, Transbaikalia and Mongolia) (Zonenshain et al., 1990; Khain et al., 2003). The Stanovoy Range in the Baikal-Sayan mobile belt forms the northeastern termination of the Central Asian fold belt (Melnikov et al., 1994).

The Central Asian fold belt is an amalgamation of several continental and micro-continental blocks that converged towards and collided with the Siberian platform (Zhao et al., 1990; Zonenshain et al., 1990; Zorin et al., 1993). The formation of this fold belt was mainly coupled to the evolution of Paleo-Asian and Mongol-Okhotsk oceans (Zonenshain et al., 1990; Delvaux et al., 1995; Dobretsov et al., 1995).

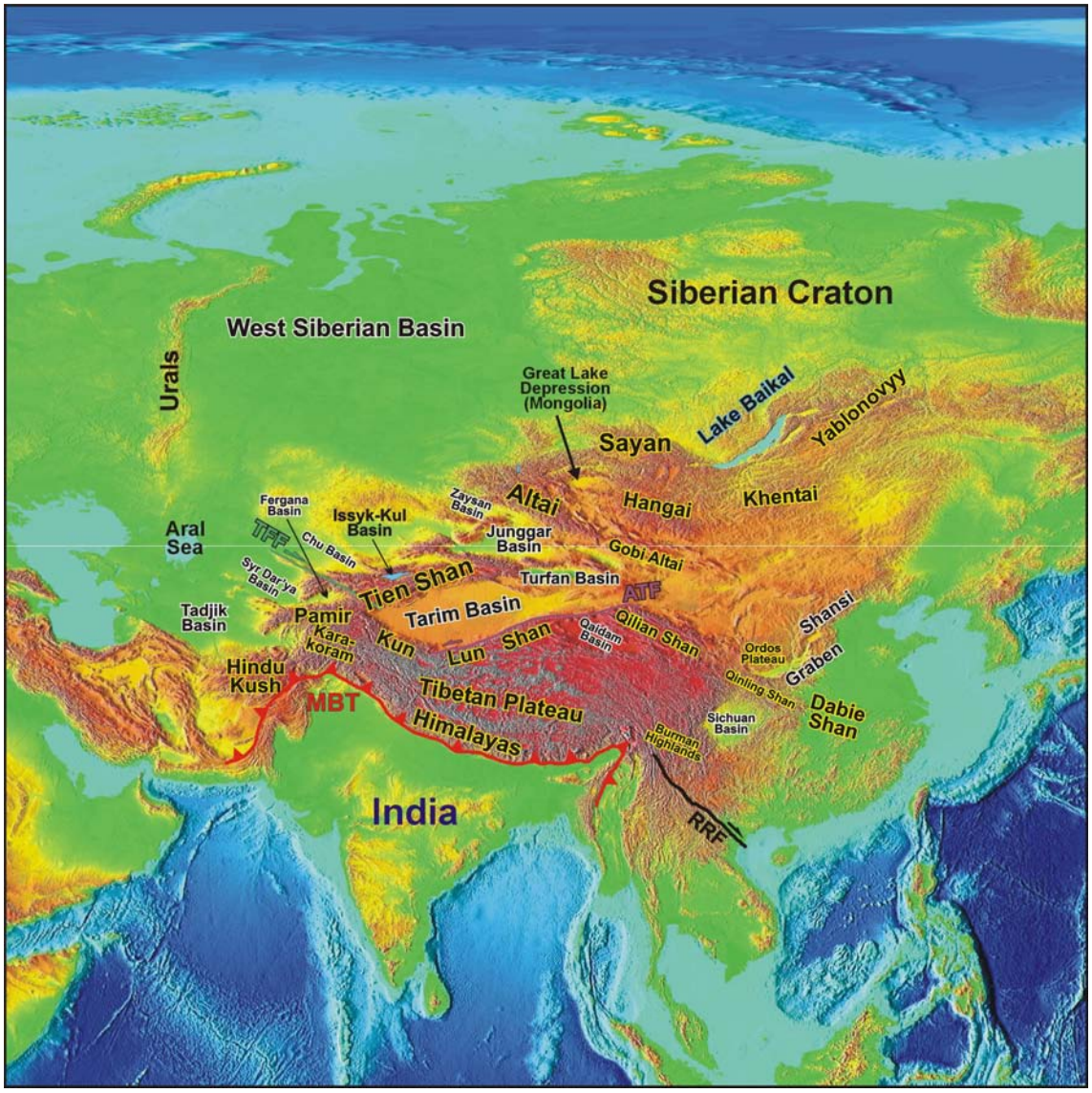

Figure 3.1: *Topographic image of Central Asia, showing the location of the major mountain ranges and (intra-montane) basins. From De Grave (2003).*

3.1.1 Paleozoic evolution

The initiation of the evolution of the Paleo-Asian Ocean dates back to the Late Proterozoic (900–1100 Ma) when in the Baikal area an oceanic basin develops with rifted margins (Dobretsov et al., 1995; Khain et al., 2003). The ophiolites in the western segment of the Baikal-Muya Belt and the Yenisei Ridge are believed to mark the onset of the opening of the Paleo-Asian Ocean (Delvaux et al., 1995; Dobretsov et al., 1995; Khain et al., 2003). This opening caused the beginning of the break-up of a super-continent which had formed in an earlier phase of major collisions (referred

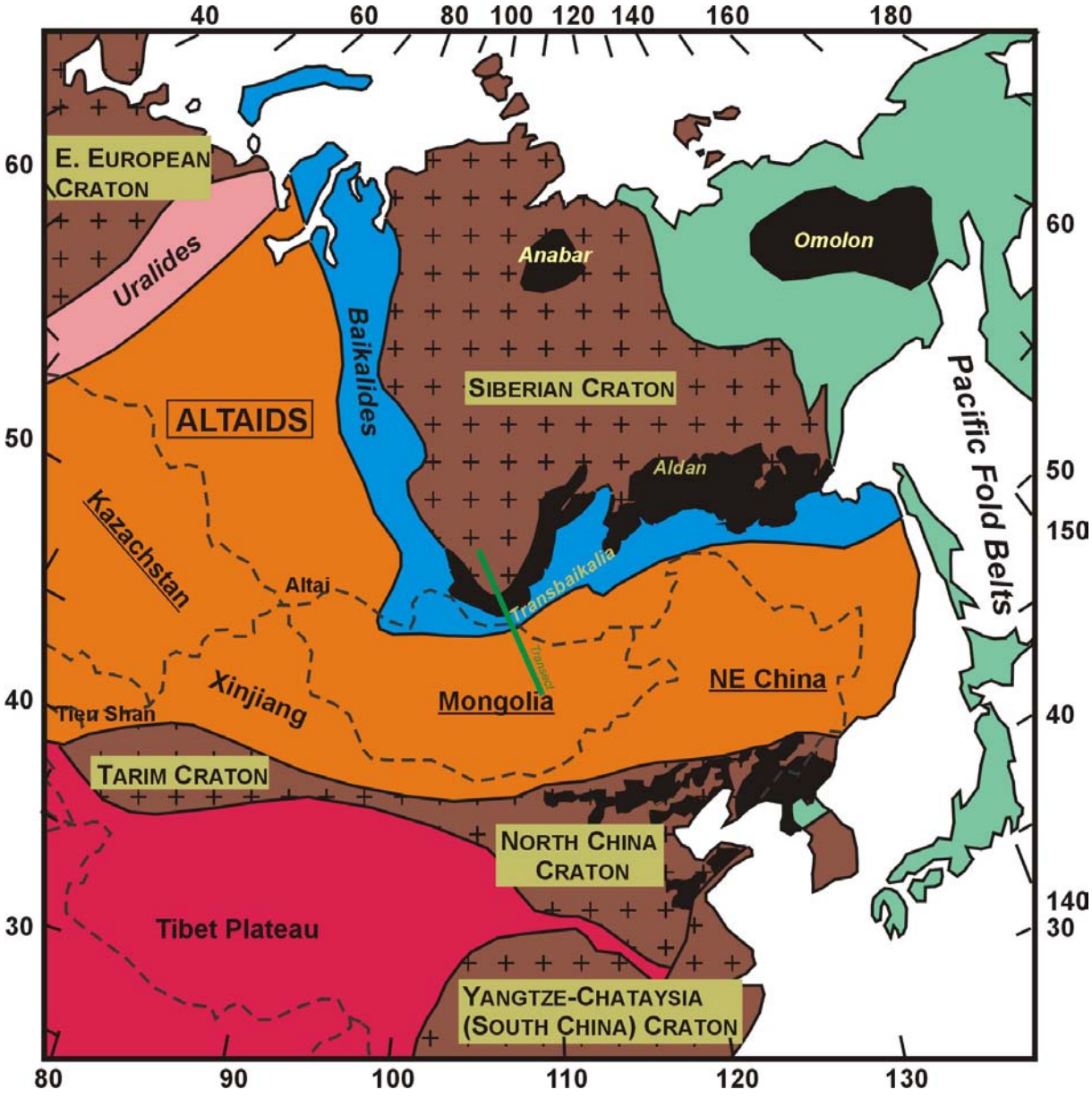

Figure 3.2: *Simplified tectonic divisions of Asia. The Altaids in this figure (as described by Şengör et al. (1993)) correspond more or less to the Central Asian Fold Belt (e.g. Jahn et al., 2000; Khain et al., 2003). This area is situated between Precambrian cratons: Siberian and North-China and Tarim. Black area's in the figure correspond to exposed Archean to early Proterozoic rocks. Figure modified from Jahn et al. (2000) and Şengör and Natal'In (1996). The NW-SE oriented green line in the Baikal rift shows the location of the crustal cross-section from figure 3.3.*

to as the Grenville orogeny). The "hypothetic" super-continent at that time was centred on

Laurentia (North America) and was called Rodinia[1] (Hoffman, 1999).

The break-up of Rodinia caused the development of a passive margin in the southern edge of the Siberian craton (Melnikov et al., 1994). Mainly clastic carbonaceous sediments accumulated here, which overlie the Pri-Baikalian volcano-plutonic belts (e.g. Melnikov et al., 1994; Khain et al., 2003).

The margins of the Paleo-Asian Ocean evolved again in a system of island arcs and back-arc basins between ∼850–650 Ma (Khain et al., 2003). Dobretsov et al. (1995) identified two different stages in this development one from ∼920 to 800 Ma and one between ∼750 and 700 Ma. At that time a series of isolated continental blocks existed in the Paleo-Asian Ocean, that had either broken off the Siberian continent or (East) Gondwana (Dobretsov et al., 1995). The collision of a first series of micro-continents (Khamar Daban – Barguzin) occurred at the end of the Precambrian (between 700–620 Ma, mostly in the Vendian – Early Cambrian) (Delvaux et al., 1995; Dobretsov et al., 1995). Also the Tuva-Mongolia terrane might have made its first contact with Siberia at that time, however, as discussed by Bachtadse et al. (2000) evidence exists that Tuva-Mongolia and Siberia formed a real coherent block only in the Early Silurian.

Notwithstanding this first accretion of micro-continents to the Siberian platform, the Paleo-Asian Ocean is believed to have attained its maximal dimensions in this time period (Vendian – Early Cambrian) (Dobretsov et al., 1995). In mid-Cambrian time the Paleo-Asian Ocean had developed in a complex system of oceanic basins, micro-continents and island arcs (Khain et al., 2003).

A new series of collisions started in the second half of the Early Cambrian, and lasted till the Middle Ordovician (Dobretsov et al., 1995). At this time also the oceanic branch between Tuva-Mongolia and Siberia closed, and this caused the oceanic subduction to migrate southward (Delvaux et al., 1995). The wedge shape of the Tuva-Mongolia terrane subdivided the Paleo-Asian Ocean in two branches (Delvaux et al., 1995; Dobretsov et al., 1995): (1) a first one has been called the *Paleo Mongol-Okhotsk ocean*, and (2) the second one was the *Western Paleo-Asian Ocean*.

Yet another collisional stage has been identified for the Late Silurian – Early Devonian, during which the Pri-Baikal fold and thrust belt was formed (Delvaux et al., 1995). This stage was followed in the Late Paleozoic by an extensional regime in the eastern part of the Paleo-Asian Ocean, related to the evolution of the Mongol-Okhotsk Ocean. On the other hand, in the western part of the Paleo-Asian Ocean new fragments were once more accreted to Siberia: in the Early – Middle Carboniferous the Altai-Mongol block and Kazakhstan collided; and in the Late Carboniferous – Early Permian the Tien Shan and Tarim blocks attached to Kazakhstan and Siberia (Zonenshain et al., 1990; Delvaux et al., 1995).

The main process during the Mesozoic was the closure of the Mongol-Okhotsk Ocean. The Amurian plate first attached to the North China continent in the Late Triassic – Early Jurassic

[1] According to Hoffman (1999) cratons of West Gondwana (Amazonia and Rio Plata) were connected to the present Atlantic margin of Laurentia, cratons of East Gondwana (South-China, Australia and East Antarctica) flanked the present Pacific margin of Laurentia, while the cratons of Baltica, Siberia and Sino-Korea were located at the northern side of Laurentia, and the Kalahari Craton at the southern margin. After the break-up of Rodinia, the East Gondwana and West Gondwana cratons were assembled again in Gondwana (Hoffman, 1999).

and together they converged towards Siberia (Zonenshain et al., 1990). The final closure of the ocean took place in the Late Jurassic – Early Cretaceous (Zonenshain et al., 1990; Delvaux et al., 1995).

The result of this series of accretions is the development of a strongly heterogeneous crust, in which rheologically strong crystalline cratons and continents are welded together by weaker deformation zones (figure 3.3). The geometry of this weaker zones has often influenced the development of later structures in central Asia. The Baikal-Sayan mobile belt is such a weaker deformation zone; it is strongly heterogeneous and contains remnants of folded structures (from the multistage collisions with the Siberian Craton) which have been affected by igneous rocks of varying composition and age (figure 3.3) (Logatchev, 1993; Melnikov et al., 1994).

During the Late Cretaceous – Paleogene, Central Asia was characterised by a long period of tectonic quiescence. In most of the area a vast peneplenation surface was formed, that developed in a laterite-kaolinite weathering crust as a result of the prevailing humid and hot subtropical climate (Mats, 1993; Delvaux et al., 1995; Mats et al., 2004). For the Baikal region, this peneplenation surface can be used as a reference level to distinguish between the pre-rift evolution and the Cenozoic rift evolution.

3.1.2 Neotectonic reactivation

It is evident that the present intra-continental deformation in Central Asia is still strongly influenced by the India-Eurasia collision and the continued penetration (e.g. Molnar et al., 1973; Molnar and Tapponnier, 1975; Tapponnier and Molnar, 1979), and therefore the timing of this collision can be considered to mark the onset of neotectonic deformation in Asia[2]. The relative importance of this collision compared to other processes (like shear traction at oceanic subductions in the Pacific, mantle dynamics, etc.), however, is still in debate (e.g. Calais et al., 2003).

There has been some discussion on the exact timing of the collision between India and Eurasia, and although some data suggest that the collision could have started in the latest Cretaceous time (∼70 Ma), most authors believe that the sudden decrease in convergence velocity between both continents, some 50–55 Ma ago, marks the actual onset of collision (Yin and Harrison, 2000).

At present the Indian plate has penetrated into Eurasia for at least 1500–2000 km (Molnar and Tapponnier, 1975; Tapponnier et al., 1982). From GPS measurements the current convergence rate between India and Eurasia is estimated to be 40–50mm/yr, of which 18±2mm/yr are accommodated by overthrusting in the Himalaya's, while 20–30mm/yr are distributed in growing mountain ranges further north (e.g. Reigber et al., 2001; Hetzel et al., 2002).

The strain that results from the collision between India and Eurasia and the continued post-collisional indentation is partitioned over two important processes (figure 3.4):

[2] *Neotectonics* has been defined by Muir Wood and Mallard (1992) as tectonic processes active in the *current tectonic regime.*

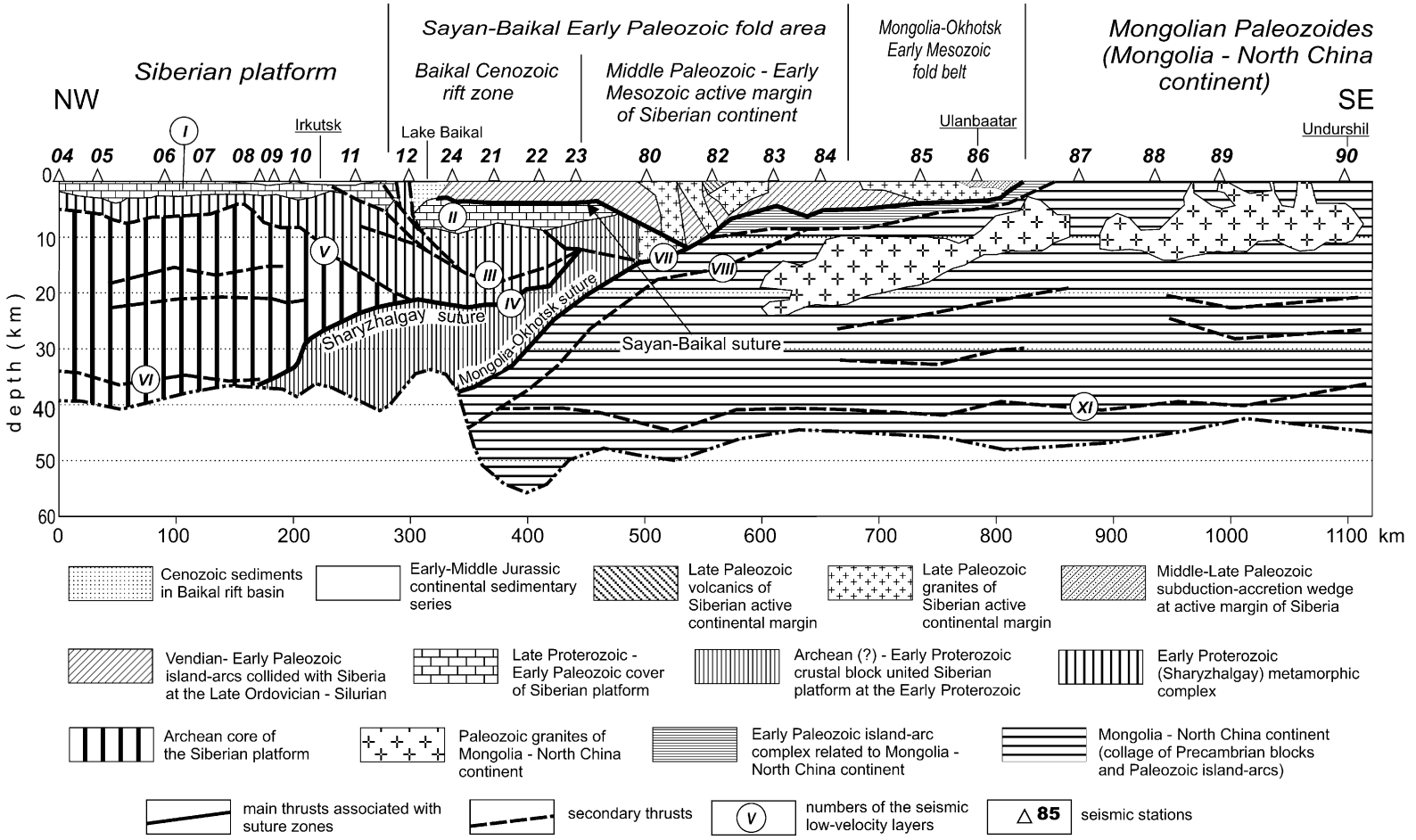

Figure 3.3: *Cross-section of the Earth's crust through the Baikal Rift. The cross-section has been constructed on the basis of the combined interpretation of seismic, gravity, and geological data. From Zorin et al. (2002). The approximate location of the transect is indicated in figure 3.2.*

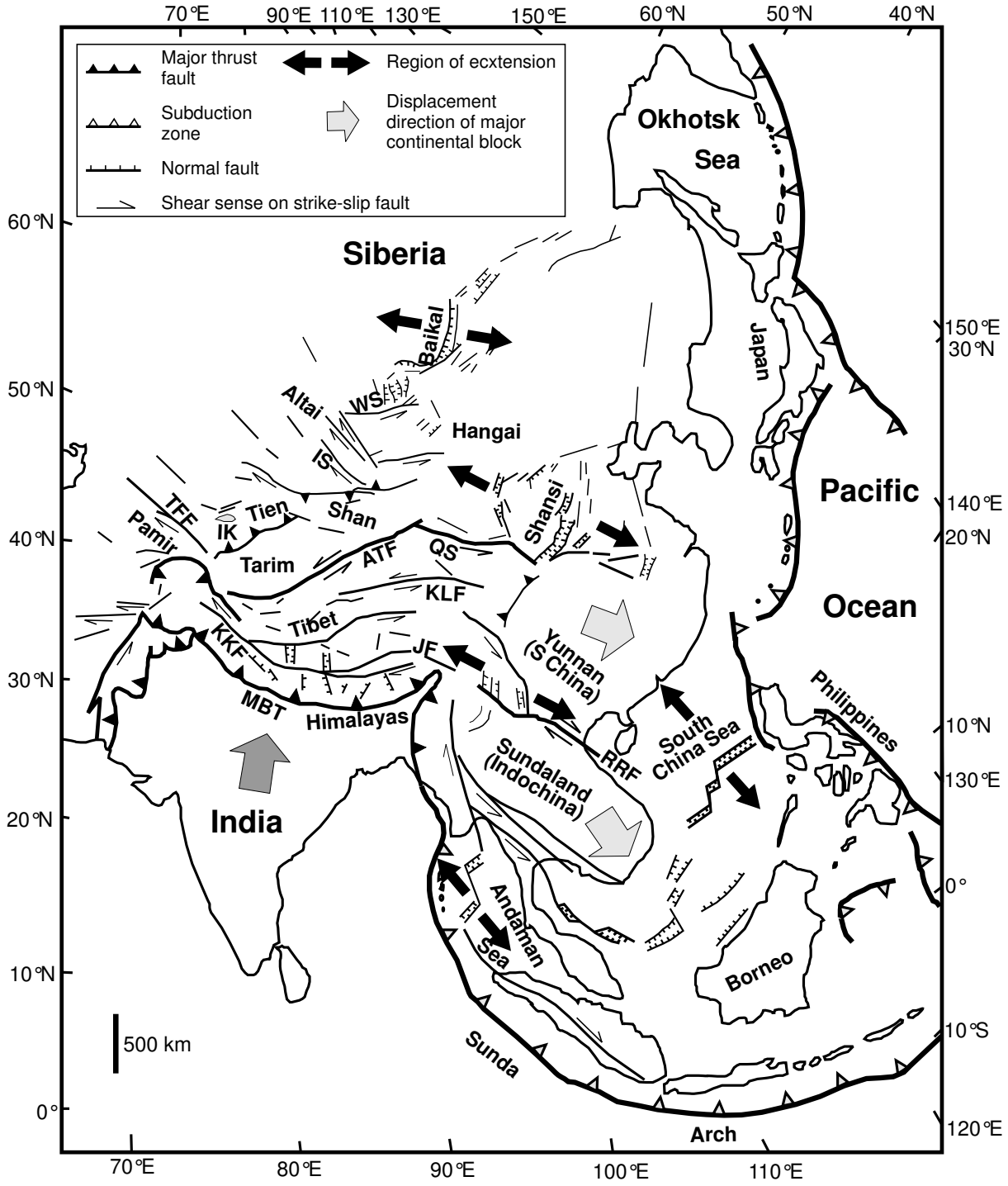

Figure 3.4: *Map of central-east Asia, showing the locations of major faults (thrust, strike-slip and normal) and subduction zones. Also displacement directions of the main continental blocks are indicated. From Tapponnier et al. (1982).*

1. thrusting and thickening of the crust, and
2. movements along large strike-slip faults causing the lateral escape of continental blocks (i.e. extrusion tectonics).

The former process is evidenced by for example the elevated topography of the Tibetan plateau and Himalaya's (with a crustal thickness of ∼70 km), as well as by major east-west oriented thrust faults which formed directly north of the suture zone between India and Eurasia (e.g. the Main Central Thrust and the Main Boundary Thrust in the Himalaya's) (e.g. Yin and Harrison, 2000).

As a result of the north-south compression, the topography of parts of Central Asia adopted a system of sub-parallel ridges and depressions, which apparently fits in a lithosphere folding model with a characteristic wavelength of ∼360 km (Nikishkin et al., 1993; Burov et al., 1993). Superimposed on this lithosphere folding a smaller scale folding has been inferred — supported by topographic data — for the upper crust, with wavelengths in the order of 30–50 km and 4–9 km (Nikishkin et al., 1993; Burov et al., 1993; Cloetingh et al., 1999).

The second process — the extrusion tectonics mechanism — is believed to accommodate as well an important part of the present convergence between both continents. Le Pichon et al. (1992) estimated the total amount of continental surface that has been lost between India and Eurasia to be larger than 57×10^5 km^2 and smaller than 68×10^5 km^2, probably even smaller than 62×10^5 km^2. Their estimated most likely amount of area that would have disappeared to create the observed topography in Asia is $\sim39\times10^5$ km^2. The deficit of $\sim19\times10^5$ km^2 between both values was attributed by Le Pichon et al. (1992) to the lateral extrusion of crustal blocks towards the east–southeast. However, because the elevation distribution in Asia prior to the indentation of India is not exactly known, estimates like the ones of Le Pichon et al. (1992) remain quite uncertain. Not surprisingly, other researchers have proposed other values for the amount of convergence accommodated by extrusion, ranging from 15% (England and Molnar, 1997b), via 30% (Repulmaz and Tapponnier, 2003) up to 50% (Avouac and Tapponnier, 1993).

Regardless the relative importance of the amount of extrusion, the model requires the presence of major strike-slip faults to accommodate the lateral block movements. The Altyn-Tagh Fault[3] and the Red River Fault[4] are believed to have been the most important in this process (e.g. Tapponnier et al., 1982).

Both processes to accommodate the lithospheric shortening have been successfully modelled by means of physical experiments. Burg et al. (1994) produced models in which "lithospheric buckling" was observed as a response to compression. The first order wavelength of this buckling corresponded to ∼200 km in nature. Tapponnier et al. (1982); Cobbold and Davy (1988); Peltzer and Tapponnier (1988) and recently Fournier et al. (2004) on the other hand, simulated the extrusion process along strike-slip faults in relation to the indentation of a rigid indenter in a plane strain environment near a free lateral boundary.

The neotectonic evolution of Central Asia mainly consists of a rejuvenation of long-lived older

[3] total sinistral Tertiary displacement of ∼500±200 km (Meng et al., 2001)
[4] total sinistral Tertiary displacement of ∼700±200 km (Leloup et al., 1995)

structures north of the India-Eurasia suture. The deformation zone extends for more than 3000 km northeast of the Himalayas, causing late Tertiary vertical motion of 2–5 km in the Pamirs, the Tien-Shan and Altay (Molnar and Tapponnier, 1975; De Grave, 2003). Two models have been proposed to explain the transmission of strain so far north in Eurasia's interior. In the first model the continental deformation is described as a result of rigid block motions, where deformation is localised in relatively narrow fault zones and fold belts that delineate the coherent blocks and micro-continents (e.g. Tapponnier et al., 1982; Peltzer and Saucier, 1996; Repulmaz and Tapponnier, 2003). In the second type of models, the lithosphere is treated as a continuum, and this results in a more diffuse deformation of the crust and upper mantle rather than the confined deformation in narrow bands (e.g. England and Jackson, 1989; England and Molnar, 1997a).

3.2 The Baikal Rift Zone (BRZ)

The Baikal Rift Zone is a typical example of a tectonically active continental rift system. It has classically been defined as the series of fault bounded Cenozoic basins between the Olekma River in the northeast and the East Sayan Mountains in the southwest (figure 3.5) (e.g. Logatchev, 1993). The grabens form a 2000 km long S-shaped strip that rims the wedge of the Siberian Craton (figure 3.5). The rheological difference between the Siberian Craton in the northwest and the Sayan-Baikal mobile belt in the southeast, has strongly influenced the structure of the Cenozoic Baikal Rift Zone. Many of the Cenozoic faults resulted from the reactivation of older faults (e.g. Zonenshain and Savostin, 1981; Theunissen et al., 1993). The Bolnai Fault (figure 3.5) is sometimes considered as the southern limit of the Baikal Rift Zone (Zonenshain and Savostin, 1981; Logatchev, 1993).

At present the Baikal rift basins are located in a domal uplift: the *Sayan-Baikal domal uplift* (Logatchev, 1993), or the *Baikalian arch* (Mats, 1993), that has a maximum height of 3000–3500 m above sea level (e.g. Logatchev, 1993). In the Baikal Rift Zone 14 different basins developed. The three largest, the southern, central and northern Lake Baikal basins, are located in the central part of the rift zone, and are occupied by the world's largest fresh water volume: *Lake Baikal* (Mats, 1993). Other basins include: Busingol Basin, Khubsugul Basin, Darkhat Basin, Tunka Basin, Barguzin Basin, Kitchera Basin, Upper Angara Basin, Muya Basin, Tsipa-Baunt Basin, Chara Basin, Tokko Basin (Zonenshain and Savostin, 1981; Logatchev and Zorin, 1992; San'kov et al., 2000). The BRZ can be divided in three zones: (1) a northern part, more or less E-W oriented, where different small basins developed arranged in an en echelon geometry, (2) a central part, including Lake Baikal and the Barguzin Basin, (3) a southern part (Tunka region) that is also more or less E-W oriented. The northern and southern parts have often been interpreted as areas of well-defined strike-slip faulting (e.g. Doser, 1991; Doser and Yarwood, 1991; Sherman et al., 2004), even to that extent that the zones have been interpreted as transform faults (Sherman and Levi, 1977; Sherman, 1978; Balla et al., 1991; Sherman, 1992; McCalpin and Khromovskih, 1995; Delvaux et al., 1997; Sherman et al., 2004). Field observations however suggest that at least for the northern area, the latest evolution (i.e. Quaternary) is best described

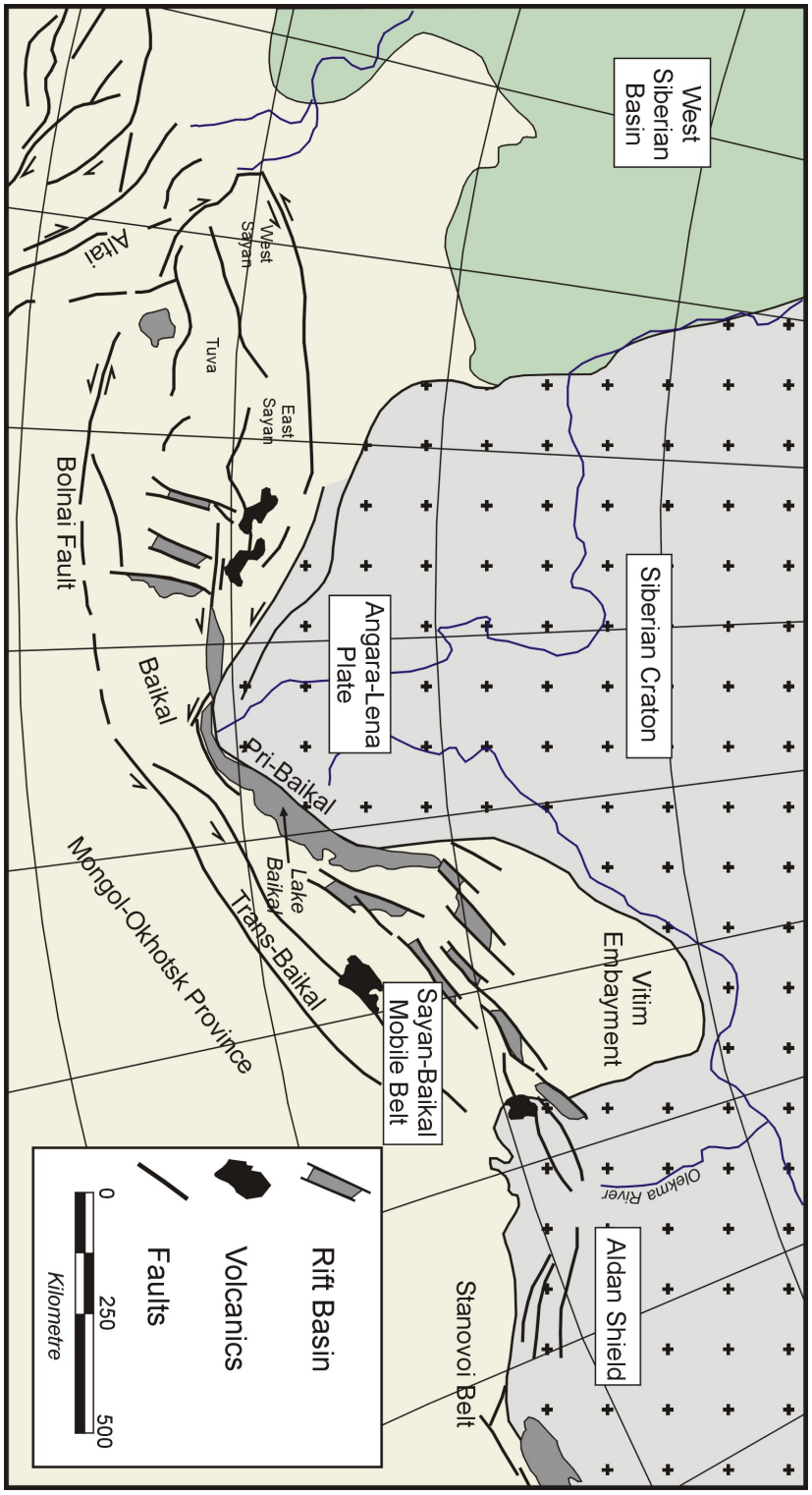

Figure 3.5: *Main structural elements of the Baikal Rift Zone (BRZ). Modified from Delvaux et al. (1997).*

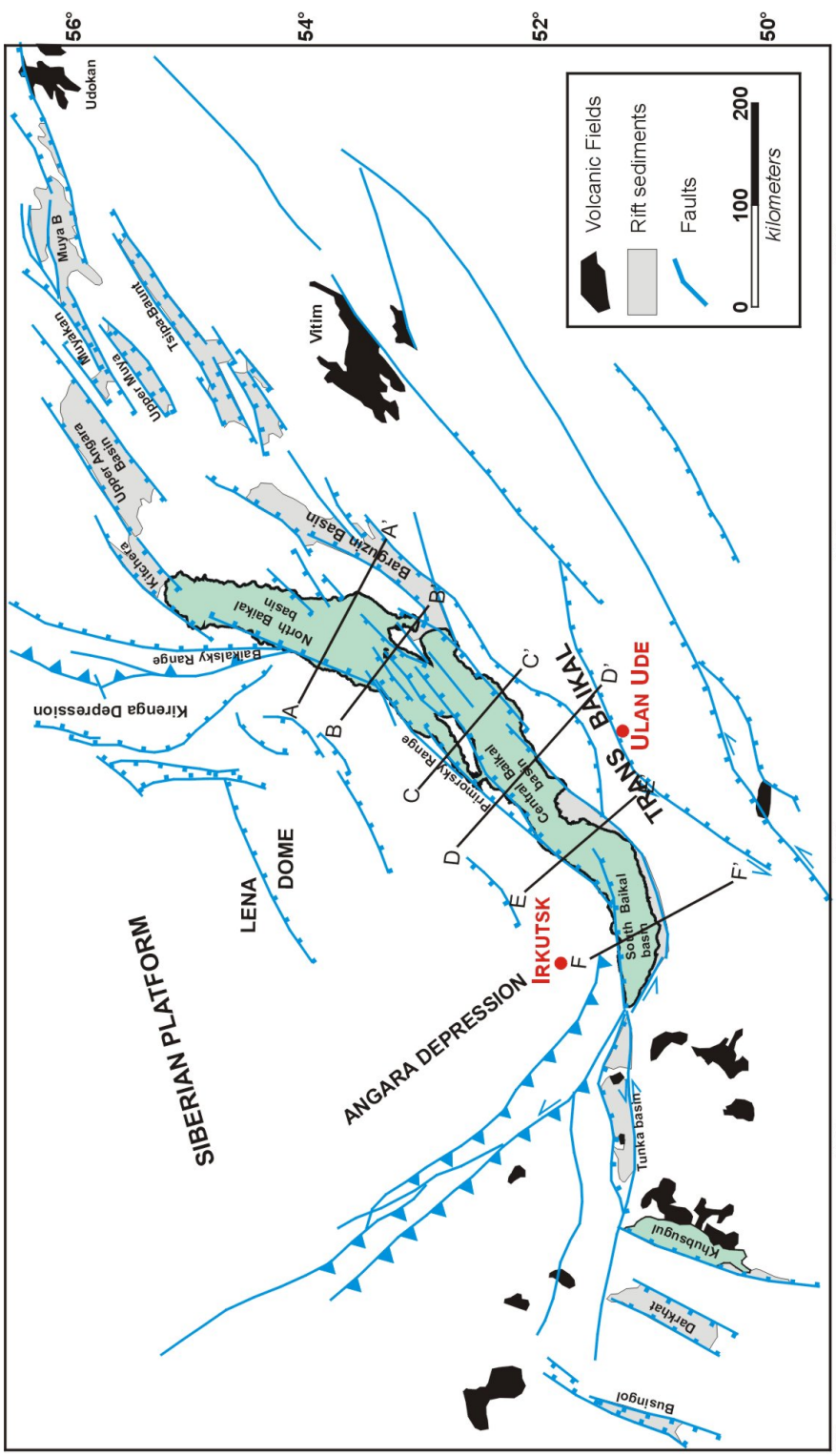

Figure 3.6: *Basic fault map of the Baikal Rift Zone. Solid lines through Lake Baikal indicate the location of the topographic profiles in figure 3.12. Modified from Delvaux et al. (1997).*

as one of oblique rifting, as the reported style of faulting is mainly dip slip, with only minor portions of left-lateral movements (San'kov et al., 2000). Strike-slip faulting on NE oriented faults has likely been more important in earlier stages of evolution (up to ∼5 Ma) (Delvaux et al., 1997; San'kov et al., 1997).

Based on GPS measurements, the present rate of extension in the southern part of the Baikal Rift Zone has been calculated to be 4.5±1.2 mm/yr (Calais et al., 1998; Sankov et al., 1999) or 4±1 mm/yr (Calais et al., 2003) in a WNW-ESE direction (azimuth ∼100°N according to Sankov et al. (1999)). This measured rate is considerably higher than the ones calculated based on kinematic models of Central Asia, in which the convergence between India and Eurasia is the sole driving mechanism for the present deformation (e.g. England and Molnar, 1997b). Such models predict extension rates in the BRZ of maximum 2 mm/yr. On the other hand, estimates based on the seismic moment release that resulted from the three large earthquakes ($M \geqslant 6.9$) on the Obruchevsky fault of the last 300 years, suggest an average slip along the fault of 5.6 mm/yr (Calais et al., 1998). This indicates that little or no aseismic slip is occurring along the fault (Calais et al., 1998). In the northern part of the BRZ, the average extension rate has been estimated to be 3.2±0.5 mm/yr in a N140°±20°E direction, based on summed Holocene displacements on major faults (San'kov et al., 2000). Zonenshain et al. (1992) reported a plate spreading rate of less than 0.1 cm/yr.

The present-day activity of the Baikal Rift Zone is evidenced by the ∼4000 seismic events occurring annually (figure 3.7). Between 1961 and 1999, ∼30000 earthquakes have been instrumentally recorded with magnitudes $2.5 \leqslant M \leqslant 7.6$ (Sherman et al., 2004). Since 1760, 27 events have been reported with magnitude $M \geqslant 6$ (Sherman et al., 2004). Déverchère et al. (2001) relocated 632 earthquakes that occurred between 1971 and 1997, and found a relative high abundance of earthquakes at depths between 15 and 25 km (≈50%). Earthquake activity persisted upto depths between 30 and 40 km (i.e. ≈7–13%), indicating that the lower crust and upper mantle are seismogenic at large depths (Déverchère et al., 1991, 2001).

The amount of horizontal extension that has occurred in the Baikal Rift is estimated by Logatchev and Florensov (1978) to be less than 10 km, but later Zonenshain et al. (1992) estimated an extension of minimum 10.6 km and a maximum of almost 15 km. These values lead to a low overall stretching factor β around 1.15 – 1.20 (Zonenshain et al., 1992).

Magmatism in the Baikal Rift zone prior to the formation of the rift has been rather limited and also the rift related volcanism resulted in only a relative small volume (∼5000–6000 km^3) of volcanic rocks as compared to other rifts. For the Rio Grande Rift, for example, this volume is believed to be an order of magnitude larger (e.g. Lipman et al., 1989) and for the Kenya Rift even 20 times larger (e.g. Logatchev et al., 1983). During the evolution of the Baikal Rift Zone two peaks of magmatic activity occurred, one in the Middle–Late Miocene, and the other in the Pliocene–Quaternary (Rasskazov, 1994; Zorin et al., 2003). This resulted in the development of three important basalt fields: Sayan-Khamar-Daban, Vitim and Udokan (figure 3.6) (Logatchev, 1993; Rasskazov, 1994). Unlike in other rifts, the volcanism in the Baikal Rift Zone occurs independently from major rift faults or basins, with the only exception being the basaltic field located near Khubsugul (Logatchev, 1993).

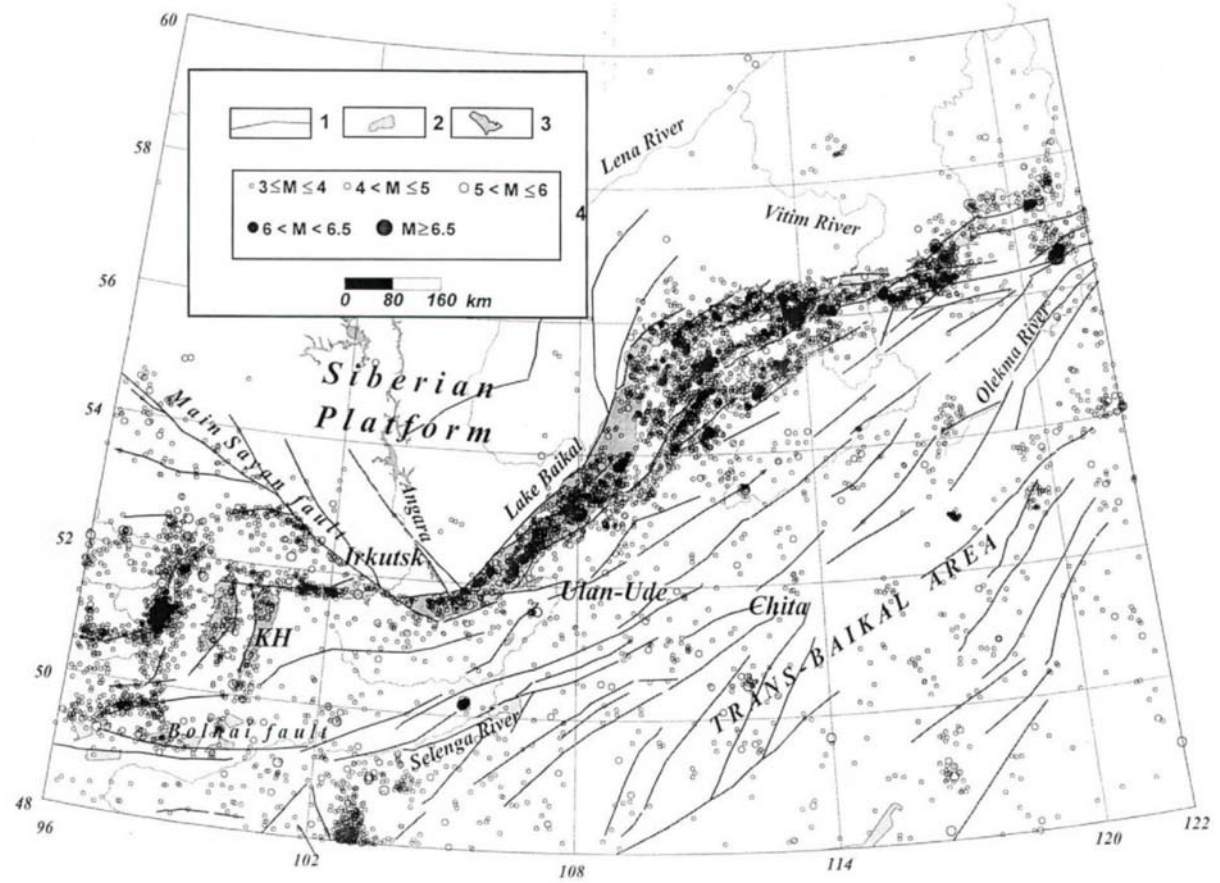

Figure 3.7: *Epicentres of recorded earthquakes in the Baikal area with magnitudes between 3 and 7 during the period 1964–1997. 1 — Faults active in the Cenozoic; 2 — Basins; 3 — Lakes; 4 — Earthquake epicentres. KH = Lake Khubsugul. From Klyuchevskii (2004).*

3.2.1 Slow rifting stage

Based on the interpretation of structural field data (e.g. Delvaux et al., 1997; San'kov et al., 1997), and of the sedimentary infill of the Baikal basins (Hutchinson et al., 1992; Moore et al., 1997), several distinct tectonic stages can be recognised in the Cenozoic evolution of the Baikal Rift Zone. Two major stages, however, include all the smaller ones: the *slow rifting stage* and the *fast rifting stage* (discussed in the next section) (Logatchev and Florensov, 1978).

The slow rifting stage lasted from ca. 30 Ma till about 3.5 Ma (e.g. Mats, 1993) or 2.5 Ma (Kuzmin et al., 2000) and lead to the formation of large depressions, mainly as a result of a relatively slow subsidence and an unimportant uplift of the rift shoulders (Logatchev, 1993; Mats, 1993). All three Baikal basins started to evolve in the slow rifting phase, but due to a difference in syn-rift sediment thickness between the south and central basins (ca. 10 km) compared to the northern basin (ca. 4 km), the latter is believed to be considerably younger (Hutchinson et al.,

1992; Mats et al., 2000). Tapponnier and Molnar (1979) suggested that the shallower depth of the northern Baikal basin might be a result of the distribution of extension over a broader zone, i.e. including the deformation in the Barguzin Basin.

Paleostress reconstructions of the early development of the Baikal region suggest that the initial evolution has been characterised by transpressional stress conditions, whereas during later stages in the slow rifting phase, a more extensional stress regime was established (Delvaux et al., 1997) (see section 3.2.4).

The slow rifting stage can be subdivided in two sub-stages, an early stage from 35-30 to 10 Ma, and a late stage from 10 to 3.5 Ma (Mats, 1993). The slow rifting stage has also been referred to as the *proto-Baikalian* evolution stage (Mats, 1993), the *proto rift stage* (Delvaux et al., 1997) or the *Early Rift Stage* or *Tankhoy Stage* (Mats et al., 2000).

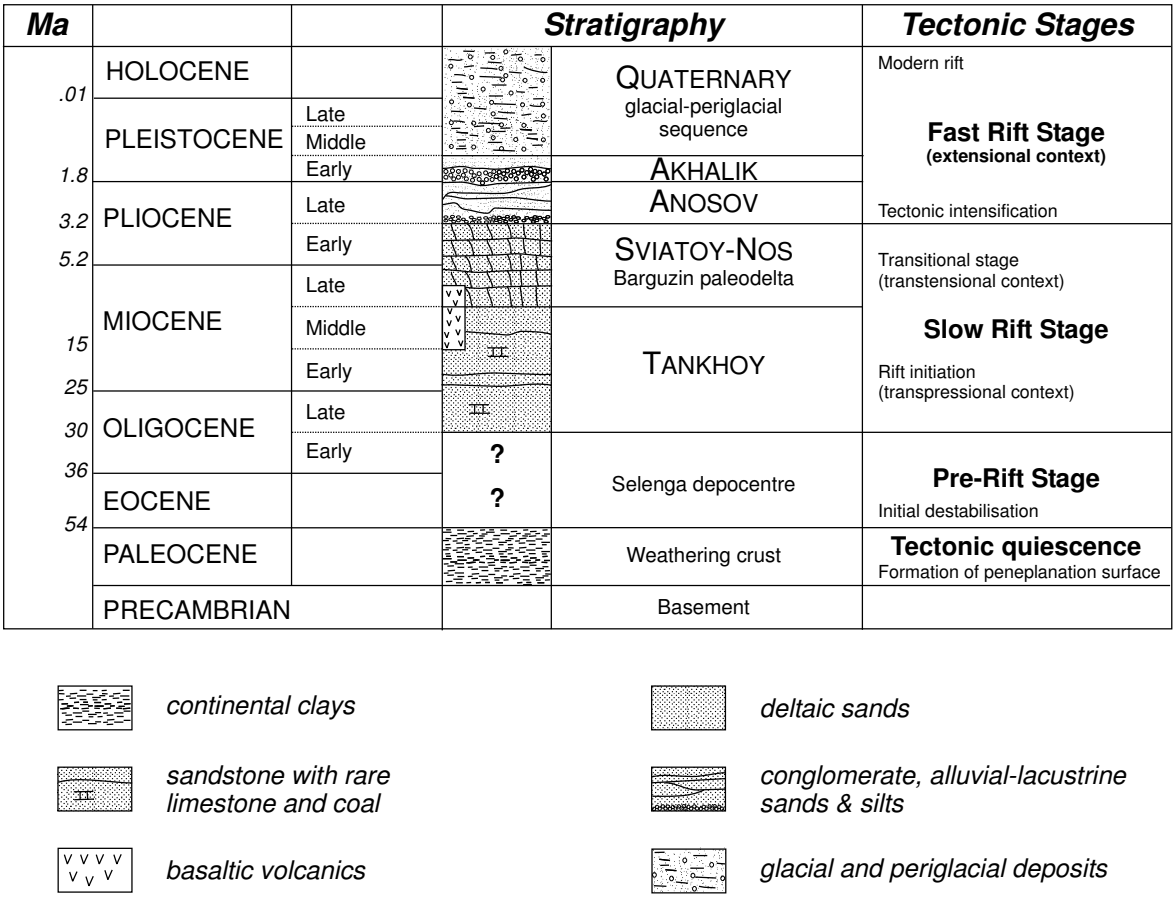

Figure 3.8: *Stratigraphic overview of the Baikal Rift Zone with the major tectonic stages. Modified from Delvaux et al. (1997).*

3.2.2 Fast rifting stage

The fast rifting stage, from 3.5–2.5 Ma to present, started with an acceleration of the tectonic movements (six-to-ten-fold increase in the strain rate according to Logatchev and Florensov (1978)), which resulted in an increased subsidence of the Baikal basins and the uplift of especially the western rift flank. The increased topography also caused an increase in the input of clastic sediments in Lake Baikal (Mats, 1993). During the fast rifting stage also the grabens located in northern Mongolia started to open (Zonenshain and Savostin, 1981; Logatchev and Zorin, 1992).

Delvaux et al. (1997) have shown that the transition to the fast rifting stage also implied a change in the stress regime. In the central part of Lake Baikal mainly normal dip slip movements occurred along the major faults (see section 3.2.4).

The fast rifting stage can be subdivided in three main tectonic stages: (1) an early stage from 3.5 to 0.8 Ma, a middle stage from 0.8 to 0.1 Ma and a late or modern stage from 0.1 Ma to present (e.g. Mats, 1993). Mats (1993) have referred to the fast rifting stage as the *Neobaikalian* evolution stage, while Delvaux et al. (1997) called it the *active rift stage*.

Recently ten Brink and Taylor (2002) explained the transition between the slow and the fast rifting stage in terms of fault segment linkage and the associated post-linkage displacement increase, similar to the model of Gupta et al. (1998) (explained in section 2.4.2). ten Brink and Taylor (2002) used this model to explain the observed increased subsidence rates in the fast rifting stage. This idea is discussed in more detail in chapter 5.

3.2.3 Active or passive rifting in the Baikal Rift Zone?

In section 2.9.1 on page 78 it was explained that rifts can be classified in 2 types based on the most important mechanism that drives the extension: active or passive rifting. In particular for the Baikal Rift Zone, the question whether it is actively or passively rifting, has been intensively debated.

Believers of the active rifting hypothesis have argued that evidence can be found for a broad asthenospheric up-welling at the location of the rift zone (e.g. Zorin and Rogozhina, 1978; Logatchev and Zorin, 1992; Gao et al., 1994; Zorin et al., 2003). Such evidence has mainly been derived from gravitational data and seismic soundings, which reveal a thinned crust underneath the Baikal Rift and an anomalous mantle (i.e. characterised by lower p-wave velocities which reflect a lower density, probably related to a hotter mantle) (Zorin and Rogozhina, 1978; Zorin et al., 2003). More recently acquired gravitational data, however, seem to contradict such interpretation (e.g. Petit, 1998; Tiberi et al., 2003). Moreover, it is unclear how much information this present-day situation might provide about the rifting mechanism during the initiation of the Baikal Rift Zone 35 Ma ago. Also the arched domal uplift in which the Baikal rift is located has been used as an indication for the rising asthenosphere and therefore as an argument for the active driving forces for rifting, however, given that the rising of the dome is dated later than the appearance of the first rift basins, this is argument is rather ambiguous (Zonenshain

and Savostin, 1981). Nevertheless, also part of the Baikal Rift Zone has been uplifted before the basin formation.

In the passive rift hypothesis, extension in the Baikal Rift is believed to result from far field stresses. The generation of such stresses could for example be related to the penetration of India into Eurasia (see section 3.1.2) (Molnar and Tapponnier, 1975). The passive rift hypothesis is supported by numerical models which have calculated that the presence of far-field stresses in combination with the favourably oriented zones of weakness in the Baikal rift could be responsible for the development of the extensional basins in Baikal (Lesne et al., 1998, 2000). Also the non-existence of a regional elevated heat flow in Lake Baikal (e.g. Lysak, 1978; Golubev, 2000; Poort and Klerkx, 2004) is easier explained in a passive rifting model. Local anomalies in heat flow values have been reported at certain locations in Lake Baikal, but these have been explained by local fluid circulations often related to faulting (e.g. the anomaly in Zavarotny) (Golubev, 2000; Poort and Klerkx, 2004).

3.2.4 Development of the Baikal Rift Zone

Several kinematic models have been proposed for the formation of the Baikal Rift Zone and the opening of Lake Baikal:

- Different authors have suggested a pull apart type of opening, in which several "gaps" are formed between major E-W trending strike-slip faults. Models of this type agree on the "transform" zones in the northern and southern part of the rift, but they differ in the location and number of other strike-slip faults within Lake Baikal (e.g. Sherman and Levi, 1977; Balla et al., 1991). A major shortcoming of these models remains however, that so far no clear evidence has been found, which proves the lateral movements on the transform faults to be indeed as important as predicted by the models[5]. And secondly, the inferred locations of some of the strike-slip zones interpreted within Lake Baikal, appear to be rather speculative. For the model of Balla et al. (1991), major faults have been inferred in Lake Baikal by correlation between outcrops on both sides of the lake. However, often no evidence exits — nor from earthquake focal mechanisms nor from seismic profiling — for the existence of such faults (e.g. Levi et al., 1997).

- Based on paleostress reconstructions, Delvaux et al. (1997) have suggested that the initial evolution of the central part of the rift zone happened in a transpressional context which later changed in one of transtension (figures 3.9a and b). The transpressional regime (before Late Miocene) involved the reactivation of the Primorsky shear zone as a wrench fault. During the transtensional regime (Late Miocene – Early Pliocene), the central part of the rift opened obliquely. At the same time the Main Sayan Fault developed in a sinistral strike-slip fault, and the East-Sayan block moved eastward relative to the Angara-Lena Plate. This movement is associated with thrusting in the Tunka Range (figure 3.9b), and

[5] See for example the discussion on page 8 of Zonenshain and Savostin (1981), where they note that important strike-slip faults in the model of Sherman and Levi (1977) have previously been interpreted as clearly normal faults by Sherman et al. (1973)

might have caused extensional deformation in the southern Baikal basin as a result of the expulsion of the Khamar-Daban block. The Tunka Basin, south of Lake Baikal, likely formed as a flexural response to the overthrusting.

In the fast rifting stage (figure 3.9c), faults in the central part of the rift zone evolved in mostly dip-slip faults, with only minor lateral movements. This resulted in the more or less orthogonal opening which is characteristic for the evolution of this part of the rift zone. The southern Baikal basin continued to open obliquely. The Tunka Fault, south of Lake Baikal, evolved into a sinistral strike-slip fault, and accommodated the opening of the southwesternmost basins of the rift zone.

In a later stage (Late Pleistocene – Holocene), also a transtensional stress regime is established in the Tunka Basin. Recently also new Mesozoic structures have been reactivated in the Angara-Lena Plate, maybe in relation to the formation of the Lena Dome (figure 3.9d).

Chemenda et al. (2002) have run simple physical experiments of uniaxial extension in a one-layer plastic material to understand the first order lithospheric-scale mechanics of rifting. They studied the strain localisation in relation to the distribution of rheologically stronger and weaker material and they used a configuration which is similar to the situation in the Baikal Rift Zone (figure 3.10). Chemenda et al. (2002) introduced a more rigid part in the model, shaped like the Siberian craton. To initiate rifting in the model near the craton they locally heated the model (dashed line in figure 3.10). After the rift initiation, further extension caused the development of 3 deformation branches oriented obliquely to the tension direction. Two of them (AB and CE in figure 3.10) correspond reasonably well to the upper and lower branches of the Baikal Rift Zone. The third branch (BK in figure 3.10) which developed as well, is in nature less well expressed, but it can be linked to a zone south of the Baikal Rift Zone, characterised by a slightly increased seismic activity (the zone which connects the cluster of earthquakes at 48°N-103°E with the westernmost extremity of Lake Baikal in figure 3.7). The experiment of Chemenda et al. (2002) has confirmed the importance of the weak suture zone near the Siberian craton in shaping and localising the Baikal Rift Zone. It also suggests that this rheological difference, together with the direction of extension, were the main parameters that determined the first-order shape of the rift zone.

3.3 Lake Baikal

As mentioned in the previous section, 14 different basins formed in the Baikal Rift Zone. The three largest are located in the central part of the rift zone, and are filled with the waters of Lake Baikal (figure 3.11). The $\int$-shaped lake has a length of 636 km, an average width of 40-50 km and an average water depth of 730 m (with a maximum of 1642 m[6]). It consists of the largest free fresh water body on earth (i.e. excluding the water stored in ice caps in other parts of the world). The lake surface is at an altitude of 455.5 m above sea level. 50% of the water inflow

[6]Maximum sounded depth in the central basin at location: N53°14'59" – E108°05'11". Data from The INTAS Project 99-1669 Team (2002).

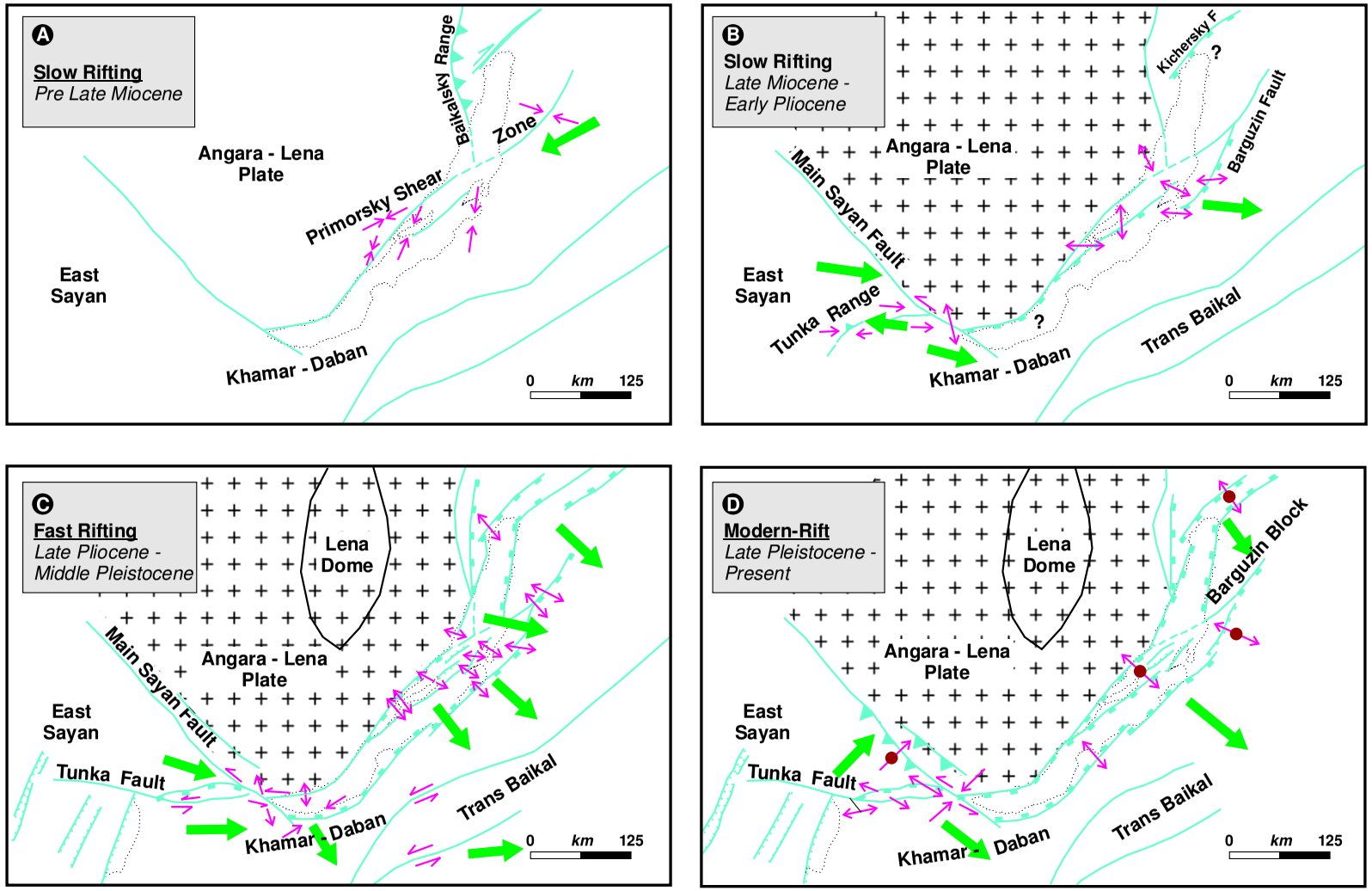

Figure 3.9: *Tectonic maps of 4 different evolutionary stages of the central Baikal rift. Large arrows represent inferred block motions relative to the adjacent block or with respect to the Angara-Lena Platform. Divergent and convergent arrows correspond to respectively normal and reverse movements, whereas arrows parallel to a fault indicate strike slip movements. The fault kinematics are inferred from slip calculations on "mean" movement planes and the related stress tensors. Arrows marked with a dot have been calculated from earthquake focal mechanisms. Blue lines indicate major faults. From Delvaux et al. (1997).*

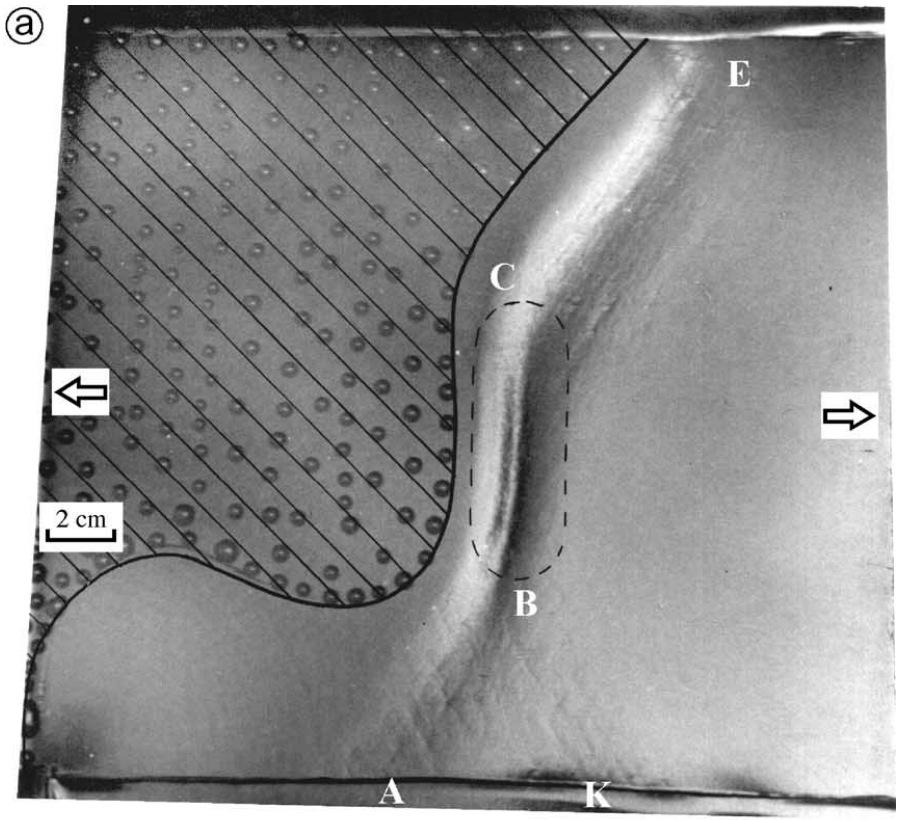

Figure 3.10: *Oblique top view of a deformed experiment of Chemenda et al. (2002). The strong "lithosphere" in the model is marked by the dashed area, and a local weak zone is contoured by the dashed line. From Chemenda et al. (2002).*

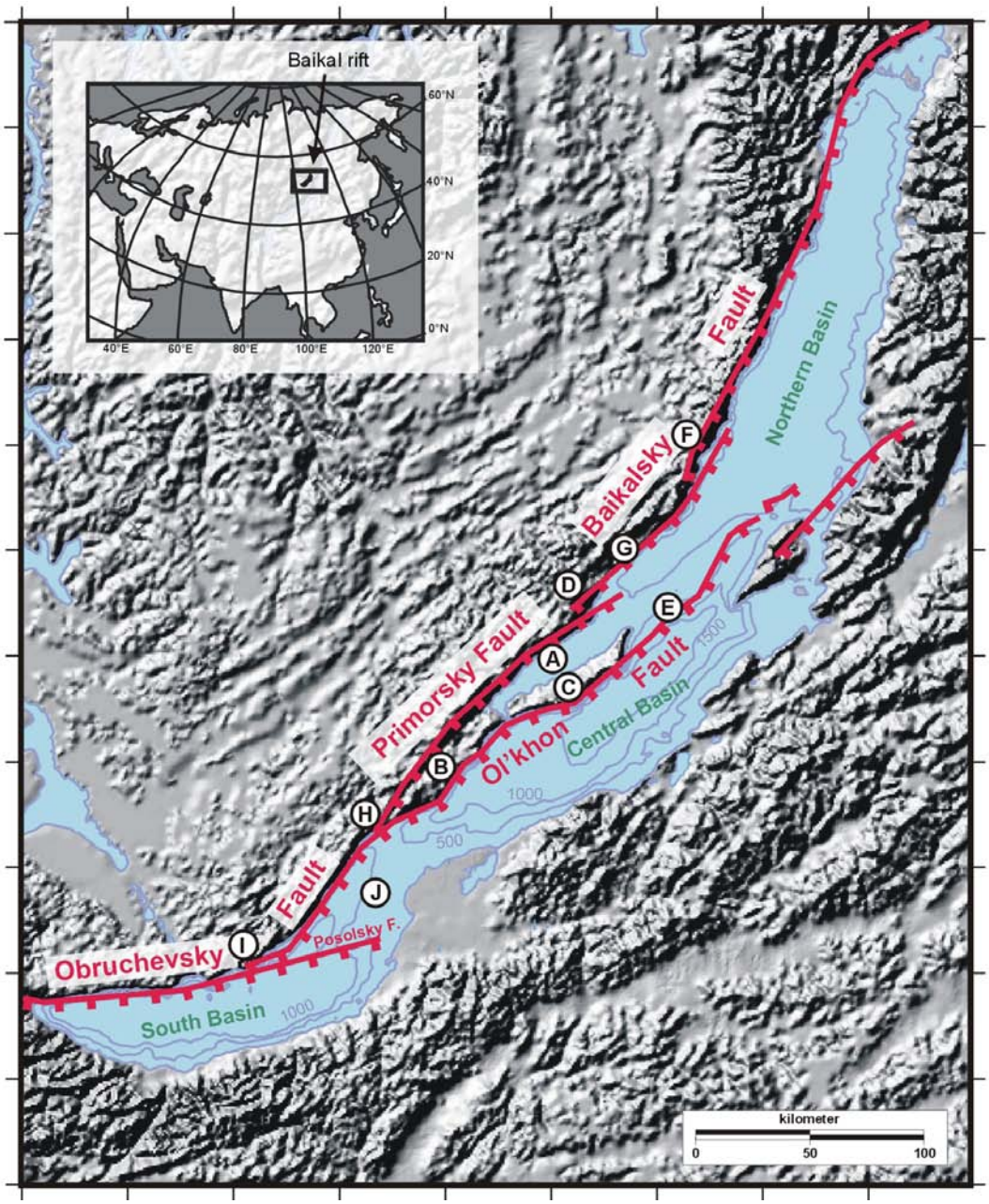

Figure 3.11: *Simplified structural map of Lake Baikal, showing the major faults of the western lake border. The map is drawn on a digital terrain model of the area. A — Maloe More; B — Pri-Ol'khon; C — Ol'khon Island; D — Zunduk; E — Academician Ridge; F — Zavarotny; G — Kocherikovo; H — Buguldeika River mouth; I — Bolshy-Koti and J — Selenga Delta Accommodation Zone. Blocks B, C and E make up the Academician Ridge Accommodation Zone.*

in Lake Baikal is accomplished by the Selenga River, and the delta that formed at the river's mouth is the world's largest continental delta (Logatchev, 1993).

The 3 Baikal basins have different orientations, which results in the clearly segmented geometry of Lake Baikal, a property that is also recognised in other extensional terrains like for example the East African Rift System (e.g. Bosworth, 1985; Rosendahl et al., 1986), the Basin and Range Province (e.g. Faulds and Varga, 1998), the Gulf Extensional Province (e.g Stock and Hodges, 1990; Axen, 1995) and other rifts. Between the different basins two large accommodation zones exist: the *Academician Ridge Accommodation Zone* between the central and the northern basin, and the *Selenga Delta Accommodation Zone* between the central and the southern basin. Logatchev (1993) refers to the ridges as *structural highs*, and he emphasises that they do not act as accommodation zones during the development of Lake Baikal. Zonenshain et al. (1992) on the other hand interpreted them as real accommodation zones. Delvaux et al. (2000) interpreted the Academician Ridge Accommodation Zone as a transfer zone between the northern and southern basin, and Scholz and Hutchinson (2000) referred to the Selenga Delta Accommodation Zone as an accommodation zone. The three Baikal basins show a clear asymmetrical shape with major large displacement faults on their western shore and a more gradual change in topography along the eastern margin (eg. Zonenshain and Savostin, 1981; Hutchinson et al., 1992; Logatchev, 1993; Mats, 1993). In the active rift hypothesis this asymmetry has been attributed to a southeastward directed flow in the upper part of the anomalous mantle that underlies the Baikal Rift Zone (Zorin and Rogozhina, 1978). The vertical displacement that took place along the western border faults in the central part of lake Baikal is estimated to be around 8000 m by Zonenshain et al. (1992), but when a assuming a sediment thickness of 8–9 km for the central basin (ten Brink and Taylor, 2002), this value should rather be around 12 km (ie. with rift shoulders reaching heights of 1500–2000 m above lake level and a water depth of 1500 m). Several topographic profiles through the Baikal Rift Zone are included in figure 3.12.

Based on the geometry of tilted blocks near the western border faults of lake Baikal, some authors do believe that these faults show listric shapes in cross-section[7] On the other hand seismological data provides evidence that the Ol'khon fault has a dip between 51–55° at depths up to 20 km as well as near the surface (Zonenshain et al., 1992). Therefore a domino-style of extension might be important in the Baikal Rift Zone (Zonenshain et al., 1992). van der Beek (1997) applied three models for extension to Lake Baikal (flexural cantilever model, necking model and detachment model) and he concluded that the flexural cantilever model was not suitable to describe the observed topography and erosion around lake Baikal. However, he was unable to discriminate between the necking and the detachment models, concluding that the latter was most probable seen the strong asymmetry of the Baikal basins.

Using multi-channel reflection seismic data, three first-order stratigraphic units have been identified in the lake's sediments (Hutchinson et al., 1992). The proto-rift deposits directly overlie the basement and have a maximum thickness of 4 to 5 km. These are overlain by the

[7]Reference in Mats et al. (2000) to Russian work of Pleshanov and Romazina (1981): Some questions on kinematics of faults development in central part of Baikal Rift. Problems of Faults Tectonics. Nauka, Novosibirsk, pp. 129–141 (in Russian).

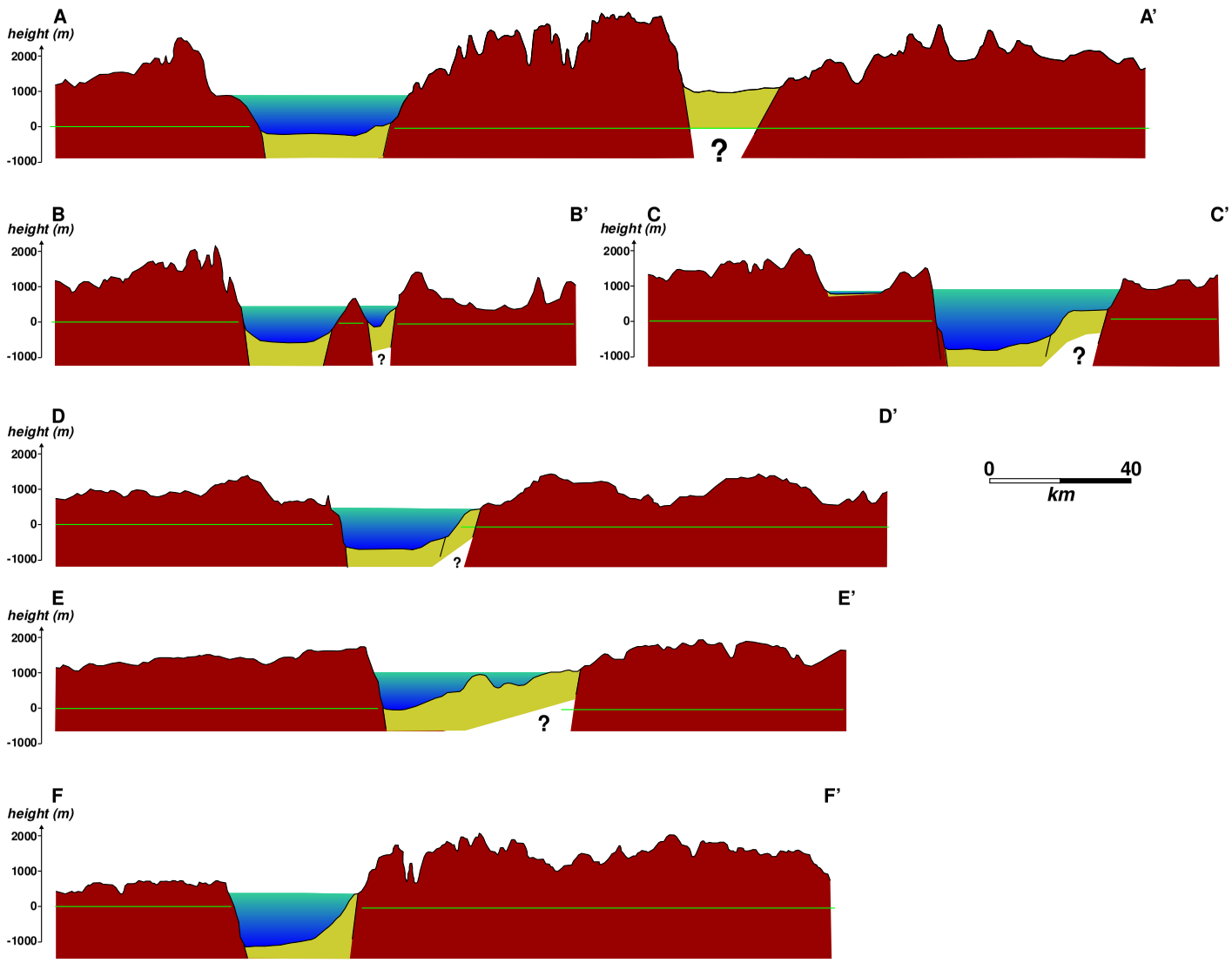

Figure 3.12: *Topographic sections through Lake Baikal, showing the morphology of the lake and the adjacent mountain ranges. The location of the different profiles can be found on figure 3.6. Modified from Mats et al. (2001).*

middle-rift deposits (1–2 km thick). The boundary between the two units has been interpreted by Hutchinson et al. (1992) as corresponding to the transition from the slow to the fast rifting phase. On top the modern-rift units have been deposited with thicknesses that are in general less than 500 m. A well-defined angular unconformity exists between the proto- and middle-rift deposits that marks the increased tectonic movements. The sedimentation rate during the deposition of the middle-rift deposits was around 5 to 10 times higher than that during deposition of the proto-rift deposits (Logatchev, 1993). The modern rift units include Pleistocene and Holocene sediments, and likely represent the last strong tectonic pulse that affected the Baikal Rift Zone (Logatchev, 1993). The middle-rift deposits, together with the modern rift deposits, represent the fast rifting stage.

3.3.1 Western Border Deflection

The orientation of the border faults along the western side of Lake Baikal changes from a ENE direction along the southern basin to an approximately NNE orientation in the northern basin. This deflection reveals clearly the different segments of the western border fault system.

The Obruchevsky Fault scarp is the northwestern border of the southern Baikal basin. Despite its sharp bend near Bolshy-Koti and a split of the fault with an eastern segment prolongating in the basin as the Posolsky Fault, it is usually traced to the mouth of the Buguldeika River. Here it splays into an eastern branch, the Ol'khon Fault, and a western branch, the Primorsky Fault, the main boundary of the central Baikal Basin (Figure 3.11). The Ol'khon Fault (or Morsky Fault according to Agar and Klitgord (1995)) cross-cuts Lake Baikal, delimiting the southern side of the Ol'khon Island and the submerged Academician Ridge, two major blocks of the Academician Ridge accommodation zone (Mats et al., 2000). Farther to the north, near Kocherikovo, the Primorsky Fault dies out, and is replaced by the Baikalsky Fault, which has a slightly different orientation and borders the northern basin.

Within these major fault segments, a smaller scale segmentation can be identified, see section 5.2 for a description of the Primorsky Fault. For the northern Baikalsky Fault, a relay structure is present in the area of Zavarotny (Matton and Klerkx, 1995; Delvaux et al., 2000). Here a southern segment dies out in Lake Baikal and its displacement is transfered to an onshore segment to the north. Both segments partly overlap, and a clear ramp structure has developed in between (Matton and Klerkx, 1995) (Figure 4.2).

Paleo-stress tensors for Lake Baikal have been calculated by Delvaux et al. (1997) and San'kov et al. (1997), based on fault slip data of the main faults. A map of the most recent stress field is represented in figure 3.13. Stress tensor maps of earlier Cenozoic evolution stages can be found in the aforementioned references. Paleozoic stress tensors for the region have been published by Delvaux et al. (1993) and Delvaux et al. (1995).

3.3.2 Evolution of Lake Baikal

The evolution of Lake Baikal itself was obviously related to the evolution of the Baikal Rift Zone (described in section 3.2.4). The following section specifically addresses how the different

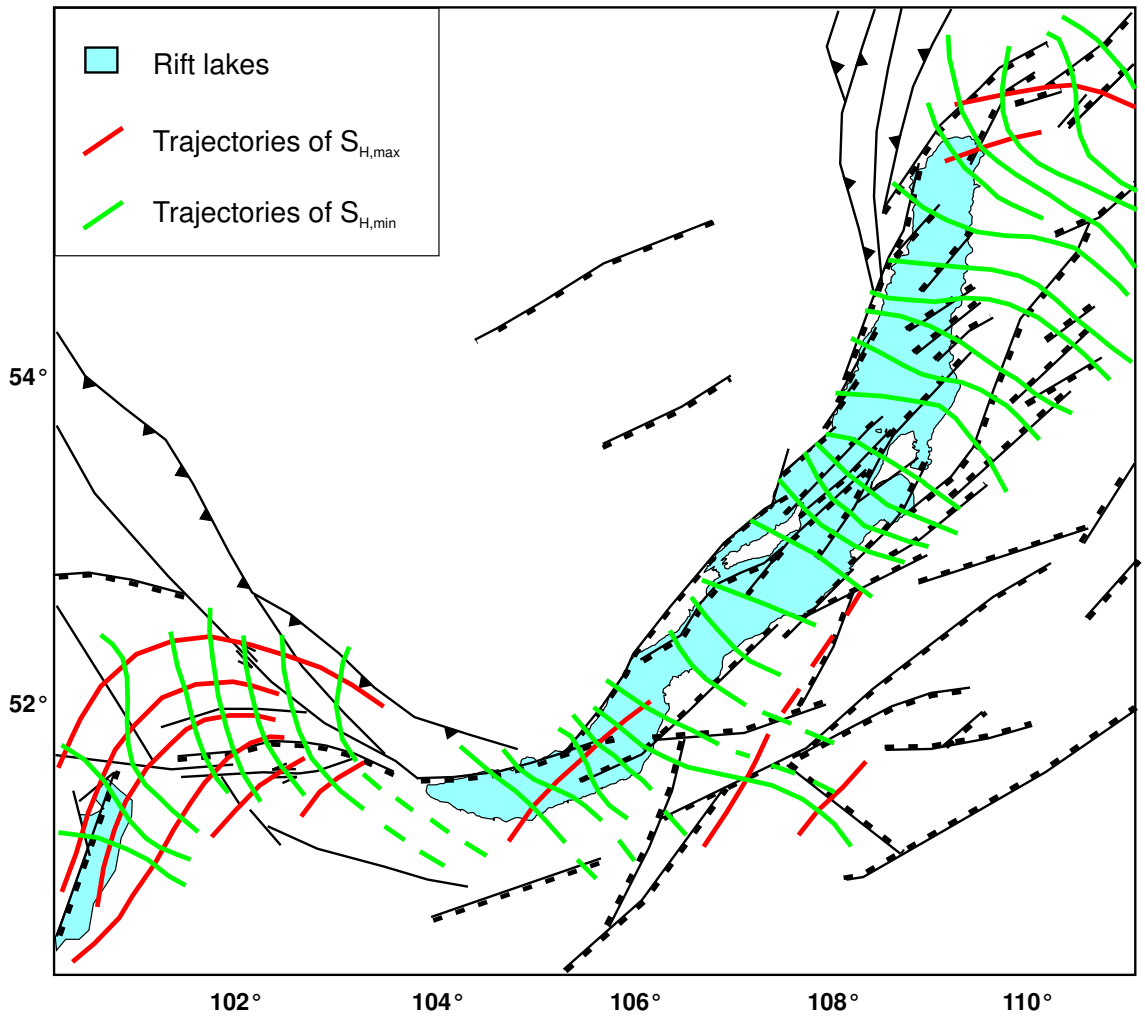

Figure 3.13: *Present-day stress field in the central part of the Baikal Rift Zone. Stress tensors are computed from earthquake focal mechanisms. From San'kov et al. (1997).*

evolution stages were expressed in Lake Baikal.

In the first part of the slow rifting stage, deep water lakes were formed in the central and southern Baikal basins. The northern basin as well as the Academician Ridge remained dry at that time (Mats, 1993; Mats et al., 2000), and the northwestern limit of Lake Baikal was formed by the Ol'khon Fault. An isolated lake could have formed in the northern extremity of the norther Baikal basin at the same time, but no connection existed with the central basin (Mats, 1993).

Later, during the Middle Miocene, the Baikal shoreline gradually moved northwestward, as a result of the subsidence of different structural blocks of the Academician Ridge (Mats et al., 2000). During the Late Miocene the transition to a transtensional regime caused a considerable enlargement of several basins. The graben between the Svyatoy Nos peninsula and the Ushkany islands was one of them, and through this strait, waters from the central Baikal basin started

to flood the northern basin and the northwestern part of Maloe More (Mats, 1993; Mats et al., 2000).

During the Late Miocene – Pliocene (10–3.5 Ma), the northern Baikal basin deepened further, and the southeastern limit of the basin advanced in relation to the tilting towards the northwest of the northwestern sub-blocks of the Academician Ridge.

The tectonic pulse at about 3.5 Ma — when the fast rifting stage started — likely caused the development of the very deep rift depressions of Lake Baikal, as a result of the combination of subsidence of the basin floor and uplift of the rift shoulders. At that time also the Ol'khon block was uplifted, and major regressions occurred in Maloe More. Also the Zunduk horst and the northwestern sub-block of Maloe More remained above lake-level during this period (Mats et al., 2000). Another period of intense uplift of the western rift shoulders took place at the beginning of the Pleistocene (Mats, 1993).

During the Late Pleistocene (0.15–0.12 Ma) a last tectonic stage started, which caused a further subsidence of the rift basins, accompanied by a further uplift of the rift shoulders. During this stage, the northwestern sub-block of the Academician Ridge finally became submerged (Mats et al., 2000).

In later chapters, the structure and evolution of the Zavarotny relay ramp (chapter 4) and the Ol'khon Region (chapter 5) are analysed and discussed.

Part I

The role of relay ramps in the evolution of a rift basin: application to Lake Baikal

Chapter 4

A large scale relay ramp in northern Lake Baikal: the area of Zavarotny

As mentioned in the previous chapter, near the village of Zavarotny a relay ramp has formed between two overlapping segments of the Baikalsky Fault (figure 4.1 and 4.2). In this chapter the internal structure of this ~400 km^2 large relay ramp is described and discussed. Published descriptions of the internal structures of relay ramps are usually based on much smaller examples (see section 2.5), and therefore analysing the ramp structure in Zavarotny provides the opportunity to make useful comparisons between observed structures in relay ramps at different scales.

In this chapter also the process of linkage between two major synthetically dipping fault segments is discussed, and further insight in the evolution of border fault systems in rifts is provided. Moreover, this chapter highlights the complexity of the internal structure of a large relay zone, including the formation of smaller basins within the ramp.

4.1 Available data and applied research methods

Due to its specific location, partly onshore and partly offshore, the relay ramp in Zavarotny can be accessed with different research techniques. The data available for the offshore part of Zavarotny were acquired during different campaigns between 1993 and 1995 by the *Royal Museum of Central Africa* (RMCA), Tervuren (Belgium) and the *Renard Centre of Marine Geology* (RCMG), Gent (Belgium). These data consists of a very fine grid of bathymetric data, obtained by echo-sounding profiling (Matton and Klerkx, 1995) and a total of 300 km of high-resolution single-channel seismic profiles, covering the whole area (Figure 4.3) (De Batist and Vanhauwaert, 1995). The seismic data were shot using a "Centipede" sparker source (frequency range of 400–1500 Hz when operated at 500 J) and a single-channel streamer as receiver. The incoming signal was filtered using a bandpass filter (400 Hz high-pass; 2000 Hz low-pass) and digitally recorded on an Elics Delph2 system. After processing with ProMax software (frequency filtering, spiking deconvolution), all the data were loaded and interpreted using the KINGDOM

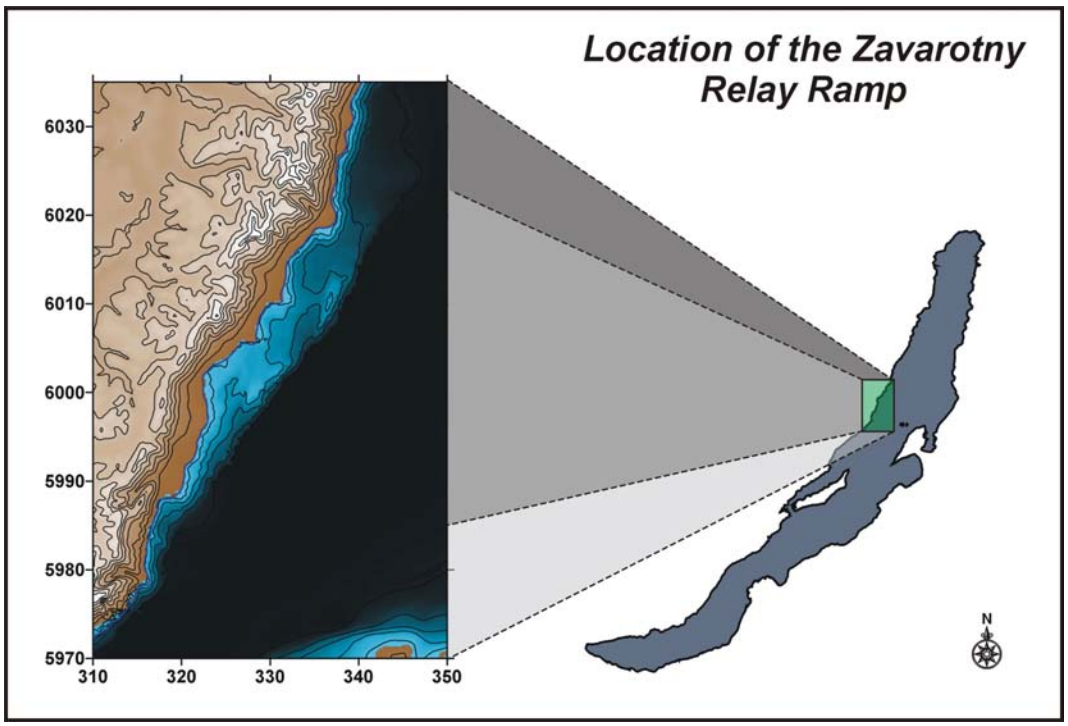

Figure 4.1: *Location of the relay ramp of Zavarotny in the northern part of Lake Baikal.*

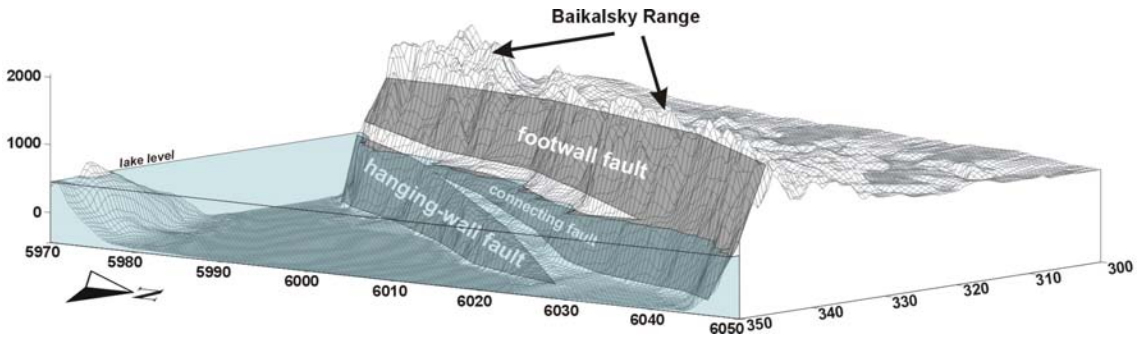

Figure 4.2: *Three dimensional representation of the relay ramp between two segments of the Baikalsky fault.*

Suite software from Seismic Micro-Technology. The seismic sections have a theoretical vertical resolution of approximately 1 m and the penetration is deep enough to allow the detection of the basement reflector in this area (up to 120 ms sub-bottom depth).

For the onshore part of the ramp, topographical maps (scale: 1/50,000) were digitised in the Royal Museum of Central Africa, and the results were merged with the echo-sounding data. This allowed for the construction of a *digital terrain model* (DTM) that provides a link between onshore and offshore structures (Figure 4.6) (e.g. Delvaux et al., 2000). In this chapter the results of the interpretation of these data sets are presented, together with the analysis of

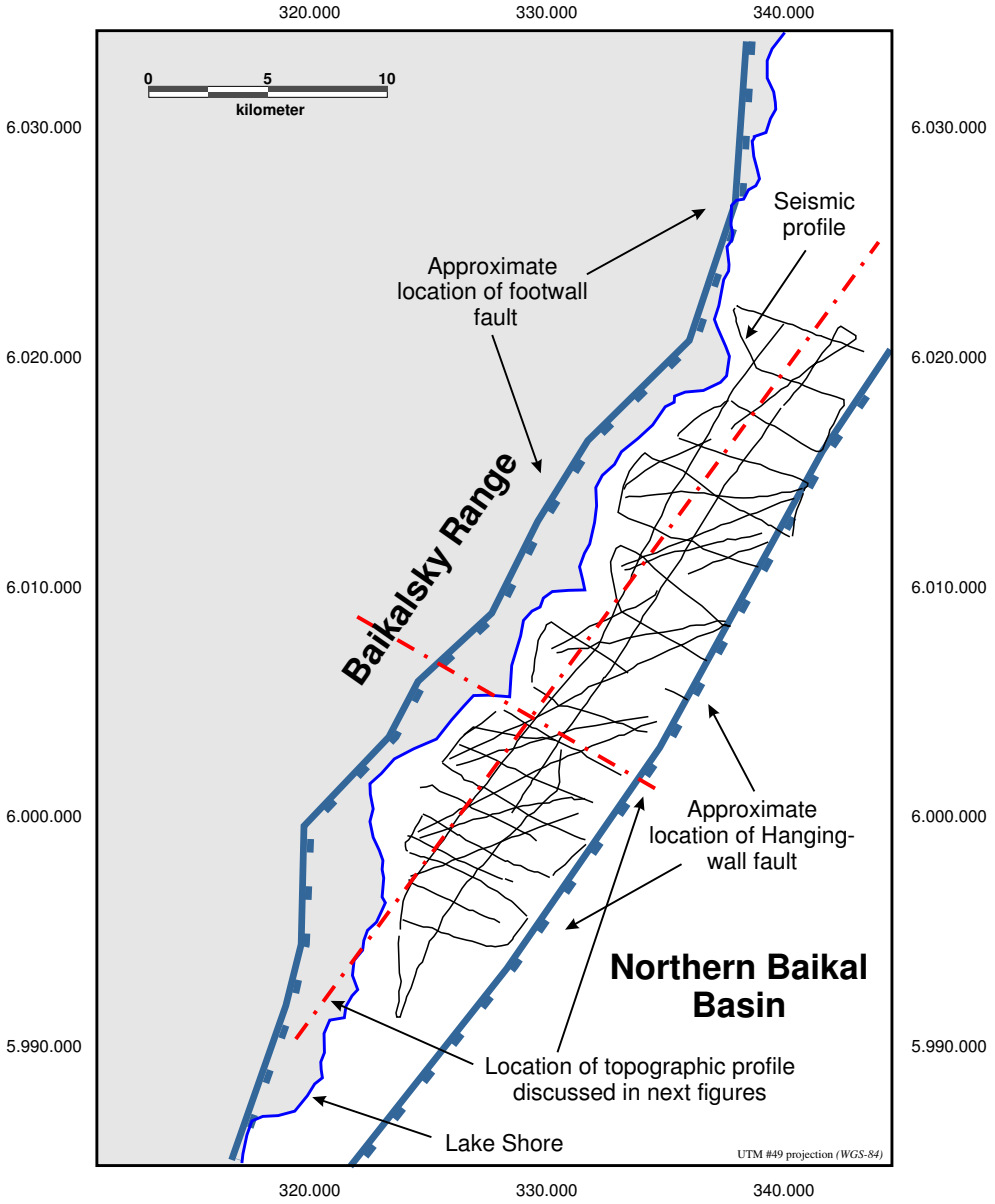

Figure 4.3: *Grid of high-resolution seismic sparker profiles in the area of Zavarotny. The approximate locations of the faults bordering the relay ramp are indicated. The total length of the profiles is ∼300 km. The dashed red lines show the location of the topographic profiles in figure 4.4 and 4.5.*

satellite imagery (RESURS mk-4 images with a 10 m spatial resolution). These images were made in 1996 and provided by the GIS-centre of the United Institute of Geology, Geophysics and Mineralogy in Novosibirsk.

4.2 Morphology of the Zavarotny area

The area of Zavarotny is a ∼40 km×∼10 km tilted ramp structure between 2 fault segments of a major large displacement rift boundary fault (Baikalsky Fault). The segment of the Baikalsky fault in the south of Zavarotny has a different orientation from that in the north (respectively N45°E and N15°E), but they are almost parallel within the zone of overlap. The southern segment (hanging-wall fault) terminates in the lake where it dies out towards the north after ∼35 km. The main fault on land (footwall fault) corresponds to the leading border fault farther to the north. Both faults dip towards the south-east.

A topographical cross-section (figure 4.4) shows the ∼10 km wide platform that has formed between the two main faults. The surface of the platform appears to be slightly tilted towards the hanging-wall fault. The cross-section also reveals the presence of a topographic step (at a distance of around 7000–8000 m in the profile), which is considered here as part of the relay ramp because of its small dimensions compared to the main faults. This topographic step corresponds more or less to the present-day lake border (figure 4.2). Matton and Klerkx (1995)

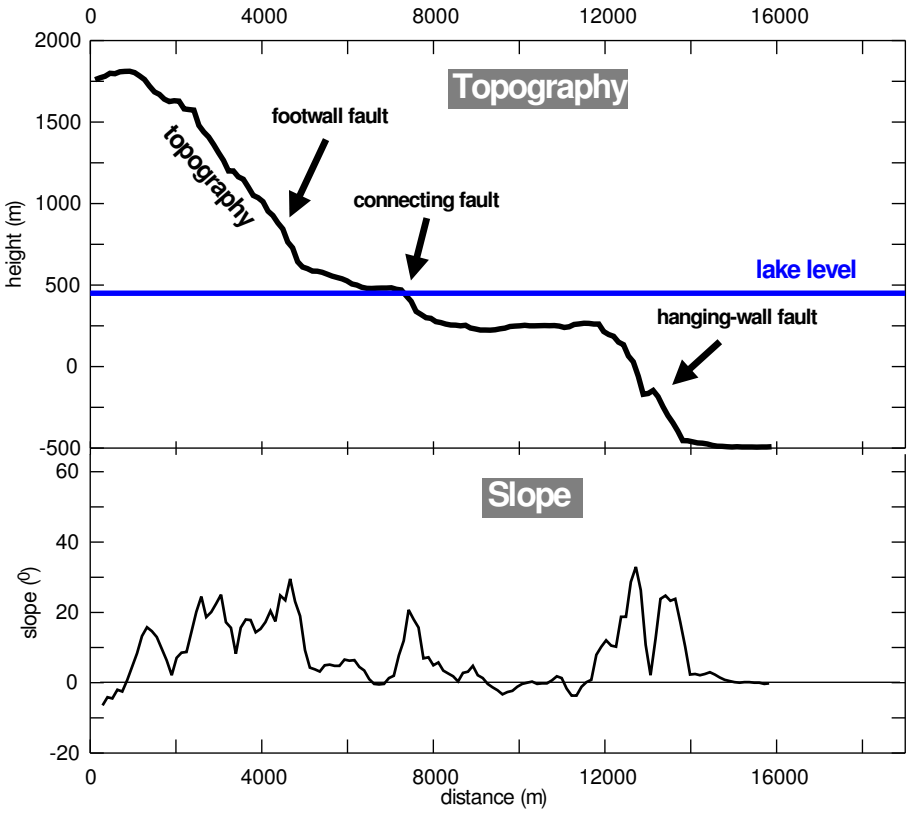

Figure 4.4: *Topographic profile crossing the ramp in Zavarotny (see figure 4.3 for its location). The lower part of the figure shows the variation in slope along the profile (the graph is a running average of the actual "noisy" slope variations). This figure shows that the connecting fault is minor compared to the major faults and therefore it can be considered as part of the ramp.*

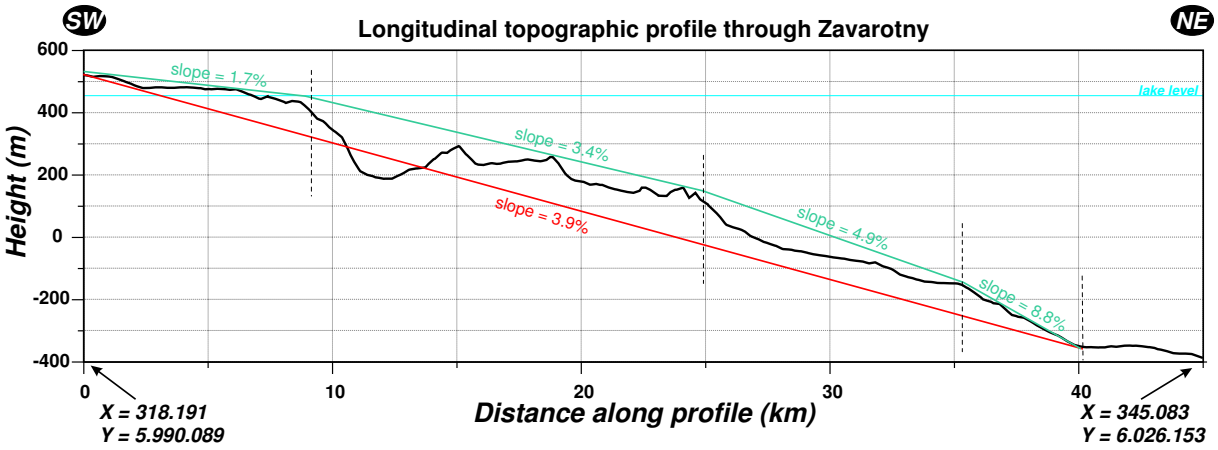

Figure 4.5: *Longitudinal topographic section through the Zavarotny relay ramp. The location of the profile is indicated in figure 4.3. Four zones illustrate the different slope values in the ramp: lowest values for the slope are found in the upper part of the structure, and the values increase towards the lower parts.*

have interpreted this step as a normal fault, and they interpreted the actual relay ramp as a structure that had formed between this "middle fault" and the hanging-wall fault, whereas the onshore part remained relatively undeformed and flat (this is discussed further in section 4.4.2). They referred to the whole structure — which in this work is interpreted as *the* relay ramp — as a complex relay zone.

A longitudinal elevation profile shows that the highest part of the ramp, which is approximately 50 m above the lake level, is located at the southwestern limit of the overlap zone (figure 4.5). The depth of the ramp gradually increases towards the northeast, where it eventually reaches a value of ∼800 m below lake level (figure 4.5). The longitudinal topographic profile of the ramp can roughly be subdivided in 4 zones, characterised by slightly different average slope values. As seen in the figure, average elevation gradients are lowest in the southwestern part of the ramp (1.7%), and they increase towards the northeast (respectively 3.4%, 4.9% and 8.8%).

On a smaller scale, local variations in topography are apparent in the ramp. These variations are superimposed on the overall elevation change, and they result in a rather rough surface morphology of the ramp. In the offshore part of Zavarotny different small basins have formed. These structures are discussed further in sections 4.3.1 and 4.3.2.

In general the morphology of the onshore part of the ramp is more smoothed than the offshore part. During field investigations in this onshore area, small surface breaks have been reported, which are caused by movements on faults with orientations oblique to the main faults of the Zavarotny ramp (Matton and Klerkx, 1995).

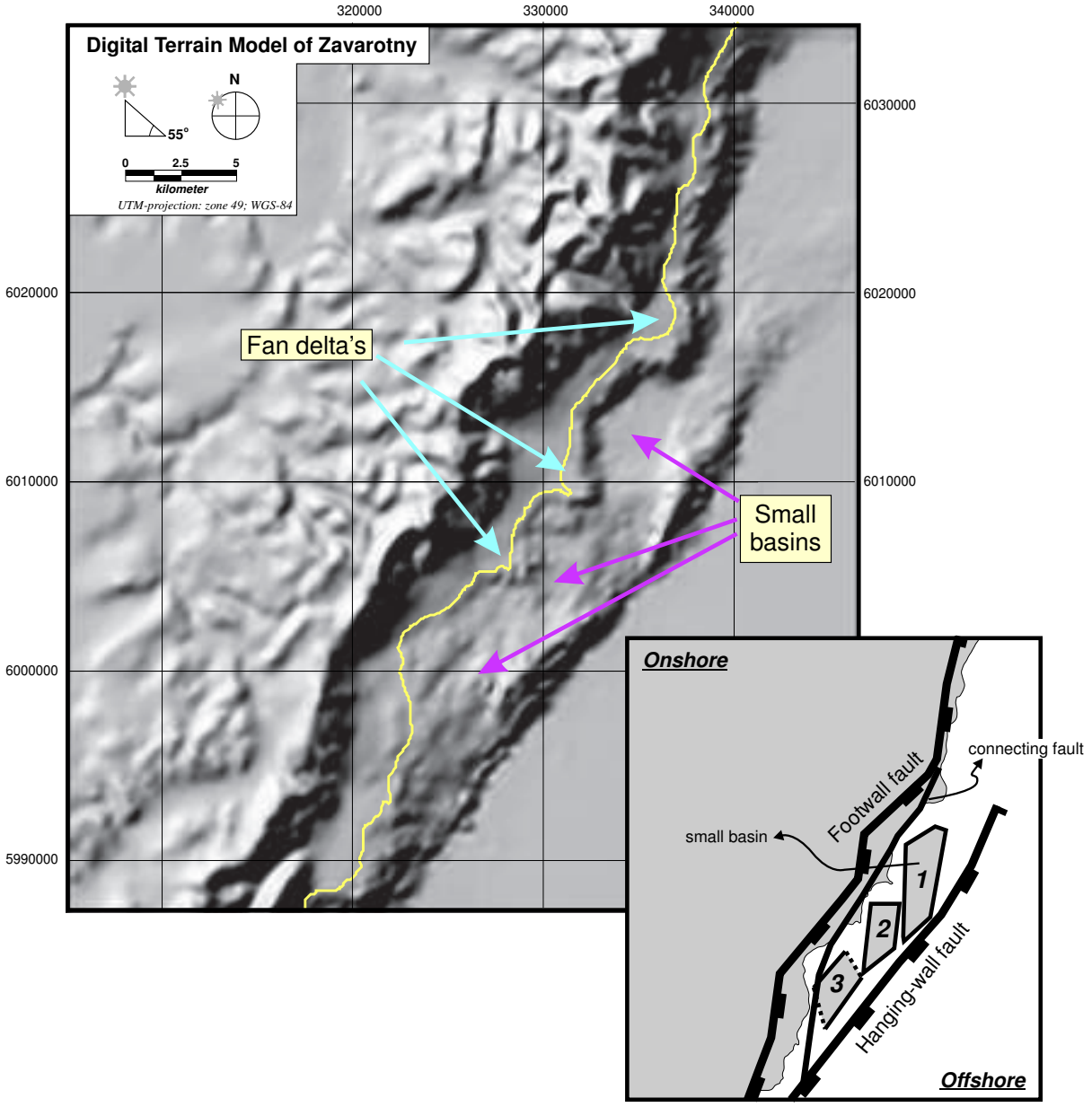

Figure 4.6: *Shaded relief representation of the digital terrain model of Zavarotny. The model was constructed by combining bathymetric data from echo-sounding profiles with digitised topographic maps (1/50.000). The inset illustrates the general structural interpretation of the area.*

4.3 Structural interpretation

4.3.1 Interpretation of Digital Terrain Models (DTM)

The general morphology of the Zavarotny relay ramp has been described in section 4.2. There,

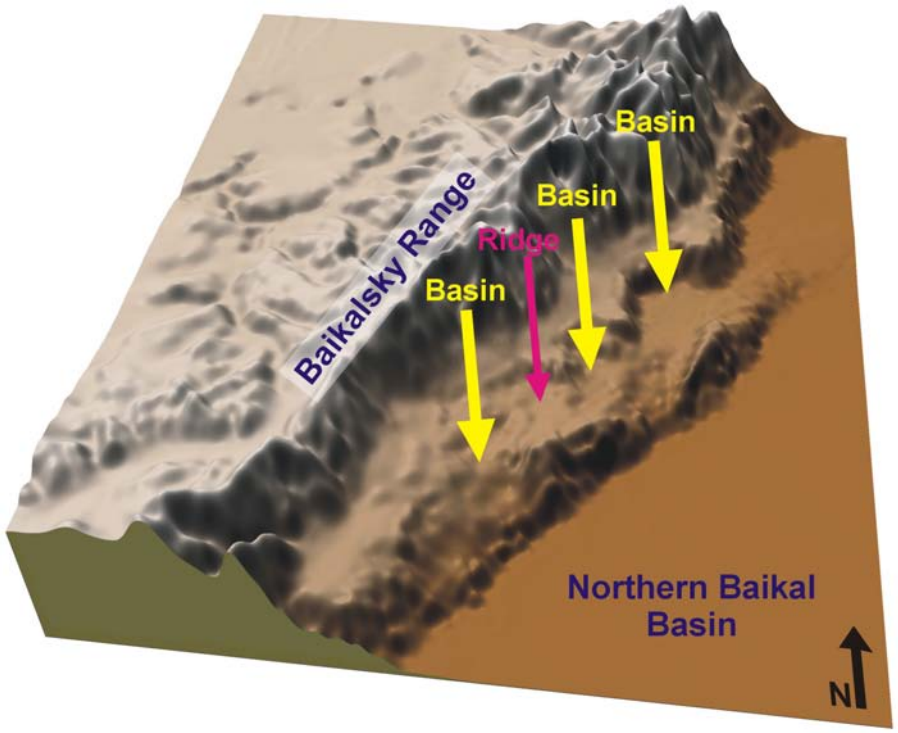

Figure 4.7: *3D surface view of the digital terrain model of Zavarotny. The different basins in the ramp are indicated (see the table below for their characteristics).*

it was already shortly mentioned that the lake-floor topography between the two offshore faults shows some distinct small basins (figures 4.6 and 4.7). These basins have been called *embryonic* basins by Matton and Klerkx (1995), and have thus been interpreted as young structures in an early evolutionary stage. A total of three relatively large basins can be recognised, which slightly change their orientation throughout the ramp, from a NE-SW orientation in the southern part to a more or less N-S orientation in the north (see inset in figure 4.6).

Basin 1[1]	**Basin 2**	**Basin 3**
width = 4.4 km	width = 2.2 km	width = 3.1 km
length = 9.1 km	length = 5.6 km	length = 5.6 km
basin axis = N2°W	basin axis = N5°E	basin axis = N35°E

[1] *Basin numbering is shown in the inset of figure 4.6*

Inside the southern basin three topographic jumps can be identified that locally delimit smaller basins. The orientation of two of these smaller basins differs slightly from the orientation of the southern basin itself and of the third small basin (respectively N20°E and N35°E). From

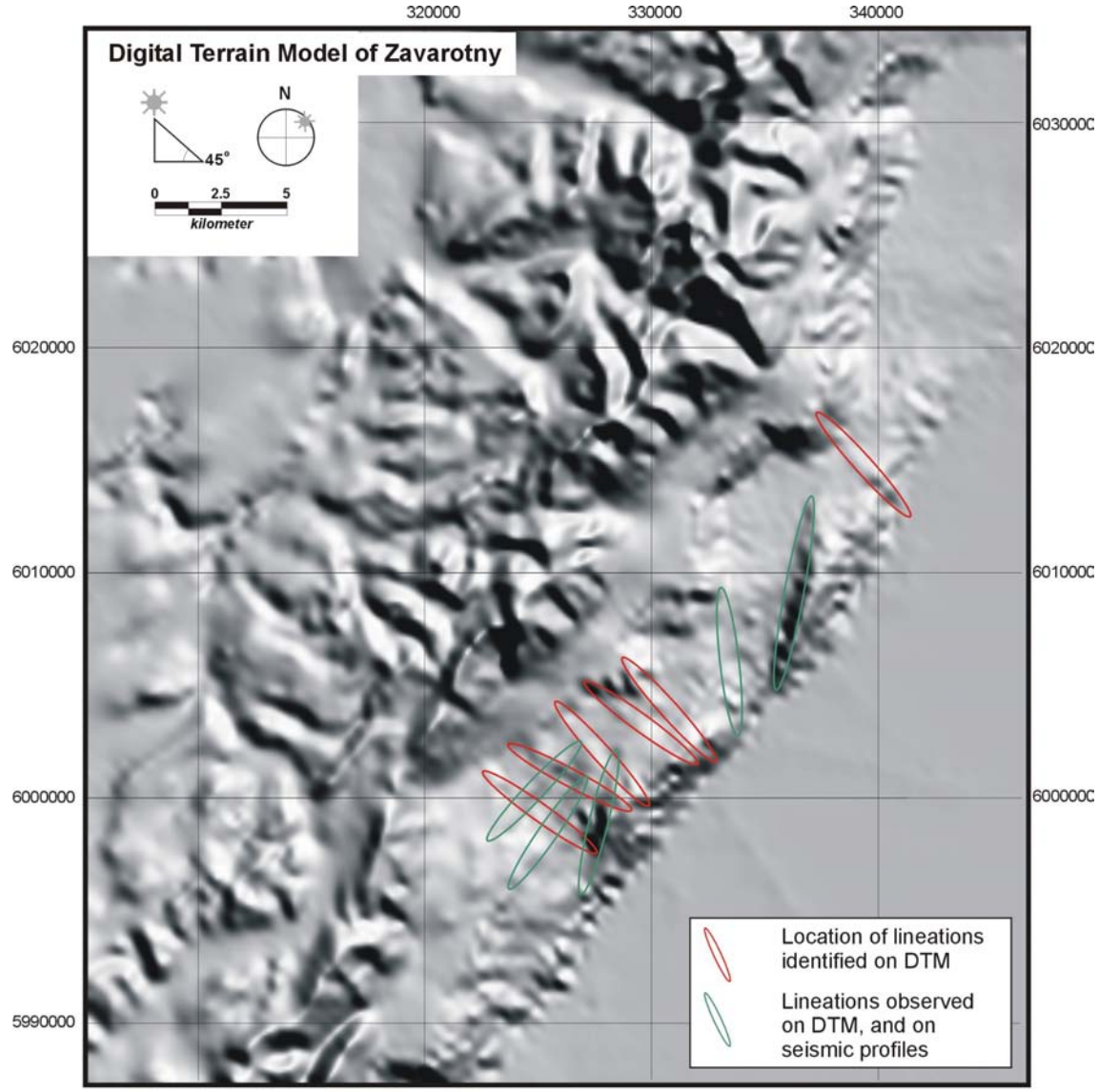

Figure 4.8: *Digital elevation model of Zavarotny, "illuminated" from a different direction compared to figure 4.6. In this figure a series of lineations are seen (some of which have been indicated), which strike almost perpendicularly to the main faults. Other illumination directions allowed to identify additional lineations in Zavarotny. A rose-diagram of all offshore and onshore directions is represented in figure 4.18.*

the interpretation of the seismic profiles, it is clear that the genesis of the different basins in Zavarotny is not the same everywhere in the ramp (see section 4.3.2).

Analysis of the bathymetric part of the digital terrain model allowed to trace linear structures that could not be correlated between different seismic profiles. In total 32 of such lineations were identified, 10 of which were also recognised as real faults on the seismic profiles (see Figure 4.14). Examples of some of these lineations are included on the DTM in figure 4.8. Because of their

limited morphological expression, the lineations could only be made visible by illuminating the elevation model from different directions. A rose diagram representation of all the directions of the observed lineations is presented in Figure 4.18 and discussed later in this chapter (section 4.3.3) parallel with the onshore interpretation.

4.3.2 Interpretation of seismic profiles

By picking the acoustic basement reflector on the high-resolution seismic profiles it has been possible to visualise the basement surface of the relay ramp. Although there has been deposition of sediments in the observed small basins described in 4.3.1 (e.g. see the seismic profiles in figures 4.9–4.13), there is still a strong resemblance between the morphology of this basement surface and that of the lake floor (compare figures a and b in 4.14). This suggests that the ramp is still actively deforming and that the sedimentary infill has not smoothed out the basement morphology. The seismic profiles also provide evidence that the "embryonic" basins observed in the ramp are bordered by a series of faults (e.g. Figure 4.9 – 4.13). The fault map (Figure 4.14d) shows the areal correlation of the most important faults that cause deformation of the basement in the ramp.

In the northern part of the ramp, a topographic step is produced by a NS-oriented fault, dipping towards the east. Also on neighbouring profiles, this fault can be traced and it links up with the major hanging-wall fault in the south. Towards the north, it dies out, not revealing any linkage with the footwall fault. The fact that it splays from one of the major faults, and propagates towards the other, strongly suggests that it is a developing through-going fault, but has not yet caused the final hard linkage stage of the relay ramp. The largest 'embryonic' basin of the ramp is bordered in the west by this fault. The eastern limit of the basin is formed by an elevated basement-high near the hanging-wall fault.

On seismic profile number 49, which strikes normal to the major faults in the southern part of the relay ramp, a series of faults is seen that dip antithetically to the main faults (Figure 4.15). The lack of corresponding synthetic faults and the tilted orientation of the thin sedimentary cover indicates a tilted block geometry. This block tilting is responsible for the formation of the small basins (half-grabens) in this part of the relay ramp (as described in 4.3.1). The strike of these faults (being more or less NNE) seems to correspond to a pre-existing basement fabric observed onshore on satellite images (see Figure 4.17). The outer faults on seismic profile 49 are interpreted here to be the most important, and the "half-graben" structures therefore form sub-basins in the larger basin of the southern part of the ramp (as interpreted in Figures 4.6 and 4.14d). In the other ramp basins the same type of half-graben geometry is not observed.

The detailed sedimentary infill of the small basins shows alternating periods of deposition and non-deposition (figure 4.16). For this reason the short gravity cores that are available from the Zavarotny area are insufficient to construct an age model for the whole sedimentary sequence. Moreover, due to the specific sedimentation environment of a relay ramp, no age information could be obtained by correlating units from inside the ramp with units outside. Therefore the different deformation stages of the ramp could not be dated (absolutely or relatively), nor correlated to other events in the evolution of the Baikalsky Fault Zone.

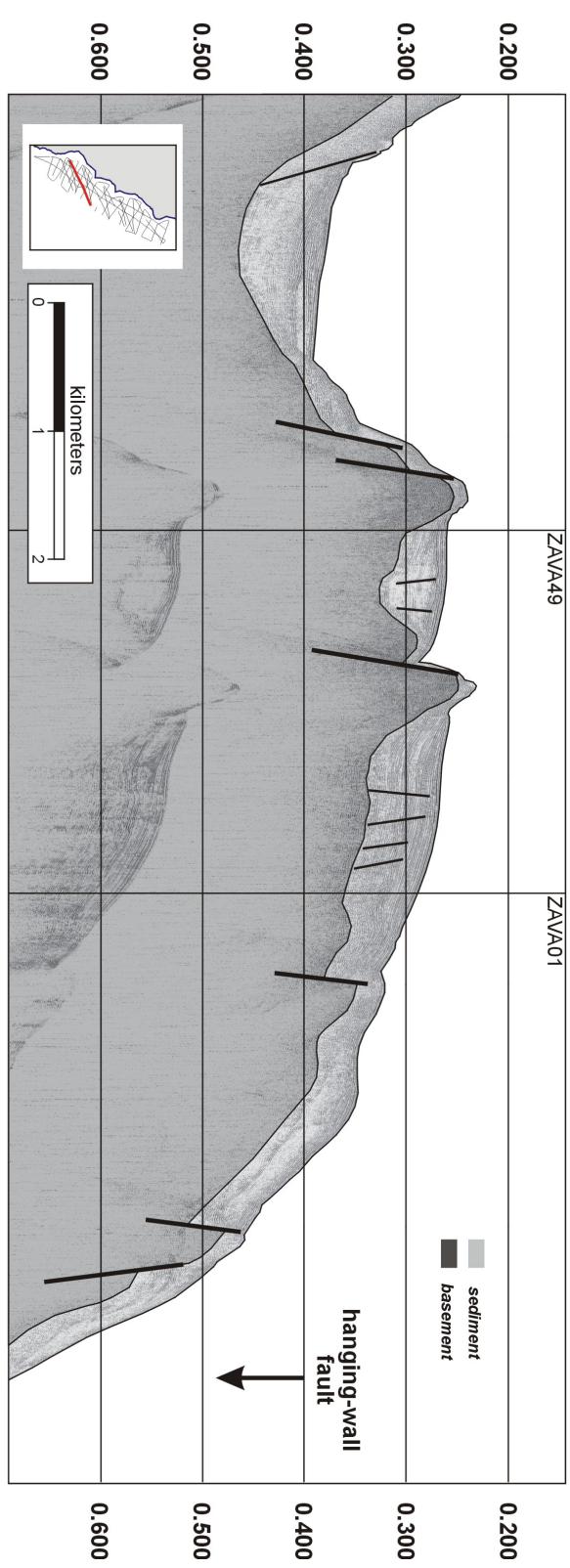

Figure 4.9: *High-resolution seismic profile (ZAVA015) showing some of the fault bounded basins within the relay-structure. Also from this profile the strong correspondence between the lake-floor morphology and the basement morphology can be seen.*

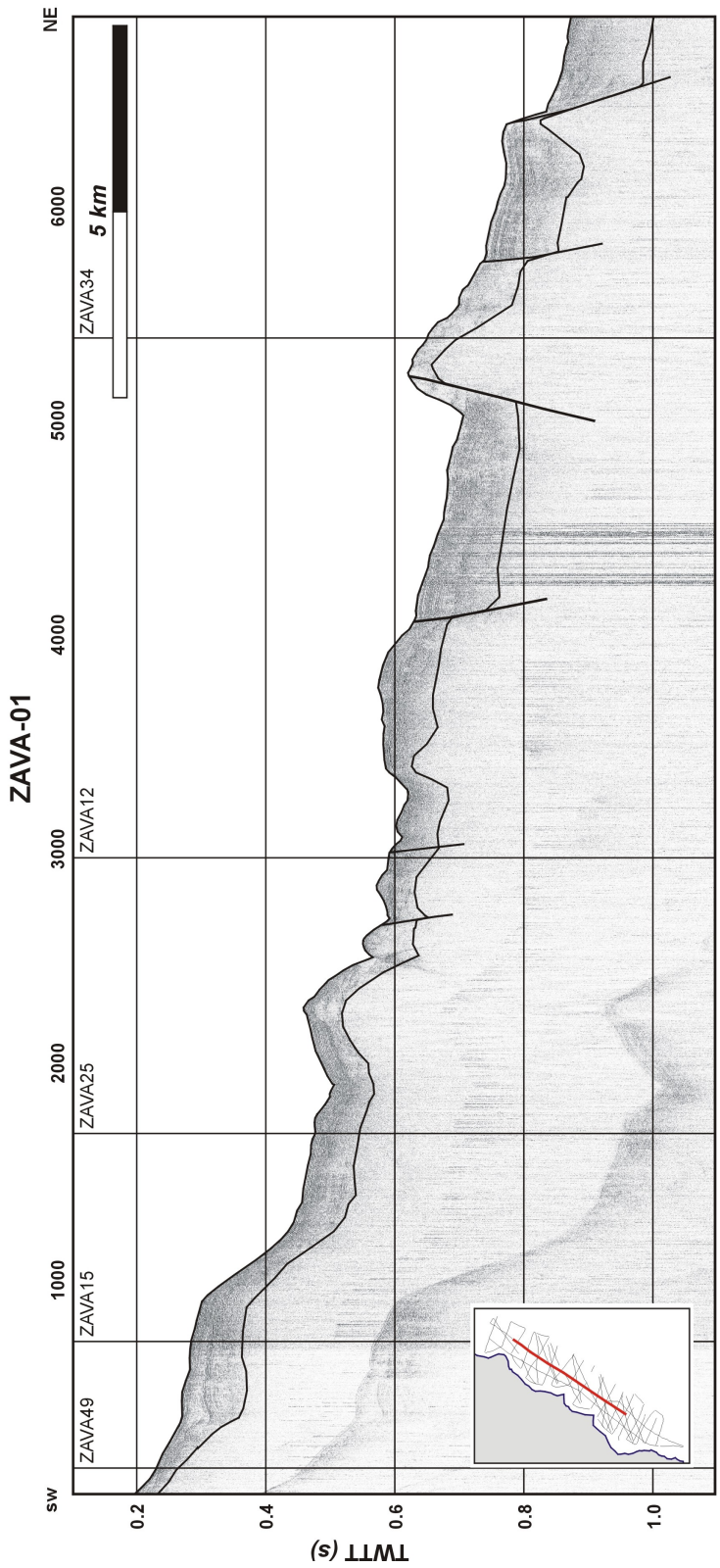

Figure 4.10: *High-resolution seismic profile (ZAVA-01). The profile crosses the relay ramp longitudinally.*

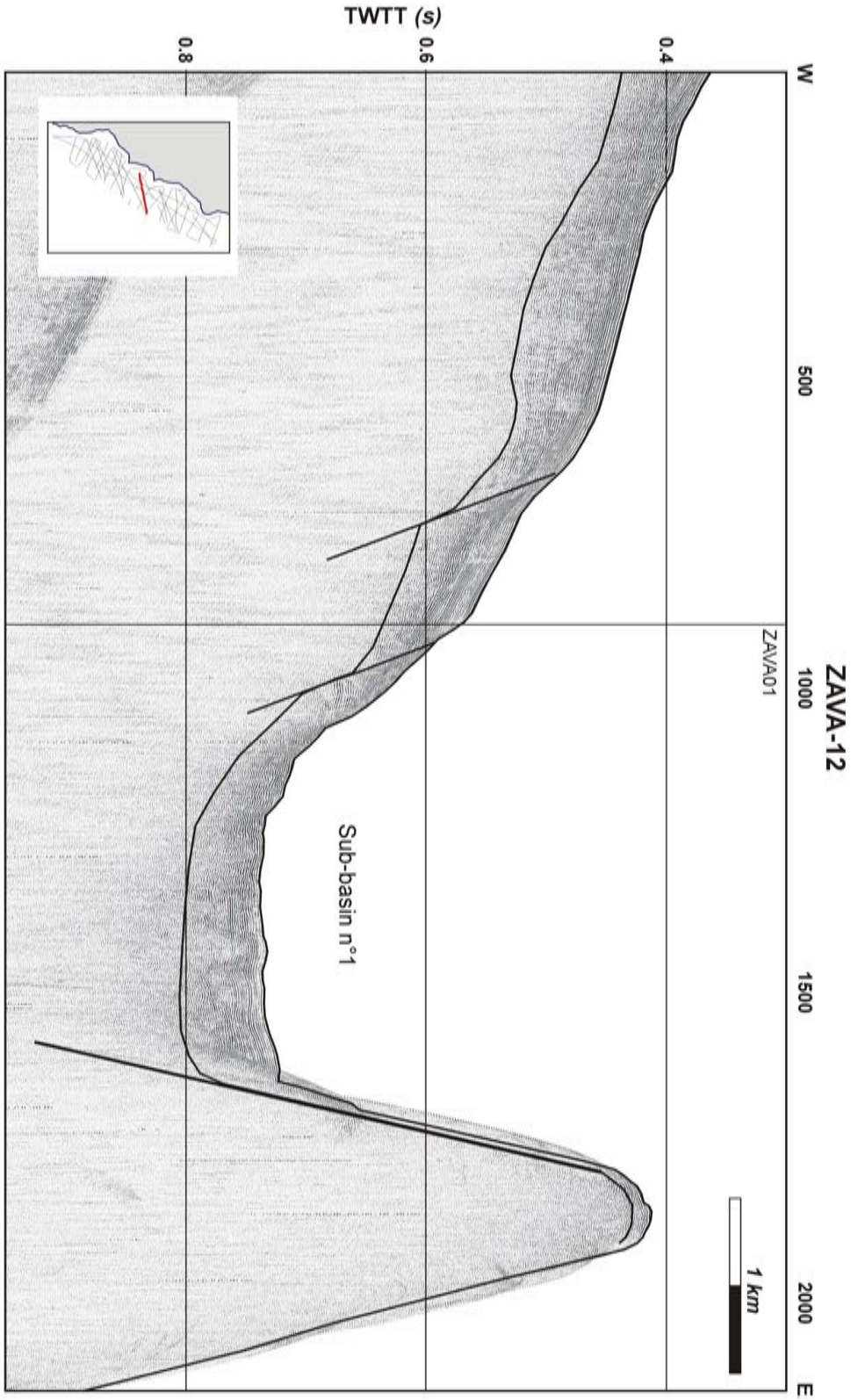

Figure 4.11: *High-resolution seismic profile (ZAVA-12). The profile was shot in sub-basin 1 of the relay ramp.*

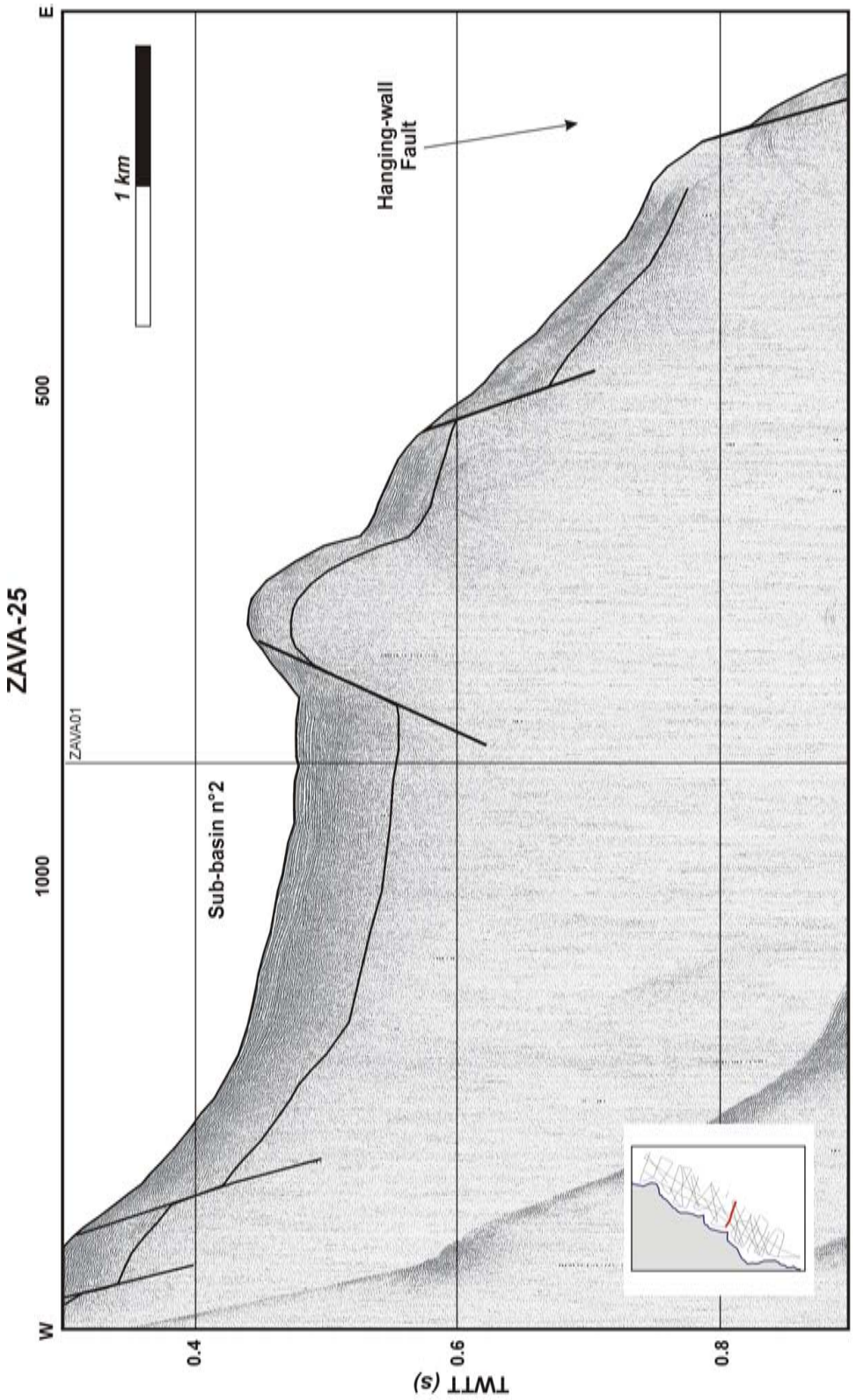

Figure 4.12: *High-resolution seismic profile (ZAVA-25). The profile was shot in sub-basin 2 of the relay ramp.*

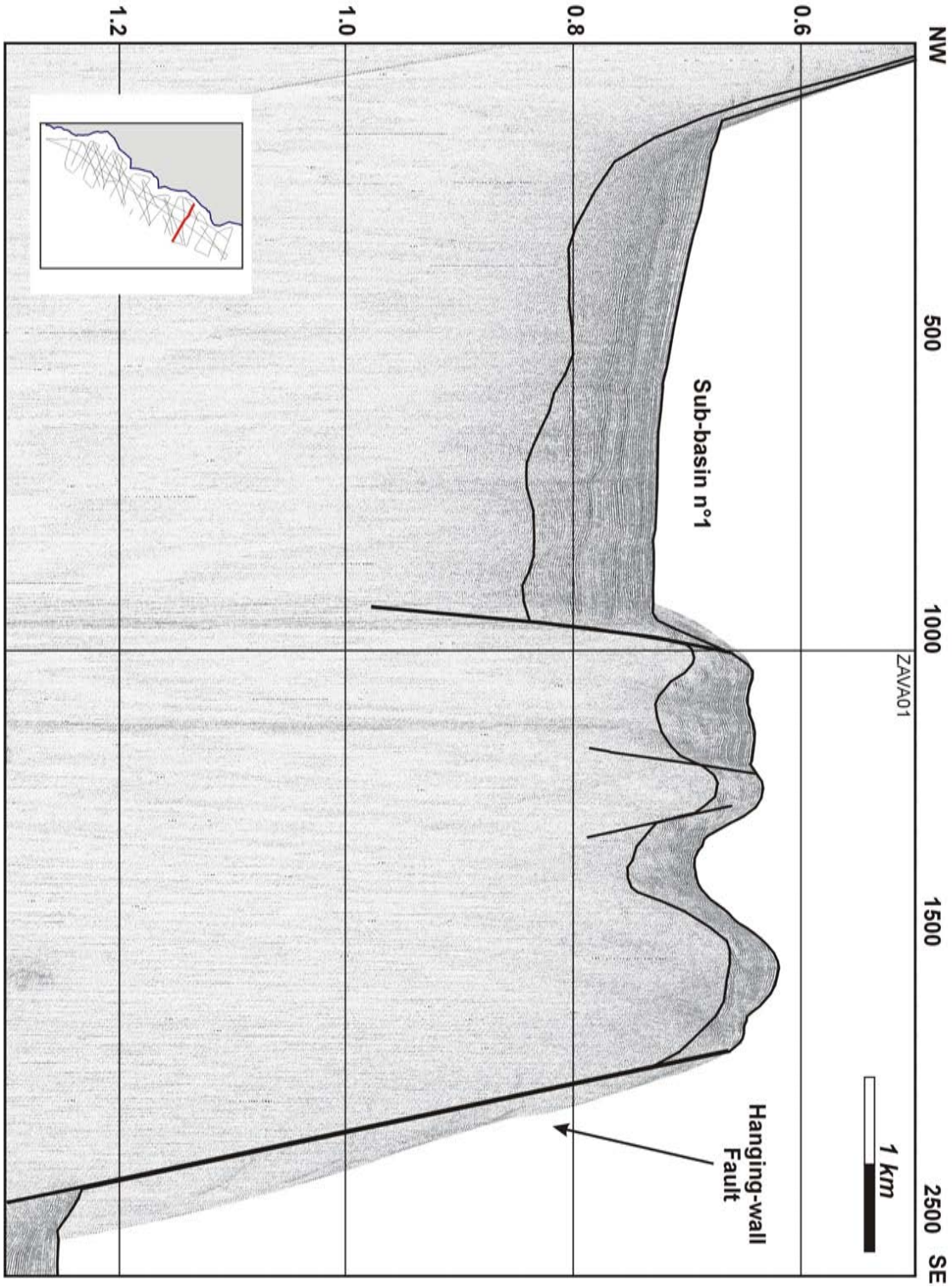

Figure 4.13: *High-resolution seismic profile (ZAVA-34). The profile was shot in sub-basin 1 of the relay ramp.*

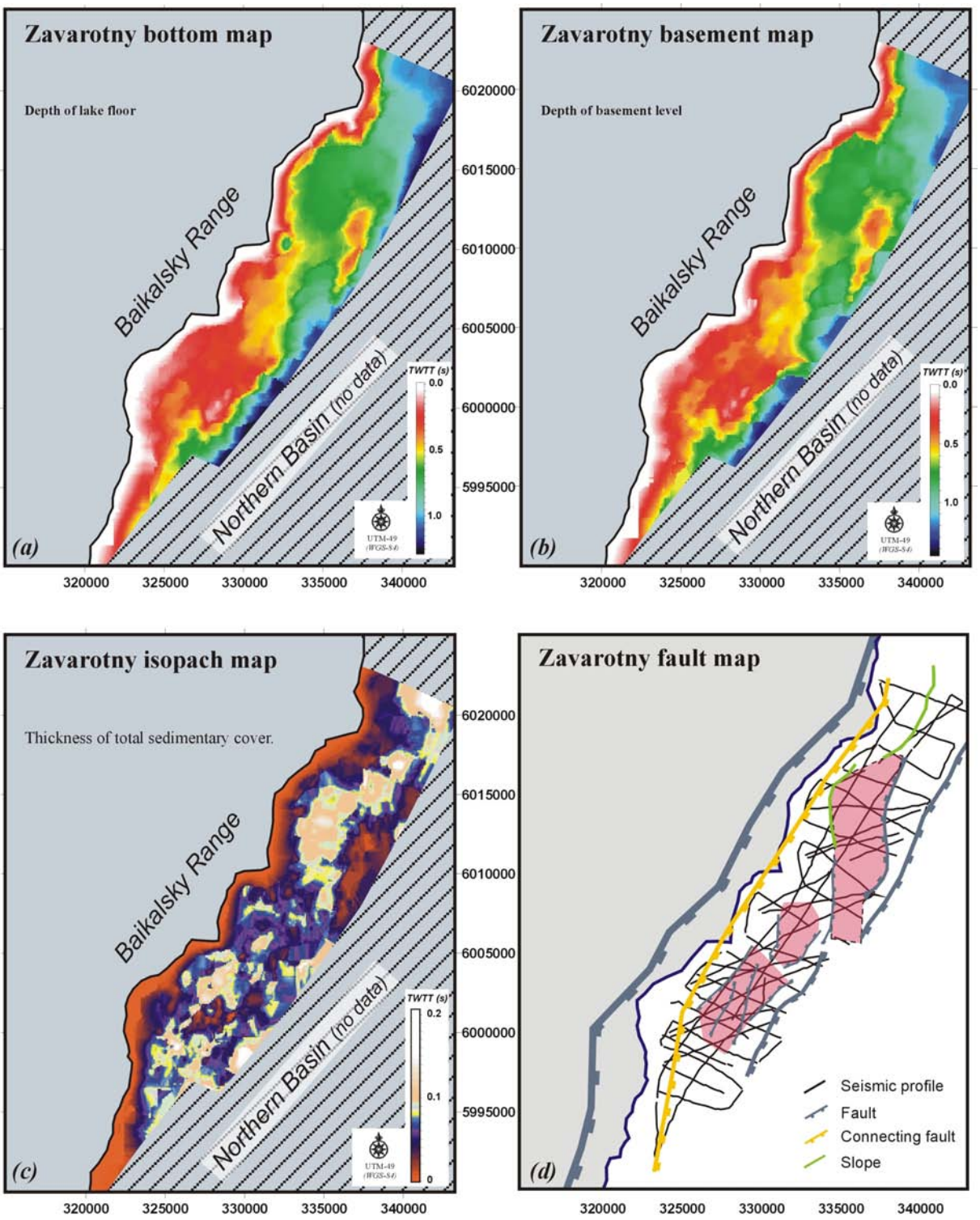

Figure 4.14: *Maps produced from the seismic profiles in Zavarotny: (a) depth of the lake floor, (b) depth of the acoustic basement level, (c) isopach map and (d) fault map. Depth and thickness are expressed in two-way-travel time. The strong similarity between the lake floor morphology (a) and the basement morphology (b) indicates that the ramp structure is actively deforming. The fault map (d) illustrates that the basins in Zavarotny are fault bounded structures.*

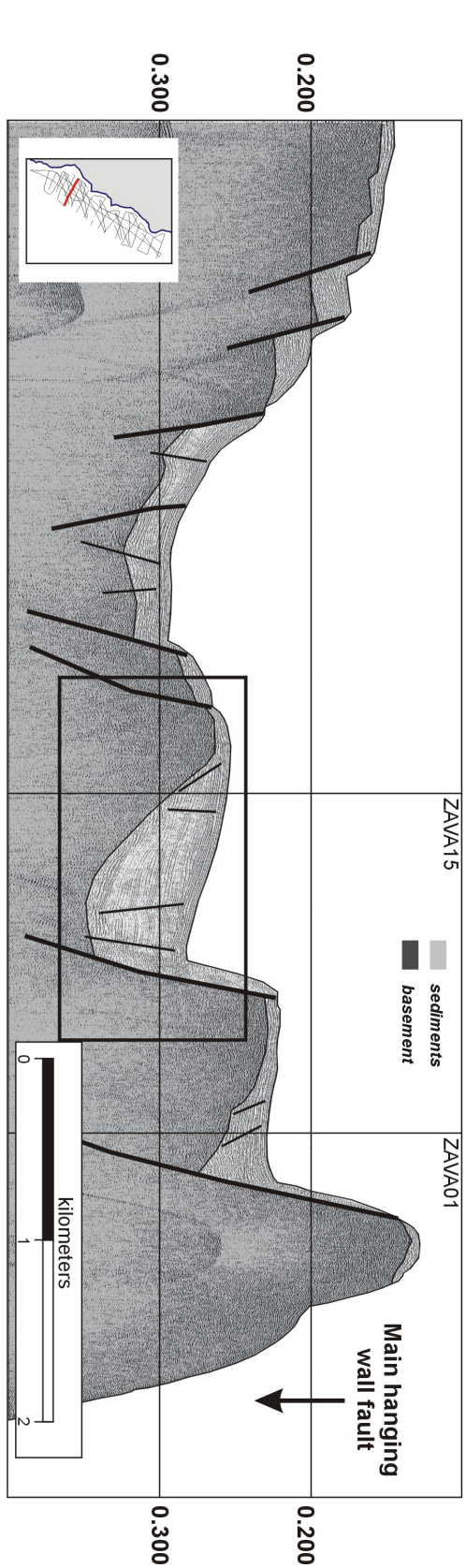

Figure 4.15: *Seismic profile ZAVA049, showing the tilted block geometry of the southern sub-basin (see figure 4.14 for its location. The rectangle marks the location of the detail view in figure 4.16.*

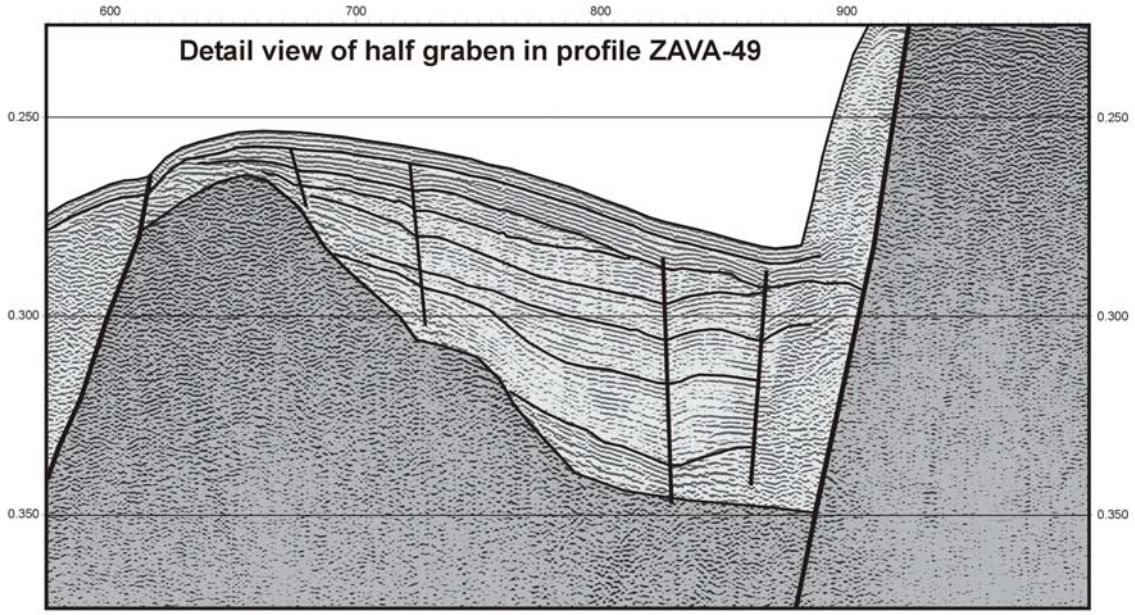

Figure 4.16: *Detailed view of one of the tilted blocks shown on profile ZAVA049. See figure 4.15 for the location.*

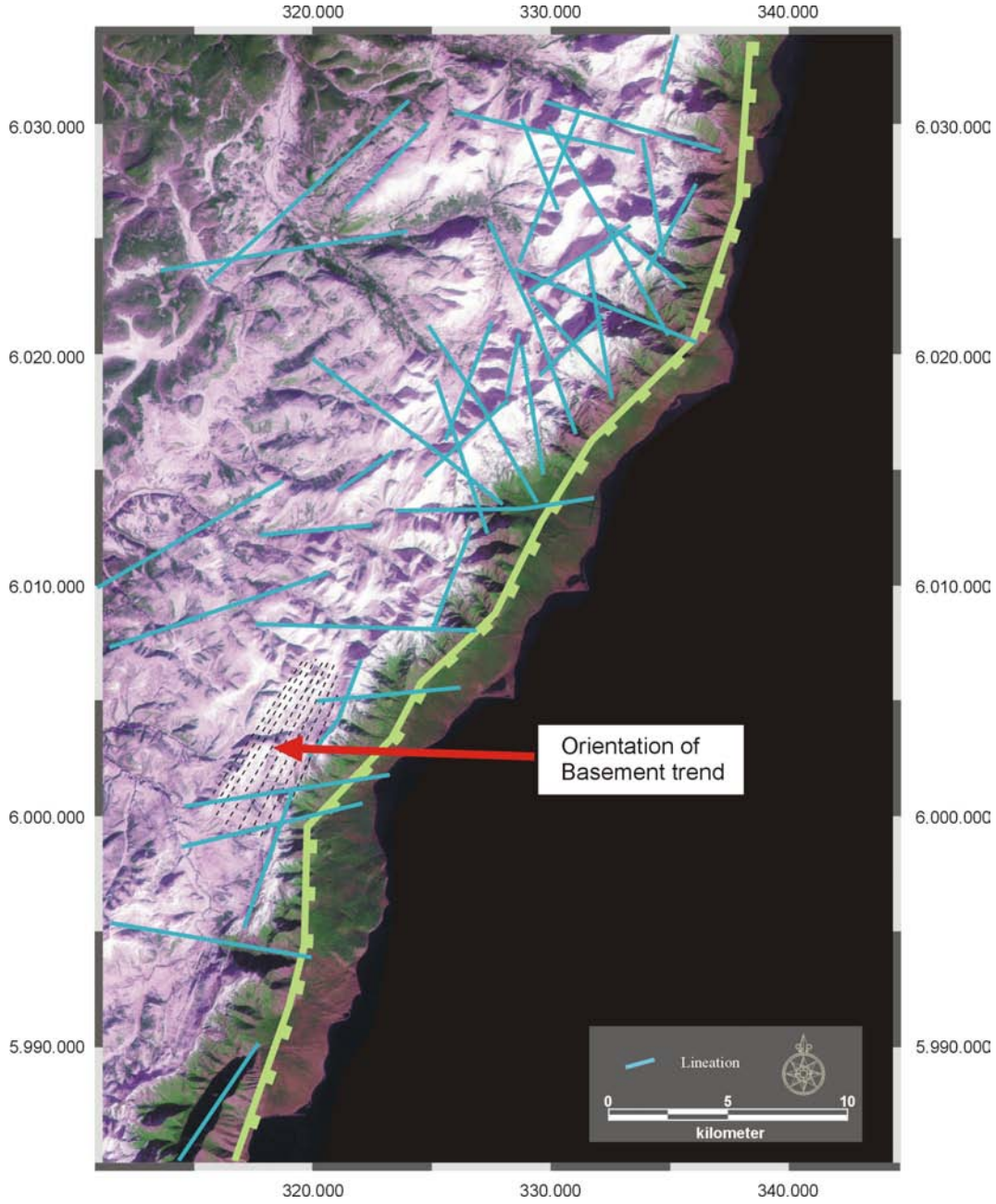

Figure 4.17: *Satellite image of the Zavarotny area, with interpreted lineations. A rose diagram of the lineations is included in figure 4.18.*

4.3.3 Satellite image interpretations

The RESURS mk-4 images illustrate that the major faults of Zavarotny parallel the direction of an older basement structure (Figure 4.17), which closely follows the border of the Siberian

craton (Melnikov et al., 1994). Given the fact that also smaller faults have adopted this basement direction, it is believed that the anisotropic character of the basement strongly influences the development of younger faults. The satellite image however also reveals linear structures striking E-W, at high-angles to the basement anisotropy (Figure 4.17 and 4.18). Although we cannot further determine the nature of these lineaments from the satellite images alone, we observe some of them on the digital terrain model, and therefore they must correspond to topographic height differences. They are, however, less expressed than the lineations that follow the main basement trend. This smaller topographic difference, together with the lower resolution of the DTM compared to the satellite image, could explain why these lineations are not all seen on the DTM.

Figure 4.18 presents a rose diagram of the onshore and offshore lineations observed on the satellite image and/or the DTM. This figure clearly illustrates that both areas have lineations that follow the direction of the main faults (i.e. the hanging-wall and footwall faults) and observed basement fabric (∼N40°E). Both areas contain, however, also a second set of lineations: in the offshore part their direction is more or less perpendicular to the major faults (∼N135°E), whereas in the onshore part they are oriented almost east-west, striking with a ∼45° angle to the main faults (figure 4.18). Because the offshore direction is rather unimportant in the onshore area, it has been interpreted as representing local deformation in the ramp.

4.4 Discussion

The following observations have been made so far in Zavarotny:

- A relay ramp has developed between an onshore footwall fault and an offshore hanging-wall fault.
- The ramp dips towards the northeast.
- A large topographic step has formed in the ramp, which links the footwall fault with the hanging-wall fault.
- In the morphology of the relay ramp, three distinct basins have been observed, which are bordered by faults.
- Some of the faults in the relay ramp have a strike direction which is more or less parallel to the main faults, whilst others strike almost perpendicularly to them.
- The relay ramp is an actively developing structure, with a surface morphology that strongly resembles the morphology of the basement.
- One of the faults in northern part of the relay ramp splays off the hanging-wall fault and propagates towards the footwall fault.

4.4.1 Determining fault interaction in Zavarotny

Strictly speaking, the term “overlap zone” should have been used so far in this chapter, because no displacement transfer between the main faults in Zavarotny has yet been demonstrated. Using “relay ramp” implicitly implies such a displacement transfer.

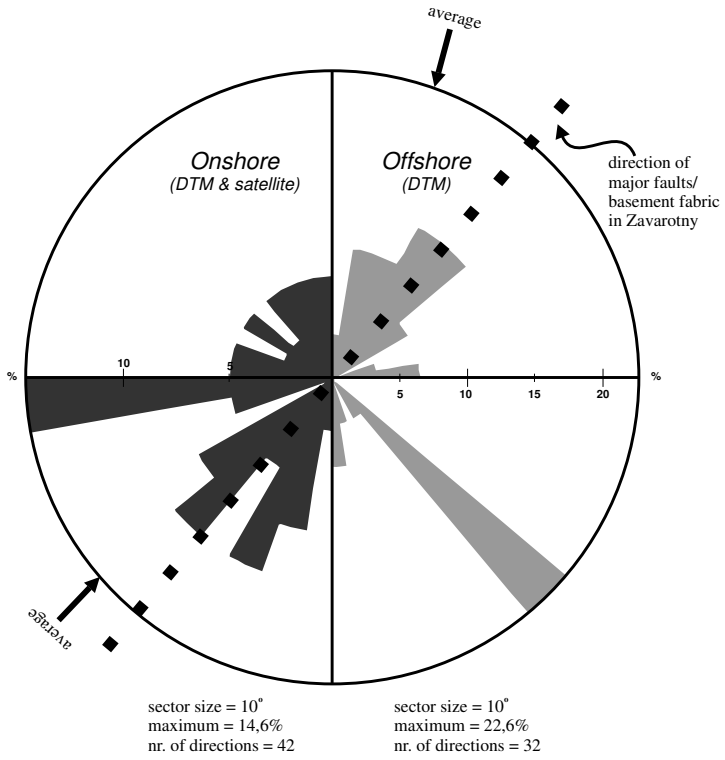

Figure 4.18: *Rose diagram to illustrate the strike direction of the different "lineaments" observed on the satellite image (left part of the diagram) and on the bathymetry of the DTM (right part). In both areas several lineaments have the same orientation as the main faults and basement fabric in Zavarotny. In the onshore part, however, also an east-west direction is important, while a N135°E direction is important in the offshore area.*

As explained in section 2.4.4 on page 54, analysing throw profiles of faults can reveal possible mechanical interaction with neighbours. By drawing height profiles from a digital terrain model of Zavarotny, the approximate throw (i.e. the vertical component of the displacement) along the two segments of the Baikalsky fault was measured (Figure 4.19). For this, only the height difference between the lake floor level on either side of the faults could be used, because due to the particular sedimentation environment in the ramp, other horizons could not be correlated with reflections outside. Figure 4.19a clearly shows that the displacement on the footwall fault is largest where there is no displacement on the hanging-wall fault. As soon as the overlap zone is reached, the displacement on the footwall fault suddenly decreases, whereas the displacement on the hanging-wall fault increases. Farther to the southwest, the displacement on the footwall fault becomes minimal. This demonstrates that in the overlap zone displacement is transferred between both faults. Within the overlap zone, the top of the footwall fault remains at an almost constant height (figure 4.19b).

In view of the strong decrease of displacement of the main faults in Zavarotny in the area of the ramp we can conclude that their throw profiles are at least "tip restricted" according to the

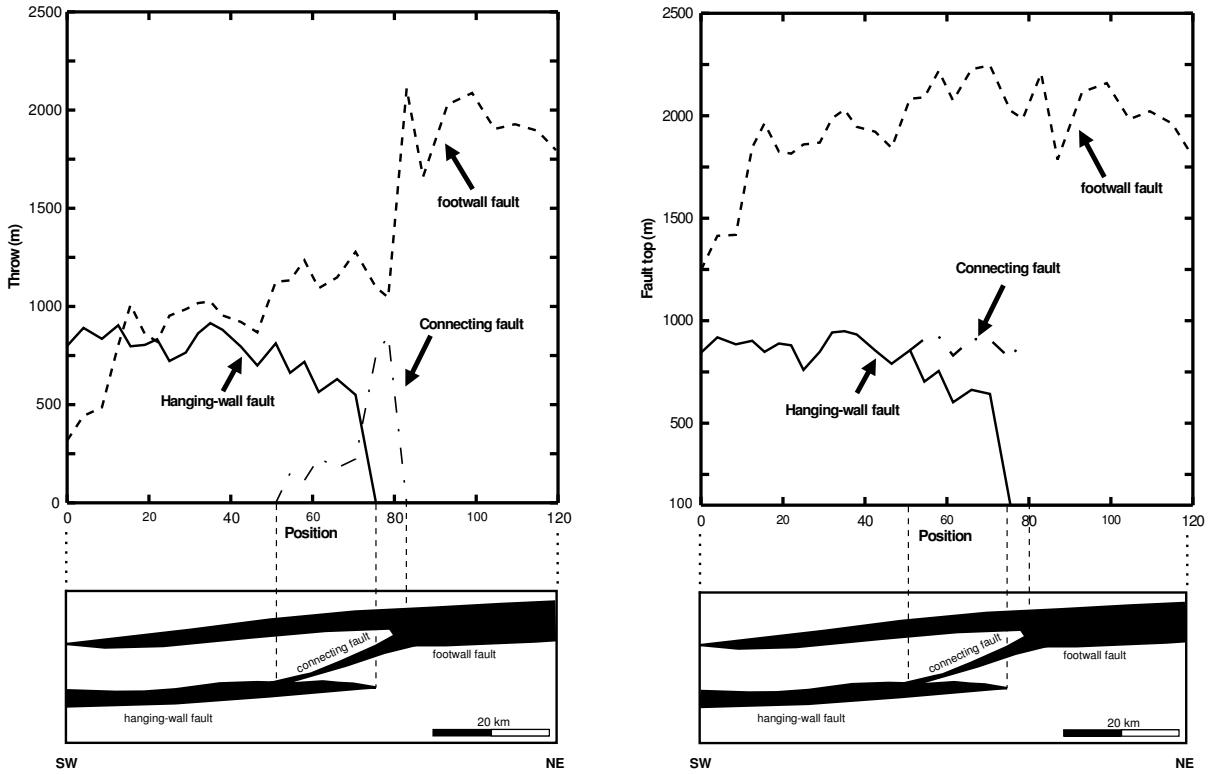

Figure 4.19: *Topographic difference between the top and the base of the main fault scarps in Zavarotny (figure a) and the height of the top of the different fault scarps (figure b). The scheme under the graphs should be considered as an illustration only, here the thickness of the black area is proportional to the throw. The 100m at the base in figure b corresponds to the depth of the lake floor above sea level (≈355 m water depth) near the tip of the hanging-wall fault. Below this value the hanging-wall fault is undefined.*

classification of Manighetti et al. (2001) (Figure 2.18), and that this is most likely the result of their mutual interaction. For these reasons it is justified to call the overlap zone in Zavarotny a relay ramp.

As also mentioned in section 2.4.4, some studies used the separation between faults and the degree of overlap as a criteria to evaluate a possible interaction (e.g. Huggins et al., 1995; An, 1997). For Zavarotny the distance of overlap is 40 km and the separation distance is 10 km, with a ratio of 4 we can assume fault interaction in this case (e.g. Willemse, 1997).

4.4.2 Is the Zavarotny ramp breached?

Important in the discussion of the Zavarotny relay ramp is whether the ramp has been breached or not. This section discusses observations mentioned in the previous sections to argue that the relay ramp is already in a breached stage, and that breaching has been achieved by the development of a connecting fault between the two main faults (see figure 2.22). This conclusion

will be corroborated further by specific observations which support the idea of faulting in the area of this connecting fault.

The difficulty in determining — and proving — whether or not the Zavarotny relay ramp is breached arises from the fact that the interpreted connecting fault is buried, and not covered by seismic profiles. In fact, the interpretation is based on morphological observations only. Matton and Klerkx (1995) have already interpreted the "topographic step" in the ramp as being a fault (their "middle fault"). They interpreted the fault to be "severely segmented by NE trending faults", to explain the observed irregular fault trace. There are, however, several indications that the actual shape of observed topographic step in Zavarotny is determined to a large extent by sedimentary input of clastic material from the nearby Baikalsky range. The main arguments for this are:

(a) the occurrence of two deltaic structures in the ramp and another one farther to the north,
(b) the fact that this relatively irregular step corresponds to the lake shore and
(c) the absence of a well expressed morphology in the onshore part of the ramp compared to that of the offshore area (Figure 4.6).

Most likely, the coarse grained sediments of the Baikalsky range are easily transported on the onshore parts of the ramp, but deposited rapidly when they reach the lake water, forming a relative steep slope ($\approx 30°$).

Although the actual shape of the topographic step is most likely determined by sedimentological processes, as mentioned above, the step is nevertheless interpreted here as being partly related to normal faulting, for the following reasons:

(a) In Figures 4.19 and 4.4 we see that the topographic difference reaches values of about 700 meters, and therefore the deposition of immense volumes of sediment would have been required. If we compare this value with the thickness of fan-delta's in other parts of the western lake border ($\pm$ 50 m e.g. Agar and Klitgord (1995)) it seems unrealistic. Faulting of basement blocks could considerably reduce the amount of sediments needed to achieve the current infill. Other evidence against major erosion of the rift flanks (ie. more than a few hundreds of meters) since the onset of rifting, comes from the analysis of apatite fission track data (Van Der Beek et al., 1996).

(b) In the onshore part of the topographic profile (Figure 4.4) there is a transition from a slightly concave to a more or less flat horizontal shape (around 6000m distance in the profile). This transition could be the result of movements along an underlying buried normal fault.

(c) Onshore topographic profiles, located in the northern part of the ramp and oriented perpendicularly to the main fault strike, reveal distinct local small increases in the slope of the ground surface in this area ($\sim$50% increase of the average slope which is $\pm$7%) (figure 4.20). This slope variation is not observed in the onshore part of the southern half of the ramp where the connecting fault is expected to be offshore. Also on the satellite image, sometimes lineations (surface breaks?) are observed at the location of this slope increase (see arrows in figure 4.21).

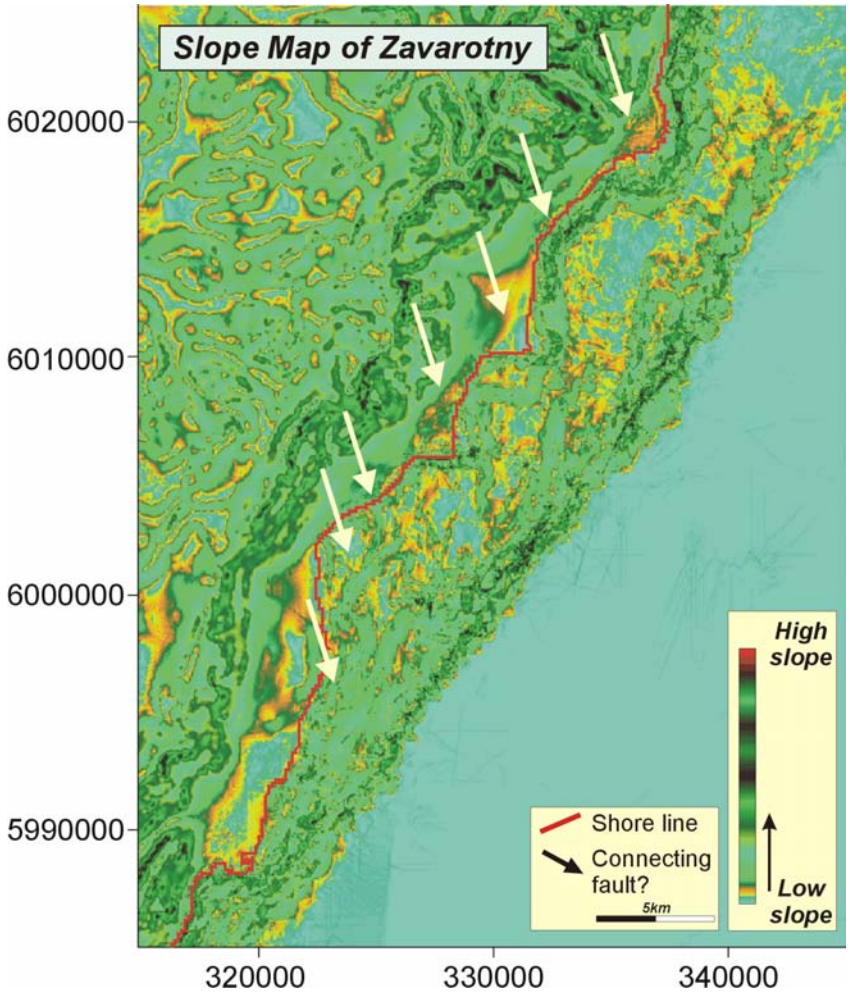

Figure 4.20: *Slope map of the Zavarotny area. In the onshore part, a line can be observed (indicated with arrows) which marks a local variation in slope. This linear pattern can correspond with the interpreted connecting fault in Zavarotny*

(d) Near the southwestern end of the ramp structure a series of north-northeast striking lineations are observed on the digital terrain model (Figure 4.6 and 4.22), which might correspond to recent faulting in this region. Moreover, their position corresponds to where we would expect the connecting fault to reach the hanging-wall fault.

4.4.3 Comparison with existing models for relay ramp evolution

Based on the data and interpretations presented so far in this chapter, a possible evolution scheme has been drawn for the Zavarotny relay ramp (figure 4.23). At least some of the characteristics of this relay ramp do not correspond to observations made in other, small scale, natural relay ramps (e.g. Peacock and Sanderson, 1991, 1994; Huggins et al., 1995); these are discussed

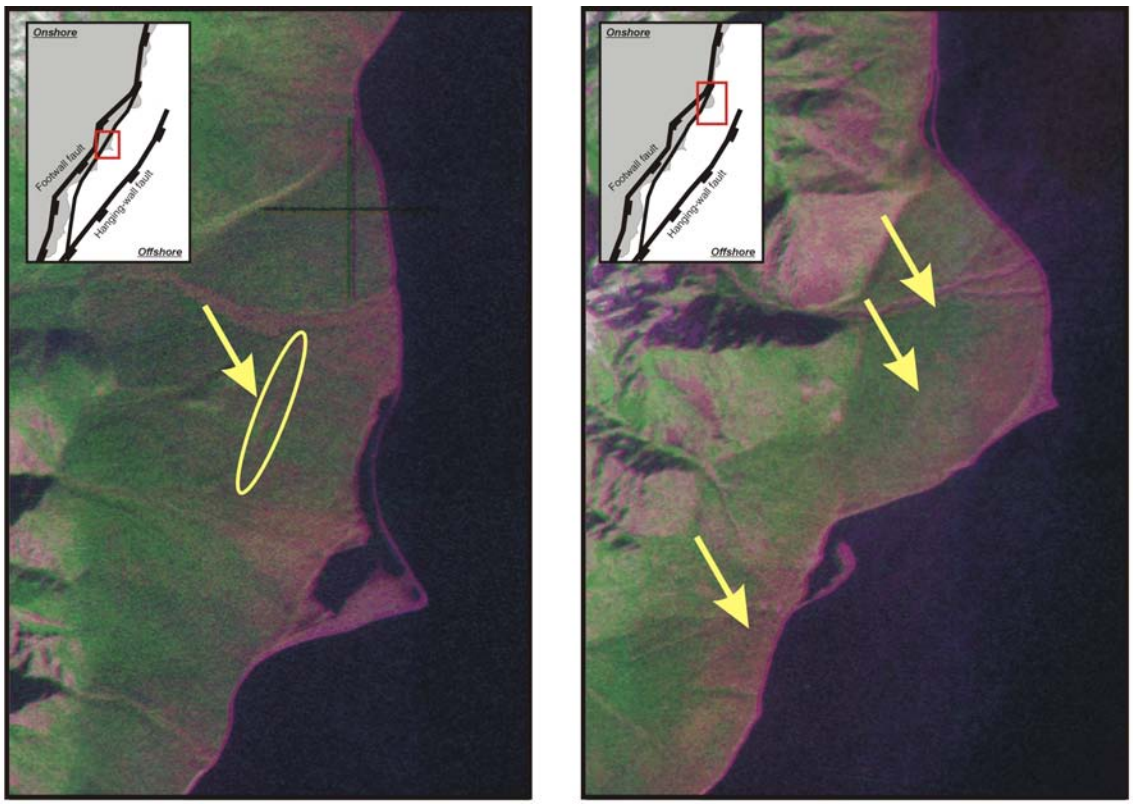

Figure 4.21: *Satellite images of two area's in the northern half of the Zavarotny relay ramp (see insets for locations). Arrows indicate possible signs of active faulting underneath the surface, related to displacements along the connecting fault. The indicated lineations correspond to a local increase in the surface slopes (from an average slope of ±7% to values of ∼10–12%).*

below. It must, however, be said that Peacock et al. (2000b) already found some deviating structures in the large *Hold With Hope* relay ramp and concluded that there is not a complete scale independency for what concerns the internal structure of a relay ramp. The length to width ratio of the Zavarotny relay ramp is ∼4, and corresponds well with published geometries of relay ramps on smaller scale (e.g. Acocella et al., 2000).

If we consider the connecting fault as being part of the whole ramp, this implies that the Baikalsky fault segments are already in the hard-linked stage. In that case one would expect the unused fault-parts to be gradually eroded and finally disappear, with later displacements confined to the new fault. This would not explain the development of the small basins between the connecting and the hanging-wall faults, nor the development of a new secondary through-going fault as observed on the seismic profiles. Therefore, it seems more likely that the main structures in Zavarotny are produced by a combination of soft linkage as well as hard linkage processes, with the development of a new soft-linking relay ramp between the major hanging-wall fault and the observed connecting fault.

The development of the first connecting fault to breach the relay ramp could also be consid-

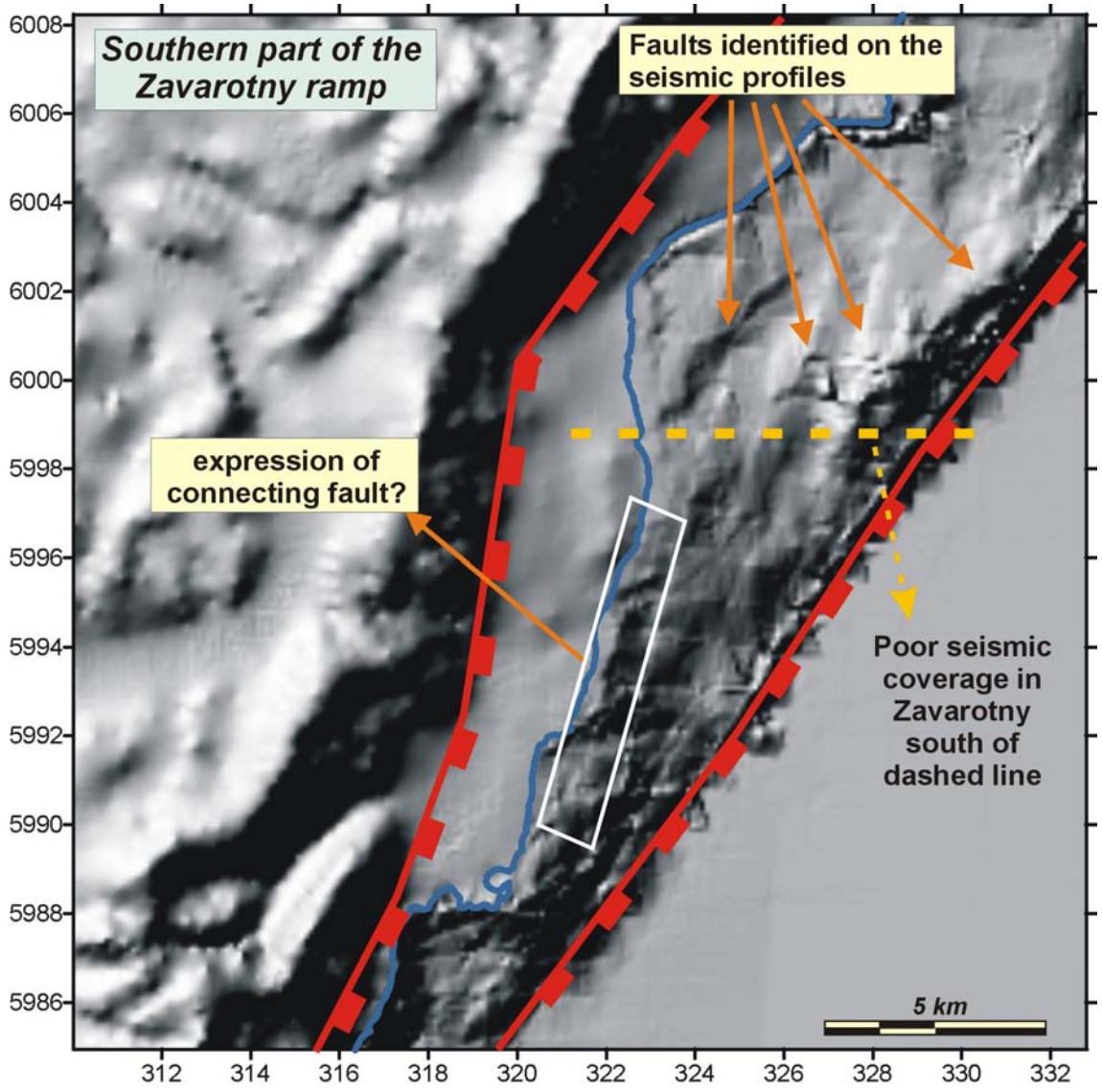

Figure 4.22: *Detailed view of the southern part of the Zavarotny ramp. The available seismic profiles in this part of the ramp are insufficient to reveal the structure in this part. Possible signs for the connecting fault are indicated on the image.*

ered peculiar, because by far the most natural examples are characterised by one of the major fault segments that slightly bends and grows towards the other segment (e.g. Childs et al., 1995) to achieve the final connection, a property that was also observed for the linking of extensional fractures (Acocella et al., 2000). As explained in section 2.5, Ferrill et al. (1999) described examples of both types of breaching, and explained the linkage in terms of the displacement gradient on the main faults. The faults that are observed inside the relay ramp at Zavarotny strike only slightly oblique to the main faults, and therefore suggest tilting and bending of the

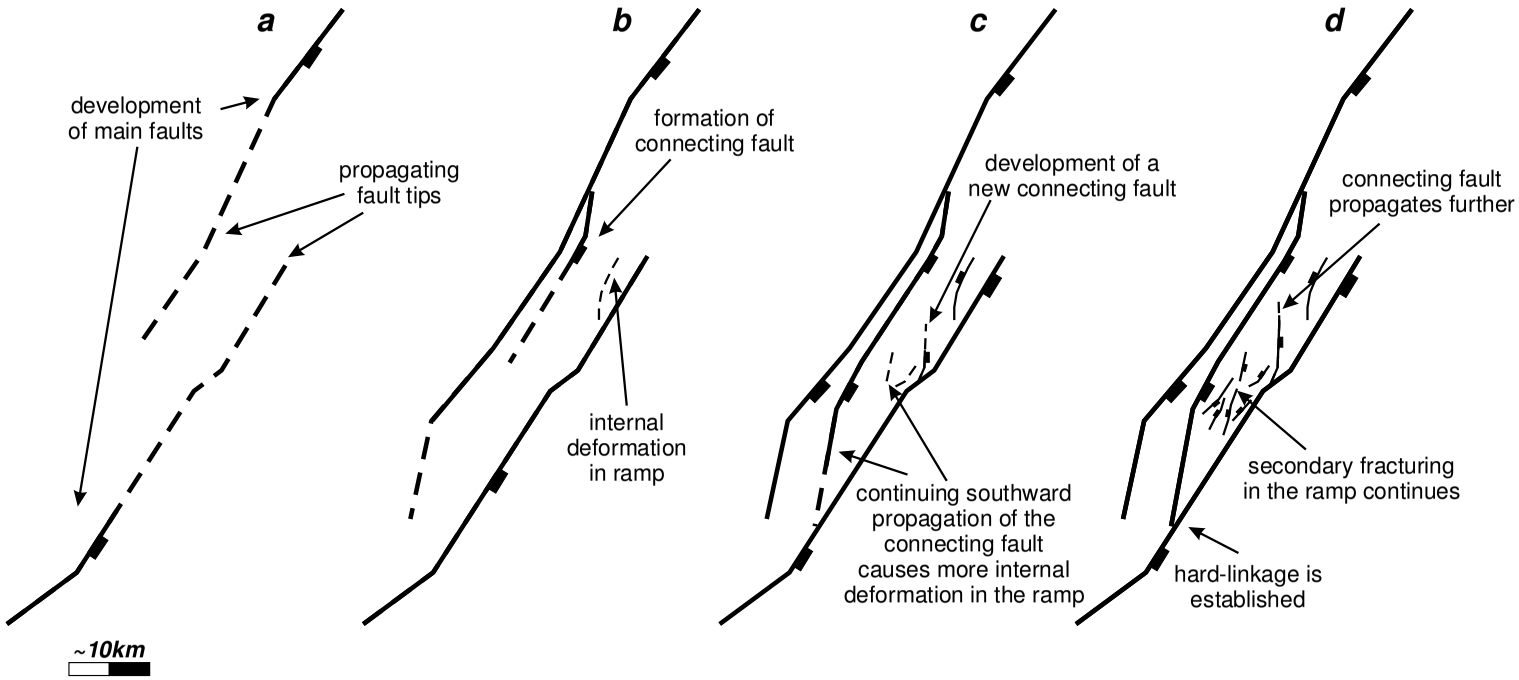

Figure 4.23: *Schematic illustration of the possible evolution of the Zavarotny relay ramp. (a) The main faults develop and propagate to form an overlap zone. (b) While the main faults overlap, a relay ramp forms. Deformation in this relay ramp results in the formation of the connecting fault, which splays off the footwall fault and propagates towards the hanging-wall fault. (c) The propagation of this connecting fault, causes additional secondary deformation in the ramp, between the connecting fault and the hanging-wall fault. This secondary deformation expands southward with in relation to the southward propagation of the connecting fault. (d) While the relay ramp in Zavarotny has been breached by the connecting fault, a new connecting fault develops in the northeastern part of the ramp. This fault splays off the hanging-wall fault and propagates towards the first connecting fault.*

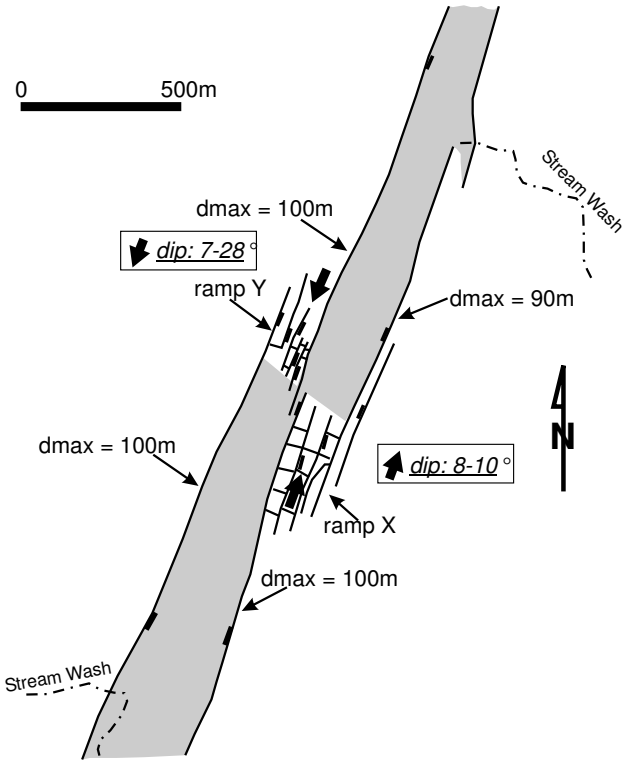

Figure 4.24: *Simplified structural map of the S.O.B Hill relay zone in the Devil's Lane graben. Two major relay ramps dip in opposite directions. Modified from Trudgill and Cartwright (1994).*

ramp along an axis parallel to the main faults. This suggests that the fault displacement does not increase disproportionally relative to the fault tip propagation, which seems to — in case the model of Ferrill et al. (1999) is correct — contradict the development of a new through-going connecting fault.

Trudgill and Cartwright (1994) observed in the S.O.B.-Hill relay zone also some features that did not obey the model of Ferrill et al. (1999). They observed two relay ramp systems between the border faults of two off-set grabens (Devil's Lane; figure 4.24). These relay ramps have an opposite dip direction, with the southern one dipping towards the north with an angle of 8–10° and the northern one dipping towards the south with an angle of 7–28°. The aspect ratio's of the two ramps are more or less the same (see Appendix A). Following the model of Ferrill et al. (1999) we would expect the ramp with the steepest dip to be characterised by more faults or fractures that strike at high angle to the main faults than the ramp with the lower dip. The steep ramp is, however, characterised by faulting parallel to the main faults, and the less steep ramp is characterised by both: faulting parallel to the main faults as well as an important amount of extension carried by joint sets that strike almost perpendicular to the main faults (Trudgill and Cartwright, 1994).

Another possibility for Zavarotny, is that the main faults result from the reactivation of

inherited basement structures, and that therefore fault lengths were determined long before the displacement reached the limit for lateral propagation (e.g. Walsh et al., 2002; Peacock, 2002). This would initially result in relatively low displacement gradients at the fault tips of the main faults, and as such the internal deformation of the relay ramp will be characterised by mainly fault parallel secondary faults. In a later stage, when the displacement increases on the main faults (without a further propagation), the displacement gradients at the fault tips increase as well, and cause the secondary deformation inside the ramp to be characterised by faults striking at higher angle to the main faults. This mechanism of fault reactivation could therefore explain the occurrence of both kind of faults (striking either parallel or at high angle to the main faults). However, in our case, this explanation is not sufficient as one would expect the parallel faults to develop prior to the connecting fault.

In the cases explained by e.g. Cartwright et al. (1996) and Ferrill et al. (1999) the connecting fault is not a single, well expressed fault, but rather a fault system resulting from the interconnection of different fault clusters in the ramp. In Zavarotny, the first connecting fault — although buried by sediments — as well as the second (developing) fault seem to consist of a single, well defined, trace. Also Young et al. (2001) observed a single, well expressed fault that links up two fault segments in the Murchison-Statfjord North Fault Zone.

It is possible that the style of linkage determines whether or not the relay ramp dies out completely after breaching. Probably the connecting fault for Zavarotny was at the stage of breaching not yet able to account for the taking over of all the displacement of the older crosscut segments. This could explain why the ramp continued its development after it got breached.

Peacock et al. (2000b) noted already that the secondary faults developed in the Hold With Hope ramp strike differently to those in smaller relay ramps (Peacock and Sanderson, 1991). The orientation of the faults that were observed in the top of the ramp corresponds to the observations from the Hold With Hope ramp, however the dip directions are opposite as the faults in Zavarotny dip antithetically to the main faults.

There are many factors that could explain the observations in Zavarotny. Probably the most important is the influence of the basement structure in the area. As seen on the satellite image (Figure 4.17) the onshore orientation of basement structures corresponds with the strike direction of the secondary offshore faults in the upper part of the ramp. Possibly these structures limit the amount of bending in the ramp (along an axis parallel to the main faults) that is required to form secondary faults in the ramp, parallel to these main faults.

Because the relay ramp in Zavarotny is relatively large, it is likely that it is subject to stress field variations on another scale, that do not only result from the local fault interactions. Smaller ramps would act as being located in a more "homogeneous" external stress field (e.g. Manighetti et al., 2001). This means that we should consider possible influences of the overall kinematic processes in Lake Baikal on the evolution of Zavarotny. Indeed, a larger scale process could be expected as the border fault segments of lake Baikal systematically deflect on left-lateral oversteps.

4.5 Conclusions

Based on the interpretation of several detailed data sets, the structure of a relative large scale relay ramp has been described in the western border fault system of Lake Baikal and a possible evolutionary scheme has been proposed.

An uncommon combination of secondary fault development in the ramp (with fault strikes that are almost parallel or at low angle to the main faults) and breaching of the ramp by a newly formed fault has been observed. It was concluded that the ramp structure in Zavarotny results from a combination of soft as well as hard linkage displacement transfer.

As the observed evolution in Zavarotny does not seem to correspond completely with smaller scale examples from other studies, it is concluded that the structure of large relay ramps cannot be determined solely based on their analogy with smaller ones. Instead additional information is needed on for example larger ongoing kinematic processes in rifts, pre-existing structures, etc.

If these influences are indeed significant, experimental modelling will be a good systematic approach to gain insight in the role that several properties of the main faults (e.g. relative orientation, their sense of movement and spacing, etc.) play in the development and subsequent evolution of the relay ramp between them. This information might then be used in natural examples to make a distinction between the expected relay ramp structures, and the structures influenced by other processes. That way, these models will surely complement the theoretical approaches of earlier research, and they can be used — like the small scale descriptions — for guiding the interpretation of larger scale natural examples that are more likely to carry exploitable hydrocarbon reserves than their small scale analogues. A modelling study of relay ramps is presented in chapter 6.

Chapter 5

The evolution of the central part of Lake Baikal: a structural study

The structural description which is presented in this chapter is focused on another relay zone example from Lake Baikal, the Pri-Ol'khon Block. This block is located in the central part of the lake, and is larger than the relay ramp in Zavarotny (described in the previous chapter). The internal structure of this relay zone will be analysed in a first part of this chapter, followed by the proposition of a new evolution model for the area. The study is based on the interpretation of new seismic profiles from Maloe More, satellite images from Central Baikal and digital terrain models.

5.1 Introduction

In the central part of Lake Baikal, a large tilted block exists between two major boundary faults of the western lake border (Primorsky Fault and Ol'khon Fault (see chapter 3)) (figure 5.1). It is believed that the area evolved and got tilted when the Primorsky Fault propagated southward and cut through the footwall of the Ol'khon Fault (eg. Agar and Klitgord, 1995) (see section 5.3). At present the footwall fault (Primorsky Fault) has linked up with the hanging-wall fault (Ol'khon Fault) (figures 3.11 & 5.2). In this chapter, new data (high resolution seismic profiles, digital terrain models and satellite images) are presented that enable us to propose a new, alternative model for the structure and evolution of this block.

The study of this structure in central Lake Baikal is interesting for several reasons:

❶ If the above mentioned evolution model is the correct one, the Primorsky and the Ol'khon Faults would have formed in an earlier evolution stage (i.e. before they merged together) a gigantic relay ramp. This relay ramp would have had a width of ∼20–30 km and a length of >80 km, making it larger than the ramp in Zavarotny (chapter 4). As such it would provide another opportunity to study the internal structure and evolution of a large scale relay structure.

❷ In chapter 2 (see section 2.4.2) the model of Gupta et al. (1998) was introduced (page 52), which explains the possible transition in rifts from a slow rifting stage to a climax stage as a result of the linkage of different faults. In Gupta et al. (1998)'s model, the increased subsidence rate that characterises the rift climax stage, is attributed to the post-linkage displacement readjustments of newly formed composite faults, rather than to an increase in the rate of regional extension. Recently ten Brink and Taylor (2002) argued that the transition from the slow rifting stage to the fast rifting stage in the Baikal Rift Zone (see section 3.2.1 and 3.2.2) could as well be related to the connection of different faults and an associated increase in subsidence, and not necessarily to a change in the tectonic regime.
Because the study in this chapter provides information on the propagation and final merging of two major boundary faults in Lake Baikal it could be a test case for the hypothesis of ten Brink and Taylor (2002). Indeed, if the model of Gupta et al. (1998) is applicable to Lake Baikal, one expects that the connection of these two *major* faults will have had a large influence on the subsequent subsidence of the hanging-wall region (i.e. Maloe More and central Lake Baikal). Therefore, by deducing the timing of the fault connection in the central part of Lake Baikal and by evaluating whether at the same time subsidence increased in the area, the hypothesis can be tested.

5.2 Outline of the Pri-Ol'khon Block

The *Pri-Ol'khon Block* is the wedge shaped area between the mouth of the Buguldeika River in the south and the village Kocherikovo in the north — bordered by the Ol'khon Fault in the south-east and the Primorsky Fault in the north-west (Mats et al., 2000) (see figures 3.11 & 5.2). The block (approximately 30 km wide and 100 km long) contains 4 areas: *Ol'khon Island*, and *Pri-Ol'khon Peninsula* which are onshore and *Maloe More* and the *Zama Depression* which are submerged beneath the present lake level (figure 3.11). Maloe More is sometimes interpreted as the southwestern extremity of the northern Baikal basin (e.g. Khlystov et al., 2001). It continues southwestward as the on-land Chernorud Graben (figure 5.1).

Mats (1993) and Agar and Klitgord (1995) identified in the Pri-Ol'khon Block three subparallel (neotectonic) structural domains. These domains extend longitudinally through the Pri-Ol'khon Block for over 120 km with varying width between 1.5–20 km (Agar and Klitgord, 1995) (figure 5.2): (1) the Primorsky Fault Footwall (PFW), (2) the Primorsky Graben (PG) and (3) the Primorsky Fault Hanging-wall (PHW). Also a lateral segmentation of the Pri-Ol'khon Block can be identified related to the along-strike segmentation of the Primorsky Fault (Agar and Klitgord, 1995). The different sub-blocks (I, II and III in figure 5.2) are all characterised by different elevation levels, and changes in morphology and surface slopes. The boundaries between these different sub-blocks might be fault related, but their present morphology (e.g. Ol'khon Gate) is strongly shaped by abandoned drainage systems that once crossed the Ol'khon Fault's footwall region (Agar and Klitgord, 1995).

The Primorsky Fault Footwall (PFW) consists mainly of the 15 km wide Primorsky Range. This mountain range has a height of 900 m in the south near Buguldeika and a maximum height

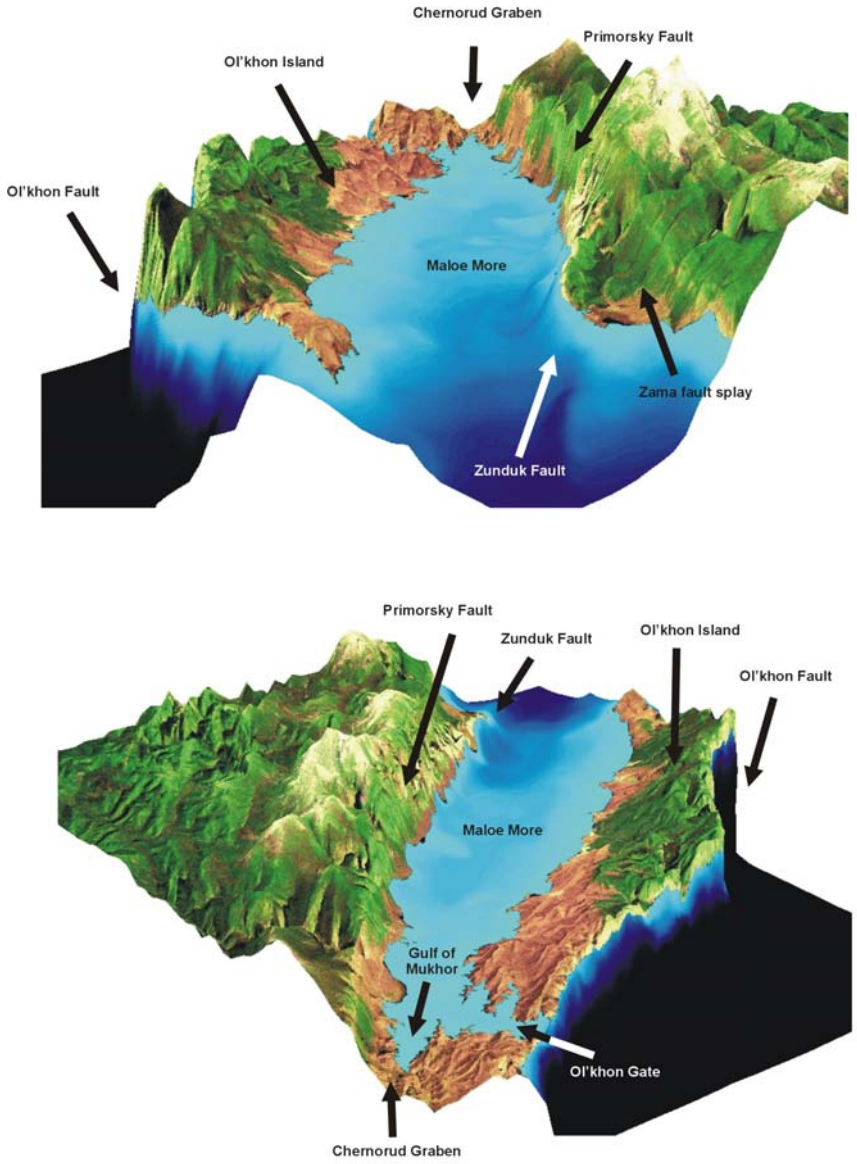

Figure 5.1: *Satellite image (RESURS mk-4) draped over the digital terrain model of Maloe More and Olkhon Region, with the main structural elements indicated. This figure clearly illustrates the tilted-block nature of the area between the Primorsky and the Olkhon Faults. In the upper image north is downward, in the lower one north is upward.*

of ∼1700 m near the mouth of the Sarma River. The fault scarp of the Primorsky Fault forms the border between the PFW-domain in the northwest and the Primorsky Graben (PG) in the southeast. The Primorsky Fault reaches a maximum vertical offset of ca. 400 m and this offset gradually diminishes towards zero near the mouth of the Buguldeika river (Mats, 1993). Field

studies have revealed a left lateral displacement on a number of subsidiary faults of the Primorsky Fault, as well as a 300-400 m horizontal offset of Late Pleistocene – Early Holocene alluvial fans (Arzhannikova and Gofman, 2000). The estimated amount of horizontal displacement along the Primorsky Fault during Cenozoic times is less than 1.0–1.2 km (Sherman, 1978), however other researchers mention values around 2 km (Arzhannikova and Gofman, 2000). The amount of Cenozoic vertical throw of the fault is estimated to be a few hundred metres (Agar and Klitgord, 1995). The Primorsky Fault is in its southwestern part characterised by a well-defined single scarp, but towards the northeast it splays in different sub-faults forming a zone containing four to five narrow steps (Mats et al., 2000). These faults accommodate the present displacement of the Primorsky Fault. In the hanging-wall domain of the Primorsky Fault, different blocks have been observed that are tilted in a northwest direction (ie. towards the fault). As discussed

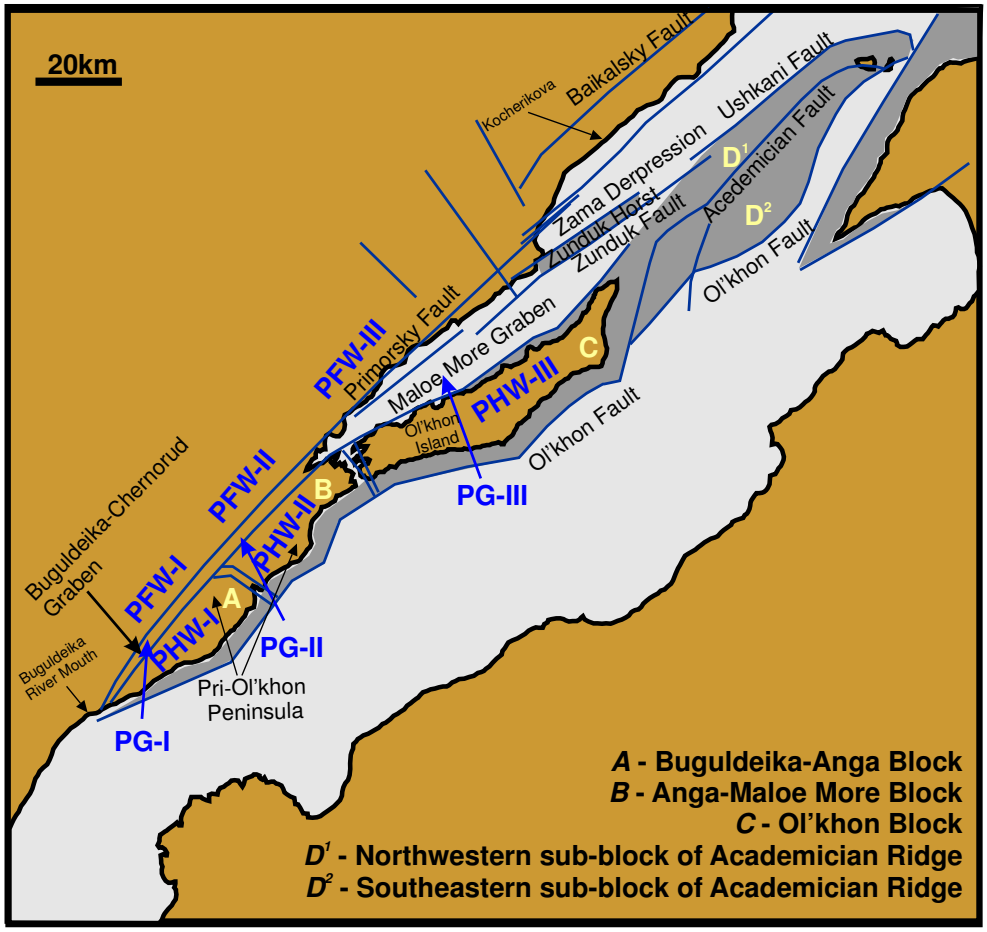

Figure 5.2: *Main structural elements of the central part of Lake Baikal. Modified from Mats et al. (2000) and completed with domains of Agar and Klitgord (1995): PFW = Primorsky Fault Footwall, PG = Primorsky Graben and PHW = Primorsky Fault Hanging-wall. Numbers I, II & III correspond to different block that result from the lateral segmentation of the Pri-Ol'khon Block .*

in section 3.3, this tilting has been used as evidence for the listric character of the Primorsky Fault.

The Primorsky Graben consists of the onshore Buguldeika-Chernorud Graben (1.5–5 km wide) and the offshore area of Maloe More (∼15 km wide) (figure 5.2). The depth of Maloe More increases from 0 m in the southwest (Gulf of Mukhor) to ∼400 m in the northeast (figure 5.1). Many authors have stated that the different islands in Maloe More are bordered on their western side by a fault (eg. Mats, 1993; Agar and Klitgord, 1995; Levi et al., 1997), and they interpreted this as being the main western boundary fault of Ol'khon Island, dipping antithetically to the Primorsky Fault. In this scheme, Maloe More has been interpreted as a graben structure inside Lake Baikal. The Primorsky Fault Hanging-wall (PHW) is the area southeast of this fault zone, upto the Ol'khon Fault (figure 5.2) (Agar and Klitgord, 1995).

On the Pri-Ol'khon Peninsula, several minor topographic steps can be observed that are caused by minor displacements on recent basement faults, indicating that in this area intra-segment neotectonic deformation has occurred (Agar and Klitgord, 1995). Whether this deformation can be attributed to the interaction between the Ol'khon and Primorsky Faults is unclear.

Cenozoic sediments (Oligocene to Quaternary age) have been deposited in Maloe More and in local depressions on the western border of Ol'khon Island. These depressions are believed to result from the tilting of small blocks in the area (Mats, 1993; Mats et al., 2000).

5.3 Models for fault propagation in Central Lake Baikal

As mentioned in the introduction, the depression of Maloe More is believed to have formed in relation to the southwestward growth of the Primorsky Fault, which caused a gradual propagating subsidence from the northeast towards the southwest. This model was well suited to explain the reigning idea that the southwestern limit of Maloe More was a young structure, overlain by only little sediments (few metres), directly on top of the crystalline basement, and this in contrast to the northeastern part of Maloe More which is deeper and covered with ∼150–180 m of sediments (e.g. references in Khlystov et al., 2001).

Subsiding of the northeastern part of Maloe More below lake level corresponds to the deposition of seismic-stratigraphic sequence B6 of Moore et al. (1997); they do, however, not have any age constraints on this. According to the seismic-stratigraphic interpretations of Mats et al. (2000), the flooding of Maloe More is recorded by the onlaps at the base of their Unit B which is estimated to be of Late Miocene age.

Based on the morphology of the Primorsky Fault scarp, Agar and Klitgord (1995) estimated the fault's reactivation to be younger than 1 Ma.

There is evidence for ongoing recent subsidence of the Maloe More Block from the submergence of an archeologic site of Neolithic age (7000 years B.P. ^{14}C dated (eg. Mats et al., 2000)), and from earthquake activity in the Primorsky Fault Zone (Arzhannikova and Gofman, 2000).

The displacement profile of the Primorsky Fault — from a maximum vertical offset of ca. 400 m that gradually diminishes towards zero to the south — supports the idea of the

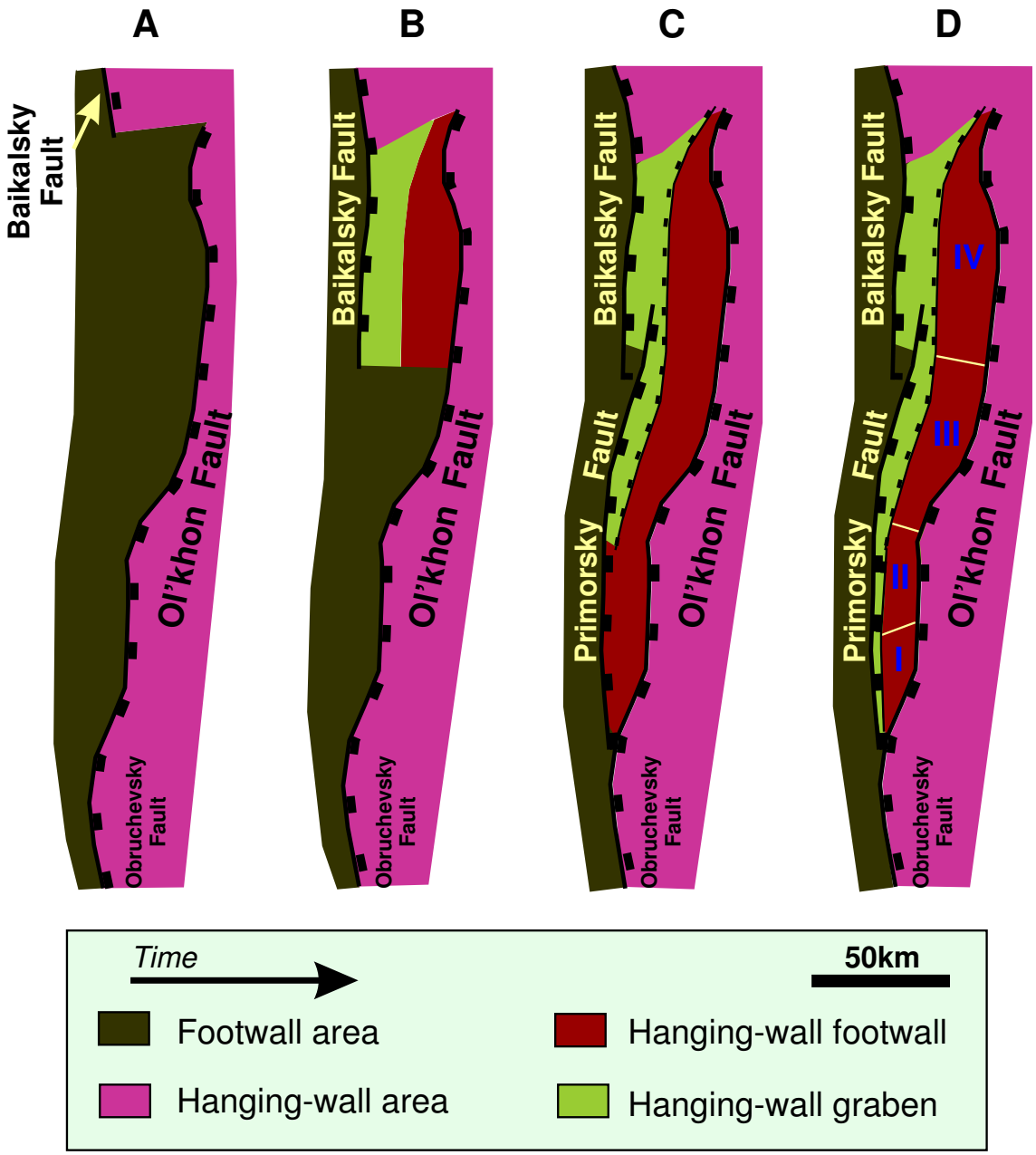

Figure 5.3: *Illustration of the existing model of fault propagation in the central part of Lake Baikal. Modified from Agar and Klitgord (1995). The evolution results from the southward propagation of the Baikalsky Fault and later the Primorsky Fault to form an overlap zone with the Ol'khon Fault (figures B and C). The block between both faults is characterised by antithetic faulting, and can be divided in 4 sub-block (figure D). I. Buguldeika-Anga Block, II. Anga Maloe More Block, III. Ol'khon Island and IV. Academician Ridge.*

southward propagating fault as proposed by Agar and Klitgord (1995). In this model the lateral segmentation of the Pri-Ol'khon Block could have resulted from a break-up caused by local tension when the northern part of the block subsided while the southern part remained initially in the same position (V. A. San'kov, *personal communication*, August 2002). Local earthquake ruptures that parallel the Ol'khon Gate (and are perpendicular to the Primorsky Fault) have been observed and are attributed to a stage of local northeastern extension throughout the Holocene (Arzhannikova and Gofman, 2000). These ruptures started to form in the Pri-Ol'khon Block around 8–9 ka ago. On the other hand, also earthquakes did occur on faults that parallel the Primorsky Fault (for example a large earthquake at Sarma, dated 10100±90 ka ago) (Arzhannikova and Gofman, 2000). The latter type of earthquakes most likely represents the activity of the Primorsky Fault, whereas the former earthquake ruptures (that appeared more recently) possibly represent the internal deformation of the Pri-Ol'khon Block related to the first series of earthquakes.

5.4 Available data-sets

For this chapter a set of recently acquired high-resolution reflection seismic profiles in Maloe More has been used, in combination with a detailed bathymetric map of Maloe More (INTAS Project 99-1669), digitised topographic maps (RMCA) and satellite images (RESURS mk-4 and Landsat) of Ol'khon Island, Pri-Ol'khon and the Primorsky Range.

The high-resolution seismic profiles were collected in the summers of 1998 and 2001 (>1000km), and were all shot with a "Centipede" sparker source and a single-channel streamer as receiver (figure 5.4). The incoming signal was filtered (200Hz high-pass; 2300Hz low-pass) and digitally recorded on an Elics Delph2 system. After acquisition, the seismic data were processed using ProMax software (frequency filtering, spiking deconvolution,...) and interpreted using the KINGDOM Suite interpretation software from Seismic Micro-Technology. Further details on the acquisition of the seismic profiles can be found in Vanneste and De Batist (1998) and Hus and De Rycker (2001). The seismic profiles have a vertical resolution of about 1 meter.

The new, higher-resolution bathymetry data (The INTAS Project 99-1669 Team, 2002) were merged with digitised topographic data (scale 1:200,000) from the Royal Museum of Central Africa (Tervuren, Belgium) in order to construct a complete digital terrain model (DTM) of the area.

Figure 5.1, produced by integration of the topographic and the bathymetric data overlain by a satellite image, illustrates the main morphostructural characteristics of the area.

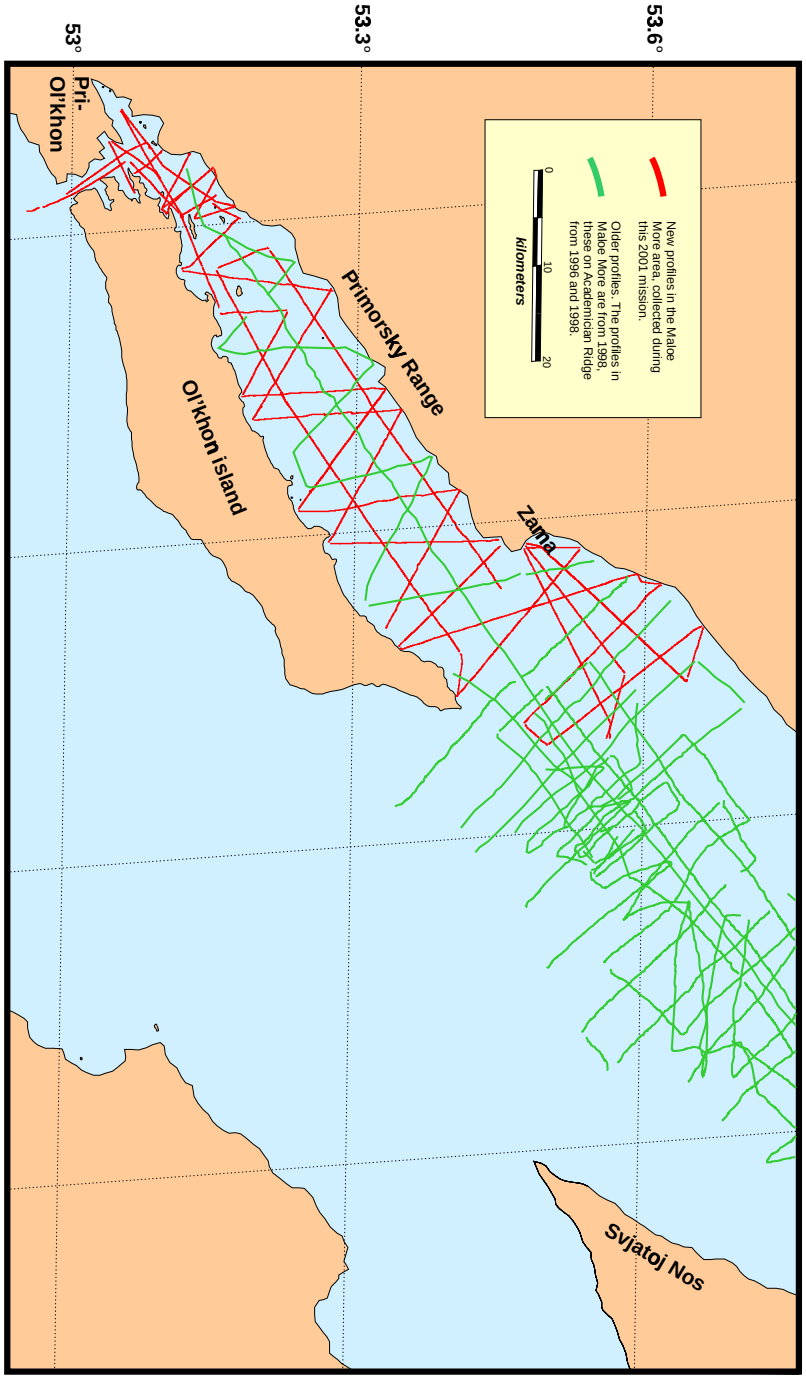

Figure 5.4: *Track-plot of the high resolution seismic profiles available in Maloe More. The profiles were collected in 1998 and 2001 and they have a total length >1000km.*

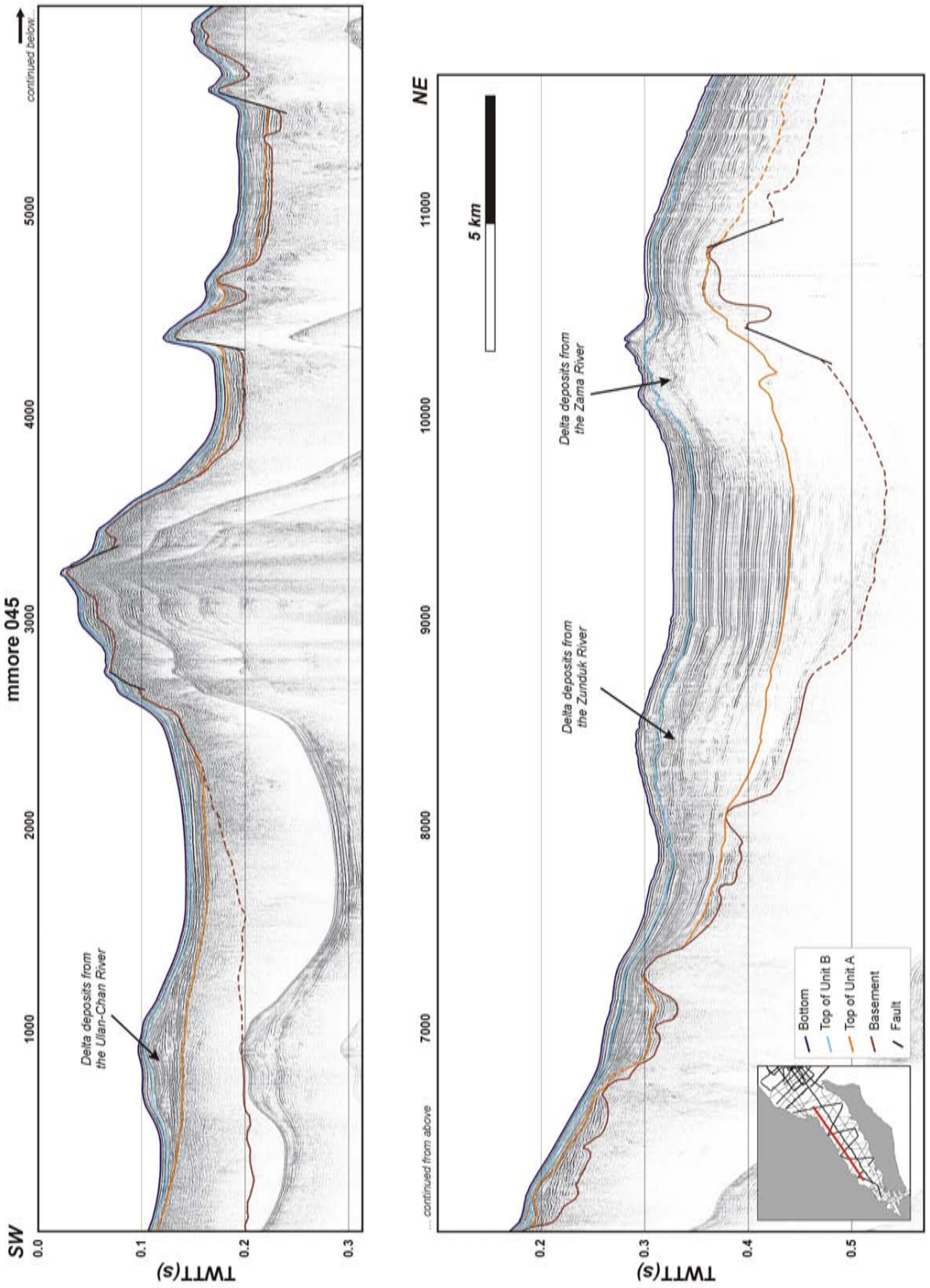

Figure 5.5: *Seismic image of the longitudinal profile mmore045 through Maloe More. The profile is located near the Primorsky Fault (see figure 5.4 for its location).*

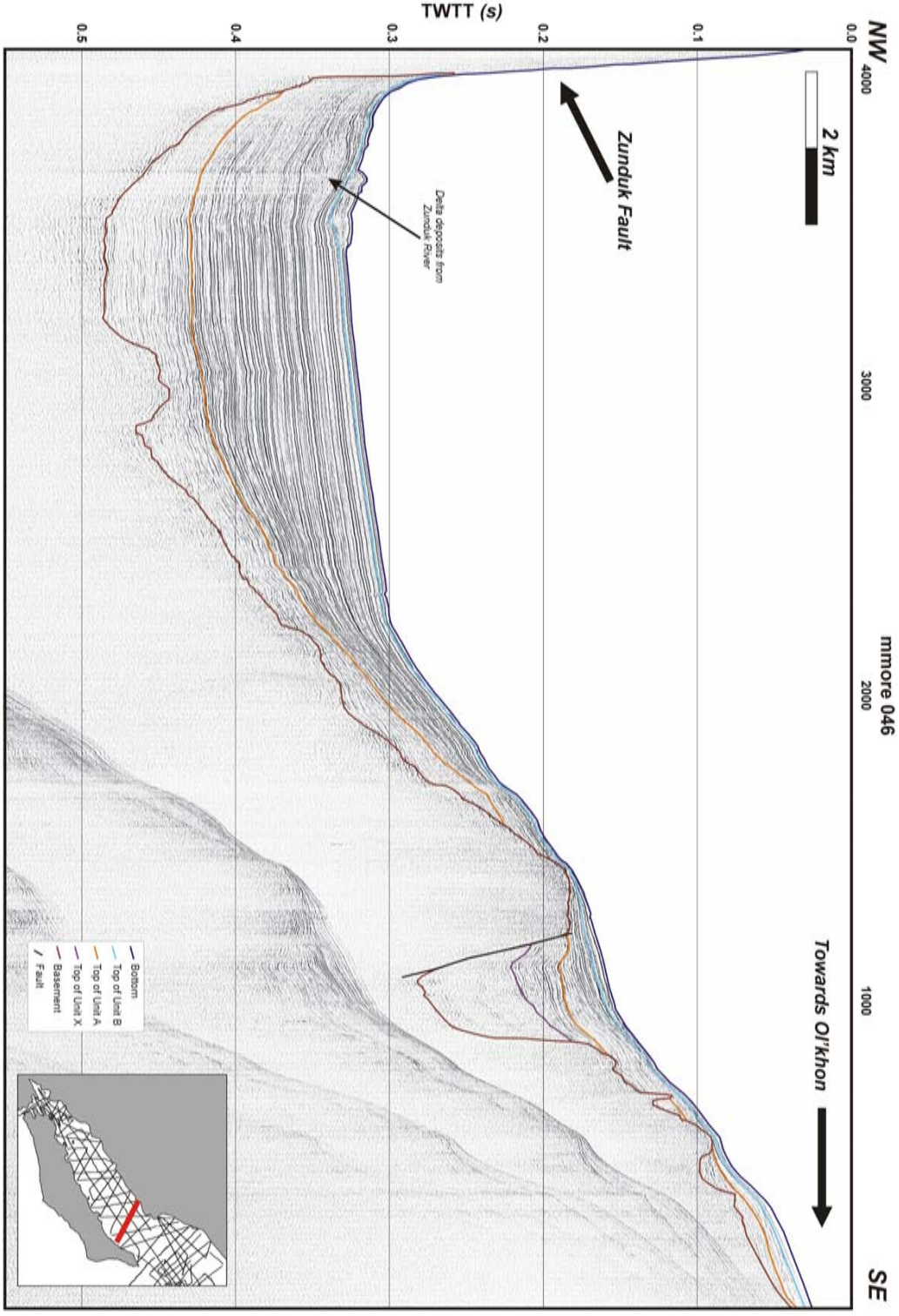

Figure 5.6: *Seismic profile mmore046 that is oriented perpendicular to the Primorsky Fault (figure 5.4). Note the thick sedimentary infill near the Primorsky Fault, and the gradual decrease in sediment thickness towards Ol'khon.*

5.5 Interpretation

5.5.1 Seismic interpretation of Maloe More

Introduction

The penetration of the seismic signal was large enough to reach the acoustic basement in most parts of Maloe More. This acoustic basement has been interpreted to represent the top of the pre-rift units, i.e. here formed by an extensive laterite-kaolinite weathering crust (Mats, 1993) (see also chapter 3). Mats et al. (2000) and Khlystov et al. (2001) identified already three first order seismic stratigraphic units in Maloe More, which overlie the basement. These units were called *Unit X*, *Unit A* and *Unit B* from old to young. Unit X is only found in Maloe More, whereas Unit A and B also occur on the submerged Academician Ridge between the northern and the southern Baikal basins. Mats et al. (2000) have correlated Unit X to the lower Lower-Middle Oligocene Ularya Formation on Ol'khon Island. Unit A, which lies discordant on Unit X, is more widespread than the latter and has been correlated to the Lower-Middle Miocene Tagai Formation on Ol'khon (Mats et al., 2000; Khlystov et al., 2001). The basal layers of Unit B were deposited around 7 Ma ago in the northern part of Maloe More, and this unit is believed to correspond to the Sasa Sequence defined at Cape Sasa on Ol'khon Island (Mats et al., 2000). Coisne (2004) identified on top of Unit B another small unit which she called *Unit R*.

A longitudinal seismic profile through Maloe More (mmore45; figure 5.5) shows the first-order geometry of units A, B and R. The oldest unit, Unit X, has only been deposited in depressions closer to Ol'khon Island and the Zunduk Horst, and is not recorded on this profile (see for example profile mmore46; figure 5.6). Seismic profile mmore45 reveals an almost stepwise pattern of the lake floor as well as for the level of the acoustic basement. Both, lake floor and basement level, deepen towards the northeastern end of Maloe More. Also the overall thickness of the sediments increases from the southwest towards the northeast (figure 5.5), where they eventually reach a thickness of more than 150 m (or 0.15–0.2 s TWTT).[1]

Basement

On profile mmore45 it is observed that the acoustic basement is characterised by a rough morphology in which basement highs alternate with depressions (figure 5.5). The depth map of the basement — derived from the interpretation of all seismic profiles — shows that these basement highs correspond to transverse ridges which are orientated at high-angle to the Primorsky Fault (figure 5.7). Near this fault, the height of the different ridges varies between 60–110 m. The isopach map of the whole sedimentary sequence in Maloe More (figures 5.8 & 5.9) reveals the presence of sedimentary depocentres between the different basement ridges. These depocentres correspond with 5 sub-basins in the area. Some of the basement ridges that delimit these basins are bounded by normal faults, whereas others are not (e.g. figure 5.5). The different ridges have

[1] To convert the thicknesses on the isopach map from two-way travel-time into meters, a value for the speed of sound in the sediments of 1600–1800m/s can be used (Antipin et al., 2001).

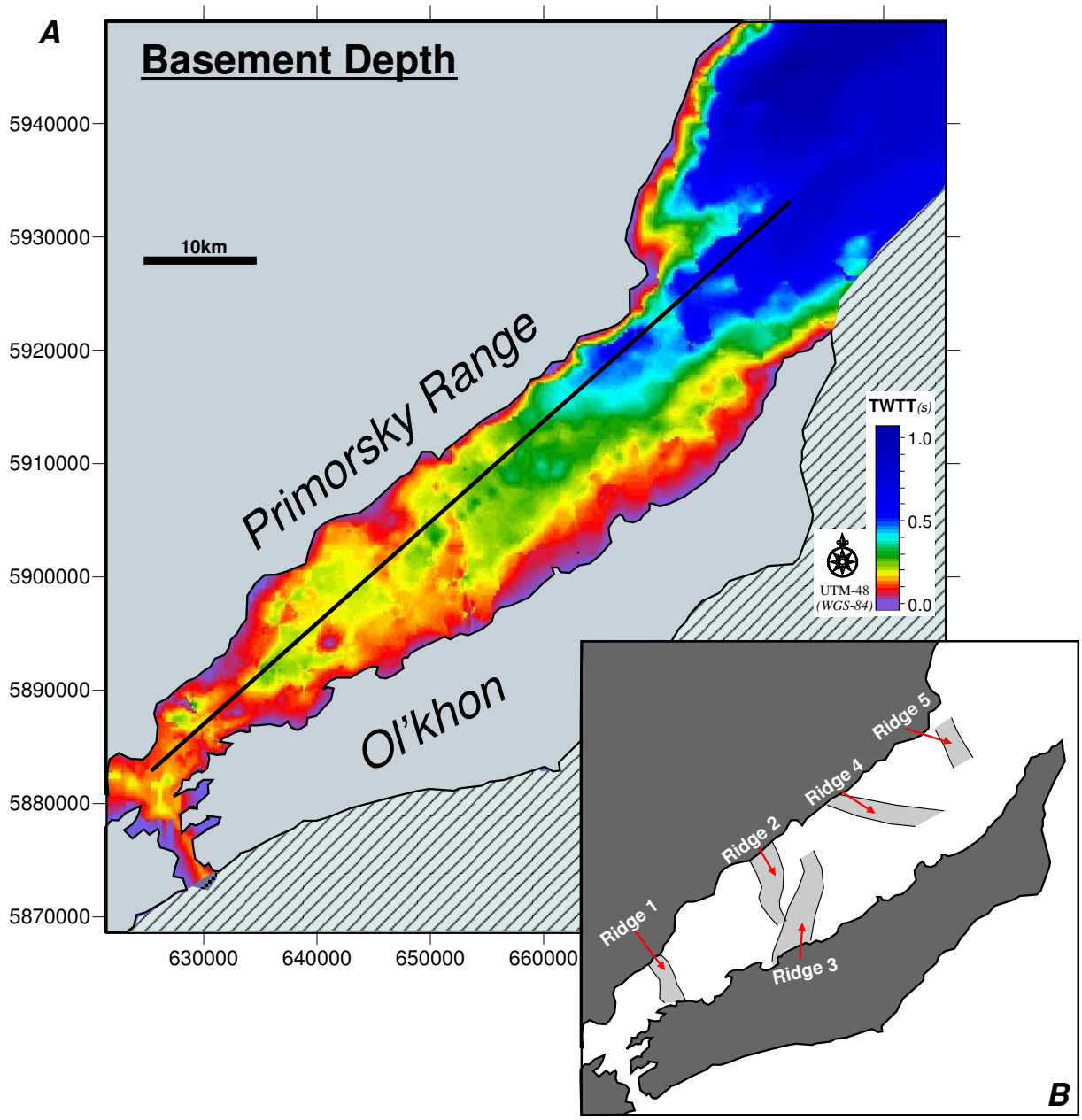

Figure 5.7: *Depth of the acoustic basement in Maloe More and Zama (two-way travel times in seconds). Different ridges in the morphology of the basement have been indicated. The line drawn through Maloe More illustrates the location of the profiles from figure 5.8*

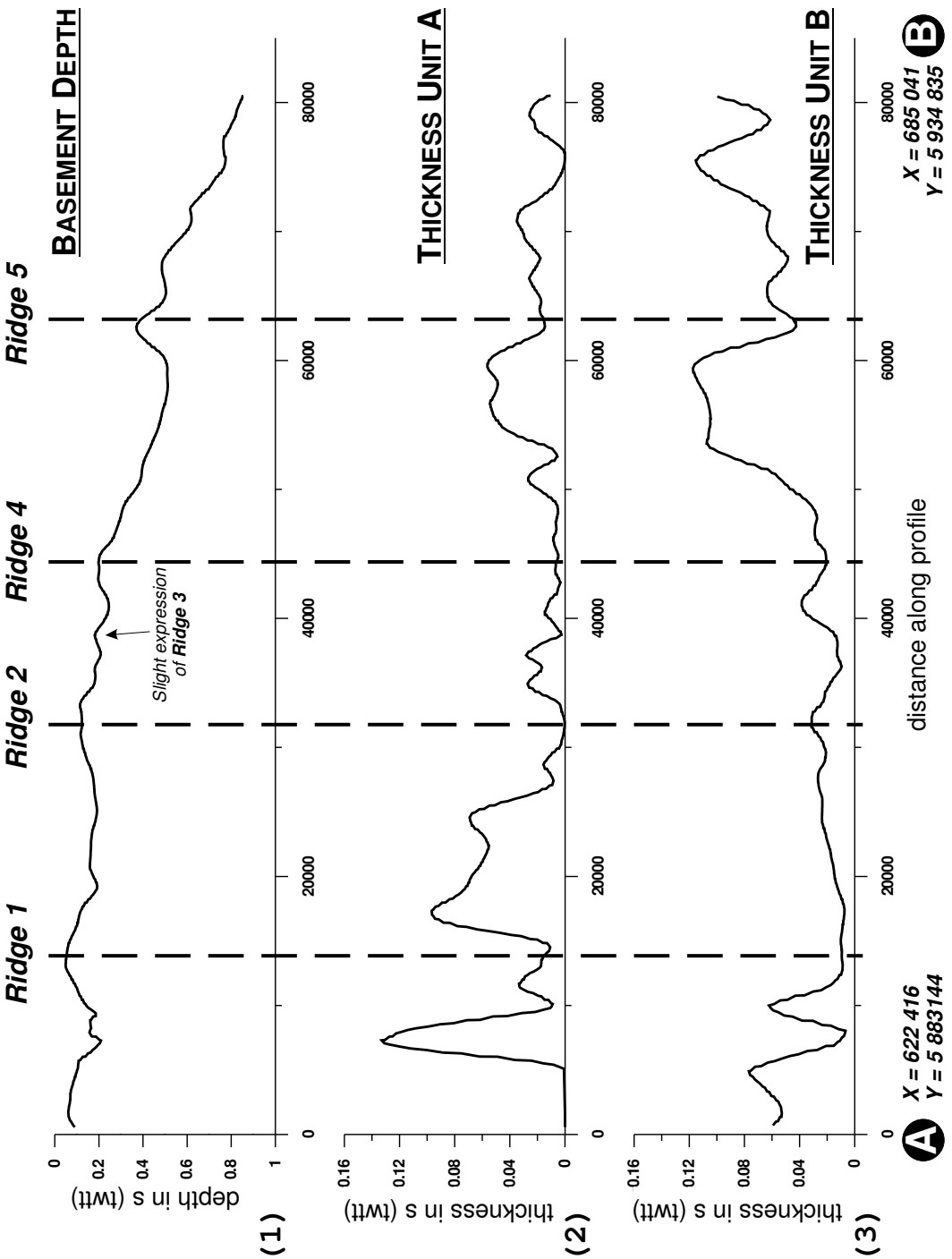

Figure 5.8: *Longitudinal profile through Maloe More, showing the depth of the basement (1), the thickness of sedimentary unit A (2) and the thickness of sedimentary unit B (3). The profile is located near the Primorsky Fault (see figure 5.7).*

been numbered from 1 to 5 in figure 5.7 & 5.8. Except from ridge 3, all of them are best expressed near the Primorsky Fault, and their morphological expression gradually decreases away from this fault. The strike of the different ridges are: ∼N35°W for ridge nr. 1, ∼N25°W for ridge nr.2, ∼N18°E for ridge nr. 3 , ∼N75°W for ridge nr. 4 and ∼N25°W for ridge nr. 5. All these directions form a high-angle with the general strike of the Primorsky Fault which is ∼N50°E. Profile mmore46, which was shot in sub-basin nr. 4 and oriented at high-angle to the Primorsky Fault, illustrates that this sub-basin is deepest near the Primorsky Fault, and gently shallows towards Ol'khon Island (figure 5.6).

In the sedimentary deposits, not much evidence is found of basement faults that propagate into the sedimentary cover. Faults that affect the sedimentary cover, without clearly cutting through the basement, are termed here "sedimentary faults". This does, however, not imply that the faults are a result of sedimentary deformation without a tectonic origin.

Unit X & A

Unit X and Unit A are not thicker than a few tens of meters, and they are mainly present in the sub-basins of the basement structure (e.g. figure 5.5 & 5.8). The highest thickness of these units is found in depocentres in the southern half of Maloe More, where locally both units together attain a total thickness of 70-80 m (figure 5.10). Also near the Zunduk Fault, in the northern part, relatively large deposits of the units occur. Deposits of unit X&A occur as more or less isolated bodies between the different basement ridges. Nevertheless, the northernmost ridges in Maloe More (nrs. 4 and 5) are covered by a thin layer of the upper part of unit A. The unit is absent, however, on the ridges located more to the south (nrs. 3, 2 and 1) (figure 5.5).

Unit B

Unit B occurs throughout the whole study area, lying either on the older sedimentary units, or directly upon the basement (mainly on the ridges) (figure 5.5). The unit is characterised by continuous reflectors. Unlike the older Unit A, the overall thickness of this unit increases from the southwestern part of Maloe More towards the northeast. In some areas its thickness exceeds a 100 m (Khlystov et al., 2001) (figure 5.11). Unit B is present on all the ridges in Maloe More, but its thickness is largest on the northern ridges, and smallest on the southern ones (figure 5.5). Numerous "sedimentary faults" affect the deposits of unit B, with often no clear relation to underlying basement faulting. The presence of the sedimentary faults is too ubiquitous to determine their 3D geometry and infer a possible formation mechanism.

On top of Unit B another sedimentary unit can be identified (Unit R), that is only about 5ms thick (twtt) or ∼4–5 m. This upper unit appears to be less faulted than the deposits of the underlying Unit B.

During the whole evolution of the area, rivers incised the Primorsky Range and brought coarse clastic sediments into Maloe More. This is evidenced by the deposits of fan delta's still present along the flanks of the Primorsky and Zunduk Faults.

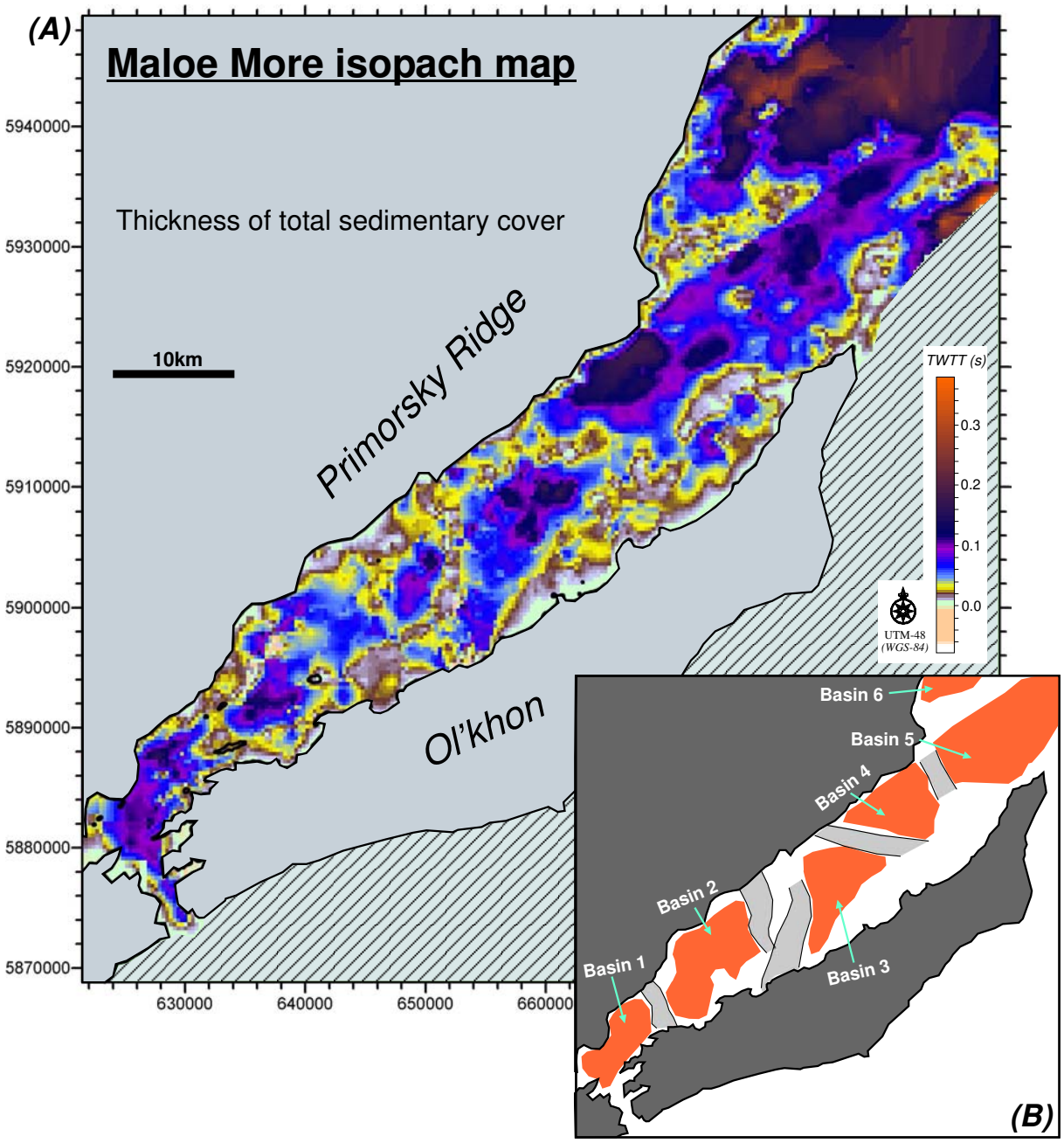

Figure 5.9: *Isopach map of the total sedimentary thickness in Maloe More. Different clear depocentres can be observed, which are bordered by the basement ridges (see figure 5.7). On the ridges less sediments have accumulated.*

Additional seismic profiles of the Pri-Ol'khon Block are included in figures 5.12–5.14.

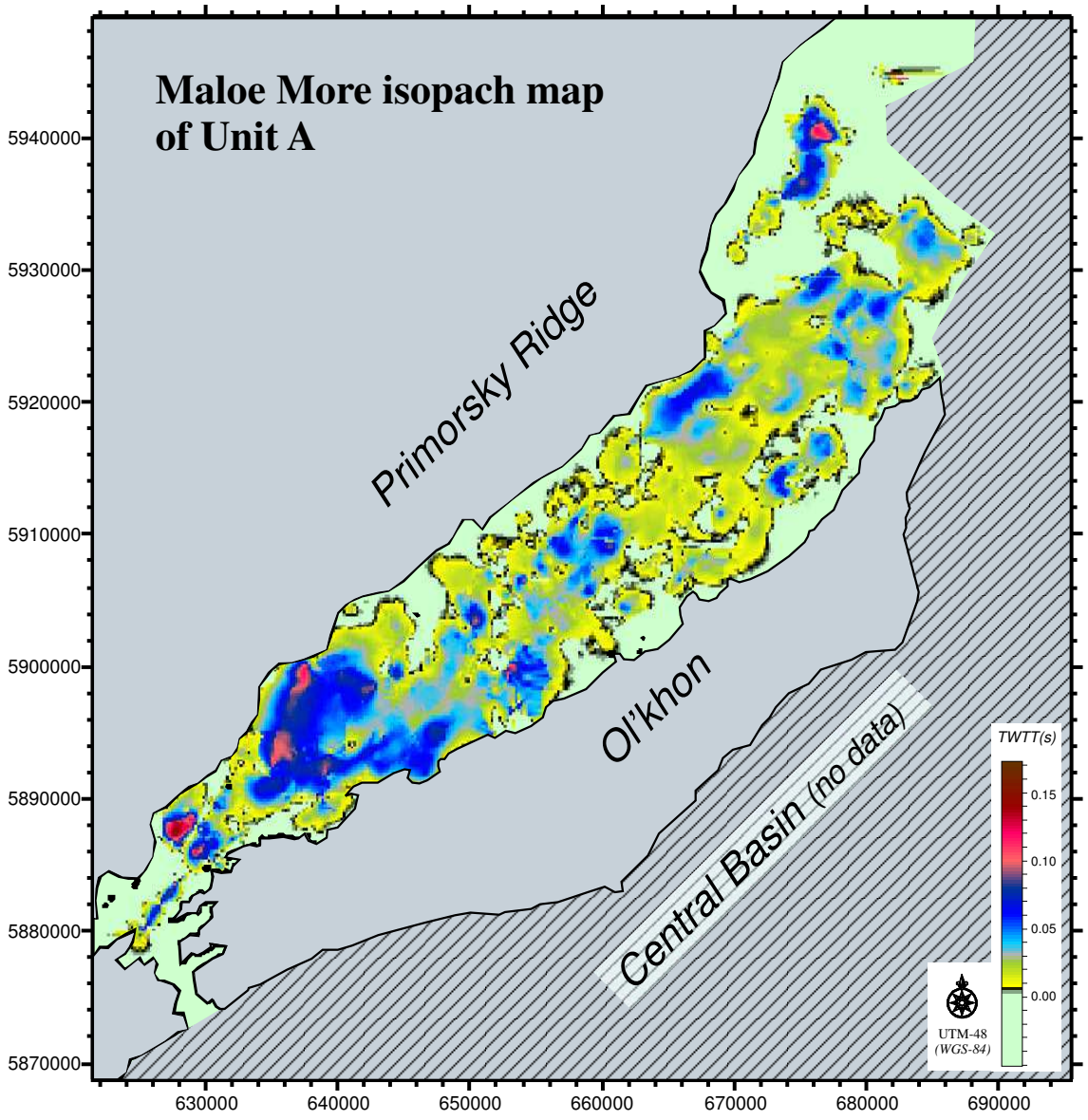

Figure 5.10: *Isopach map of Unit A in Maloe More. The thickest deposits of this unit occur in the southwestern part of Maloe More, as well as near the Zunduk Fault.*

5.5.2 DTM and Satellite image interpretation

As mentioned above (section 5.2), Agar and Klitgord (1995) have identified distinct segments in the trace of the Primorsky Fault and they have related this segmentation with 3 sub-blocks in the Pri-Ol'khon Block (I, II, III in figure 5.2). In this scheme they did, however, consider the area of Maloe More to constitute one of such sub-blocks. For this study, the Primorsky Fault area has been investigated in more detail, using satellite images in combination with the

digital terrain model and a slope map (figures 5.15 and 5.16). The interpretation of the onshore segmentation of the western border fault system along Maloe More is illustrated in figure 5.16. The geometry of the derived fault pattern suggests that during the evolution of this border fault system different fault segments have connected. The arrows in figure 5.15 indicate such inferred "connecting points". Based on the slope map in figure 5.15 and the DTM in figure 5.17, an additional possible segment boundary has been identified offshore, where the trace of the Zunduk Fault is characterised by a kink (indicated by the uppermost arrow in figure 5.15). In

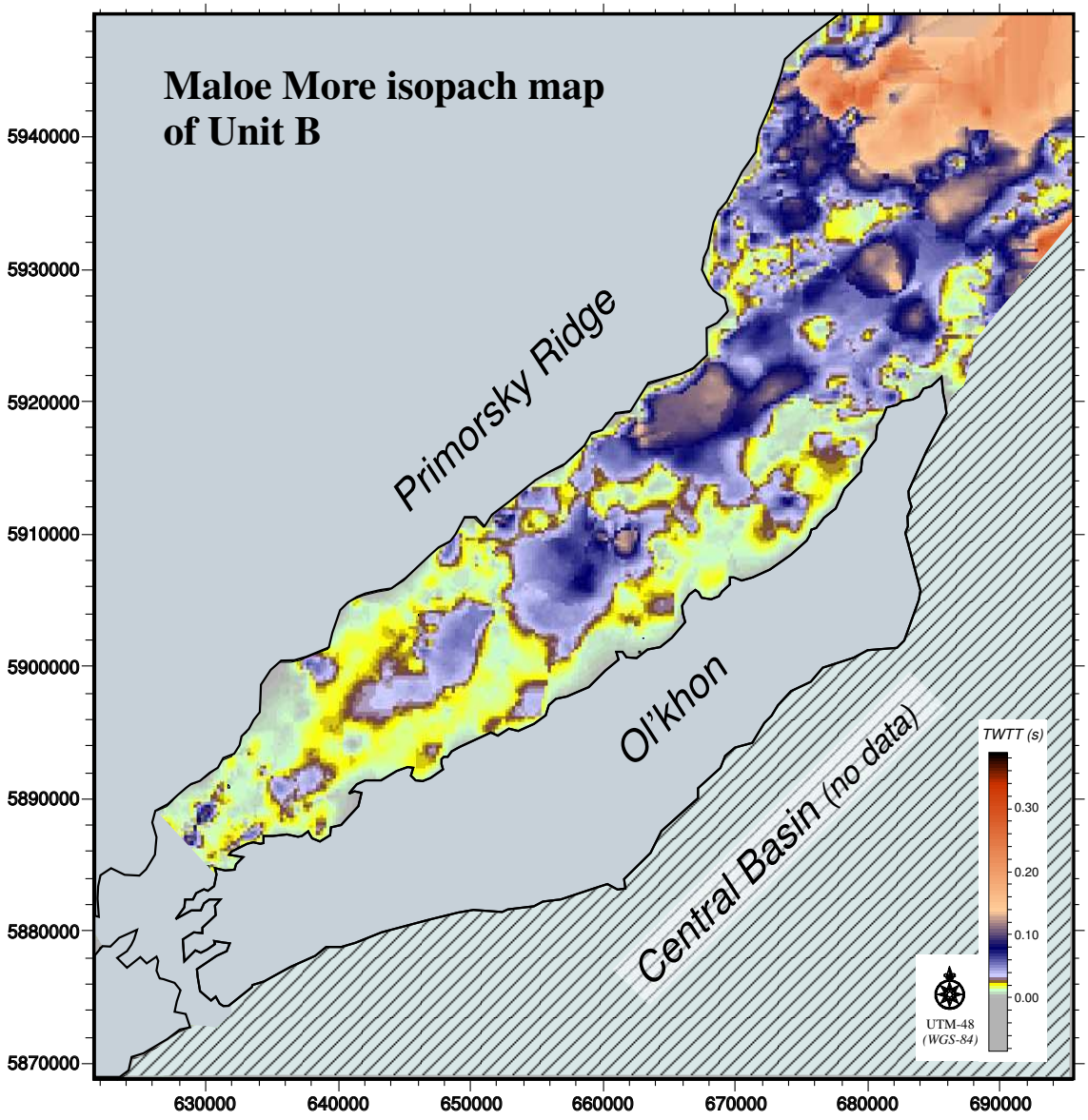

Figure 5.11: *Isopach map of Unit B in Maloe More. Superimposed on the local variations an overall increase in the thickness of this unit is observed from the southwest towards the northeast.*

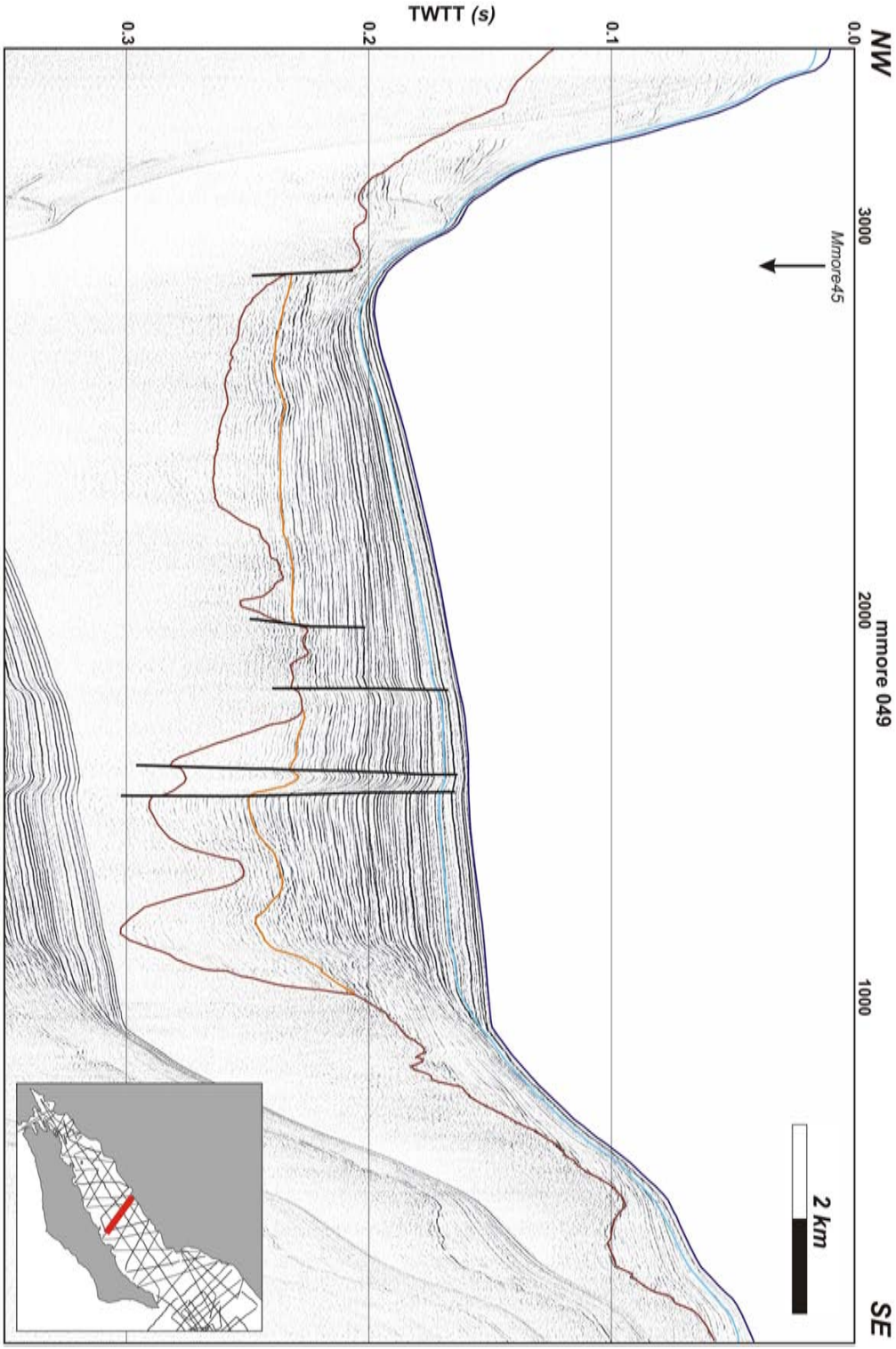

Figure 5.12: *Seismic profile mmore49*

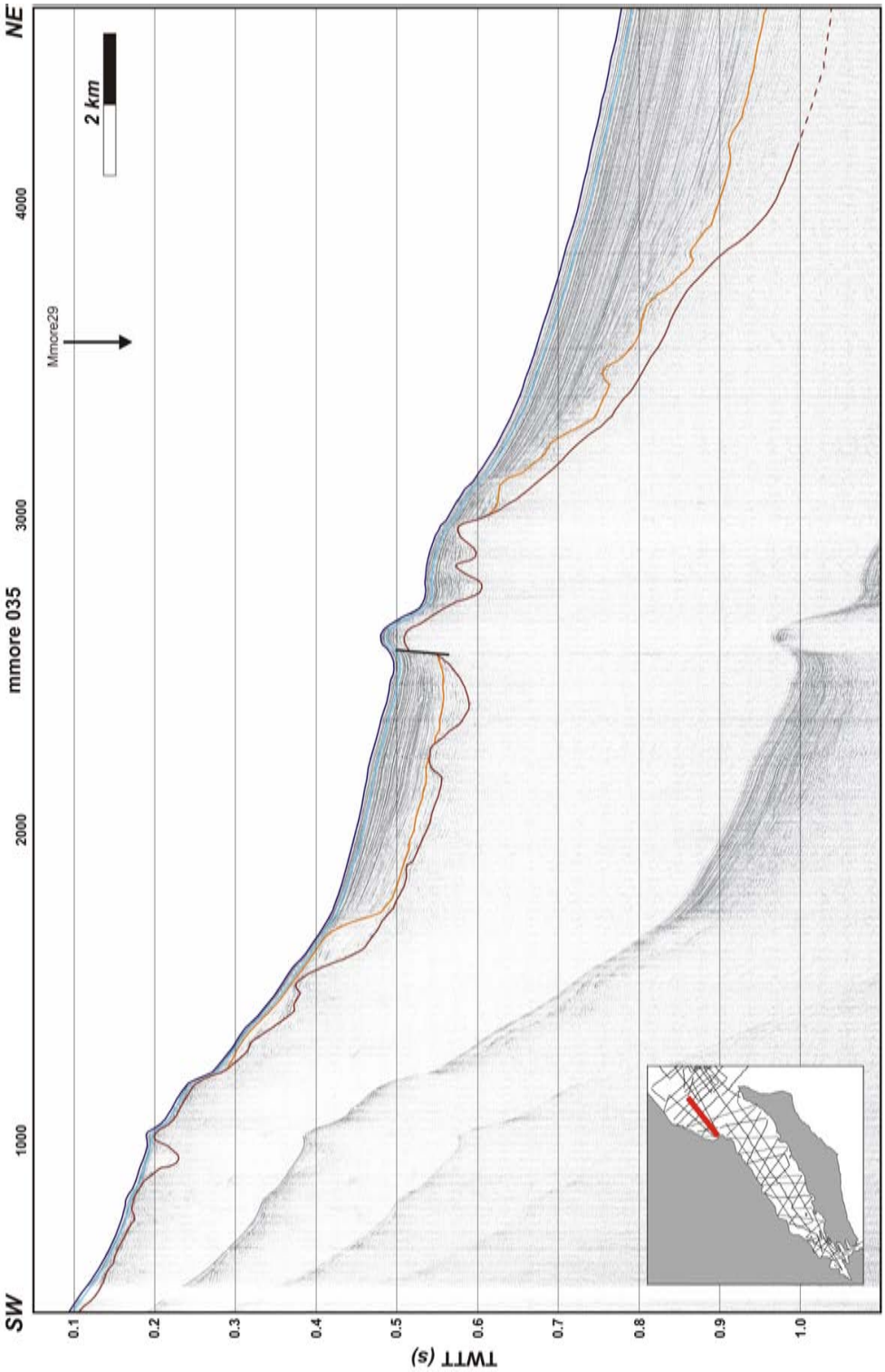

Figure 5.13: *Seismic profile mmore35, which was shot longitudinally throug the fault splay at Zama.*

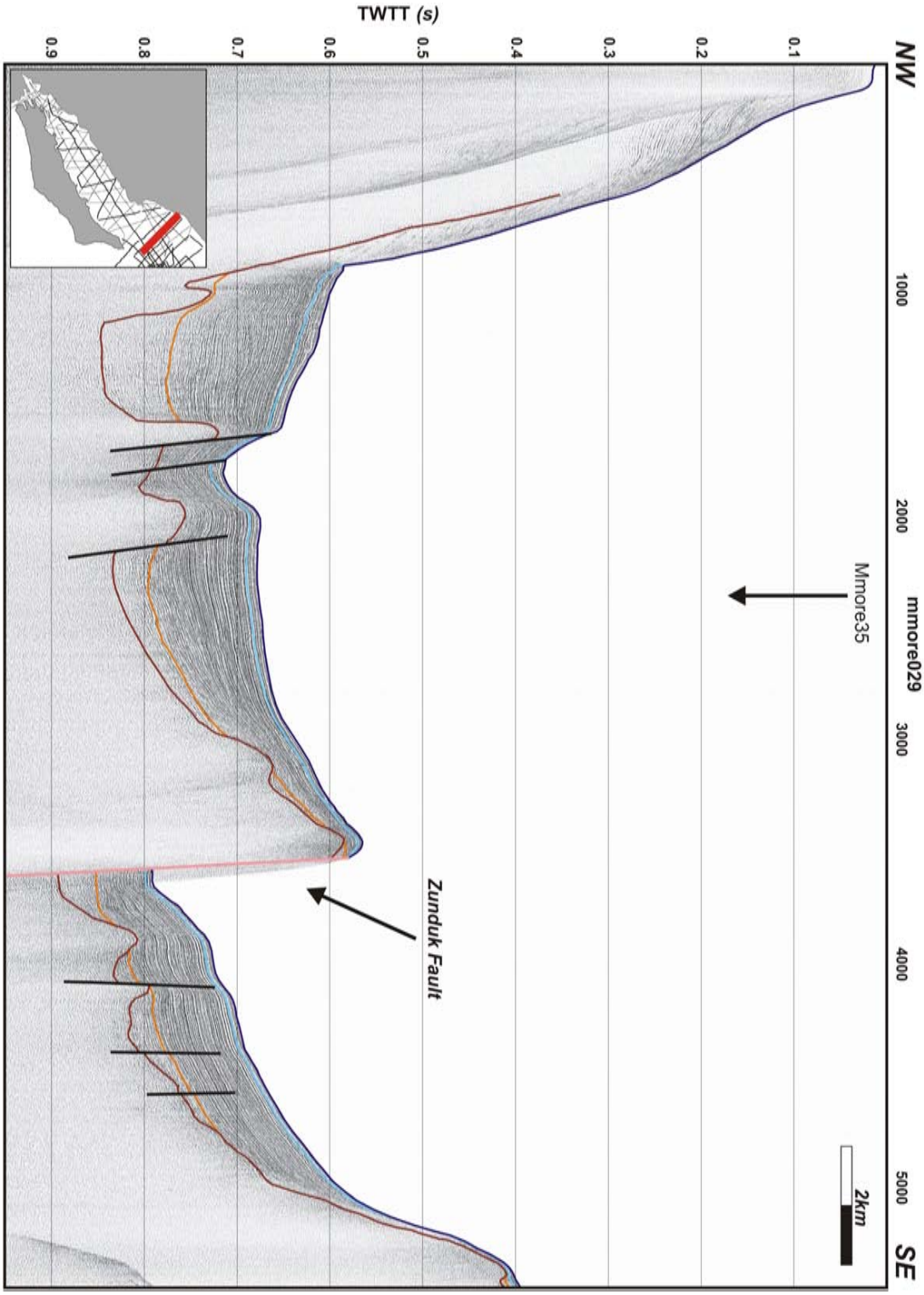

Figure 5.14: *Seismic profile mmore29.*

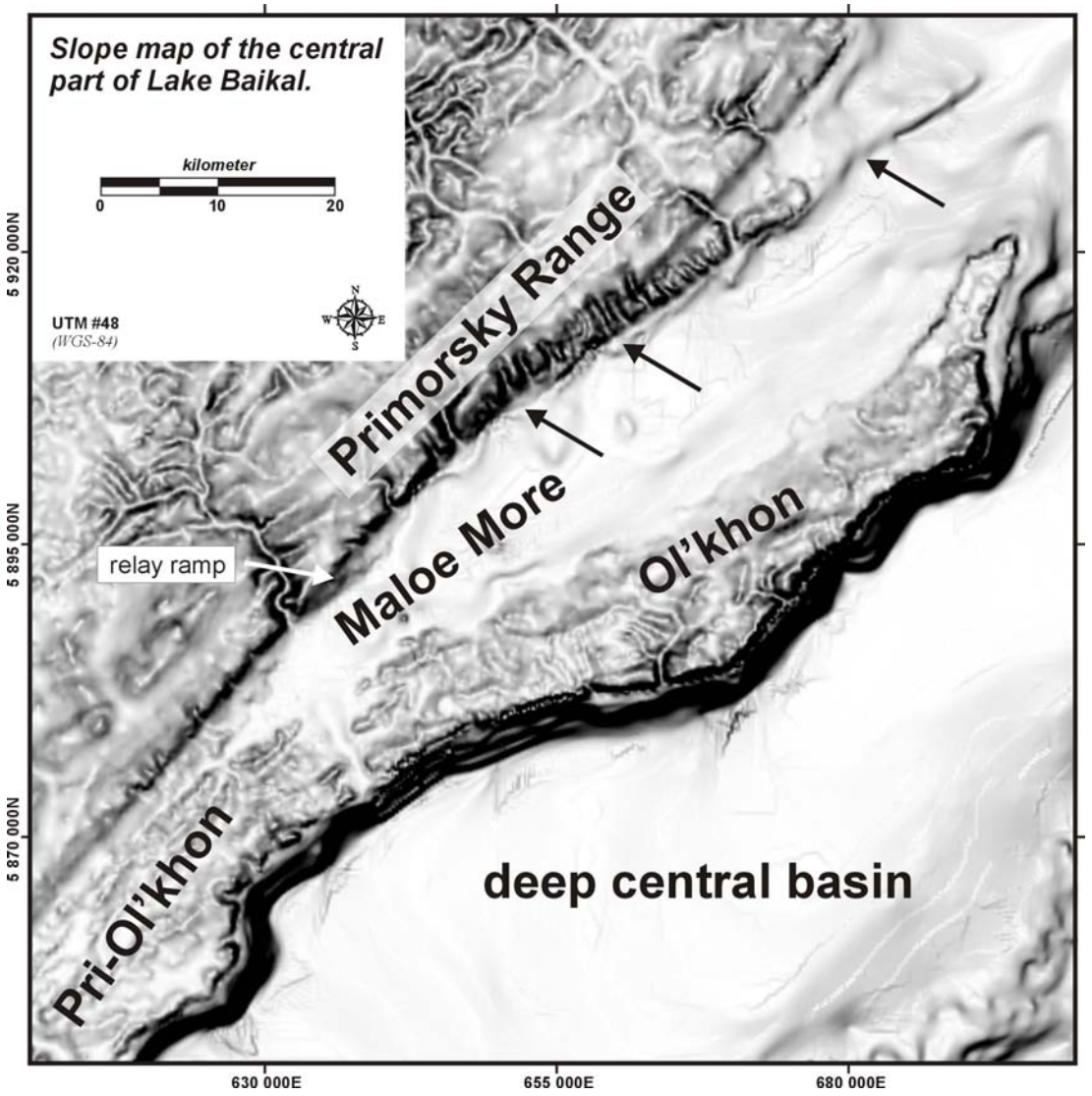

Figure 5.15: *Slope map of the central part of lake Baikal. The arrows indicate the different locations along the trace of the western border fault that might correspond to areas where different segments of this fault system grew together.*

total 4 such connecting points have been inferred along the northwestern border fault system of the Pri-Ol'khon Block.

A compilation of the interpreted structures, onshore and offshore, is presented in figure 5.18 in which a satellite image has been merged with the basement map of Maloe More. It was already mentioned (section 5.5.1) that the ridges in the basement morphology of Maloe More were oriented at high-angle to the main strike of the Primorsky Fault, from this combined figure, it is moreover clear that 4 of the 5 basement ridges are located near the "connecting

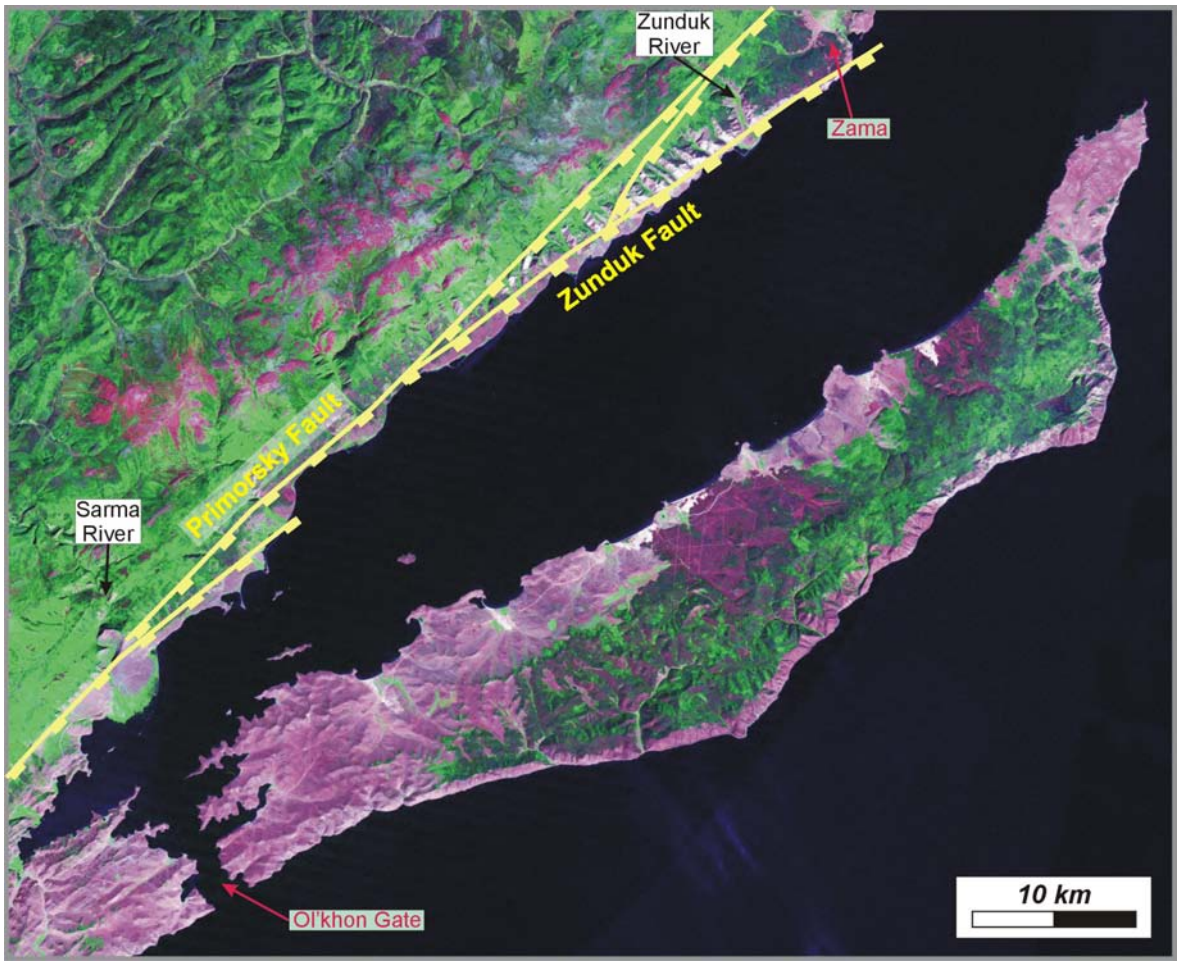

Figure 5.16: *Landsat image containing the onshore interpretation of the Primorsky and Zunduk Faults in Maloe More. The derived fault pattern suggests that during the evolution of this border fault different segments have grown together.*

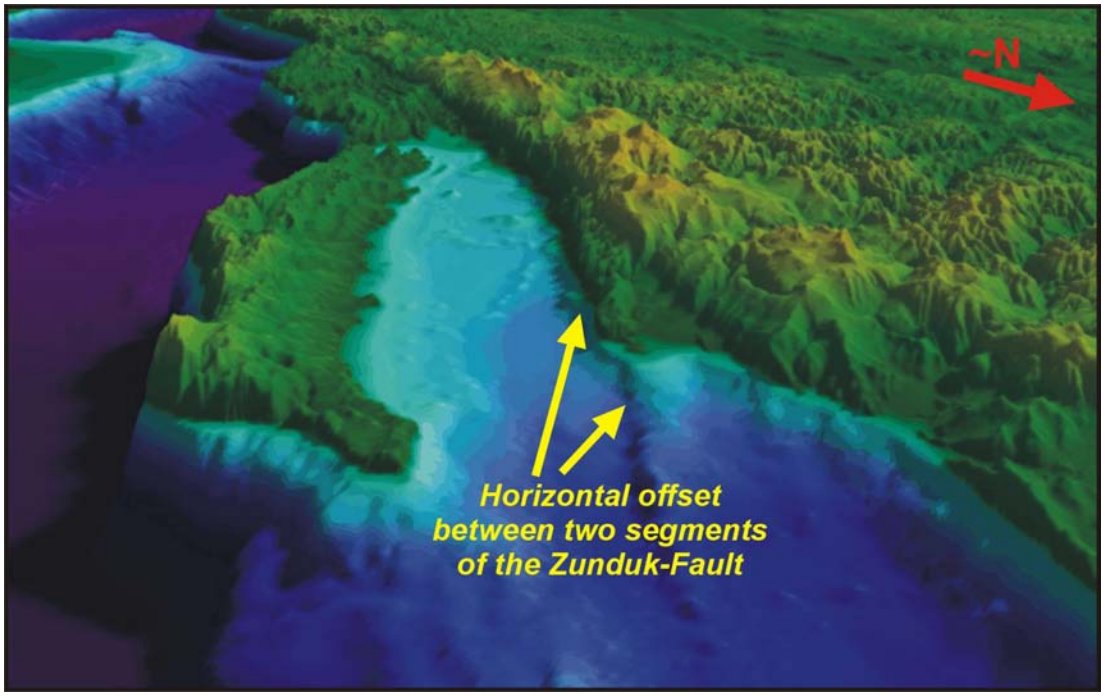

Figure 5.17: *Approximately north-south oriented view of the digital terrain model of the Pri-Ol'khon Block. A clear offset between two segments of the Zunduk Fault is indicated. At this location, the two segments likely connected.*

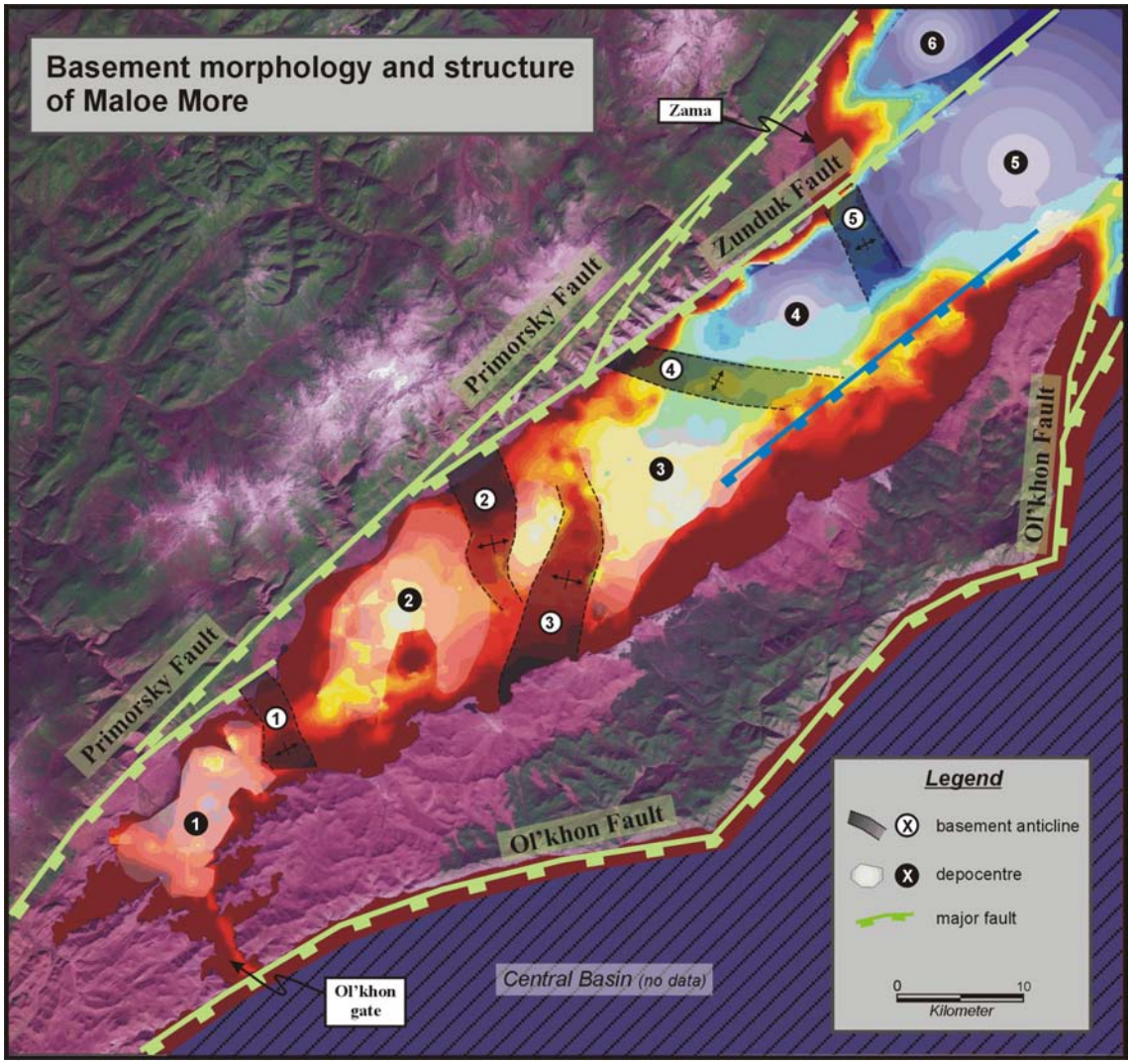

Figure 5.18: *The depth of the basement of Maloe More mosaic-ked with a satellite image of Ol'khon Island and the Primorsky Range. On the satellite image, the segmentation of the Primorsky and Zunduk Faults is indicated. The offshore part shows the different ridges and basins in Maloe More as interpreted with the seismic profiles.*

points" of the Primorsky Fault system (figure 5.18). On the satellite image of Ol'khon Island and Pri-Ol'khon, no other basement structures are observed with orientations similar to those of the basement ridges in Maloe More. Most prominent lineaments onshore have strike directions which are comparable to the strike of the Primorsky Fault.

5.5.3 Structural interpretation.

Because the orientation of the transverse ridges in Maloe More (∼N25°W) does not correspond to directions that could have been inherited from pre-rift evolutionary stages (∼N50°E), a "modern" mechanism — which relates to the development of the Cenozoic Lake Baikal — is most likely responsible for their formation. The adequate formation mechanism should explain the ridge-like morphology in Maloe More, but it should also account for the absence of this morphology on Ol'khon Island.

Concerning the transverse basement ridges different observations have been made so far:

1. From the interpretation of the seismic profiles, it is known that:
   - the ridges have stood out in the lake floor morphology during most of the evolution of Maloe More,
   - the ridges bordered different isolated depocentres, and
   - — except from ridge 3 in figure 5.18 — all the ridges in Maloe More are best expressed near the Primorsky Fault, and gradually disappear towards Ol'khon Island.
2. The interpretation of the onshore fault geometry from the satellite image and slope map suggests that:
   - during the evolution of the northwestern border fault system several faults have grown together.
3. The combination of the satellite image and the basement map revealed that:
   - Many of the ridges (ridges nr. 1, 2, 4 and 5) are located near the zones where different segments of the western border fault connected (figure 5.18).

These points indicate that the ridges could represent so-called *intra basin highs* or *transverse basement highs* (eg. Schlische, 1995). Such antiform highs result from the difference in the amount of hanging-wall subsidence near the tips of interacting fault segments (where a relative small subsidence occurred) as compared to the centres of the segments (characterised by a relative large subsidence). Based on this interpretation, a modified evolution model will be postulated for Maloe More in a later section (section 5.6.1).

As outlined in section 5.2, Maloe More has for a long time been interpreted as being a graben structure in the rift system, bounded on both sides by faults (the Primorsky Fault in the northwest and the Maloe Fault in the southeast) (e.g. Mats, 1993; Agar and Klitgord, 1995; Levi et al., 1997). Not on the seismic profiles nor on Ol'khon Island however, this Maloe Fault has been observed (see also Coisne, 2004). For this reason, Maloe More is interpreted here as being just the submerged part of the large tilted block that forms the Ol'khon Region. The in some

places well-expressed western shore of Ol'khon Island often corresponds to erosional processes along steeply dipping foliation surfaces, without indications for recent faulting. In other places, however, the western shore is characterised by a gradual transition into the lake, without a sudden change in topography (Coisne, 2004).

The seismic profiles have revealed that some of the islands in Maloe More, are indeed fault bounded on their western side, but there is no evidence for the existence of a common fault for all, being the boundary fault of the eastern side of Maloe More and the western side of Ol'khon Island.

5.6 Discussion

The data presented in the previous sections have illustrated that — even in the earliest stage of the evolution of Maloe More — depocentres had already formed in its southwestern part. This finding somehow contradicts the model of a gradual propagation of the Primorsky Fault towards the south which would have caused the subsidence of Maloe More (e.g. Agar and Klitgord, 1995).

Also the proposed timing for the reactivation of the Primorsky Fault (ca. 1 Ma ago according to Agar and Klitgord (1995)) is contradicted by the occurrence of old sedimentary deposits (units X&A, with an Oligocene–Miocene age) in different depressions all along Maloe More.

5.6.1 Evolution of Maloe More

Based on the interpretations made in this chapter, it is possible to postulate an evolution model for Maloe More that is different from older models. This model is outlined below (see also figure 5.19):

During the deposition of Unit X&A in Maloe More (Oligocene–Miocene) isolated depocentres existed whose formation was directly related to the activity of different fault segments of the Primorsky and Zunduk Faults. These fault segments formed the northwestern border of these depocentres, which were separated from each other by basement highs (transverse ridges). At that time, the basement ridges corresponded with the areas between the adjacent fault segments. The formation of such depocentres must have occurred along the whole length of Maloe More, to explain the present distribution of the deposits of unit X&A (figure 5.10 & 5.19a).

With continuing extension in the region, the different segments of the western border fault system increased their length and displacement, causing the depocentres to become larger. Eventually the segments approached neighbouring segments close enough to allow for interaction and a later coalescence (similar to the process described in section 2.4.1) (figure 5.19b).

The first two segments to coalesce were from the Zunduk Fault causing the gradual lowering of ridge number 6 especially near the fault trace itself. When unit B was deposited in this area, there was already a connection between depocentres 4 and 5 (figure 5.18). This connection was located near the Zunduk Fault, whereas the southeastern end of ridge 6 remained a barrier during this period. The early connection of these two fault segments, and the subsequent displacement on this long fault, are the reasons for the basement being at that time more

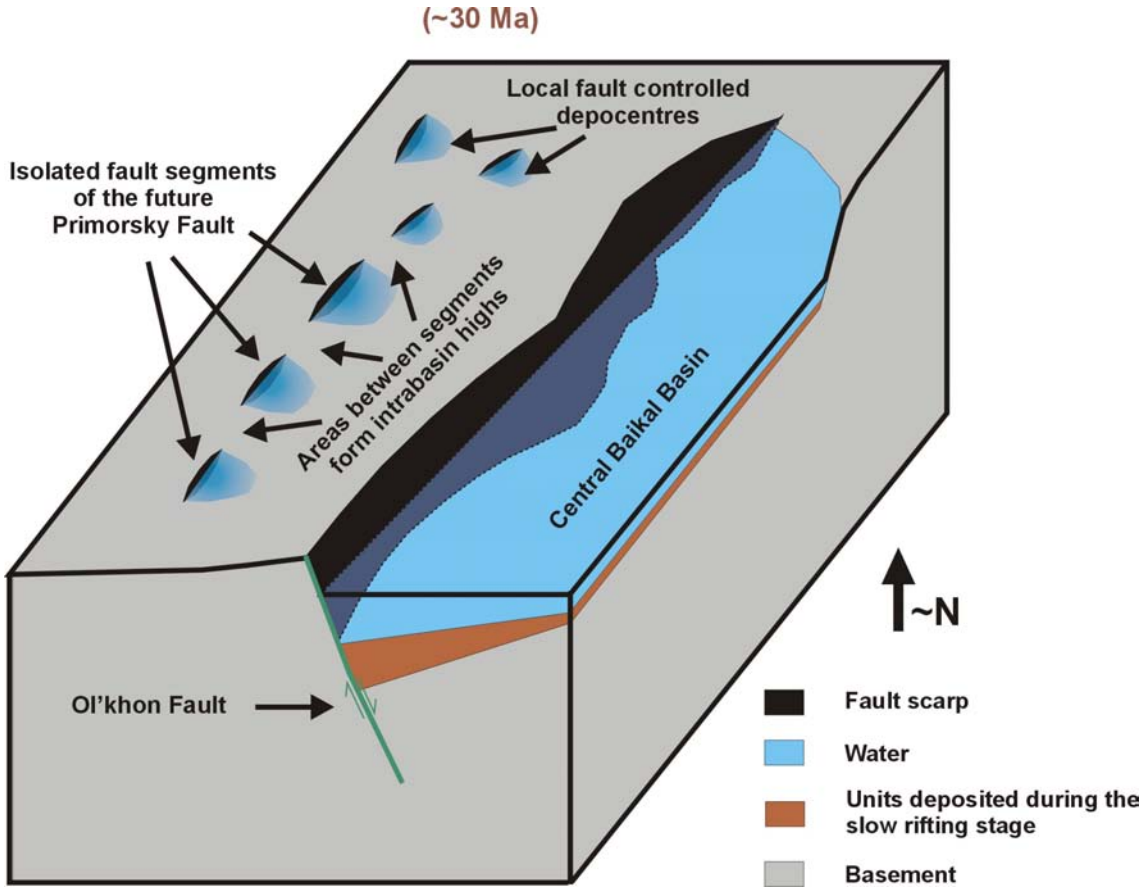

Figure 5.19: **(a)** *Conceptual model of the evolution of Maloe More. First evolution stage: Different isolated fault segments develop in the hanging-wall region of the Ol'khon Fault. These segments delimit small half-graben basins in which unit X&A have been deposited. These basins are separated by transverse intra-basin highs that correspond to the locations of minimal subsidence between different fault segments.*

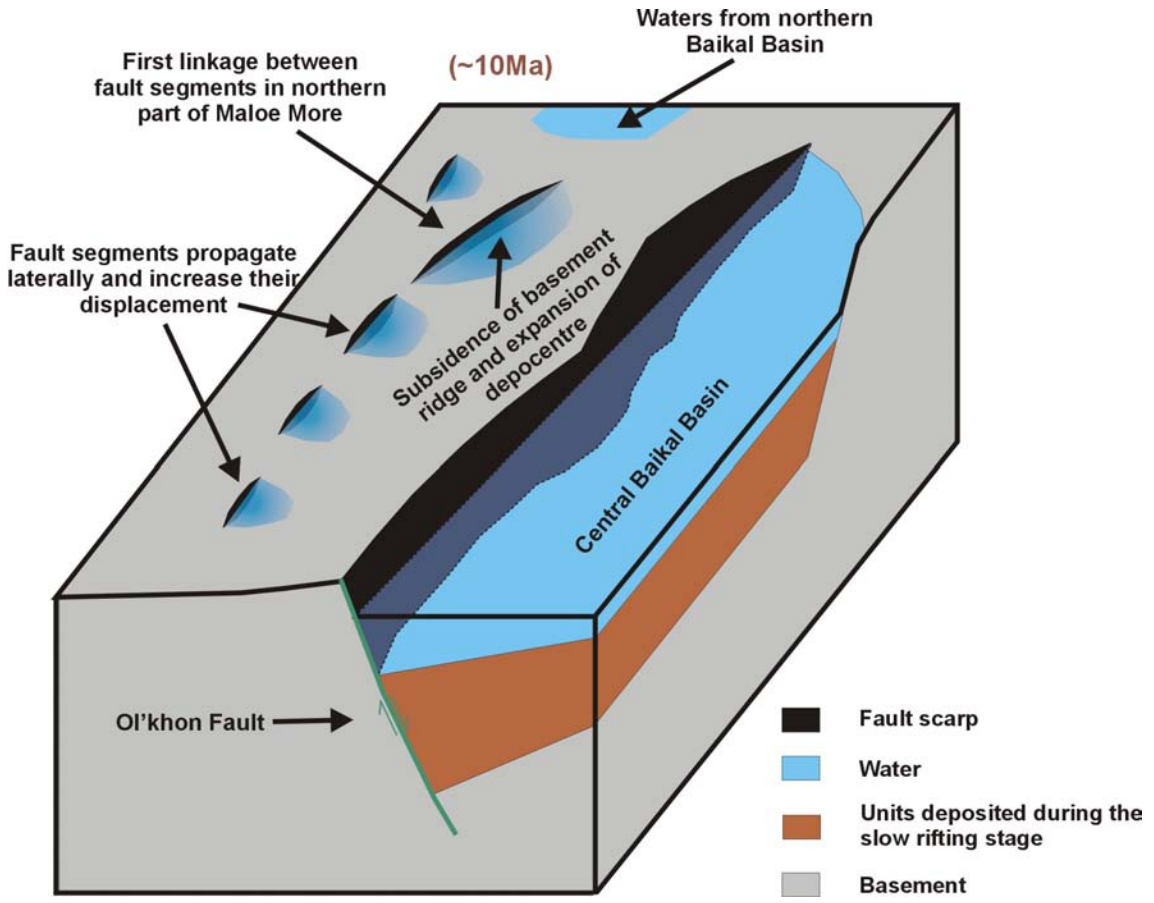

Figure 5.19: ***(continued, b)*** *Conceptual model of the evolution of Maloe More. Second evolution stage: During this stage, the isolated fault segments increase their displacement and propagate further. In the northernmost part of Maloe More, this lateral propagation caused the connection between 2 such fault segments. This linkage resulted in an expansion of the half-graben basin and the gradual disappearance of the intra-basin high between the segments.*

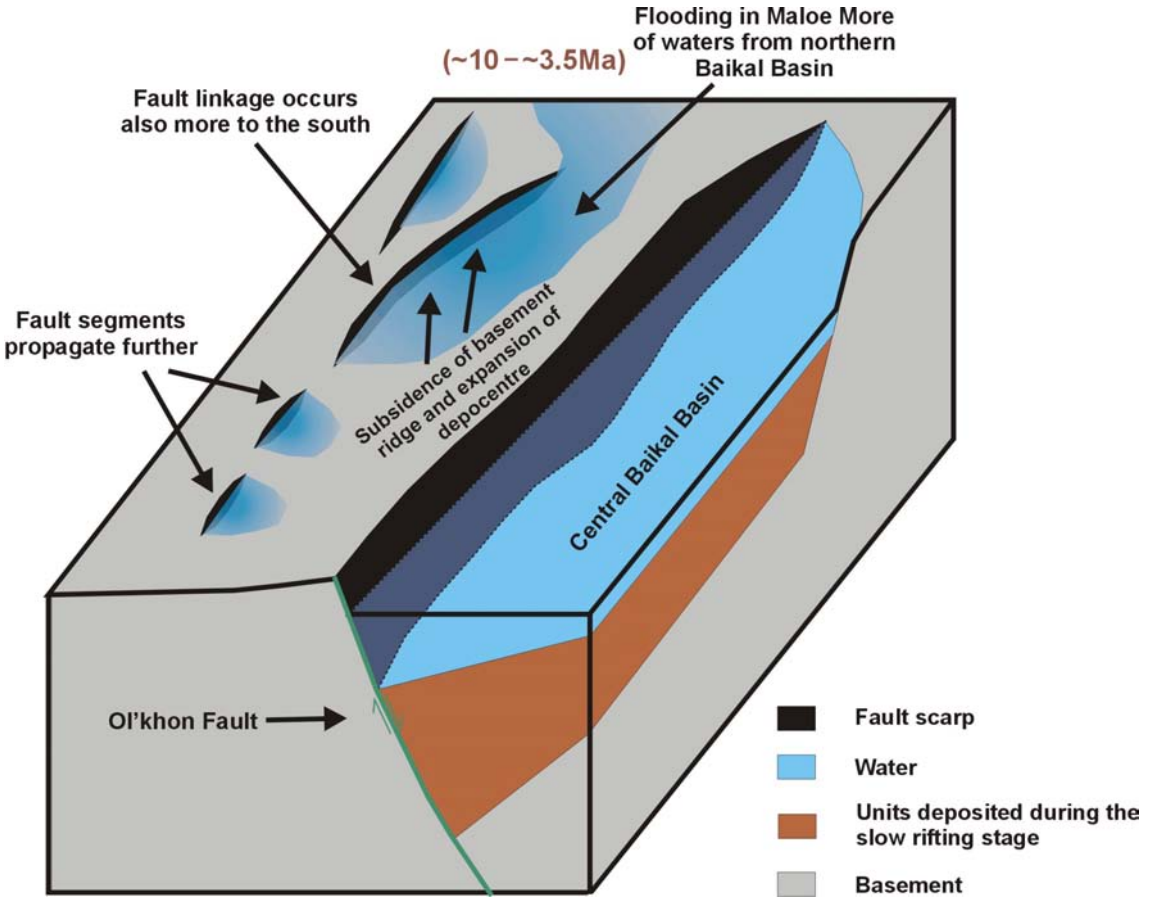

Figure 5.19: ***(continued, c)*** *Conceptual model of the evolution of Maloe More. Third evolution stage: Segments propagate further, and start to link-up also more to the south in Maloe More. During this time, also the waters of the northern Baikal Basin start to flood the northern half of Maloe More.*

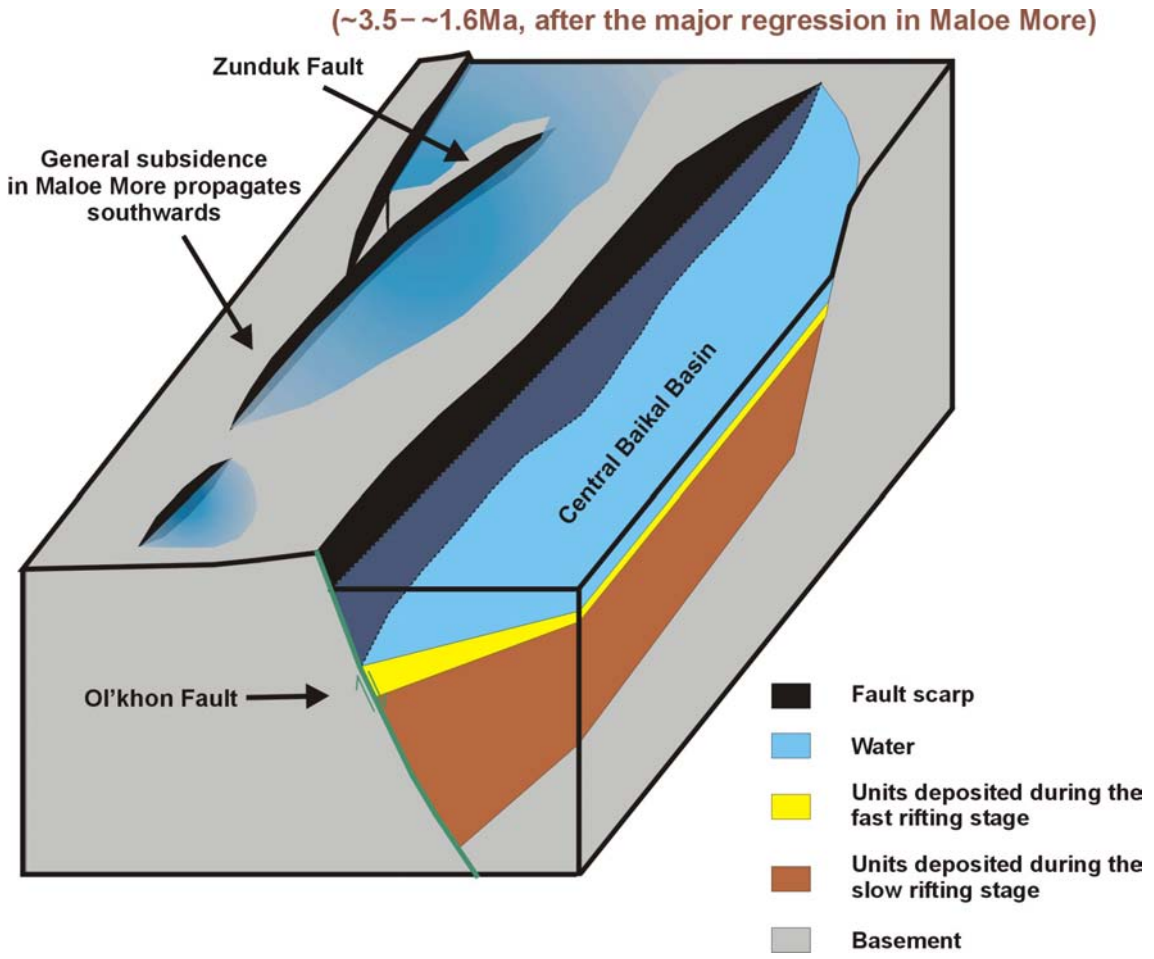

Figure 5.19: ***(continued, d)*** *Conceptual model of the evolution of Maloe More. Southern fault segments connect, while the overall displacement increases.*

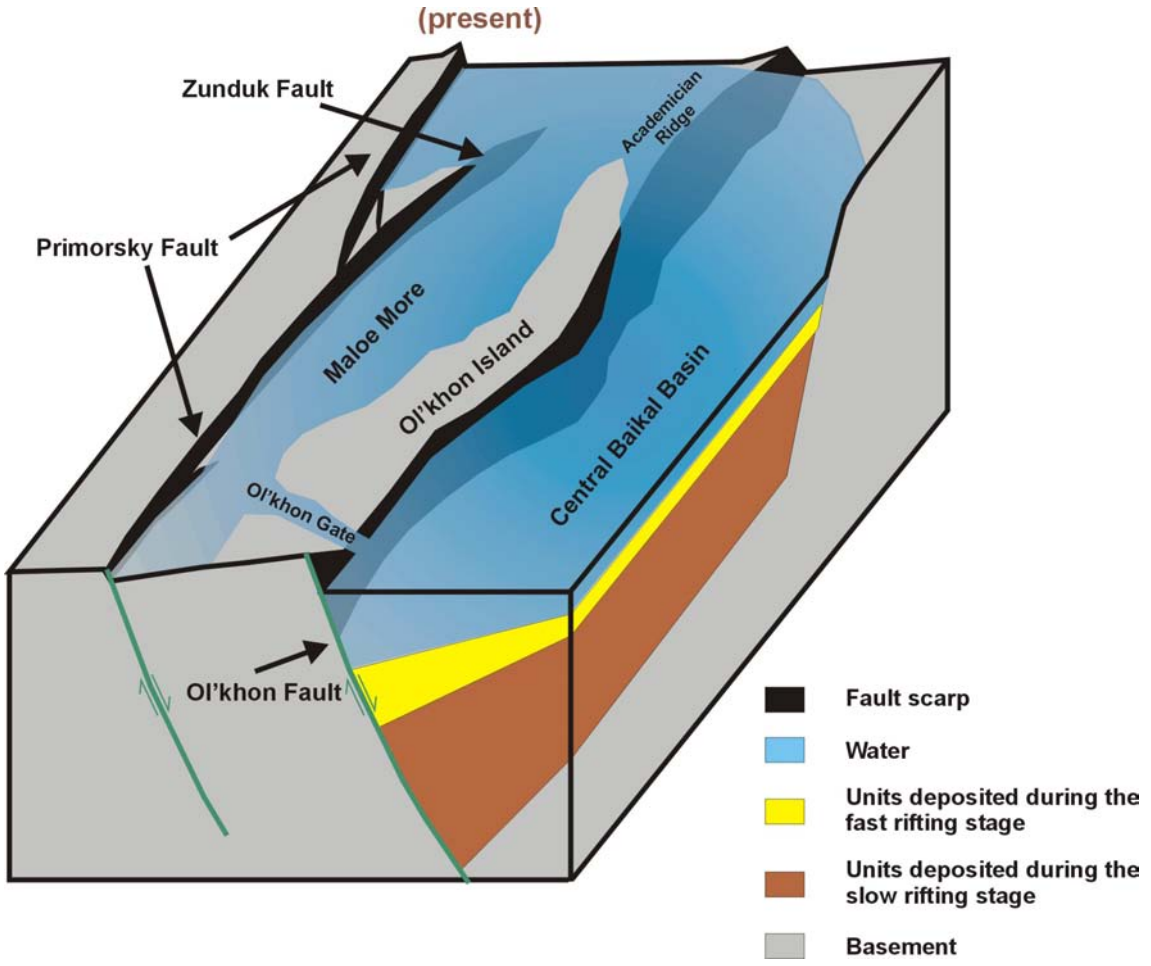

Figure 5.19: ***(continued, e)*** *Conceptual model of the evolution of Maloe More. Present situation.*

submerged here than in the other parts of Maloe More. The same scenario occurred in later times for the other segments of the Primorsky Fault in the southwestern part of Maloe More (figure 5.19c–e). However, as these segments grew together only later, the basin highs that had formed between them persisted longer, strongly influencing the distribution of the deposits of unit B. This explains why these ridges are still clearly visible on the isopach map of the whole sedimentary sequence in Maloe More (figure 5.9).

The fact that the highs between the different segments of the Primorsky Fault seem to gradually disappear after fault segments connect (e.g. ridge 5 in figure 5.18) suggests that the Primorsky Fault grew by the "coherent fault model" of Childs et al. (1996) and Walsh et al. (2003). Therefore, the different fault segments were likely already connected at depth (see section 2.4.3).

A final connection of the Primorsky and the Ol'khon Faults might have occurred when the uppermost unit in Maloe More was deposited (unit R). One might indeed expect that a final connection of these two faults would have reduced the intra-block deformation of the area, as observed by the decrease in the number of faults cutting through the upper unit (eg. Gawthorpe et al., 2003).

The idea of the Zunduk Fault playing an important role in the initial subsidence of Maloe More, as suggested by the proposed evolution model, is consistent with the relative late submerging of the Zunduk Fault footwall block (Mats et al., 2000).

In the light of the evolution scheme presented above, the most feasible explanation for the uplift of Ol'khon Island around 3.5 Ma ago (see section 3.3.2) — when the fast rifting stage started in the Baikal Rift Zone — might be that this uplift was related to footwall uplift of the Ol'khon Fault associated with the at that time increased subsidence rate of the Ol'khon Fault's hanging-wall. Moreover as at that time also major regressions occurred in Maloe More (Mats et al., 2000) this uplift seems to have affected the Pri-Ol'khon Block as a whole, confirming that it actually is one structural block. The uplift of the Pri-Ol'khon Block also forms an indication for the Primorsky Fault not yet being linked with the Ol'khon Fault at that time because, if that were the case, one would expect a subsidence in Maloe More instead of an uplift. The Primorsky Fault should have been at that time only of "minor" importance, i.e. with a restricted trace length.

5.6.2 Comment on the two-stage rifting model

Agar and Klitgord (1995) refer to seismic profiles of the USGS to illustrate that since around 1 Ma ago there has been a decrease in the amount of faulting in the deep central Baikal basin, ie. in the hanging-wall of the Ol'khon Fault. They further state that this period also corresponds to the time of linking between the Primorsky Fault with the Ol'khon Fault. If indeed the connection of the two main faults in Central Lake Baikal results in a decrease in the activity in its hanging-wall, this would mean that the model of ten Brink and Taylor (2002) to explain subsidence intensification in Baikal by the readjustment of displacement profiles along its main faults doesn't hold. And therefore it remains questionable that this is the most suitable explanation for the

transition of the slow rifting stage to the fast rifting stage around 3.5 Ma ago in the Baikal Rift Zone. Indications have been found (and discussed above) that two of the major faults in the central part of Lake Baikal connected only after the transition into the fast rifting stage. If the model of ten Brink and Taylor (2002) is the right one, it still needs to be answered which other fault connections could have been so important as to cause the transition ∼3.5 Ma ago, which was observed in the whole Baikal Rift Zone.

Moreover, paleostress reconstructions in the Baikal Rift Zone have illustrated that the transition between the two rifting stages in the central part of the rift marked a change in the stress field from a strike-slip or transpressional regime in the slow rifting stage to a pure extensional regime in the fast rifting stage (Delvaux et al., 1997; San'kov et al., 1997). As there were at that time clear changes in the orientation of the stress field, it is not unlikely that they were accompanied by changes in the magnitude of the stress field as well. Therefore stating that the increased subsidence rates in the fast rifting stage are not related to an increase in the rate of extension is for the Baikal Rift probably running ahead of the observations.

5.6.3 Note on fault reactivation

The Primorsky Fault has been a long-lived deformation zone (Proterozoicum and Paleozoicum) that was reactivated in the Cenozoic (Theunissen et al., 1993; Arzhannikova and Gofman, 2000). Unlike the idea proposed by Walsh et al. (2002) — that a reactivated fault is characterised by a length equal to the inherited fault length, but with initially only minor displacements (section 2.6.2) — the evolution model described in this chapter suggests that the Primorsky Fault reactivation did originally not involve the whole fault. Instead different patches of the old shear zone were initially reactivated and grew laterally with increasing displacement. The reactivation of the whole Primorsky Fault has only been the final result of this.

The irregular fault trace of the Ol'khon Fault, also suggests that the fault grew by the connection of different fault segments (C. K. Morley *personal communication*, September 2001), also indicating that the fault was not reactivated at once along whole its length, but rather as different smaller segments.

5.6.4 Note on the scale independence of relay ramps

Regardless the fact whether or not the Pri-Ol'khon Block formed a relay ramp in earlier times before the actual merging of the Primorsky and the Ol'khon Faults (e.g. Agar and Klitgord, 1995; Delvaux et al., 2000), observations from the study in this chapter can be used to argue that large scale relay ramps are likely to be structurally different from small scale ramps. Where for smaller relay ramps it is possible that they are fully controlled by two overlapping fault segments that grew themselves by the radial propagation process, this is unlikely for relay ramps that are controlled by large-scale faults. As observed in this chapter, the main faults of such large ramps might have formed as a result of fault segment linkage, causing the relay ramp to be shaped by local depocentres and transverse ridges. This structure can in a later stage be further complicated by the superposition of similar deformations as those recognised in smaller

ramps (secondary fracturing, layer bending, etc.).

5.7 Conclusions

In this chapter a new model has been proposed for the development of the Pri-Ol'khon Block. This model can be used to explain more observations that were made in the area than the previous model of Agar and Klitgord (1995). For example:

- The model provides an explanation for the occurrence of different basement ridges in Maloe More, striking highly oblique to the direction of the main western boundary fault.
- The model explains the presence of relatively thick deposits of old sedimentary units in the southwestern part of Maloe More (Unit X&A).

In the model presented, the Primorsky Fault did not propagate gradually in a southwestward direction to create the Maloe More depression. Instead, in a first phase, extension was distributed more or less equally over different segments that make up the present-day Primorsky and Zunduk Faults. The linkage of these segments increased the amount of displacement, causing a further subsidence. This linkage process was established first between the northernmost segments in Maloe More and only later more to the south. As a result the overall subsidence in Maloe More also propagated from north to south.

During the evolution of Maloe More and Lake Baikal, different fault segments evidently grew together, increasing locally subsidence rates for certain time spans. However it remains unclear whether this mechanism is a good explanation for the two rifting stages in the Baikal Rift Zone. At present there are no clear indications confirming that the connection of major fault segments occurred everywhere at the same time during the evolution of the lake. Moreover, as there also seems to be an increase in tectonic activity around 3.5 Ma ago in other areas of Asia, probably a more regional explanation might be required to explain the two rifting stages that are observed in Lake Baikal.

Part II

Sandbox modelling of relay ramps between normal faults

Robert Hus, December 2004

Chapter 6

Analogue Modelling of relay ramps

The analogue modelling experiments discussed in this chapter, belong to the first category of models mentioned on page 25 in section 1.1 of the introduction. In these first models, the geometry of 2 faults was varied to see how this affected the relay ramp structure that formed between them, and the further evolution of the ramp. The observed real time evolution of the ramps in the sandbox models has subsequently been compared to conceptual evolution models inferred from static relay ramp examples. This chapter also contains the theoretical background of scaled experiments. In a later chapter on the second category of models (chapter 7), there will be referred to this section.

The models presented in this chapter have all been run in the analogue modelling laboratory of the University of Rome (Università Roma Tre) under the supervision of Dr. Valerio Acocella.

6.1 Introduction

Although the first reported analogue modelling experiments in earth science date back to almost 200 years ago[1], the technique has only been widely used since the pioneering models of Cadell in 1889[2] to study the geometric, kinematic and dynamic evolution of geological structures (e.g. McClay, 1996).

In general the study of geologic structures encompasses the observation and inspection of final structures without having a chance to observe the initial situation or to witness the actual evolution (Ramberg, 1981). Ramberg (1981) has stated the role of experimental modelling in tectonics as:

> The significance of scale-model work in tectonic studies lies in the fact that a correctly constructed dynamic scale model passes through an evolution which simulates exactly

[1]These experiments were done by Sir James Hall and presented to the Royal Society of Edinburgh: Hall Sir, J. 1812. Account of a series of experiments, showing the effects of compression in modifying the action of heat. *Trans. R. Soc. Edin.,*6,71–185; Hall Sir, J. 1815. On the vertical position and convolution of certain strata, and their relation with granite. *Trans. R. Soc. Edin.,*7,79–108. References from Koyi (1997) and Ranalli (2001).

[2]Cadell, H. M. 1889. Experimental researches in mountain building. *Trans. R. Soc. Edin.,*35,337–357. Reference from McClay (1996).

that of the original (the prototype), though on a more convenient geometric scale (usually smaller) and with a conveniently changed rate (usually faster).

It is, however, not the aim of modelling experiments to accurately simulate a complex geological situation because this would require the precise knowledge of the boundary geometries and conditions that have determined the process in nature (Mandl, 2000). Mandl (2000) has emphasised that, in a study of tectonic fault structures by scaled models, relatively simple boundary geometries should be imposed, and that rather than attempting to simulate the full complexity of a natural fault system at once, the combination of simple models should be used to analyse the complex situations in nature.

Scaled analogue models provide visual images of how complex geological structures evolve in time and space, and are therefore useful tools for guiding the interpretation of natural structures. In addition, correctly scaled physical models deform according to the same mechanical laws as natural structures. Unlike numerical models, analogue models of brittle deformation in the upper crust easily include the formation and growth of new faults in 3 dimensions during the experimentation (McClay, 1996).

Analogue models have been used to simulate and understand geologic structures in different regimes: e.g. extensional deformation (Horsfield, 1977; Vendeville et al., 1987; Ellis and McClay, 1988; McClay, 1990b; Tron and Brun, 1991; Childs et al., 1993; McClay and White, 1995; Mauduit and Dauteuil, 1996; Higgins and Harris, 1997; Acocella et al., 1999a; Clifton et al., 2000; Mart and Dauteuil, 2000; Gabrielsen and Clausen, 2001; McClay et al., 2002), thrust faulting (Mulugeta and Koyi, 1987; Colletta et al., 1991; Cobbold et al., 2001; Schreurs et al., 2001; Lickorish et al., 2002), strike-slip deformation (Emmons, 1969; Tchalenko, 1970; Richard and Krantz, 1991; Schreurs, 1994; Dooley and McClay, 1997; McClay and Bonora, 2001; Schöpfer and Steyrer, 2001), inversion (Buchanan and McClay, 1991, 1992), etc... The similarities observed between the structures in the models and those from nature, confirm the usefulness of scaled physical models.

6.2 Theoretical background of scaled experiments

6.2.1 Scaling

In order for a model to be a good analogue for a natural structure, the model should be scaled correctly. A correct scaling requires that basically three conditions are fulfilled: (1) *geometric similarity* between the model and the prototype, (2) *kinematic similarity* between them and (3) *dynamic similarity* between them (Hubbert, 1937; Ramberg, 1981).

geometric similarity: a model and a prototype are geometrically similar if all corresponding lengths are proportional and all corresponding angles are equal (Hubbert, 1937). This implies that the ratio of the distances between any two corresponding points in the model and prototype is constant,

$$\frac{L_m}{L_p} = \lambda \tag{6.1}$$

as well as the ratio of corresponding surfaces between model and prototype and corresponding volumes:

$$\frac{S_m}{S_p} = \lambda^2 \quad \text{and} \quad \frac{V_m}{V_p} = \lambda^3$$

Symbols marked with the sub-script m denote values for the model, whereas those with the sub-script p correspond to values for the prototype.

kinematic similarity: a model and a prototype are kinematically similar if the model remains geometrically similar to the prototype during the evolution of both structures, provided that the evolutionary stages are compared at corresponding times (Ramberg, 1981). This requires that the model ratio of time remains constant throughout the evolution:

$$\frac{t_m}{t_p} = \tau \tag{6.2}$$

with t_p the time needed for a given transformation of the prototype and t_m the time required for the model to undergo a corresponding transformation (Hubbert, 1937; Ramberg, 1981).

dynamic similarity: Dynamic similarity is fulfilled if for each force F_p that acts on a mass dm_p of the prototype, a corresponding force F_m exists in the model that acts upon a mass dm_m. This force must have the same orientation as F_p and the ratio of their magnitudes should be equal to the model ratio of force:

$$\frac{F_m}{F_p} = \phi$$

This ratio should be the same for all kinds of mechanical forces that act on the model and prototype (e.g. gravity, inertia, viscous, elastic and frictional) (Ramberg, 1981):

$$\phi = \frac{F_{m,g}}{F_{p,g}} = \frac{F_{m,i}}{F_{p,i}} = \frac{F_{m,v}}{F_{p,v}} = \frac{F_{m,e}}{F_{p,e}} = \frac{F_{m,f}}{F_{p,f}} \tag{6.3}$$

In all experiments for this work well rounded dry quartz sand has been used. Dry quartz sand obeys the limit condition of Coulomb-Mohr and has an angle of internal friction that is more or less the same to that of sedimentary rocks (ie. 30°–40°) (Schellart, 2000). This means that to scale the model — in the earth's gravitational field — the cohesion of the modelling analogue should be scaled down with the same factor as the dimensions of the model compared to the prototype. This is required because in normal gravity, the ratio between corresponding stresses in the model and the prototype equals the ratio between corresponding lengths (i.e. λ) (eg. Hubbert, 1937; Mandl, 2000). Indeed, for the overburden stress:

$$\frac{\sigma_m}{\sigma_p} = \frac{\rho_m.g_m.L_m}{\rho_p.g_p.L_p}$$

As $g_p = g_m$ and $\rho_p \approx \rho_m$ this equation reduces to

$$\frac{\sigma_m}{\sigma_p} \approx \frac{L_m}{L_p} = \lambda$$

Correct scaling of a model moreover requires that the same deformation mechanism is active in model and prototype, and that faulting starts in both cases at the same critical conditions (kinematic similarity). If both, prototype and model, follow the limit condition of Coulomb-Mohr (see equation 2.3 on page 32) this means that:

$$\left(\frac{\sigma'_I - \sigma'_{III}}{2}\right)_m = \lambda\left(\frac{\sigma'_I - \sigma'_{III}}{2}\right)_p$$

or

$$\left(\frac{\sigma'_I - \sigma'_{III}}{2}\right)_m = \lambda(\tau_{0,p} + \sigma_p.\tan\varphi)$$

therefore, apart from the stresses, also the cohesion of the modelling material should be scaled down with the same scaling factor λ:

$$\tau_{o,m} = \lambda.\tau_{o,p}$$

with:

φ = the angle of internal friction
τ_0 = the cohesion

With cohesion values for well-rounded dry quartz sand ranging from a few Pa to about 520 Pa (McClay and Ellis, 1987; Vendeville et al., 1987; Krantz, 1991) and one of 10^7 – 7.10^7 Pa for most sedimentary rocks (eg. Schellart, 2000), this results in a scaling factor λ of around 10^5, or 1 cm in the model corresponds to 1 km in the prototype (eg. Horsfield, 1977; Dooley and McClay, 1997, amongst others).

6.2.2 Properties of sand as a modelling analogue

From equation 2.3 it is clear that the 2 mechanical properties that determine the deformation of a material that obeys the Mohr-Coulomb criteria are the cohesion of the material *(τ_0)* and the angle of internal friction *(φ)*. These values can be determined experimentally with shear rigs, in which shear stresses and normal stresses are measured at failure (e.g. McClay, 1990a). Weijermars et al. (1993) argued that for models in a normal gravity field cohesion values should be 300 Pa or less, in order to fulfil the scaling criteria discussed above. Angles of internal friction should be between 40° and 30° to correspond to natural values (Weijermars et al., 1993). Under such conditions the mechanical behaviour of dry quartz sand in the model is similar to that of a brittle upper crust in nature.

As a response to the tensional stresses in a model, sand will form granular shear zones of which the width is directly proportional to the grain size of the material (McClay, 1990a). Such shear zones are formed by a process that is called *shear dilation* (Mandl, 1988). The sliding of

grains over each other increases the pore space in the shear zone (volume increase of typically 12% (e.g. McClay, 1990a)) and decreases the number of point contacts between the grains (figure 6.1). McClay (1990a) showed that the width of the shear zones is approximately 5 times the average grain size of the modelling material. In sand models with an averaged grain size of 300μm shear zones had widths of around 1.5 mm, whereas for clay layers with a significantly smaller grain size, the shear zone widths could be as small as 0.2 mm (McClay, 1990a). Once a fault forms in a sandbox model, it becomes weaker than the surrounding unfaulted sand, causing it to be the preferred location for further failure.

Cohesionless sand is suitable as a modelling material because of its bulk mechanical properties. Scaling back individual sand grains in a model to unrealistic large boulders in nature therefore makes little sense (Weijermars et al., 1993).

The deformation of a *brittle* material is characterised by an initial stage of predominantly elastic deformation, that converts in a sudden shear failure as stresses build up and attain a critical value. This shear failure is practically independent of the rate at which the material was strained (Mandl, 1988). This implies that the deformation rate in an analogue model containing only quartz sand for the simulation of brittle processes in nature does not affect the final result.

6.2.3 Polymers as modelling material

Several of the experiments in this work contained apart from the brittle sand layers also polymers. For the experiments presented in this chapter basal bars of bouncing putties were used (see section 6.4) to localise the fault formation. The second type of the rift models described in chapter 7 contained a 1 cm thick base-layer of SGM-36 polymer.

Both polymers are high viscosity silicone oils that are widely used in analogue modelling studies because of their viscous flow behaviour. SGM-36 is a *polydimethylsiloxane* (PDMS), 1 molecule of the polymer is composed of a chain of 8664 units of Me_2SiO. SGM-36 has a density of 965 kg/m^3, and it is liquid between 200 and 500 K (Weijermars, 1986). Bouncing putties on the

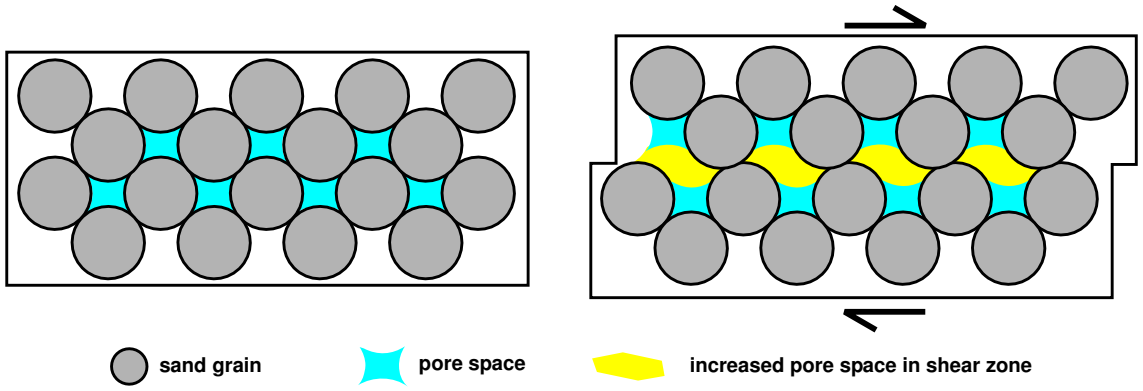

Figure 6.1: *Increase in pore space and decrease in number of point contacts caused by the sliding of grains past each other in a shear zone in a sandbox model. After White (1993).*

other hand are built from a boron derivate of PDMS: PBDMS or *polyborondimethylsiloxane* and subsequently "contaminated" with various fillers (Weijermars, 1986). The exact composition of bouncing putties is unknown, and their rheology is unpredictable because of the different fillers that are used. Bouncing putties and PDMS show viscoelastic behaviour, but only their viscous response should be used in modelling experiments (Weijermars, 1986).

SGM-36 is a Newtonian fluid with a viscosity $\eta_0 = 5{\times}10^4$ Pa s below strain rates of $3{\times}10^{-3}\mathrm{s}^{-1}$ at 24°C (Weijermars, 1986). The bouncing putty used in this chapter had a viscosity $\eta_0 = 10^4$ Pa s.

In a Newtonian viscous fluid, deviatoric stresses are linearly proportional to the strain rate and the viscosity (e.g. Ramsay and Lisle, 2000). Therefore the mechanical behaviour of a viscous material includes a time related parameter. For the dynamic similarity of the model and the prototype, the ratio between these deviatoric stresses must equal the ratio between the other stresses in model and prototype (Childs et al., 1993) (see equation 6.3). Thus:

$$\frac{\dot{\epsilon}_m.\eta_{0,m}}{\dot{\epsilon}_p.\eta_{0,p}} = \phi \tag{6.4}$$

with $\dot{\epsilon}$ the strain rate and η_0 the viscosity. ϕ can for example be determined from the ratio of overburden stresses in model and prototype:

$$\frac{\dot{\epsilon}_m.\eta_{0,m}}{\dot{\epsilon}_p.\eta_{0,p}} = \frac{\rho_m.g_m.L_m}{\rho_p.g_p.L_p} \tag{6.5}$$

The model ratio of time (τ or t^*) of the model is the inverse of the model ratio of strain rate ($\dot{\epsilon}^*$):

$$\frac{t_m}{t_p} = \frac{\dot{\epsilon}_p}{\dot{\epsilon}_m} = \frac{\rho_p.g_p.L_p.\eta_{0,m}}{\rho_m.g_m.L_m.\eta_{0,p}} \tag{6.6}$$

This model ratio of time is important when the viscous flow in the model represents a true simulation of rock flow in the prototype (for example to simulate salt flow (Childs et al., 1993) or magma injection (Merle and Vendeville, 1995)). In the experiments in this study, the polymers have been used solely for the localisation of fault displacement. Nevertheless, the models were deformed with sufficiently low strain rates to stay in the Newtonian flow regime.

6.2.4 Limitations

Although the results of scaled physical experiments show many similarities with larger natural geological structures, several limitations to such models exist. The boundary conditions at the base and the sides of the model may strongly influence the deformation in the sand, therefore these boundary conditions should be chosen carefully as to closely represent the natural situation (e.g. McClay, 1996). Dissimilarities between the boundary conditions of the model and the prototype is one of the reasons why a 100% correct scaling of models can never be perfectly achieved in the natural gravity field (Mandl, 2000). Other scaling problems arise from, for example (Mandl, 2000):

1. the elastic stiffness of the model material that is not exactly scaled by the same factor as the length dimensions (when scaled back, the elasticity of sand would turn out to be too low compared to that of natural rocks).

2. the softening processes in the model and prototype that are difficult to assess and virtually impossible to be properly scaled,

3. abnormal pore pressures and compaction in the prototype that are not accounted for in the model,

4. the possible role of inertial forces in the formation of faults that is poorly understood which means that there is still a lack of scaling rules,

5. also the widths of shear zones in sandbox models are, when scaled back, much larger than those of natural faults.

Another limitation of analogue models is that they are yet unsuitable for the simulation of thermal, flexural and isostatic effects related to faulting in the upper crust (McClay, 1996; Dooley and McClay, 1997).

Within the known limitations we may, however, safely assume that faults generated in sand models have the initial orientations and shapes of the corresponding faults in the up-scaled natural process. We may also expect the same sequential development of the faults in the model and prototype (Mandl, 2000).

6.3 Small-scale modelling of relay ramps: Introduction

The existing conceptual models of relay ramp evolution (see section 2.5 on page 60) have proven to be good guides for structural interpretations of relay ramps. However, from the descriptions in chapter 4, it is clear that they do not appropriately describe all aspects of natural examples. The mechanical modelling studies of Willemse et al. (1996), Willemse (1997) and Crider and Pollard (1998), in which they deduced the influence of several starting parameters on the stress distribution between overlapping normal fault segments, can be considered as a more systematic approach for gaining insight in the evolution of relay ramps. However, also a modelling study using scaled sandbox models could help to investigate relay ramps in a more systematic way.

Despite the abundance of field data and mechanical models, very limited attempts have been made to specifically simulate and understand the formation of relay ramps between normal faults through analogue modelling (e.g. Peacock and Parfitt, 2002). With the modelling presented here, it was tried to fill that gap.

In the experiments two fault segments were created, of which parameters like fault overlap, fault spacing, segment length, etc. could be varied systematically. By imposing such a controlled geometry of the main faults, and by investigating how a change in this geometry results in a change in the development and evolution of a relay ramp between these faults, the models differ from other experimental works, where relay ramps have been sporadically described during the

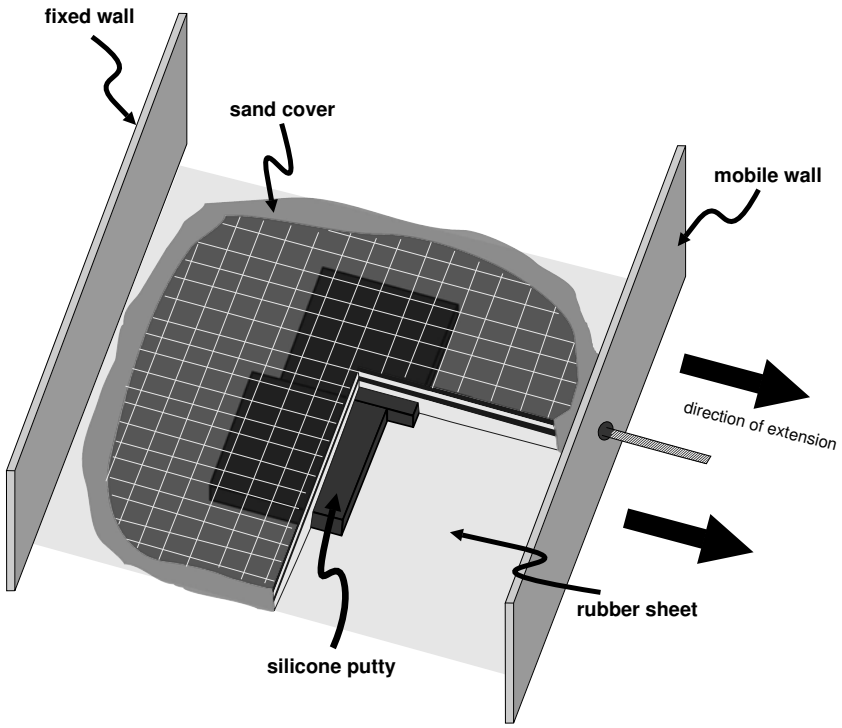

Figure 6.2: *Sketch of the experimental apparatus.*

interaction of "arbitrary" normal fault segments that evolved in an extensional fault system (eg. Childs et al., 1993; McClay and White, 1995; Clifton et al., 2000; Gupta and Scholz, 2000; Mansfield and Cartwright, 2001; McClay et al., 2002). To the best of my knowledge, only few experiments have been published in which overlap zones between extensional cracks were the main objects of investigation (Mauduit and Dauteuil, 1996; Peacock and Parfitt, 2002; Acocella, 2002; Tentler, 2003)

6.4 Small-scale modelling of relay ramps: Experimental set-up

The models were carried out with a typical sandbox set-up consisting of a rubber sheet attached between a mobile and a fixed wall (figure 6.2). On top of the rubber sheet a dry quartz sand cover of 4 to 6 cm thickness was sifted by mechanical sieving. By moving the mobile plate away from the fixed one, the rubber sheet was stretched and extension in the model was achieved. Sand with a mean grain size of 200×10^{-6}m and an internal friction angle of 37.6° has been used.

In experiments on thrust faulting, Faccenna et al. (1995) and Schreurs et al. (2001) used silicone putty layers that did not extend over their entire model and they observed that the main faults formed at the boundary between the brittle-viscous domain (ie. with sand and putty) and the purely brittle domains (ie. with only sand). The same technique was used

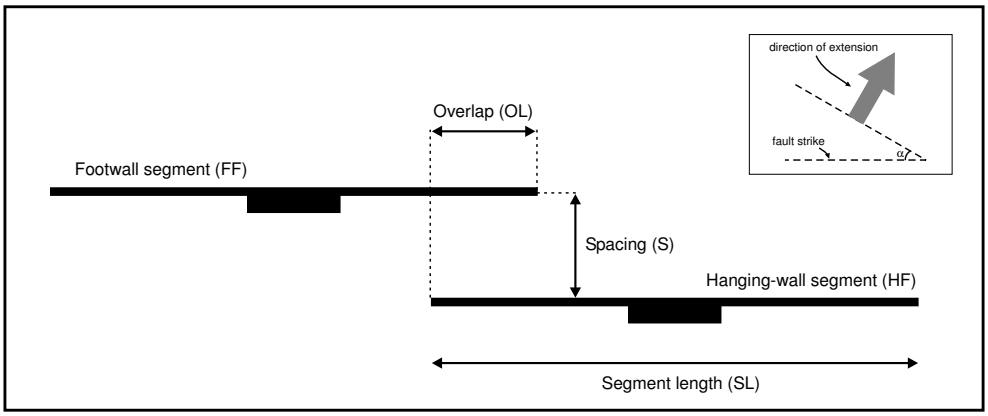

Figure 6.3: *Parameters that define the geometry of the 2 fault segments in a relay ramp. These nomenclature is used for the fault segments that we observed during the modelling, but also to explain the geometry of the silicone putty bars at the base of the model.*

here in an extensional environment (see figure 6.2) by putting two silicone bars at the base of the model before adding the sand. The width of the silicone bars typically was around 10 cm, and the length varied between the experiments. The silicone had a viscosity of 10^4 Pa s. Because of the presence of the viscous putty, the models were deformed with a slow strain rate ($0.0139\,\mathrm{cm.s^{-1}}$). However, it should be noted that the silicone was only used to induce the main faults in the models and that, therefore, it did not correspond to any specific analogue in nature. The introduced silicone putty ridges represent initial instabilities that are small compared to the faults that form in the models (Le Calvez and Vendeville, 2002). Therefore, after the formation of the faults, their further evolution and interaction occurred in the brittle environment of the sand cover. This technique, to trigger fault formation with silicone putty bars, has also been used recently to model off-set grabens (Le Calvez and Vendeville, 2002).

The use of silicone bars in the experiments permits to avoid the complications arising from the use of a basal moving plate, with a shaped velocity discontinuity, at the base of the sand-pack, as for example in Mauduit and Dauteuil (1996) and Acocella et al. (1999a). In fact, the presence of offset basal velocity discontinuities in these experiments implied the presence of a connecting segment which always affected the geometry and kinematics of the resulting interaction zone.

By varying the geometry of the silicone putty bars it was possible to change the geometry of the two interacting main fault segments in the model (figure 6.2). In each model faults developed on both sides of the silicone bars, what allowed to study 2 relay zones during one run (dipping antithetically to each other). The width of the silicone bars was chosen large enough to prevent the interaction of the faults on opposing sides of the bars. At the end of the experiments (after 10 cm of extension, corresponding to 20% stretching) the models were impregnated with water and sliced parallel to the direction of extension.

The main parameters that were varied during the experiments are (see figure 6.3): a) the spacing between the fault segments *(S)*, b) their length *(SL)*, c) the degree of overlap *(OL)*

and d) the orientation of the segments; both relative to each other and also with regard to the direction of extension *(α)*. Moreover, some models with "left overstepping" and "right overstepping" relay ramps have been run, and in some experiments the maximum displacement on the fault segments was shifted towards the fault tip to investigate if this had an influence on the way the ramps evolved. This increase in displacement could easily be achieved by increasing the thickness of the silicone bars at the border where the ramp was going to form.

6.5 Small-scale modelling of relay ramps: Results

6.5.1 Description of selected experiments

In this first section some of the experiments are described, and specific observations are emphasised. A more systematic analysis of the experimental relay ramps starts on page 193. Within the description the main faults that formed in each experiment were termed:

- footwall fault *(FF)*,
- hanging-wall fault *(HF)*,
- footwall fault of the A-ramp *(AFF)*, and
- hanging-wall fault of the A-ramp *(AHF)*.

In this convention, the footwall fault was the fault that formed closest to the fixed wall of the modelling rig (figure 6.4). The *main* ramp or M-ramp of the model is the relay ramp that formed closest to the fixed wall. The A-ramp is the *antithetic* ramp to the main ramp, and formed closest to the mobile wall. Sometimes this letters (M or A) are included in the experiment's name to specifically refer to one of the ramps that formed (see figure 6.4). The 2 grabens that formed in the models were called the footwall graben *(FWG)* and the hanging-wall graben *(HWG)* for respectively the graben closest to the fixed wall, and the one closest to the mobile wall (figure 6.4).

Experiment ZAV02

Set-up: Silicone bars with a length of 22 cm, a width of 5 cm and a height of 1.5 cm were used in this experiment. They were off-set for 5 cm (figure 6.5). The thickness of the overlying sand cover was 4.5 cm.

Results: HF formed at 25 mm of extension, followed by AFF at 27 mm. Only at 37 mm of extension, FF and AHF started to form. At this stage in the modelling, two off-set, relatively narrow (4–5 cm), grabens have formed in the model. Because the silicone bars were chosen too small (1.5 cm), the main interaction in model ZAV02 occurred between the HF and AHF faults. The transfer zone that formed in this model therefore corresponded to an approaching divergent conjugate transfer zone rather than to a relay ramp.

The fault tips of HF and AFF have become segmented, with the segments rotating slightly anticlockwise. This way the fault linkage seems to have been achieved (figure 6.6).

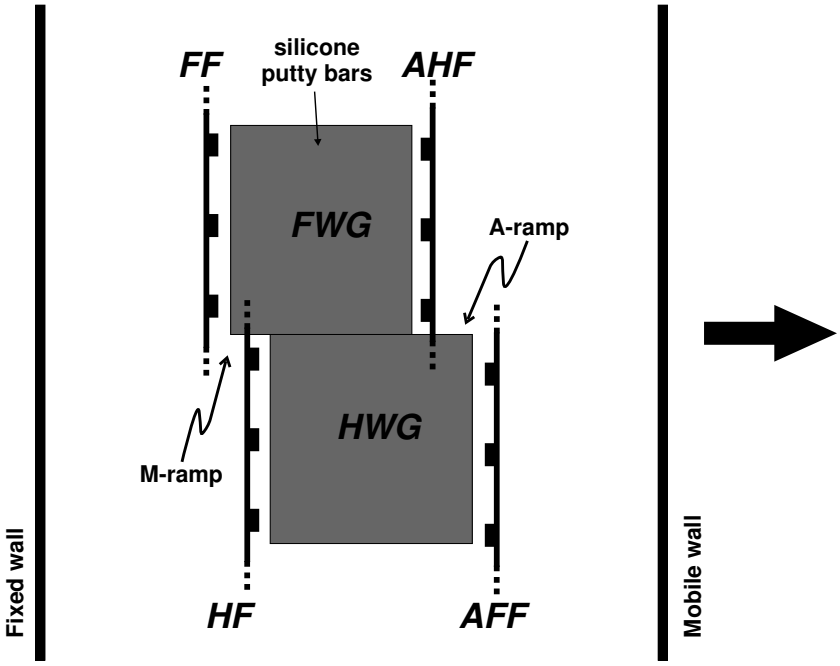

Figure 6.4: *The main faults and grabens that formed in the experiments. FF = footwall fault of M-ramp, HF = hanging-wall fault of M-ramp, AFF = footwall fault of A-ramp, AHF = hanging-wall fault of A-ramp, HWG = hanging-wall fault graben, FWG = footwall fault graben. This figure does not refer to the set-up of any particular experiment.*

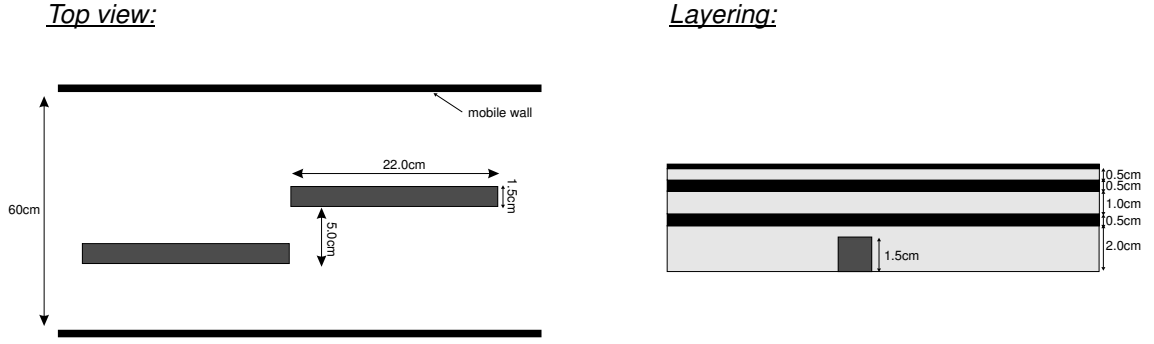

Figure 6.5: *Set-up characteristics of experiment ZAV02. The width of the silicone bars in this experiment is much smaller than in other experiments.*

Trudgill and Cartwright (1994) published a similar geometry between two offset grabens in the Canyonlands National Park, Utah (figure 4.24). Unlike in our model, the main fault interaction in the S.O.B Hill relay zone in the Devil's Lane Graben is between the offset synthetically dipping normal faults, rather then the more closely spaced antithetic faults (figure 4.24 on page 141).

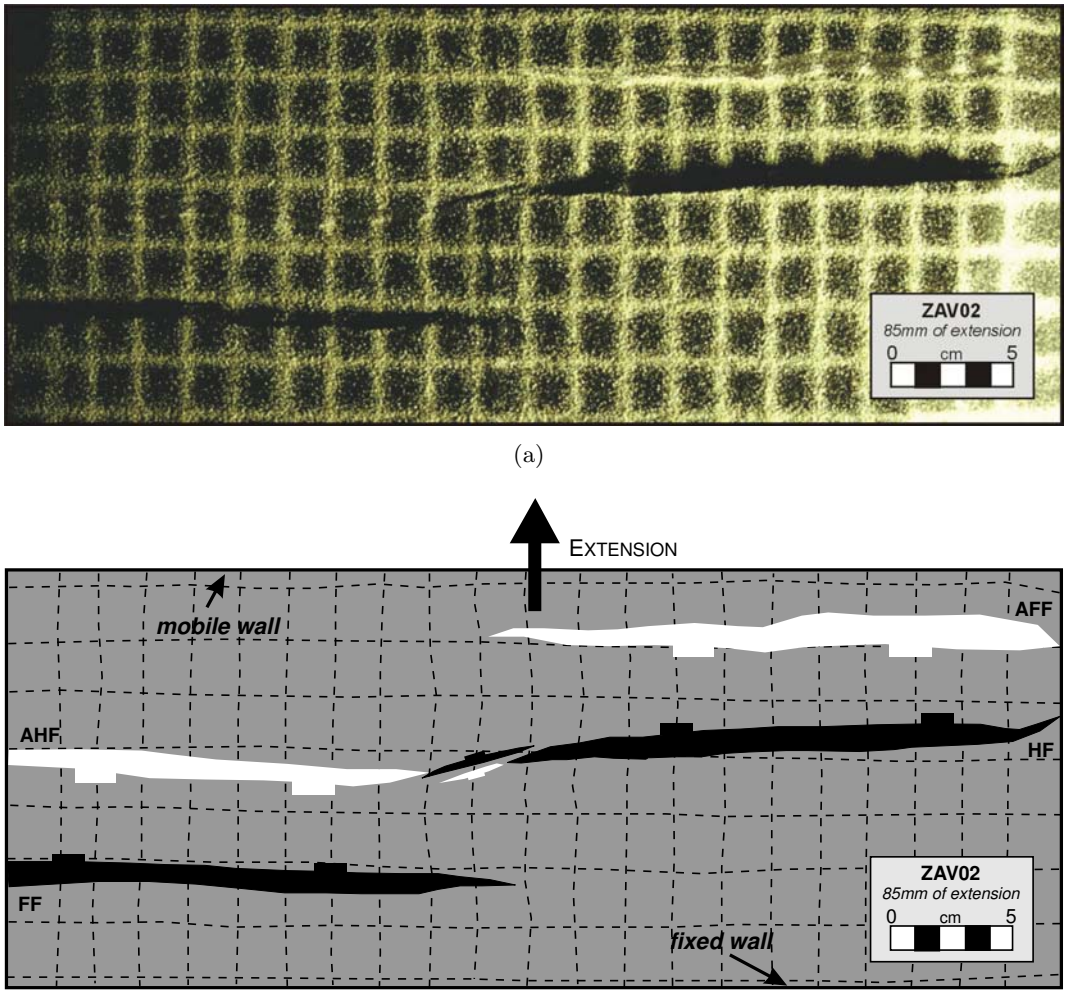

Figure 6.6: *Running shot of experiment ZAV02 after 85 mm of extension (a), and the interpretation (b). In this figure, white faults dip towards the fixed wall, whereas black faults dip towards the mobile wall.*

Experiment ZAV06

Set-up: In this experiment, two wedge-shaped silicone pieces were added to one side of the silicone bars (figure 6.7). The purpose of this was to increase the displacement gradient at the relay ramp side of the faults that would form in the model. To prevent the interaction of the M and A ramps, like in model ZAV02, the silicone bars used here had a width of 8 cm, and the offset between them was 1.5 cm. The height of the silicone bars was 3 cm, but at the location of the wedge, a maximum height of 4 cm was reached (figure 6.7).

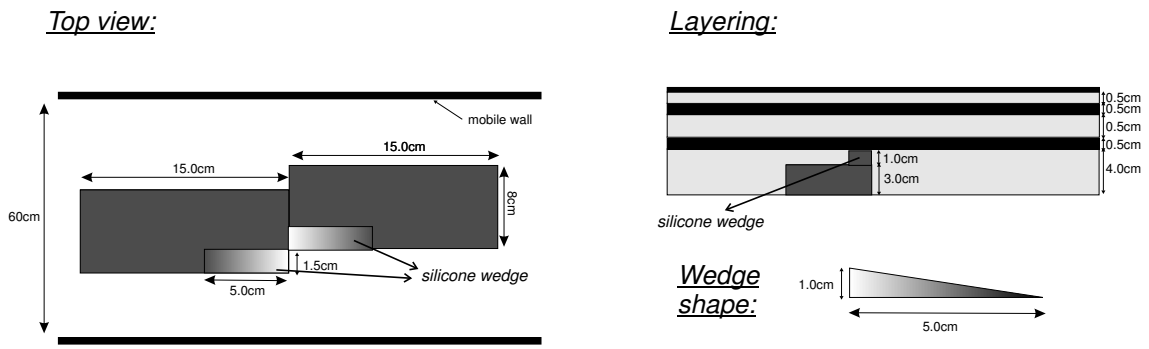

Figure 6.7: *Set-up characteristics of experiment ZAV06*

Results: After 10 mm of extension, the first slight surface expression of the FF segment appears. After 15 mm also the HF segment is observed. Both segments (FF and HF) are connected and a continuous fault is formed, without the development of a relay ramp. The maximal displacement on this continuous fault occurs at the centre of the fault, where the silicone is thickest.

At 30 mm of extension also the AHF and AFF have formed, and a small relay ramp develops between both faults. The offset of 1.5 cm between both faults, was however the same as for the M-faults. The evolution of the A-ramp is illustrated in figure 6.8.

At 40 mm of extension, AFF slightly bends towards AHF. At an extension of 51 mm, the overlap distance between the A-faults is 6 cm, and at 59 mm of extension, breaching is achieved by the development of a new connecting fault. The connecting fault has formed close to the end of the AHF, near the border of the 2 putty bars.

At 69 mm of extension, the short-cut tip of AHF seems to become offset by a lateral displacement component on the connecting fault. The overall vertical displacement of the connecting fault remains relatively low, and the main fault segments continue to accommodate displacement, and to slightly propagate further.

The model was stopped after 102 mm of extension. A vertical cross-section through the relay ramp is included in figure 6.9.

6.5.2 Analysis of the different experiments

General evolution of the experiments

The results of the different experiments are listed in table 6.1, that shows the characteristics of the observed ramps after the final amount of extension (10 cm) was reached. The final overlap (FO) and the fault system length (FSL) were measured on the surface of the model, the displacement (D) was measured along the cross-sections.

The general evolution of the relay ramps was characterised by three different stages (figure 6.10), here described:

1. *Immature stage:* This stage consists of the onset of faulting, marked by the development of isolated fault traces at the surface (figure 6.10,a). The onset of faulting at surface was usually observed after approximately 2 cm of extension (corresponding to ≈4% of extension). The top view pictures of the experiments at early stages (≈ 2 cm of extension) show that the faults started to form in the centre of the silicone bar and subsequently propagated towards both sides. However, small-displacement faults with the same lengths

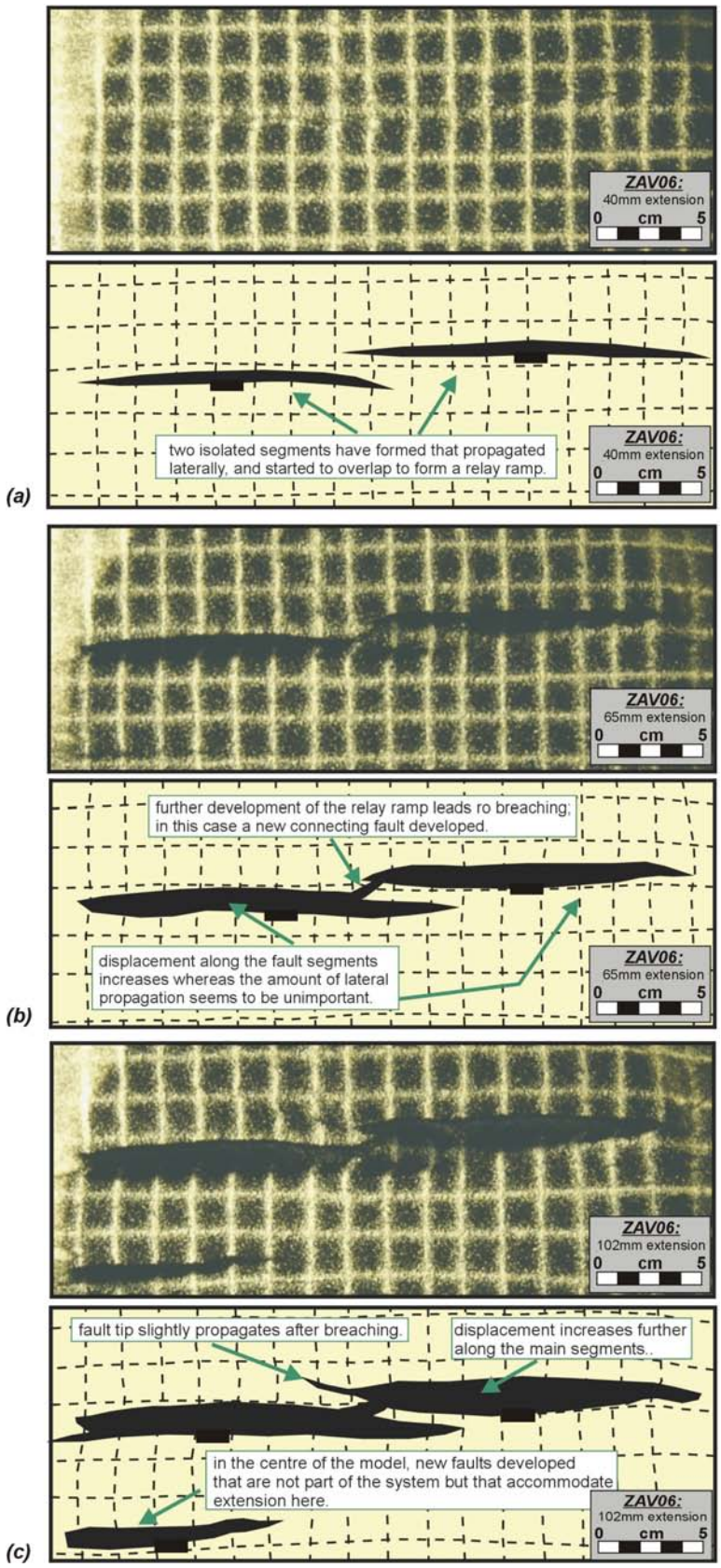

Figure 6.8: *Running-shots of experiment ZAV06A. The model is characterised by two silicone bars that do not overlap, and with a spacing of 1.5 cm. The observed structures during the evolution are indicated in the figures. The first fault started to develop after 1.4 cm of extension.*

Robert Hus, December 2004

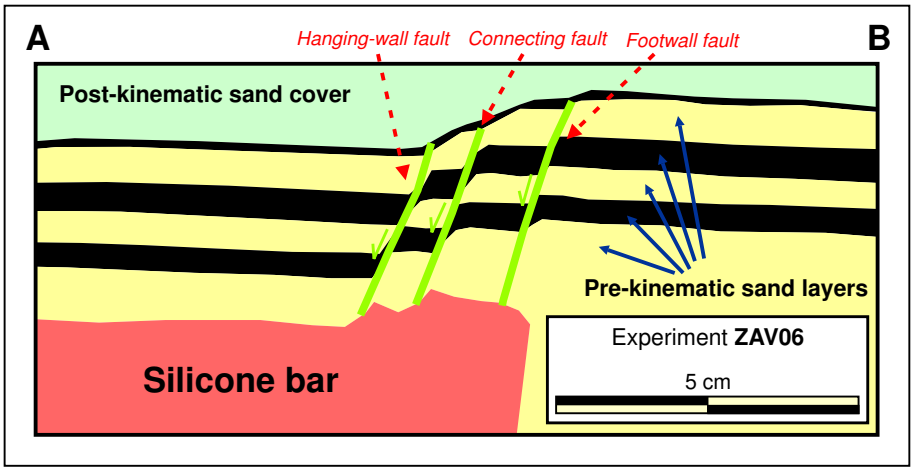

Figure 6.9: *Vertical section through the A-ramp of model ZAV06. The section was made after 102 mm of extension, and is located in the HWG-area, 1 cm before the transition to the FWG silicone.*

Exp. n°		FO	S	ST	FSL	AR	D	OO	Remarks
ZAV03	M	4.0	2.0	4.0				0	interaction between M and A
	A	3.0	2.5	4.0				0	ramps
ZAV04	M	6.5	2.5	5.5	34	3.7	2.0	0	FF deflects away from HF
	A	6.5	2.5	5.5	38	4.4	1.5	0	HF propagates towards FF
ZAV05	M	6.0	2.5	4.0	36	5.2	1.0	0	no breaching
	A	4.5	2.5	4.0	34	4.8	0.7	0	FF propagates towards HF
ZAV06	M	—	1.5	6.0	30	2.5	1.3	0	no ramp, continuous fault
	A	8.5	1.5	6.0	34	3.5	1.0	0	breaching through splaying
ZAV07	M	—	1.5	5.8	34	2.9	1.0	0	no ramp, continuous fault
	A	—	2.0	5.8	36	3.1	1.7	0	no ramp, continuous fault
ZAV08	M	16.0	5.0	5.5	35	4.6	1.3	0	interaction but no breaching
	A	—	2.0	5.5	40	3.6	1.0	0	no ramp, continuous fault
ZAV09	M	5.0	7.0	4.2	20	2.9	0.3	0	no interaction
	A	9.0	2.0	4.2	22	3.7	0.6	0	HF connects with FF
ZAV10	M	10.0	2.5	4.0	26	4.5	0.5	2	relay ramp but no breaching
	A	7.0	2.5	4.0	26	4.1	0.7	0	FF propagates to HF
ZAV11	M	10.0	1.5	5.0	22	3.2	?	4	no signs of breaching
	A	11.0	2.5	5.0	22	3.3	?	4	no signs of breaching
ZAV12	M	—	1.5	5.0	20	2.0	1.2	4	HF too big; links with FF before latter developed
	A	12.0	4.5	5.0	23	3.5	1.0	4	no interaction
ZAV13	M	7.0	3.0	5.0	20	2.7	0.5	4	curved faults due to interaction
	A	9.0	3.0	5.0	20	2.9	0.5	4	curved faults due to interaction
ZAV14	M	7.0	4.0	4.8	22	3.0	0.33	0	interaction??
	A	6.5	2.5	4.8	23	3.1	0.66	0	HF links with FF
ZAV15	M	10.5	3.5	3.7	25	4.8	0.8	0	
	A	5.0	2.5	3.7	23	3.8	0.8	0	
ZAV16	M	7.0	2.5	4.3	25	3.7	1.0	0	
	A	6.5	2.5	4.3	24	3.5	1.0	0	
ZAV17	M	12.0	5.0	4.3	24	4.2	1.0	0	
	A	5.0	1.5	4.3	24	3.4	0.8	0	breaching through splaying
ZAV18	M	4.0	1.5	4.5	24	3.1	0.7	0	small ramp breached by FF linking with HF

FO = final overlap
S = spacing
ST = thickness of sand cover
FSL = fault system length
AR = aspect ratio of faults
D = displacement
OO = original overlap of silicone bars

all dimensional units are in cm.

HF = hanging-wall fault
FF = footwall fault

Table 6.1: *Summary of the different parameters of the experiments. The original overlap (OO) and the spacing (S) were imposed by the configuration of the silicone bars, the other parameters resulted from the extension.*

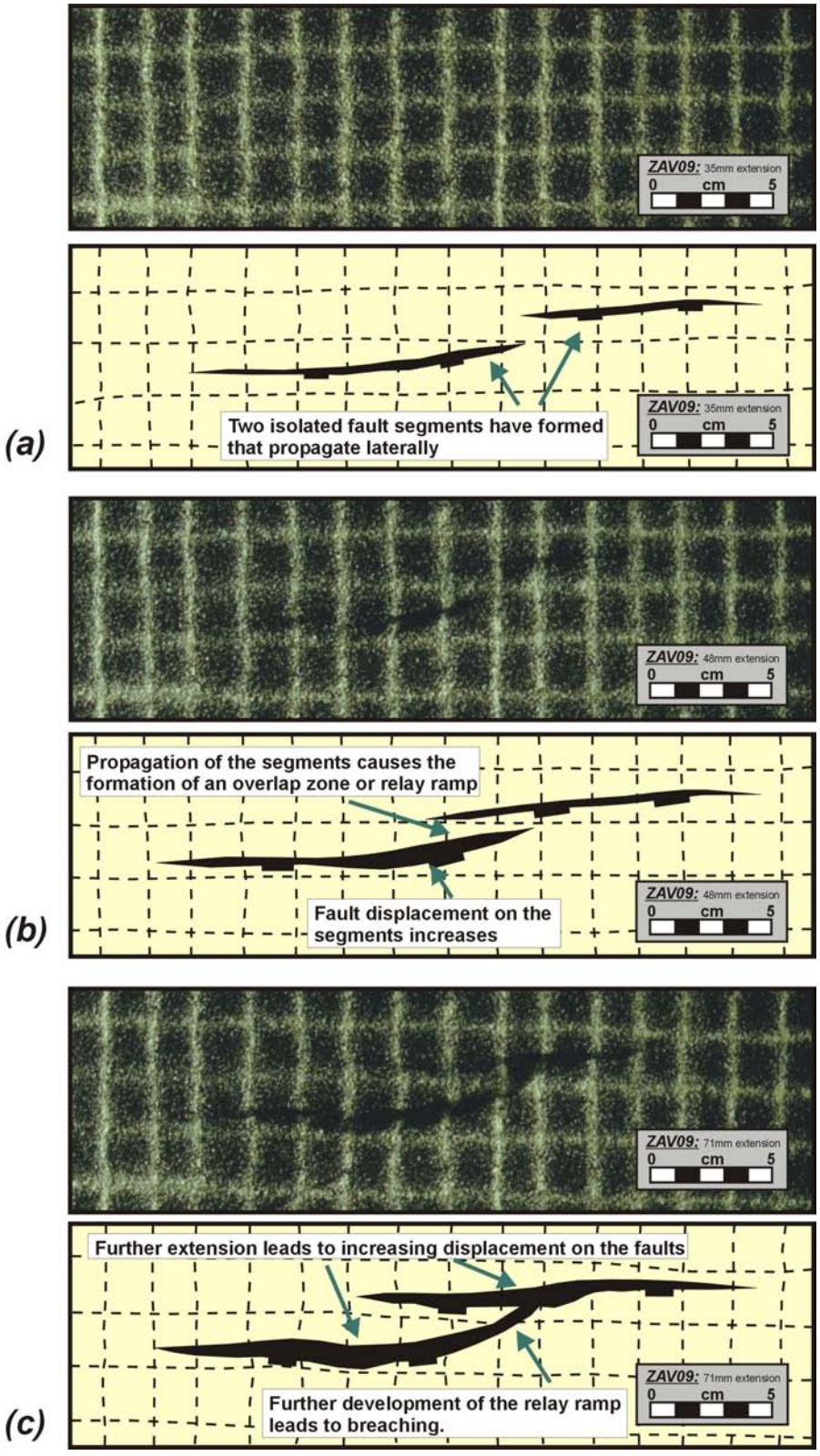

Figure 6.10: *Running-shots of experiment ZAV09A, showing the three different evolutionary stages, typically observed in the modelling: the* immature stage *(a), the* overlapping stage *(b) and the* linkage stage *(c). The linkage in this experiment was achieved through the propagation of the hanging-wall fault towards the footwall fault.*

as the silicone bars formed even after a relative small amount (2-3 cm) of extension. This indicates that the faults in the immature stage were probably "under-displaced" according to scaling laws (see equation 2.12), or that the faults were characterised by a considerable vertical propagation before they reached the model's surface (e.g. Walsh et al., 2002). Further extension of the model increased the displacement along these under-displaced fault, causing them to propagate laterally afterwards. When this propagation started, the fault length was no longer restricted to the length of the silicone bars, and free propagation outside the bar area started.

2. *Interacting stage:* The second evolution stage was reached when the propagation of the segments had been large enough to create an overlapping configuration of the faults (figure 6.10,b). Interaction between the two fault segments in each experiment was inferred when: (a) in cross-section, a continuous bend or tilt of the layers could be observed between the two faults or, (b) in map view, a deflection of the trace of one or both of the faults was observed (excluding the examples where this deflection was clearly result of side-effects). When this mechanical interaction occurred, we termed the resulting structure a relay ramp. Tilting of the layers inside the ramp was usually towards the footwall fault, with the angle of tilting being around 5°.

3. *Linkage stage:* The final stage in the evolution was reached when the two originally isolated faults got connected and the ramp structure became breached. This stage was characterised by either the propagation of one of the main faults towards the other, or by the development of a new connecting fault that splayed from one of the main faults and subsequently cut through the ramp. The final linkage in the evolution of the two segments was not reached for all experiments, but most of them showed after 10 cm of extension at least signs of a near breaching (e.g. the propagation of one of the main faults towards the other).

Relationship between length, displacement and spacing

As mentioned in the description of the immature evolution stage, the faults in the models were under-displaced early in the experiments. To determine whether or not this remained the case during further evolution of the models, the relation between fault length and displacement was determined and the observations were linked to known scaling laws (figure 6.11). As such it has been possible to test if there was any influence of the fault's triggering mechanism (i.e. using the basal silicone bars) on the actual final fault shapes in the models. Although natural examples of relay zones are often marked by a shift of the maximum displacement from the centre of the trace towards the relay zone (see section 2.5), the displacement was measured in the centre of the silicone bars. Moreover it was assumed that the displacement, as well as the length, of both segments were similar. This is justified as in each experiment 2 silicone bars were used that had the same length and thickness. Measuring the displacement in the centre of the silicone bars is also justified, as this is the place where the faults are expected to have nucleated. Moreover it

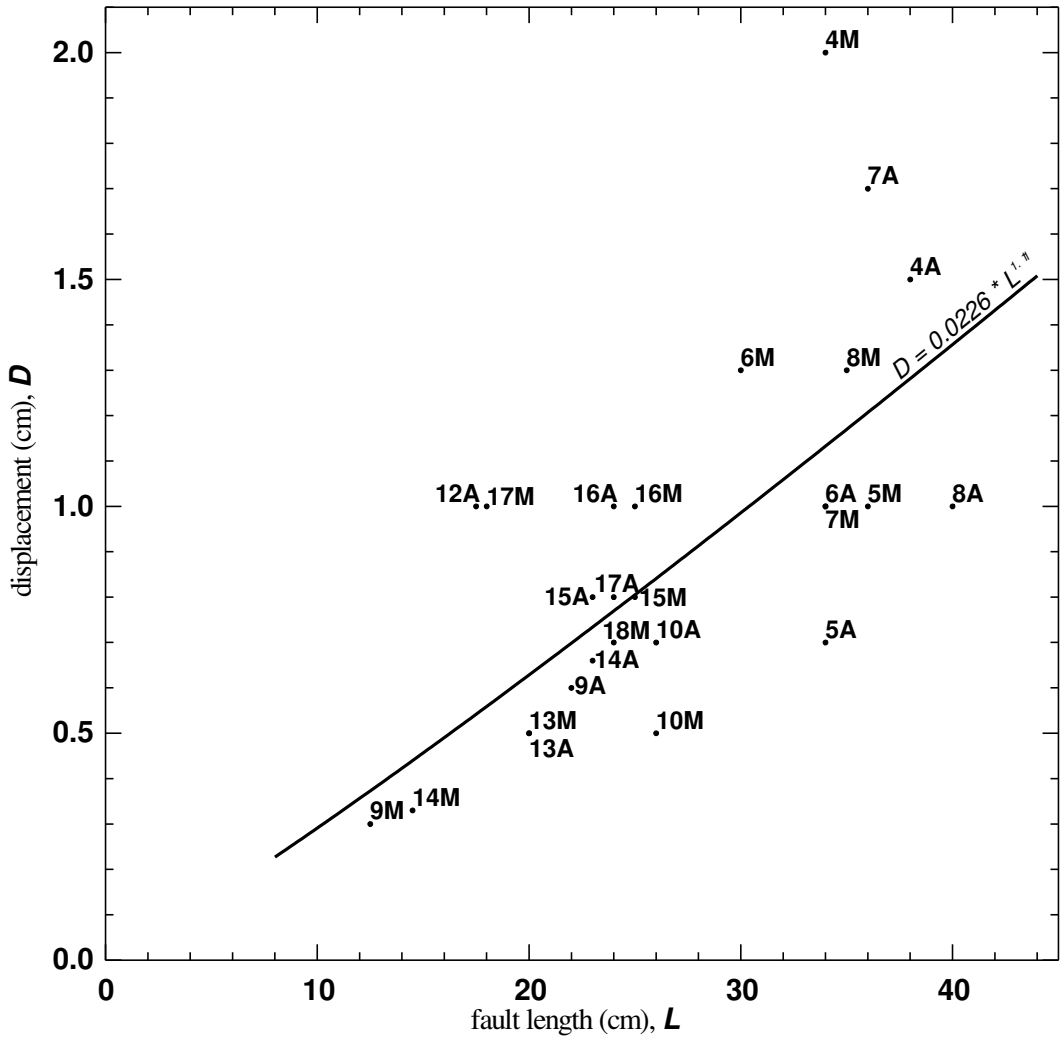

Figure 6.11: *Relation between the segment lengths of the modelled faults and the displacement along that fault. Displacement was measured on a cross-section through the centre of one of the segments.*

was much easier to produce a slice of the model exactly at the centre of the silicone bar than at the (arbitrary) location of the maximum displacement.

For 27 faults, the obtained relationship between segment length (L) and displacement (D) after 10 cm of extension is:

$$D = 0.0226 \times L^{1.11} \tag{6.7}$$

For interacting fault segments, the fault system length (FSL) has been used for L, whereas for non-interacting faults L equalled the length of the individual faults (Gillespie et al., 1992). Faults which had reached the lateral boundaries of the sandbox have not been included in the calculation of this relation, because in such cases the fault growth would have been censored. In figure 6.12 the relationships are shown between the spacings of the modelled faults and their total

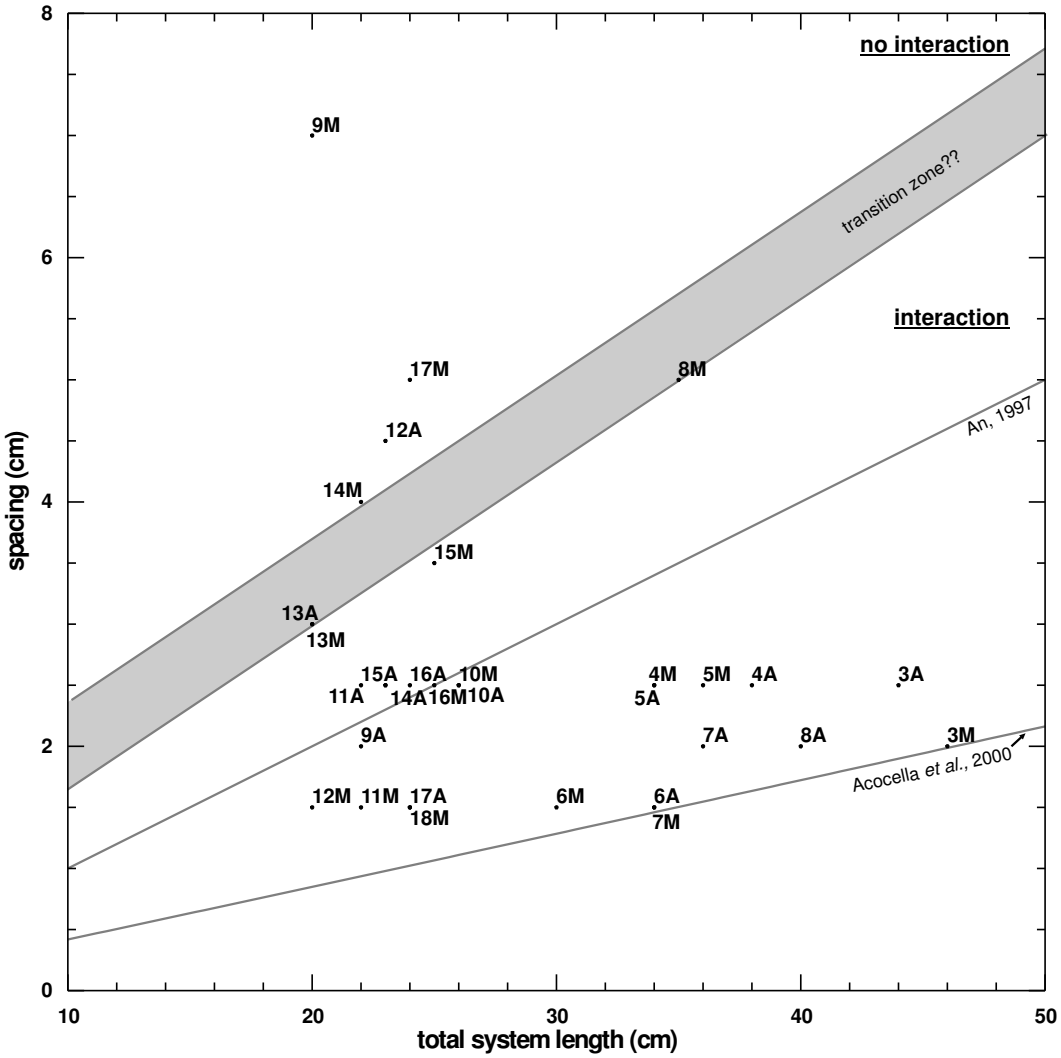

Figure 6.12: *Relation between the spacing of two fault segments and the length of the total system. The upper left corner of the graph corresponds to an area where no interaction occurs, the lower right corner is marked by interaction. The grey zone is a transition zone between both areas. The line curves correspond to transitions observed in other studies.*

length (fault system length *FSL* in table 6.1). The experiments show two distinct behaviours that depend on the combination of these values. Given a certain total length of the faults, interaction between the faults does occur up to a certain value of the spacing, larger spacings result in no interaction for the same fault system length. The 'interaction' and 'no-interaction' domains in the graph are separated by a transition zone. This zone represents an area for which it is unsure from the experiments alone whether or not interaction occurs. The best fit line that goes through the centre of the area is given by the equation:

$$S = 0.135 \times FSL + 0.68 \tag{6.8}$$

Figure 6.12 also contains two lines marking the transition between the interacting (below) and non-interacting (above) domains between experimental strike-slip faults (An, 1997) and normal faults in Iceland (Acocella et al., 2000). The line from Acocella et al. (2000) shows that the minimum length of a fault system should be around 14 times the value of the spacing for interaction to occur, whereas the line from An (1997) suggests that this length is 10 times the spacing for strike-slip faults. Our data shows that the critical fault length is about 8 times the spacing, slightly lower than the previous results.

Relationship between overlap and spacing

Although similar overlap to spacing relations have been observed between overstepping strike-slip faults in nature and overstepping strike-slip faults in laboratory experiments (An, 1997), here the 'layer bending' and 'trace deflection' criteria, as mentioned above, has been used to infer fault interaction. This allowed to directly compare the experimentally observed relation between overlap and spacing with normal faults from natural examples (eg. Acocella et al., 2000), something that would not have been possible if the relation between overlap and spacing from natural examples had been used to infer fault interaction in the models (eg. Huggins et al., 1995; Peacock, 2003).

During the propagation of the faults in the experiments it was observed that an initial overlap of the segments was reached relatively early (around 3–4 cm of extension) in the model's run. Figure 6.13 shows the variation of the overlap distance of the normal faults as a function of the amount of extension. The decrease in the slope of the curves in figure 6.13 indicates that, when a certain overlap was attained (mostly between 40 and 70 cm of extension), during the second evolutionary stage, the rate of propagation of the segments at the side of the relay ramp decreased, often becoming zero before the final amount of extension had been reached.

In experiments 3 to 9 the initial overlap of the silicone putty's was 0 cm (ie. lying against each other without overlapping). This allowed to study the relation between the overlap and the spacing. The observed relation does not seem to be too straightforward (figure 6.14):

1. In general the overlap (OL) is larger when the distance between the segment (S) increases.
2. This is not true when the spacing is too large to allow for interaction between two segments. In that case one would expect no hindering to fault propagation and therefore large overlaps (exp. 9M in figure 6.14).
3. In some experiments, small spacings (<2.0 cm) lead to the formation of a continuous fault, without the formation of a relay ramp (points plotted on the x-axis of figure 6.14); in other experiments with the same spacing, ramps did form (eg. ZAV06A, ZAV17A and ZAV18M).

Because mechanical modelling has shown that the aspect ratio of the fault (i.e. length/height) has an influence on the overlap to spacing ratio of a relay ramp (Willemse, 1997), the for this study useful theoretical curves for the overlap to spacing (i.e. for aspect ratio's of 2 and 4) have been added to figure 6.14. The aspect ratio's from the faults in our models varied between

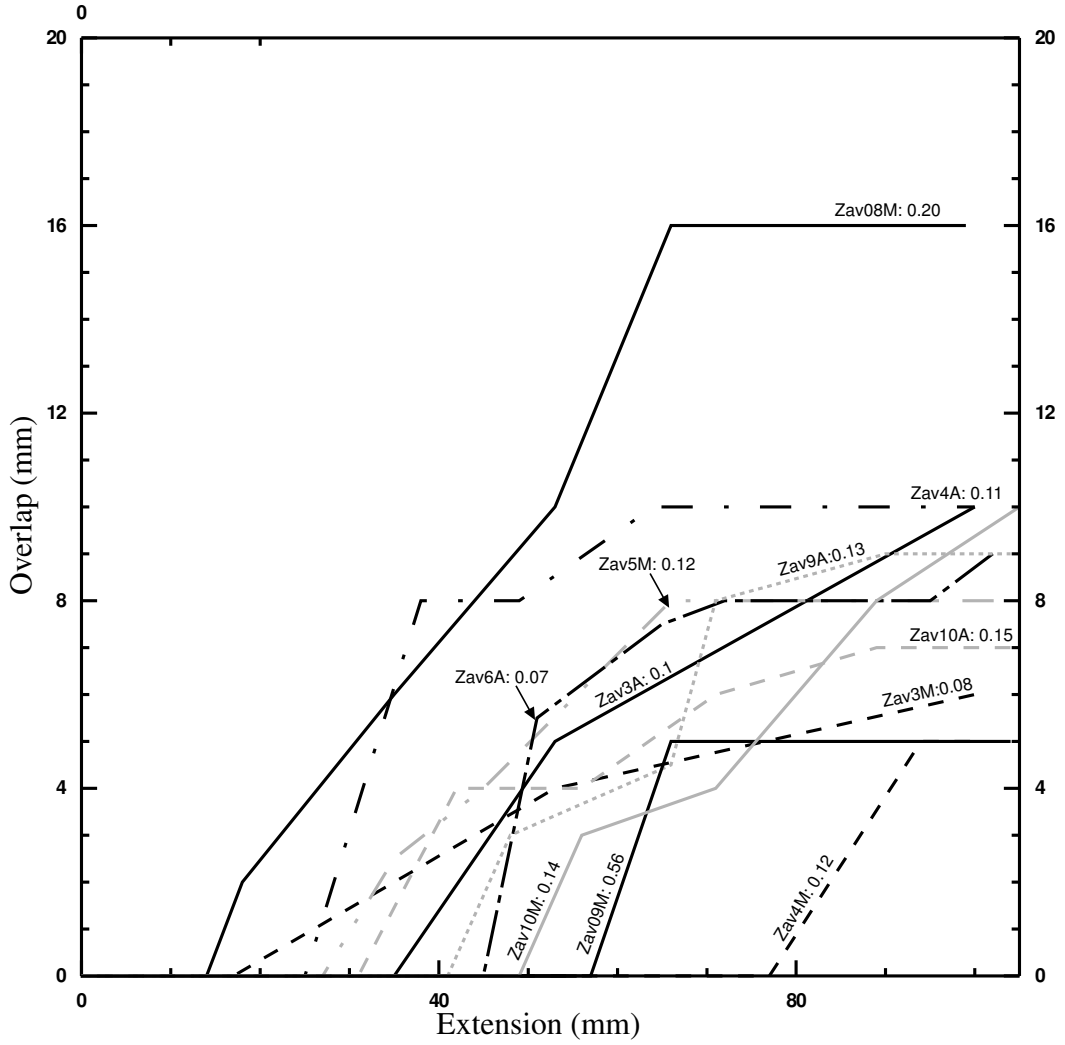

Figure 6.13: *Degree of overlap of the two fault segments of the relay ramp in function of the amount of extension. The numbers after the experiment names, correspond to the ratio of fault spacing and segment length.*

the different experiments from 2.5 to 5.2, however large uncertainties about these values exist because they could not be properly measured. In figure 6.14 the experimental results for the spacing to overlap relation plot around the theoretical curve of Willemse (1997) corresponding to faults with aspect ratio's = 4. For non-interacting segments (eg. ZAV9M) the points plot in another region of the graph. Nevertheless, there is a large scattering of the data around the theoretical curves. For example points with aspect ratio around 3 (11M, 11A, 17A) plot far to the left of the theoretical curve for an aspect ratio of 4. To check the dependence of the overlap to spacing ratio on the aspect ratio, their relation has been plotted in figure 6.15a. This graph shows, that an increase in the aspect ratio of the faults indeed allows for the overlap to

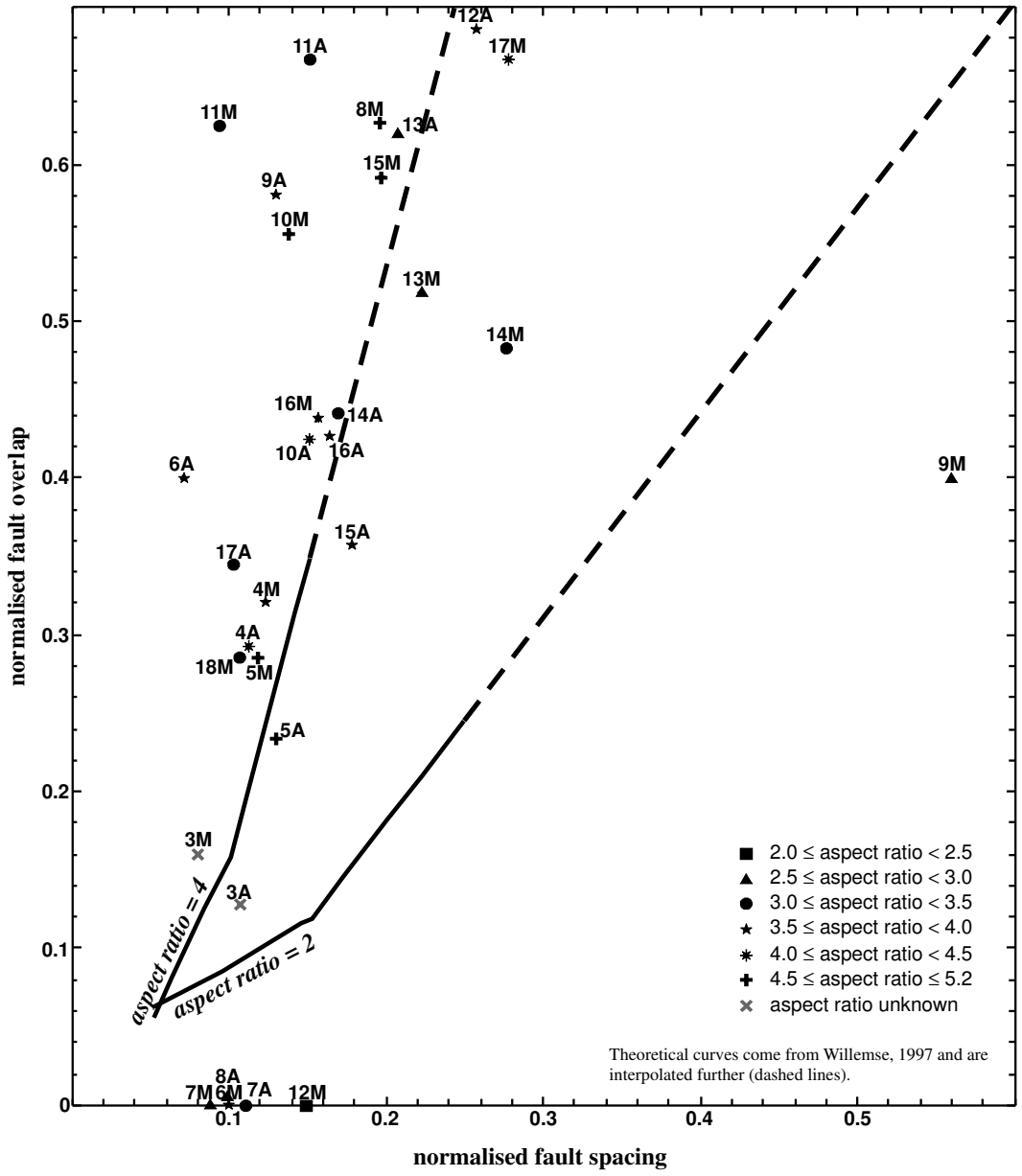

Figure 6.14: *Relation between fault overlap and spacing. Both are normalised to the segment length. The line curves were calculated by Willemse (1997) and correspond to the theoretical relationship for faults with a certain aspect ratio that are characterised by a uniform stress drop along the fault trace.*

become larger for the same amount of spacing. There is however a large scattering of the data, indicating that the relation might not be that simple.

Figure 6.15b shows the distribution of the length to width ratio of the experimental overlapping zones during the evolutionary stage 2. The mean ratio is 3.12 and 95% of the examples have a ratio between 1.75 and 6. This is with the continuous faults and the non-interacting

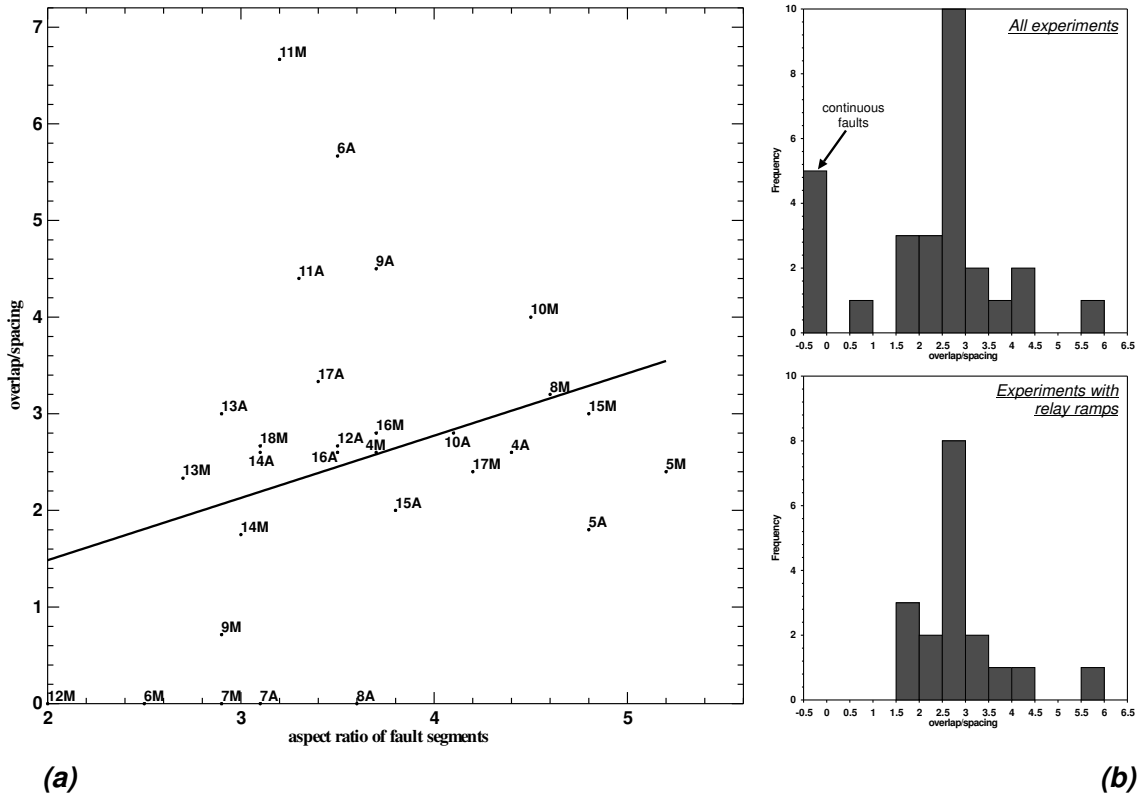

Figure 6.15: *Relation between the overlap to spacing ratio of a relay ramp, and the aspect ratio of the main faults (a), and histograms showing the distribution of the different overlap to spacing ratio's observed in the models (b).*

examples excluded.

Relay ramp breaching

50% of the experimental relay ramps had breached — or were getting breached — before the final amount of extension (ie. 20%) was reached (eg. Figure 6.16). We observed the different modes of breaching as mentioned by Childs et al. (1995): 1) 55% of the breaching occurred by the propagation of the hanging-wall fault towards the footwall fault, 2) for 27% it was the footwall fault that propagated towards the hanging-wall fault, and 3) in 2 cases (18%) the breaching was accomplished by a new fault that cut through the ramp.

Hanging-wall fault to footwall fault propagation was thus the most common way of linking. In this case, the hanging-wall and the footwall faults started to form at the same time, but as soon as the first faulting was observed, the hanging-wall fault often developed in the most important fault of the two, taking up more displacement than the footwall fault. In a first stage this resulted in the development of a depression in the centre of the hanging-wall fault trace. After the hanging-wall fault had propagated to the footwall fault in a later stage, a

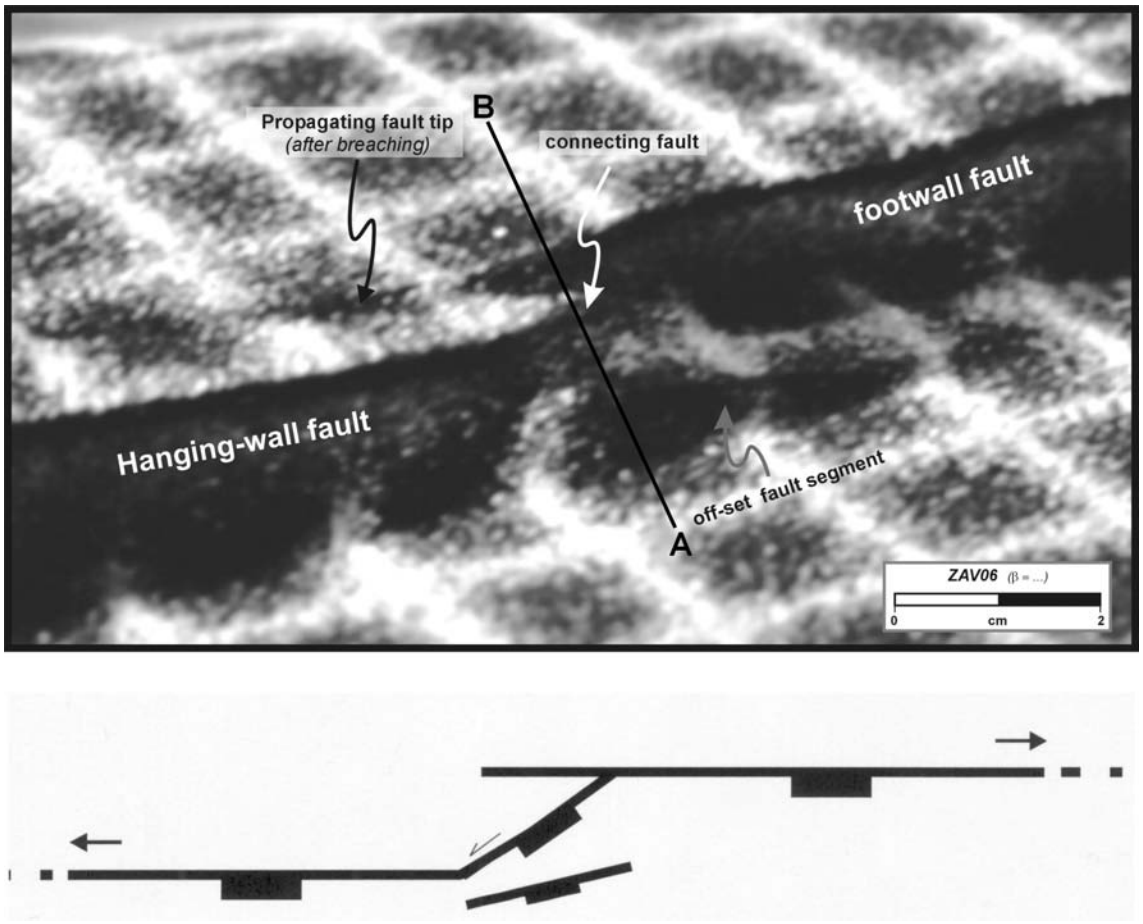

Figure 6.16: *Oblique photograph of experiment ZAV06A. This model is an example of a ramp that breached by a connecting fault. The picture illustrates the propagation of the fault tips after the ramp got breached. The scheme underneath is a line drawing of the observed fault geometry. Note that the geometry actually becomes more complex through the breaching.*

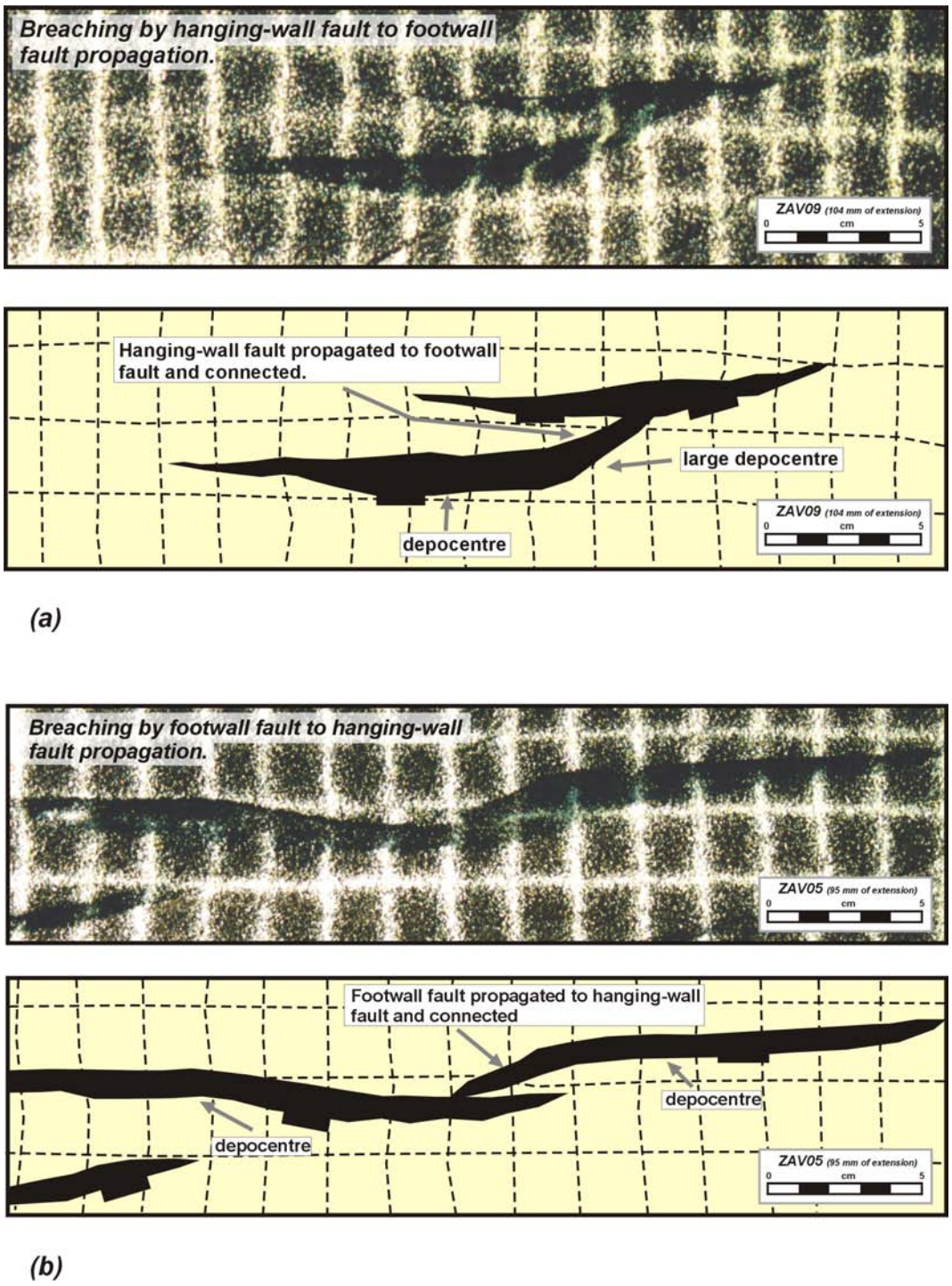

Figure 6.17: *Example of a relay ramp breached by the propagation of the hanging-wall fault towards the footwall fault in experiment ZAV09A (a), and one where breaching occurred through the propagation of the footwall fault to the hanging-wall fault in experiment ZAV05A (b). The different depressions that formed in the models are indicated.*

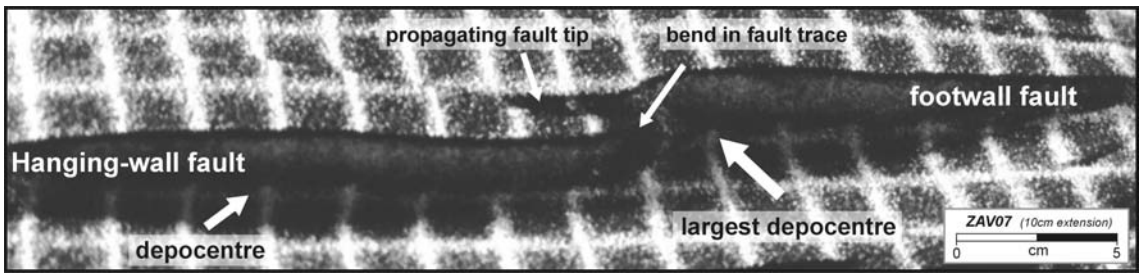

Figure 6.18: *Oblique photograph of experiment ZAV07A. The experiment was characterised by a connection of the two off-set fault segments before the faults reached the surface of the sand cover. Note the occurrence of the two depressions and the propagation of the fault tip of the footwall segment.*

second depression developed near the connecting point. Often this central depression became the largest of the whole system (figure 6.17a).

When the footwall fault propagated towards the hanging-wall fault none of the two faults seemed to become larger and more important than the other during the extension process. Therefore this resulted in the development of two similar depressions, one at the centre of the footwall fault and the other at the hanging-wall fault. After the footwall connected with the hanging-wall fault, the development of a similar large depression in the linking area, as described above, was not observed. This part of the hanging-wall remained more elevated compared to the adjacent depressions, and formed as such a kind of intra basin high (Schlische, 1995) (figure 6.17b).

A connecting fault has been observed in cases where the faults were spaced close (ie. <2 cm) to each other (ZAV06A and ZAV17A but not in ZAV09A). In the case of experiment ZAV17A the displacement gradient started to increase just outside the relay ramp, but it decreased again in the relay ramp itself. It was at this location that later the new breaching fault splayed off and linked up with the footwall fault.

In those cases where the modelled faults were characterised by an early-stage linkage between the offset segments before the actual fault reached the surface of the sand cover, a continuous fault formed with a clear bend in the centre. Figure 6.18 shows an example of such an experiment (ZAV07A). Although the linkage occurred early in the evolution, there are still 2 separate depressions along the fault. One is located in the centre of the hanging-wall segment, and the other one — which is the biggest one — is located at the footwall segment, but shifted towards the bend (figure 6.18).

After breaching of the ramps the relict fault tips did not die out directly. Instead the fault tips continued to propagate although at a lower propagation rate, still accounting for some of the extensional deformation in the model (see figure 6.16). Similar observations were made for the continuous faults (e.g. figure 6.18) where at the bend in the fault trace a clear propagation of the originally offset faults could be observed. In the case of figure 6.18 it is the footwall fault segment that propagates further and cuts through the footwall of the hanging-wall fault segment.

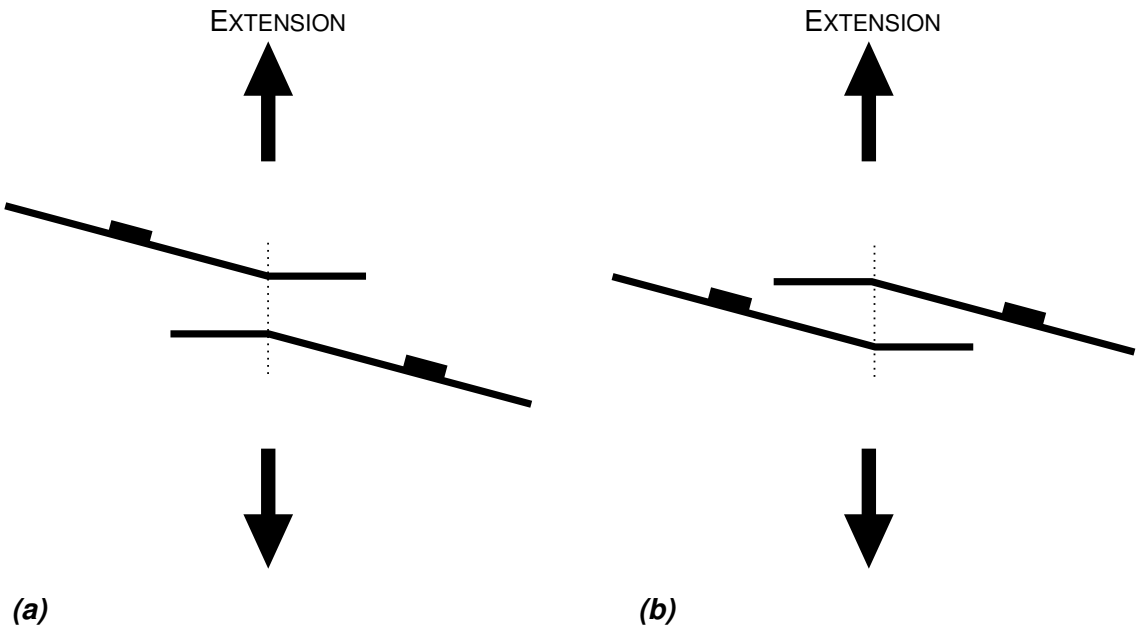

Figure 6.19: *Between left-oblique right-stepping faults an "open" relay ramp geometry developed (a), whereas the geometry of the ramp between left-oblique left-stepping faults was more "closed" (b).*

When we imposed a strike of the main faults that was oblique to the extension directions, the faults adopted a geometry outside the silicone putty bars that was again more or less perpendicular to the direction of extension. We doubt that the applied boundary conditions in these experiments are realistic, because pre-existing "weakness zones" in nature are not expected to suddenly stop at overlap zones. However, in the experiments this resulted for left-oblique left-stepping faults and right-oblique right-stepping faults to form a more closed geometry of the ramps (faults growing towards each other), whereas for right-oblique left-stepping faults and left-oblique right-stepping faults, the relay zones were more "open" i.e. faults slightly diverging (e.g. figure 6.19). This did however not modify the overlap/spacing ratio of the ramps.

6.6 Small-scale modelling of relay ramps: Discussion

6.6.1 Discussion of the experiments

Evolution of the models

For the evolution of the modelled relay ramps only 3 clear different stages were identified: the immature stage, the interacting stage and the linkage stage. These stages correspond respectively to stage 1, 2 and 4 in the evolution scheme proposed by Peacock and Sanderson (1991) from the study of natural relay ramps (see section 2.5 on page 60). In the models it was not possible to observe the development of the secondary fractures in the ramps that marks the start of the breaking down of the relay ramp and which forms the 3^{rd} evolutionary stage of Peacock and

Sanderson (1991).

Figure 6.13 shows that after relatively small amounts of extension (3–4 cm) overlap zones started to form, meaning that the immature stage in the experiments was only of minor importance. After the transition to the interacting stage, the length of the overlap zones still increased for a certain amount of extension, but most curves in figure 6.13 reach a plateau even when extension increases further. The fact that the fault tips in the relay zone stop propagating, is most likely caused by propagation impediment, resulting from the interaction of two faults with an overlap geometry (section 2.4.1).

Relationship between length, displacement and spacing

As illustrated in figure 6.11 an empirical displacement-length scaling has been found for the faults in the models given by:

$$D = 0.0226 \times L^{1.11} \tag{6.9}$$

It has been explained in section 2.3.3 that the value of the exponent n in the general displacement-length relation of faults (eq. 2.12) varies in natural systems between 1 and 2, but that so far no consensus exists (e.g. Walsh and Watterson, 1988; Gillespie et al., 1992; Cowie and Scholz, 1992b; Gudmundsson, 1992; Dawers et al., 1993). Taking into account that the value of the exponent also depends on material properties (Cowie and Scholz, 1992b), the value of $n = 1.11$ appears to be consistent with the ones obtained from natural systems. This indicates that the above described initial "under-displacement" of the faults in the models is readjusted to a normal displacement profile in later stages of the experiment. As such, the technique of triggering normal faults by adding a silicone bar at the base of the model seems to be suitable. In the displacement-length graph (figure 6.11) there is a large scatter of the data ($R^2 = 0.5$) that might be explained by the dependence of the scaling relation on many different factors (Bürgmann et al., 1994; Mansfield and Cartwright, 2001), not the least important being measurement errors when determining the values of D and L. More accurate ways to determine the maximum displacement along a fault would be to use shadow lengths of the fault scarp as a measure of throw (e.g. Mansfield and Cartwright, 2001), or to make detailed laser scans of the surface of the model after its evolution. In the latter case, however, measurements could be complicated by degradation of the fault scarp when displacements become too large.

Similar to An (1997) and Acocella et al. (2000), the models allowed to link the interaction between two faults to a combination of the total system length and the spacing between the faults (figure 6.12). This would mean that inferring interaction based on the overlap to spacing ratio alone (ie. on the geometry of the overlap zone) might be insufficient. In figure 6.12 a gray transition zone has been drawn between the "interaction area" and the "no interaction area". This zone is rather broad, but based on the available data it was impossible to refine it. The reason why the slope of the interaction to no-interaction zone is larger than that of Acocella et al. (2000) for normal faults is unclear, but it could be that it is influenced by the nucleation points of the faults in the models. In the experiments, faults never nucleated far from each other, as the silicone bars lie next to each other. This means that overlap zones are formed relatively

fast in the model's run. If for example in Iceland the average distance between nucleation points of the fractures was larger, one might expect the faults to have in general larger lengths before they start interacting.

Relationship between overlap and spacing

The trend in the experimental data that the overlap distance (OL) is generally larger when the spacing (S) between the segments increases (figure 6.14), is easily explained by the mechanical interaction between the two segments. It was already described in section 2.4.1 that the magnitude of the variation in propagation force for fractures and faults with a closely spaced geometry is larger than for more widely spaced fractures (figure 2.11). This means that the closely spaced faults in the experiments are more subject to the propagation impediment that results from the interaction, and that finally causes the faults not to propagate further in the relay zone. Faults that are spaced more widely will only feel the same propagation impediment when larger overlap zones have formed (see figure 2.11).

As observed in the experiments, small spacings of the silicone bars can either result in the formation of a relay ramp or a continuous fault. This indicates that in such cases defining a unique solution for the fault linkage process in the models remains difficult. In a "critical situation" between the transition from one stage to another (e.g. the transition between the formation of a continuous fault and a relay ramp), the actual shift to either stage might be influenced by small disturbances in the model (C. Faccenna, *personal communication*). For example Mansfield and Cartwright (2001) argued that small mechanical heterogeneities in their models might have had large influences on shaping the final fault displacement geometries of their experiments. The presence of analogous small mechanical heterogeneities might have been such a small disturbance in the models that caused the occurrence of either the development of a continuous fault or a relay ramp.

Influence of the aspect ratio on the interaction

The aspect ratio of the faults in the models (i.e. length/height) is believed to have a considerable influence on their mechanical interaction, as the stress field perturbation around a fault is larger for vertically tall faults (i.e. with a low aspect ratio) than for vertically small faults (i.e. with a high aspect ratio) (e.g. figure 2.10 on page 47). For the interpretations of the influence of the aspect ratio's on the interaction in the models we should, however, be very careful, as there is an uncertainty in determining the aspect ratio. The fault heights in the experiments were determined by the thickness of the sand pack and therefore the aspect ratio calculated at the end of an experiment somehow overestimates the aspect ratio of the faults during the modelling. Earlier in the experiments, the fault lengths would have been smaller, while the fault height had already reached its maximum value. For this reason it was impossible to properly measure the aspect ratio's in all stages of the modelling. Therefore it is difficult to accurately couple experimental observations with the theoretical ideas of the aspect ratio.

Using the final fault length and the thickness of the sand cover to determine the aspect

ratio's of the modelled faults, values that range from 2.5 to 5.2 in the different experiments were found.

Although there were difficulties in accurately determining the aspect ratio, some of the observations do not seem to follow the known relation between interaction and aspect ratio. In ramp ZAV09A for example (table 6.1), for a spacing of 2 cm of the silicone bars, a little ramp formed, whereas in other experiments (ZAV07A and ZAV08A) this spacing resulted in a continuous fault. In the beginning of the experiment, however, the fault segments in ZAV09A had a length of 7 cm each (imposed by the 7 cm long silicone bars in that experiment), which results in an aspect ratio of 1.67 in the early stages of the experiment, just before the ramp started to form. In experiments ZAV07A and ZAV08A, the initial segment length was 15 cm, resulting in aspect ratios of respectively 2.59 and 2.73 in the beginning of that experiment. The fact that the two segments in the ZAV07A and ZAV08A models linked in an early stage (before forming a relay ramp), might suggest stronger interaction in the beginning of the experiment here than in experiment ZAV09A, although the aspect ratio of the fault segments is smaller in the latter. The non-correlation ($R^2 = 0.09$) in figure 6.15 between the overlap to spacing ratio of the ramps and the aspect ratio of the faults also indicates that for these models there is no clear relation between both: an increase in the aspect ratio of the faults allows for an increase in the degree of overlap compared to the spacing — and as such indicates less mechanical interaction between the segments — but there is a large scattering of the data in the graph. Also in figure 6.14 there is a large scattering of the data points around the theoretical curves for spacing to overlap relations, suggesting that probably other processes influenced the relation, and the interaction between neighbouring segments, as well. Obviously, also the difficulties encountered in determining the aspect ratio's greatly contributes to the scatter in this graph.

Length to width ratio of overlap zones

The length to width ratio's of the overlap zones that formed in the experiments, correspond well with observations from Acocella et al. (2000) for extensional fractures in Iceland. They found that for 88% of their examples the ratio was lying between 2 and 6, with an average of 3.5. The observation from natural fault systems that the geometry of the overlap zones is similar over a broad range of scales has already been mentioned earlier in this work (see section 2.5.2 and appendix A).

Breaching

In the models 55% of the breached relay ramps were characterised by hanging-wall fault to footwall fault propagation, 27% by footwall fault to hanging-wall fault propagation, and only 18% by the development of a new connecting fault. Also in nature the breaching of a relay ramp by the development of a new cross-cutting fault is probably the least common, as its occurrence has been least described. The most frequent way of breaching in the examples of appendix A is however the propagation of the footwall fault towards the hanging-wall fault, and not the other way round as in the experiments. Also the examples described in Childs et al. (1995) were all

breached by a footwall fault to hanging-wall fault propagation, and therefore this mechanism is likely to be the most common in nature. However, it is hard to determine accurate percentages on this.

The development of a new fault to connect the two offset main segments, has only been observed in cases where the spacing was rather small (1.5 cm). Recently Tentler (2003) found from analogue models of overlapping spreading centres that only in cases where the spreading ridges were spaced at larger distance from each other new fractures developed inside the overlap zone and as such caused the final breaching. This somehow seems to contradict the observations here, but it should be mentioned that in the models here the new connecting fault that cut through the ramp corresponded to a splay fault of one of the major faults. However, also for larger spacings the nucleation of new fractures in the ramp to finally accomplish the breaching was not observed.

In section 2.5.1, the model of Ferrill et al. (1999) was introduced that states that the mode of breaching is related to the displacement gradients on the main faults. Steep displacement gradients that result from large displacements at the fault tips without proportional propagation of this tip would favour breaching by a connecting fault, whereas in the other cases one of the main faults is more likely to propagate to achieve the linkage. In some of the models (ZAV04A & ZAV06M) the displacement gradient of the faults at the relay zone tip had been increased, however this did not result in a breaching by a connecting fault in these experiments. Experiments ZAV06A & ZAV17A on the other hand were not characterised by any imposed displacement increase at the fault tips in the relay zone.

6.6.2 Comparison of specific observations with existing conceptual models

Although the overall evolution of the relay ramps in the experiments corresponds well with the existing conceptual models of relay ramp evolution, some specific observations do not seem to follow the existing models as described in section 2.5. These observations are shortly mentioned in this paragraph.

A first observation that was made in several experiments is the propagation of the main fault tips even after the relay ramp is breached. As explained, existing models of relay ramp evolution state that as soon as a hard connection is formed between the main faults, this connection will take over all displacement in the ramp, causing the ramp and the unused fault tips to disappear. In the descriptive section of the modelling results (starting at page 190) several experiments were described, which were characterised by a post-linkage propagation of the fault tips at the relay zone (e.g. ZAV06A in figure 6.16). Even experiments where a continuous fault was formed before it reached the surface of the model (e.g. ZAV07A in figure 6.18) sometimes showed a clear propagation of one or both of the main faults at the bend. In nature, the final geometry of both described systems would be very similar (figure 6.20) although the formation history would be different. If the main faults continue to propagate even after a hard linked structure has formed, this would mean that shortly after breaching, the new hard connection is not yet able of taking over all the displacement in the ramp, and that the system evolves further for some time before the ramp structure will finally disappear.

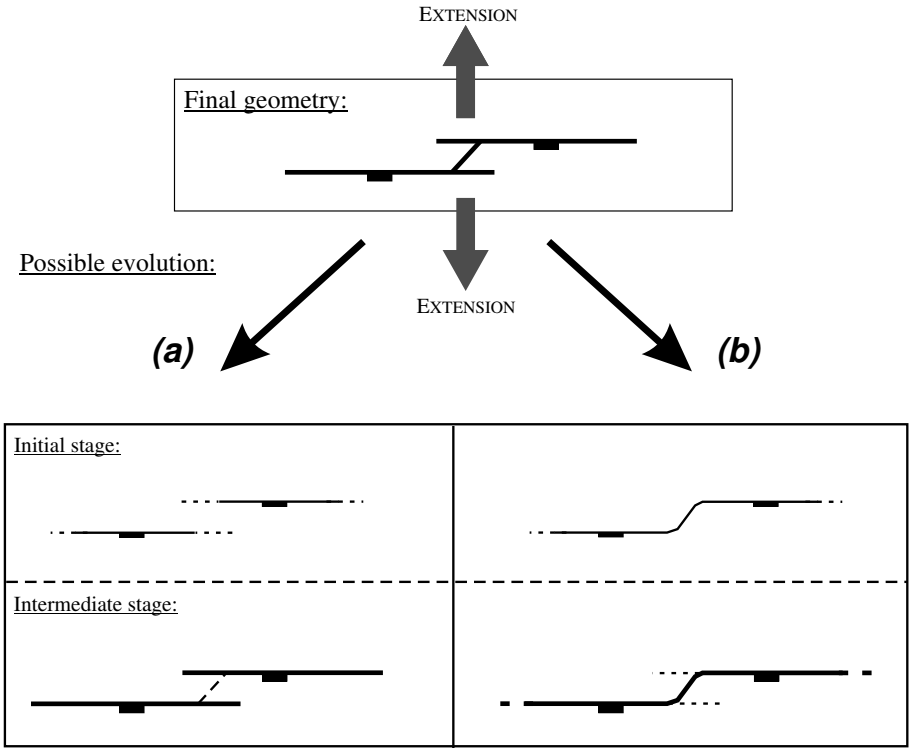

Figure 6.20: *The same final geometry might result from relay ramps breaching by a connecting fault, or fault propagation at bends in a continuous fault.*

In chapter 4, it was already noticed that in the area of Zavarotny the relay ramp did seem to evolve further even after breaching. There, it was suggested that the breaching mode in Zavarotny could be the reason for this. This was based on the idea that if the connecting fault was a newly developed fault, it could very well be that in the beginning it was unable to transfer all the displacement between the two faults. From the models presented here, it is clear that also the other breaching modes do not necessarily imply the sudden cessation of activity in the ramp. As such, the breaching of a relay ramp is certainly not an instantaneous process. In the light of this it could be useful to propose a fifth evolution stage in the evolution scheme of Peacock and Sanderson (1991), being the *post-breaching stage*, although strictly speaking the relay ramp does no longer exist in that stage (see section 2.5). The displacement on the fault tips that propagated after the ramps had breached usually remained rather small compared to the main faults. Nevertheless, the fact that the faults — which often had stopped or at least decreased their propagation rate while forming the overlap zone — "restart" to propagate further, indicates that in the end the relay ramp system is no longer capable of accommodating all the deformation and that — despite the propagation impediment caused by the nearby fault — the faults need to propagate. This might be an indication that only a limited amount of displacement transfer can be achieved along a relay ramp.

Another observation that is worth mentioning is the evolution of model ZAV17A, where the

Normal situation for relay ramp

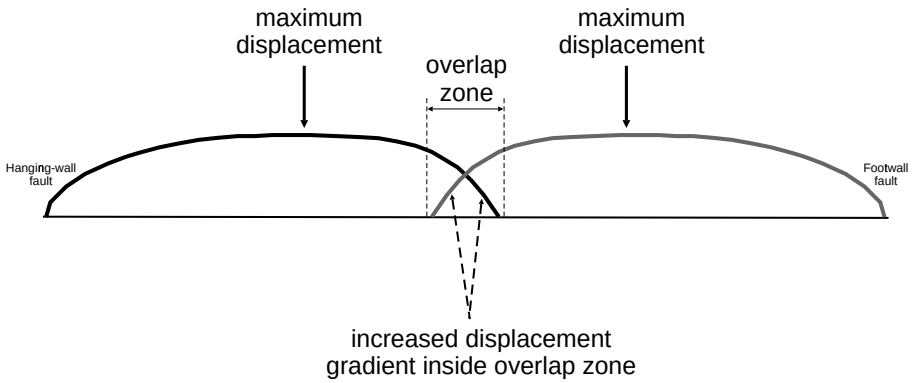

Situation for ZAV17A

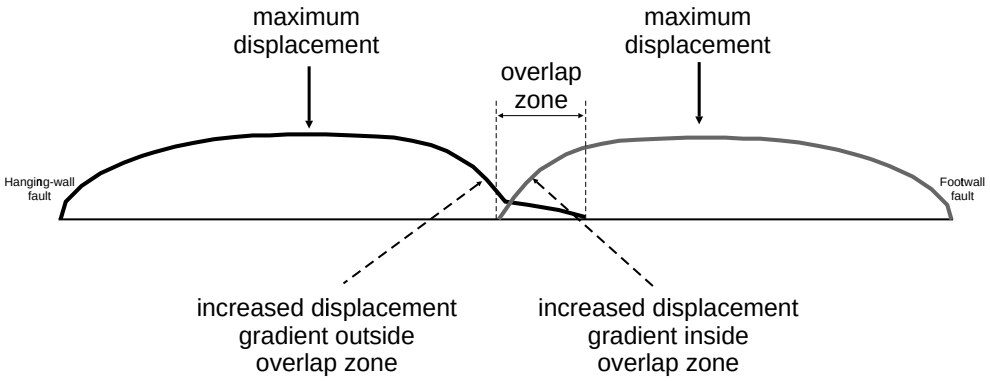

Figure 6.21: *Unlike most natural examples (upper figure), the hanging-wall fault of experiment ZAV17A showed a clearly increased displacement gradient just outside the overlap zone, and only a gentle displacement gradient inside (lower figure). In a later evolution stage a connecting fault splayed of from the hanging-wall at this point.*

hanging-wall fault showed a clear increase in the displacement gradient just outside the overlap zone, rather than inside the overlap zone as usually reported in nature (figure 6.21). Inside the overlap zone the hanging-wall fault of ZAV17A showed only a gentle displacement decrease. In a later stage of the experiment, a fault splayed off from the hanging-wall fault, exactly at the point where the displacement gradient suddenly decreases. This splay-fault propagated through the ramp, and accomplished the final breaching of ramp ZAV17A. This experiment illustrates that the arrestment of the fault tip can occur outside the overlap zone, and that this might have a profound influence on the internal structure of the relay ramp.

It has only been possible to observe the fault evolution at the surface of the models, and this is a limitation. The vertical propagation of the faults from the base of the model (at the silicone bars, where the faults nucleated) to the top surface could explain the initially large fault lengths that have been observed in the models (e.g. Walsh et al., 2002). Also in later evolution stages the observed fault growth at the model's surface could still be characterised by propagation out of the inspection plane, however, seen the large aspect ratio's of the faults in the models, it is believed that mainly in-plane propagation has been observed (e.g. Walsh et al., 2003).

6.7 Conclusions

Relay ramps with initially controlled fault geometries can be simulated using sandbox models containing basal silicone bars.

The experimental ramps evolved in three stages, characterised by the growth of the normal faults, their interaction and linkage. Interaction and linkage occurred only when the total length of the faults was larger than 8 times their spacing. The length to width ratio of the relay ramps during the interaction stage showed preferred geometries, clustering around 3.

Three common ways of relay ramp breaching have been reported in the experiments: i.e. hanging-wall fault to footwall fault propagation, footwall fault to hanging-wall fault propagation and the development of a new connecting fault. Unlike in natural examples, hanging-wall fault to footwall fault propagation was the most common in the experiments.

The propagation of the fault tips was observed both before and after the linkage stage, even though the final deformation pattern was identical.

The models evolved like structures reported in nature and therefore are considered reliable analogues. Nevertheless, the further propagation of the fault tips after the linkage has not been described in nature and constitutes a new observation in the evolution of extensional relay ramps.

Chapter 7

Scaled physical models of Lake Baikal and the Baikal Rift Zone

With the models presented in this chapter, a possible mechanism that could influence the stepwise border fault deflection in Lake Baikal was tested, and it was evaluated whether the process could be responsible for the creation of the different relay zones between the border fault segments.

First the different models will be described, and subsequently the similarities with and the implications for the Baikal Rift Zone will be discussed. At this stage no attempt will be made to discuss the structures which have no direct implication for our understanding of Lake Baikal.

All models presented in this chapter have been run in the structural modelling laboratories of Royal Holloway, University of London under the supervision of Prof. Dr. Ken McClay.

7.1 Introduction

Despite the huge progress that has been made over the last decades in understanding the development of Lake Baikal, several questions regarding the rift's evolution still remain largely unanswered:

- Why is there a systematic stepwise deflection of the western boundary fault along the length of the lake?
- How did the different Baikal basins evolve, and how did the accommodation zones between the basins develop?
- Has the location of the relay zones between the different boundary faults been predetermined? Or do they occur at "arbitrary" locations?
- Did the faults evolve in a similar fashion as predicted by the models described in chapter 2?

In this chapter, one of the possible controls on the deflection of the western border fault in Lake Baikal is examined by means of a sandbox modelling study. For this purpose, a series of models

were run with differently shaped rigid basal plates. The boundary conditions that were chosen for the modelling are obviously an over simplification of the natural situation (for example one constant direction of extension), but nevertheless, the experiments can provide insight in how changes in the orientation of pre-existing structures can complicate the fault geometries in an area.

The geometry of the base-plates that were used in the different experiments ranged from a simple linear shape to shapes mimicking the Siberian Craton. This modelling gave insight into the extent to which the present-day surface faulting in Lake Baikal could be related to pre-existing basement structures.

Including pre-shaped velocity discontinuities in rift models has been a commonly used approach to test the influence of pre-existing *discrete structures* on the subsequent rifting. However, one should bear in mind that only limited conclusions can be drawn from such models, mainly because they normally don't include the influence of *pervasive* pre-existing basement *fabrics* on the subsequent rifting (Morley, 1999c).

7.2 Analogue models of rift systems

Many experimental studies have successfully reproduced small-scale analogues of extensional structures that are characteristic for rift systems (Horsfield, 1977; Tron and Brun, 1991; McClay and White, 1995; Keep and McClay, 1997; Acocella et al., 1999a; Brun, 1999; McClay et al., 2001, 2002; Corti et al., 2003). These reproductions have focused on different aspects of the rifting, for example three or four-layer models have been used to simulate lithospheric deformation (e.g. Davy and Cobbold, 1988; Allemand and Brun, 1991; Gartrell, 2001; Michon and Merle, 2003), whereas other models mainly concentrated on surficial deformation of the brittle crust in relation to the rifting (e.g. McClay and Ellis, 1987; McClay and White, 1995; Acocella et al., 1999a; McClay et al., 2002). The first category addressed problems like the influence of lithospheric rheology on the width of rift systems, whereas in the latter complex fault patterns were produced that are readily comparable with natural examples (McClay et al., 2002).

Models on both scales have illustrated that the angle between the rift trend and the direction of extension exerts a major influence on the surface faulting and basin development in the model (Tron and Brun, 1991; McClay and White, 1995; Mart and Dauteuil, 2000; McClay et al., 2002).

7.2.1 Orthogonal rifts

An orthogonal rift is characterised by a rift trend that is oriented perpendicularly to the direction of extension. Physical models of such rifts are in general characterised by the development of long linear fault traces (e.g. Mart and Dauteuil, 2000; McClay et al., 2002) (figure 7.1). Both, basin margin faults as well as intra-rift faults, have a strike more or less orthogonal to the direction of extension. With increasing extension, deformation tends to increase in the central part of the rift system, but a significant reorganisation of the fault system is uncommon (McClay et al., 2002).

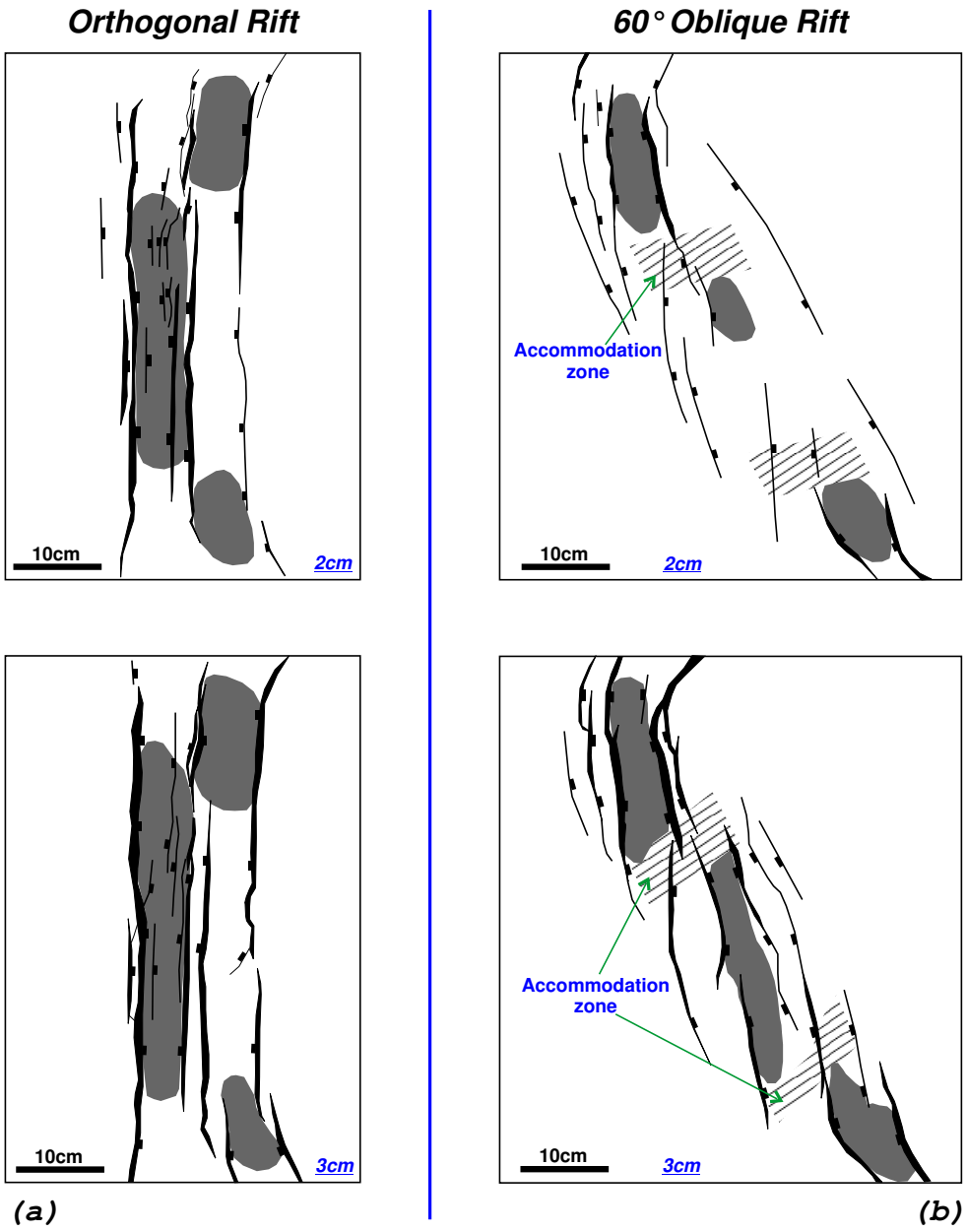

Figure 7.1: *Line-drawings of the sequential development of an orthogonal rift (a) and a 60° oblique rift (b). From McClay and White (1995). In the orthogonal rift long linear faults develop that are oriented perpendicular to the direction of extension, whereas in the oblique model, different smaller faults form in an en echelon geometry. Grey shadings in the figure represent local depocentres. See also figures 7.27 and 7.29.*

7.2.2 Oblique rifts

Oblique rifts are characterised by a rift trend that is not perpendicular to the direction of extension. Rift obliquity is usually quantified by the angle between the rift trend and the extension vector.

The length of fault segments in rifts has been found to be inversely proportional to the degree of obliquity of the rift (e.g. McClay et al., 2002). Highly oblique rifts form a series of short rift boundary fault segments with an en echelon geometry. Lateral propagation of these segments, results in the merging of the different rift basins in one single rift, in which the initial en echelon geometry remains visible (Mart and Dauteuil, 2000). McClay and White (1995) have emphasised that they didn't observe the presence of discrete transfer faults in their rift models (both orthogonal and oblique), not near the surface, nor in the lower parts.

7.3 Experimental procedure

The rift experiments in this study can be classified in 2 categories: (1) experiments with only sand layers that were extended above a rubber sheet detachment and metal base-plates (experiments BAIK-01 to BAIK-07), and (2) experiments containing a basal polymer covered by brittle sand layers (experiments EP-01, EP-02 and EP-03). The modelling rigs for both types of experiments are shown in figure 7.2 and 7.3 respectively. The rubber sheet detachment models (first category of experiments) are a standard type of sandbox models for the simulation of brittle deformation. The polymer models (second category of experiments) were chosen in a later stage, because these models better localise the active deformation in the centre of the model. The scaling of analogue models has been explained earlier in chapter 6.

For the first category of experiments, dry quartz sand was sprinkled on top of a basal detachment formed by a 5–10 cm wide rubber sheet attached between two shaped metal plates (figure 7.2 and 7.4). This sand pack (i.e. pre-kinematic) was made-up of alternating 4–5 mm thick blue, black or white coloured layers, totalling a thickness of 7.5 cm. The metal base-plates were attached to the end-walls of the model. Extension in the model was achieved by pulling one of the end-walls (and thus the metal plates) away from the other. The strain rate in this category of models was 0.0053 cm/s. During the extension process, the surfaces of the models were carefully monitored by 35-mm digital photography, with shots taken every 1 mm of extension. Created accommodation space was filled with red and white syn-kinematic sand layers every 1 or 2 cm of extension. Deformation of the models was stopped after 100% of extension.

Finished models were impregnated with a gelatine solution and sectioned either horizontally (1.5 cm interval) or vertically (1 cm or 0.5 cm interval) to reveal their internal structure.

The second category of models (experiments EP-01 to EP-03) were deformed using a different technique. Here the brittle sand layers were sprinkled on top of a 1 cm thick layer of SGM-36 polymer. The polymer was put on top of a basal plastic sheet, attached to one of the end-walls of the rig. By sliding the end-wall away, the plastic sheet was pulled out of a shaped slot in the centre of the rig (figure 7.3). To assure the same basal friction in the whole model, the base of

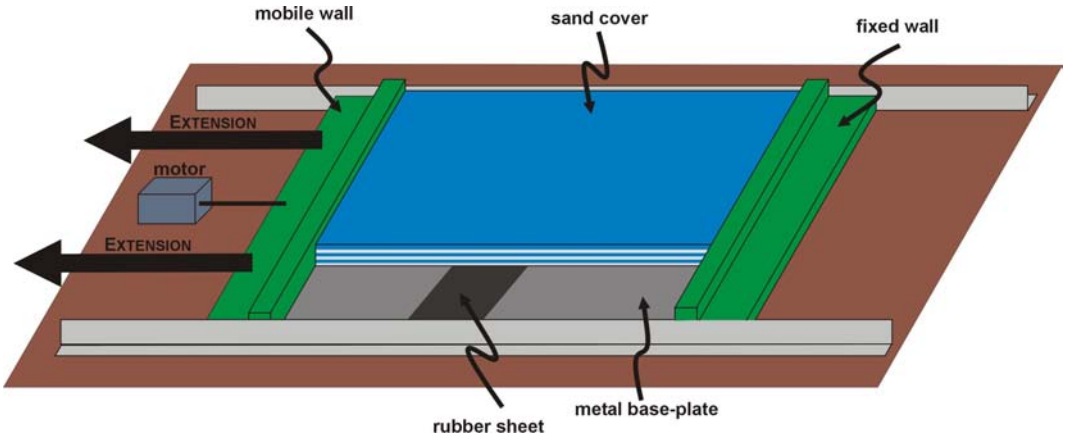

Figure 7.2: *3D-modelling apparatus used to run the first set of experiments (a). The different types of base-plates that were attached to the walls of the rig are shown in figure 7.4. Because only one of the end-walls was moved, the rift basins that formed in the models had an asymmetric shape. The distance between the metal side-walls is 60 cm.*

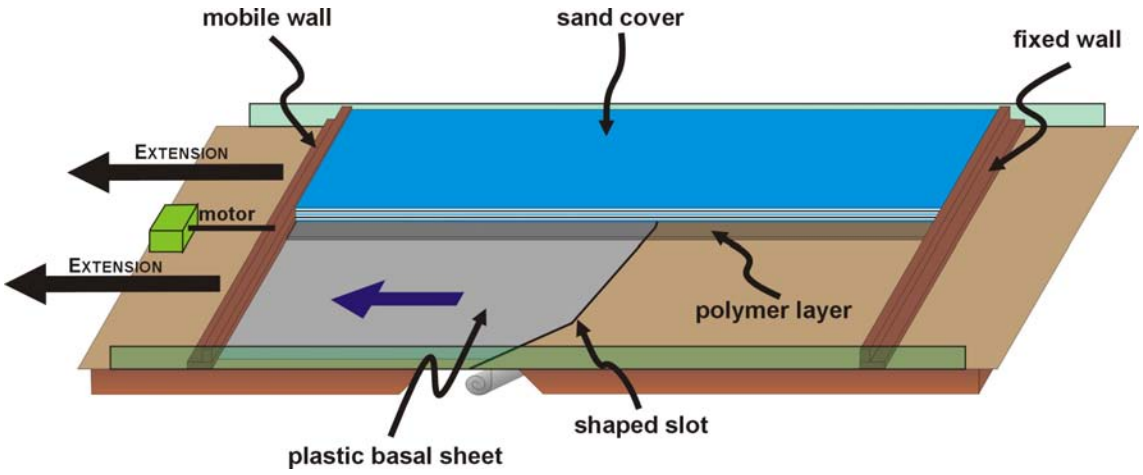

Figure 7.3: *Modelling rig for experiments EP-01 to EP-03. Here a basal polymer layer was used to localise the deformation in the overlying sand cover. Extension was achieved by pulling a plastic sheet out of a shaped central slot. The distance between the side-walls is 92.5 cm. During the experiments the right half of the rig was covered with a fixed plastic sheet to assure the same basal friction in both parts of the model (not indicated in the figure).*

the other half of the model (i.e. from the central shaped slot to the fixed wall) consisted of the same — although here immobile — plastic sheet (not drawn in figure 7.3). Before adding the sand layers, the polymer rested 3 days in the rig to allow for the escape of even the smallest air bubbles that could influence the polymer's deformation during the modelling. The procedure

Figure 7.4: *Different types of base plate geometries used in the first set of sandbox experiments. Detailed dimensions can be found in the illustrations in Appendix B (page 305). Grey areas represent the metal plates, black zones correspond to the rubber sheet. The arrow at the right indicates the slicing direction for the vertical slices. Characters O, P and B are used in the descriptions of* `type 2` *and* `type 4` *models to refer to the location of faults (see section 7.4.1).*

for layering, monitoring and sectioning the models, was identical to the first category of models. The strain rate however, was lowered to 0.0033 mm/s to stay in the Newtonian flow regime of the polymer (see section 6.2.3 on page 185).

In models EP-01 and EP-02 a 2.5 mm thick white clay layer was added under a 1 mm surface layer of coloured sand. The addition of this tiny clay layer allowed for the visualisation of small fractures that affected the model's surface before the actual development of faults. This clay layer has only been used in two rift models, and the obtained results appeared consistent to models containing only sand. However, as a result of the large cohesion of clay, the precursor fractures in the models are not correctly scaled to fractures in the brittle crust.

Animations of the top-photographs were made to investigate the evolution of the models through time. These movies are included on the accompanying CD-ROM. Also the series of cross-sections was animated to visualise the geometric changes in the models.

The structural modelling laboratories at Royal Holloway University of London also have 2D modelling rigs, in which the evolution of cross-sections of models can be observed through glass side-walls. Two examples of such models are included in Appendix C, and the animation of the different running shots can be found on the CD-ROM as well.

Three dimensional surfaces of the models could be produced by digitising certain levels in the different cross-sections of a model. This has been done for the pre-kinematic level in selected experiments. The technique is outlined in appendix D.

7.4 Results

7.4.1 Conventions

To describe the observations that were made during the modelling the following conventions has been used:

- The modelled rift zones contain a *fixed wall side* and a *mobile wall side*. These terms refer to the approximate half of the rift zone that is located closest to respectively the fixed wall and the mobile wall of the modelling rig. The *fixed wall side faults* usually dip towards the mobile wall, whereas the *mobile walls side faults* dip towards the fixed wall. The pulling side of the model, which corresponds to the mobile wall side, is either indicated in the different figures, or reported in the captions.

- Some of the base-plates that were used in the modelling had shapes that mimicked the geometry in Lake Baikal. To describe the fault geometries (from left to right) in these models the previous convention is used, but additionally fault segments have been termed "O", "P" and "B" faults, respectively, to refer to their distribution from the lower part of the model to the upper part. These "O", "P" and "B" parts correspond respectively to the parts of the base-plates that correspond to the Obruchevsky, Primorsky and Baikalsky Faults in the Baikal Rift Zone (see figure 7.4 and figure 3.11 on page 106).

- Only when discussing vertical cross-sections terms like "lower" and "upper" refer to the location in the model in depth. On surface views these terms refer to the approximate lower and upper half of the photograph and/or model.

7.4.2 Baikal experiment nr 1: BAIK-01

Characteristics

The first Baikal model has a simple geometry of the base plates and was performed as a reference experiment for later models with more complex base plate geometries. The model has the following set-up characteristics:

- base plate geometry: `Type 1`,
- dimensions: 70 cm × 60 cm,
- extension achieved by pulling one of the base plates (asymmetric rift),
- 10 cm wide rubber sheet in the centre of the model,
- 7.5 cm of pre-kinematic layers. A total of 13 layers all being 0.55 cm thick. From base to top the colours used were: black – white – blue – white – black – white – blue – white – black – white – blue – white – blue.
- After extension the model was sliced vertically, with 0.5 cm spacing between the first 10 slices and 1 cm spacing between the following. On both sides of the model, the first 5 cm have been skipped as these parts are strongly influenced by side effects.

The model was extended for 10 cm with a picture taken every 1 mm of extension. Syn-kinematic layers of sand were added after every 2 cm of extension. In total 5 syn-kinematic layers (red and white) were added.

Description

The following table summarises the observations that were made during the model's run (see also figure 7.5):

Extension	Observations
0.6 cm	Formation of the first surface depression in the model in the zone of the rubber sheet.
0.9 cm	Formation of the first faults in the model. These faults parallel the orientation of the base plates. In the centre of the model, also faults develop that strike more perpendicularly to the direction of extension. Faults are clearly segmented and relay ramps form between different segments

continued on the next page...

...continued from the previous page

1.1 cm	A rather broad graben (≈20 cm) has formed with in its central part a deeper graben. The boundary faults of the broad graben are oriented parallel to the base plates (ie. with an ∼80° angle to the direction of extension), whereas the faults of the central graben form angles between 80–90° to the direction of extension. 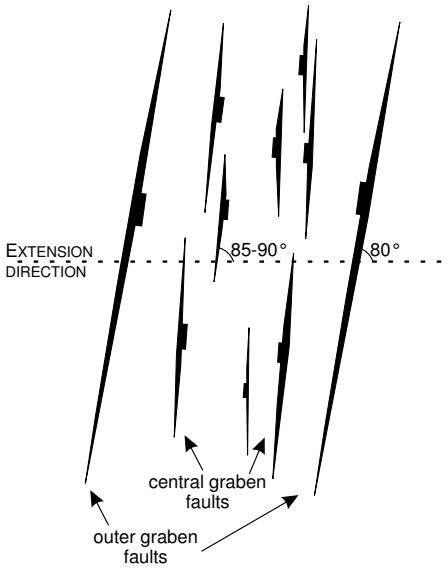
1.3 cm	New faults striking with the 80–90°-angle, develop close to the outer faults. Existing faults propagate laterally and their displacement increases.
2.0 cm	A clear asymmetry has formed: the faults on the side of the mobile wall all dip towards the fixed wall, and are distributed in an approximately 5 cm wide zone, whereas the faults on the opposite side of the graben are spread over a 10 to 12 cm zone. The mobile wall side faults have larger displacements than the fixed wall side faults. Red syn-kinematic layer added.
	Later stages are characterised by the formation of new faults, mainly in the centre of the model. Also these faults consist of different segments, that gradually link up as extension increases. The outer faults of the model attain an almost uniform displacement along their length.
4.0 cm	White syn-kinematic layer added.
6.0 cm	Red syn-kinematic layer added.

continued on the next page...

...continued from the previous page	
8.0 cm	White syn-kinematic layer added. In this stage, some of the central faults curve towards a neighbour larger fault in their footwall, and form as such horse blocks: 
10.0 cm	Final amount of extension reached. Final red syn-kinematic layer added.

The final fault geometry of experiment BAIK-01 is illustrated in figures 7.5 and 7.9. This surface views reveal the presence of relatively long linear outer faults on both sides of the model. Due to the pulling at only one side of the model (indicated by the arrows on the left in figure 7.9) the grabens in the model had an asymmetric shape. This explains the occurrence of fewer, but larger displacement faults, on the left side of the model as compared to the right side. An interpreted cross-section through the centre of the model is presented in figure 7.6, other sections are included in figure 7.7. Also from these figures the asymmetrical shape of the rift basin is clear.

On the cross-sections selected levels could be digitised to create elevation models (see Appendix D). Figure 7.8 shows a 3D visualisation of the pre-rift level of the model after 10 cm of extension. There is a good correspondence between the geometry of the pre-rift level and the geometry of the model's top surface after the deformation (see figure 7.9). However, at locations where many small faults cut the top surface, usually fewer faults are observed in the pre-rift level. This could indicate that some of the smaller faults resulted from the bifurcation of larger faults at depth. This bifurcation is clearly observed on some of the cross-sections (see for example figure 7.10).

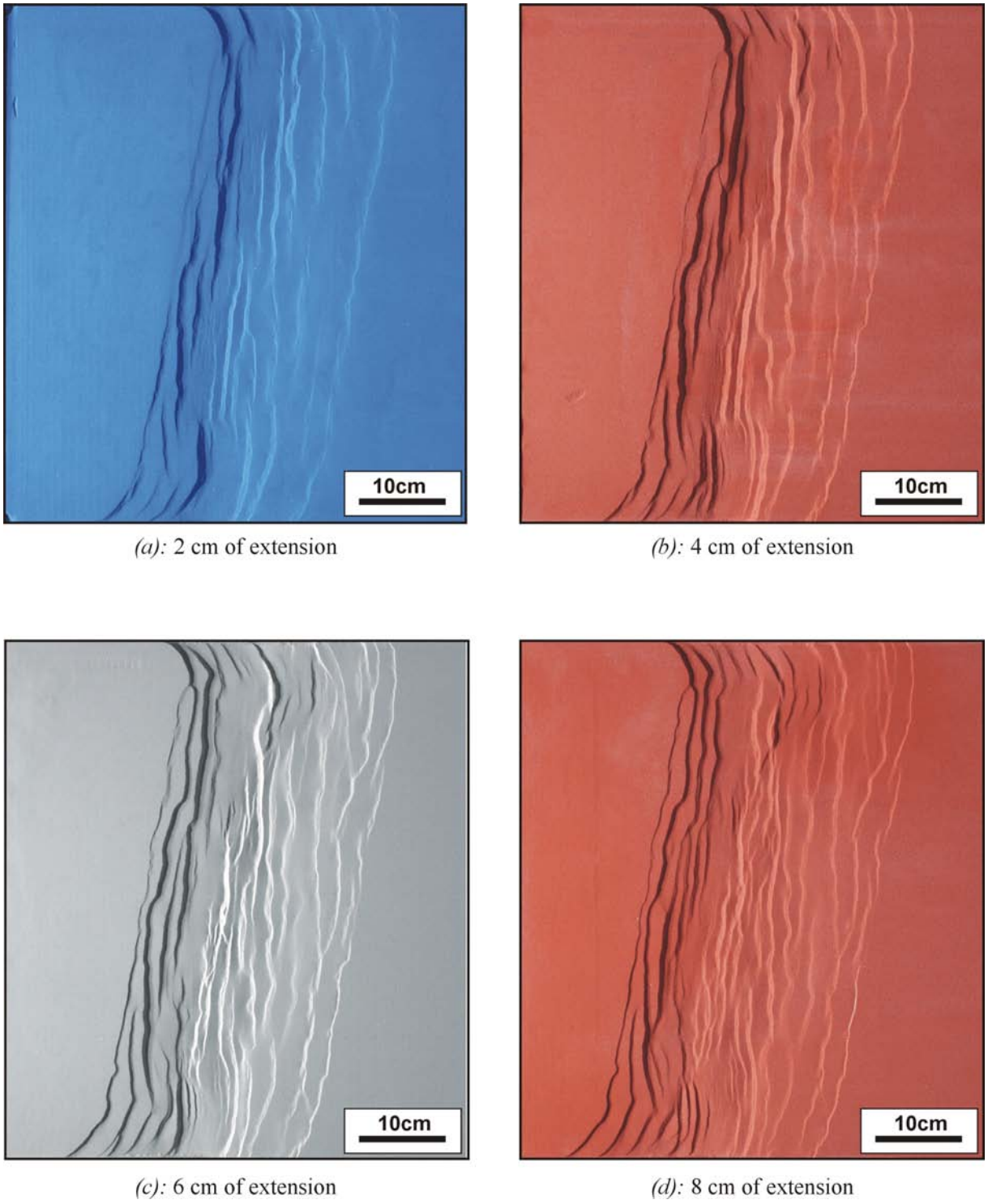

(a): 2 cm of extension

(b): 4 cm of extension

(c): 6 cm of extension

(d): 8 cm of extension

Figure 7.5: *Running shots of model BAIK-01 after different amounts of extension. The mobile wall was on the left side.*

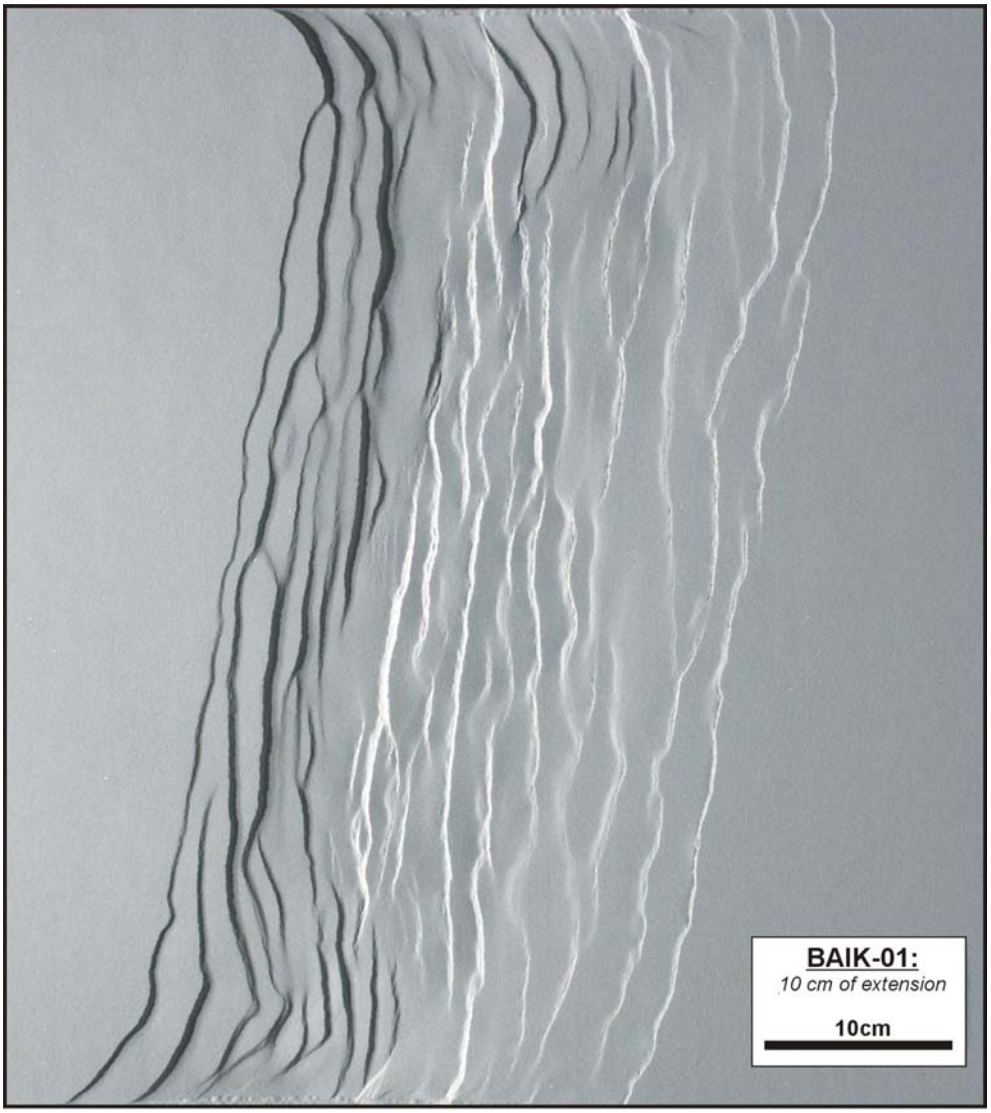

(e): 10 cm of extension

Figure 7.5: ***(continued)*** *Last running shot of experiment BAIK-01, after 10 cm of extension. Note the clear asymmetry which developed between the mobile wall side and the fixed wall side in the model. At the mobile wall side (left), few large displacement faults occur, which are spread over a ∼10 cm wide zone, whereas on the fixed wall side more, smaller displacement faults, formed that occupy a ∼20 cm wide deformation zone.*

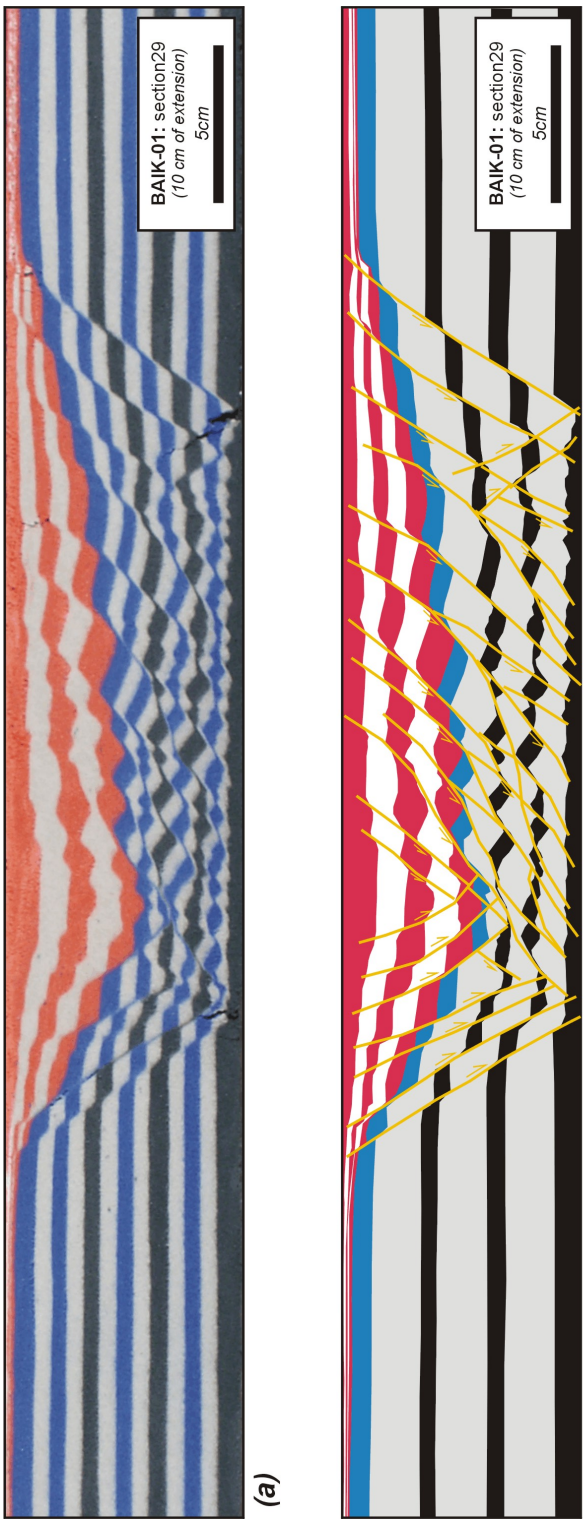

Figure 7.6: *Central cross-section (nr. 29) of experiment BAIK-01 after 10 cm of extension (see figure 7.9 for location). The original photograph is presented in figure (a) and an interpretation in figure (b). Note the asymmetry of the modelled basin, with few major faults on the left side, and more smaller faults on the right side. Black and blue layers correspond to pre-kinematic sand layers, red and white layers are the syn-kinematic infill.*

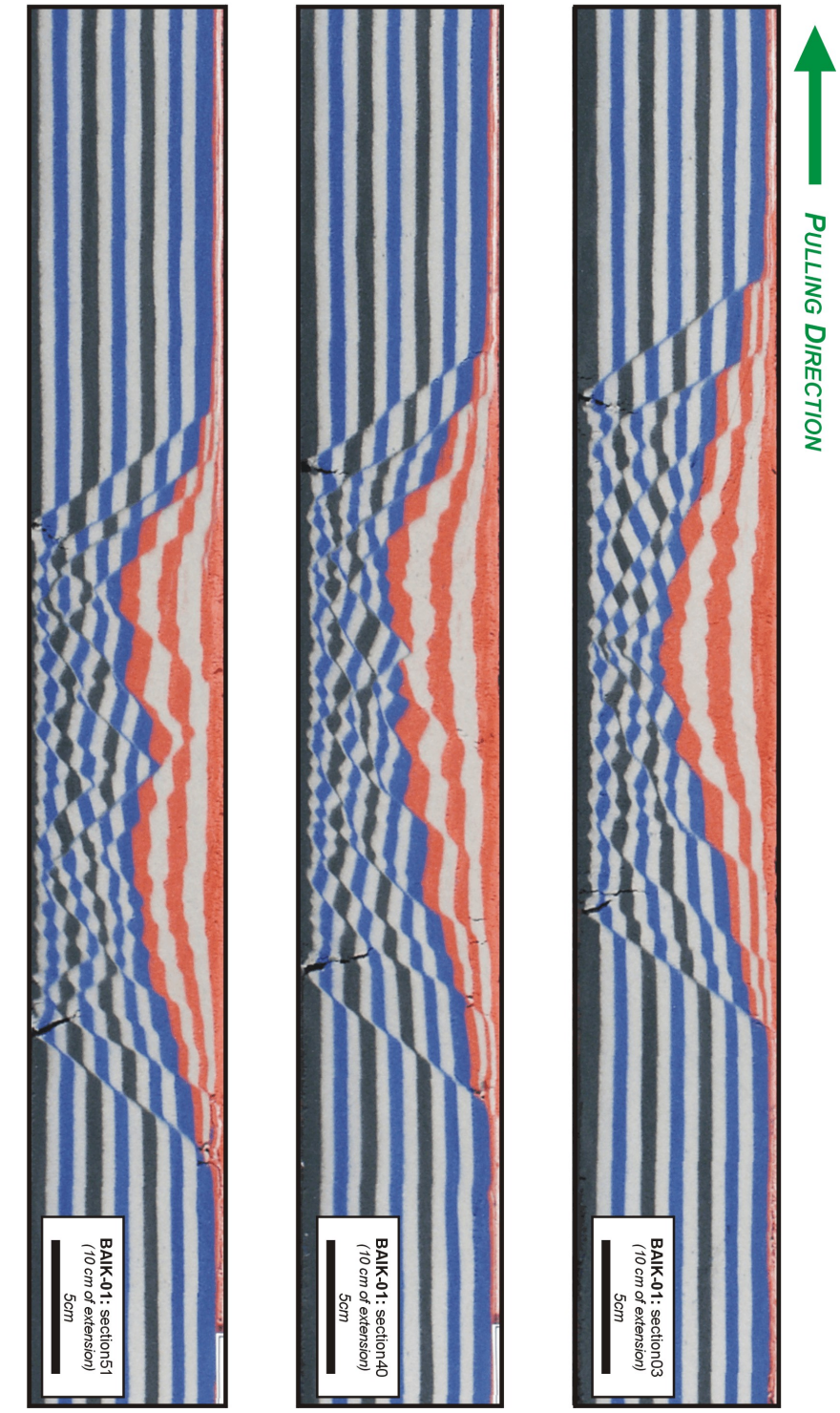

Figure 7.7: *Three cross-sections through model BAIK-01: (a) section 03, (b) section 40 and (c) section 51 (see figure 7.9 for the locations). Black and blue layers correspond to pre-kinematic sand layers, red and white layers are the syn-kinematic infill.*

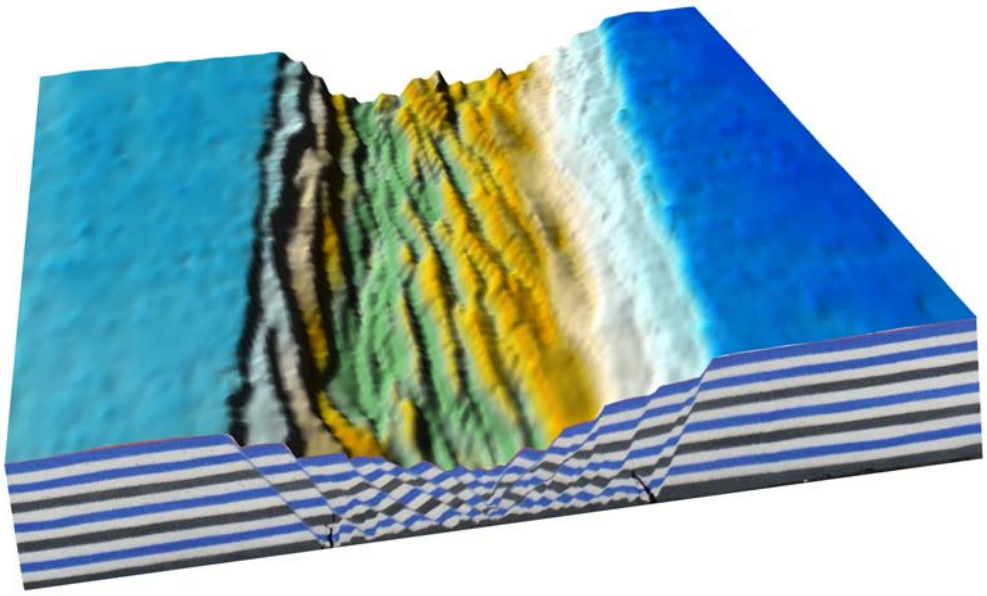

Figure 7.8: *3D visualisation of the pre-rift level in model BAIK-01 after 10 cm of extension. The mobile wall was on the left side.*

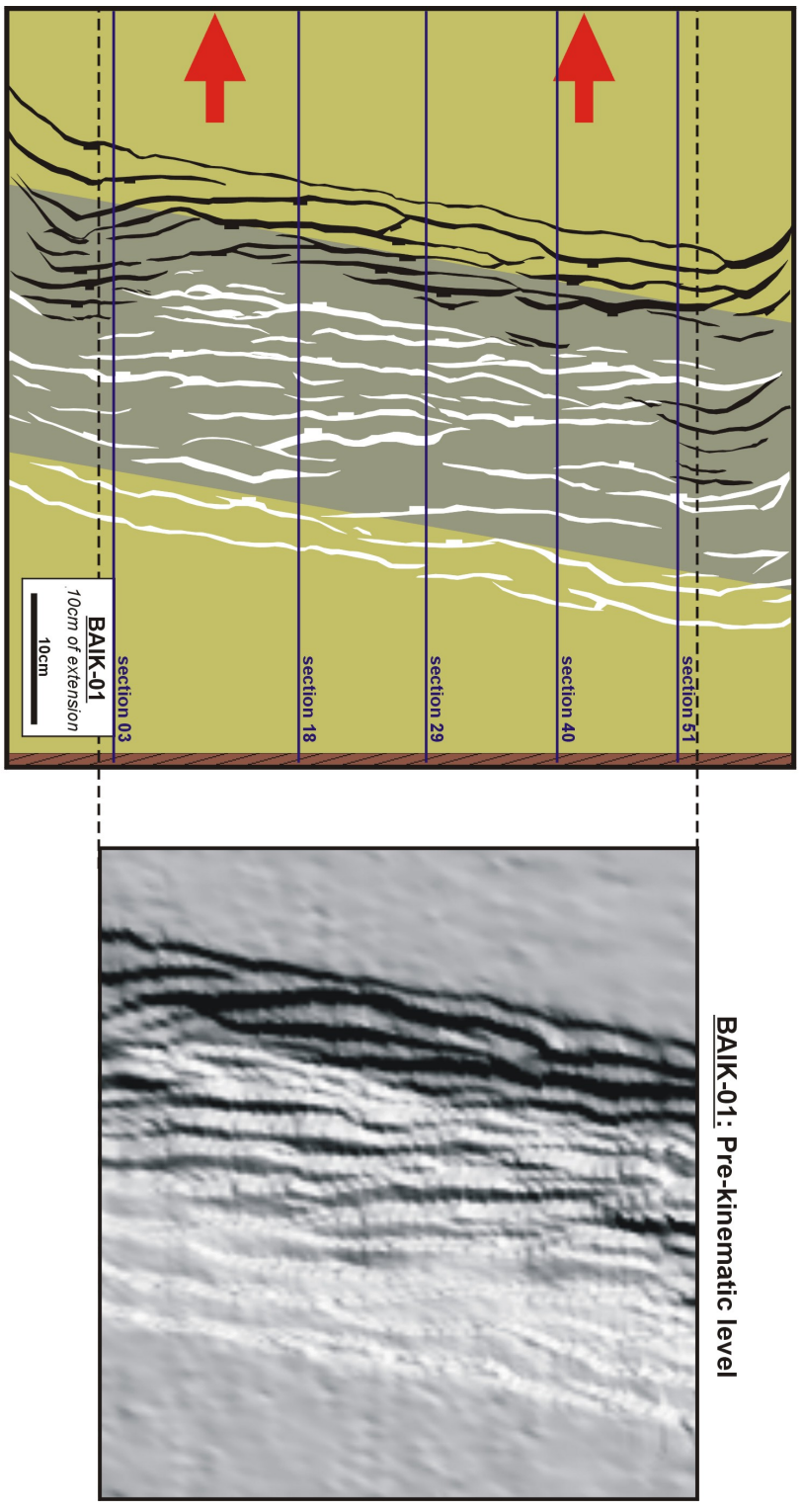

Figure 7.9: *Interpretation of the top surface structure of experiment BAIK-01 after 10 cm of extension (a), and shaded relief representation of the pre-kinematic level of the model after the same amount of extension (b). Arrows indicate the pulling direction.*

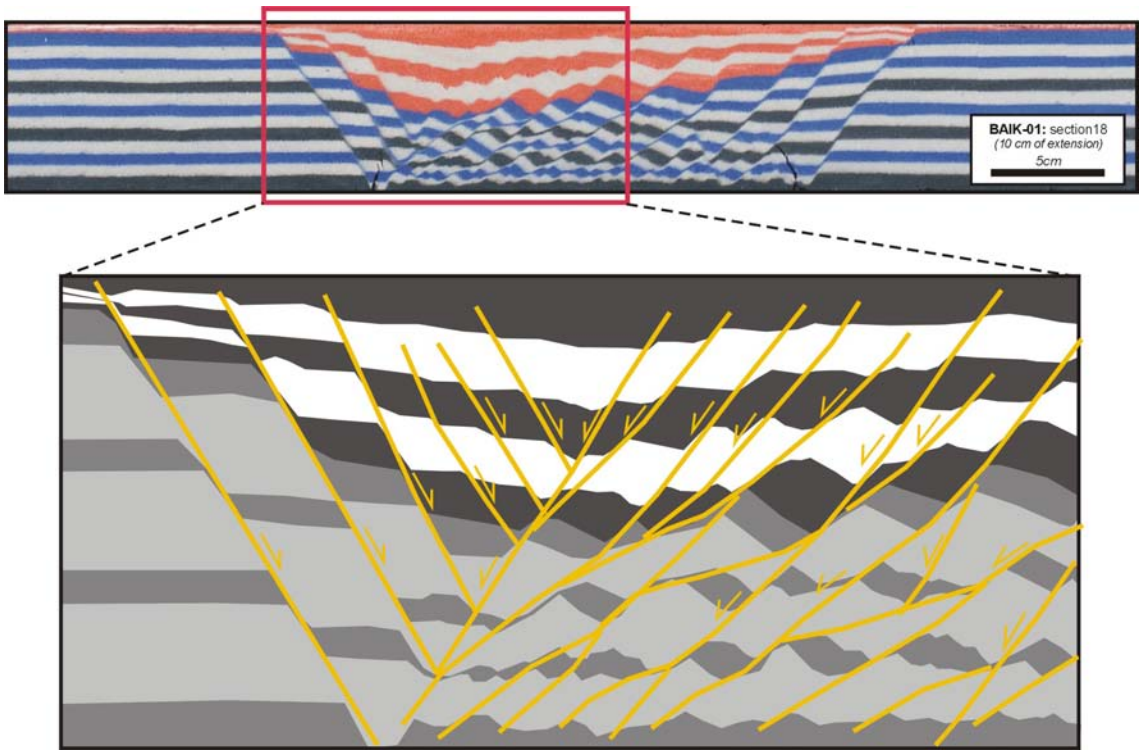

Figure 7.10: *Cross-section 18 of model BAIK01 (see figure 7.9 for its location), and the interpretation of part of it. This part clearly illustrates that some of the faults splay into several faults near the surface.*

7.4.3 Baikal experiment nr 6: BAIK-06

This model has a linear base-plate geometry with a 5 cm wide detachment. The model has the following set-up characteristics:

Characteristics

- base plate geometry: `Type 1`,
- dimensions: 65 cm × 60 cm × 7.5 cm,
- extension achieved by pulling one of the base plates (asymmetric rift),
- 5 cm wide rubber sheet in the centre of the model,
- 7.5 cm of pre-kinematic layers. A total of 13 layers all being 0.55 cm thick. From base to top the colours used were: black – white – blue – white – black – white – blue – white – black – white – blue – white – blue.
- After extension the model was sliced vertically, with 1 cm spacing. On both sides of the model, the first 5 cm have been skipped.

The model was extended for 5 cm with a picture taken every 1 mm of extension. The first syn-kinematic layer was added after 2 cm of extension, the following after every centimetre of extension. In total 4 syn-kinematic layers (red and white) were added.

Description

The following table summarises the observations that were made during the model's run (see also figure 7.11):

Extension	Observations
0.5 cm	First surface faulting occurs in the model.
0.6 – 1 cm	Long linear outer faults develop first in the model, followed by the development of an intra-rift fault system at the mobile wall side. These intra-rift faults develop along the whole length of the model more or less at the same time. This fault system is more segmented than the outer faults.
1 – 2 cm	The mobile wall side faults increase their displacement. On the fixed wall side also intra-rift faults start to form which are distributed more widely than the faults on the mobile wall side. At the mobile wall side, two long faults accommodate the displacement. A central intra-rift graben has formed that has the same orientation as the base-plate geometry (i.e. 80°).
2 cm	Red syn-kinematic layer added.
2 – 3 cm	Few more intra-rift faults develop on both sides of the model.

continued on the next page...

...continued from the previous page	
3 cm	White syn-kinematic layer added.
3 – 4 cm	No new faults seem to develop. The graben in the model widens.
4 cm	Red syn-kinematic layer added.
4 – 5 cm	In the region of the fixed-wall side faults, also faults form that dip towards the fixed wall. As a result a small horst structure develops. Faulting at the fixed wall side is concentrated in 2 fault zones, one being the outer fault system, and another one located more or less in the centre of the model. In between the area is relatively undeformed.
5 cm	Final amount of extension reached.

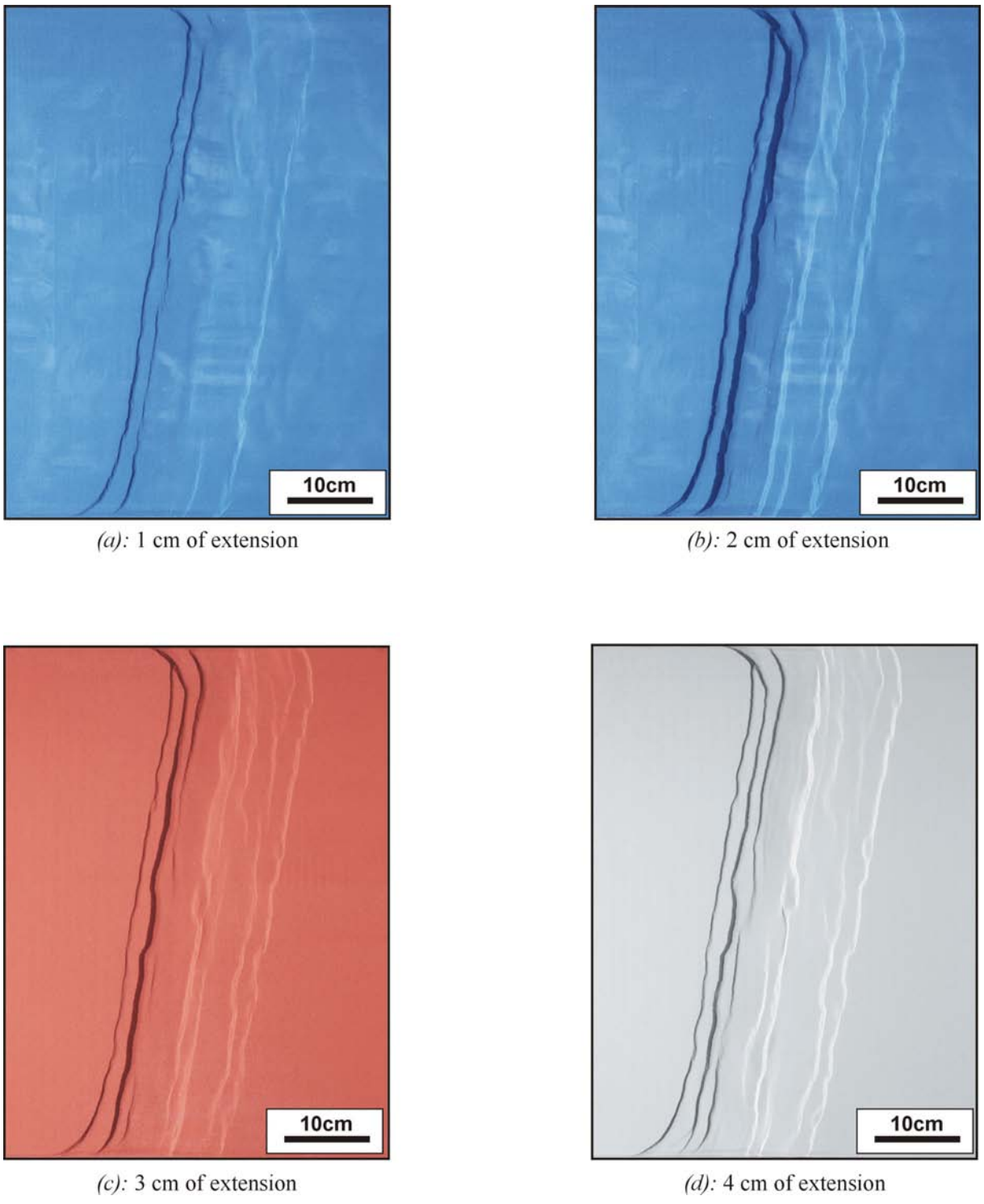

(a): 1 cm of extension

(b): 2 cm of extension

(c): 3 cm of extension

(d): 4 cm of extension

Figure 7.11: *Running shots of model BAIK-06 after different amounts of extension. Base-plates had a type 1 geometry. The mobile wall was on the left side.*

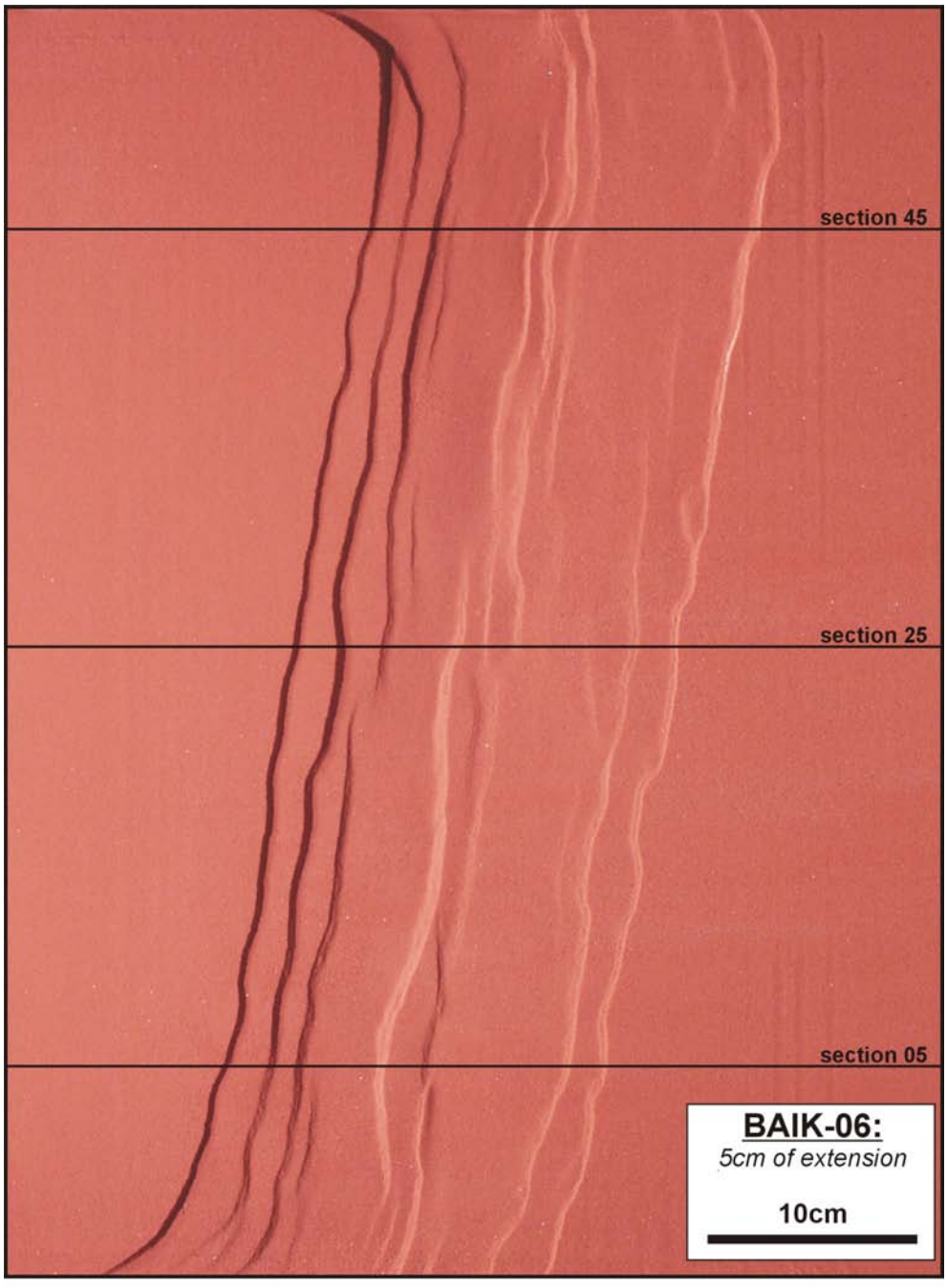

(e): 10 cm of extension

Figure 7.11: ***(continued)*** *Last running shot of experiment BAIK-06, after 5 cm of extension. Cross-sections are included in figure 7.12.*

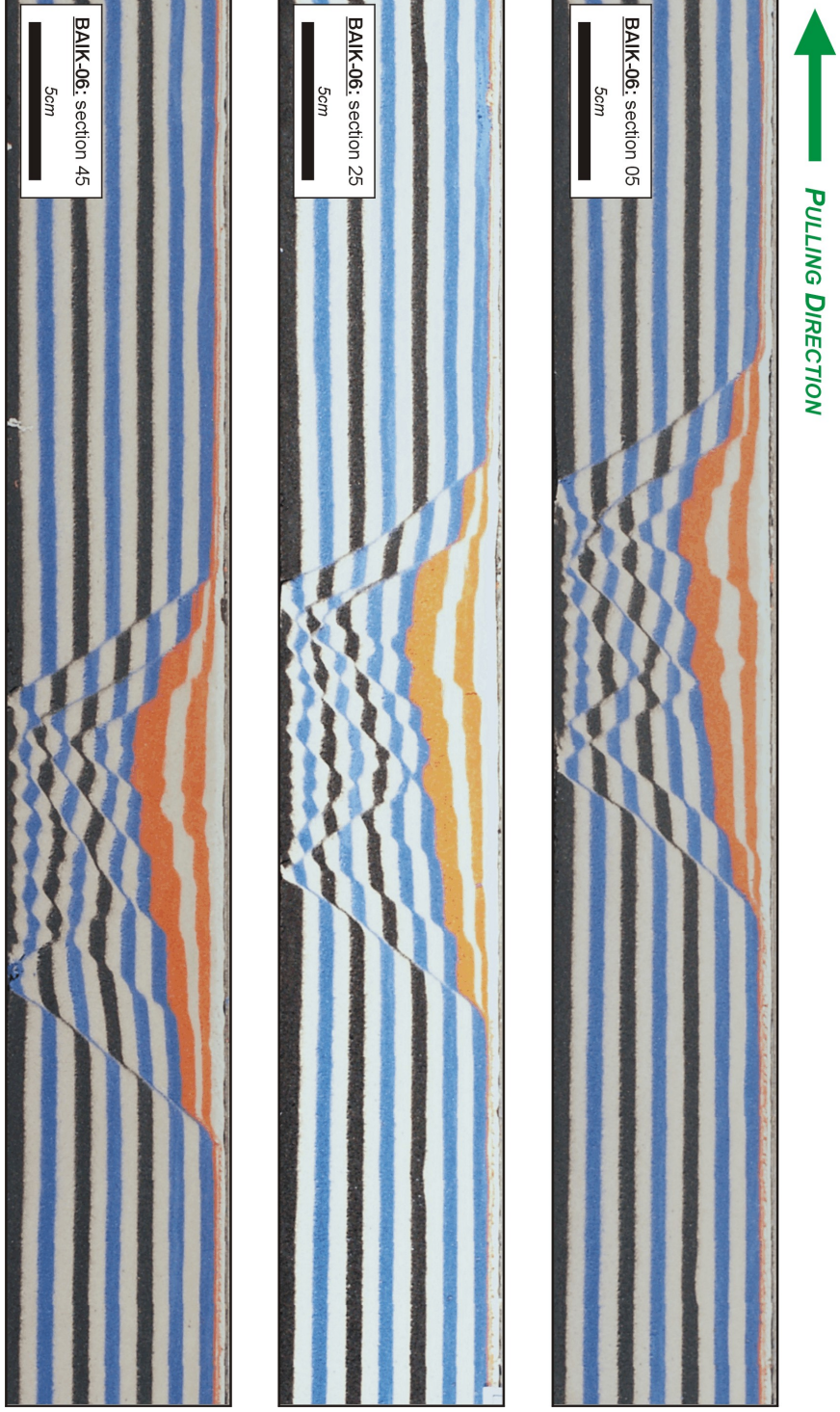

Figure 7.12: *Three cross-sections through model BAIK-06: (a) section 05, (b) section 25 and (c) section 45 (see figure 7.11 for the locations). Black and blue layers correspond to pre-kinematic sand layers, red and white layers are the syn-kinematic infill.*

7.4.4 Baikal experiment nr 2: BAIK-02

Characteristics

The base-plate border in the second model changes its orientation in four steps, similar to the western border faults in Lake Baikal. The two lower segments correspond to the Obruchevsky Fault, the third segment to the Primorsky Fault and the upper segment to the Baikalsky Fault.

- base plate geometry: `Type 2`,
- dimensions: 72 cm × 60 cm × 7.5 cm,
- extension achieved by pulling one of the base plates (⟶ asymmetric rift),
- 10 cm wide rubber sheet in the centre of the model,
- 7.5 cm of pre-kinematic layers. A total of 13 layers all being 0.55 cm thick. From base to top the colours used were: black – white – blue – white – black – white – blue – white – black – white – blue – white – blue.
- After extension the model was sliced vertically, with 1 cm spacing between the different slices. On both sides of the model, the first 5 cm have been skipped.

The model was extended for 10 cm with a picture taken every 1 mm of extension. Syn-kinematic layers of sand were added after every 2 cm of extension. In total 5 syn-kinematic layers (red and white) were added.

Description

The following table summarises the observations that were made during the model's run (see also figure 7.13):

Extension	Observations
0.7 cm	First expression of surface subsidence.
0.8 cm	Surface becomes slightly faulted.
0.8 – 1.5 cm	Many faults form, but they are striking mainly perpendicular to the extension direction. The base-plate geometry is only slightly expressed by the outer faults in the model. Faults again form as different segments that propagate laterally and link up with neighbouring segments as displacement increases.
2.0 cm	Grabens have formed next to the upper two segments of the base plate. The main boundary faults however strike perpendicularly to the direction of extension, and the grabens are not off-set.

continued on the next page...

...continued from the previous page

	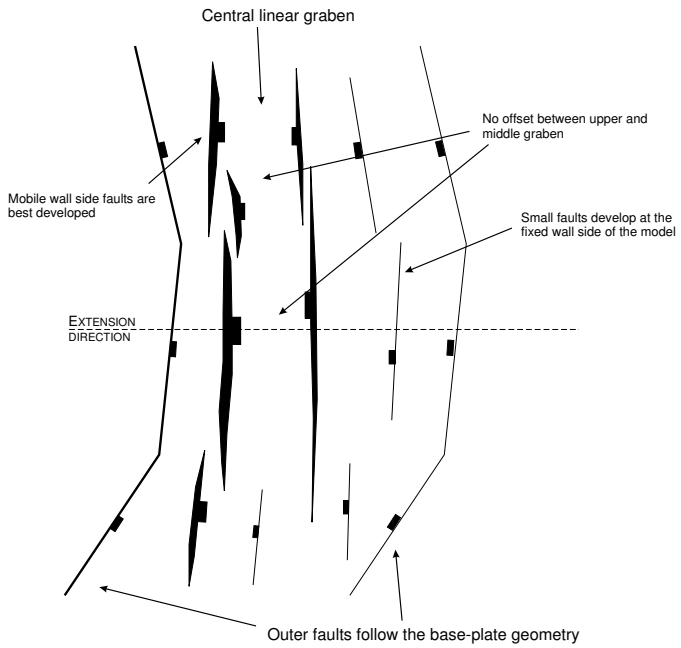
	Red syn-kinematic sand layer added.
2.0 – 4.0 cm	The displacement on the faults at the mobile wall side of the model increases with further extension, whereas at the fixed wall side, also the number of faults increases. The expression of the base-plate geometry becomes more evident.
4.0 cm	White syn-kinematic sand layer added.
5.0 – 6.0 cm	The faults on the fixed wall side were in the previous stage well expressed, and more or less straight. In this stage, especially in the central part of the model, they evolve in a network of shorter fault traces that interconnect with neighbours.
6.0 cm	Red syn-kinematic sand layer added.
7.0 – 8.0 cm	The faults on the fixed wall side evolve again in more continuous faults, with displacement localised on few, but highly irregular faults. On the other hand, the well-developed faults of the mobile wall side become more irregular and complicated by new faults.
8.0 cm	White syn-kinematic sand layer added.
8.0 – 10.0 cm	New faults have developed in the central part of the model, dipping towards both the fixed and the mobile walls.
10.0 cm	Final amount of extension reached. Red syn-kinematic sand layer added.

Cross-sections of the model are included in figure 7.14. Note that the changes in orientation of the base-plate has almost no effect on the geometry of the cross-sections.

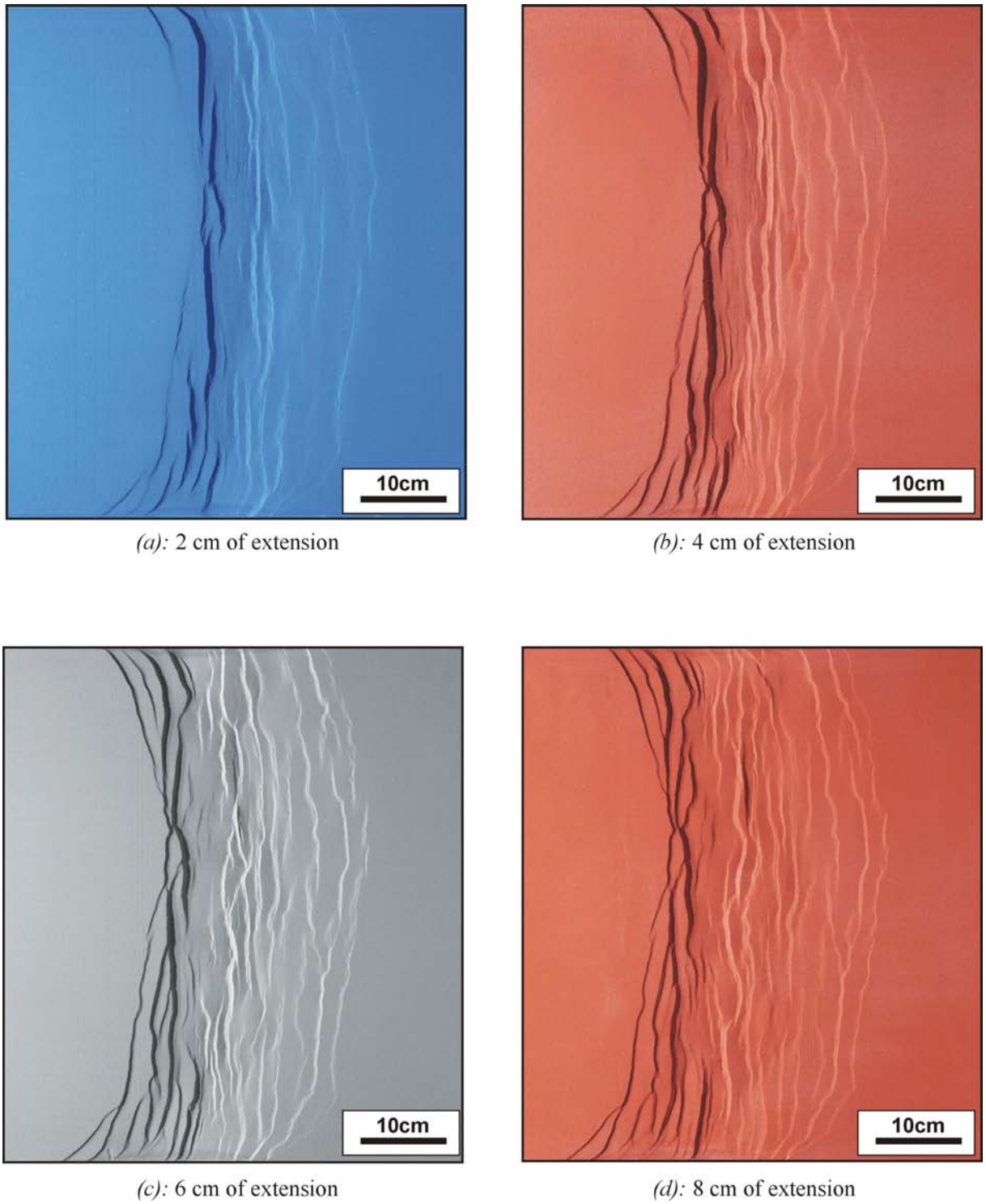

(a): 2 cm of extension

(b): 4 cm of extension

(c): 6 cm of extension

(d): 8 cm of extension

Figure 7.13: *Running shots of model BAIK-02 after different amounts of extension. Base-plates had a type 2 geometry. The mobile wall was on the left side.*

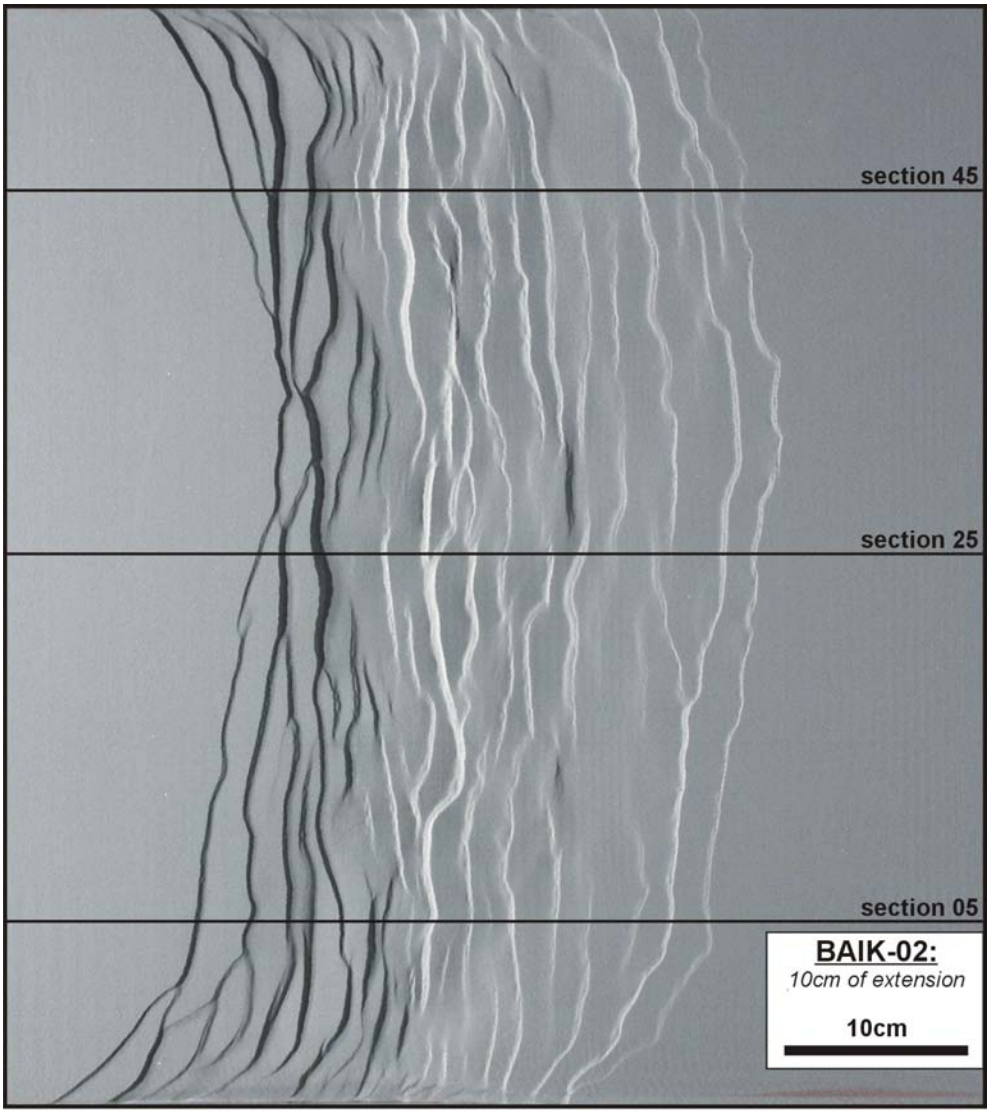

(e): 10 cm of extension

Figure 7.13: ***(continued)*** *Last running shot of experiment BAIK-02, after 10 cm of extension. Cross-sections are included in figure 7.14. Note the clear difference between the central faults (intra-rift faults), which strike at high-angle to the extension vector, and the outer faults of the model, which mainly follow the base-plate geometry. The outer faults are characterised by less displacement than the intra-rift faults.*

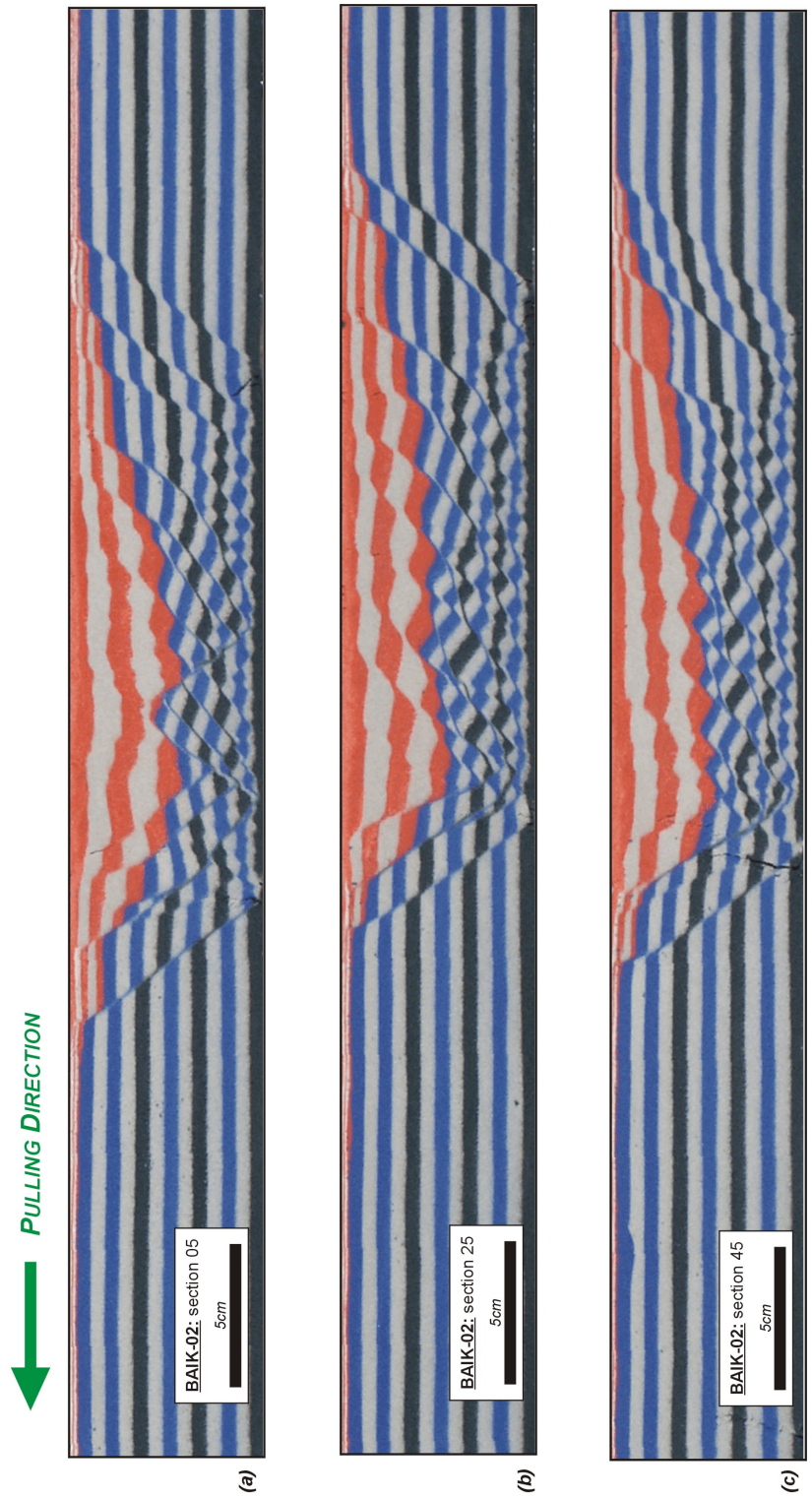

Figure 7.14: *Three cross-sections through model BAIK-02: (a) section 05, (b) section 25 and (c) section 40 (see figure 7.13e for the locations). Black and blue layers correspond to pre-kinematic sand layers, red and white layers are the syn-kinematic infill.*

7.4.5 Baikal experiment nr 3: BAIK-03

This rift model is similar to experiment BAIK-02, but it has a 5 cm wide rubber detachment. The model has the following set-up characteristics:

Characteristics

- base plate geometry: `Type 2`,
- dimensions: 67 cm × 60 cm × 7.5 cm,
- extension achieved by pulling one of the base plates (asymmetric rift),
- 5 cm wide rubber sheet in the centre of the model,
- 7.5 cm of pre-kinematic layers. A total of 13 layers all being 0.55 cm thick. From base to top the colours used were: black – white – blue – white – black – white – blue – white – black – white – blue – white – blue.
- After extension the model was sliced vertically, with 1 cm spacing. On both sides of the model, the first 5 cm have been skipped.

The model was extended for 5 cm with a picture taken every 1 mm of extension. The first syn-kinematic layer was added after 2 cm of extension, the following after every centimetre of extension. In total 4 syn-kinematic layers (red and white) were added.

Description

The following table summarises the observations that were made during the model's run (see also figure 7.15):

Extension	Observations
0.4 cm	First faults affect the model's surface Faults are clearest at the locations where the base-plate strike is oriented at high angle to the direction of extension (i.e. at the "P" segment).
0.5 – 1 cm	At the mobile side of the model a relay zone develops between the "O" and the "P" fault segments, but not between the "P" and "B" segments. Faulting is best expressed at the mobile side of the model. At the fixed wall side, irregularities are formed between the "P" and "B" segments. Also intra-rift faults start to form.
1 – 2 cm	An intra-rift graben forms that does not follow the orientations of the outer faults in the upper part of the model ("B" segment), instead it strikes more or less perpendicular to the direction of extension (figure 7.15). Lower in the model, the intra-rift graben bounding faults strike more or less parallel to the "P" segment. The faults bounding this intra-rift graben are highly segmented.

continued on the next page...

...continued from the previous page	
2 cm	Red syn-kinematic layer added.
2 – 3 cm	Many of the fault segments have linked, and this results in a highly irregular trace of the intra-rift graben faults. This irregularity is stronger on the fixed wall side of the model, although the initial segmentation was similar in both cases.
3 cm	White syn-kinematic layer added.
3 – 4 cm	More faults develop inside the intra-rift graben. These faults mainly develop at the mobile wall side.
4 cm	Red syn-kinematic sand layer added.
4 – 5 cm	In the lower part of the model deformation is concentrated on large displacement faults (one is the original outer fault of the rift zone at the mobile wall side). In the upper part on the other hand, displacement is distributed over a fan-like geometry of faults. 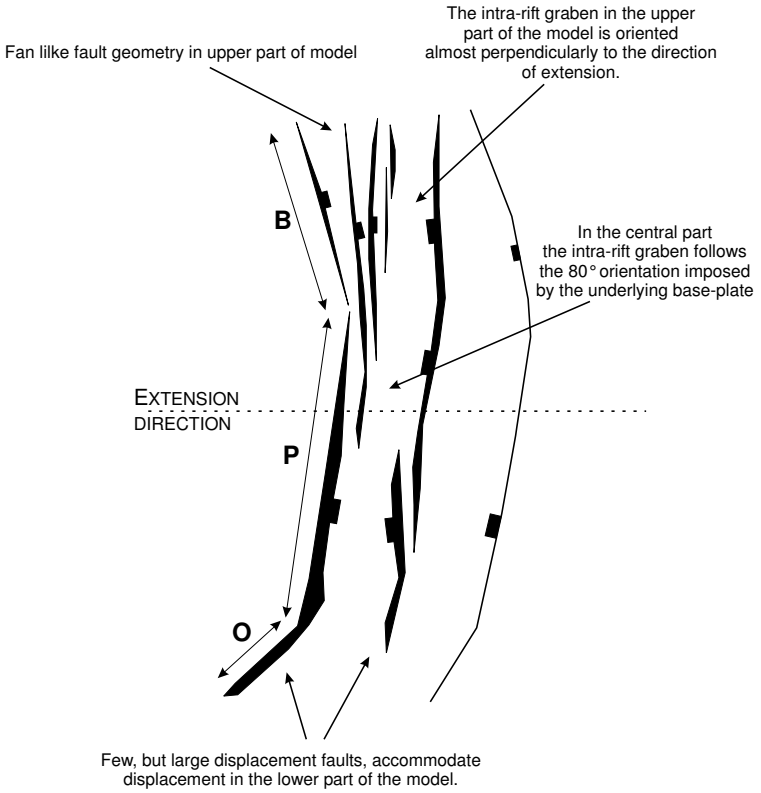
5 cm	Final amount of extension reached.

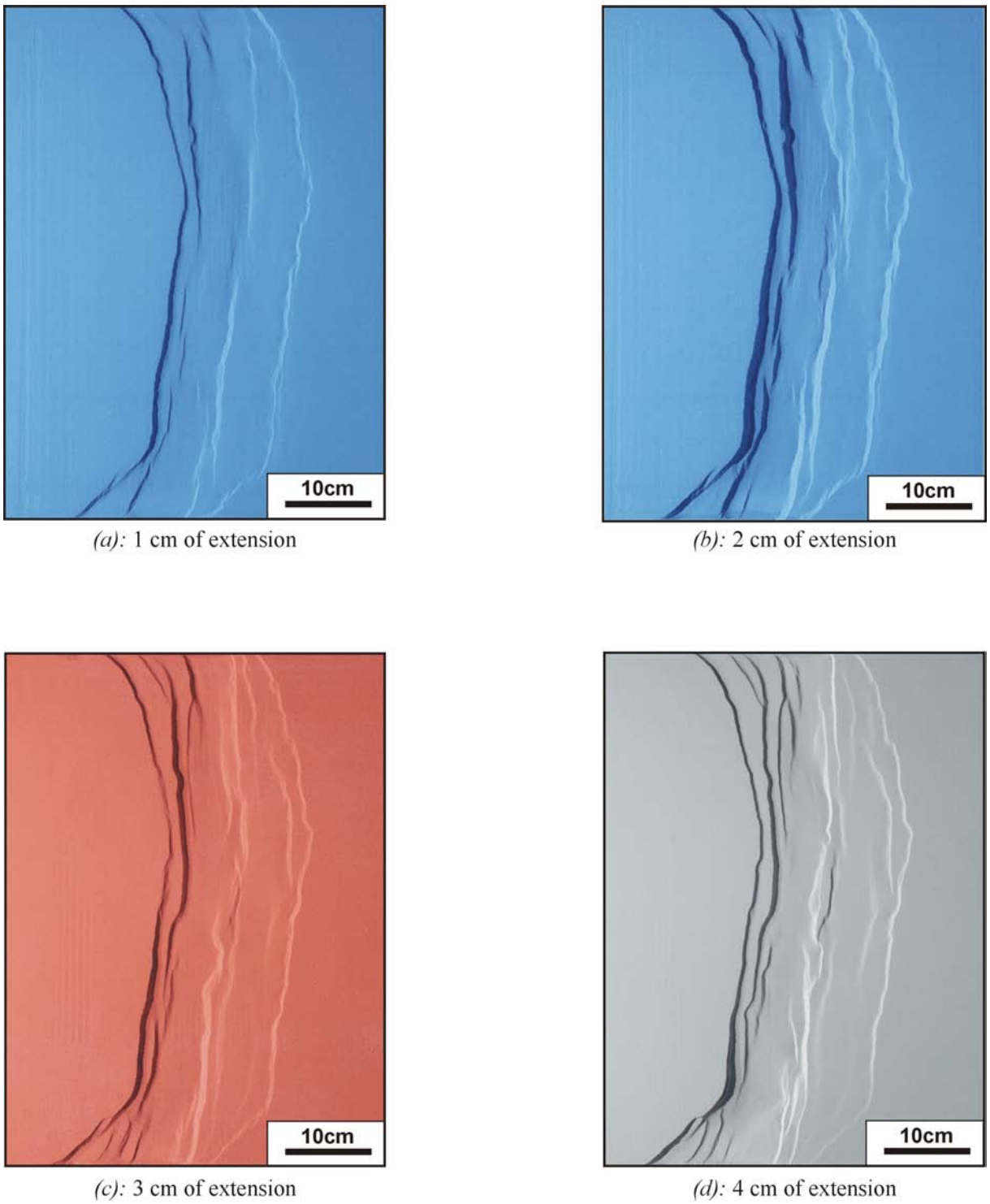

(a): 1 cm of extension

(b): 2 cm of extension

(c): 3 cm of extension

(d): 4 cm of extension

Figure 7.15: *Running shots of model BAIK-03 after different amounts of extension. Base-plates had a type 2 geometry. The mobile wall was on the left side.*

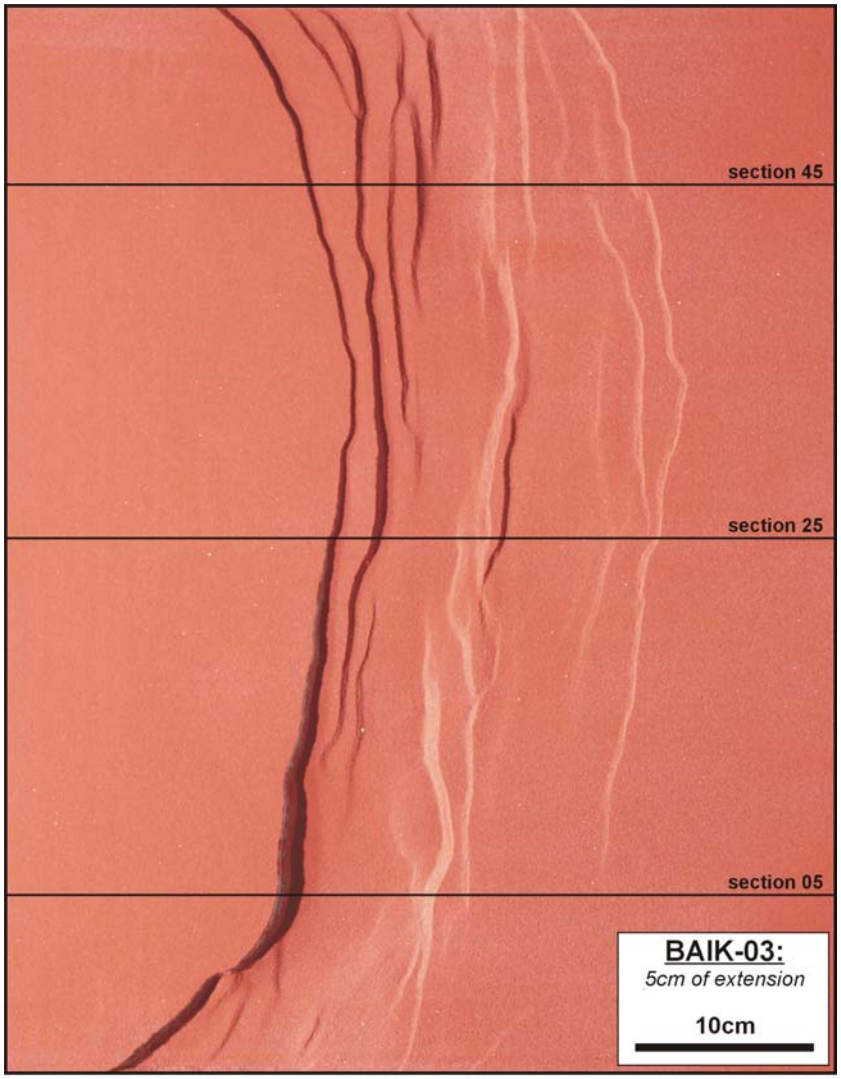

(e): 10 cm of extension

Figure 7.15: ***(continued)*** *Last running shot of experiment BAIK-03, after 5 cm of extension. Cross-sections are included in figure 7.16.*

Figure 7.16: *Three cross-sections through model BAIK-03: (a) section 05, (b) section 25 and (c) section 40 (see figure 7.15 for the locations). Black and blue layers correspond to pre-kinematic sand layers, red and white layers are the syn-kinematic infill. The rift basins in this model are narrower than those in the detachment models with a 10 cm wide rubber sheet, but their depth is similar.*

7.4.6 Baikal experiment nr 7: BAIK-07

Characteristics

The seventh model mimics the geometry of Lake Baikal, and the adjacent Khubsugul and Angara basins. This model is simplified compared to later models (BAIK-04 and BAIK-05) in that Lake Baikal is simulated by a straight line that is oriented like the Primorsky Fault.

- base plate geometry: `Type 3`,
- dimensions: 72 cm × 60 cm × 7.5 cm,
- extension achieved by pulling one of the base plates (asymmetric rift),
- 10 cm wide rubber sheet in the centre of the model,
- 7.5 cm of pre-kinematic layers. A total of 13 layers all being 0.55 cm thick. From base to top the colours used were: black – white – blue – white – black – white – blue – white – black – white – blue – white – blue.
- After extension the model was sliced vertically, with 1 cm spacing between the different slices. On both sides of the model, the first 5 cm have been skipped.

The model was extended for 10 cm with a picture taken every 1 mm of extension. Syn-kinematic layers of sand were added after every 2 cm of extension. In total 5 syn-kinematic layers (red and white) were added.

Description

The following table summarises the observations that were made during the model's run (see also figure 7.17):

Extension	Observations
0.7 cm	Formation of the first surface depression in the model in the zone of the rubber sheet.
0.8 cm	First faults develop in the centre of the model and near the borders of the base plates (although less well expressed).
1.2 cm	In the lower part of the model, faults tend to be perpendicular to the direction of extension, whereas in the upper part, the faults strike with the 80° direction of the base plate (relative to the pulling direction). Faults are clearly segmented.
2.0 cm	The overall fault geometry remains the same. In the lower part, a well expressed central graben has formed, that strikes perpendicularly to the direction of extension. In the upper part a slightly more diffuse deformation takes place along structures that clearly follow the 80° trend. Red layer of syn-kinematic sand added.

continued on the next page...

...continued from the previous page

2.0 – 4.0 cm	The graben that had formed in the lower part of the model is cross-cut by an accommodation zone which links the left (ie. mobile wall side) faults of the "lower graben" with the right (ie. fixed wall side) faults of the "upper graben". The lower graben is more asymmetric towards the fixed wall, whereas the upper graben is clearly asymmetric towards the mobile wall. Although faults developed inside this upper graben, there are no faults that cross-cut the graben. 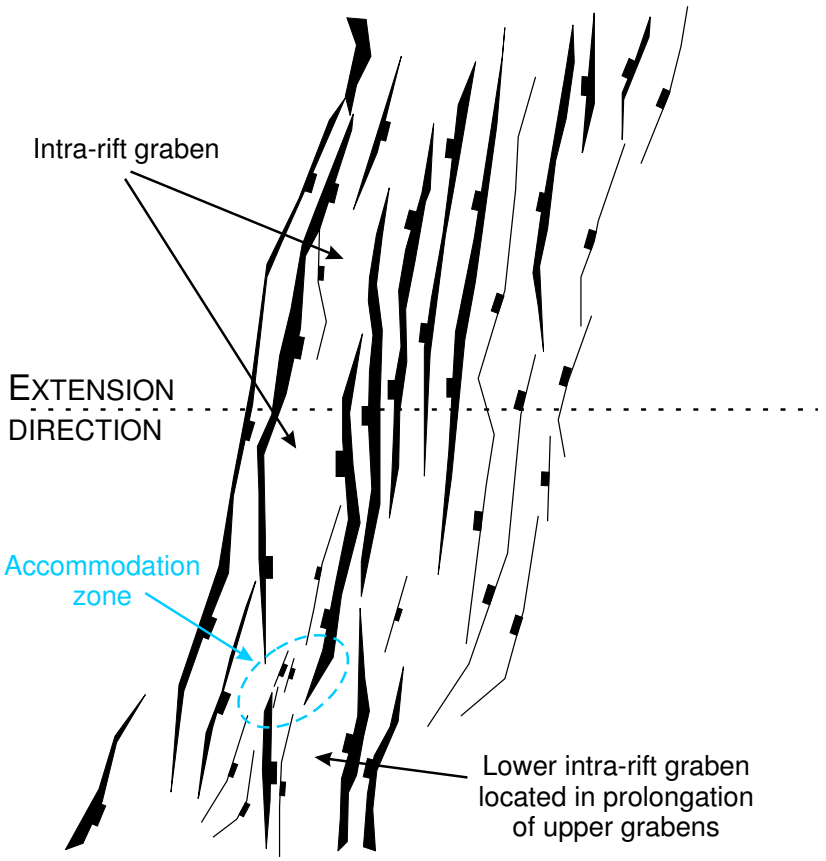
4.0 cm	White layer of syn-kinematic sand added.
4.0 – 6.0 cm	In the previous stage, the upper and the lower graben had a different polarity, but were located in prolongation of each other. In this stage the grabens become clearly off-set: the lower graben's depocentre is located near the fixed wall and the upper graben's depocentre formed near the mobile wall.

continued on the next page...

<table>
<tr><td colspan="2">...continued from the previous page</td></tr>
<tr><td>6.0 cm</td><td>Red layer of syn-kinematic sand added.</td></tr>
<tr><td>6.0 – 8.0 cm</td><td>The previously described off-set becomes stronger, and the faults of the lower graben tend to adopt the orientation of the base-plate in this part.
 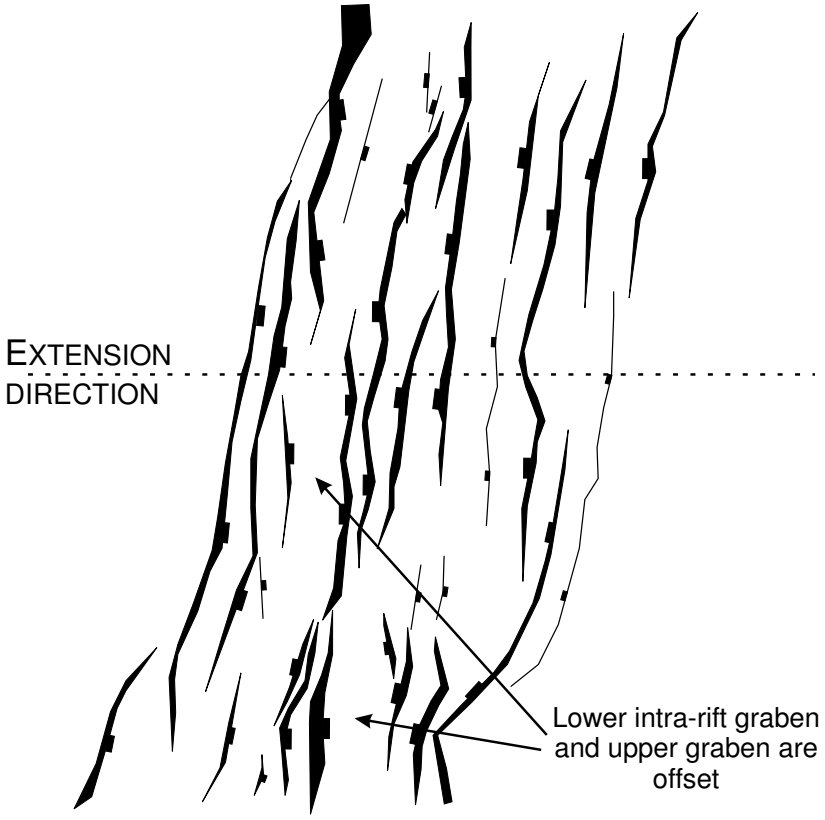
</td></tr>
<tr><td>8.0 cm</td><td>White layer of syn-kinematic sand added.</td></tr>
<tr><td>10.0 cm</td><td>Final amount of extension reached. Last red layer of syn-kinematic sand added.</td></tr>
</table>

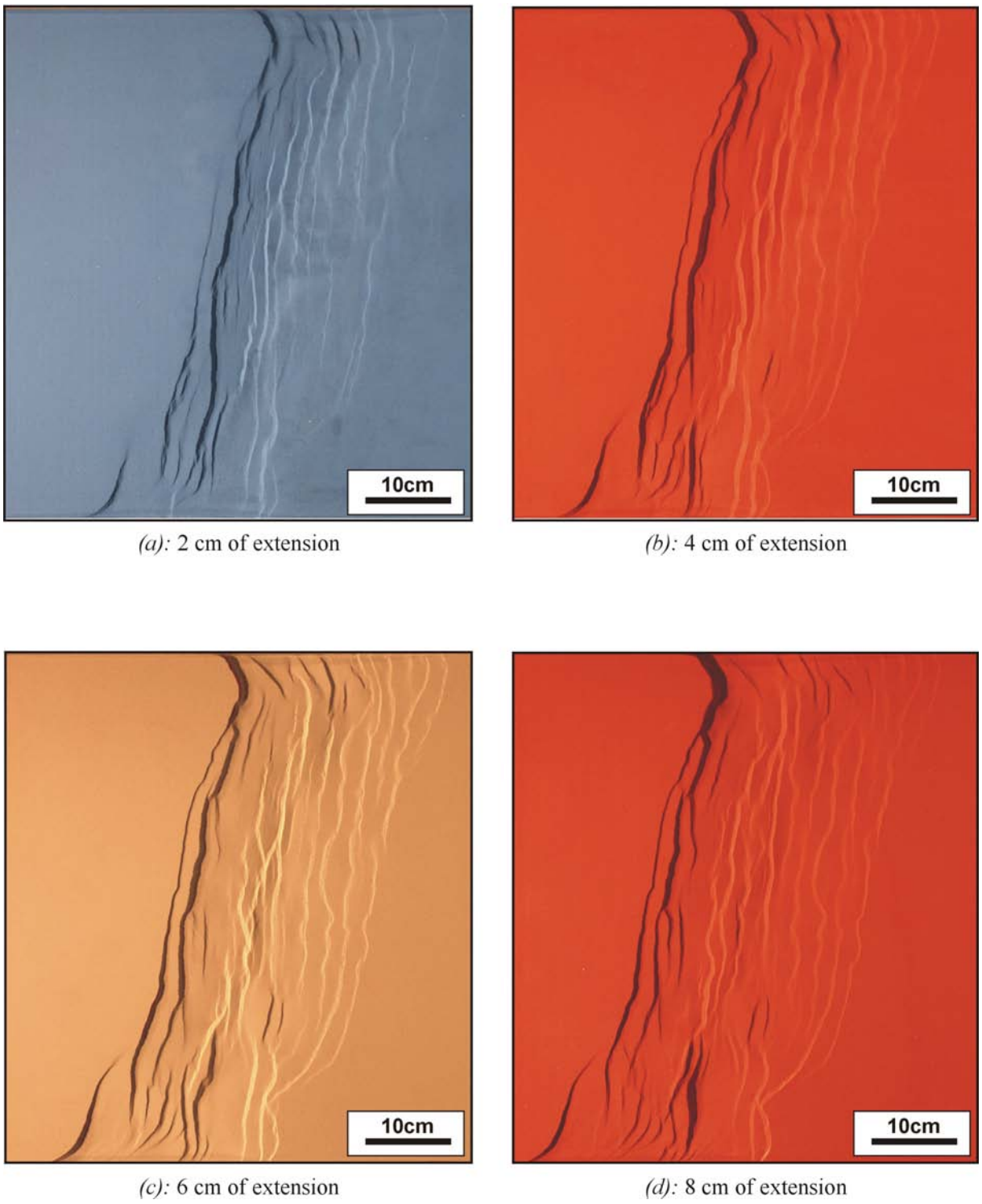

(a): 2 cm of extension

(b): 4 cm of extension

(c): 6 cm of extension

(d): 8 cm of extension

Figure 7.17: *Running shots of model BAIK-07 after different amounts of extension. Base-plates had a type 3 geometry. The mobile wall was on the left side.*

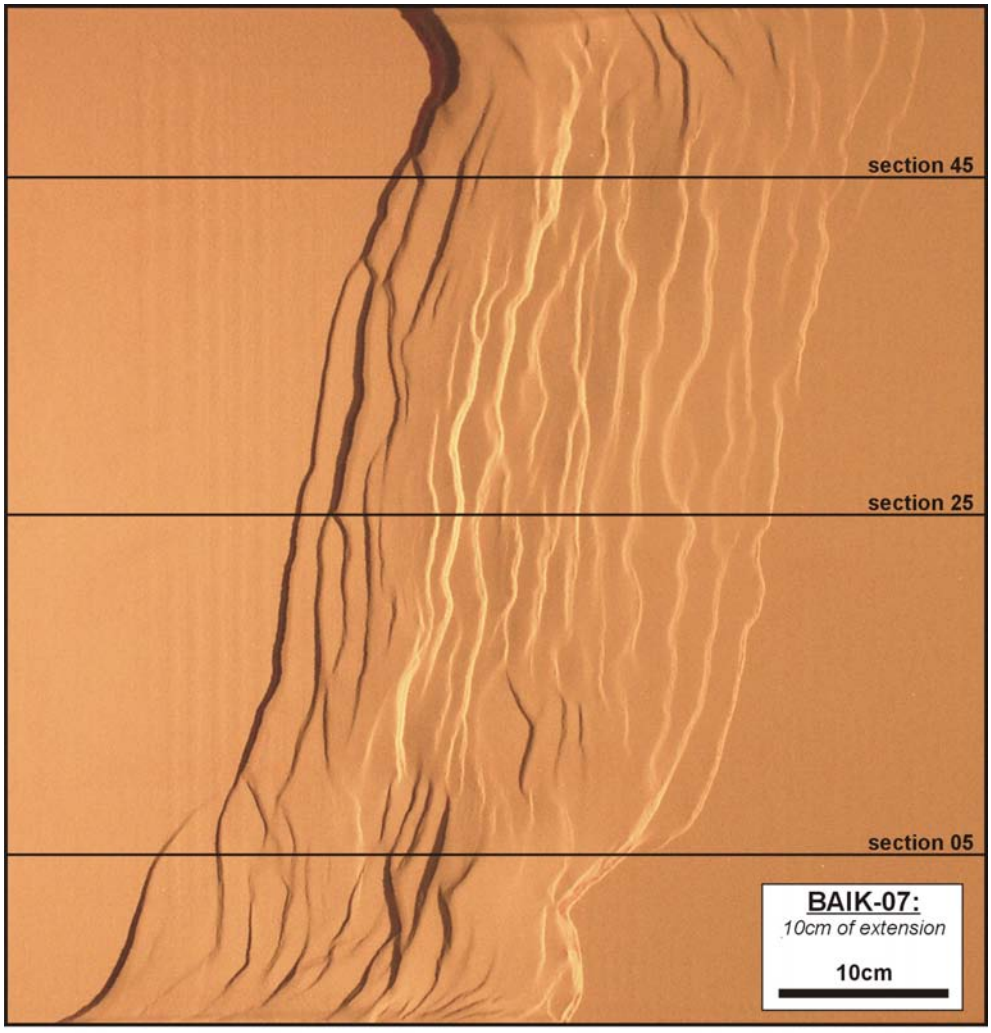

(e): 10 cm of extension

Figure 7.17: ***(continued)*** *Last running shot of experiment BAIK-07, after 10 cm of extension. Cross-sections are included in figure 7.18.*

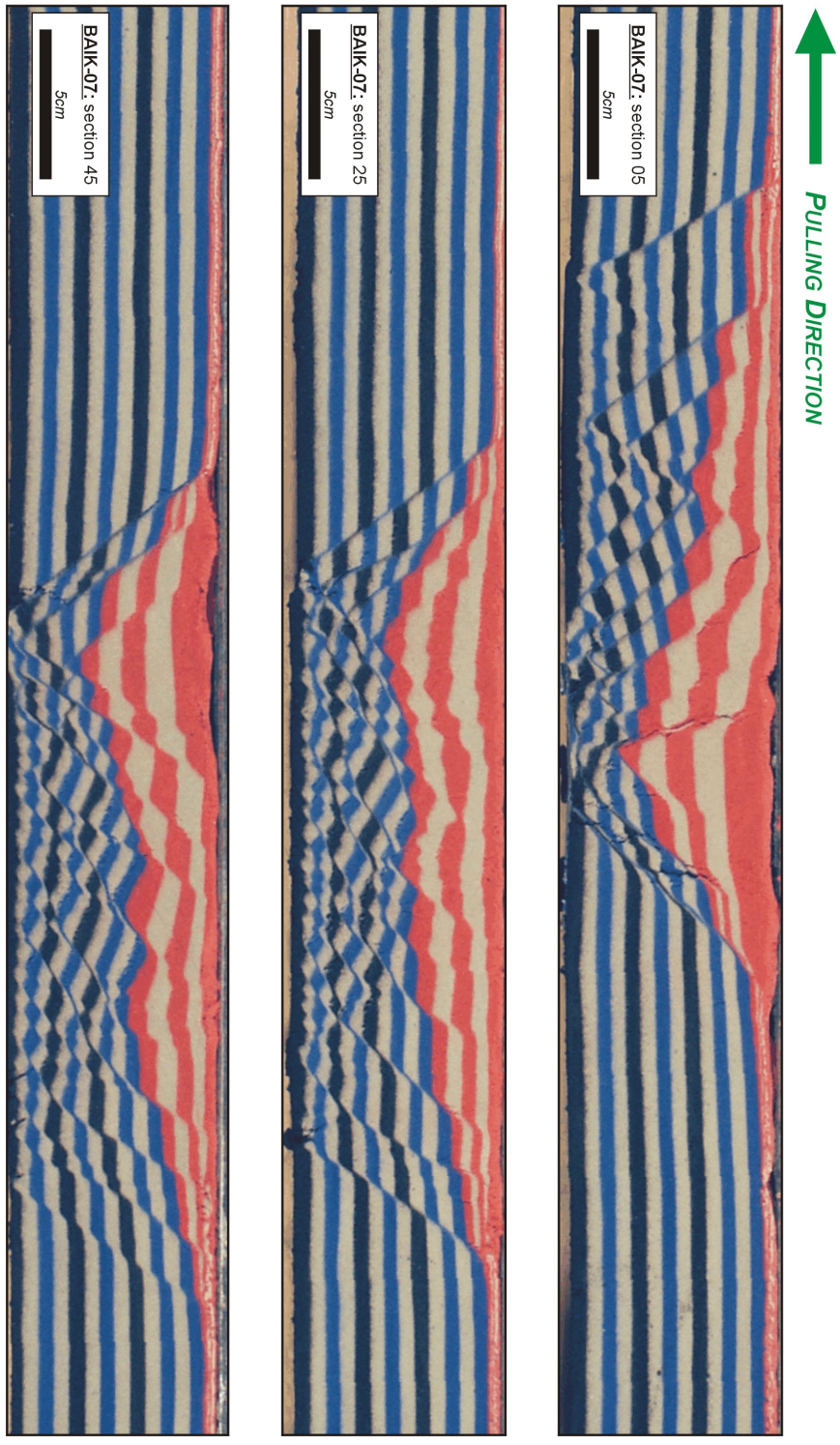

Figure 7.18: *Three cross-sections through model BAIK-07: (a) section 05, (b) section 25 and (c) section 45 (see figure 7.17 for the locations). Black and blue layers correspond to pre-kinematic sand layers, red and white layers are the syn-kinematic infill. Note the difference in asymmetry between the lower part of the model (a) and the upper parts (b&c)*

7.4.7 Baikal experiment nr 4: BAIK-04

The base-plates in this model include the main trend of the Khubsugul and Upper-Angara basins. The model has the following set-up characteristics:

Characteristics

- base plate geometry: `Type 4`,
- dimensions: 66 cm × 60 cm × 7.5 cm,
- extension achieved by pulling one of the base plates (asymmetric rift),
- 5 cm wide rubber sheet in the centre of the model,
- 7.5 cm of pre-kinematic layers. A total of 13 layers all being 0.55 cm thick. From base to top the colours used were: black – white – blue – white – black – white – blue – white – black – white – blue – white – blue.
- After extension the model was sliced, with 1 cm spacing. On both sides of the model, the first 5 cm have been skipped.

The model was extended for 5 cm with a picture taken every 1 mm of extension. The first syn-kinematic layer was added after 2 cm of extension, the following after every centimetre of extension. In total 4 syn-kinematic layers (red and white) were added.

Description

The following table summarises the observations that were made during the model's run (see also figure 7.19):

Extension	Observations
0.6 cm	First surface faulting observed in the model. The first faults that develop are located in the parts of the model where the base-plate border is oriented at high angle to the direction of extension.
0.6 – 1 cm	Faults with other strikes develop as well. Where fault segments with different orientations meet, relay structures are formed (figure 7.20). The faults at the mobile wall side of the model are best developed. Intra-rift faults start to develop.
1 – 2 cm	The intra-rift faults delineate a central graben that has no linear shape, but instead adopts slightly different orientations along the rift zone. Many of the earlier formed relay structures disappear as larger faults develop. More intra-rift faults are formed, mainly at the fixed-wall side of the model.

continued on the next page...

...continued from the previous page

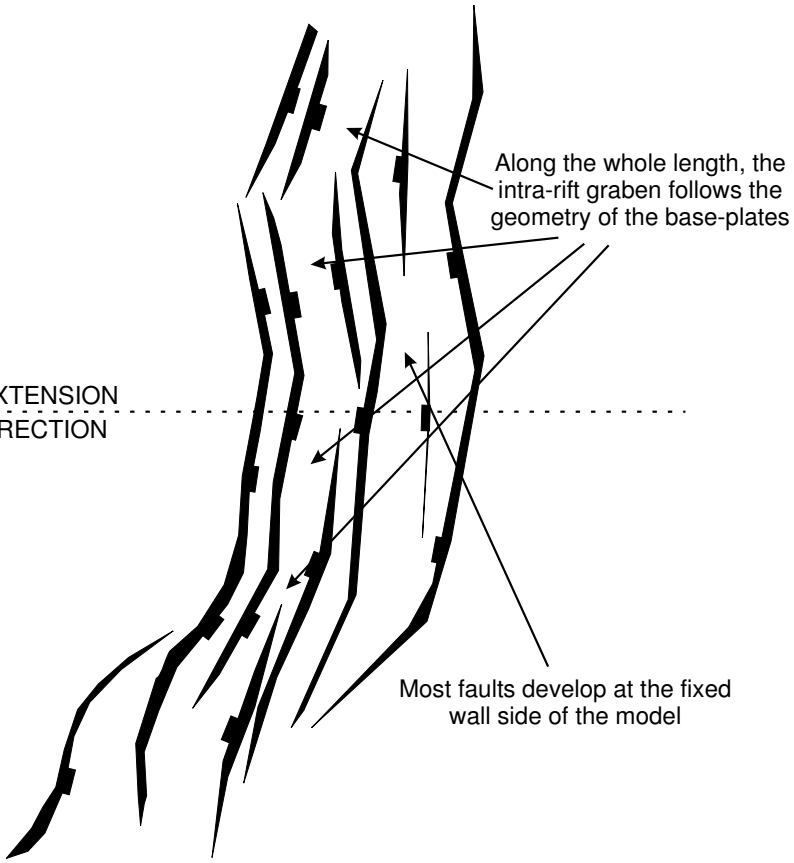

2 cm	Red syn-kinematic layer added.
2 – 3 cm	During this stage the existing faults increase their displacement. No new faults develop.
3 cm	White syn-kinematic layer added.
3 – 4 cm	Few new intra-rift faults form, mainly in the upper part of the model at the location of the sharp bend in the base-plate.
4 cm	Red syn-kinematic layer added.
4 – 5 cm	Further increase in displacement on existing faults, without a further increase in the number of faults.
5 cm	Final amount of extension reached.

Throughout the evolution of the model several relay zones formed, developed and disappeared. Between two intra-rift fault segments in the upper part of the model, the evolution of a relay ramp can be observed. This evolution is described in figure 7.25.

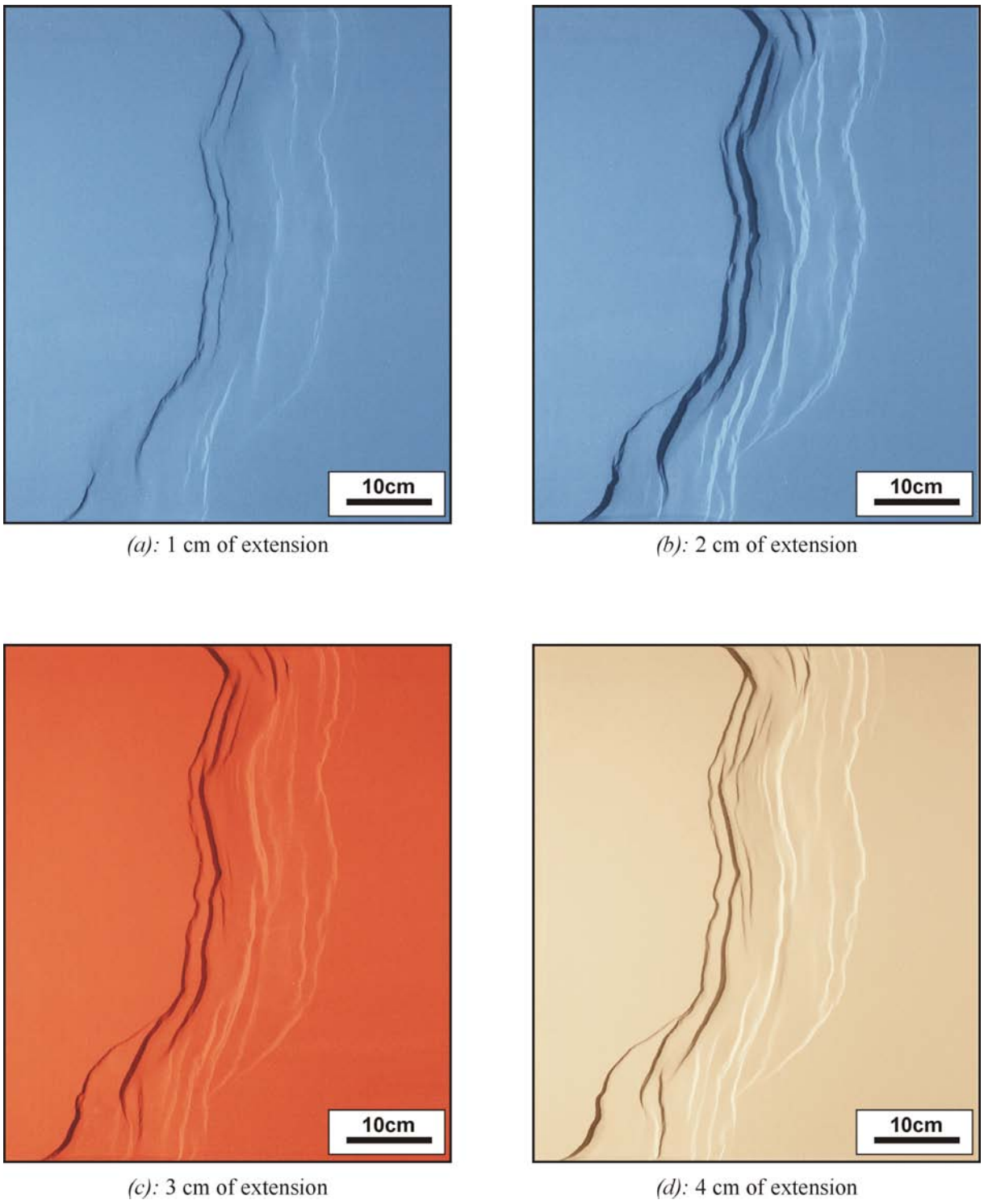

(a): 1 cm of extension

(b): 2 cm of extension

(c): 3 cm of extension

(d): 4 cm of extension

Figure 7.19: *Running shots of model BAIK-04 after different amounts of extension. Base-plates had a type 4 geometry. The mobile wall was on the left side.*

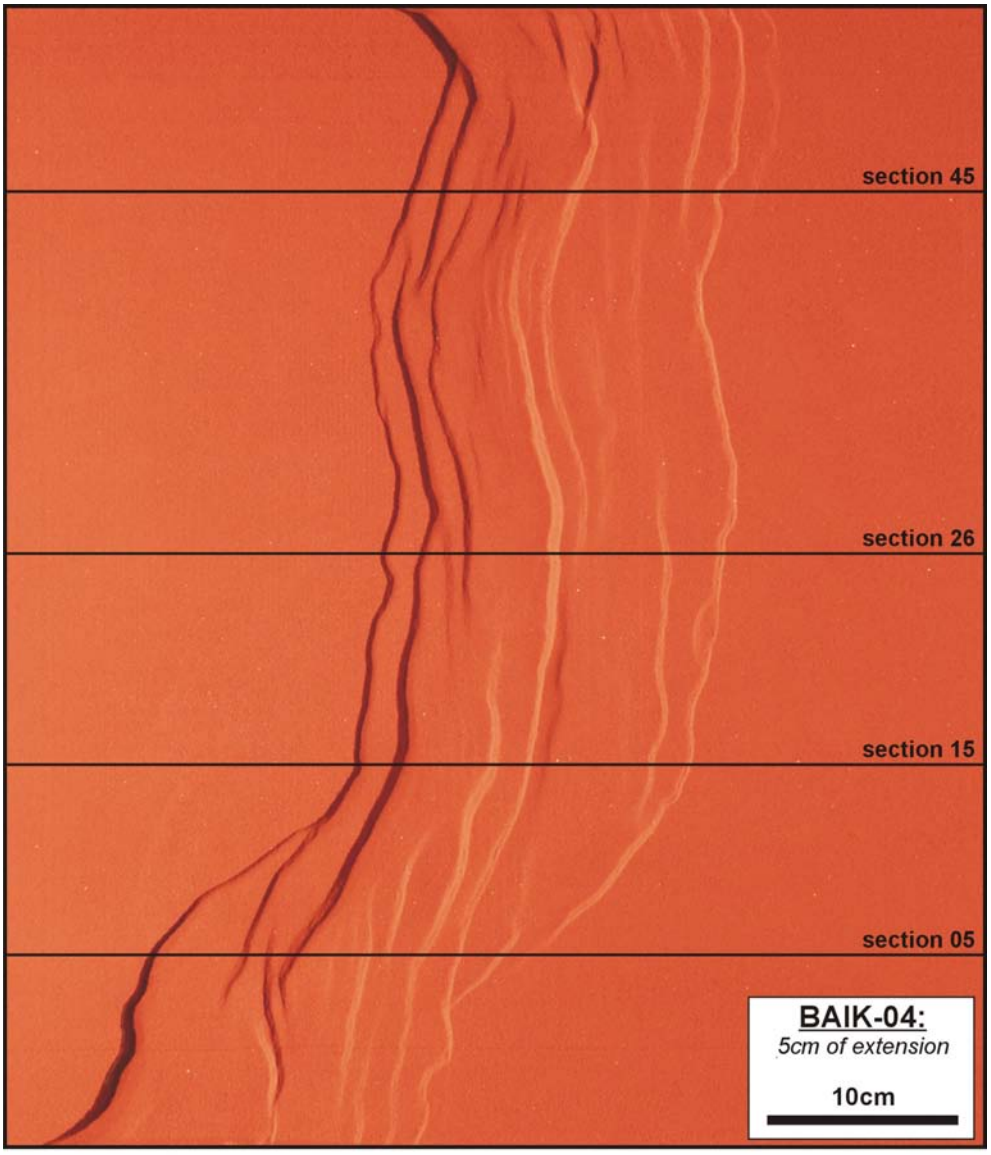

(e): 10 cm of extension

Figure 7.19: ***(continued)*** *Last running shot of experiment BAIK-04, after 5 cm of extension. Indicated cross-sections are included in figure 7.22 and 7.23.*

Figure 7.20: *Running shot of experiment BAIK-04 after 9 mm of extension (a) and an interpretation (b). Black faults dip towards the bottom of the page, and white fault towards the top. The grey zone in the middle of figure b represents the geometry of the rubber sheet. Yellow circles indicate overlapping fault tips or relay ramps, and the red rectangles correspond to underlapping fault tips. Note that the relay ramps or more common in the outer (larger) faults, whereas the underlapped geometry is more frequent in the, in this stage smaller, inner faults. A later evolution stage of the model are illustrated in figure 7.21.*

Figure 7.21: *Running shot of experiment BAIK-04 after 20 mm of extension (a) and an interpretation (b). Black faults dip towards the bottom of the page, and white fault towards the top. The grey zone in the middle of figure b represents the geometry of the underlying rubber sheet. The evolution of the relay ramp in the red circle, is outlined in figure 7.25.*

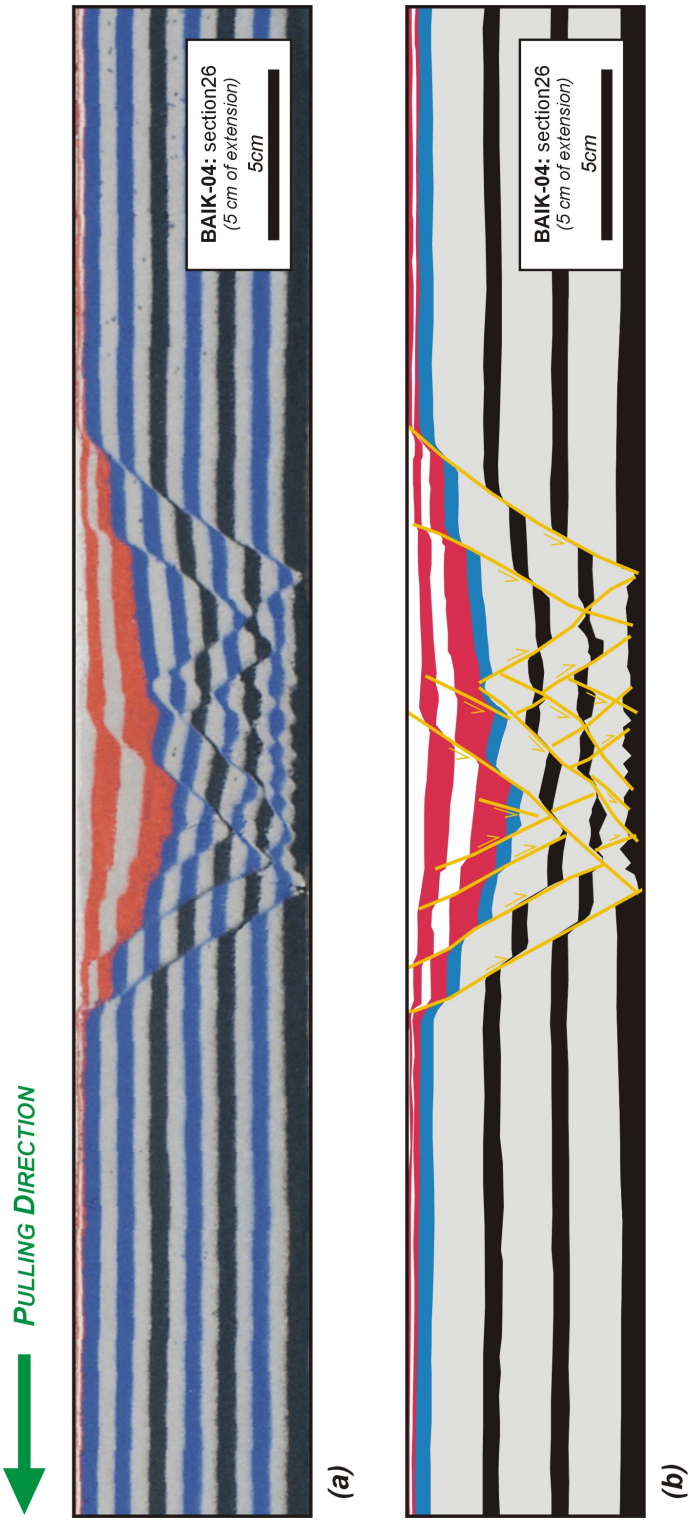

Figure 7.22: *Cross-section nr. 26 of experiment BAIK-04 after 5cm of extension (see figure 7.19e for the location). The original photograph is presented in figure (a) and an interpretation in figure (b).*

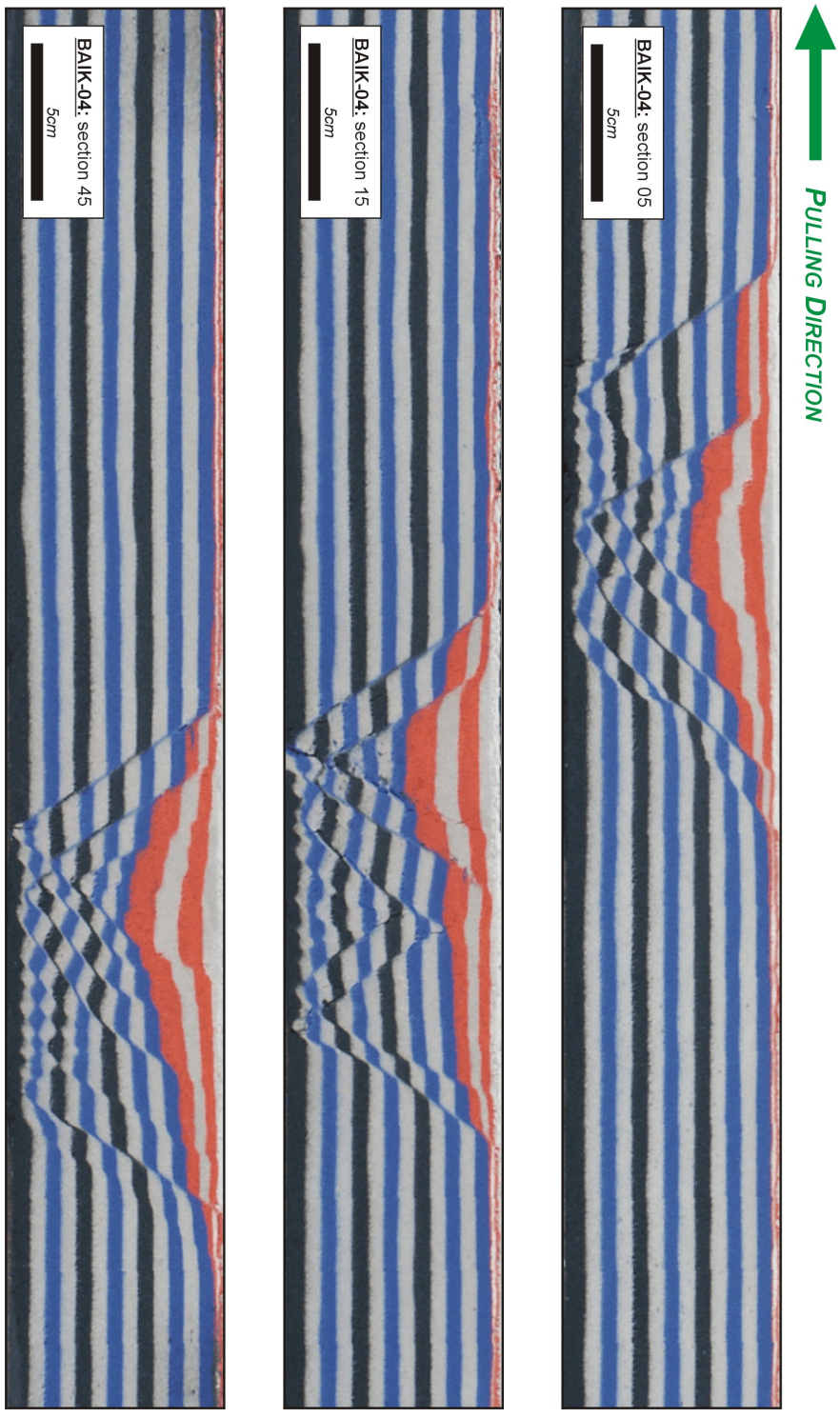

Figure 7.23: *Three cross-sections through model BAIK-04: (a) section 05, (b) section 15 and (c) section 45 (see figure 7.19e for the locations). Black and blue layers correspond to pre-kinematic sand layers, red and white layers are the syn-kinematic infill.*

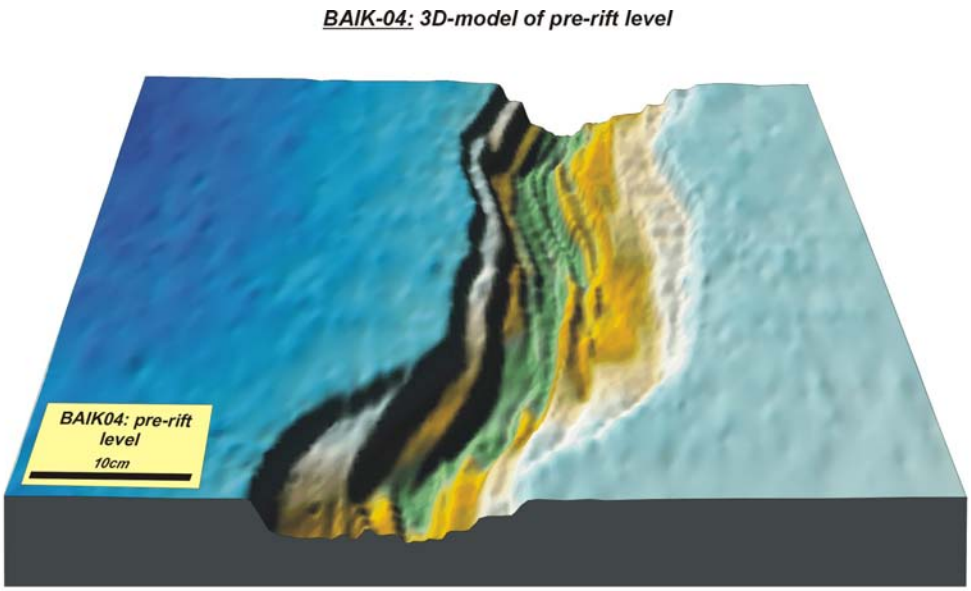

Figure 7.24: *3D surface of the pre-rift level of model BAIK-04 after 5 cm of extension. The mobile wall was on the left side. Note the absence in the model of different individual basins, separated by accommodation zones.*

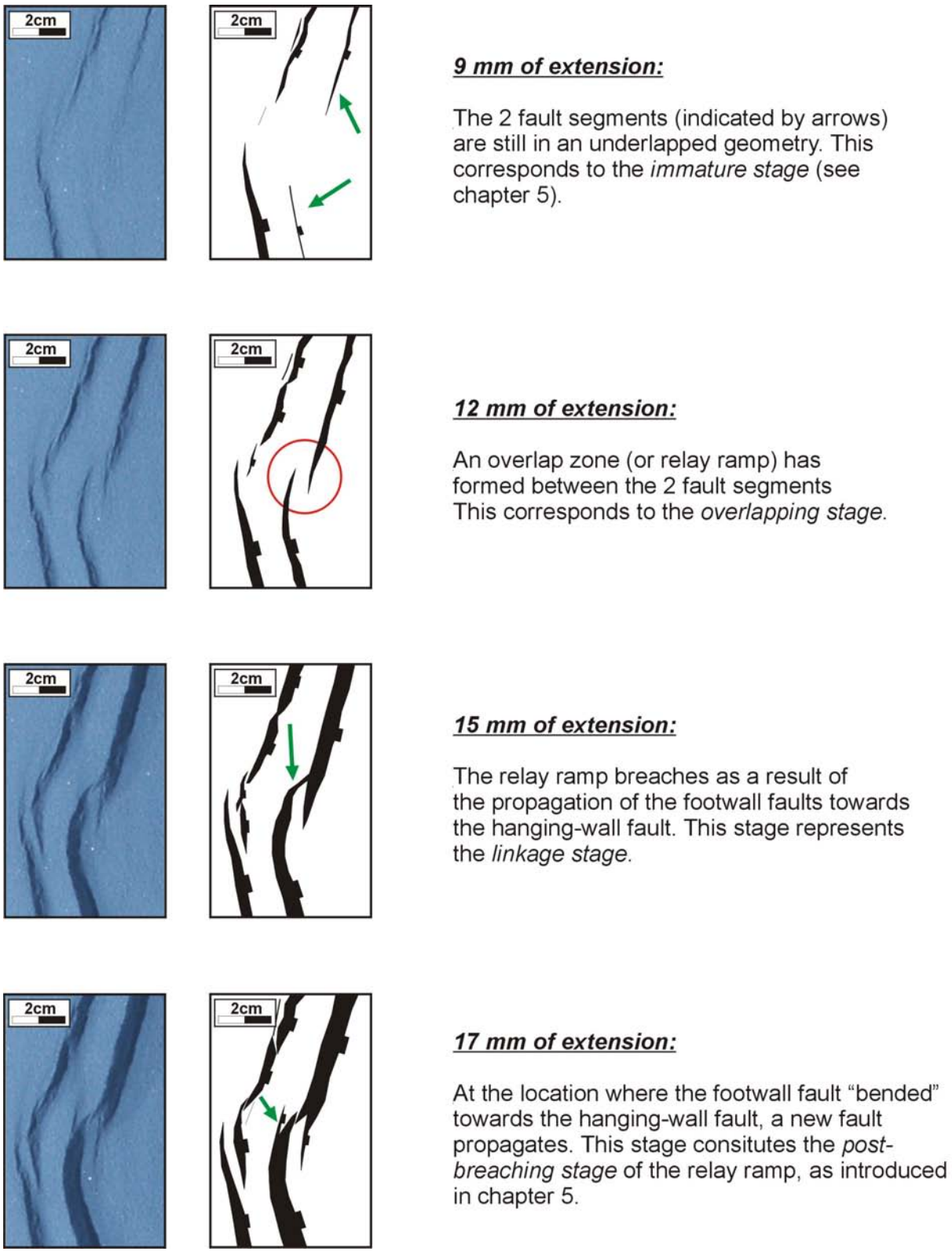

Figure 7.25: *Evolution of a relay ramp in BAIK-04. The location of the ramp in the model is indicated in figure 7.21. The evolution of this relay ramp confirms the diagram in figure 2.20 where it has been illustrated that the different stages in relay ramp evolution can be observed both in time and in depth. Also in this model a post-breaching evolution of the relay ramp is observed.*

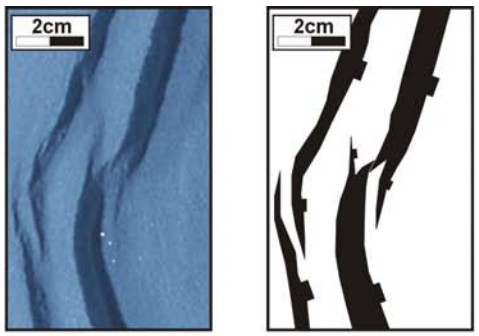

20 mm of extension:

Fault displacement increases, but the geometry remains unchanged.

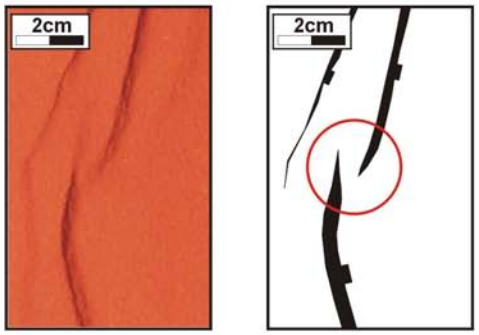

24 mm of extension:

Faults cut through the added red syn-kinematic layer with a normal overlap geometry.

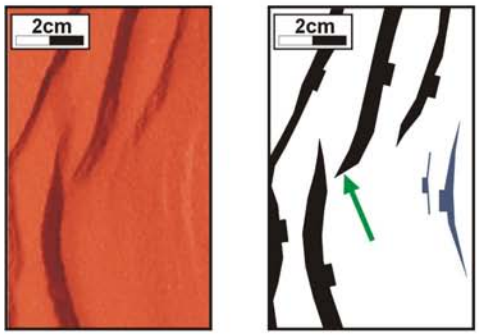

30 mm of extension:

The hanging-wall fault of the relay ramp propagates towards the footwall fault, and almost makes a connection.

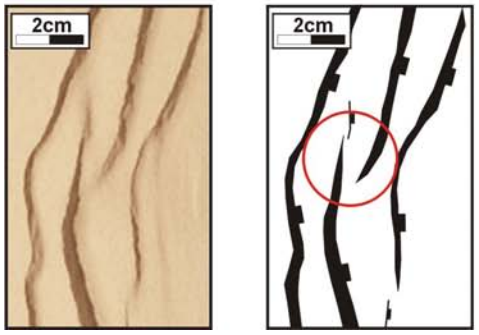

40 mm of extension:

Faults propagate trough the added white syn-kinematic sand layer with a normal overlap geometry.

Figure 7.25: *(continued)*

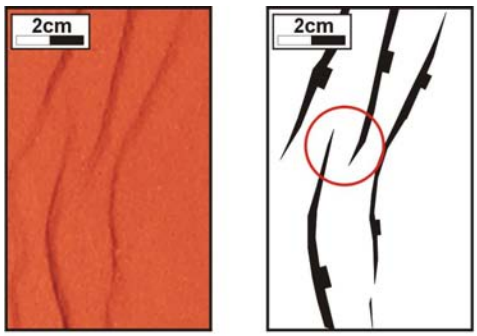

45 mm of extension:

Faults cut through the added red syn-kinematic layer with a normal overlap geometry.

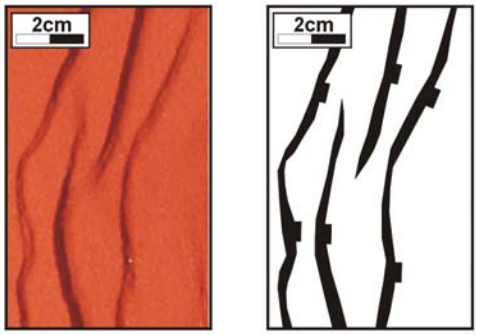

50 mm of extension:

Final amount of extension. The faults at the surface remain in the normal relay ramp geometry.

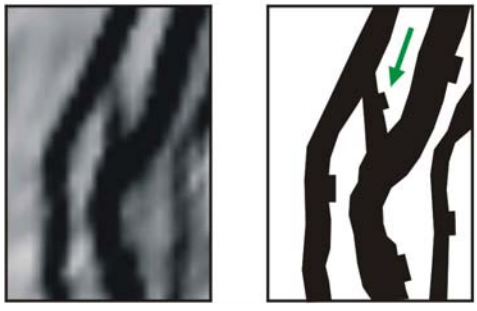

50 mm of extension:

From this reconstruction of the pre-kinematic level after 5cm of extension, it is clear that the fault tip that was found to propagate after the breaching (see blue photographs above) has connected with the neighbouring fault.

Figure 7.25: *(continued)*

7.4.8 Baikal experiment nr 5: BAIK-05

This model has the same characteristics as model BAIK-04:

Characteristics

- base plate geometry: `Type 4`,
- dimensions: 66 cm × 60 cm × 7.5 cm,
- extension achieved by pulling one of the base plates (asymmetric rift),
- 5 cm wide rubber sheet in the centre of the model,
- 7.5 cm of pre-kinematic layers. A total of 13 layers all being 0.55 cm thick. From base to top the colours used were: black – white – blue – white – black – white – blue – white – black – white – blue – white – blue.
- After extension the model was sliced horizontally, with 1.5 cm between each slice.

The model was extended for 5 cm with a picture taken every 1 mm of extension. The first syn-kinematic layer was added after 2 cm of extension, the following after every centimetre of extension. In total 4 syn-kinematic layers (red and white) were added.

Description

The following table summarises the observations that were made during the model's run (see also figure 7.26):

Extension	Observations
0.6 cm	First surface faulting is observed at the mobile wall side.
0.7 – 1 cm	Faults also develop at the fixed wall side. Again relay structures form at some of the locations where the strike of the underlying base-plate changes. The first intra-rift faults start to develop.
1 – 2 cm	In the northern and the middle part of the model, the intra rift faults delineate different basins. Unlike in previous models, these basins do not form a continuous graben structure, but rather are offset along strike. The intra-rift faults are largest where the outer faults of the model are least developed (i.e. near the angles in the base-plates) and vice versa. In the lower part of the model, an accommodation zone develops between two offset basins.
	continued on the next page...

...continued from the previous page

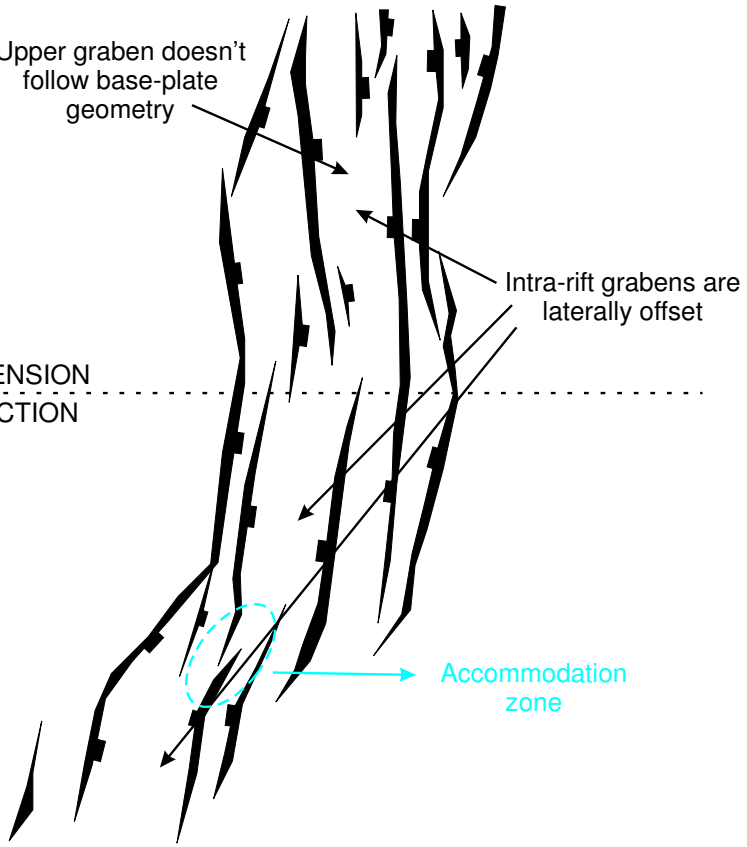

2 cm	Red syn-kinematic layer added.
2 – 3 cm	Grabens in the model widen and the accommodation zone in the lower part develops further. No new faults seem to form in this stage.
3 cm	White syn-kinematic layer added.
3 – 4 cm	The different intra-rift grabens increase their width, and few new intra-rift faults develop.
4 cm	Red syn-kinematic layer added.
4 – 5 cm	Few new faults are formed in this stage. The offset between the intra-rift graben in the upper part and that in the middle part of the model becomes larger.
5 cm	Final amount of extension reached.

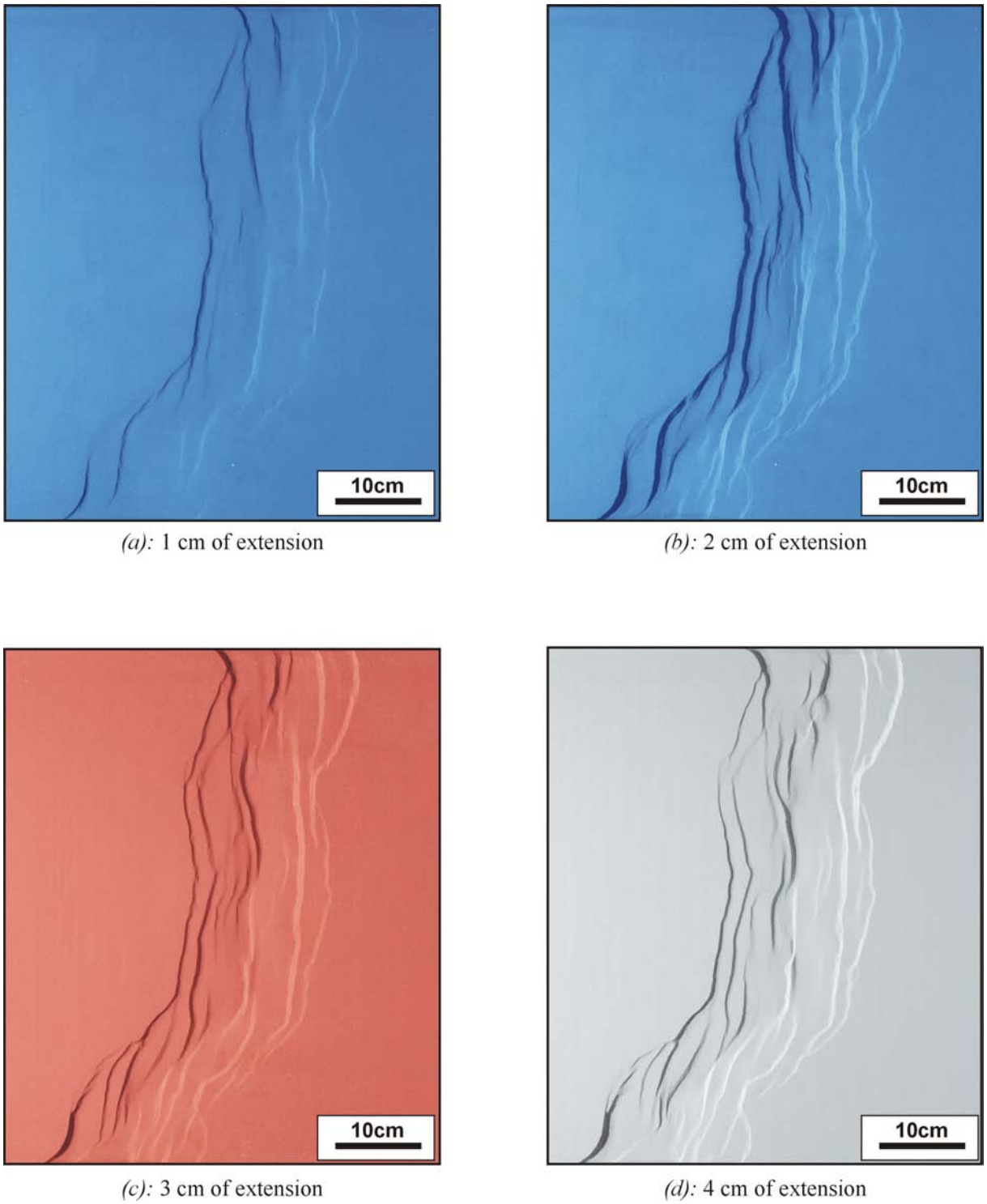

(a): 1 cm of extension

(b): 2 cm of extension

(c): 3 cm of extension

(d): 4 cm of extension

Figure 7.26: *Running shots of model BAIK-05 after different amounts of extension. Base-plates had a type 4 geometry. The mobile wall was on the left side.*

Figure 7.26: ***(continued)*** *Running shot of experiment BAIK-05 after 50 mm of extension (a), and an interpretation (b). Black faults dip towards the bottom of the page, and white faults towards the top. The grey zone in the middle of figure b represents the geometry of the underlying rubber sheet.*

7.4.9 Polymer experiment nr. 1: EP-01

Characteristics

Model EP-01 is an orthogonal rift model, which contains a polymer layer at the base. The model has been deformed in the deformation rig illustrated in figure 7.3.

- slot geometry: linear, perpendicular to the direction of extension,
- rig dimensions: 45 cm × 92.5 cm × 7 cm,
- extension achieved by pulling from one side a basal plastic sheet out of the central slot (asymmetric rift),
- 1 cm thick basal SGM36 polymer layer
- 6 cm of pre-kinematic sand layers:
  - 11 layers with a thickness of 0.50 cm each. From base to top the colours used were: white – blue – white – black – white – blue – white – black – white – blue – white,
  - 1 mm black layer,
  - 2.5 mm clay layer,
  - 1 mm blue surface layer.
- After extension the model was sliced vertically, with 0.5 cm spacing between the different slices. On both sides of the model, the first 15 cm have been skipped.

The model was extended for 10 cm with a picture taken every 1 mm of extension. A first syn-kinematic sand layer was added after 4 cm of extension. Additional syn-kinematic layers were added every 2 cm of extension. In total 4 syn-kinematic layers (red and white) were added.

Description

The following table summarises the observations that were made during the model's run (see also figure 7.27):

Extension	Observations
0.3–0.4 cm	First surface fracturing appear in the thin clay layer. Fractures concentrate in two parallel zones in the centre of the model.
0.8–0.9 cm	Faults start to form in the zones of fracturing. These faults appear to grow independently from the fractures. Faults are segmented, with segments located more or less in each other's prolongation. Between the two fault zones a ∼10 cm wide graben forms along the whole length of the model. Initially there is almost no internal deformation in the graben. Also outside the graben, the model remains relatively undeformed.
1 cm	New fractures develop in the undeformed parts of the model.

continued on the next page...

...continued from the previous page	
1.5–2.5 cm	At the mobile wall side, the graben boundary fault increases its displacement, whereas on the fixed wall side the boundary fault displacement doesn't increase significantly. Instead, an intra-graben fault develops on this side (figure 7.27a). At the fixed wall side of the model, also faults develop outside the central graben.
2.5–3.5 cm	Also near the mobile wall side fault, a fault starts to develop inside the central graben.
4 cm	Red syn-kinematic layer added.
4–5 cm	On the fixed wall side of the model, the existing faults propagate through the red layer and increase their displacement further. In the undeformed part near the mobile wall side, a second graben develops. This graben is separated from the central graben by a ∼5 cm wide horst.
5–6 cm	The boundary faults of this developing second graben are still strongly segmented. The initial development is more irregular than that of the central graben faults.
6 cm	White syn-kinematic layer added.
6–10 cm	The boundary fault segments have connected and long linear faults have formed. So far the displacement on the fixed wall side of the model has been distributed over different small-displacement faults. In this stage of the evolution, some of these small displacement faults become inactive, and the displacement localises again on the central graben faults (figure 7.27).

Throughout the evolution of the model, the width of the central graben has remained more or less constant. The active graben boundary fault at the mobile wall side has continuously been shifted inward to achieve this constant width. Older faults, which were "moved" outside the central graben zone with increasing extension, became inactive. This can also be observed on the cross-sections of the model (figure 7.28), where faults that created a large off-set of the pre-rift level, cause no (or only a minor) displacement of the model's top surface.

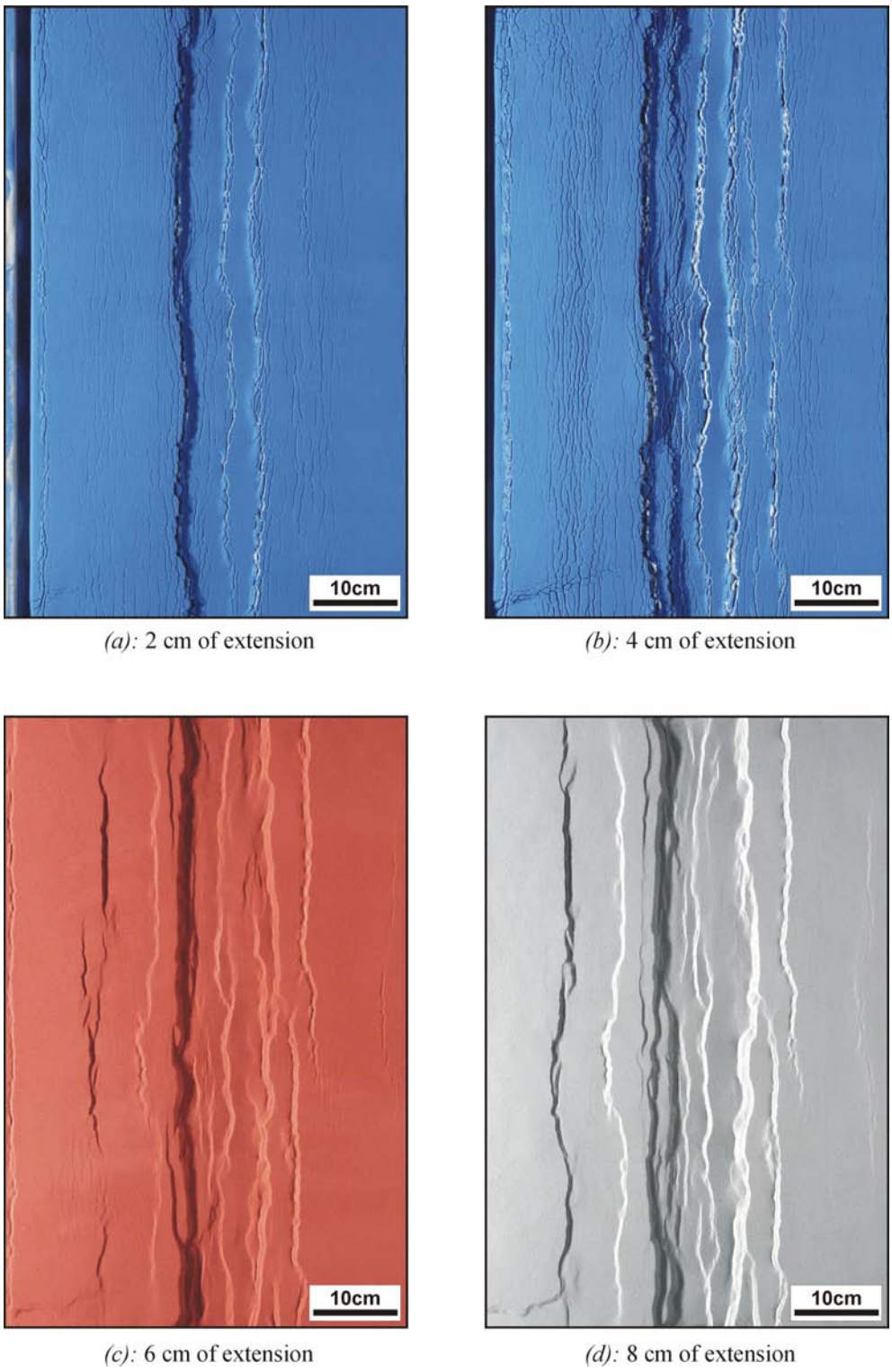

(a): 2 cm of extension

(b): 4 cm of extension

(c): 6 cm of extension

(d): 8 cm of extension

Figure 7.27: *Running shots of experiment EP-01 (orthogonal rift model) after different amounts of extension. The mobile wall is on the left side of the figures, the fixed wall side is on the right. Note the numerous small fractures in the model's surface that are made visible by the addition of a thin clay layer (pictures* a *and* b*).*

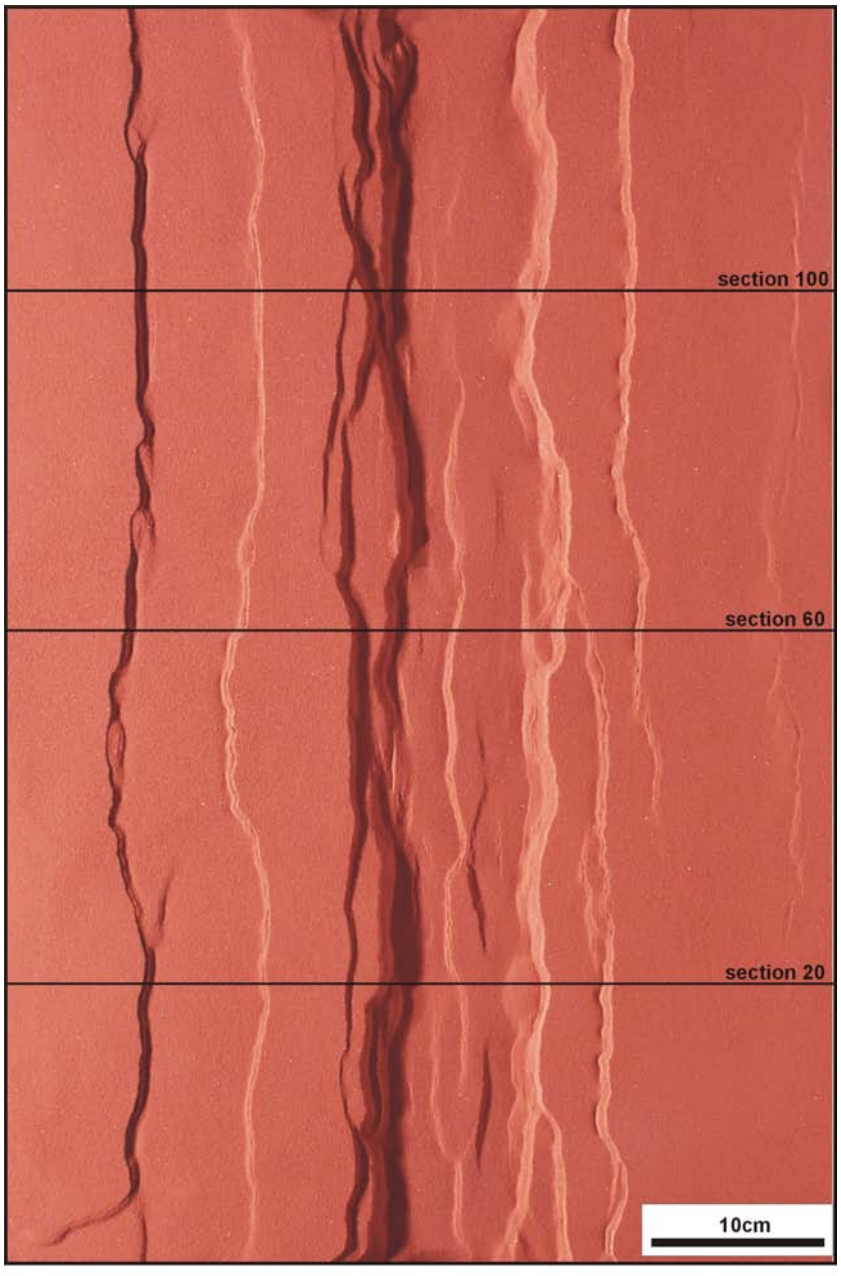

(e): 10 cm of extension

Figure 7.27: ***(continued)*** *Last running shot of experiment EP-01, after 10 cm of extension. Cross-sections are included in figure 7.28.*

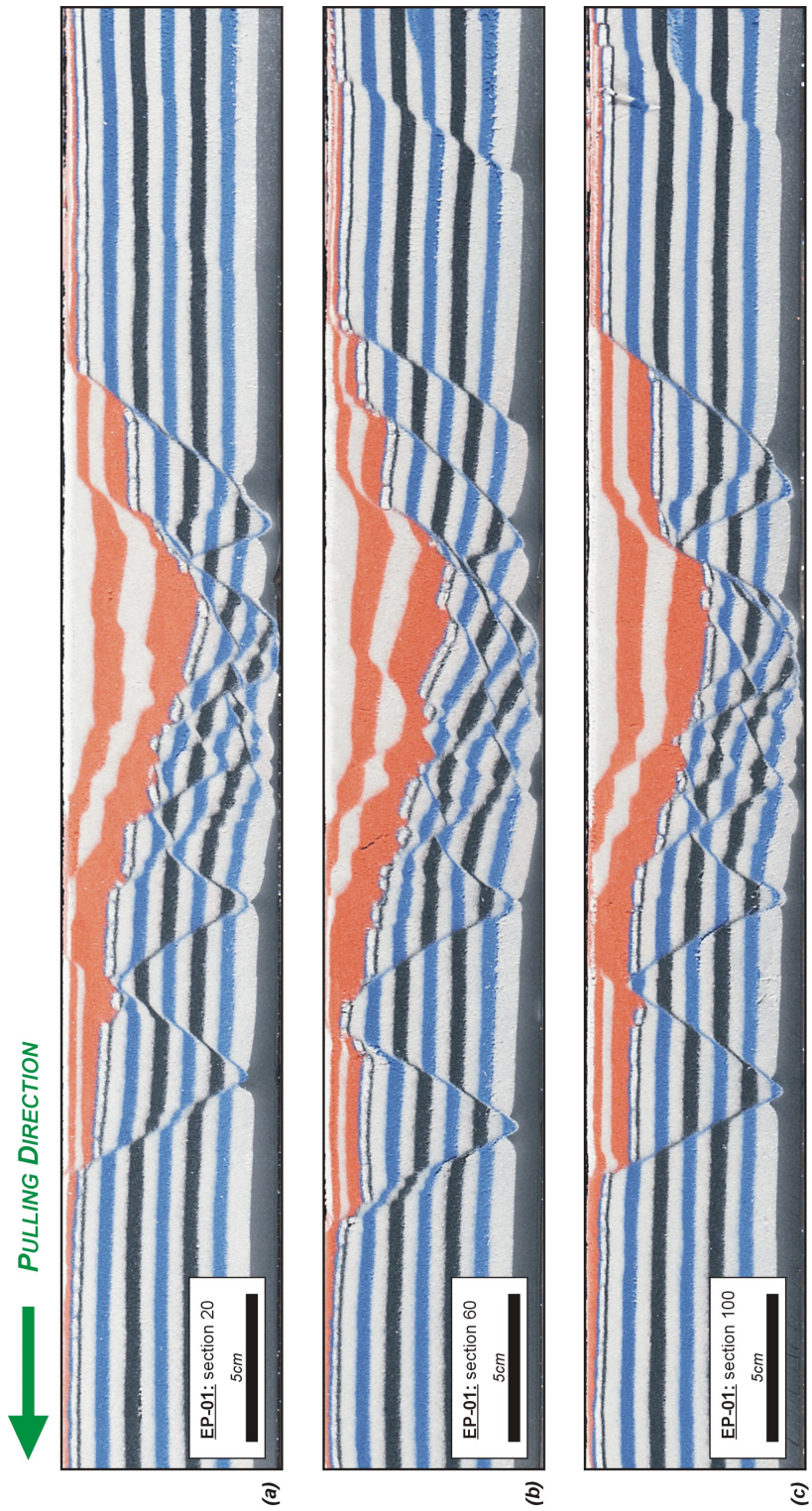

Figure 7.28: *Three cross-sections through model EP-01: (a) section 20, (b) section 60 and (c) section 100 (see figure 7.27 for the locations). Black and blue layers correspond to pre-kinematic sand layers, red and white layers are the syn-kinematic infill.*

7.4.10 Polymer experiment nr. 2: EP-02

Characteristics

Model EP-02 is a 60° oblique rift model, which contains a basal polymer layer.

- slot geometry: linear, 60° oblique to the direction of extension,
- rig dimensions: 96 cm × 92.5 cm × 7 cm,
- extension achieved by pulling from one side a basal plastic sheet out of the central slot (asymmetric rift),
- 1 cm thick basal SGM36 polymer layer
- 6 cm of pre-kinematic sand layers:
  - 11 layers with a thickness of 0.50 cm each. From base to top the colours used were: white – blue – white – black – white – blue – white – black – white – blue – white,
  - 1 mm black layer,
  - 2.5 mm clay layer,
  - 1 mm blue surface layer.
- After extension the model was sliced vertically, with 0.5 cm spacing between the different slices. On both sides of the model, the first 15 cm have been skipped as they are likely to be strongly influenced by side effects.

The model was extended for 11.55 cm (corresponds to 10 cm of extension perpendicular to the slot) with a picture taken every 1 mm of extension. A first syn-kinematic sand layer was added after 4 cm of extension. Additional syn-kinematic layers were added every 2 cm of extension. In total 5 syn-kinematic layers (red and white) were added.

Description

The following table summarises the observations that were made during the model's run (see also figure 7.29):

Extension	Observations
0.5–1 cm	Rift formation starts with the development of 6 clearly offset en echelon rift segments.
1–2 cm	The lower parts of rift segments at the mobile wall side are oriented parallel to the central slot, whereas the upper parts adopt an orientation that is more perpendicular to the direction of extension. For the fixed wall side, the upper parts of the different segments follow the 60° orientation of the slot, while the lower parts of the segments are oriented at higher angle to the direction of extension.

continued on the next page...

...continued from the previous page

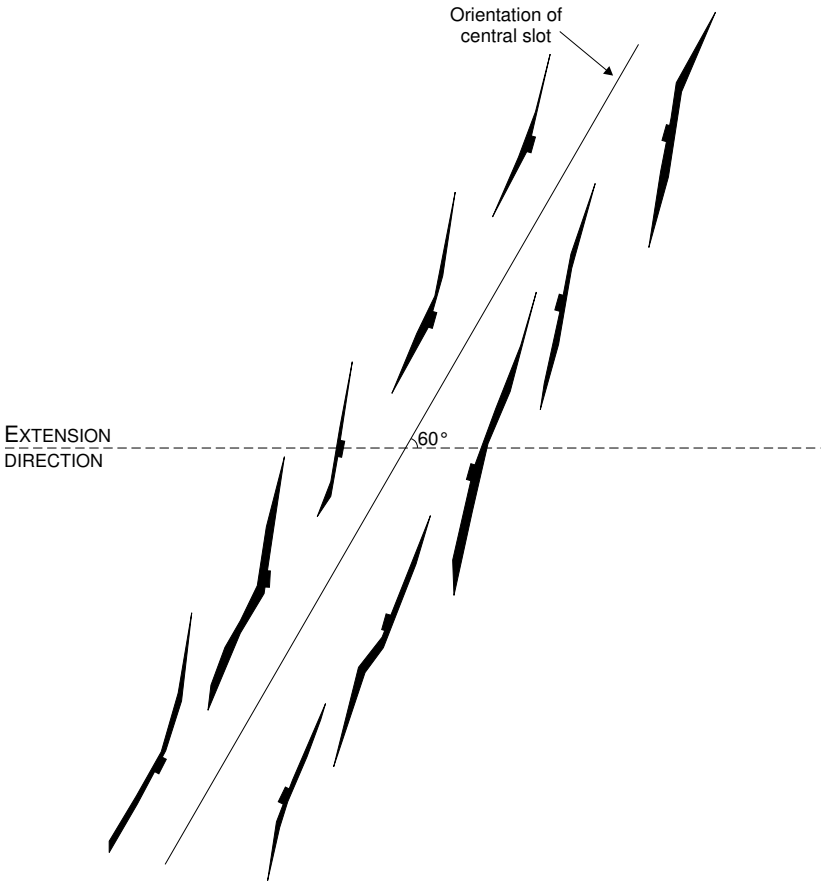

2–4 cm	With increasing extension, the faults develop further. At this stage, no longer a clear connection between the different grabens exists. Instead the system develops into different small, offset grabens. Opposed dipping faults start to interact and connect with each other, or pass by each other to cut through the central rift zone. This coalescence of en echelon faults results in sigmoidally shaped grabens.
4 cm	Red syn-kinematic layer added. Although the main deformation is concentrated near the central slot, the outer faults remain active as well and cut through the red sand layer.
6 cm	White syn-kinematic layer added.

continued on the next page...

...continued from the previous page	
6 – 10 cm	The geometry of the outer faults remains relatively simple (consisting of several en echelon segments). The central deformation zone on the other hand is rather complex: here a large number of small faults occur with varying strike directions (forming angles between 60° and 90° with the direction of extension).

Figure 7.29: *Running shots of experiment EP-02 (60° degree oblique rift model) after different amounts of extension. The mobile wall is on the left side of the figures, the fixed wall side is on the right.*

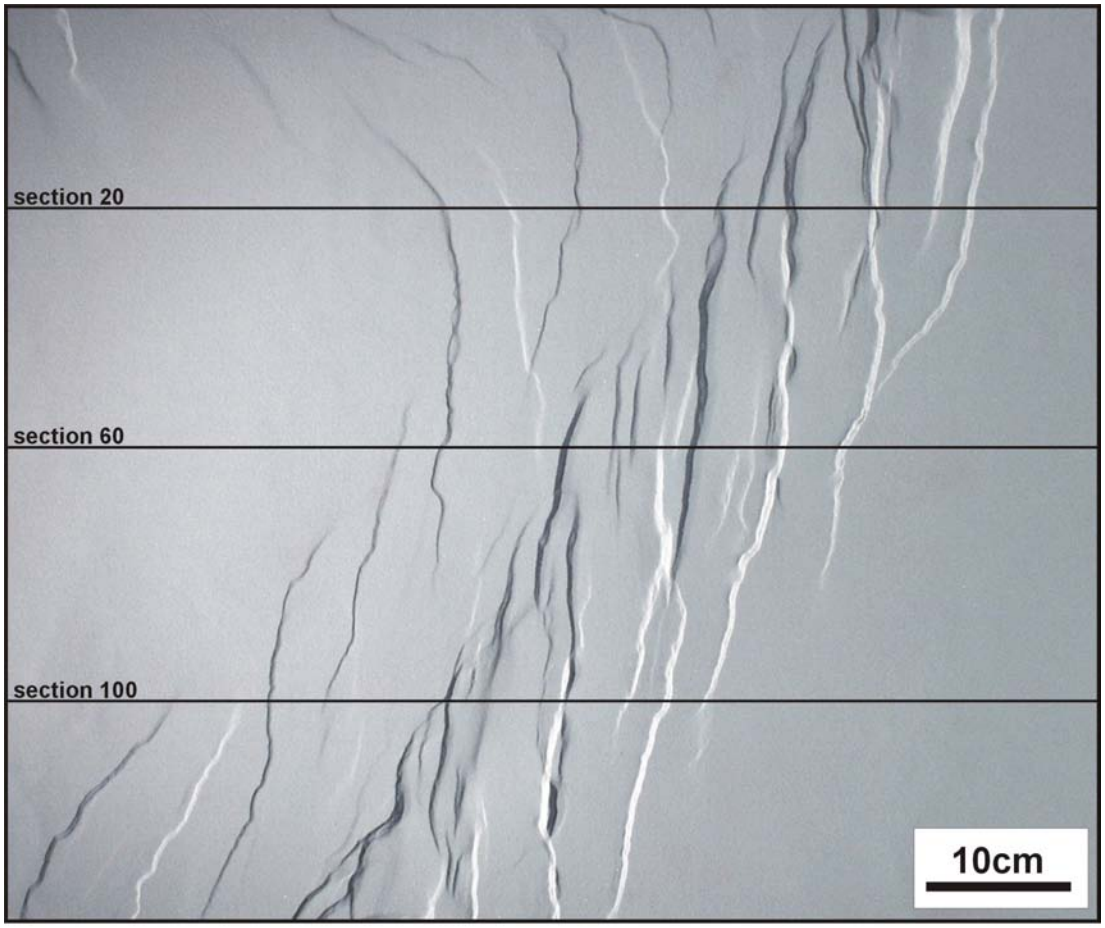

(e): 10 cm of extension

Figure 7.29: ***(continued)*** *Last running shot of experiment EP-02, after 10 cm of extension. Cross-sections are included in figure 7.30.*

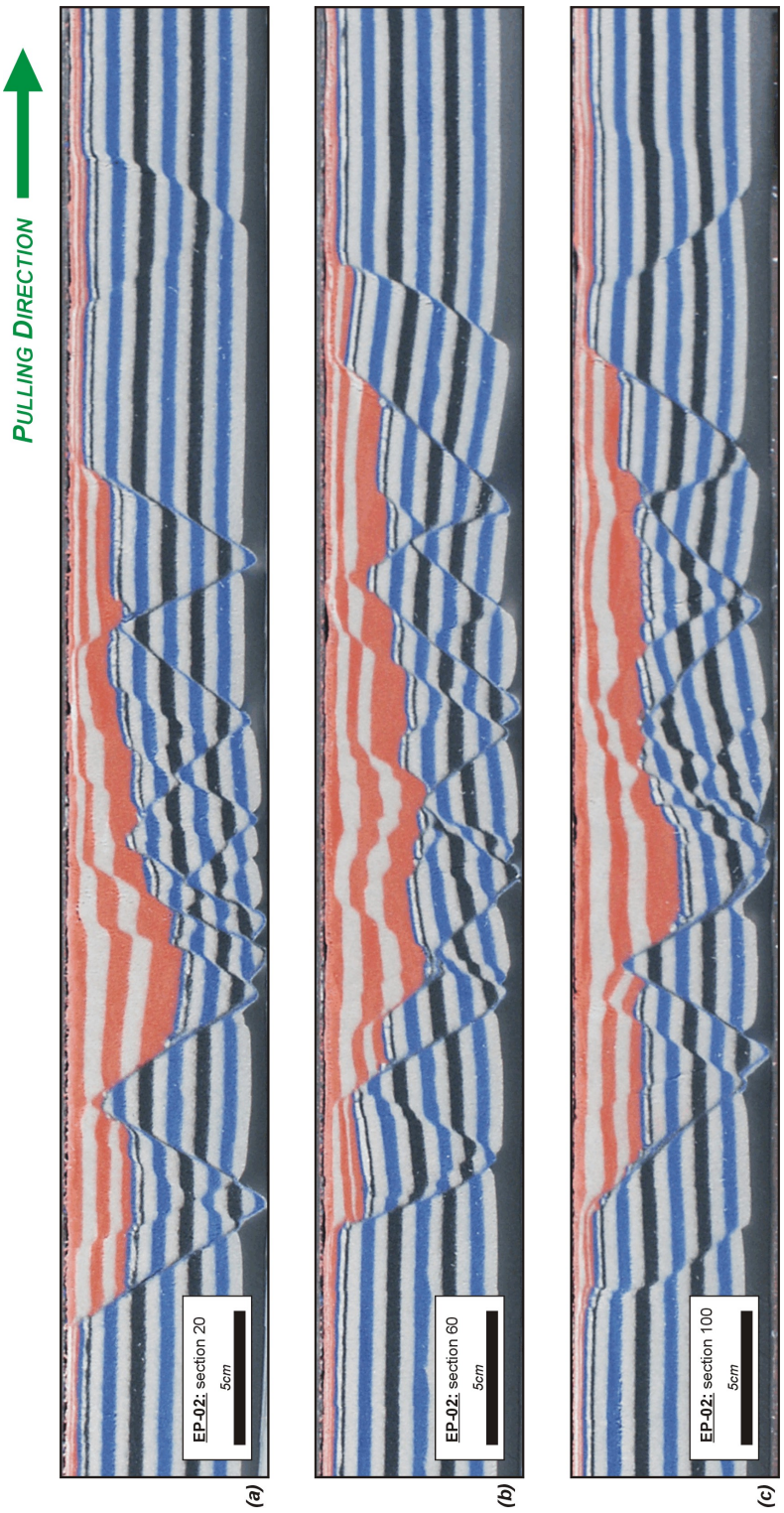

Figure 7.30: *Three cross-sections through model EP-02: (a) section 20, (b) section 60 and (c) section 100 (see figure 7.29 for the locations). Black and blue layers correspond to pre-kinematic sand layers, red and white layers are the syn-kinematic infill.*

7.4.11 Polymer experiment nr. 3: EP-03

Characteristics

Model EP-03 is a rift model which contains a basal polymer layer. In this model the central slot had a shape similar to the `type 2` experiments above.

- slot geometry: similar to `type 2` base plates.
- rig dimensions: 72.5 cm × 92.5 cm × 7 cm,
- extension achieved by pulling from one side a basal plastic sheet out of the central slot (asymmetric rift),
- 1 cm thick basal SGM36 polymer layer
- 6 cm of pre-kinematic sand layers: 12 layers with a thickness of 0.50 cm each. From base to top the colours used were: white – blue – white – black – white – blue – white – black – white – blue – white – blue,
- After extension the model was sliced vertically, with 0.5 cm spacing between the different slices. On both sides of the model, the first 15 cm have been skipped as they are likely to be strongly influenced by side effects.

The model was extended for 10 cm with a picture taken every 1 mm of extension. A first syn-kinematic sand layer was added after 4 cm of extension. Additional syn-kinematic layers were added every 2 cm of extension. In total 4 syn-kinematic layers (red and white) were added.

Description

Extension	Observations
1–1.3 cm	First expression of surface faulting, in the P & B segments of the model.
1.5–1.7 cm	The O segment develops as 2 en echelon segments.
1.7–4 cm	At the mobile wall side a second intra-graben fault system develops. In the lower part of the model, deformation is distributed over many faults, whereas in the central and upper parts the displacement is accommodated on fewer but high-displacement faults.
4 cm	Red syn-kinematic layer added.
4–6 cm	The position of the major faults remains constant. The initial boundary faults are "pulled" out of the central deformation zone with increasing extension. As a result their activity decreases (only a small off-set of the red syn-kinematic sand layer).

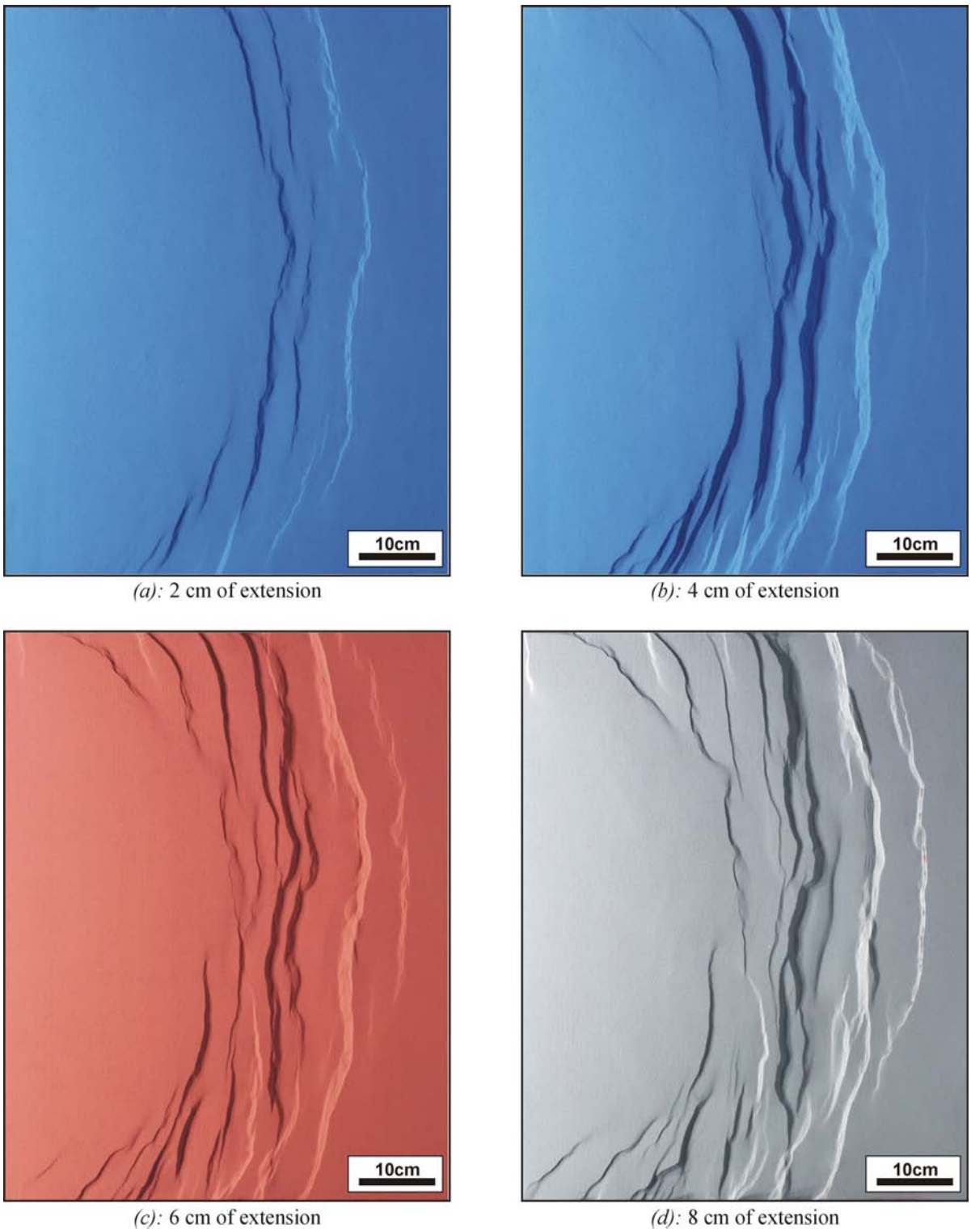

(a): 2 cm of extension

(b): 4 cm of extension

(c): 6 cm of extension

(d): 8 cm of extension

Figure 7.31: *Running shots of experiment EP-03 after different amounts of extension. The mobile wall is on the left side of the figures, the fixed wall side is on the right.*

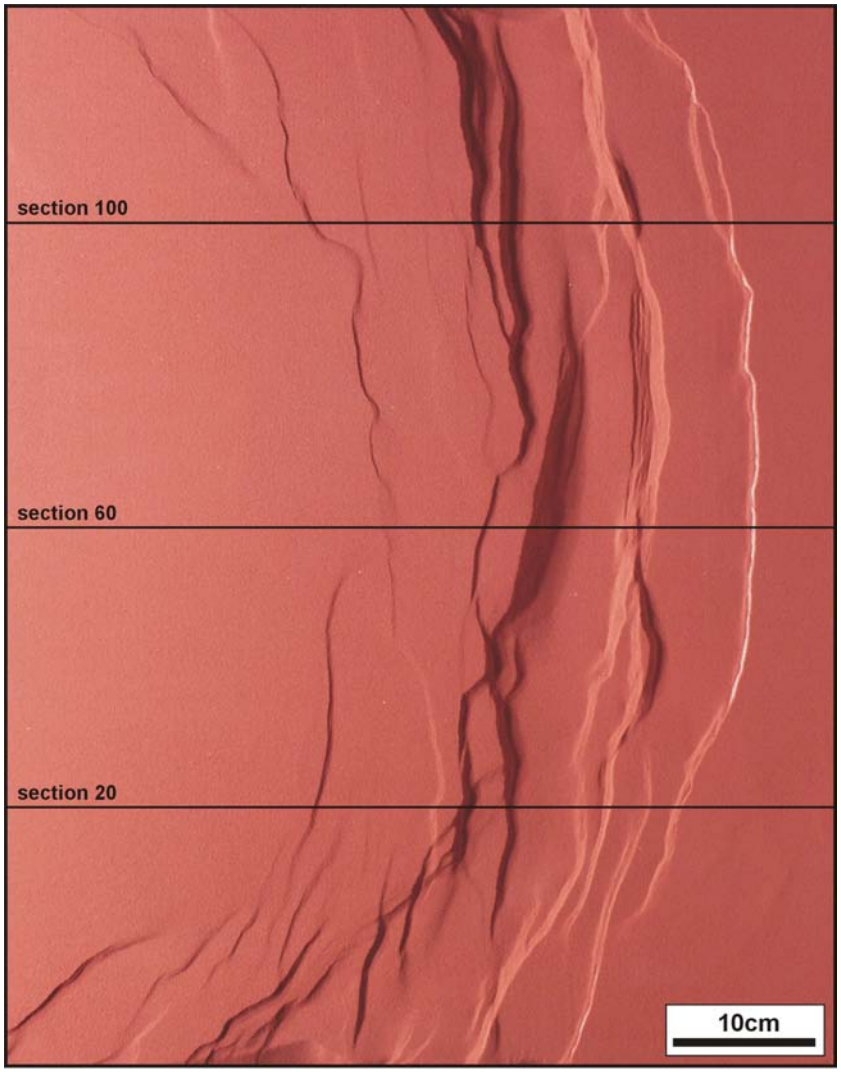

(e): 10 cm of extension

Figure 7.31: ***(continued)*** *Last running shot of experiment EP-03, after 10 cm of extension. Cross-sections are included in figure 7.32.*

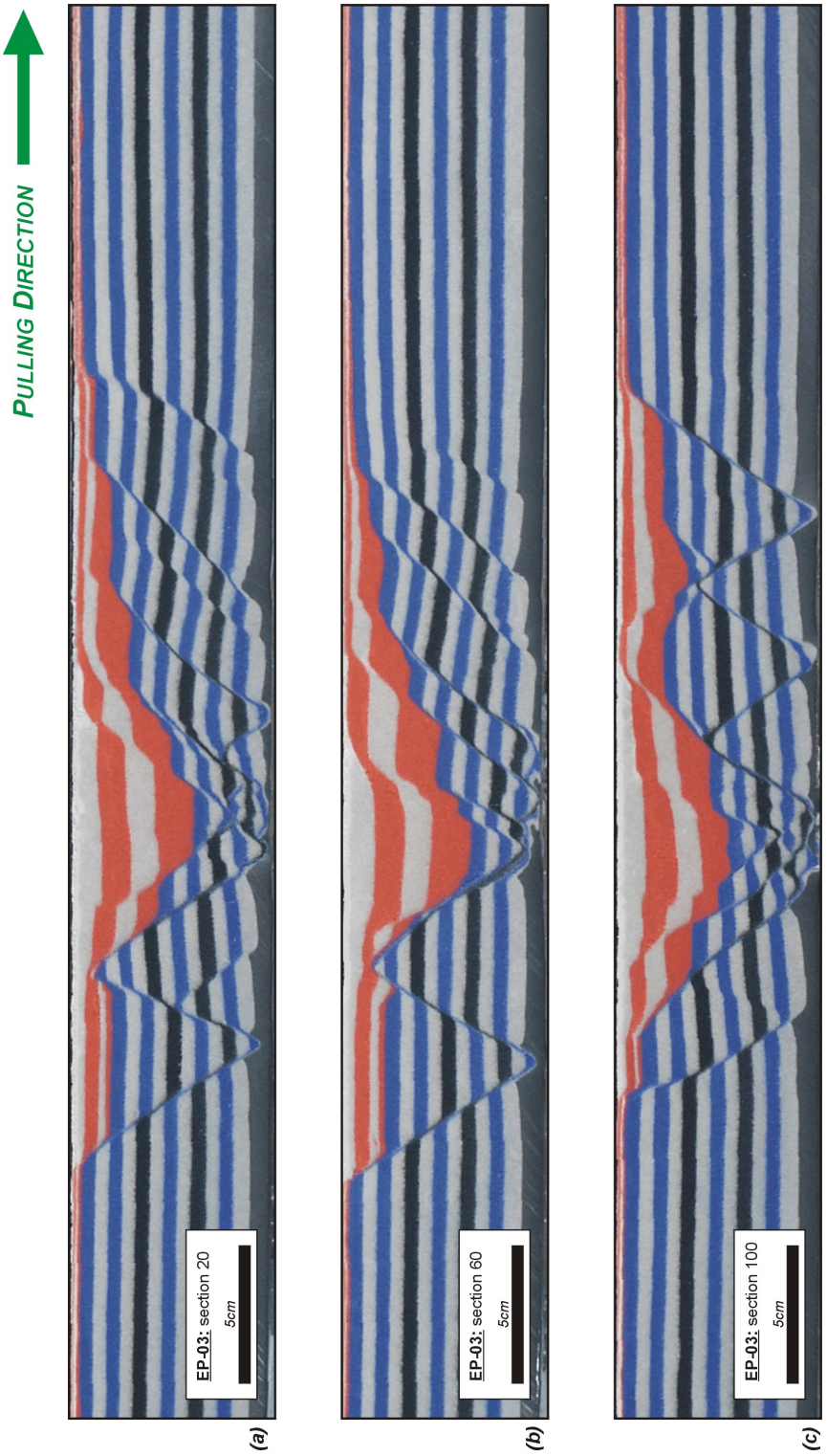

Figure 7.32: *Three cross-sections through model EP-03: (a) section 20, (b) section 60 and (c) section 100 (see figure 7.31 for the locations). Black and blue layers correspond to pre-kinematic sand layers, red and white layers are the syn-kinematic infill.*

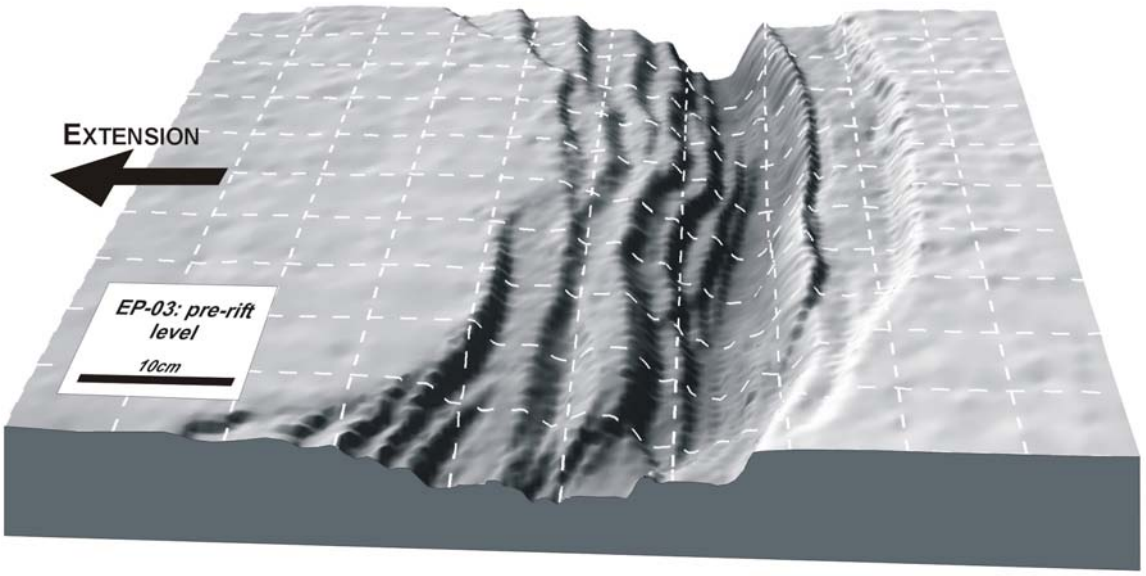

Figure 7.33: *3D surface view of the pre-rift level of experiment EP-03 after 10 cm of extension.*

7.5 Discussion

7.5.1 Rubber sheet detachment models

Before the actual faulting in the models was observed, deformation typically involved a broad subsidence at the location of the detachment. This depression was bordered by a slightly expressed bending of the surface layers. This bending has been the only observed precursor to the surface faulting in this type of models. With increasing extension, the first faults developed exactly at the location of these bends. As soon as the first faults affected the model's surface, they were characterised by long trace lengths, and only minor surface displacement. Throughout the further evolution of the models these faults remained the "outer" faults of the rift. Two-dimensional rift models, where the evolution has been observed in cross-section (through a glass side-wall) rather than in top-view (see appendix C), reveal that this bending is associated with fault propagation folding. The first faults in the model initiate at the detachment level, and subsequently propagate upward, causing the observed folding at the surface. This mechanism is illustrated in figure 7.34.

In chapter 6, this mechanism of upward fault propagation has been invoked as a possible explanation for the development of initial long fault lengths, characterised by only a minor offset of the top-surface of the model. The observations in figure 7.34 illustrate that also in these rift models upward fault propagation likely influenced the observed fault shapes at the model's surface. The amount of extension that was required to cause the formation of the first faults in the models depended on the angle between the orientation of the base-plate and the direction of extension, and typically varied around 0.6 cm or 0.8 cm for respectively 5 and 10 cm wide rubber

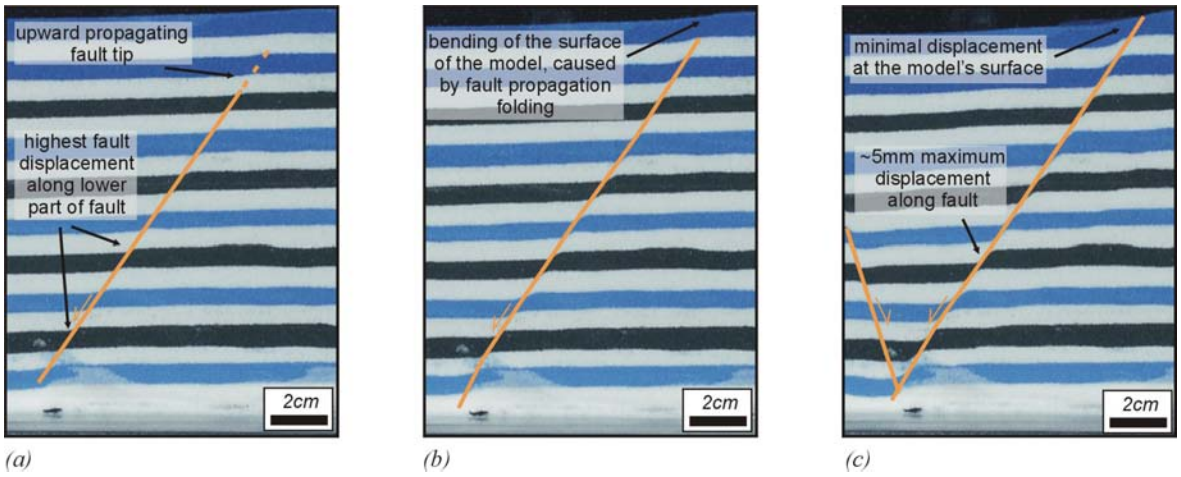

Figure 7.34: *Different evolution stages (observed in cross-section) in the formation of a rift boundary fault in the rubber sheet detachment models. The model depicted is the two-dimensional Asymmetric Rift Model 2 from Appendix C (page 316). (a) 1 cm of extension: lower layers in the model become off-set. (b) 1.25 cm of extension: fault propagates further upward, causing the formation of a fault-propagation fold at the model's top surface. (c) 1.75 cm of extension: the fault has reached the surface of the model.*

sheets. The strike direction of the outer rift faults followed in general the orientation of the underlying base-plate border. Only when the angle between the orientation of the base-plate and the direction of extension became too small, the faults in the sand cover did not follow this orientation, but rather developed as structures with a strike more or less perpendicular to the direction of extension.

It is useful to distinguish between two type of faults in the models:

(1) A first type, corresponding to the outer rift model faults, described so far in this discussion. These faults propagate directly from the well-defined linear velocity discontinuity, which exists between the border of the solid metal base-plate and the rubber detachment, and
(2) A second type of faults, which form in a later stage above the uniformly stretching detachment and which represent the internal deformation in the modelled rift. Although the latter type of faults often also originate at the base of the model, this is not always the case (e.g. see appendix C).

The largest displacement faults in the models corresponded with such intra-rift faults. Similar observations have been made by McClay et al. (2001) who found that the growth of the intra-rift faults was often arrested at locations of interlocking fault tips. This arrestment resulted in anomalous large displacements on the faults in relation to the fault lengths.

Both types of faults (rift border faults and intra-rift faults) have been observed to result from the growth and connection of different segments, through a mechanism similar to the one described in chapter 2 (section 2.4). Only the timing of linkage seems to differ between both types of faults. For the first type, linkage appears to occur very early in the evolution (mostly within the first 2–3 cm), whereas the pre-linkage fault evolution for the intra-rift faults can last significantly longer (till the final amount of extension). One way to explain this observation might be that the outer faults evolved from their initiation as one coherent fault system; possibly made up of one major fault plane. If true, the observed relay zones would correspond to irregularities in this fault plane (e.g. bifurcations or branching) near the model's surface. The second type of faults would, on the other hand, correspond to different, initially isolated segments that accidentally start to interact with neighbours. This difference in evolution can also explain the difference in scale of the relay zones. In the former case, the relay zones usually are small (small overlap and small spacings), whereas for the latter faults the relay zones evolve as larger structures. Like in previous models of rifting (e.g. McClay and White, 1995) no discrete transfer faults have been observed between offset fault segments in the models.

With increasing extension, the rift system developed in an asymmetric structure. Dominant large rift boundary faults were observed on the mobile wall side of the models, whereas at the fixed wall side, the extensional deformation was distributed over a broader area, consisting of several smaller displacement faults. The overall complexity of the rift is directly related to the complexity of the base-plate geometry. In many rift models a distinct intra-rift graben developed that did not follow the geometry (and complexity) of the underlying base-plates. This intra-rift graben usually consisted of a linear graben, oriented more or less perpendicular to the direction of extension. Occasionally, an off-set has been observed between different segments of such

an intra-rift graben, and sometimes a slight variation in the orientation of the intra-rift graben could be observed between different parts of the model. This variation in orientation was mainly observed in the models with a 5 cm wide detachment. The width of the rubber sheet further determines the width of the overall rift zone in the models, however, it does not seem to influence the width of the different grabens that develop within the rift.

A shortcoming of the detachment models is that the rigid base of the model does not permit the formation of keels to the fault blocks (unlike the polymer models discussed below). This restriction can result in the formation of a distinct listric fault geometry in the pre-kinematic sand layers, as observed on several cross-sections (McClay, 1990b). Another important restriction is the pre-defined width of the rubber sheet in the models, which directly determines the width of the modelled rift zone.

7.5.2 Polymer models

The polymer models differ from the rubber sheet detachment models, in three ways:

1. They do not have a pre-defined width of the rift zone, and therefore the width of the deformation zone solely depends on the amount of extension. The width of the "active" rift graben remains more or less constant, and appears to be independent of the amount of extension.
2. The presence of the polymer at the base of the model does not create a sharp linear velocity discontinuity at the base of the sand pack. The polymer somehow smooths the introduced velocity discontinuity that exists at the slot in the modelling rig.
3. In the polymer models keels to fault blocks can be formed. This results in the absence of listric fault geometries in the pre-rift sand layers in these models.

The absence of the sharp velocity discontinuity allows the outer faults to develop as originally isolated faults, which are not part of a single fault system. As a result of this, the outer faults are at large strains remarkably more segmented in the polymer models, compared to the outer faults in the detachment models (compare for example figures 7.27 & 7.5 and 7.31 & 7.15).

Unlike in the detachment models, the velocity discontinuity in the polymer models remained at fixed position (the location of the central slot). This boundary condition could account for the constant location of the main active graben faults in the centre of the model (near the slot), whereas older faults are "pulled" out of the central zone with increasing strain, and as a result become less important. This rifting mechanism is comparable to the one observed at oceanic spreading centres.

The inclusion of a tiny clay layer close to the model's surface has made the presence of extensional fractures visible that preceded the faulting. These fractures developed in a relatively broad, although well-defined, zone with orientations that parallel the strike of the future fault that cross-cuts them. Normal faults developed in many of the fracture zones, although not in all of them.

The polarity of the rift asymmetry in the polymer models was opposite to that of the rubber

sheet detachment models. In the polymer models, highest displacement faults and the deepest basins formed at the fixed wall side, rather than at the mobile wall side.

7.5.3 Comparison of the models with the structure of Lake Baikal

Our models did not produce the three distinct sub-basins, separated by accommodation zones that are characteristic for Lake Baikal. Rather than following the imposed basement geometry, the intra-rift faults and grabens developed almost perpendicularly to the direction of extension. This often resulted in a central, more or less linear graben within the wider rift zone. Only in the `Type 4` experiments with a 5 cm wide basal detachment, a stepwise orientation of the sub-basins has been observed that resembles the natural situation in Lake Baikal. Nevertheless, the accommodation zones between these basins did not form in the models.

The rift models containing a 10 cm wide rubber basal detachment, are too wide and they create fault geometries, which are too complex to correspond to the situation in the Baikal Rift Zone. Instead the main structure in the Baikal Rift Zone is determined by fewer but larger faults.

In general, the outer faults in the models did follow the orientation of the underlying base-plates, and as such they were characterised by a stepwise orientation change, similar to the situation in Lake Baikal. As discussed above, relay zones have played an important role in the growth and evolution of the faults in the models. The detachment models show that relay zones between segments of the outer rift faults often occur where the orientation of the underlying base-plates changes. This observation therefore suggests a strong control of the base-plate geometry on the development of relay zones.

The cross-sectional views of the models showed a distinct asymmetric shape of the rift basins, with few large displacement faults on one side, and more but smaller displacement faults on the other. The models did not produce half-grabens as the principal rift units. Similar asymmetric cross-sections (probably a bit stronger) are observed in Lake Baikal, where also clear faults are observed on both sides of the lake, with the western boundary faults being the most important. Also in Lake Baikal no real half-graben rift basins developed.

7.5.4 Shortcomings

The modelling presented in this chapter is obviously an over-simplification of the development of the Baikal Rift Zone in nature. Apart from the general limitations of analogue sandbox models (see section 6.2.4), this over-simplification puts additional constraints on the applicability of the models presented here.

- a recent direction of extension in the central part of Lake Baikal (at the location of the Primorsky Fault) has been used to deform the whole Baikal Rift Zone. As a result, no account has been taken for the influence of different stress fields in earlier stages in the evolution of the rift zone. These stress regimes have changed considerably during the evolution of the Baikal Rift Zone (Delvaux et al., 1997). Also no account has been taken for other stress regimes that or active in other parts of the rift zone.

- the models simulate only the deformation in the upper, brittle parts of the crust. They do not include the influence of deformation processes that can act in the lower parts of the lithosphere and affect the deformation near the surface, or vice versa.
- the scaling factor of the rift models in this chapter ($\lambda \approx 10^{-5}$) does not allow to adequately model the whole Baikal Rift Zone in one single sandbox experiment. This means that these models will unlikely answer all questions regarding the exact formation of the rift zone as a whole, but nevertheless, they serve as good visualisation means for many aspects of the evolution of faults in rifts, with in particular the complex structural geometries of boundary fault systems.

7.6 Conclusions

An important observation from the experiments has been that during the evolution of the boundary faults, different relay zones occurred at the locations where the base-plate direction changed its orientation. This observation confirms that in natural rifts the geometry of basement anisotropies can influence the location of intrabasin transfer zones between fault segments that are located on the same side of a rift. This conclusion complements the conclusions from previous modelling studies of rifts, which have demonstrated a strong basement control on the development of interbasin transfer zones (like accommodation zones) (e.g. Acocella et al., 1999a).

The accommodation zones between the different basins in Lake Baikal have not been reproduced, and therefore it is still unclear which mechanism has been responsible for their development. Whether the formation of the accommodation zones has been related to changes in the stress regimes throughout the evolution of the lake or to a possibly more complex geometry of pre-existing structures needs to be investigated further.

Chapter 8

Discussion & Conclusions

For this dissertation different examples of relay ramps have been investigated, either as natural examples or by experiments. In the different chapters short discussions were included. In this chapter all observations and discussions will be put together to come to a final overview.

8.1 Discussion on the structure and evolution of relay ramps

8.1.1 Are relay ramps scale independent?

In both relay ramp examples from Lake Baikal (Zavarotny and Pri-Ol'khon Block), several observations were made, which have not been reported in other relay ramps on a smaller scale.

In the relay ramp in Zavarotny (chapter 4), an unusual combination of relay ramp breaching by a newly developed fault occurred together with secondary faulting inside the relay ramp, with strikes that are almost parallel to the main faults. The combination of both features is uncommon because the development of a new connecting fault to breach the ramp requires that σ_3 inside the ramp is oriented more or less parallel to the main faults. The development of secondary fractures which parallel the main faults on the other hand, requires the orientation of σ_3 to be more or less perpendicular to the main faults.

A possible explanation for this observation has been suggested in chapter 4. There it was suggested that the internal structure of the relay ramp is strongly influenced by the presence of a pre-existing basement fabric and structures inside the ramp. For Zavarotny it could for example be possible that due to the presence of pre-existing structures, the secondary faults in the southern half of the relay ramp did not require the same amount of bending in the ramp as would have been required to form new faults. The exact influence of such a basement fabric on the internal structure of a relay ramp has not been studied so far, so it is hard to assess its importance. It is, however, very well possible that pre-existing fabrics will also influence relay ramps on a smaller scale, but for smaller scale ramps the fabric will most likely appear to be uniform, whereas in larger ramps different trends might be observed in different parts of the relay ramps.

Additional to the possibility of having a non-uniform fabric distribution in large relay ramps,

another factor which might play in large ramps is a variation in the regional stress field. The prevailing stress field inside a relay ramp results from the combination of a local stress field that is caused by the fault interaction and the regional stress field. Small relay zones will very likely be located in a homogeneous regional stress field, which implies that all "relay zone specific" structures, result from the fault interaction. However, when the size of a relay zone increases, the chances increase that it is no longer located in such a homogeneous stress field. This also might result in the formation of different structural geometries in different parts of the ramp.

Whether the last process of a varying regional stress field really had an influence on the architecture of the Zavarotny relay ramp is unclear. An influence of pre-existing structures on the other hand can be inferred from the angle between the first connecting fault and the main faults in Zavarotny. This angle is 10–15° and is much smaller than angles reported from other studies (typically ∼45–60°). Another indication for the reactivation of pre-existing structures in Zavarotny is that the connecting fault appears to have a well-defined single fault trace. This is in contrast with many other breaching faults that are irregular, and that result from the connection of different clusters of secondary faults within a relay ramp. It is important to re-emphasise that the first order geometry of relay ramps (length to width ratio) was found to be invariant of scale (Peacock, 2003). The relay ramp in Zavarotny has a length to width ratio of 4, which is very common. Therefore, the reactivation of the Baikalsky fault segments has had no influence on the first order shape of the relay ramp.

As a result of the observations mentioned above, it was concluded that large scale relay ramps are likely to be structurally different from smaller scale examples. In chapter 5 another observation was made that can cause very large relay ramps to have different internal structures. As observed in the Pri-Ol'khon Block, it is possible that for large relay ramps, the main faults themselves grew by the connection of different smaller fault segments. This growth process can cause the presence of transverse ridge structures and different depocentres within the relay ramp, and as such it creates an additional deformation, which can further complicate the more "normal" internal deformation that is associated with smaller relay ramps of which the main faults grow by a lateral propagation process. The transverse ridges on their turn can be bordered by so-called release faults. This are faults which are formed as a result of the increase in length of hanging-wall by bending or flexure along the strike of a normal fault (Destro, 1995). Release faults are characterised by mainly normal movement, and are oriented at high angle to the main fault.

It should be stressed here that — as mentioned in chapter 2 — fault growth by segment linkage is a process which is also observed on small scales, and that as such the "transverse ridge" and "depression" morphology might be observed in smaller ramps as well. The relation between fault length and fault displacement (equation 2.12; $D = c \times L^n$ with $1 \leq n < 2$), however, shows that the morphology is expected to be relatively better expressed for large faults compared to smaller faults ($n \geq 1$). This could explain why the observation has never been reported on a smaller scale. Another requirement to observe this morphology, be it for small or large relay ramps, is that the different segments of the faults need to have a length that is

comparable to the width of the relay ramp. If not, the area that is affected by the depressions and ridges would be too small compared to the surface area of the ramp.

Another possibility for the scale dependence of very wide relay ramps (width > 100 km) has been suggested by Peacock et al. (2000b) who mentioned the possibility that large basin margin faults might be connected by a shallow dipping detachment fault (see also Larsen, 1988) or shear zone which transfers the strain between both faults, or that they are physically unconnected, but pass downward into the lower crust in a zone of distributed ductile extension.

What the exact effect of these processes is on the internal structure of relay ramps is at this stage not clear, however, it has been found that large relay ramps mostly dip towards their footwall fault (e.g. Maloe More and examples in Larsen (1988) and Peacock et al. (2000b)), whereas smaller ramps are usually tilted towards their hanging-wall fault (e.g. Peacock and Sanderson, 1991; Childs et al., 1995).

8.1.2 Breaching of relay ramps

An important conclusion reached in chapter 4 has been that the Zavarotny Relay Ramp continued to deform after a hard-linkage connection was established. This continuing deformation has been inferred from the development of the new connecting fault, and the young morphology inside the ramp. In chapter 4 it was suggested that a new ramp structure might have formed between the first connecting fault and the hanging-wall fault, and that as such the strain transfer in Zavarotny occurred through a combination of soft-linkage and hard-linkage displacement transfer. This post-breaching deformation in the ramp was explained in chapter 4 as being likely related to the breaching mode. Indeed one might expect that initially a developing (small) connecting fault is not capable of transferring all displacement between two major faults. The models from chapter 6, and the explained example in chapter 7, however, show that such a post-breaching evolution may occur for the other breaching modes as well, and that it appears to be a common process. Recently similar observations were made in the evolution of smaller ramps (Soliva and Benedicto, 2004), and in relay ramps simulated by 3D distinct element models (Imber et al., 2004). These studies concluded that relay ramp evolution only stops when the faults are fully hard-linked in 3 dimensions. The models in chapter 6, however, have shown that a "relay ramp geometry" might evolve from a continuous fault as well, which in fact implies that fault connection in 3D will not necessarily cause a cessation of the relay ramp evolution. From these observations a post-breaching evolution stage has been added to the classical evolution stages of a relay ramp (see chapter 2). Therefore, relay ramp evolution can be described in basically 5 stages:

Stage 1: Subparallel offset faults are isolated and do not interact.

Stage 2: A relay ramp forms when the two faults have propagated to form an overlap zone. A tilted area forms between both faults.

Stage 3: Stresses inside the relay ramp cause the formation of secondary fractures inside the ramp.

Stage 4: The relay ramp is breached when the two, originally isolated faults, are connected by the propagation of one of the main faults towards the other, or by the development of a connecting fault.

Stage 5: A post-breaching evolution may start when the all displacement transfer is not established completely by the hard connection. This post-breaching evolution involves a slight continued propagation of the main faults, often after an initial decrease in fault propagation rate when the faults enter the overlap zone (see chapter 6).

8.1.3 Evolution of the central part of Lake Baikal

The study of the Pri-Ol'khon Block in chapter 5 has illustrated that the evolution of large relay zones can be a lengthy process, which in the case of the central part of Lake Baikal has been started early in the rift's evolution and still continues at present. Evidently the maturity of the Pri-Ol'khon Block is related to the overall tectonic activity in Lake Baikal, the slow deformation in the early evolution for example likely reflects the slow development during the first rifting stage of the Baikal Rift Zone (see figure 5.19).

The evolution model which has been proposed for the Pri-Ol'khon Block in chapter 5 differs from a previous model, but it is able to explain the observed ridge-like morphology in Maloe More, as well as the occurrence of old sedimentary deposits in isolated depressions, distributed in the area.

The new model implies that the Primorsky Fault has initially been reactivated in different small segments, and not as a single long fault. The displacement along these individual segments caused the formation of different depressions in Maloe More, which were separated by areas of less subsidence. These area's correspond to the transverse ridges. Only after a lateral propagation of the different segments in relation to a displacement increase, fault segments coalesced. This resulted in the expansion of the depressions, caused by an adjustment in the displacement profile of the composite fault. The apparently gradual recent subsidence in Maloe More is in this model explained by the sequence in which this fault coalescence occurred: first the segments in the north of Maloe More were connected, followed later by segments more to the south.

No indications have been found that after the connection of two major faults in Lake Baikal (the Primorsky and Ol'khon faults) a major subsidence occurred in the hanging-wall region of the fault (i.e. the Pri-Ol'khon Block and the central Baikal basin). Therefore, the hypothesis of ten Brink and Taylor (2002), in which they stated that the transition from the slow rifting to the fast rifting stage in the Baikal Rift Zone is caused by the connection of different faults and a subsequent readjustment of displacement profiles, rather than by a real intensification of the stress field, is not supported by data from the central part of the rift zone.

8.1.4 The creation of relay zones in Lake Baikal

In a second modelling study (chapter 7), an attempt has been made to simulate the border fault deflection and the formation of relay zones, which are observed in Lake Baikal. These models

tested the influence of pre-existing zones of weakness on the formation of a rift structure. In the models it has been observed that the outer rift faults mostly adopted the direction of the underlying base plates. Moreover, at locations in the model where the orientation of the base plates changed, often relay zones developed. This indicates a strong control of orientation changes in the strike of pre-existing zones of weakness, on the location of relay zones between rift border faults in nature.

A stronger correspondence between the models and Lake Baikal or the Baikal Rift Zone, however, has not been observed. The models failed to reproduce important characteristics of Lake Baikal, and as such they could not be used to come to better constraints on the evolution and formation of the different sub-basins in Lake Baikal, or the different accommodation zones in the lake. To achieve this, it might be necessary to introduce additional pre-existing structures in the models, or to introduce a multistage deformation process as has been proposed for the Baikal Rift Zone. Despite their lack of direct applicability to Lake Baikal, the models can give interesting insights in the mechanisms of faulting in other rifts, and although this topic is beyond the scope of the present thesis, it will be analysed in future.

8.2 Final Conclusions

The main aims of this work have been to unravel the architecture of relay zones between rift boundary faults and to determine their evolution path. It has, moreover, been tried to evaluate the role of the relay zones in the rifting process. Additional insights have been gained through a modelling study, where the structural evolution of relay ramps has been observed in real time, in a controlled environment where the geometry of two main faults was systematically varied. Another modelling study has aimed to determine whether the presence of pre-existing zones of weakness could be responsible for the observed deflection of the border faults of Lake Baikal, and if this deflection results in the formation of relay zones between the different segments.

Determining the internal structure of large relay zones has been possible through a multi-disciplinary investigation of two natural examples from Lake Baikal.

8.2.1 Overview of the different conclusions

The relay ramp in Zavarotny

It has been possible to determine the internal structure of a large-scale relay ramp between two boundary faults of Lake Baikal. This study has highlighted the complex nature of such large relay ramps, and it has demonstrated that the evolution of large-scale relay ramps is likely influenced or controlled by more factors than the evolution of small-scale examples.

- Large-scale relay ramps between major border faults can have a considerably different structure than examples on a smaller scale. An unusual observation in Zavarotny includes the occurrence of secondary faulting in the relay ramp, with fault strikes almost parallel to the main faults, in combination with a breaching of the ramp by a newly developed fault.

- The angle between the connecting fault, and the main faults in Zavarotny is much lower than in other examples of relay ramps that are breached by a connecting fault. This suggests the reactivation of preferential basement structures
- Indications have been found for a continuing evolution of the relay ramp in Zavarotny after its breaching. The displacement transfer in Zavarotny is accomplished by a combination of hard linkage and soft linkage processes.

The study of the Pri-Ol'khon Block

A new model has been proposed for the evolution of the Pri-Ol'khon Block, which is a large tilted block between two boundary faults in Lake Baikal. The model is able to describe the following (new) observations:

- It explains the occurrence of different isolated depocentres of old sedimentary units throughout Maloe More.
- It explains the occurrence of most of the observed transverse basement ridges that have been recognised in Maloe More.

In the new model, the reactivation of the Primorsky Fault comprised an initial stage in which different segments of the fault evolved as seemingly isolated structures (at least near the surface), which propagated laterally with increasing extension. The basement depressions corresponded with the centres of these fault segments, whereas the transverse basement ridges were located between the ends of the segments. Only in a later stage, these different segments started to link-up, and this caused the gradual submergence of the transverse ridges as a result of the adjustment of the displacement profile of the composite fault.

Sandbox models of relay ramps

This work has presented a first set of analogue sandbox models of relay ramps, in which overlap zones were created between faults with a controlled geometry. The influence of this geometry on the subsequent evolution of the ramps has been tested.

- Silicone bars are well suited to initiate normal faulting at precise locations in sandbox models.
- Fault interaction between overlapping faults has only been observed if the total length of the fault system was larger than 8 times the spacing between the faults.
- The ratio between the length and the width of the experimental overlap zones clustered around 3.
- The three common ways of relay ramp breaching that occur in nature have been observed in the experiments. Hanging-wall fault to footwall fault propagation was the most common breaching style in the experiments, followed by footwall fault to hanging-wall fault

propagation. The least common mode has been breaching by the development of a new connecting fault in the ramp. This mode has only been observed in case the spacing between both main faults was small.

- In the models also indications have been found for a continuing evolution of the overlap zone after breaching. Therefore a *post-breaching stage* has been added to the different evolution stages of a relay ramp.

This modelling study has allowed to observe the real time evolution of relay ramps. It has demonstrated that this evolution might be more complex than has been inferred so far from "static" natural examples.

Sandbox models of Lake Baikal

The sandbox models of Lake Baikal have demonstrated that relay zones often occur at the locations where the orientation of the base-plates changes. This reflects a strong control of pre-existing structures on the location of intrabasinal transfer zones between major boundary faults at the same side of a rift in nature.

A final conclusion which should be mentioned is that every research technique that has been applied in this study has contributed to the understanding of the structural evolution of the relay zones in Lake Baikal. Using the observations from natural structures, boundary conditions could be defined to first start and later evaluate a modelling study. Such a multidisciplinary approach, combining observations from nature and investigations from modelling might be necessary to tackle similar problems in future.

8.2.2 Future work

Although the amount of research that focused upon the growth and evolution of normal fault systems has increased considerably the last decade, there are still several unanswered questions. In the field of the present work, an important topic that requires further attention is how the fault growth process is influenced by the 3D geometry of the fault system. For example, does the internal structure of a relay zone change when the faults are connected at depth in a single fault or in a common detachment fault? Also little is known about the timing of the different stages in normal fault evolution.

The following questions for example remain largely unanswered like:

- How long does the fault linkage process take in nature, and how does this linkage relate to the 3D geometry of the fault system?
- When does the displacement readjustment occur (i.e. before or after the fault connection), and how long does it take to be accomplished? What influences this timing?

Also the use of more accurate analysing tools could considerably enlarge the usefulness of scaled models. In relay ramp models for example, accurate laser scans of the surface morphology might reveal slight variations in fault displacement along the fault traces, or they could be used to follow the tilting and bending of the surface layer in the model in relation to the propagation of the main faults. On a larger scale, possibly also a rift climax stage can be observed in analogue models in relation to the linkage of faults, as has been demonstrated in numerical models (e.g. Gupta et al., 1998).

It would also be useful to investigate in a systematic way the influence of a pervasive basement fabric on the internal structure of relay ramps. The introduction of such a fabric in scaled analogue models, however, is not too straightforward (e.g. Morley, 1999c).

Finally it would be interested to analyse the presented rift models in more detail. Mapping for example the displacement variations on the faults in relation to nearby faults or in relation to intersection with other faults, or comparing fault orientations in modelled accommodation zones with natural ones can provide further insight in the intriguing complexity of fault interaction.

Appendix A

Overlap to spacing data of natural normal fault systems

In this appendix a compilation is included of the geometries of several overlap zones between normal faults in nature. The table is mainly based on measurements of overlap zone dimensions on published maps, completed with field measured data if available.

Similar tables have been published for overlap zones between strike-slip faults by for example Aydin and Nur (1982), Aydin and Schultz (1990) and An (1997).

Area	Location	Geometry (m)		BT[1]	Reference
		Overlap	Spacing	(m)	
Canyonlands, Utah	SOB Hill relay zone	360	120	N	Trudgill and Cartwright (1994)
		360	140	N	
	Twin Valleys region	100	66.67		
Greenland	Hold With Hope	250000	100000		Peacock et al. (2000b)
North Sea Rift	Moray Firth	58536	29268		Morley et al. (1990)
	Argyll and Auk Fields	24390	12195		
	Argyll field	9600	4000		
Northeast Idaho	Beaverhead fault	16666	4583	F	Anders and Schlische (1994)
Newark Basin		14444	7777	N	
Hawaii	Kilauea Volcano	1034	689	N	Peacock and Parfitt (2002)
		1379	603	C	
Atalanti		1666	1666	N	Gawthorpe and Hurst (1993)
Northern North Sea	Strathspey-Brent-Statfjord	2941	1470	F	McLeod et al. (2000)
		1666	1111	F	
		3333	2222	F	
		122	44.44	F	Walsh et al. (1999)
		1200	250	B	
		1333	111	N	
Kenia	Lokichar Fault	4210	3684	F	Morley (2002)
Cumbria, England		34.72	8.33	N	Barnett et al. (1987)
Lancashire	Nook Colliery	40.00	20.00	F	Walsh et al. (2003)Walsh et al. (2003)
Kilve, Somerset		0.90	0.15	C	Peacock and Sanderson (1994)
		0.75	0.08	N	
		0.27	0.03	F	
		0.90	0.26	F	
Watchet		0.64	0.14	B	

Area	Location	Geometry (m)		BT[1]	Reference
		Overlap	Spacing	(m)	
Central Graben	Olaf Fault	5454	3333	N	Cartwright (1991)
Central Graben	Gorm Fault Zone	1818	2424	N	
	Coffee Soil Fault	2424	1212	F	
Feda Graben		1818	1515	N	
North Gulf of Evvia		2083	1250	N	Roberts and Jackson (1991)
Gulf of Corinth		2500	833	N	
		1666	833	N	
		5416	1666	N	
Aegean Region	Lastros fault zone	263	200	C?	Stewart and Hancock (1991)
Aegean Region	Yavansu fault zone	242	136	H	
Abruzzo	Fiamignano fault	17727	9545	N	Cowie and ROberts (2001)
Abruzzo		27272	8181	N	
Abruzzo		13636	7500	N	
Karstryggen	Marcusdal Ramp	5294	4411	N	Larsen (1988)
South Yorkshire	Rockingham Colliery	52.63	105	N	Huggins et al. (1995)
Derbyshire	Glapwell Colliery	44.44	22.22	N	Huggins et al. (1995)
South Yorkshire	Denaby Main Colliery	14.71	11.76	N	
South Yorkshire	Silverwood Colliery	130	16.00	N	
Northumberland	Daisyhill coal site	166	72.22	N	
North Debryshire	Markham Colliery	194	41.18	N	
Central North Sea		642	164	N	Childs et al. (1995)
Northern North Sea		1043	565	F	

[1] Breaching Type: N = no breaching; C = connecting fault; H = Hangingwall fault to footwall fault propagation; F = Footwall fault to hanging-wall fault propagation; B = Both faults propagated towards each other.

Appendix B

Geometry of the base plates used for the modelling

This appendix includes detailed illustrations of the base plates that were used during the different modelling experiments of Lake Baikal. As described in the set-up section 7.3 on page 220, both base plates were connected by a rubber sheet with an initial width of either 5 or 10 centimetres, depending on the experiments.

The metal plates were first cleaned with LOCTITE *7070* cleaner and LOCTITE *770* polyolefin primer after which the rubber sheets were glued to them with LOCTITE *480* instant adhesive.

The rubber sheet was pre-stretched for 0.7 to 1.5 cm (depending on the starting width), before the edges were cut off. Only after that stage the sand layers were added. This procedure minimizes the contraction of the rubber sheet in a direction perpendicular to the direction of extension.

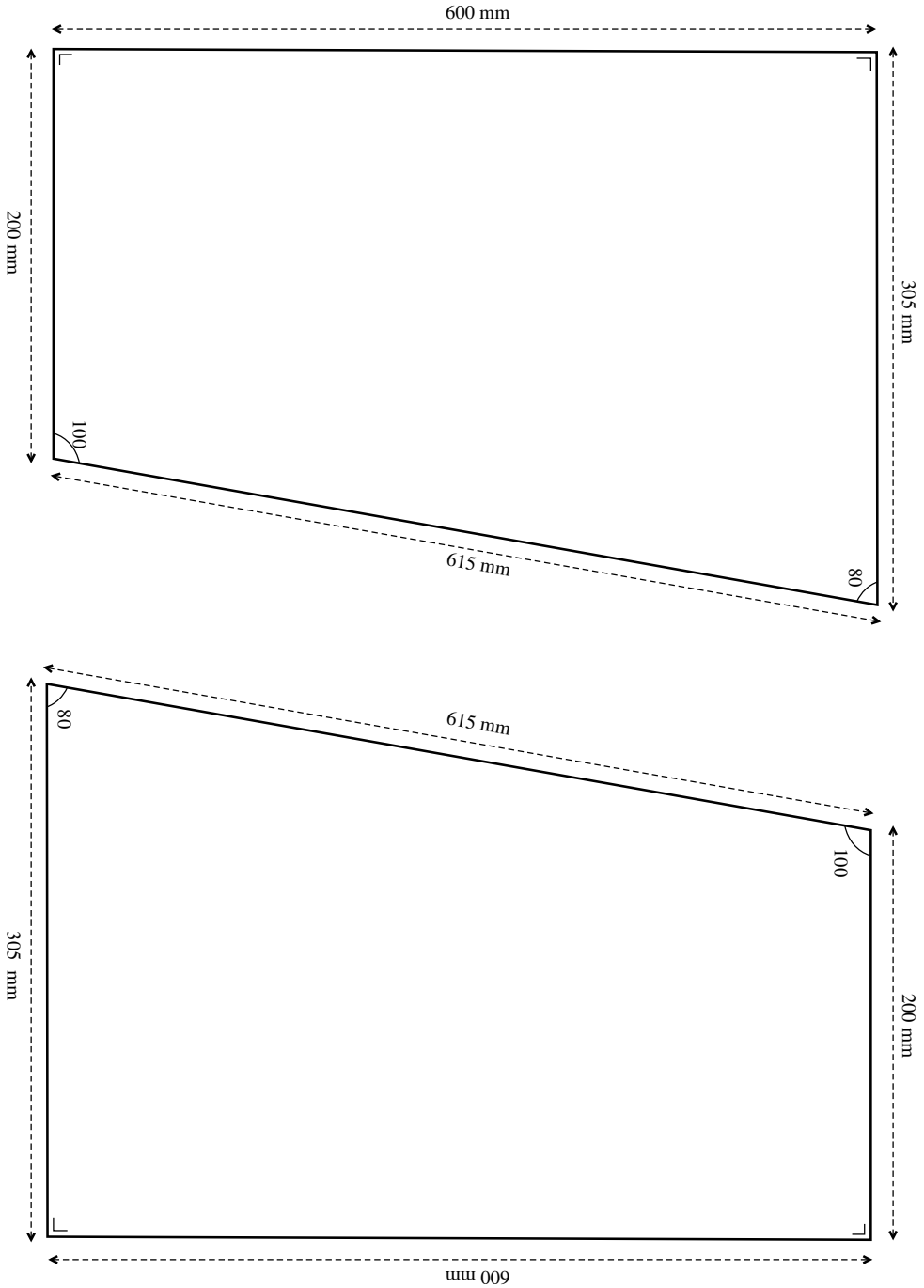

Figure B.1: *Baseplate geometry of Type 1 experiments. These experiments were meant as reference experiments.*

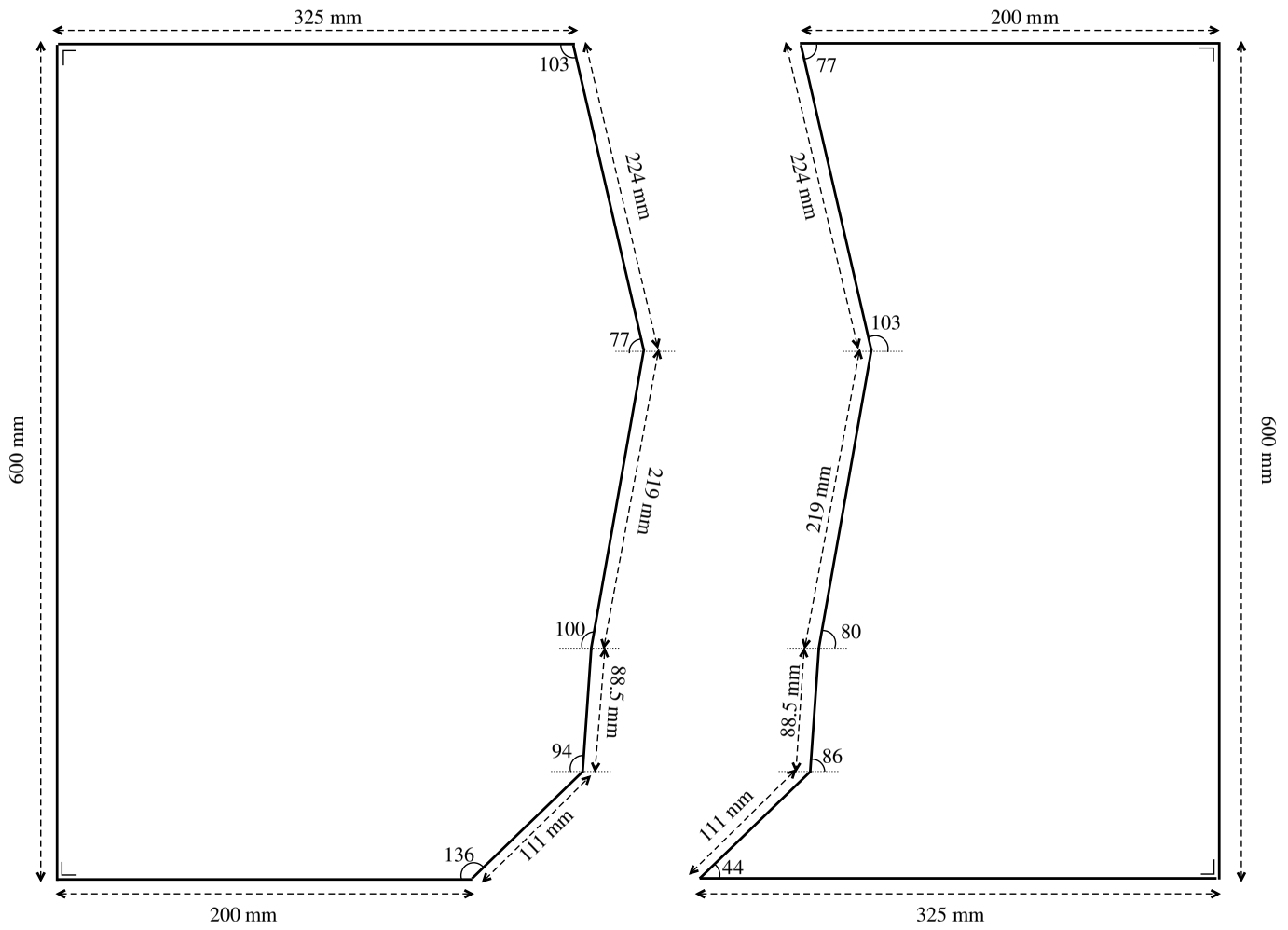

Figure B.2: *Baseplate geometry of* `Type 2` *experiments. The baseplate mimics the shape of Lake Baikal, and was used to test the influence of pre-existing structural trends in the area on subsequent rifting.*

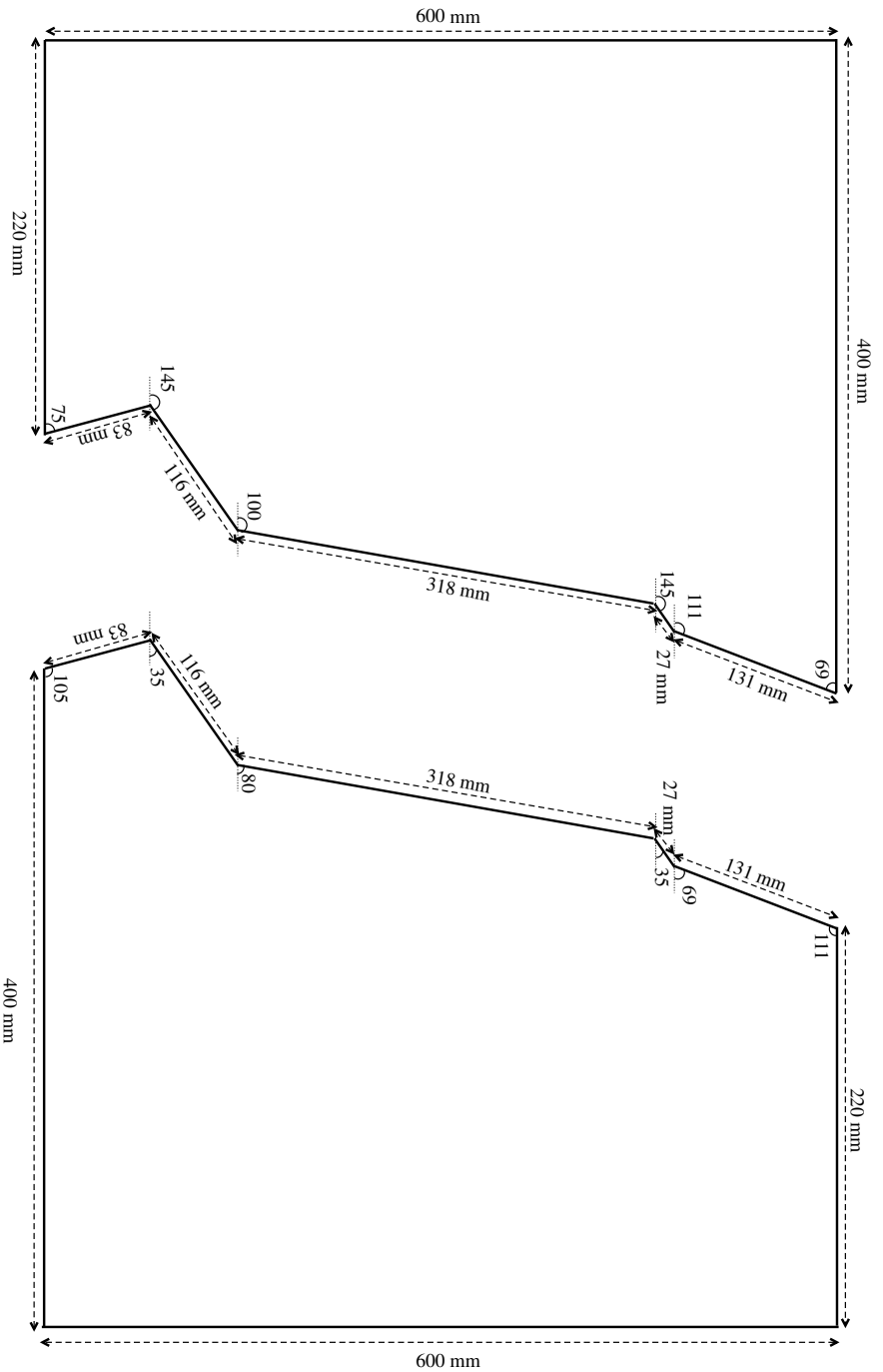

Figure B.3: *Baseplate geometry of* Type 3 *experiments. These experiments were meant as reference experiments for simulations of the Baikal Rift Zone. It includes the positions and orientations of the Khubsugul basin and the Angara basin.*

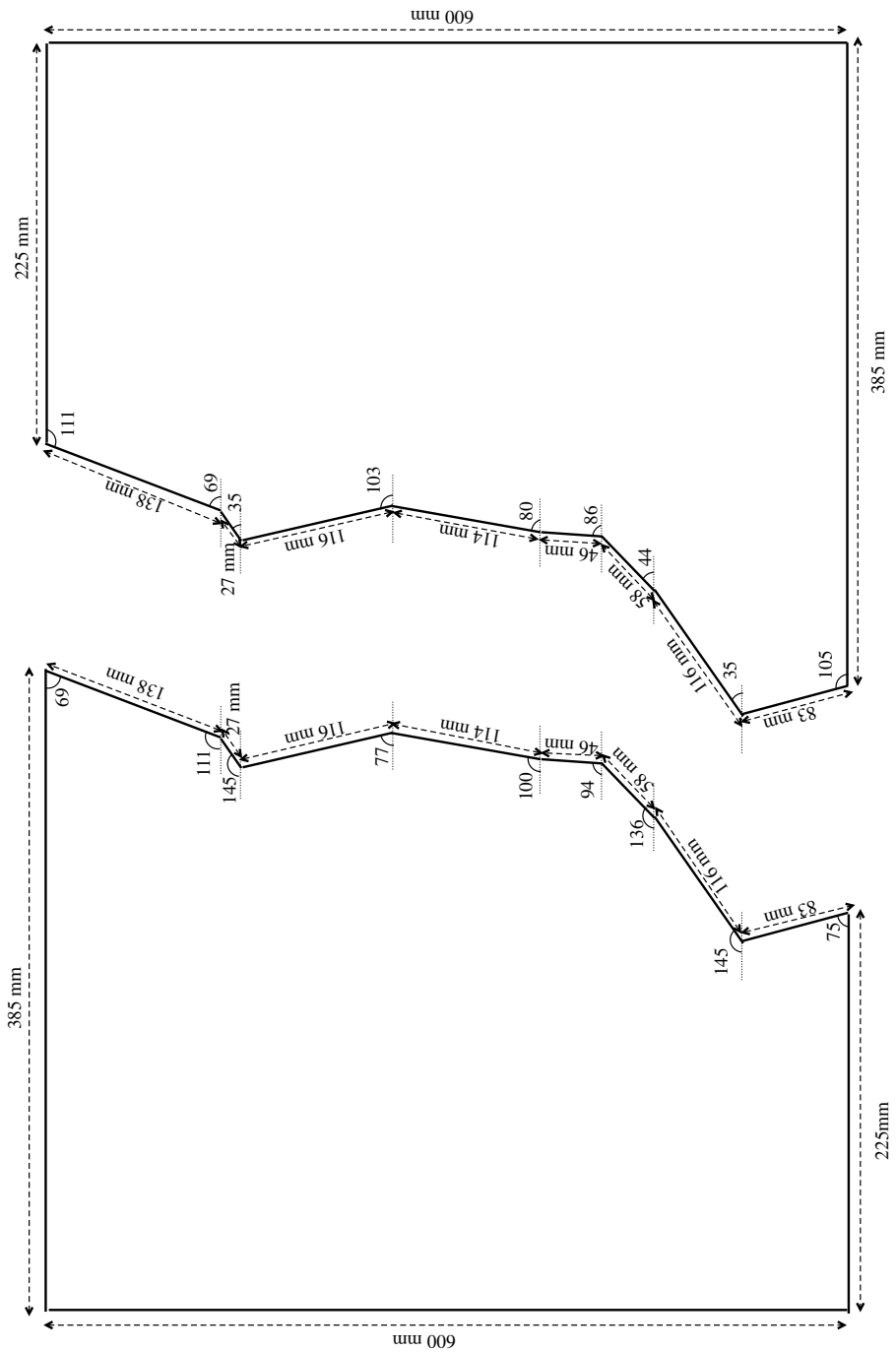

Figure B.4: *Baseplate geometry of* **Type 4** *experiments. This base-plate includes the shape of Lake Baikal together with the positions of the Khubsugul and Angara basins in the Baikal Rift Zone.*

Appendix C

2D models of asymmetric rifts

This appendix contains the description of 2 orthogonal asymmetric rift models that were run in a 2D deformation rig (figure C.1). Such rigs allow for the visualisation of the evolution of the cross-sections of a model. The models were run and interpreted in Royal Holloway University of London, together with Soledad Anadon Ruiz.

C.1 Asymmetric rift model 1

C.1.1 Characteristics

The first rift model has the following set-up characteristics:

- dimensions: 40cm $\times$ 25cm,
- 10cm wide rubber sheet in the centre of the model,
- 5cm of pre-kinematic layers. A total of 10 layers all being 0.5cm thick. From base to top the colours used were: white – blue – white – blue – white – black – white – blue.

The model was extended for 10cm with a picture taken every 2.5mm of extension. Syn-kinematic layers of sand were added after every centimetre of extension. With the first layer added after 2 centimetre (red layer).

C.1.2 Description

The following table summarises the observations that were made during the model's run.

Extension	Observations
1–2cm	The first surface expressions of faulting develop in the central part of the model, related to a gentle bending of the layers. As extension progresses, the rift gets broader. The first border fault develops in the margin close to the mobile end of the model at 1.75 cm of extension. It's soon followed by the formation of a conjugated fault in an inner position to the rift.
2–3cm	A new conjugated fault develops right below the central part of the syn-rift basin. At 2.75 cm of extension the first border faults appear in the margin close to the fixed wall of the model. At 3 cm of extension an antithetic fault develops related to the one in the middle of the rift.
3-4cm	The previous faults continue to grow. At 3.75 cm of extension a fault begins to form in the footwall of the middle-rift fault, and it propagates upwards.
4cm	See figure C.2. The activity is focused in the central part of the rift. The fault developed in the footwall of the middle-rift fault has propagated upwards through it, and new ones are now starting to form. An antithetic fault develops in relation to an inner fault dipping towards the mobile wall.
4–7cm	Extension continues taking place through the already existing faults. A second fault developed in the footwall of the middle-rift fault has propagated upwards through it, and the first one starts to displace it. At 5.5 cm of extension this second fault begins also to displace the middle-rift fault. A new conjugated fault develops in the margin close to the mobile end of the model at 6.5 cm of extension.
7–10cm	At 7 cm of extension a fault starts to develop in the side of the central graben close to the fixed wall of the model. It nucleates in the syn-kinematic layers, on the contrary than the previous faults. At 7.75 cm of extension one fault developed in the footwall of the middle-rift fault, which has propagated upwards through it, becomes one boundary of the central graben. The same process takes place at 9.5 cm of extension when another fault becomes the limit of the central graben on the side of the fixed wall of the model as the result of the reactivation of an older one.
10cm	See figure C.3. Final amount of extension reached. Figure C.3 corresponds to a slice along the internal part of the model. The described structural evolution doesn't fit well with the final morphology that can be observed in figure C.3. There is a notable difference between this and the final stage observed in the glass wall (figure C.4).

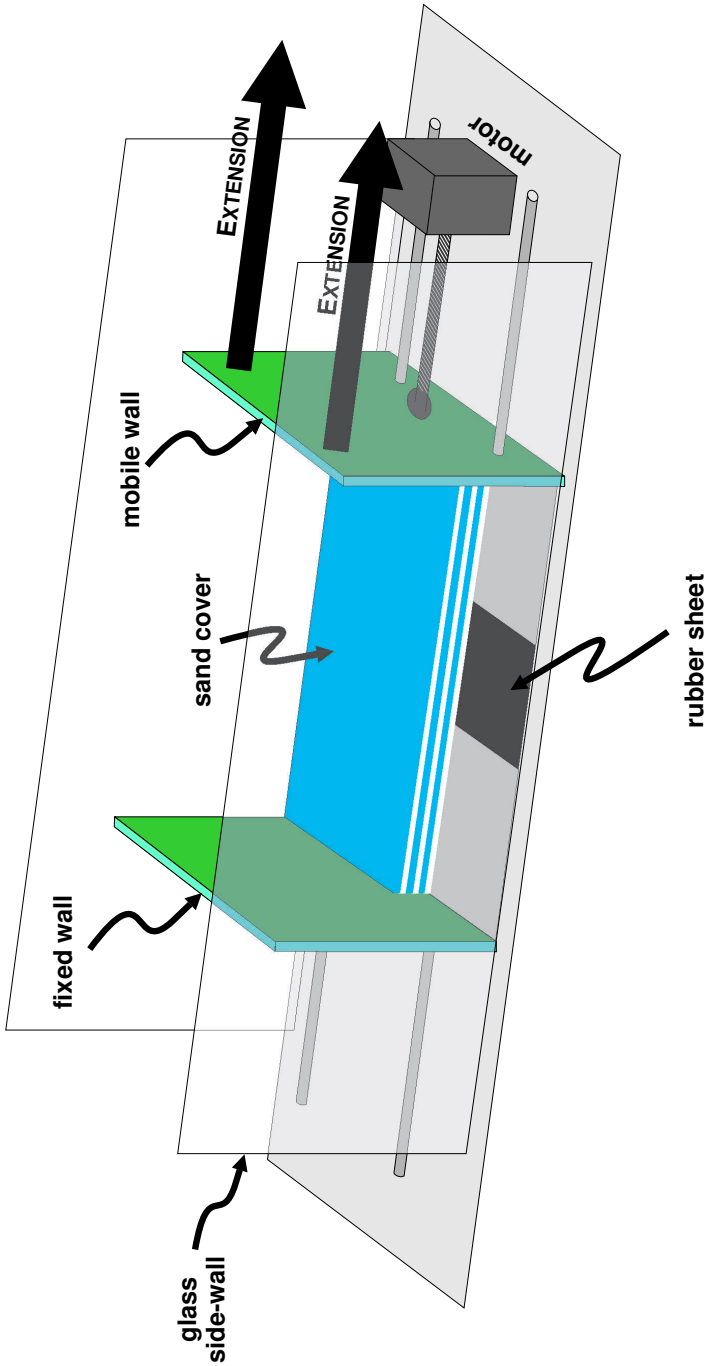

Figure C.1: *Schematic representation of the 2D rig that was used for the rift models in this appendix*

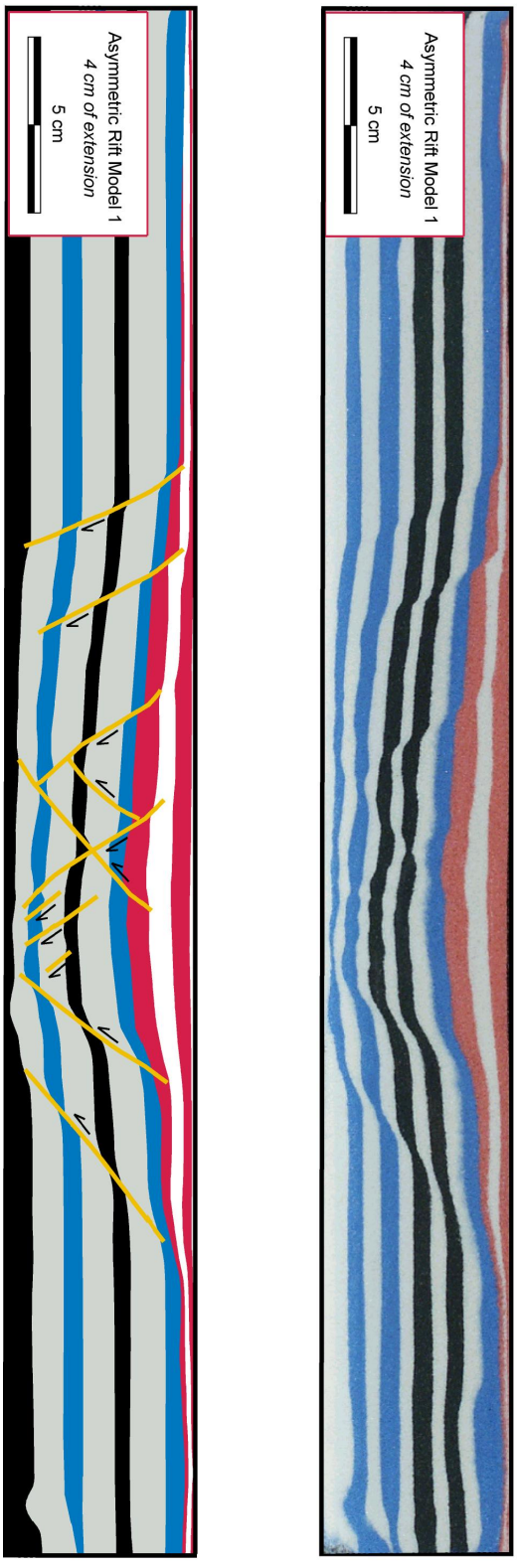

Figure C.2: *Original photograph and interpreted section of Asymmetric Rift Model 1 after 4cm of extension. The main boundary faults have formed.*

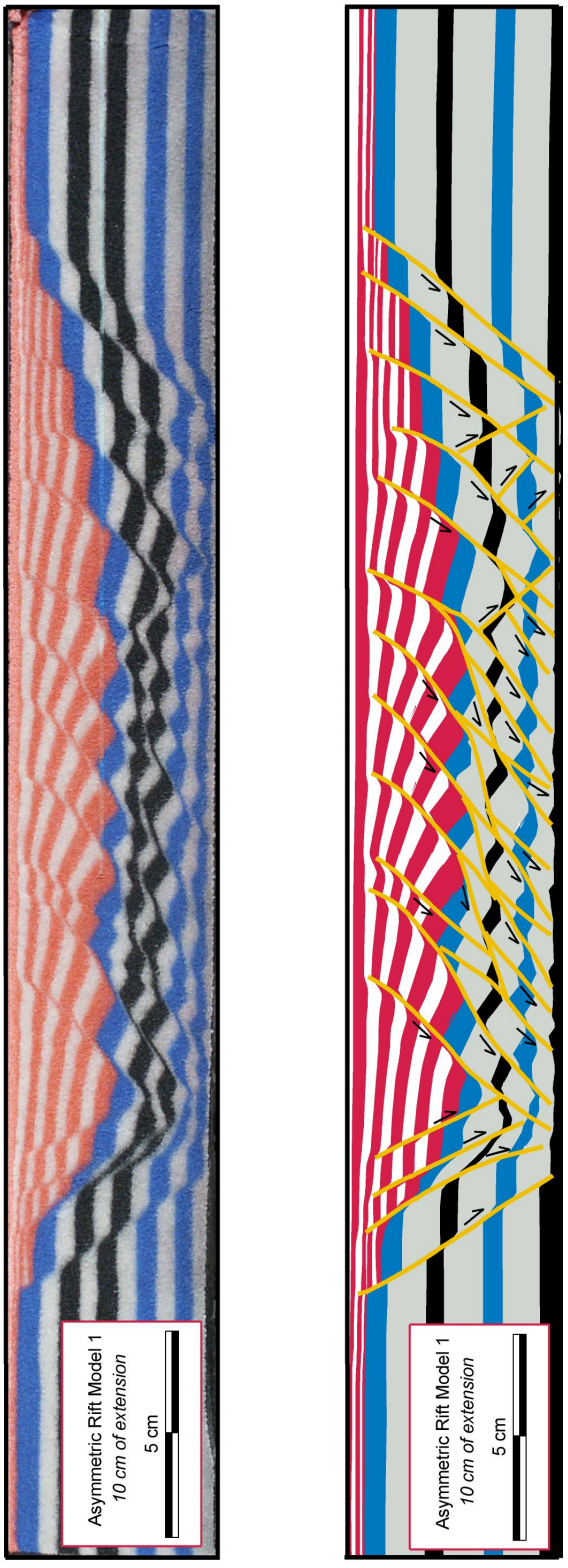

Figure C.3: *Original photograph and interpreted section of Asymmetric Rift Model 2 after 10cm of extension. This cross-section was taken in the middle of the model.*

Figure C.4: *Digital photograph of the model after 10cm of extension. This picture is the last running shot, and corresponds to the model slice near the glass wall.*

C.2 Asymmetric rift model 2

C.2.1 Characteristics

The second rift model has the following set-up characteristics:

- dimensions: 40cm × 25cm,
- 10cm wide rubber sheet in the centre of the model,
- 10cm of pre-kinematic layers. A total of 20 layers all being 0.5cm thick. From base to top the colours used were: white – blue – white – black – white – blue – white – black – white – blue – white – black – white – blue – white – black – white – blue – white – blue.

The model was extended for 10cm with a picture taken every 2.5mm of extension. Syn-kinematic layers of sand were added after every centimetre of extension. With the first layer added after 2 centimetre (red layer).

C.2.2 Description

The following table summarises the observations that were made during the model's run.

Extension	Observations
1–2cm	First border fault forms at the side of the mobile wall. Immediately followed by the formation of a big antithetic fault (at 1.25cm of extension). There is not yet any sign of the boundary faults at the fixed wall in cross-section, however a flexural bending of the layers could be observed at 1.75cm of extension. At this amount of extension also a new fault forms at the mobile wall, conjugate to the first antithetic fault.
2–3cm	The last fault that forms clearly consists of two segments that overlap in cross-section (eg. figure C.5). Also a new boundary fault starts to form in the footwall of the first one (ie. closer to the mobile wall). At 2.5cm of extension, the first signs of the fixed wall faults show up in cross section. A total of six faults form near that side. They all dip towards the mobile plate. At 3.0 cm of extension antithetic faults form to these ones.

continued on the next page...

...continued from the previous page	
3–4cm	The central depression of the rift is till located between the first "antithetic fault" and its conjugate, although at this stage new faults start to form in this central depression.
4cm	See figure C.5 The model has clearly evolved enough to observe the main boundary faults on both sides of the rift system. The central part of the rift is still located where the first faults formed. On both sides, faults have grown in the footwall of previous ones.
4–7cm	New extension is accommodated by increasing displacements on the faults that already existed in the model. Only at 6cm of extension new faults form in the central part of the rift.
8–9 cm	New faults form in the central depression as well as just outside near the fixed wall side. The latter dips antithetically to the main faults here. At 9 cm the fixed wall the fault geometry near the fixed wall side becomes complicated due to a series of antithetic faults, that slightly displace the main faults that formed earlier. At the same time the mobile wall fault system remains relatively simple. This process continues up to the final amount of extension.
10cm	See figure C.6 Final amount of extension reached. This interpreted section corresponds to a slice half-way in the model. Compared to the 10cm-shot during the models run (figure C.7) there is a remarkable difference between the two.

C.3 Discussion

When we look to the interpreted 10cm sections of the two asymmetric rift models (figure C.3 and C.6), it seems that the direction of asymmetry is different in both models. Model 1 (ARM-1) has clear steep closely spaced boundary faults at its western side, directly delimiting what seems to be the biggest depocentre in the model. The eastern side corresponds to a series of more than 10 parallel faults, that rotated during extension in a clockwise direction. Especially in the central part of the rift this rotation resulted in low-angle normal faults in the pre-rift layers, adopting a more listric profile in the syn-kinematic "deposits".

On the contrary the Model 2 (ARM-2) does not show this contrast. Here a series of closely spaced parallel faults borders the rift on the eastern side, with the main depocentre lying on this side of the rift. Throughout the whole model faults occur that dip in both directions (east and west) as well in the pre- as in the syn-kinematic layers. The listric shape of the faults — as described for ARM-1 — is not as obvious in ARM-2.

The fact that the listric fault profiles in ARM-1 are only observed in the syn-kinematic infill on a set of parallel faults, suggests that they result from a domino-style of deformation. The

already formed faults would become more and more tilted, but they would cut in the newly added undeformed syn-kinematic sand layers with a constant dip angle ($\approx 60°$). Further extension of the model would therefore result in rotation of the fault last syn-kinematic sand layer as well, slightly changing the fault's dip angle here compared to the dip angle in the new syn-kinematic layer that is to be added. This process results therefore in fault profiles that become gradually more listric with continuing extension and syn-kinematic "sedimentation" (eg. Vendeville and Cobbold, 1988). We do not know whether the absence of the "listric" faults in ARM-2 therefore means that there was no domino-style faulting there during the extension of the model.

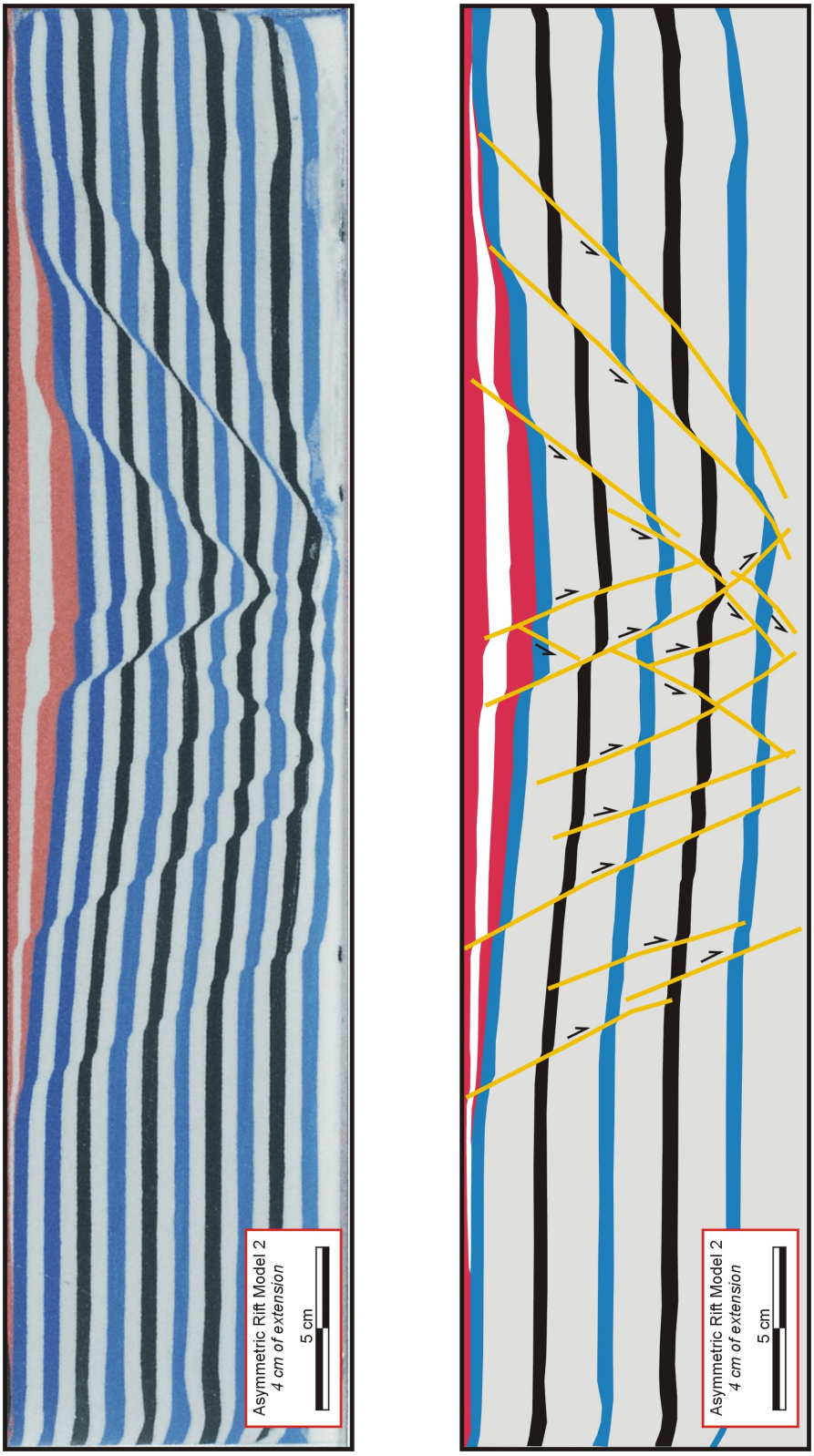

Figure C.5: *Original photograph and interpreted section of Asymmetric Rift Model 2 after 4cm of extension. The main boundary faults have formed.*

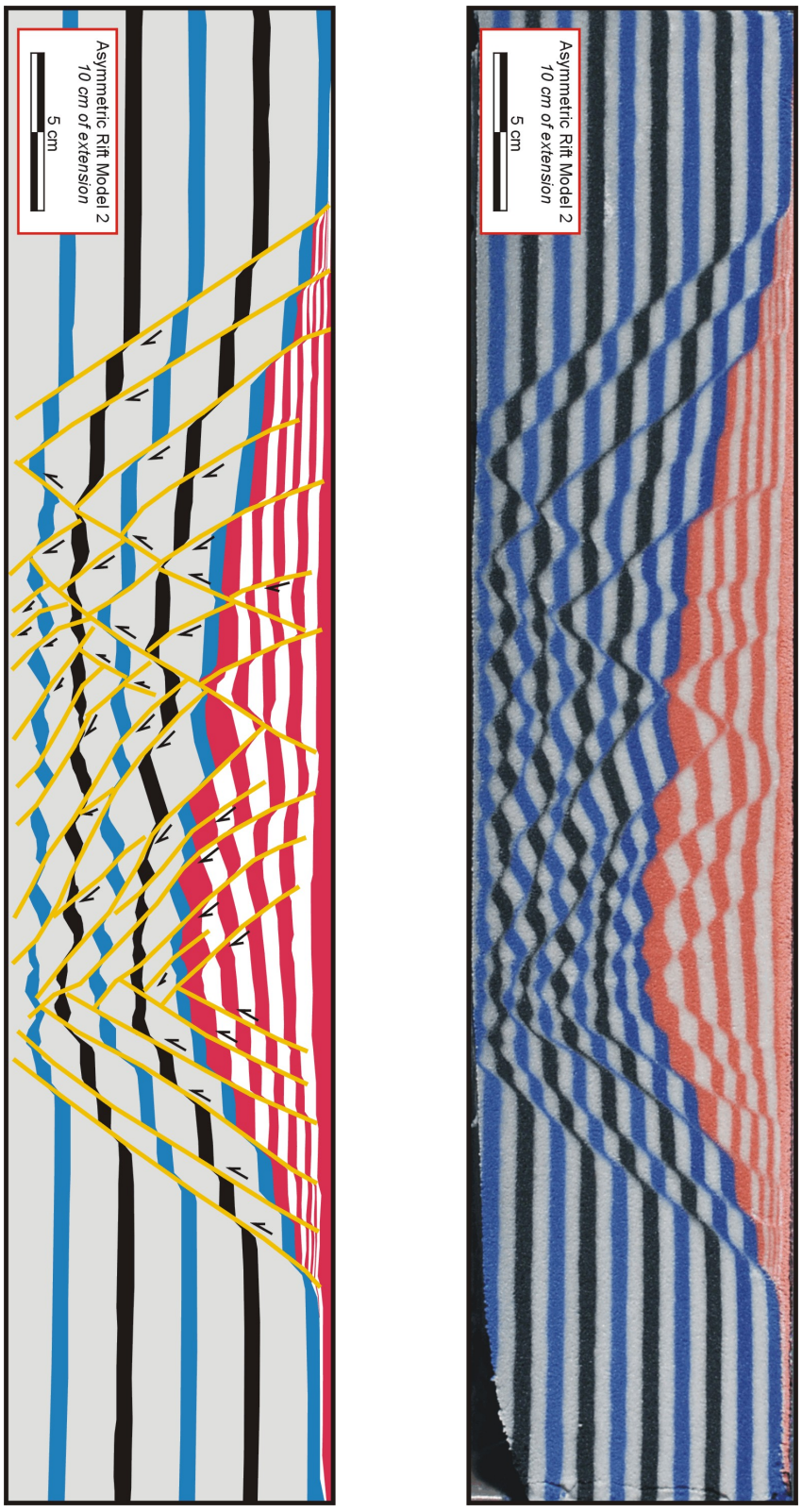

Figure C.6: *Original photograph and interpreted section of Asymmetric Rift Model 2 after 10cm of extension. This cross-section was taken in the middle of the model.*

Figure C.7: *Photograph of model 2 after 10cm of extension. This picture is the last running shot, and corresponds to the model slice near the glass wall.*

Appendix D

Constructing 3D surface views of sectioned analogue models in SURFER

D.1 Introduction

In SURFER the possibility exists to open a *base map* which can be any standard image processing format like for example jpeg, tiff, bmp, etc... or a vectorial format like dxf, shp, wmf, etc... Opening a base map is done in the map-tab in the main menu of SURFER .

When a bitmap image is opened as a base map, it is not geo-referenced. The "coordinates" of the map are derived from the pixels in the bitmap file. Geo-referencing the map by defining coordinates for the corners of the image is possible, but is for this purpose not necessary. Unless not all sections are taken from the same position and with the same zooming.

D.2 Digitising the sections

If we consider all sections being photographed in exactly the same position, we can use the image's pixels as "coordinates" for the final 3D image. Therefore by just digitising in SURFER a level on a certain section one gets 2D-data for that section. In the final 3D image this data would consist of an X-position and a height value (Z-value). To be able to construct an actual 3D image, a Y-value should be added to the data later (see next section).

Digitising a section in SURFER is done by opening the section as a base map, then select it and in the map-tab choose the option *digitize*. Every mouse click will from that moment on produce a coordinate pair in a separate window. After having digitised the desired level, the window can be saved in a file and closed. To automate the addition of a Y-value to the data, I suggest you use the name `sectionxx.dat` with xx being the number of the section for example 01 or 15.

D.3 Adding an Y-value

As every section is a straight line in the original model, adding the 3rd coordinate consists of adding a constant value as the y-coordinate for every digitised point of thea certain section. The value of this Y-coordinate depends on the number of the section (being the depth of the section in the model).

As all data points are digitised using pixels as unit values, also the y-coordinate should be included as "pixels". If for example the spacing between 2 sections is 1cm, the difference between the y-values of the 2 different section is let's say 35pixels. The exact value can be calculated by digitising the end of the photographed scale bar on the section and the beginning and making the difference between the two x-values.

If all subsequent digitised sections were saved as a file `sectionxx.dat`, the xx contains information on how far the section was located in the model and therefore on what value should be added as a y-value. For example a simple AWK-script can automatically evaluate the value of XX and add a column containing the appropriate Y-value to the file (free versions of Gnu-AWK are available on the internet[1]):

```
BEGIN { FS = ","}


NF > 0 { split(FILENAME,ARR,".")
      slice = substr(ARR[1],8,2)
      printf("%.2f\t%.2f\t%.3f\n",-$1,slice*35,-$2) }
```

The 35 in `slice*35` in the script, is the factor to convert a section's depth in the model to pixel values.

By making a batch file, containing the command line argument to run this AWK-script on a section. The y-value can easily be added for all sections, and the output can be written in one common file containing 3D-data for the whole model. For example in DOS this batch-file would look like:

```
gawk-w32 -f script.awk section01.dat > surferlevel.dat
gawk-w32 -f script.awk section02.dat >> surferlevel.dat
gawk-w32 -f script.awk section03.dat >> surferlevel.dat
gawk-w32 -f script.awk section04.dat >> surferlevel.dat
 ⋮
gawk-w32 -f script.awk sectionXX.dat >> surferlevel.dat
```

[1] See `http://www.gnu.org/software/gawk/gawk.html` for the source code and a manual, and `http://www.ibiblio.org/pub/micro/pc-stuff/freedos/gnuish/gnuish.htm` for pre-compiled executables for most common oparating systems.

In this particular case, script.awk is the file in which the awk-script is written. Gawk-w32 is the WINDOWS executable for AWK. SectionXX.dat are the different digitised data-files, and surferlevel.dat is the final file containing all 3D-data.

D.4 Calculating the grid

In the SURFER menu under the Grid-tab is an option *data*. When selecting this, SURFER asks a file name containing data to calculate a grid (for example surferlevel.dat). In a next dialog, the properties of the grid can be chosen (eg. number of lines and columns, gridding algorithm etc...).

When the grid is calculated it can be visualised by selecting in the map-menu a desired map type (eg. 3D surface, contour, etc...). Every map type has its own properties that can be changed.

Uitgebreide Nederlandse samenvatting

1 Inleiding

In gebieden van extensie, in de bovenste delen van de aardkorst, wordt het begrip transferzone gebruikt om te verwijzen naar de complexe vervormingszones waarlangs bewegingsoverdracht gebeurt tussen verschillende breuken. Met de invoering van het begrip transferzone bij de interpretatie van riftsystemen (tijdens de jaren '80), werd een grote stap voorwaarts gemaakt. Vanaf dat moment beseften onderzoekers dat verschillende gebieden van een rift — soms met verschillende structurele kenmerken — toch met elkaar in verbinding konden staan en in feite één coherent dynamisch systeem konden vormen. Aangezien een regionale extensie nooit geconcentreerd wordt op één grote normaalbreuk, maar eerder verdeeld wordt over verschillende kleinere breuken, komen transferzones in zulke gebieden frequent voor.

Transferzones zijn zogenaamde *zachte verbindingsstructuren*, wat wil zeggen dat ze de beweginsoverdracht tussen breuken voltrekken zonder dat een goed-gedefinieerde (secundaire) breuk de breuken verbindt. Deze laatste vormt immers een *harde verbindingsstructuur* en wordt een transferbreuk genoemd (zie figuur 1.2).

Transferzones hebben een belangrijke invloed op verschillende geologische processen en verschijnselen, zoals: (a) het groeiproces van breuken, (b) de ontwikkeling van koolwaterstofreservoirs, (c) het sedimentatiepatroon langsheen breuken, alsook (d) het drainagenetwerk, (e) de ontwikkeling van tektonische bekkens en (f) de locatie van vulkanische activiteit. Dit verklaart het groot aantal recente studies waarin transferzones bestudeerd zijn.

1.1 Doelstellingen van het onderzoek

De bestaande studies van transferzones kunnen ruwweg ingedeeld worden in 2 categorieën. In een eerste categorie is vooral de detailstructuur van een bepaald type van transferzones zeer nauwkeurig bestudeerd, en dit aan de hand van kleinschalige (van kleiner dan een meter tot enkele 10-tallen meters) natuurlijke voorbeelden. De tweede categorie van studies daarentegen, omvat studies waarin grotere voorbeelden van transferzones onderzocht werden, maar waarbij nauwelijks naar de interne structuur is gekeken. In deze categorie van studies onderzocht men eerder de geometrie van de aangrenzende breuken en bekkens, en keek men naar hoe deze

geometrie door de transferzone beïnvloed werd.

Ondanks de recente aandacht die uitging naar transferzones, zijn er toch een aantal vragen die onbeantwoord bleven:

1. Wat is de interne structuur van grootschalige transferzones in riftbekkens, en hoe evolueren zulke grootschalige transferzones?

2. Is de interne structuur en evolutie van een grootschalige transferzone vergelijkbaar met die van een kleinschalige? En bestaat er aldus een onafhankelijkheid van de schaal?

3. Kunnen we bepalen hoe een initiële breukgeometrie het verder verloop van de transferzone-evolutie beïnvloedt? En wordt hun evolutie bepaald door de manier waarop het riftbekken evolueert?

Met dit werk is geprobeerd om de bovengenoemde vragen te helpen beantwoorden. Hiervoor werd de interne structuur van een aantal grootschalige transferzones uit de Baikal-Rift onderzocht, en werd getracht om een model te postuleren voor hun evolutie.

De bepaling van de structuur van de transferzones in dit werk is gebaseerd op de toepassing van verschillende onderzoekstechnieken zoals: analyse van hoge-resolutie reflectieseismische profielen, satellietbeeldinterpretatie en de interpretatie van digitale terreinmodellen. Waar mogelijk is een bijkomend onderzoek gebeurd aan de hand van experimentele simulaties van soortgelijke structuren in geschaalde zandbakmodellen.

1.2 Belang van het onderzoek

Door de specifieke locatie en eigenschappen van de transferzones in de Baikal-Rift, heeft deze studie kunnen genieten van een aantal belangrijke voordelen t.o.v. andere studies. Zo zijn de transferzones grootschalige voorbeelden, die al een zekere mate van evolutie ondergingen. Zij bevinden zich in het Baikal-Meer gedeeltelijk onder water, en gedeeltelijk op het land, waardoor het aantal aanwendbare onderzoeksmethoden vergroot werd. In tegenstelling tot veel andere grootschalige transferzones liggen de transferzones in het Baikal-Meer niet begraven onder kilometers dikke sedimentpaketten, waardoor ze bereikbaar blijven voor hoge-resolutie geofysische observatiemethoden. Gedurende het laatste decennium werden er op het Baikal-Meer verschillende expedities georganiseerd wat resulteerde in de beschikbaarheid van zéér uitgebreide data-sets. Bovendien hebben enkele van deze expedities zich volledig toegespitst op aan aantal van de verschillende transferzonegebieden.

1.3 Classificatie van transferzones

In de literatuur kan een groot aantal verschillende (Engelse) termen teruggevonden worden die allemaal betrekking hebben op transferzones of op bepaalde types van transferzones. De voor deze studie meest belangrijke zijn: *relay ramp, relay zone* en *accommodation zone*. Een relay ramp (zie figuur 1.3) is een transferzone tussen 2 overlappende normaalbreuken, die beide dezelfde hellingsrichting hebben. In dit werk is de term relay ramp gebruikt als de overlappende

breukeinden parallel waren. In het andere geval werd het begrip relay zone verkozen. Een accommodatiezone is een structuur die zich ontwikkeld heeft tussen overlappende normaalbreuken met een tegenovergestelde hellingsrichting. De term wordt vaak gebruikt om naar een bepaald type transferzone te verwijzen, hoewel striktgenomen voor een accommodatiezone de vereiste niet bestaat dat de 2 breuken op hetzelfde moment actief waren. Deze vereiste is er wel vooraleer gesproken kan worden van een transferzone.

Een systematisch indelingsschema voor transferzones is voorgesteld geweest door Morley et al. (1990) (zie figuur 1.4). Een eerste onderscheid in deze indeling is gebaseerd op de hellingsrichting van de breuken waartussen de verplaatsingsoverdracht gebeurt. Hellen de twee breuken in dezelfde richting dan vormen zij een *synthetische* transferzone. Hellen zij in tegenovergestelde richting dan spreekt men van een *geconjugeerde* transferzone. De geconjugeerde transferzones kunnen aldus verder onderverdeeld worden; in het geval de breuken naar elkaar toehellen wordt het een *convergente* transferzone, hellen de breuken weg van elkaar, dan wordt het een *divergente* transferzone. Tot slot is er een laatste onderverdeling in het indelingsschema van Morley et al. (1990) gebaseerd op de mate waarin de breuken elkaar overlappen. Is er nog geen overlap dan spreken Morley et al. (1990) van een *naderende* transferzone, bestaat er reeds een zekere overlap dan spreken ze van een *overlappende* transferzone, en in het geval van een volledige overlapping, spreken ze van een *collaterale* transferzone.

2 Eigenschappen van extensiebreuken

De laatste 20 jaar zijn normaalbreuken uitvoerig bestudeerd geweest, en dit heeft geleid tot betere inzichten in de geometrie van normaalbreuken, de groei en evolutie van normaalbreuken, hun invloed op de ontwikkeling van tektonische bekkens, enz...

Voor deze studie zijn vooral de ideeën die zich ontwikkelden over de groei van normaalbreuken van belang, en deze worden in de volgende sectie kort toegelicht.

2.1 De groei van geïsoleerde breuken

Omdat verplaatsingsprofielen van geïsoleerde breuken gewoonlijk gekenmerkt worden door een maximale verplaatsing in het centrum en een geleidelijke afname naar de breukeinden, is het idee ontstaan dat breuken zich uitbreiden door zgn. “radiale propagatie”. In dit model verhoogt een verplaatsing langsheen de breuk de spanningen aan de breukuiteinden, wat op zijn beurt leidt tot een verdere laterale uitbreiding van de breuk.

Eén van de eerste modellen die de groei van geïsoleerde breuken volgens dit mechanisme beschreef was het “cumulatieve verschuivingsmodel” van Walsh en Watterson (1987). Dit model veronderstelde dat hoeveelheid verschuiving langsheen een breuk toenam volgens een eenvoudige rekenkundige rij. Walsh en Watterson (1987) leidden op basis van deze veronderstelling een eenvoudige schalingsrelatie af voor normaalbreuken die het verband weergaf tussen de maximale verplaatsing langsheen een breuk en de lengte van de breuk.

Een meer algemene schalingsrelatie voor breuken is geformuleerd in vergelijking 2.12. De

waarden die voor de exponent n in deze vergelijking zijn berekend op basis van de studie van natuurlijke breuksystemen, variëren tussen 1 en 2.

2.2 Breukgroei door het aaneenkoppelen van breuken

Een belangrijke observatie bij normaalbreuken was dat hun verloop soms zeer onregelmatig was, gekenmerkt door verschillende knikken of verspringingen. Deze bevinding, die moeilijk verklaarbaar was met het radiale propagatie-mechanisme van geïsoleerde breuken, leidde tot de ontwikkeling van het idee dat breuken kunnen groeien door zich met elkaar te verbinden.

Bij dit mechanisme van "breukgroei door segmentverbinding", groeien breuksegmenten in een eerste fase als geïsoleerde breuken, die zich bij toenemende extensie lateraal zullen uitbreiden. Op een bepaald ogenblik zullen 2 breuken elkaar dicht genoeg genaderd hebben zodat er een interactie zal ontstaan tussen hun verschillende spanningsvelden. Het gevolg van deze interactie is dat de twee breuken met elkaar gaan overlappen en er zich een relay ramp tussen de breuken zal vormen. Deze ramp zal bij verdere extensie gebroken worden, en de breuksegmenten zullen met elkaar verbonden geraken. Op dat moment heeft er zich een breuk gevormd die een lengte heeft, gelijk aan de som van de twee oorspronkelijke breuken, en een verplaatsing gelijk aan de maximale verplaatsing van de twee breuken. Het idee bestaat dat zo'n breuk die "onderverplaatst" is volgens de schalingsrelatie uit vergelijking 2.12, zal gekenmerkt worden door een plotse toename in verplaatsing, vooral in het centrum van de breuk zonder een toename in lengte, tot de schalingrelatie weer voldaan is. Op regionale schaal, wanneer verschillende breuken volgens dit mechanisme groeien, kan dit leiden tot een plotse algehele subsidentietoename in een gebied, zonder een toename in de vervormingssnelheid.

2.3 Relay ramps

Zoals hierboven vermeld is een relay ramp een bijzonder type van transferzone, namelijk een overlapzone tussen twee normaalbreuken die beiden in dezelfde richting hellen, en waartussen zich een gekantelde structuur ontwikkeld heeft (figuur 2.19). Zo'n structuur die de verplaatsing van de ene breuk naar de andere overdraagt is een tijdelijke structuur in de evolutie van normaalbreuken. Een relay ramp is onderhevig aan hoge spanningen, en zal als gevolg hiervan intern vervormen. Uiteindelijk zal de structuur gebroken worden, en verdwijnt ze. Deze breking kan op verschillende manieren verwezenlijkt worden; enerzijds kan een van de grote breuken zich naar de andere breuk uitbreiden en zich uiteindelijk verbinden, of er kan zich in de ramp een nieuwe breuk ontwikkelen die door de ramp snijdt, en zo de twee hoofdbreuken met elkaar verbindt.

De geometrie van relay ramps (verhouding tussen de overlaplengte en de afstand tussen de breuken) is gelijk over verchillende grootte-ordes.

2.4 Reactivatie van breuken

De geometrie van extensiestructuren kan sterk beïnvloed worden door de aanwezigheid van reedsbestaande oudere structuren. De reactivatie van zo'n oudere structuur — ook al heeft ze

niet volledig de juiste oriëntatie — zal in bepaalde gevallen eenvoudiger gebeuren dan de vorming van nieuwe breuken in intacte gesteenten. Wanneer een breuk gereactiveerd wordt, zal ze haar oorspronkelijke lengte behouden. Initieel zal zo'n breuk dus ook "onderverplaatst" zijn volgens de schalingsrelatie voor normaalbreuken.

3 Geologische achtergrond van het Baikal-Meer

De Baikal Riftzone ontwikkelde zich sinds het Boven Oligoceen langsheen de rand van het Siberische Craton in de verzwakte korst van de Sayan-Baikal *mobile belt*. Het ontstaan van de riftzone was waarschijnlijk gekoppeld aan de botsing tussen Indië en Eurazië zo'n 55–50 Ma geleden. In totaal ontwikkelden zich 14 verschillende riftbekkens in de riftzone, waarvan de 3 grootste — die centraal in de riftzone gelegen zijn — opgevuld zijn met de waters van het Baikal-Meer.

In de evolutie van de Baikal Riftzone worden twee duidelijke fasen onderscheiden: een trage en een snelle riftingsfase. De trage riftingsfase (van zo'n 35 tot 10 Ma geleden) leidde tot de vorming van grote depressies, gerelateerd aan een trage subsidentie en een onbelangrijke opheffing van de riftschouders. Tijdens de snelle riftingsfase (van 3.5 Ma tot op heden) verhoogde de tektonische activiteit in de regio, wat leidde tot snelle toename in subsidentie en een bijkomende opheffing van de riftschouders.

3.1 Het Baikal-Meer

Het Baikal-Meer heeft een lengte van 636 km, een gemiddelde breedte van 40–50 km, een maximale diepte van 1642 m en het is het grootste zoetwatermeer op aarde. Het  -vormige Baikal-Meer is opgebouwd uit 3 riftbekkens: het noordelijk, centraal en zuidelijk Baikal-Bekken. Deze bekkens zijn van elkaar gescheiden door 2 accommodatiezones: de Academician-Ridge-Accommodatiezone tussen het noordelijk en het centraal bekken, en de Selenga-Delta-Accommodatiezone tussen het centraal en het zuidelijk bekken.

De drie Baikal-Bekkens vertonen een duidelijk asymmetrische vorm die voortvloeit uit de aanwezigheid van een duidelijke grote randbreuk aan de westelijke kant, en een serie van minder uitgesproken breuken aan de oostelijke kant. De oriëntatie van de westelijke randbreuk verandert stapsgewijs van een ONO-richting in het zuidelijk bekken naar een NNO-richting in het noordelijk bekken. De Obruchevsky-Breuk is de randbreuk van het zuidelijk bekken, ter hoogte van de monding van de Buguldeika-Rivier splitst deze breuk op in een westelijke arm, de Primorsky-Breuk en een oostelijke arm, de Ol'khon-Breuk. De Ol'khon-Breuk vormt de randbreuk van het centraal Baikal-Bekken. Ter hoogte van Kocherikovo gaat de Primorsky-Breuk over in de Baikalsky-Breuk, die de randbreuk vormt van het noordelijk Baikal-Bekken. Tussen de verschillende randbreuken, en tussen verschillende segmenten van de randbreuken hebben zich een serie relay zones ontwikkeld. De studiegebieden van deze scriptie zijn een relay ramp tussen twee segmenten van de Baikalsky-Breuk (de Zavarotny relay ramp), en een gekanteld blok tussen de Ol'khon en Primorsky Breuken (het Pri-Ol'khon-Blok).

4 Een grootschalige relay ramp in het noordelijk Baikal-bekken: het gebied van Zavarotny

Ter hoogte van Zavarotny heeft er zich een relay ramp gevormd tussen twee segmenten van de Baikalsky-Breuk. Deze relay ramp heeft een oppervlakte van zo'n 400 km^2. De interne structuur van deze ramp werd bestudeerd aan de hand van hoge-resolutie reflectieseismische profielen, digitale terreinmodellen en een satellietbeeld.

4.1 Analyse van digitale terreinmodellen: Morfologie van de relay ramp

Een longitudinaal profiel door de ∼40 km lange relay ramp toont aan dat de structuur het hoogste is in het zuidwestelijk deel. Hier bereikt de ramp een hoogte van zo'n 50 m boven het meeroppervlak. Naar het noordoosten toe verdiept de ramp en bereikt uiteindelijk een diepte van zo'n 800 m onder het wateroppervlak. In het offshore gedeete van de relay ramp is een duidelijke ruwe morfologie waarneembaar, waarin drie sub-bekkens voorkomen met elk een licht verschillende oriëntatie. In vergelijking met het offshore gedeelte is de morfologie van het onshore gedeelte van de relay ramp veel vlakker. Op dwarsprofielen is een duidelijke topografische sprong waarneembaar die de voetblokbreuk van de relay ramp verbindt met de hangende-blok-breuk.

4.2 Interpretatie van seismische profielen

De hoge-resolutie reflectieseismische profielen hebben aangetoond dat de verschillende sub-bekkentjes in de relay ramp van Zavarotny afgelijnd worden door breuken. Deze breuken zijn gekarteerd in figuur 4.14. Deze figuur laat ook zien dat er een zeer sterke gelijkenis is tussen de morfologie van het meerbodemoppervlak in Zavarotny, en de morfologie van de sokkel, wat aantoont dat de relay ramp een actieve structuur is.

Seismische profielen in het zuidelijk deel van de relay ramp laten een duidelijke structuur van gekantelde blokken zien (figuur 4.15). Deze kanteling gebeurde langsheen een serie breuken die quasi parallel zijn aan de hoofdbreuken in Zavarotny. Meer in het noorden wordt een sub-bekken afgelijnd door een breuk die van de hangende-blok-breuk is afgesplitst en zich naar de voetblok-breuk toe beweegt. Deze breuk werd in dit werk geïnterpreteerd als een zich ontwikkelende verbindingsbreuk.

4.3 Discussie

Op basis van verschillende argumenten is de topografische sprong die in de morfologie van de relay ramp te Zavarotny waarneembaar is, geïnterpreteerd als breukgebonden. Dit wil zeggen dat de relay ramp zich reeds in het gebroken stadium bevindt. Bestaande modellen die de evolutie van relay ramps beschrijven vermelden dat in dit stadium de ramp afsterft omdat de verbindingsbreuk de verplaatsing tussen de twee oorspronkelijke hoofdbreuken zal overdragen. De observaties in Zavarotny, nl. de goede gelijkenis tussen de sokkelmorfologie en die van de meerbodem, alsook de ontwikkeling van een nieuwe verbindingsbreuk in de relay ramp, tonen aan dat deze ramp nog verder evolueert en dus niet is afgestorven.

Er wordt verondersteld dat relay ramps zullen gebroken worden door de ontwikkeling van een nieuwe verbindingsbreuk wanneer de verplaatsingsgradiënten aan de uiteinden van de hoofdbreuken zeer groot zijn. In zo'n geval krijgt men een sterke verbuiging in de ramp langsheen een as loodrecht op de hoofdbreuken. Als gevolg hiervan ontwikkelen zich secundaire breuken in de relay ramp die een grote hoek vormen met de hoofdbreuken. Wanneer de verplaatsingsgradiënten aan de uiteinden van de hoofdbreuken niet groot zijn, zullen zich in de relay ramp eerder secundaire breuken ontwikkelen die min of meer parallel zijn aan de hoofdbreuken. De breking van de relay ramp zal in zo'n geval eerder gebeuren doordat een van de hoofdbreuken naar de ander toegroeit. De combinatie in Zavarotny, van secundaire breuken die parallel zijn aan de hoofdbreuken en de ontwikkeling van een nieuwe verbindingsbreuk die de relay ramp breekt, is dus ongewoon.

Doordat op het satellietbeeld van Zavarotny preferentiële richtingen in de sokkel waar te nemen zijn die parallel zijn aan de hoofdbreuken, is het mogelijk dat zulke preferentiële richtingen ook de oriëntatie van de verbindingsbreuk en de secundaire breuken in Zavarotny beïnvloed hebben.

4.4 Conclusies

De studie van de grote relay ramp in Zavarotny heeft aangetoond dat zulke grote ramps door meer factoren beïnvloed kunnen worden dan structuren op kleinere schaal. En dat de interne structuur dus niet volledig schaalonafhankelijk is.

Er zijn in Zavarotny aanwijzingen gevonden voor het verder evolueren van de relay ramp, nadat deze gebroken werd.

5 De evolutie van het centrale deel van het Baikal-Meer: een structurele studie

Het Pri-Ol'khon-Blok is een wigvormig gekanteld blok tussen de Ol'khon-Breuk en de Primorsky-Breuk in het centraal deel van het Baikal-Meer. Het blok bestaat uit een offshore gedeelte, Maloe More, en een onshore gedeelte, Ol'khon-Eiland en Pri-Ol'khon. Bestaande evolutiemodellen van het Pri-Ol'khon-Blok veronderstellen dat een recente graduele propagatie van de Primorsky-Breuk in een zuidwestwaartse richting de geleidelijke kanteling en inzakking van het blok heeft veroorzaakt. Voor de Primorsky-Breuk en de Ol'khon-Breuk zich uiteindelijk verbonden hebben, zou dus tussen beide breuken een grote overlapzone of relay ramp bestaan hebben.

Het Pri-Ol'khon-Blok is hier bestudeerd door middel van een uitgebreid netwerk van reflectieseismische profielen in Maloe More, digitale terreinmodellen en satellietbeelden.

5.1 Seismische interpretatie

De penetratie van het seismisch signaal was groot genoeg om in het gehele studiegebied een akoestische sokkel te bereiken. Deze sokkel vertoont een ruwe morfologie, met een afwisseling van transverse ruggen en depressies. De diepte van de sokkel neemt geleidelijk toe van het

zuidwesten in Maloe More naar het noordoosten. In totaal zijn er 5 sokkelruggen en 6 bekkentjes geïdentificeerd.

Bovenop deze sokkel hebben zich vier grote seismisch stratigrafische eenheden afgezet: Eenheid X, Eenheid A, Eenheid B en Eenheid R. De oudste eenheden (X en A) komen vooral voor in de verschillende sub-bekkens in de sokkel. De grootste diktes zijn gevonden in bekkens in het zuidwestelijke deel van Maloe More, alsook aan de Zunduk-Breuk. Het voorkomen van deze oude afzettingen in het zuidwesten en in geïsoleerde depocentres over heel Maloe More is onverklaarbaar met het bestaande evolutiemodel van het Pri-Ol'khon-Blok.

Eenheid B ligt hetzij rechtstreeks op de sokkel, hetzij op Eenheid A. Deze eenheid komt zowel in de verschillende depressies voor als op de sokkelruggen. De algehele dikte van Eenheid B neemt toe van het zuidweten naar het noordoosten, en de eenheid bereikt op sommige plaatsen diktes van >100 m. De eenheid is aangetast door een groot aantal sedimentbreuken.

Bovenop Eenheid B heeft zich Eenheid R afgezet. Deze slechts enkele meters dikke recente eenheid is opvallend minder aangetast door sedimentbreuken dan Eenheid B.

5.2 Satellietbeeld- en DTM-analyse

Aan de hand van satellietbeelden en digitale terreinmodellen is de Primorsky-Breuk bestudeerd. Deze onshore-interpretatie laat een duidelijke segmentatie van de breuk zien, wat laat vermoeden dat ze ontstaan is door het aaneengroeien van verschillende segmenten. Op basis van die geometrie zijn 4 locaties geïdentificeerd die waarschijnlijk overeenkomen met zulke verbindingspunten.

5.3 Discussie

Wanneer men de offshore en onshore interpretaties van het Pri-Ol'khon-Blok naast elkaar legt, wordt het duidelijk dat de verschillende transverse sokkelruggen in Maloe More voorkomen ter hoogte van de onshore afgeleide verbindingspunten. Dit laat vermoeden dat de ruggen overeenkomen met zgn. *transverse basement highs*. Wanneer twee afzonderlijke breuken elk een bekken aflijnen, komen zulke ruggen voor tussen de bekkens waar de verplaatsing langsheen de (rand-)breuken minimaal is.

5.3.1 Evolutiemodel voor het Pri-Ol'khon-Blok

Op basis van de gemaakte interpretaties is het mogelijk geweest om een nieuw evolutiemodel voor het Pri-Ol'khon-Blok voor te stellen dat verschilt van het oude model waarin de Primorsky-Breuk zich gradueel naar het zuidwesten uitbreidde. Dit nieuw evolutiemodel bestaat uit 2 stadia:

1. Tijdens een eerste fase (tijdens de afzetting van eeheden X&A) bestond de Primorsky-Breuk uit verschillende kleine geïsoleerde segmenten die elk kleine depocentres aflijnden. Door een toenemende extensie, breidden deze segmenten zich lateraal uit en vergrootten de depocentres.

2. Op een bepaald ogenblik (tijdens de laatste afzettingen van Eenheid A) naderden 2 breuksegmenten in het noordoosten van Maloe More elkaar dicht genoeg om met elkaar te interageren en uiteindelijk te vergroeien. Deze vergroeiing leidde tot een graduele subsidentie van de sokkelruggen tussen de 2 noordelijke depocentres. Gelijkaardige situaties deden zich vervolgens voor meer naar het zuiden, en gradueel geraakten de verschillende segmenten van de Primorsky-Breuk met elkaar verbonden. Het is door de volgorde waarmee de segmenten zich met elkaar verbonden (van het noordoosten naar het zuidwesten) dat de subsidentie van Maloe More gradueel leek te gebeuren tijdens de afzetting van Eenheid B.

6 Analoge modellering van relay ramps

Door middel van een serie zandbakmodellen zijn relay ramps bestudeerd waarvan de geometrie van de hoofdbreuken gedeeltelijk vooraf bepaald was. De lengte en oriëntatie van de breuken, alsook de afstand tussen de overlappende breuken varieerden tussen de verschillende experimenten. Vervolgens is bestudeerd hoe deze variaties de ontwikkeling en evolutie van de relay ramps beïnvloedden.

De modellen werden uitgevoerd in een typische modelleringszandbak, bestaande uit een rubberen basis die verbonden is met een beweegbare plank en een vaste plank. Op het rubber werden verschillende lagen zand gestrooid. Door de beweegbare plank weg te bewegen van de vaste plank rekte de rubberen basis uit, en ontstond er extensie in het zandpakket. De locatie van de normaalbreuken die zich in het zand vormden werd bepaald door 2 siloconenrepen onder het zand. Door de geometrie van de siliconenrepen te veranderen kon de geometrie van de normaalbreuken gewijzigd worden (figuur 6.2).

6.1 Analyse van de experimenten

Vier verschillende evolutiefasen werden onderscheiden in de ontwikkeling van de experimentele relay ramps:

1. *Immatuurstadium:* In dit stadium ontwikkelden de breuken zich als geïsoleerde structuren die zich lateraal uitbreidden.

2. *Interactiestadium:* Dit stadium ontstond wanneer de twee breuken elkaar voldoende dicht genaderd hadden om met elkaar te interageren. Vrij vlug in dit stadium ontwikkelde zich een relay ramp.

3. *Verbindingsstadium:* Dit stadium behelsde de afbraak van de relay ramp en het met elkaar verbonden geraken van de twee breuken.

4. *Post-breekstadium:* Nadat de oorspronkelijk geïsoleerde breuken met elkaar verbonden raakten, werd er nog een aanzienlijke verdere evolutie van het systeem waargenomen. Deze verdere evolutie is in dit post-breekstadium ingedeeld.

Om te testen of het gebruik van de siliconenrepen in de modellen een eventuele invloed had op de vorm van de gevormde breuken is de relatie bepaald tussen de verplaatsing van de breuken en hun lengte. Deze relatie is $D = 0.0226.L^{1.11}$, en komt goed overeen met de schalingsrelatie van normaalbreuken.

Interactie tussen de breuksegmenten in de modellen is waargenomen wanneer de totale lengte van het breuksysteem groter of gelijk was aan 8 keer de afstand tussen de breuken.

Het verband tussen de breedte en de lengte van de experimentele relay ramps is niet eenduidig:

1. In het algemeen is de overlaplengte (lengte van de relay ramp) groter naarmate de afstand tussen de breuken groter is.

2. Dit is niet meer het geval wanneer de afstand te groot wordt om nog interactie tussen de breuken toe te laten.

3. In sommige experimenten leidden zeer kleine afstanden tussen de breuken tot de ontwikkeling van een smalle relay ramp, maar in andere gevallen leidde dezelfde afstand tot de ontwikkeling van een continue breuk.

De verhouding tussen de lengte en de breedte van de experimentele relay ramps was gemiddeld 3.

50% van de relay ramps werden gebroken of waren quasi gebroken voor het einde van het experiment. 55% van deze breking gebeurde door de uitbreiding van de hangende-blok-breuk naar de voetblokbreuk, 27% van de breking door uitbreiding van de voetblokbreuk naar de hangende-blok-breuk en 18% door de ontwikkeling van een nieuwe verbindingsbreuk.

7 Schaalmodellen van het Baikal-Meer en van de Baikal Riftzone

In een tweede serie van analoge zandbakmodellen is geprobeerd om inzicht te krijgen in mechanismen die verantwoordelijk kunnen zijn voor de stapsgewijze oriëntatieverandering van de randbreuken in het Baikal-Meer, of die geleid hebben tot de vorming van de verschillende Baikal-Bekkens die begrensd zijn door accommodatiezones. Waarschijnlijk de meest voor de hand liggende factor die de oriëntatie van de breuken beïnvloed heeft is het voorkomen van reedsbestaande zwaktezones aan de rand van het meer. De invloed van zulke structuren is gestest in deze modellering.

Er werden twee categorieën modellen uitgevoerd. In een eerste categorie werden voorgevormde metalen basisplaten gebruikt die met een stuk rubber met elkaar verbonden waren. Bovenop deze platen werden vervolgens verschillende lagen zand gestrooid. In totaal werden 4 verschillende platen gebruikt, waarvan de vorm varieerde tussen een eenvoudige rechte lijn en een vorm die de grens van de Siberische Craton nauwkeurig nabootste.

De tweede categorie van modellen bevatten een 1 cm dikke basislaag van SGM-36 polymeer, waarop de verschillende zandlagen gestrooid werden. Extensie in het model werd veroorzaakt

door een plastieken film uit een centrale gleuf te trekken. De vorm van deze gleuf verschilde tussen de verschillende experimenten.

7.1 Resultaten

Zeven modellen werden uitgevoerd van de eerste categorie van experimenten. In deze modellen ontwikkelden de breuken zich als verschillende smalle segmenten die met elkaar interageerden, en uiteindelijk vergroeiden. Op die wijze werden er op verschillende plaatsen langsheen het verloop van de randbreuken relay ramps ontwikkeld. Opvallend hierbij was dat ook op de locaties waar de onderliggende metalen plaat van oriëntatie veranderde meestal relay zones aanwezig waren. Met toenemende extensie ontstonden continue breuken en verdwenen de meeste relay zones.

De eerste breuken die zich in de modellen vormden waren de riftrandbreuken. Wanneer ze het oppervlakte van het model bereikten, kenden deze breuken een grote lengte, en slechts een geringe verplaatsing. Dit wijst erop dat de breuken vanuit de diepte naar boven propageerden. De riftrandbreuken volgden over het algemeen goed de geometrie van de onderliggende basisplaten. Enkel wanneer de hoek tussen de richting van extensie en de richting van de basisplaat te groot was, ontstonden er afwijkende oriëntaties. Bij toenemende extensie werd het belang van intra-rift breuken groter. Deze breuken ontwikkelden zich meestal min of meer loodrecht op de richting van extensie. Het gevolg hiervan was dat er zich intra-rift grabens ontwikkelden die niet de vooropgestelde geometrie van de basisplaten volgden. Dwarssecties door de rifts in de modellen hadden, net zoals in het Baikal-Meer, een duidelijke asymmetrisch vorm.

In de polymeermodellen zijn de riftrandbreuken opvallend minder continu, en blijven ze onregelmatig bij verdere extensie. De intra-rift breuken zijn ook in de polymeermodellen quasi loodrecht op de richting van extensie. Een verschil met de eerste categorie modellen is dat het actieve riftbekken smaller is. Bij toenemende extensie worden de randbreuken steeds verder van de centrale gleuf getrokken, en worden daardoor minder belangrijk. Aan de gleuf ontwikkelen zich continu nieuwe breuken die de extensie opvangen.

7.2 Conclusies

De stapsgewijze oriëntatieverandering van de randbreuken, zoals die zich in het Baikal-Meer voordoet, werd waargenomen in de modellen. Op de locaties waar de strekking van de randbreuken veranderde ontwikkelden zich relay structuren. Aldus kan er besloten worden dat voorbestaande structuren een belangrijke invloed hebben op de localisatie van relay zones in een randbreuk systeem.

De randvoorwaarden in de modelleringsstudie waren zeer eenvoudig, en de experimentele rifts komen niet volledig overeen met de Baikal Riftzone. Zo zijn niet de 3 verschillende Baikal-Bekkens waargenomen die elk een verschillende oriëntatie hebben, en die van elkaar gescheiden worden door accommodatiezones. Deze eenvoudige riftmodellen laten dus niet toe om het onderliggende mechanisme voor de vorming van deze structuren te bepalen.

8 Conclusies

Verschillende voorbeelden van transferzones werden in dit werk onderzocht, zowel uit het Baikal-Meer als uit zandbakmodellen.

De studie van een grote relay ramp in de buurt van Zavarotny heeft aangetoond dat zo'n relay ramp een verschillende interne structuur heeft dan deze op een kleinere schaal. Zo werd in Zavarotny een ongebruikelijke combinatie waargenomen van secundaire breuken die parallel lopen aan de hoofdbreuken en het breken van de ramp door een nieuwe verbindingsbreuk. Verder werden aanwijzingen gevonden voor het voort evolueren van de relay ramp nadat ze gebroken was.

Deze voortdurende evolutie werd ook waargenomen in experimentele relay ramps, en leidde tot het invoeren van een post-breekstadium in de evolutie van relay ramps. Daarnaast werd aangetoond dat breukinteractie in de experimenten pas optrad wanneer de totale lengte van het systeem groter of gelijk was aan 8 keer de afstand tussen de breuken.

In dit werk werd een nieuw model voorgesteld voor de evolutie van een gekanteld blok in het centraal deel van het Baikal-Meer. Dit blok zou voor de uiteindelijke verbinding van de twee randbreuken een grote relay ramp geweest zijn. Het voorgestelde evolutiemodel suggereert dat de reactivatie van de Primorsky-Breuk in verschillende segmenten gebeurde, die elk een uitgesproken invloed hadden op de morfologie van het gekantelde blok.

Tot slot werd in een laatste modelleringsstudie aangetoond dat de locatie van relay zones tussen segmenten van een riftrandbreuk bepaald kan zijn door de oriëntatie van reeds bestaande structuren. Op de plaatsen waar deze oriëntatie verandert vormt zich meestal een relay zone. Het voorkomen van de accommodatiezones tussen de verschillende bekkens in het Baikal-Meer kon met deze eenvoudige modellen niet verklaard worden.

Bibliography

Ackermann, R. V. and Schlische, R. W. (1997). Anticlustering of small normal faults around larger faults. *Geology*, 25(12):1127–1130.

Acocella, V. (2002). Analogue models of overlapping oceanic ridges. *Bolletino di Geofisica*, 42(1/2 suppl.):257–261. Proceedings of the REALMOD 2002 Conference.

Acocella, V., Faccenna, C., Funiciello, R., and Rossetti, F. (1999a). Sand-box modelling of basement-controlled transfer zones in extensional domains. *Terra Nova*, 11:149–156.

Acocella, V., Gudmundsson, A., and Funiciello, R. (2000). Interaction and linkage of extension fractures and normal faults: examples from the rift zone of Iceland. *Journal of Structural Geology*, 22:1233–1246.

Acocella, V., Salvini, F., Funiciello, R., and Faccenna, C. (1999b). The role of transfer structures on volcanic activity at Campi Flegrei (Southern Italy). *Journal of Volcanology and Geothermal Research*, 91:123–139.

Agar, S. M. and Klitgord, K. D. (1995). Rift flank segmentation, basin initiation and propagation: a neotectonic example from Lake Baikal. *Journal of the Geological Society of London*, 152:849–860.

Allemand, P. and Brun, J. (1991). Width of continental rifts and rheological layering of the lithosphere. *Tectonophysics*, 188:63–69.

Allen, P. A. and Densmore, A. L. (2000). Sediment flux from an uplifted fault block. *Basin Research*, 12:367–380.

An, L. (1997). Maximum link distance between strike-slip faults: observations and constraints. *Pure and Applied Geophysics*, 150:19–36.

Anders, M. H. and Schlische, R. W. (1994). Overlapping Faults, Intrabasin Highs, and the Growth of Normal Faults. *The Journal of Geology*, 102:165–180.

Anderson, E. M. (1951). *The Dynamics of Faulting and dyke formation with applications to Britain*. Oliver and Boyd, second edition. 206pp.

Antipin, V., Afonina, T., Badalov, O., Bezrukova, E., Bukharov, A., Bychinsky, V., Dmitriev, A. A., Dorofeeva, R., Duchkov, A., Esipko, O., Fileva, T., Gelety, V., Golubev, V., Goreglyad,

A., Gorokhov, I., Gvozdkov, A., Hase, Y., Ioshida, N., Ivanov, E., Kalashnikova, I., Kalmychkov, G., Karabanov, E., Kashik, S., Kawai, T., Kerber, E., Khakhaev, B., Khlystov, O., Khursevich, G., Khuzin, M., King, J., Konstantinov, K., Kochukov, V., Krainov, M., Kravchinsky, V., Kudryashov, N., Kukhar, L., Kuzmin, M., Nakamura, K., Nomura, S., Oksenoid, E., Peck, J., Pevzner, L., Prokopenko, A., Romashov, V., Sakai, H., Sandimirov, I., Sapozhnikov, A., Seminsky, K., Soshina, N., Tanaka, A., Tkachenko, R., Ushakovskaya, M., and Williams, D. (2001). The new BDP-98 600-m drill core from Lake Baikal: a key late Cenozoic sedimentary section in continental Asia. *Quaternary International*, 80-81:19–36.

Arzhannikova, A. V. and Gofman, L. E. (2000). Neotectonics in the primorsky fault zone. *Russian Geology and Geophysics*, 41(6):785–791.

Atkinson, B. K. (1987). Introduction to fracture mechanics and its geophysical applications. In Atkinson, B. K., editor, *Fracture Mechanics of Rocks*, pages 1–26. Academic Press, London.

Avouac, J.-P. and Tapponnier, P. (1993). Kinematic model of active deformation in Asia. *Geophysical Research Letters*, 20:895–898.

Axen, G. J. (1995). Extensional segmentation of the Main Gulf Escarpment, Mexico and United States. *Geology*, 23:515–518.

Aydin, A. and Nur, A. (1982). Evolution of pull-apart basins and their scale independence. *Tectonics*, 1:91–105.

Aydin, A. and Nur, A. (1985). The types and role of stepovers in strike-slip tectonics. In Biddle, K. T. and Christie-Blick, N., editors, *Strike-slip deformation, basin formation, and sedimentation*, pages 35–44. Society of Economic Paleontologists and Mineralogists, Special Publication No. 37.

Aydin, A. and Schultz, R. (1990). Effect of mechanical interaction on the development of strike-slip faults with echelon patterns. *Journal of Structural Geology*, 12(1):123–129.

Bachtadse, V., Pavlov, V. E., Kazansky, A. Y., and Tait, J. A. (2000). Siluro-Devonian paleomagnetic results from the Tuva Terrane (southern Siberia, Russia: implications for the paleogeography of Siberia. *Journal of Geophysical Research*, 105(B6):13509–13518.

Balla, Z., Kuzmin, M., and Levi, K. (1991). Kinematics of the Baikal opening: results of modeling. *Annales Tectonicæ*, 5(1):18–31.

Barnett, J. A. M., Mortimer, J., Rippon, J. H., Walsh, J. J., and Watterson, J. (1987). Displacement geometry in the volume containing a single normal fault. *AAPG-bulletin*, 71(8):925–937.

Barton, C. M., Evans, D. J., Bristow, C. R., Freshney, E. C., and Kirby, G. A. (1998). Reactivation of relay ramps and structural evolution of the Mere Fault and Wardour Monocline, northern Wessex Basin. *Geological Magazine*, 135(3):383–395.

Bassi, G. (1995). Relative importance of strain rate and rheology for the mode of continental extension. *Geophysical Journal International*, 122:195–210.

Bonnet, E., Bour, O., Odling, N. E., Davy, P., Main, I., Cowie, P., and Berkowitz, B. (2001). Scaling of fracture systems in geological media. *Reviews of Geophysics*, 39(3):347–383.

Bosworth, W. (1985). Geometry of propagating rifts. *Nature*, 316:625–627.

Bourne, S. J. and Willemse, E. J. M. (2001). Elastic stress control on the pattern of tensile fracturing around a small fault network at Nash Point, UK. *Journal of Structural Geology*, 23:1753–1770.

Brun, J. P. (1999). Narrow rifts versus wide rifts: inferences for the mechanics of rifting from laboratory experiments. *Philosophical Transactions of the Royal Society of London Series A — Mathematical Physical and Engineering Science*, 357:695–712.

Buchanan, P. G. and McClay, K. R. (1991). Sandbox experiments of inverted listric and planar fault systems. *Tectonophysics*, 188:97–115.

Buchanan, P. G. and McClay, K. R. (1992). Experiments on basin inversion above reactivated domino faults. *Marine and Petroleum Geology*, 9:486–500.

Buck, R. W. (1988). Flexural rotation of normal faults. *Tectonics*, 7:959–973.

Buck, R. W. (1991). Modes of continental litospheric extension. *Journal of Geophysical Research*, 96(B12):20161–20178.

Burbank, D. W. and Anderson, R. S. (2001). *Tectonic Geomorphology*. Blackwell Science. pp. 274.

Burg, J. P., Davy, P., and Martinod, J. (1994). Shortening of analogue models of the continental lithosphere: New hypothesis for the formation of the Tibetan plateau. *Tectonics*, 13(2):475–483.

Bürgmann, R., Pollard, D., and Martel, S. J. (1994). Slip distributions on faults: Effects of stress gradients, inelastic deformation, heterogeneous host-rock stiffness, and fault interaction. *Journal of Structural Geology*, 16:1675–1690.

Burov, E., Lobkovsky, L. I., Cloetingh, S., and Nikishkin, A. M. (1993). Continental lithosphere folding in Central Asia (Part II): constraints from gravity and topography. *Tectonophysics*, 226:73–87.

Calais, E., Lesne, O., Déverchère, J., San'kov, V., Lukhnev, A., Miroshnitchenko, A., Buddo, V., Levi, K., Zalutsky, V., and Bashkuev, Y. (1998). Crustal deformation in the Baikal rift from GPS measurements. *Geophysical Research Letters*, 25(21):4003–4006.

Calais, E., Vergnolle, M., San'kov, V., Lukhnev, A., Miroshnitchenko, A., Amarjargal, S., and Déverchère, J. (2003). GPS measurements of crustal deformation in the Baikal-Mongolia area (1994–2002): Implications for current kinematics of Asia. *Journal of Geophysical Research*, 108(B10):doi:10.1029/2002JB002373.

Cartwright, J. (1991). The kinematic evolution of the Coffee Soil Fault. In Roberts, A. M., Yielding, G., and Freeman, B., editors, *The Geometry of Normal Faults*, pages 29–40. Geological Society Special Publication No 56.

Cartwright, J. A., Mansfield, C., and Trudgill, B. (1996). The growth of normal faults by segment linkage. In Buchanan, P. G. and Nieuwland, D. A., editors, *Modern developments in structural geology, interpretation, validation and modelling*, volume 99, pages 163–177. Geological Society Special Publication.

Cartwright, J. A. and Mansfield, C. S. (1998). Lateral displacement variation and lateral tip geometry of normal faults in the Canyonlands National Park, Utah. *Journal of Structural Geology*, 20(1):3–19.

Cartwright, J. A., Trudgill, B. D., and Mansfield, C. S. (1995). Fault growth by segment linkage: an explenation for scatter in maximum displacement and trace length data from the Canyonlands grabens of SE Utah. *Journal of Structural Geology*, 17:1319–1326.

Chemenda, A., Déverchère, J., and Calais, E. (2002). Three-dimensional laboratory modelling of rifting: application to the baikal rift, russia. *Tectonophysics*, 356:253–273.

Childs, C., Easton, S. J., Vendeville, B. C., Jackson, M. P. A., Lin, S. T., Walsh, J. J., and Watterson, J. (1993). Kinematic analysis of faults in a physical model of growth faulting above a viscous salt analogue. *Tectonophysics*, 228:313–329.

Childs, C., Walsh, J. J., and Watterson, J. (1990). A method for estimation of the density of fault displacements below the limits of seismic resolution in reservoir formations. In The Norwegian Institute of Technology, editor, *North Sea Oil and Gas Reservoirs II*, pages 309–318. Graham & Trotman, London.

Childs, C., Watterson, J., and Walsh, J. J. (1995). Fault overlap zones within developing normal fault systems. *Journal of the Geological Society of London*, 152:535–549.

Childs, C., Watterson, J., and Walsh, J. J. (1996). A model for the structure and development of fault zones. *Journal of the Geological Society, London*, 153:337–340.

Clifton, A. E., Schlische, R. W., Withjack, M. O., and Ackermann, R. V. (2000). Influence of rift obliquity on fault-population systematics: results of experimental clay models. *Journal of Structural Geology*, 22:1491–1509.

Cloetingh, S., Burov, E., and Poliakov, A. (1999). Lithosphere folding: Primary response to compression? (from Central Asia to Paris basin). *Tectonics*, 18(6):1064–1083.

Cobbold, P. R. and Davy, P. (1988). Indentation tectonics in nature and experiment. 2. Central Asia. *Bulletin of the Geological Institutions of Uppsala*, 14:143–162.

Cobbold, P. R., Durand, S., and Mourgues, R. (2001). Sandbox modelling of thrust wedges with fluid-assisted detachments. *Tectonophysics*, 334:245–258.

Coffield, D. Q. (1987). Surface expression and internal structure of an Accommodation Zone, Gulf of Suez, Egypt. *Bulletin of the American Association of Petroleum Geologists*, 71(5):540.

Coisne, V. (2004). Structurele studie van het gebied rond ol'khon-eiland en maloe more (centraal baikal): inzicht in de evolutie van een gekanteld blok tussen twee grote riftrandbreuken. Master's thesis, Universiteit Gent. pp. 151.

Colletta, B., Letouzey, J., Pinedo, R., Ballard, J. F., and Bale, P. (1991). Computerized X-ray tomography analysis of sandbox models - examples of thin-skinned thrust systems. *Geology*, 19(11):1063–1067.

Collier, R. E. L., Pantosti, D., D'Addezio, G., Marco De Martini, P., Masana, E., and D., S. (1998). Paleoseismicity of the 1981 Corinth earthquake fault: Seismic contribution to extensional strain in central Greece and implications for seismic hazard . *Journal of Geophysical Research*, 103(B12):30001–30019.

Contreras, J., Anders, M., and Scholz, C. H. (2000). Growth of a normal fault system: observations from the Lake Malawi basin of the east African rift. *Journal of Structural Geology*, 22:159–168.

Contreras, J., Scholz, C. H., and King, G. C. P. (1997). A model of rift basin evolution constrained by first-order stratigraphic observations. *Journal of Geophysical Research*, 102(B4):7673–7690.

Corti, G., Bonini, M., Conticelli, S., Innocenti, F., Manetti, P., and Sokoutis, D. (2003). Analogue modelling of continental extension: a review focused on the relations between the patterns of deformation and the presence of magma. *Earth-Science Reviews*, 63(3-4):169–247.

Coskun, B. (1997). Oil and gas fields — transfer zone relationships, Thrace Basin, NW Turkey. *Marine and Petroleum Geology*, 14(4):401–416.

Cowie, P. and Roberts, G. P. (2001). Constraining slip rates and spacings for active normal faults. *Journal of Structural Geology*, 23:1901–1915.

Cowie, P. A. (1998). A healing-reloading feedback control on the growth rate of seismogenic faults. *Journal of Structural Geology*, 20(8):1075–1087.

Cowie, P. A., Gupta, S., and Dawers, N. H. (2000). Implications of fault array evolution for synrift depocentre development: insights from a numerical fault growth model. *Basin Research*, 12:241–261.

Cowie, P. A. and Scholz, C. H. (1992a). Growth of faults by accumulation of seismic slip. *Journal of Geophysical Research*, 97(B7):11085–11095.

Cowie, P. A. and Scholz, C. H. (1992b). Physical explanation for the displacement-length relationships of faults using a post-yield fracture mechanics model. *Journal of Structural Geology*, 14(10):1133–1148.

Cowie, P. A. and Shipton, Z. K. (1998). Fault tip displacement gradients and process zone dimensions. *Journal of Structural Geology*, 20(8):983–997.

Crider, J. G. (2001). Oblique slip and the geometry of normal-fault linkage: mechanics and a case study from the Basin and Range in Oregon. *Journal of Structural Geology*, 23:1997–2009.

Crider, J. G. and Pollard, D. D. (1998). Fault linkage: Three-dimensional mechanical interaction between echelon normal faults. *Journal of Geophysical Research*, 103(B10):24373–24391.

Crone, A. J. and Haller, K. M. (1991). Segmentation and the coseismic behavior of Basin and Range normal faults: examples from east-central Idaho and southwest Montana, U.S.A. *Journal of Structural Geology*, 13:151–164.

Dahlstrom, C. D. A. (1970). Structural geology in the eastern margin of the Canadian Rocky Mountains. *Bulletin of Canadian Petroleum Geology*, 18:332–406.

d'Alessio, M. A. and Martel, S. J. (2004). Fault terminations and barriers to fault growth. *Journal of Structural Geology*. in press.

Darros de Matos, R. M. (1993). Geometry of the hanging wall above a system of listric normal faults — a numerical solution. *Bulletin of the American Association of Petroleum Geologists*, 77(11):1839–1859.

Davison, I. (1994). Linked Fault Systems; Extensional, Strike-Slip and Contractional. In Hancock, P. L., editor, *Continental Deformation*, pages 121–141. Pergamon Press.

Davy, P. and Cobbold, P. (1988). Indentation tectonics in nature and experiment. 1. Experiments scaled for gravity. *Bulletin of the Geological Institutions of Uppsala*, 14:129–141.

Dawers, N. H. and Anders, M. H. (1995). Displacement-length scaling and fault linkage. *Journal of Structural Geology*, 17(5):607–614.

Dawers, N. H., Anders, M. H., and Scholz, C. H. (1993). Growth of normal faults: displacement-length scaling. *Geology*, 21:1107–1110.

De Batist, M. and Vanhauwaert, P. (1995). Lake Baikal 1995: Expedition Report. Internal note of the Renard Centre of Marine Geology, University of Gent.

De Grave, J. (2003). *Apatite fission-track thermochronology of the Altai Mountains (South Siberia, Russia) and the Tien Shan Mountains (Kyrgyzstan): relevance to Meso-Cenozoic tectonics and denudation in Central Asia*. PhD thesis, University of Gent. pp. 289.

Delvaux, D., Fronhoffs, A., Hus, R., and Poort, J. (2000). Normal fault splays, relay ramps and transfer zones in the central part of the Baikal rift basin: insight from digital topography and bathymetry. *Bull. Centre Rech. Elf Explor. Prod.*, 22(2):341–358.

Delvaux, D., Mazukabzov, A. M., Melnikov, A. I., and Alexandrov, V. K. (1993). Early Paleozoic compressive stress field and imbricated thrust structures along the north-western coast of Lake Baikal (Khibelen Cape). *Royal Museum for Central Africa, Tervuren (Belgium), Dépt. Géol. Min., Annual Report 1991 & 1992*, pages 123–136.

Delvaux, D., Moeys, R., Stapel, G., Melnikov, A., and Ermikov, V. (1995). Paleostress reconstructions and geodynamics of the Baikal region, Central Asia, Part I. Paleozoic and Mesozoic pre-rift evolution. *Tectonophysics*, 252:61–101.

Delvaux, D., Moeys, R., Stapel, G., Petit, C., Levi, K., Miroshnichenko, A., Ruzhich, V., and San'kov, V. (1997). Paleostress recontstructions and geodynamics of the Baikal region, Central Asia, Part 2. Cenozoic rifting. *Tectonophysics*, 282:1–38.

dePolo, C. M., Clark, D. G., Burton Slemmons, D., and Ramelli, A. R. (1991). Historical surface faulting in the Basin and Range province, western North America: implications for fault segmentation. *Journal of Structural Geology*, 13(2):123–136.

Destro, N. (1995). Release fault: A variety of cross fault in linked extensional fault systems, in the Sergipe-Alagoas Basin, NE Brazil. *Journal of Structural Geology*, 17(5):615–629.

Destro, N., Alkimin, F. F., Magnavita, L. P., and Szatmari, P. (2003). The jeremoabo transpressional transfer fault, recôncavo-tucano rift, ne brazil. *Journal of Structural Geology*, 25:1263–1279.

Déverchère, J., Houdry, F., Diament, M., Solonenko, N. V., and Solonenko, A. V. (1991). Evidence for a seismogenic upper mantle and lower crust in the Baikal rift. *Geophysical Research Letters*, 18(6):1099–1102.

Déverchère, J., Petit, C., Gileva, N., Radziminovitch, N., Melnikova, V., and San'kov, V. (2001). Depth distribution of earthquakes in the Baikal rift system and its implications for the rheology of the lithosphere. *Geophysical Journal International*, 146:714–730.

Dobretsov, N. I., Buslov, M. M., Delvaux, D., Berzin, N. A., and Ermikov, V. D. (1996). Meso- and Cenozoic tectonics of the Central Asian Mountain Belt: effects of lithospheric plate interaction and mantle plumes. *International Geology Review*, 38:430–466.

Dobretsov, N. L., Berzin, N. A., and Buslov, M. M. (1995). Opening and tectonic evolution of the Paleo-Asian Ocean. *International Geology Review*, 37:335–360.

Dooley, T. and McClay, K. (1997). Analog modeling of pull-apart basins. *Bulletin of the American Association of Petroleum Geologists*, 81(11):1804–1826.

Doser, D. (1991). Faulting within the western Baikal rift as characterised by earthquake studies. *Tectonophysics*, 196(1–2):87–107.

Doser, D. I. and Yarwood, D. R. (1991). Strike-slip faulting in continental rifts: examples from Sabukia, East Africa (1982), and other regions. *Tectonophysics*, 197:213–224.

Dou, L. and Chang, L. (2003). Fault linkage patterns and their control on the formation of the pertroleum systems of the Erlian Basin, Eastern China. *Marine and Petroleum Geology*, 20:1213–1224.

Dresen, G., Gwildis, U., and Kluegel, T. (1991). Numerical and analogue modelling of normal fault geometry. In Roberts, A. M., Yielding, G., and Freeman, B., editors, *The geometry of normal faults*, volume 56, pages 207–217. Geological Society Special Publication.

Du, Y. and Aydin, A. (1991). Interaction of multiple cracks and formation of echelon crack arrays. *International Journal for Numerical and Analytical Methods in Geomechanics*, 15:205–218.

Ebinger, C. J. (1989). Geometric and kinematic development of border faults and accommodation zones, Kivu-Rusizi rift, Africa. *Tectonics*, 8:117–137.

Ebinger, C. J., Jackson, J. A., Foster, A. N., and Hayward, N. J. (1999). Extensional basin geometry and the elastic lithosphere. *Philosophical Transactions of the Royal Society of London, Series A*, 357:741–765.

Ellis, P. G. and McClay, K. R. (1988). Listric extensional fault systems — results of analogue model experiments. *Basin Research*, 1:55–70.

Emmons, R. C. (1969). Strike-slip rupture patterns in sand models. *Tectonophysics*, 7(1):71–87.

England, P. and Jackson, J. (1989). Active deformation of the continents. *Annual Review of Earth and Planetary Sciences*, 17:197–226.

England, P. and Molnar, P. (1997a). Active deformation of asia: from kinematics to dynamics. *Science*, 278:647–650.

England, P. C. and Molnar, P. (1997b). The field of crustal velocity in Asia calculated from Quaternary rates of slip on faults. *Geophysical Journal International*, 130:551–582.

Erickson, S. G., Strayer, L. M., and Suppe, J. (2001). Mechanics of extension and inversion in the hanging walls of listric normal faults. *Journal of Geophysical Research*, 106(B11):26655–26670.

Etheridge, M. A. (1986). On the reactivation of extensional fault systems. *Philosphycal Transactions of the Royal Society of London, Series A*, 317:179–194.

Faccenna, C., Nalpas, T., Brun, J. P., and Davy, P. (1995). The influence of pre-existing thrust faults on normal fault geometry in nature and experiments. *Journal of Structural Geology*, 17(8):1139–1149.

Faulds, J. E. and Varga, R. J. (1998). The role of accommodation zones and transfer zones in the regional segmentation of extended terranes. In Faulds, J. E. and Stewart, J. H., editors, *Accomodation zones and transfer zones; the regional segmentation of the Basin and Range Province*, volume 323, pages 1–45. Geological Society of America, Special Paper.

Ferrill, D. A., Stamatakos, J. A., and Sims, D. (1999). Normal fault corrugation: implications for growth and seismicity of active normal faults. *Journal of Structural Geology*, 21:1027–1038.

Fournier, M., Jolivet, L., Davy, P., and Thomas, J. C. (2004). Backarc extension and collision: an experimental approach to the tectonics of Asia. *Geophysical Journal International*, 157:871–889.

Freeman, B., Yielding, G., and Badley, M. (1990). Fault correlation during seismic interpretation. *First Break*, 8(3):87–95.

Gabrielsen, R. H. and Clausen, J. A. (2001). Horses and duplexes in extensional regimes: A scale-modeling contribution. In Koyi, H. A. and Mancktelow, N. S., editors, *Tectonic Modeling: A volume in honor of Hans Ramberg*, Geological Society of America Memoir 193, pages 207–220.

Gao, S., Davis, P. M., Liu, H., Slack, P. D., Zorin, Y. A., Logatchev, N. A., Kogan, M., Burkholder, P. D., and Meyer, R. P. (1994). Assymetric upwarp of the asthenosphere beneath the Baikal rift zone, Siberia. *Journal of Geophysical Research*, 99(B8):15319–15330.

Gartrell, A. P. (2001). Crustal rheology and its effect on rift basin style. In Koyi, H. A. and Mancktelow, N. S., editors, *Tectonic Modeling: A volume in honor of Hans Ramberg*, Geological Society of America Memoir 193, pages 221–233.

Gauthier, B. D. M. and Lake, S. D. (1993). Probabilistic modeling of faults below the limit of seismic resolution in Pelican Field, North Sea, offshore United Kingdom. *Bulletin of the American Association of Petroleum Geologists*, 77(5):761–777.

Gawthorpe, R. L. and Hurst, J. M. (1993). Transfer zones in extensional basins: their structural style and influence on drainage development and stratigraphy. *Journal of the Geological Society of London*, 150:1137–1152.

Gawthorpe, R. L., Jackson, C. A. L., Young, M. J., Sharp, I. R., Moustafa, A. R., and Leppard, C. W. (2003). Normal fault growth, displacement localisation and the evolution of normal fault populations: the Hammam Faraun fault block, Suez rift, Egypt. *Journal of Structural Geology*, 25:883–895.

Gawthorpe, R. L. and Leeder, M. R. (2000). Tectono-sedimentary evolution of active extensional basins. *Basin Research*, 12:195–218.

Gibbs, A. D. (1984). Structural evolution of extensional basin margins. *Journal of the Geological Society of London*, 141:609–620.

Gibbs, A. D. (1987). Development of extension and mixed-mode sedimentary basins. In Coward, M. P., Dewey, J. F., and Hancock, P. L., editors, *Continental extensional tectonics*, volume 28, pages 19–33. Geological Society Special Publication.

Gibson, J. R., Walsh, J. J., and Watterson, J. (1989). Modelling of bed contours and cross-sections adjacent to planar normal faults. *Journal of Structural Geology*, 11(3):317–328.

Gillespie, P. A., Walsh, J. J., and Waterson, J. (1992). Limitations of dimension and displacement data from single faults and the consequences for data analysis and interpretation. *Journal of Structural Geology*, 14(10):1157–1172.

Goldsworthy, M. and Jackson, J. (2000). Active normal fault evolution in Greece revealed by geomorphology and drainage patterns. *Journal of the Geological Society, London*, 157:967–981.

Golubev, V. A. (2000). Conductive and convective heat flow in the bottom of Lake Baikal and in the surrounding mountains. *Bull. Centre Rech. Elf Explor. Prod.*, 22(2):323–340.

Groshong Jr, R. H., Pashin, J. C., Chai, B., and Schneeflock, R. D. (2003). Predicting reservoir-scale faults with area balance: application to growth stratigraphy. *Journal of Structural Geology*, 25:1645–1658.

Gudmundsson, A. (1992). Formation and growth of normal faults at the divergent plate boundary in Iceland. *Terranova*, 4:464–471.

Gupta, A. and Scholz, C. H. (2000). A model of normal fault interaction based on observations and theory. *Journal of Structural Geology*, 22:865–879.

Gupta, S., Cowie, P. A., Dawers, N. H., and Underhill, J. R. (1998). A mechanism to explain rift-basin subsidence and stratigraphic patterns through fault-array evolution. *Geology*, 26(7):595–598.

Gupta, S., Underhill, J. R., Sharp, I. R., and Gawthorpe, R. L. (1999). Role of fault interactions in controlling synrift sediment dispersal patterns: Miocene, Abu Alaqa Group, Suez Rift, Sinai, Egypt. *Basin Research*, 11:167–189.

Hardman, R. F. P. and Booth, J. E. (1991). The significance of normal faults in the exploration and production of North Sea hydrocarbons. In Roberts, A. M., Yielding, G., and Freeman, B., editors, *The Geometry of Normal Faults*, volume 56, pages 1–13. Geological Society Special Publication.

Harris, R. A. and Day, S. M. (1993). Dynamics of fault interaction: parallel strike-slip faults. *Journal of Geophysical Research*, 98(B3):4461–4472.

Henry, C. D. (1998). Basement-controlled transfer zones in an area of low-magnitude extension, eastern Basin and Range province, Trans-Pecos Texas. In Faulds, J. E. and Stewart, J. H., editors, *Accomodation zones and transfer zones; the regional segmentation of the Basin and Range Province*, volume 323, pages 75–88. Geological Society of America, Special Paper.

Hertzberg, R. W. (1989). *Deformation and Fracture Mechanics of Engineering Materials*. John Wiley & Sons, third edition edition. 682pp.

Hetzel, R., Niedermann, S., Tao, M., Kubik, P. W., Ivy-Ochs, S., Gao, B., and Strecker, M. R. (2002). Low slip rates and long-term preservation of geomorphic features in Central Asia. *Nature*, 417:428–432.

Higgins, R. I. and Harris, L. B. (1997). The effect of cover composition on extensional faulting above re-activated basement faults: results from analog modeling. *Journal of Structural Geology*, 19:89–98.

Hodgkinson, K. M., Stein, R. S., and King, G. C. P. (1996). The 1954 Rainbow Mountain-Fairview Peak-Dixie Valley earthquakes: A triggered normal faulting sequence. *Journal of Geophysical Research*, 101(B11):25459–25471.

Hoffman, P. F. (1999). The break-up of Rodinia, birth of Gondwana, true polar wander and the snowball Earth. *Journal of African Earth Sciences*, 28(1):17–33.

Holdsworth, R. E., Butler, C. A., and Roberts, A. M. (1997). The recognition of reactivation during continental deformation. *Journal of the Geological Society, London*, 154:73–78.

Horsfield, W. T. (1977). An experimental approach to basement-controlled faulting. *Geologie en Mijnbouw*, 56(4):363–370.

Hubbert, M. K. (1937). Theory of scale models as applied to the study of geologic structure. *Geological Society of America Bulletin*, 48:1459–1520.

Hubbert, M. K. (1951). Mechanical basis for certain familiar geological structures. *Bulletin of the Geological Society of America*, 62:355–372.

Huggins, P., Watterson, J. J., Walsh, J. J., and Childs, C. (1995). Relay zone geometry and displacement transfer between normal faults recorded in coal-mine plans. *Journal of Structural Geology*, 17(12):1741–1755.

Huismans, R. S., Podladchikov, Y. Y., and Cloetingh, S. (2001). Transition from passive to active rifting: relative importance of asthenospheric doming and passive extension of the lithosphere. *Journal of Geophysical Research*, 106:11271– 11291.

Hus, R. and De Rycker, K. (2001). Lake Baikal 2001: Logbook of the Maloe More Expedition. Internal note of the Renard Centre of Marine Geology.

Hutchinson, D. R., Golmshtok, A. J., Zonenshain, L. P., Moore, T. C., Scholtz, C. A., and Klitgord, K. D. (1992). Depositional and tectonic framework of the rift basins of Lake Baikal from multichannel seismic data. *Geology*, 20:589–592.

Huyghe, P. and Mugnier, J. L. (1992). The influence of depth on reactivation in normal faulting. *Journal of Structural Geology*, 14(8/9):991–998.

Imber, J., Childs, C., Nell, P. A. R., Walsh, J. J., Hodgetts, D., and Flint, S. (2003). Hanging wall fault kinematics and footwall collapse in listric growth fault systems. *Journal of Structural Geology*, 25:197–208.

Imber, J., Tuckwell, G. W., Childs, C., Walsh, J. J., Manzocchi, T., Heath, A. E., Bonson, C. G., and Strand, J. (2004). Thress-dimensional distinct element modelling of relay growth and breaching along normal faults. *Journal of Structural Geology*, 26:1897–1911.

Jackson, C. A. L., Gawthorpe, R. L., and Sharp, I. A. (2002). Growth and linkage of the East Tanka fault zone, Suez rift: structural style and syn-rift stratigraphic response. *Journal of the Geological Society, London*, 159:175–187.

Jackson, J. (1999). Fault death: a perspective from actively deforming regions. *Journal of Structural Geology*, 21:1003–1010.

Jackson, J. A. (1987). Active normal faulting and crustal extension. In Coward, M. P., Dewey, J. F., and Hancock, P. L., editors, *Continental Extensional Tectonics*, volume 28, pages 3–17. Geological Society Special Publication.

Jackson, J. A. and White, N. J. (1989). Normal faulting in the upper continental crust: observations from regions of active extension. *Journal of Structural Geology*, 11(1/2):15–36.

Jahn, B., Wu, F., and Chen, B. (2000). Massive granitoid generation in Central Asia: Nd isotope evidence and implication for continental growth Phanerozoic. *Episodes*, 23:82–92.

Kattenhorn, S. A. and Pollard, D. D. (2001). Integrating 3-D seismic data, field analogs, and mechanical models in the analysis of segmented normal faults in the Wytch Farm oil field, southern England, United Kingdom. *AAPG-Bulletin*, 85(7):1183–1210.

Keep, M. and McClay, K. R. (1997). Analogue modelling of multiphase rift systems. *Tectonophysics*, 273:239–270.

Khain, E. V., Bibikova, E. V., Salnikova, E. B., Kröner, A., Gibsher, A. S., Didenko, A. N., Degtyarev, K. E., and Fedotova, A. A. (2003). The Palaeo-Asian ocean in the Neoproterozoic and early Palaeozoic: new geochronological data and palaeotectonic recontstructions. *Precambrian Research*, 122:329–358.

Khalil, S. M. and McClay, K. (2001). Tectonic evolution of the NW Red Sea – Gulf of Suez rift system. In Wilson, R. C. L., Whitmarsh, R. B., Taylor, B., and Froitzheim, N., editors, *Non-Volcanic Rifting of Continental Margins*, volume 187, pages 453–473. Geological Society Special Publication.

Khlystov, O. M., Mats, V. D., and De Batist, M. (2001). Southwestern termination of north Baikal basin: Geology and correlation with Cenozoic sections of Ol'khon and BDP-96 and BDP-98 cores. *Russian Geology and Geophysics*, 42(2):362–371.

Kim, Y. S., Peacock, D. C. P., and Sanderson, D. J. (2004). Fault damage zones. *Journal of Structural Geology*, 26:503–517.

Kim, Y. S. and Sanderson, D. J. (2004). The relationship between displacement and length of faults: a review. *Earth-Science Reviews*. in press.

King, G. C. P. (1986). Speculations on the geometry of the initiation and termination process of earthquake rupture and its relation to morphology and geological structure. *Pure and Applied Geophysics*, 124:567–585.

King, G. C. P. and Nábělek, J. L. (1985). Role of fault bends in the initiation and termination of seismic rupture. *Science*, 228:984–987.

King, G. C. P., Stein, R. S., and Rundle, J. B. (1988). The growth of geological structures by repeated earthquakes, 1, conceptual framework. *Journal of Geophysical Research*, 93:13307–13319.

Klyuchevskii, A. V. (2004). Seismic moments of earthquakes in the Baikal rift zone as indicators of recent geodynamic processes. *Journal of Geodynamics*, 37:155–168.

Kornsawan, A. and Morley, C. K. (2002). The origin and evolution of complex transfer zones (graben shifts) in conjugate fault systems around the Funan Field, Pattani Basin, Gulf of Thailand. *Journal of Structural Geology*, 24:435–449.

Koukouvelas, I. K., Asimakopoulos, M., and Doutsos, T. T. (1999). Fractal characteristics of active normal faults: an example of the eastern Gulf of Corinth, Greece. *Tectonophysics*, 308:263–274.

Koyi, H. (1997). Analogue modelling: from a qualitative to a quantitative technique — a historical outline. *Journal of Petroluem Geology*, 20(2):223–238.

Krantz, R. W. (1988). Multiple fault sets and three-dimensional strain. *Journal of Structural Geology*, 10:225–237.

Krantz, R. W. (1991). Measurements of friction coefficient and cohesion for faulting and fault reactivation in laboratory models using sand and sand mixtures. *Tectonophysics*, 188:203–207.

Kusznir, N. J., Marsden, G., and Egan, S. S. (1991). A flexural-cantilever simple-shear/pure-shear model of continental lithosphere extension: applications to the Jeanne d'Arc Basin, Grand Banks and Viking Graben, North Sea. In Roberts, A. M., Yielding, G., and Freeman, B., editors, *The Geometry of Normal Faults*, pages 41–60. Geological Society Special Publication No 56.

Kuzmin, M. I., Karabanov, E. B., Prokopenko, A. A., Gelety, V. F., Antipin, V. S., Williams, D. F., and Gvozdkov, A. N. (2000). Sedimentation processes and new age constraints on rifting stages in Lake Baikal: results of deep-water drilling. *International Journal of Earth Sciences*, 89:183–192.

Lambiase, J. J. and Bosworth, W. (1995). Structural controls on sedimentation in continental rifts. In Lambiase, J., editor, *Hydrocarbon Habitat in Rift Basins.*, volume 80, pages 117–144. Geological Society Special Publication.

Larsen, P. H. (1988). Relay structures in a Lower Permian basement-involved extension system, East Greenland. *Journal of Structural Geology*, 10:3–8.

Le Calvez, J. H. and Vendeville, B. C. (2002). Experimental designs to model along-strike fault interaction. *Journal of the Virtual Explorer*, 7:1–17. In dynamic review.

Le Pichon, X., Fournier, M., and Jolivet, L. (1992). Kinematics, topography, shortening and extrusion in the India-Eurasia collision. *Tectonics*, 11(6):1085–1098.

Le Turdu, C., Richet, J. P., Xavier, J. P., Renaut, R. W., Tiercelin, J. J., Rolet, J., E., L. K., and Coussement, C. (1999). Influence of preexisting oblique discontinuities on the geometry and evolution of extensional fault patterns: Evidence from the Kenya Rift using SPOT imagery . In Morley, C. K., editor, *Geoscience of Rift Systems — Evolution of East Africa*, volume 44 of *AAPG Studies in Geology*, pages 173–191.

Leeder, M. R. and Jackson, J. A. (1993). The interaction between normal faulting and drainage in active extensional basins, with examples from the western United States and central Greece. *Basin Research*, 5:79–102.

Leeder, M. R., Seger, M. J., and Stark, C. P. (1991). Sedimantation and tectonic geomorphology adjacent to major active and inactive normal faults, Southern Greece. *Journal of the Geological Society of London*, 148:331–343.

Leloup, P. H., Lacassin, R., Tapponnier, P., Schärer, U., Dalai, Z., Xiaohan, L., Z., L., Shaocheng, J., and Trinh, P. T. (1995). The Ailo Shan – Red River shear zone (Yunnan, China), Tertiary transform boundary of Indochina. *Tectonophysics*, 251:3–84.

Lesne, O., Calais, E., and Deverchère, J. (1998). Finite element modelling of the crustal deformation in the Baikal rift zone: new insights into the active-passive rifting debate. *Tectonophysics*, 289:327–340.

Lesne, O., Calais, E., Deverchère, J., Chéry, J., and Hassani, R. (2000). Dynamics of intracontinental extension in the north Baikal rift from two-dimensional numerical deformation modeling. *Journal of Geophysical Research*, 105(B9):21727–21744.

Levi, K. G., Miroshnichenko, A. I., San'kov, V. A., Babushkin, S. M., Larkin, G., Badardinov, A. A., Wong, H. K., Coleman, S., and Delvaux, D. (1997). Active faults of the Baikal Basin. *Bull. Centre Rech. Elf Explor. Prod.*, 21(2):399–434.

Lezzar, K. E., Tiercelin, J. J., Le Turdu, C., Cohen, A. S., Reynolds, D. J., Le Gall, B., and Scholz, C. A. (2002). Control of normal fault interaction on the distribution of major Neogene sedimentary depocentres, Lake Tanganyika, East African Rift. *Bulletin of the American Association of Petroleum Geologists*, 86(6):1027–1059.

Lickorish, W. H., Ford, M., Bürgisser, J., and Cobbold, P. R. (2002). Arcuate thrust systems in sandbox experiments: a comparison to the external arcs of the Western Alps. *Bulletin of the Geological Society of America*, 114(9):1089–1107.

Lipman, P. W., Logatchev, N. A., Zorin, Y. A., Chapin, C. E., Kovalenko, V., Morgan, P., Cordell, L. E., Dungan, M. A., Ingersoll, R. V., Keller, G. R., Machette, M. N., Sanford, A. R., Kromovskikh, V. S., Leitnikov, F., Rasskazov, V., S., Sharkov, Y. V., Tsvetkov, A. A., and Yarmolyuk, V. V. (1989). Intracontinental rift comparisons Baikal and Rio Grande rift systems. *EOS*, 70:578–579, 586–588.

Lister, G. S. and Davis, A. D. (1989). The origin of metamorphic core complexes and detachement faults formed during Tertiary continental extension in the northern Colorado River region, U.S.A. *Journal of Structural Geology*, 11(1/2):65–94.

Logatchev, N., Zorin, Y., and Rogozhina, V. (1983). Baikal rift: Active or passive? Comparison of the Baikal and Kenya rift zone. *Tectonophysics*, 94:223–240.

Logatchev, N. A. (1993). History and geodynamics of the Lake Baikal Rift in the context of the Eastern Rift System: a review. *Bull. Centr. Rech. Explor. Prod. Elf Aquitaine*, 17:353–370.

Logatchev, N. A. and Florensov, N. A. (1978). The Baikal system of rift valleys. *Tectonophysics*, 45:1–13.

Logatchev, N. A. and Zorin, Y. A. (1992). Baikal rift zone: structure and geodynamics. *Tectonophysics*, 208:273–286.

Lysak, S. V. (1978). The Baikal Rift heat flow. *Tectonophysics*, 45:87–93.

Maerten, L., Gillespie, P., and Pollard, D. D. (2002). Effects of local stress perturbation on secondary fault development. *Journal of Structural Geology*, 24:145–153.

Maerten, L., Pollard, D. D., and Karpuz, R. (2000). How to constrain 3-D fault continuity and linkage using reflection seismic data: a geomechanical approach. *Bulletin of the American Association of Petroleum Geologists*, 84(9):1311–1324.

Mandl, G. (1987). Discontinuous fault zones. *Journal of Structural Geology*, 9:105–110.

Mandl, G. (1988). *Mechanics of Tectonic Faulting*. Elsevier. pp. 407.

Mandl, G. (2000). *Faulting in Brittle Rocks. An Introduction to the Mechanics of Tectonic Faults*. Springer. p. 434.

Manighetti, I., King, G. C. P., Gaudemer, Y., Scholz, C. H., and Doubre, C. (2001). Slip accumulation and lateral propagation of active normal faults in Afar. *Journal of Geophysical Research*, 106(B7):13667–13696.

Mansfield, C. and Cartwright, J. (2001). Fault growth by linkage: observations and implications from analogue models. *Journal of Structural Geology*, 23:745–763.

Marchal, D., Guiraud, M., and Rives, T. (2003). Geometric and morphologic evolution of normal fault planes and trace from 2D to 4D data. *Journal of Structural Geology*, 25:135–158.

Marrett, R. and Allmendinger, R. W. (1991). Estimates of strain due to brittle faulting: sampling of fault populations. *Journal of Structural Geology*, 13(6):735–738.

Mart, Y. and Dauteuil, O. (2000). Analogue experiments of propagation of oblique rifts. *Tectonophysics*, 316:121–132.

Martel, S. J. (1999). Mechanical controls on fault geometry. *Journal of Structural Geology*, 21:585–596.

Martel, S. J. and Boger, W. A. (1998). Geometry and mechanics of secondary fracturing around small three-dimensional faults in granitic rock. *Journal of Geophysical Research*, 103(B9):21299–21314.

Mats, V. D. (1993). The structure and development of the Baikal rift depression. *Earth-Science Reviews*, 34:81–118.

Mats, V. D., Khlystov, O. M., De Batist, M., Ceramicola, S., Lomonosova, T. K., and Klimansky, A. (2000). The evolution of the Akademichesky Ridge Accomodation Zone in the central part of the Baikal Rift, from high-resolution reflection seismic profiling and geological field investigations. *International Journal of Earth Sciences*, 89:229–250.

Mats, V. D., Lomonosova, T. K., Vorobyova, G. A., and Granina, L. Z. (2004). Upper Cretaceous–Cenozoic clay minerals of the Baikal region (eastern Siberia). *Applied Clay Science*, 24:327–336.

Mats, V. D., Ufimtsev, G. F., and Mandelbaum, M. M. (2001). *The Baikal Basin in the Cenozoic: Structure and geologic history.* SB RAS PRESS, Novosibirsk. pp. 252. In Russian.

Matton, C. and Klerkx, J. (1995). Basin structure in the Western part of Northern Lake Baikal: the Zavorotny Area. *Russian Geology and Geophysics*, 36(10):168–174.

Mauduit, T. and Dauteuil, O. (1996). Small-scale models of oceanic transform zones. *Journal of Geophysical Research*, 101(B9):20195–20209.

McCalpin, J. P. (1996). Application of paleoseismic data to seismic hazard assessment and neotectonic research. In McCalpin, editor, *Paleoseismology*, chapter nine, pages 439–493. Academic Press.

McCalpin, J. P. and Khromovskih, V. S. (1995). Holocene paleoseismicity of the Tunka fault, Baikal rift, Russia. *Tectonics*, 14(3):594–605.

McClay, K. R. (1990a). Deformation mechanics in analogue models of extensional fault systems. In Knipe, R. J. and Rutter, E. H., editors, *Deformation Mechanisms, Rheology and Tectonics*, volume 54, pages 445–453. Geological Society Special Publication.

McClay, K. R. (1990b). Extensional fault systems in sedimentary basins. A review of analogue models. *Marine and Petroleum Geology*, 7:206–233.

McClay, K. R. (1996). Recent advances in analogue modelling: uses in section interpretation. In Buchanan, P. and Nieuwland, D., editors, *Modern developments in structural geology, interpretation, validation and modelling*, volume 99, pages 201–225. Geological Society Special Publication.

McClay, K. R. and Bonora, M. (2001). Analogue models of restraining stepovers in strike-slip fault systems. *Bulletin of the American Association of Petroleum Geologists*, 85(2):233–260.

McClay, K. R., Dooley, T., Gloaguen, R., Whitehouse, P., and Khalil, S. (2001). Analogue modelling of extensional fault architecture: comparisons with natural rift fault systems. In *PESA Eastern Australasian Basins Symposium, Melbourne Victoria*, pages 573–584.

McClay, K. R., Dooley, T., Whithouse, P., and Mills, M. (2002). 4-D evolution of rift systems: Insight from scaled physical models. *Bulletin of the American Association of Petroleum Geologists*, 86(6):935–959.

McClay, K. R. and Ellis, P. G. (1987). Geometries of extensional fault systems developed in model experiments. *Geology*, 15:341–344.

McClay, K. R., Waltham, D. A., Scott, A. D., and Abousetta, A. (1991). Physical and seismic modelling of listric normal fault geometries. In Roberts, A. M., Yielding, G., and Freeman, B., editors, *The Geometry of Normal Faults*, pages 231–239. Geological Society Special Publication No 56.

McClay, K. R. and White, M. J. (1995). Analogue modelling of orthogonal and oblique rifting. *Marine and Petroleum Geology*, 12:137–151.

McGrath, A. (1982). Fault propagation and growth; a study of the Triassic and Jurassic from Watchet and Kilve, North Somerset. Master's thesis, Royal Holloway, University of London, London.

McGrath, A. G. and Davison, I. (1995). Damage zone geometry around fault tips. *Journal of Structural Geology*, 17(7):1011–1024.

McLeod, A. E., Dawers, N. H., and Underhill, J. R. (2000). The propagation and linkage of normal faults: insights from the Strathspey-Brent-Statfjord fault array, northern North Sea. *Basin Research*, 12:263–284.

McLeod, A. E., Underhill, J. R., Davies, S. J., and Dawers, N. H. (2002). The influence of fault array evolution on synrift sedimentation patterns: Controls on deposition in the Strathspey-Brent-Statfjord half graben, northern North Sea. *Bulletin of the American Association of Petroleum Geologists*, 86(6):1061–1093.

Meghraoui, M., Camelbeeck, T., Vanneste, K., Brondeel, M., and Jongmans, D. (2000). Active faulting and paleoseismology along the Bree fault, lower Rhine graben, Belgium. *Journal of Geophysical Research*, 106(B6):13809–13841.

Melnikov, A. I., Mazukabzov, A. M., Sklyarov, E. V., and Vasiljev, E. P. (1994). Baikal rift basement: structure and tectonic evolution. *Bull. Centre Rech. Elf Explor. Prod.*, 18(1):99–122.

Meng, Q. R., Hu, J. M., and Yang, F. Z. (2001). Timing and magnitude of displacement on the Altyn Tagh fault: constraints from stratigraphic correlation of adjoining Tarim and Qaidam basins, NW China. *Terra Nova*, 13:86–91.

Merle, O. and Vendeville, B. C. (1995). Experimental modelling of thin-skinned shortening around magmatic intrusions. *Bulletin of Volcanology*, 57:33–43.

Meyer, V., Nicol, A., Childs, C., Walsh, J. J., and Watterson, J. (2002). Progressive localisation of strain during the evolution of a normal fault population. *Journal of Structural Geology*, 24:1215–1231.

Michon, L. and Merle, O. (2003). Mode of lithospheric extension: Conceptual models from analogue modeling. *Tectonics*, 22(4):1028, doi:10.1029/2002TC001435.

Milani, E. J. and Davison, I. (1988). Basement control and transfer tectonics in the Recôncavo-Tucano-Jatobá rift, Northeast Brasil. *Tectonophysics*, 154:41–70.

Molnar, P., Fitch, T. J., and Wu, F. T. (1973). Fault plane solutions of shallow earthquakes and contemporary tectonics in Asia. *Earth and Planetary Science Letters*, 19:101–112.

Molnar, P. and Tapponnier, P. (1975). Cenozoic Tectonics of Asia: Effects of a Continental Collision. *Science*, 4201:419–426.

Moore, J. M. and Schultz, R. A. (1999). Processes of faulting in jointed rocks of Canyonlands National Park, Utah. *GSA Bulletin*, 111(6):808–822.

Moore, T. C. J., Klitgord, K. D., Golmshtok, A. J., and Weber, E. (1997). Sedimentation and subsidence patterns in the central and north basins of Lake Baikal from seismic stratigraphy. *GSA Bulletin*, 109(6):746–766.

Morewood, N. C. and Roberts, G. P. (2000). The geometry, kinematics and rates of deformation within an en échelon normal fault segment boundary, central Italy. *Journal of Structural Geology*, 22:1027–1047.

Morley, C. K. (1995). Developments in the structural geology of rifts over the last decade and their impact on hydrocarbon exploration. In Lambiase, J. J., editor, *Hydrocarbon Habitat in Rift Basins.*, volume 80, pages 1–32. Geological Society Special Publication.

Morley, C. K. (1999a). Aspects of transfer zone geometry and evolution in East African Rifts. In Morley, C. K., editor, *Geoscience of Rift Systems — Evolution of East Africa*, volume 44 of *AAPG Studies in Geology*, pages 161–171.

Morley, C. K. (1999b). Basin evolution trends in East Africa. In Morley, C. K., editor, *Geoscience of Rift Systems — Evolution of East Africa*, volume 44 of *AAPG Studies in Geology*, pages 131–150.

Morley, C. K. (1999c). How successful are analogue models in addressing the influence of pre-existing fabrics on rift structure? *Journal of Structural Geology*, 21(8-9):1267–1274.

Morley, C. K. (1999d). Influence of preexisting fabrics on rift structure. In Morley, C. K., editor, *Geoscience of Rift Systems — Evolution of East Africa*, volume 44 of *AAPG Studies in Geology*, pages 151–159.

Morley, C. K. (2002). Evolution of large normal faults: Evidence from seismic reflection data. *Bulletin of the American Association of Petroleum Geologists*, 86(6):961–978.

Morley, C. K., Nelson, R. A., Patton, T. L., and Munn, S. G. (1990). Transfer Zones in the East African Rift System and Their Relevance to Hydrocarbon Exploration in Rifts. *Bulletin of the American Association of Petroleum Geologists*, 74(8):1234–1253.

Morley, C. K., Vanhauwaert, P., and De Batist, M. (2000). Evidence for high-frequency cyclic fault activity from high-resolution seismic reflection survey, Rukwa Rift, Tanzania. *Journal of the Geological Society, London*, 157:983–994.

Morley, C. K. and Wonganan, N. (2000). Normal fault displacement characteristics, with particular reference to synthetic transfer zones, Mae Moh mine, northern Thailand. *Basin Research*, 12:307–327.

Moustafa, A. R. (2002). Controls on the geometry of transfer zones in the Suez rift and northwest Red Sea: Implications for the structural geometry of rift systems. *Bulletin of the American Association of Petroleum Geologists*, 86(6):979–1002.

Muir Wood, R. and Mallard, D. J. (1992). When is a fault 'extinct'? *Journal of the Geological Society (London)*, 149:251–255.

Mulugeta, G. (1985). Dynamic models of continental rift valley systems. *Tectonophysics*, 113:49–73.

Mulugeta, G. and Koyi, H. (1987). Three-dimensional geometry and kinematics of experimental piggyback thrusting. *Geology*, 15:1052–1056.

Muroaka, H. and Kamata, H. (1983). Displacement distribution along minor fault traces. *Journal of Structural Geology*, 5:483–495.

Needham, T., Yielding, G., and Fox, R. (1996). Fault population description and prediction using examples from the offshore U.K. *Journal of Structural Geology*, 18(2/3):155–167.

Nelson, R. A., Patton, T. L., and Morley, C. K. (1992). Rift-segment interaction and its relation to hydrocarbon exploration in continental rift systems. *AAPG bulletin*, 76(8):1153–1169.

Neugebauer, H. J. (1983). Mechanical aspects of continental rifting. *Tectonophysics*, 94:91–108.

Nicol, A., Walsh, J. J., Watterson, J., and Gillespie, P. A. (1996). Fault size distributions — are they really power-law? *Journal of Structural Geology*, 18(2/3):191–197.

Nikishkin, A. M., Cloetingh, S., Lobkovsky, L. I., Burov, E. B., and Lankreijer, A. C. (1993). Continental lithosphere folding in Central Asia (Part I): constraints from geological observations. *Tectonophysics*, 226:59–72.

Ofoegbu, G. I. and Ferrill, D. A. (1998). Mechanical analyses of listric normal faulting with emphasis on seismicity assessment. *Tectonophysics*, 284:65–77.

Olsen, J. and Pollard, D. D. (1989). Inferring paleostress from natural fracture patterns: a new method. *Geology*, 17:345–348.

Opheim, J. A. and Gudmundsson, A. (1989). Formation and geometry of fractures, and related volcanism of the Kafka fissure swarm, northeast Iceland. *Geological Society of America Bulletin*, 101:1608–1622.

Peacock, D. C. P. (1991). Displacements and segment linkage in strike-slip fault zones. *Journal of Structural Geology*, 13(9):1025–1035.

Peacock, D. C. P. (2002). Propagation, interaction and linkage in normal fault systems. *Earth-Science Reviews*, 58:121–142.

Peacock, D. C. P. (2003). Scaling of transfer zones in the British Isles. *Journal of Structural Geology*, 25:1561–1567.

Peacock, D. C. P., Knipe, R. J., and Sanderson, D. J. (2000a). Glossary of normal faults. *Journal of Structural Geology*, 22:291–305.

Peacock, D. C. P. and Parfitt, E. A. (2002). Active relay ramps and normal fault propagation on Kilauea Volcano, Hawaii. *Journal of Structural Geology*, 24:729–742.

Peacock, D. C. P., Price, S. P., Whitham, A. G., and Pickles, C. S. (2000b). The World's biggest relay ramp: Hold With Hope, NE Greenland. *Journal of Structural Geology*, 22:843–850.

Peacock, D. C. P. and Sanderson, D. J. (1991). Displacements, segment linkage and relay ramps in normal fault zones. *Journal of Structural Geology*, 13(6):721–733.

Peacock, D. C. P. and Sanderson, D. J. (1994). Geometry and Development of Relay Ramps in Normal Fault Systems. *Bulletin of the American Association of Petroleum Geologists*, 78(2):147–165.

Peacock, D. C. P. and Sanderson, D. J. (1995). Strike-slip relay ramps. *Journal of Structural Geology*, 17(10):1351–1360.

Peacock, D. C. P. and Sanderson, D. J. (1996). Effects of propagation rate on displacement variations along faults. *Journal of Structural Geology*, 18(2/3):311–320.

Peltzer, G. and Saucier, F. (1996). Present-day kinematics of Asia derived from geologic fault rates. *Journal of Geophysical Research*, 101(B12):27943–27956.

Peltzer, G. and Tapponnier, P. (1988). Formation and evolution of strike-slip faults, rifts and basins during the India-Asia collision: an experimantal approach. *Journal of Geophysical Research*, 93(B12):15085–15117.

Petit, C. (1998). Style of active intraplate deformation from gravity and seismicity data: the Baikal Rift, Asia. *Terra Nova*, 10:160–169.

Pivnik, D. A., Ramzy, M., Steer, B. L., Thorseth, J., El Sisi, Z., Gaafar, I., Garing, D., and Tucker, R. S. (2003). Episodic growth of normal faults as recorded by syntectonic sediments, July oil field, Suez rift, Egypt. *Bulletin of the American Association of Petroleum Geologists*, 87(6):1015–1030.

Poliakov, A. N. B., Dmowska, R., and Rice, J. R. (2002). Dynamic shear rupture interactions with fault bends and off-axis secondary faulting. *Journal of Geophysical Research*, 107(B11):2995,doi:10.1029/2001JB000572.

Pollard, D. D. and Aydin, A. (1984). Propagation and linkage of oceanic ridge segments. *Journal of Geophysical Research*, 89(B12):10017–10028.

Pollard, D. D. and Aydin, A. (1988). Progress in understanding jointing over the past century. *Bulletin of the Geological Society of America*, 100:1181–1204.

Pollard, D. D. and Segall, P. (1987). Theoretical displacements and stresses near fractures in rock: with applications to faults, joints, veins, dikes and solution surfaces. In Atkinson, B. K., editor, *Fracture Mechanics of Rocks*, pages 277–349. Academic Press, London.

Pollard, D. D., Segall, P., and Delaney, P. T. (1982). Formation and interpretation of dilatant echelon cracks. *Bulletin of the Geological Society of America*, 93:1291–1303.

Poort, J. and Klerkx, J. (2004). Absence of a regional surface thermal high in the Baikal rift; new insights from detailed contouring of heat flow anomalies. *Tectonophysics*, 383:217–241.

Poulimenos, G. (2000). Scaling properties of normal fault populations in the western Corinth Graben, Greece: implications for fault growth in large strain settings. *Journal of Structural Geology*, 22:307–322.

Ramberg, H. (1981). *Gravity, Deformation and the Earth's Crust.* Academic Press, second edition. 452pp.

Ramsay, J. G. and Huber, M. I. (1987). *The Techniques of Modern Structural Geology. Volume 2: Folds and Fractures.* Academic Press.

Ramsay, J. G. and Lisle, R. J. (2000). *The Techniques of Modern Structural Geology. Volume 3: Applications of continuum mechanics in structural geology.* Academic Press.

Ranalli, G. (2000). Rheology of the crust and its role in tectonic reactivation. *Journal of Geodynamics*, 30:3–15.

Ranalli, G. (2001). Experimental tectonics: from Sir James Hall to present. *Journal of Geodynamics*, 32:65–76.

Rasskazov, S. V. (1994). Magmatism related to the eastern Siberia rift system and the geodynamics. *Bull. Centre Rech. Elf Explor. Prod.*, 18(2):437–452.

Reigber, C., Michel, G. W., Galas, R., Angermann, D., Klotz, J., Chen, J. Y., Papschev, A., Arslanov, R., Tzurkov, V. E., and Ishanov, M. C. (2001). New space geodetic constraints on the distribution of deformation in Central Asia. *Earth and Planetary Science Letters*, 1991:157–165.

Repulmaz, A. and Tapponnier, P. (2003). Reconstruction of the deformed collision zone between India and Asia by backward motion of lithospheric blocks. *Journal of Geophysical Research*, 108(B6):2285, doi:10.1029/2001JB000661.

Richard, P. and Krantz, R. W. (1991). Experiments on fault reactivation in strike-slip mode. *Tectonophysics*, 188:117–131.

Rippon, J. H. (1985). Contoured patterns of the throw and hade of normal faults in the Coal Measures (Westphalian) of north-east Derbyshire. *Proceedings of the Yorkshire Geological Society*, 45(3):147–161.

Roberts, A. and Yielding, G. (1994). Continental extensional tectonics. In Hancock, P. L., editor, *Continental deformation*, pages 223–250. Pergamon Press.

Roberts, A. M. and Yielding, G. (1991). Deformation around basin-margin faults in the North Sea/mid-Norway rift. In Roberts, A. M., Yielding, G., and Freeman, B., editors, *The Geometry of Normal Faults*, pages 61–78. Geological Society Special Publication No 56.

Roberts, A. M., Yielding, G., and Freeman, B., editors (1991). *The Geometry of Normal Faults*, volume 56. Geological Society Special Publication. pp. 264.

Roberts, S. and Jackson, J. (1991). Active normal faulting in central Greece: an overview. In Roberts, A. M., Yielding, G., and Freeman, B., editors, *The Geometry of Normal Faults*, pages 125–142. Geological Society Special Publication No 56.

Rosendahl, B. R., Reynolds, D. J., Lorber, P. M., Burgess, C. F., McGill, J., Scott, D., Lambiase, J. J., and Derksen, S. J. (1986). Structural expression of rifting: lessons from Lake Tanganyika, Africa. In Frostick, L. E. e. a., editor, *Sedimentation in the African Rifts*, pages 29–43. Geological Society Special Publication No 25.

Rosendahl, R. B. (1987). Architecture of continental rifts with special reference to East Africa. *Annual Review of Earth and Planetary Sciences*, 15:445–503.

Rudnicki, J. W. (1980). Fracture mechanics applied to the earth's crust. *Annual Review of Earth and Planetary Sciences*, 8:489–525.

Ruppel, C. (1995). Extensional processes in the continental litosphere. *Journal of Geophysical Research*, 100(B12):24187–24215.

San'kov, V., J., D., Gaudemer, Y., Houdry, F., and Filippov, A. (2000). Geometry and rate of faulting in the North Baikal Rift, Siberia. *Tectonics*, 19(4):707–722.

Sankov, V. A., Levi, K. G., Calais, E., Déverchère, J., Lesne, O., Lukhnev, A. V., Miroshnichenko, A. I., Buddo, V. Y., Zalutskii, V. T., and Bashkuev, Y. B. (1999). Historic and Holocene horizontal movements measured at the Baikal geodynamic test ground. *Russian Geology and Geophysics*, 40(3):414–421.

San'kov, V. A., Miroshnichenko, A. I., Levi, K. G., Lukhnev, A., Melnikov, A. I., and Delvaux, D. (1997). Cenozoic stress field evolution in the Baikal Rift Zone. *Bull. Centre Rech. Elf Explor. Prod.*, 21(2):435–455.

Savage, J. C. and Hastie, L. M. (1966). Surface deformation associated with dip-slip faulting. *Journal of Geophysical Research*, 71(20):4897–4904.

Schellart, W. P. (2000). Shear test results for cohesion and friction coefficients for different granular materials: scaling implications for their usage in analogue modelling. *Tectonophysics*, 324:1–16.

Schlische, R. W. (1991). Half-graben basin filling models: New constraints on continental extensional basin development. *Basin Research*, 3:123–141.

Schlische, R. W. (1995). Geometry and origin of fault-related folds in extensional settings. *Bulletin of the American Association of Petroleum Geologists*, 79(11):1661–1678.

Schlische, R. W., Young, S. S., Ackermann, R. V., and Gupta, A. (1996). Geometry and scaling relations of a population of very small rift-related normal faults. *Geology*, 24(8):683–686.

Scholz, C. A. and Hutchinson, D. R. (2000). Stratigraphic and structural evolution of the Selenga Delta Accommodation Zone, Lake Baikal Rift, Siberia. *International Journal of Earth Sciences*, 89:212–228.

Scholz, C. H. (1990). *The mechanics of earthquakes and faulting*. Cambridge University Press, first edition. pp. 439.

Scholz, C. H. (2002). *The mechanics of earthquakes and faulting*. Cambridge University Press, second edition. pp. 469.

Scholz, C. H. and Cowie, P. A. (1990). Detremination of total strain from faulting using slip measurements. *Nature*, 346:837–838.

Scholz, C. H., Dawers, N. H., Yu, J. Z., and Anders, M. H. (1993). Fault growth and fault scaling: preliminary results. *Journal of Geophysical Research*, 98(B12):21951–21961.

Scholz, C. H. and Gupta, A. (2000). Fault interactions and seismic hazard. *Journal of Geodynamics*, 29:459–467.

Schöpfer, M. P. J. and Steyrer, H. P. (2001). Experimental modeling of strike-slip faults and the self-similar behavior. In Koyi, H. A. and Mancktelow, N. S., editors, *Tectonic Modeling: A volume in honor of Hans Ramberg*, Geological Society of America Memoir 193, pages 21–27.

Schreurs, G. (1994). Experiments on strike-slip faulting and block rotation. *Geology*, 22:567–570.

Schreurs, G., Hänni, R., and Vock, P. (2001). Four-dimensional analysis of analog models: Experiments on transfer zones in fold and thrust belts. In *Tectonic Modelling: A volume in honor of Hans Ramberg*, pages 179–190. Geological Society of America, Memoir 193.

Schultz, R. A. (1999). Understanding the process of faulting: selected challenges and opportunities at the edge of the 21st century. *Journal of Structural Geology*, 21:985–993.

Schultz, R. A. and Fossen, H. (2002). Displacement-length scaling in three dimensions: the importance of aspect ratio and application to deformation bands. *Journal of Structural Geology*, 24:1389–1411.

Schwartz, D. P. and Coppersmith, K. J. (1984). Fault behavior and characteristic earthquakes: examples from the Wasatch and San Andreas Fault Zones. *Journal of Geophysical Research*, 89(B7):5681–5698.

Scott, D. L. and Rosendahl, B. R. (1989). North Viking graben: an East African perspective. *Bulletin of the American Association of Petroleum Geologists*, 73:155–165.

Segall, P. and Pollard, D. D. (1980). Mechanics of discontinuous faults. *Journal Of Geophysical Research*, 85(B8):4337–4350.

Şengör, A. M. C. and Burke, K. (1978). Relative timing of rifting and volcanism on Earth and its tectonic implications. *Geophysical Research Letters*, 5:419–421.

Şengör, A. M. C. and Natal'In, B. A. (1996). Paleotectonics of Asia: fragments of a synthesis. In Yin, A. and Harrison, M., editor, *The Tectonic Evolution of Asia*, pages 486–640. Cambridge Univerity Press.

Şengör, A. M. C., Natal'In, B. A., and Burtman, V. S. (1993). Evolution of the Altaid tectonic collage and Paleozoic crustal growth in Eurasia. *Nature*, 364:299–307.

Sherman, S. I. (1978). Faults of the Biakal Rift Zone. *Tectonophysics*, 45:31–39.

Sherman, S. I. (1992). Faults and tectonic stresses of the Baikal rift zone. *Tectonophysics*, 208:297–307.

Sherman, S. I., Dem'yanovich, V. M., and Lysak, S. V. (2004). Active faults, seismicity and recent fracturing in the lithosphere of the Baikal rift system. *Tectonophysics*. in press.

Sherman, S. I. and Levi, K. G. (1977). Transform faults of the Baikal rift zone. *Transactions of the USSR Academy of Sciences*, 233(1-6):79–82.

Sherman, S. I., Medvedev, M. E., Ruzhich, V. V., Kiselev, A. I., and Shmotov, A. P. (1973). *Tectonics and volcanism of the southwestern part of the Baikal Rift Zone*. Nauka, Novosibirsk. 136 pp. (in Russian).

Sibson, R. H. (1989). Earthquake faulting as a structural process. *Journal of Structural Geology*, 11(1/2):1–14.

Soliva, R. and Benedicto, A. (2003). Can normal fault segment linkage increase seismic hazard? *Geophysical Research Abstracts*, 5:01110.

Soliva, R. and Benedicto, A. (2004). A linkage criterion for segmented normal faults. *Journal of Structural Geology*, 26:2251–2267.

Stein, R. S. (1999). The role of stress transfer in earthquake occurrence. *Nature*, 402:605–609.

Stewart, I. S. and Hancock, P. L. (1991). Scales of structural heterogeneity within neotectonic normal fault zones in the Aegean region. *Journal of Structural Geology*, 13(2):191–204.

Stock, J. M. and Hodges, K. V. (1990). Miocene to recent structural development of an extensional accommodation zone, northeastern Baja California, Mexico. *Journal of Structural Geology*, 12:315–328.

Tapponnier, P. and Molnar, P. (1979). Active faulting and cenozoic tectonics of the Tien-Shan, Mongolia and Baykal Regions. *Journal of Geophysical Research*, 84(B7):3425–3459.

Tapponnier, P., Peltzer, G., Le Dain, A. Y., Armijo, R., and Cobbold, P. (1982). Propagating extrusion tectonics in Asia: new insights from simple experiments with plasticine. *Geology*, 10:611–616.

Tchalenko, J. S. (1970). Similarities between shear zones of different magnitudes. *Geological Society of America Bulletin*, 81:1625–1640.

Tchalenko, J. S. and Ambraseys, N. N. (1970). Structural Analysis of the Dasht-e Baỹaz (Iran) earthquake fractures. *Geological Society of America Bulletin*, 81:41–60.

ten Brink, U. S. and Taylor, M. H. (2002). Crustal structure of central Lake Baikal: Insights into intracontinental rifting. *Journal of Geophysical Research*, 107(B7):ETG 2–1 – ETG 2–15.

Tentler, T. (2003). Analogue modeling of overlapping spreading centers: insights into their propagation and coalescence. *Tectonophysics*, 376:99–115.

The INTAS Project 99-1669 Team (2002). A new bathymetric map of Lake Baikal. Open-File Report on CD-Rom.

Thenhaus, P. C. and Barnhard, T. P. (1989). Regional termination and segmentation of Quaternary fault bends in the Great Basin, Nevada and Utah. *Bulletin of the Seismological Society of America*, 79:1426–1438.

Theunissen, K., Melnikov, A., Sklyarov, E., Mazukabov, A., and Mruma, A. (1993). The Primorsky dislocation zone in the basement of the Cenozoic Baikal Rift (Russia). *Royal Museum for Central Africa, Tervuren (Belgium), Dépt. Géol. Min., Annual Report 1991 & 1992*, pages 137–151.

Tiberi, C., Diament, M., Déverchère, J., Petit-Mariani, C., Mikhailov, V., Tikhotsky, S., and Achauer, U. (2003). Deep structure of the Baikal rift zone revealed by joint inversion of gravity and seismology. *Journal of Geophysical Research*, 108(B3):2133, doi:10.1029/2002JB001880.

Tron, V. and Brun, J. P. (1991). Experiments on oblique rifting in brittle-ductile systems. *Tectonophysics*, 188:71–84.

Trudgill, B. D. (2002). Structural controls on drainage development in the Canyonlands grabens of southeast Utah. *Bulletin of the American Association of Petroleum Geologists*, 86(6):1095–112.

Trudgill, B. D. and Cartwright, J. A. (1994). Relay ramp forms and normal fault linkages — Canyonlands National Park, Utah. *Bulletin of the Geological Society of America*, 106:1143–1157.

Turcotte, D. L. and Schubert, G. (2002). *Geodynamics*. Cambridge University Press, second edition. 456pp.

van der Beek, P. (1997). Flank uplift and topography at the central Baikal rift (SE Siberia): A test of kinematic models for continental extension. *Tectonics*, 16:122–136.

Van Der Beek, P. A., Delvaux, D., Andriessen, P. A. M., and Levi, K. G. (1996). Early Cretaceous denudation related to convergent tectonics in the Baikal region, SE Siberia. *Journal of the Geological Society, London*, 153:515–523.

Vanneste, M. and De Batist, M. (1998). Lake Baikal 1998: Expedition Report. Internal note of the Renard Centre of Marine Geology, University of Gent.

Vendeville, B. (1991). Mechanism generating normal fault curvature: a review illustrated by physical models. In Roberts, A. M., Yielding, G., and Freeman, B., editors, *The Geometry of Normal Faults*, pages 241–249. Geological Society Special Publication No 56.

Vendeville, B. and Cobbold, P. R. (1988). How normal faulting and sedimentation interact to produce listric fault profiles and stratigraphic wedges. *Journal of Structural Geology*, 10(7):649–659.

Vendeville, B., Cobbold, P. R., Davy, P., Brun, J. P., and Choukroune, P. (1987). Physical models of extensional tectonics at various scales. In Coward, M. P., Dewey, J. F., and Hancock, P. L., editors, *Continental Extensional Tectonics*, pages 95–107. Geological Society Special Publication No 28.

Vermilye, J. M. and Scholz, C. H. (1999). Fault propagation and segmentation: insight from the microstructural examination of a small fault. *Journal of Structural Geology*, 21:1623–1636.

Versfelt, J. and Rosendahl, B. (1989). Relationships between pre-rift structure and rift architecture in Lakes Tanganyika and Malawi, East Africa. *Nature*, 337:354–357.

Villemin, T., Angelier, J., and Sunwoo, C. (1995). Fractal distribution of fault length and offsets: implications of brittle deformation evaluation – the Loraine coal basin. In Barton, C. C. and LaPointe, P. R., editors, *Fractals in the Eath Sciences*, pages 205–225. New York: Plenum.

Walsh, J., Watterson, J., Bailey, W., and Childs, C. (1999). Fault relays, bends and branch-lines. *Journal of Structural Geology*, 21:1019–1026.

Walsh, J. J., Bailey, W. R., Childs, C., Nicol, A., and Bonson, C. G. (2003). Formation of segmented normal faults: a 3-D perspective. *Joural of Structural Geology*, 25:1251–1262.

Walsh, J. J., Nicol, A., and Childs, C. (2002). An alternative model for the growth of faults. *Journal of Structural Research*, 24:1669–1675.

Walsh, J. J. and Watterson, J. (1987). Distributions of cumulative displacement and seismic slip on a single normal fault surface. *Journal of Structural Geology*, 9:1039–1046.

Walsh, J. J. and Watterson, J. (1988). Analysis of the relationship between displacement and dimensions of faults. *Journal of Structural Geology*, 10:239–247.

Walsh, J. J. and Watterson, J. (1991). Geometric and kinematic coherence and scale effects in normal fault systems. In Roberts, A. M., Yielding, G., and Freeman, B., editors, *The geometry of normal faults*, volume 56, pages 193–203. Geological Society Special Publication.

Walsh, J. J. and Watterson, J. (1992). Populations of faults and fault displacements and their effects on estimates of fault-related regional extension. *Journal of Structural Geology*, 14(6):701–712.

Walsh, J. J., Watterson, J., and Yielding, G. (1991). The importance of small-scale faulting on regional extension. *Nature*, 351:391–393.

Waltham, D. (2002). Folding and faulting in coulomb materials. *Basin Research*, 14:319–328.

Watterson, J. (1986). Fault dimensions, displacements and growth. *Pure and Applied Geophysics*, 124(1/2):365–373.

Watterson, J., Walsh, J. J., Gillespie, P. A., and Easton, S. (1996). Scaling systematics of fault sizes on a large-scale range fault map. *Journal of Structural Geology*, 18(2/3):199–214.

Weijermars, R. (1986). Flow behavior and physical chemistry of bouncing putties and related polymers in view of tectonic laboratory applications. *Tectonophysics*, 124:325–358.

Weijermars, R., Jackson, M. P. A., and Vendeville, B. (1993). Rheological and tectonic modeling of salt provinces. *Tectonophysics*, 217:143–174.

Wernicke, B. (1981). Low-angle normal faults in the Basin and Range province: Nappe tectonics in an extending orogen. *Nature*, 291:645–648.

Wernicke, B. and Axen, G. J. (1988). On the role of isostasy in the evolution of normal fault systems. *Geology*, 16:848–851.

Westaway, R. (1995). Deformation around stepovers in strike-slip fault zones. *Journal of Structural Geology*, 17(6):831–846.

White, M. J. (1993). *Physical modelling and analysis of the geometries and kinematics of orthogonal and oblique rifting*. PhD thesis, Royal Holloway University of London.

Wilkins, S. J. and Gross, M. R. (2002). Normal fault growth in layered rocks at Split Mountain, Utah: influence of mechanical stratigraphy on dip linkage, fault restriction and fault scaling. *Journal of Structural Geology*, 24:1413–1429.

Willemse, E. J. M. (1997). Segmented normal faults: correspondence between three-dimensional mechanical models and field data. *Journal of Geophysical Research*, 102(B1):675–692.

Willemse, E. J. M., Pollard, D. D., and Aydin, A. (1996). Three-dimensional analyses of slip distributions on normal fault arrays with consequences for fault scaling. *Journal of Structural Geology*, 18(2/3):295–309.

Williams, G. D. and Vann, I. (1987). The geometry of listric normal faults and deformation in their hangingwalls. *Journal of Structural Geology*, 9(7):789–795.

Withjack, M. O. and Peterson, E. T. (1993). Prediction of normal fault geometries — a sensitivity analysis. *Bulletin of the American Associaton of Petroleum Geologists*, 77(11):1860–1873.

Wojtal, S. F. (1994). Fault scaling laws and temporal evolution of fault systems. *Journal of Structural Geology*, 16:603–612.

Xiao, H. and Suppe, J. (1992). Origin of rollover. *Bulletin of the American Association of Petroleum Geologists*, 76(4):509–529.

Yielding, G., Needham, T., and Jones, H. (1996). Sampling of fault populations using sub-surface data: a review. *Journal of Structural Geology*, 18(20):135–146.

Yielding, G. and Roberts, A. (1992). Footwall uplift during normal faulting — implications for structural geometries in the North Sea. In Larsen, R. M., Brekke, H., Larsen, B. T., and Talleraas, E., editors, *Structural and Tectonic Modelling and its Application to Petroleum Geology*, volume 1 of *NPF Special Publication*, pages 289–303. Elsevier, Amsterdam.

Yielding, G., Walsh, J., and Watterson, J. (1992). The prediction of small-scale faulting in reservoirs. *First Break*, 10(12):449–460.

Yin, A. and Harrison, T. M. (2000). Geologic evolution of the Himalayan-Tibetan Orogen. *Annual Review of Earth and PLanetary Sciences*, 28:211–280.

Younes, A. I. and McClay, K. (2002). Development of accommodation zones in the Gulf of Suez – Red Sea rift, Egypt. *Bulletin of the American Association of Petroleum Geologists*, 86(6):1003–1026.

Young, M. J., Gawthorpe, R. L., and Hardy, S. (2001). Growth and linkage of a segmented normal fault zone: the Late Jurassic Murchison – Statfjord North Fault, northern North Sea. *Journal of Structural Geology*, 23:1933–1952.

Zhang, P., Slemmons, D. B., and Mao, F. (1991). Geometric pattern, rupture termination and fault segmentation of the Dixie Valley-Pleasant Valley active normal fault system, Nevada, U.S.A. *Journal of Structural Geology*, 13:165–176.

Zhao, X., Coe, R. S., Zhou, Y., Wu, H., and Wang, J. (1990). New paleomagnetic results from nothern China: collision and suturing with Siberia and Kazakhstan. *Tectonophysics*, 181:43–81.

Ziegler, P. A. and Cloetingh, S. (2004). Dynamic processes controlling evolution of rifted basins. *Earth Science Reviews*, 64:1–50.

Zonenshain, I. P. and Savostin, L. A. (1981). Geodynamics of the Baikal rift zone and plate tectonics of Asia. *Tectonophysics*, 76:1–45.

Zonenshain, L. P., Golmshtok, A. Y., and Hutchinson, D. (1992). Baikal rift structure. *Geotectonics*, 26(5):396–407.

Zonenshain, L. P., Kuzmin, M. I., and Natapov, L. (1990). *Geology of the USSR: A Plate-tectonic Synthesis*. Geodynamics Series, Volume 21. American Geophysical Union. Washington, D.C.

Zorin, Y. A., Belichenko, V. G., Turutanov, E. K., Kozhevnikov, V. M., Ruzhentsev, S. V., Dergunov, A. B., Filippova, I. B., Tomutogoo, O., Arvisbaatar, N., Bayasgalan, T., Biambaa, C., and Khosbayar, P. (1993). The South Siberia–Central Mongolia transect. *Tectonophysics*, 225:361–378.

Zorin, Y. A., Mordvinova, V. V., Turutanov, E. K., Belichenko, B. G., Artemyev, A. A., Kosarev, G. L., and Gao, S. S. (2002). Low seismic velocity layers in the Earth's crust beneath Eastern Siberia (Russia) and Central Mongolia: receiver function data and their possible geological implication. *Tectonophysics*, 359:307–327.

Zorin, Y. A. and Rogozhina, V. A. (1978). Mechanism of rifting and the deep-seated structure of the Baikal rift zone. *Tectonophysics*, 45:23–30.

Zorin, Y. A., Turutanov, E. K., Mordvinova, V. V., Kozhevnikov, V. M., Yanovskaya, T. B., and Treussov, A. V. (2003). The Baikal rift zone: the effect of mantle plumes on older structure. *Tectonophysics*, 371:153–173.